



**Old drugs with new tricks:
repurposing small molecules to promote
lysosomal escape of
small nucleic acid therapeutics**

Thijs Van de Vyver

Pharmacist

Master of Science in Drug Development

2020

Thesis submitted to obtain the degree of
Doctor in Pharmaceutical Sciences

Proefschrift voorgedragen tot het bekomen van de graad van
Doctor in de Farmaceutische Wetenschappen

Dean

Prof. dr. apr. Jan Van Bocxlaer

Promotor

Prof. dr. apr. Koen Raemdonck

Co-promotor

Prof. dr. apr. Stefaan De Smedt

Members of the Evaluation Committee:

Prof. dr. **Serge Van Calenbergh** (chairman)

Ghent University

Prof. dr. **Tom Coenye** (secretary)

Ghent University

Prof. dr. **Pieter Mestdagh**

Ghent University

Prof. dr. **Véronique Pr at**

Catholic University of Louvain

Prof. dr. **Roy van der Meel**

Eindhoven University of Technology

Prof. dr. **Arwyn Tomos Jones**

Cardiff University

The author and the (co-)promoters give the authorization to consult and to copy parts of this thesis for personal use only. Any other use is limited by the Laws of Copyright, especially the obligation to refer to the source whenever results from this thesis are cited.

De auteur en de (co-)promotoren geven de toelating dit proefschrift voor consultering beschikbaar te stellen en delen ervan te kopiëren voor persoonlijk gebruik. Elk ander gebruik valt onder de beperkingen van het auteursrecht, in het bijzonder met betrekking tot de verplichting uitdrukkelijk de bron te vermelden bij het aanhalen van resultaten uit dit proefschrift.

Ghent, December 13th 2020

The promoters:

Prof. dr. apr. Koen Raemdonck

Prof. dr. apr. Stefaan De Smedt

The author:

Apr. Thijs Van de Vyver

“True knowledge exists in knowing that you know nothing.”

Socrates

TABLE OF CONTENTS

List of abbreviations	1
Aims and outline of the dissertation	7
Chapter 1 Modulating intracellular pathways to improve the non-viral delivery of RNA therapeutics	11
Chapter 2 Screening a drug repurposing library for adjuvants that induce lysosomal siRNA escape in nanogel transfected cells	97
Chapter 3 Cationic amphiphilic drugs boost the lysosomal escape of small nucleic acid therapeutics in a nanocarrier-dependent manner	137
Chapter 4 Repurposing prazosin as a cell death inducer and lysosomal escape enhancer of siRNA	185
Chapter 5 Broader international context, relevance and future perspectives	253
Summary and conclusions	283
Samenvatting en conclusies	287
Curriculum vitae	291

LIST OF ABBREVIATIONS

A	AAT	alpha-1 antitrypsin	
	Abs	antibodies	
	ADAR	RNA-specific adenosine deaminase	
	ADRB2	adrenoceptor beta 2	
	AF647	alexa fluor® 647	
	Ago2	argonaute RISC catalytic component 2	
	AHR	aryl hydrocarbon receptor	
	ALAS1	delta-aminolevulinate synthase 1	
	AMI	amitriptyline	
	AMPK	adenosine monophosphate-activated protein kinase	
	AP(s)	adaptor protein(s)	
	APC(s)	antigen-presenting cell(s)	
	APG(s)	autophagosome(s)	
	API	apilimod	
	ApoE	apolipoprotein E	
	APY	APY-0201	
	ASGPR(s)	asialoglycoprotein receptor(s)	
	ASM	acid sphingomyelinase	
	ASO(s)	antisense oligonucleotide(s)	
	ASO-CTRL	negative control gapmer ASO	
	ASO-Cy5®	ASO-eGFP labeled with Cy5® dye	
	ASO-eGFP	eGFP-targeting gapmer ASO	
	ASO-NG(s)	ASO-loaded NG(s)	
	AT	antithrombin	
	ATG	autophagy-related	
	ATP	adenosine triphosphate	
	ATP6 V	V-type proton ATPase subunit 6	
	AUC	area under the curve	
	AutoLYS	auto(phago)lysosomes	
	AZE	azelastine	
	B	BADGE	bisphenol A diglycidyl ether
		Bcl-2	B-cell lymphoma 2 protein
		BMP	bis(monoacylglycero)phosphate
C	CAD(s)	cationic amphiphilic drug(s)	
	Cas9	CRISPR associated protein 9	
	CAV1	caveolin-1	
	CCB(s)	calcium channel blocker(s)	
	CCM	complete cell culture medium	
	CD	cluster of differentiation	
	CD45	protein tyrosine phosphatase receptor type C	
	CHMP1B	charged multivesicular body protein 1B	
	Chol-siRNA(s)	cholesterol-conjugated siRNA(s)	
	CI	confidence interval	
	clogP	calculated logP	
	CLQ	chloroquine	
	CMA	chaperone-mediated autophagy	
	CMap	Connectivity Map	
	COP	coatamer protein complex	
	COVID-19	coronavirus disease 2019	
	CP(s)	coat protein(s)	
	cp-asiRNA(s)	cell-penetrating asymmetric siRNA(s)	
	CPP(s)	cell-penetrating peptide(s)	
	CPSF30	cleavage and polyadenylation factor 30	

	Cre	Cre recombinase
	CRISPR	clustered regularly interspaced short palindromic repeats
	CRISPRa	CRISPR activation
	CRISPRi	CRISPR interference
	CRISPRko	CRISPR knockout
	CTL(s)	cytotoxic T lymphocyte(s)
D	DC(s)	dendritic cell(s)
	DCGR8	DiGeorge syndrome critical region gene 8
	DES	desloratadine
	DEX	dexamethasone
	dex-HEMA	dextran hydroxyethyl methacrylate
	dex-MA	dextran methacrylate
	DEXS	10 kDa dextran sulphate
	DFO	deferoxamine
	DHA	docosahexaenoic acid
	DHP	dihydropyridine
	DLin-MC3-DMA	heptatriaconta-6,9,28,31-tetraen-19-yl 4-(dimethylamino)butanoate
	DLs	dynamic light scattering
	DMD	Duchenne muscular dystrophy
	DMEM	Dulbecco's Modified Eagle Medium
	DMG-PEG₂₀₀₀	1,2-dimyristoyl-rac-glycero-3-methoxypolyethylene glycol-2000
	DMSO	dimethyl sulfoxide
	DN	dominant negative
	DNA	deoxyribonucleic acid
	DOPE	1,2-dioleoyl- <i>sn</i> -glycero-3-phosphoethanolamine
	DOTAP	1,2-dioleoyl-3-trimethylammonium-propane
	DOX	doxazosin
	DPC(s)	dynamic polyconjugate(s)
	ds	double-stranded
	DS	degree of substitution
	DsieGFP	Dicer substrate siRNA targeting eGFP
	DsiFLuc	Dicer substrate siRNA targeting <i>firefly</i> luciferase
	DsiRNA(s)	Dicer substrate siRNA(s)
	DSPC	1,2-distearoyl- <i>sn</i> -glycero-3-phosphocholine
	DSPE-PEG₂₀₀₀	1,2-distearoyl- <i>sn</i> -glycero-3-phosphoethanolamine-N-[methoxy(polyethylene glycol)-2000]
	dsRNA	double-stranded RNA
E	EC	extracellular
	ECM	EC matrix
	EDTA	ethylenediaminetetraacetic acid
	EE(s)	early endosome(s)
	EEA1	early endosome antigen 1
	eGFP	enhanced green fluorescent protein
	EL(s)	endolysosome(s)
	EMA	European Medicines Agency
	EPR	enhanced permeability and retention
	ER	endoplasmic reticulum
	ESC	enhanced stability chemistry
	ESCRT	endosomal sorting complex required for transport
	EVs	extracellular vesicle(s)
F	FBS	fetal bovine serum
	FDA	US Food and Drug Administration
	FDs	FITC-labeled dextrans
	FER-1	ferrostatin-1
	FFS	fluorescence fluctuation spectroscopy
	FIASMA(s)	functional inhibitor(s) of ASM
	FITC	fluorescein isothiocyanate

	FSC	forward scatter	
G	GABA	gamma-amino-butyrac acid	
	GalNAc	N-acetylgalactosamine	
	GCC2	GRIP and coiled-coil domain-containing protein 2	
	GLUT	glucose transporter	
	GPX4	glutathione peroxidase 4	
	GSK-3α/β	glycogen synthase kinase 3 α/β	
	GTP	guanosine triphosphate	
H	HAO1	hydroxyacid oxidase 1	
	hATTR	hereditary transthyretin amyloidosis	
	HCLQ	hydroxychloroquine	
	HDAC(6)	histone deacetylase (6)	
	HEPES	4-(2-hydroxyethyl)-1-piperazineethanesulfonic acid	
	HG	high glucose	
	HOPS	homotypic fusion and protein-sorting	
	HPS4	Hermansky–Pudlak Syndrome 4	
	HSP70	heat shock protein 70	
	HTS	high-throughput screening	
	I	I.V.	intravenous
IC		intracellular	
IC₅₀		half maximal inhibitory concentration	
IFN(s)		interferon(s)	
IKK		I κ B kinase	
IKKϵ		inhibitor of nuclear factor kappa B kinase subunit epsilon	
IL(s)		interleukin(s)	
ILV(s)		intraluminal vesicles	
I.P.		intraperitoneal	
IRF(s)		interferon regulatory factor(s)	
ISG(s)		IFN-stimulated gene(s)	
ISRIB		integrated stress response inhibitor	
iTOP		induced transduction by osmocytosis and propanebetaine	
ITR		itraconazole	
IVT		<i>in vitro</i> transcribed	
J		JP	<i>in vivo</i> -jetPEI [®]
K		KET	ketotifen
	KIF	kinesins gene family	
	ko	knockout	
	KRAS	Kirsten rat sarcoma	
L	LAMP1	lysosomal-associated membrane protein 1	
	LBPA	lysobisphosphatidic acid	
	LCD	lysosomal cell death	
	LDHA	lactate dehydrogenase A	
	LDLR	low density lipoprotein receptor	
	LDR	lysotracker [®] deep red	
	LE(s)	late endosome(s)	
	LF	lipofectamine [®]	
	LIP(s)	liposome(s)	
	LMP	lysosomal membrane permeabilization	
	LNA	locked nucleic acid	
	LNP(s)	lipid nanoparticle(s)	
	LOF	lofepramine	
	LOP	loperamide	
	LPX(s)	lipoplex(es)	
	LSD	lysosomal storage disease	
	LUC	luciferase	
LYS	lysosomes		
M	M6P(R)	mannose 6-phosphate (receptor)	

	MC3	DLin-MC3-DMA
	MC3 (D)siLNP(s)	(D)siRNA-loaded MC3-containing LNP(s)
	MC3 LNP(s)	LNP(s) containing the ionizable lipid MC3
	MDR-1	multidrug resistance protein 1
	MEF(s)	mouse embryonic fibroblast(s)
	MFI	mean fluorescence intensity
	MHC	major histocompatibility complex
	miRNA	microRNA
	MoA	mode-of-action
	MPS	mononuclear phagocyte system
	mRNA	messenger RNA
	MSNP(s)	mesoporous silica NP(s)
	MTOC	microtubule-organizing center
	mTOR	mammalian target of rapamycin
	mTOR-i	mTOR-independent
	MUG1	murinoglobulin-1
	MVB	multivesicular body
	MVBs	multivesicular bodies
	MW	molecular weight
	MyD88	myeloid differentiation primary response gene 88
	Ma2M	murine α -2-macroglobulin
N	NA(s)	nucleic acid(s)
	NAION	non-arteritic anterior ischemic optic neuropathy
	NDP52	nuclear domain 10 protein 52
	NDSB(s)	non-detergent sulfobetaine(s)
	NE	nuclear envelope
	NEC-1	necrostatin-1s
	NF-κB	nuclear factor- κ B
	NG(s)	nanogel(s)
	NGS	next-generation sequencing
	NIHCC	National Institutes of Health Clinical Collection
	NLR(s)	NOD-like receptor(s)
	NLRP3	NLR pyrin domain containing 3
	NLS-GFP	nuclear-localized signaling expressing GFP
	NOD	nucleotide oligomerization domain
	Norm EE	normalized eGFP expression vs. siNG-DMSO control
	NP(s)	nanoparticle(s)
	NPC1	Niemann-Pick type C protein 1
	NPD	Niemann-Pick disease
	ns	not significant
	NS1	non-structural protein 1
	NSCLC	non-small cell lung cancer
	nt	nucleotide
	NTC	not treated control
O	OA	oleic acid
	OAS(s)	2'-5'-oligoadenylate synthetase(s)
	ON(s)	oligonucleotide(s)
	ON-NG(s)	ON-loaded NG(s)
P	PAINS	pan-assay interference compounds
	PBS	phosphate buffered saline
	PCA	principal component analysis
	PCI	photochemical internalization
	PCR	polymerase chain reaction
	PCSK9	proprotein convertase subtilisin/kexin type 9
	PDI	polydispersity Index
	PDMAEMA	poly(2-(dimethylamino)ethyl methacrylate)
	pDNA	plasmid DNA

	PEG	polyethylene glycol
	PEI	polyethylenimine
	PFA	paraformaldehyde
	PH1	primary hyperoxaluria type 1
	PI(3,4,5)P₃	phosphatidylinositol-3,4,5-triphosphate
	PI(3,5)P₂	phosphatidylinositol-3,5-bisphosphate
	PI3K	phosphatidylinositol 3-kinase
	PI3P	phosphatidylinositol-3-phosphate
	PIKfyve	FYVE domain-containing phosphatidylinositol 3-phosphate 5-kinase
	pKa1	pKa of the conjugated acid of the most basic amine
	PKC(-α)	(α isoform of) protein kinase C
	PKR(s)	dsRNA-dependent protein kinase(s)
	PLD	phospholipidosis
	PLGA	poly(lactic-co-glycolic acid)
	PLK1	polo-like kinase 1
	PNA	peptide nucleic acid
	PO	phosphodiester
	PPX(s)	polyplex(es)
	PRA	prazosin
	pre-miRNA(s)	precursor miRNA(s)
	pri-miRNA(s)	primary miRNA(s)
	PRR(s)	pattern recognition receptor(s)
	PS	phosphorothioate
	PS-ASO(s)	PS-containing ASO(s)
	PTX	paclitaxel
R	R&D	research and development
	Rab	Ras-related in brain
	REs	recycling endosomes
	RIG-I	retinoic acid-inducible gene I
	RISC	RNA-induced silencing complex
	RLR(s)	RIG-I-like receptor(s)
	RLU	relative light units
	rMFI	relative mean fluorescence intensity
	RNA(s)	ribonucleic acid(s)
	RNAi	RNA interference
	RNP	ribonucleoprotein
	ROS	reactive oxygen species
	RPMI	Roswell Park Memorial Institute
	RyR	ryanodine receptor
S	S.C.	subcutaneous
	SAL	salmeterol
	SAM	self-amplifying RNA
	SAR	structure activity relationship
	saRNA	short activating RNA
	SARS-CoV-2	severe acute respiratory syndrome coronavirus 2
	SD	standard deviation
	SDC	spinning disk confocal
	SEM	standard error of the mean
	sgRNA(s)	single-guide RNA(s)
	shRNA(s)	short hairpin RNA(s)
	siATG5	ATG5-directed siRNA
	siCD45	CD45-directed siRNA
	siCTRL	siRNA scrambled control
	siCy5®	siCTRL labeled with Cy5® dye
	siEGFP	siRNA targeting eGFP
	siLIP(s)	siRNA-loaded LIP(s)
	siLNP(s)	siRNA-loaded LNP(s)

	siMSNP(s)	siRNA-loaded MSNP(s)
	siNG(s)	siRNA-loaded dextran nanogel(s)
	siNPC1	NPC1-targeted siRNA
	siNP(s)	siRNA-loaded NP(s)
	siRab27b	Rab27b-directed siRNA
	SIRC	stress-induced response complex
	siRNA	small interfering RNA
	siTFEB	TFEB-directed siRNA
	SLC2A	solute carrier family 2
	SM	sphingomyelin
	SNALP(s)	stable NA-lipid NP(s)
	SP-B	surfactant protein B
	SSC	side scatter
	SSO(s)	splice switching oligonucleotide(s)
T	TA(s)	tumor antigen(s)
	TAM	tamoxifen
	TAP	transporter for antigen presentation
	TBE	TRIS/Borate/EDTA
	TBK1	TANK-binding kinase 1
	TCR(s)	T-cell receptor(s)
	TER	terazosin
	TF(s)	transcription factor(s)
	TFEB	transcription factor EB
	TGN	<i>trans</i> -Golgi network
	TIR	Toll/IL-1 receptor
	TLR(s)	Toll-like receptor(s)
	TMAEMA	[2-(methacryloyloxy)ethyl]-trimethyl-ammonium
	TNF-α	tumor necrosis factor- α
	TRBP	transactivating response RNA-binding protein
	TRIF	TIR domain-containing adaptor inducing IFN- β
	TRPML1	transient receptor potential mucolipin 1
	TRVP1	transient receptor potential cation channel subfamily V member 1
	TSC	tuberous sclerosis complex
	TSG101	tumor susceptibility gene 101
	TTR	transthyretin
U	UGCG	UDP-glucose ceramide glucosyltransferase
	ULK1	Unc-51 like autophagy activating kinase 1
	US\$	United States dollar
V	v-/t-SNARE(s)	vesicle-/target- soluble N-methylmaleimide sensitive factor attachment protein receptor(s)
	VAC-1	vacuolin-1
	VEGFR1	vascular endothelial growth factor receptor 1
	vLDLR	very low density lipoprotein receptor
	VPS28	vacuolar protein sorting-associated protein 28 homolog
	VV	Vaccinia virus
W	WT	wild type
Y	YM	YM-201636
Z	zVAD	zVAD-fmk
	zVAD-fmk	N-Benzoyloxycarbonyl-Val-Ala-Asp(O-Me) fluoromethyl ketone
N.A.	α-TOC	α -tocopherol
	2/3D	two-/three-dimensional
	3-MA	3-methyladenine
	6BIO	6-bromo-indirubin-3O-oxime
	5mC	5-methylcytosine
	Ψ	pseudouridine

AIMS AND OUTLINES

There is no doubt about the therapeutic potential of several RNA(-based) therapeutics. For example, small interfering (si)RNA is able to induce specific gene silencing of key disease targets. However, given the plethora of extra- and intracellular barriers upon *in vivo* administration, appropriate delivery systems are required to efficiently and safely deliver these nucleic acid (NA) molecules to the interior of target cells. In this context, several non-viral delivery strategies, such as encapsulation in nanoparticles (NPs) or conjugation of chemically stabilized NA strands to targeting ligands (*e.g.* for small NAs such as small interfering (si)RNA), have been successfully developed. Indeed, the recent approvals of both a siRNA-loaded lipid nanoparticle (LNP) and GalNAc-siRNA conjugates for liver-related diseases represented important milestones for the NA delivery field. However, even for these state-of-the-art delivery systems, efficient intracellular delivery remains a major bottleneck. Upon internalization by target cells, the therapeutic cargo is typically sequestered in endocytic compartments and the bulk of the endocytosed NA drug, generally exceeding 99% of the internalized amount, is rapidly trafficked towards the degradative lysosomes that are considered as a dead end for NA therapeutics. Opposed to this paradigm, we recently reported that cationic amphiphilic drugs (CADs) could strongly promote the cytosolic delivery of lysosomal sequestered siRNA in dextran nanogel-transfected non-small cell lung cancer (NSCLC) cells. Due to their lysosomotropic properties, these drugs accumulate inside the lysosomal compartment where they induce phospholipidosis (PLD), lysosomal swelling and a transient lysosomal membrane permeabilization (LMP), allowing improved cytosolic delivery of siRNA. In this thesis, we aim to further unravel the broader applicability and the mechanistic insights of this adjuvant approach.

In **Chapter 1**, we will provide an overview of the plethora of RNA(-based) therapeutics and the numerous extra- and intracellular barriers encountered by these therapeutic molecules upon *in vivo* administration. Additionally, we will describe how several delivery systems have been developed to improve both biodistribution and the intracellular delivery in target cells. However, the latter remains a largely inefficient process for current drug delivery vehicles. As an increased understanding of the biological mechanisms behind intracellular delivery can foster the rational development of the next generation of NA carriers, we will discuss how several non-genetic (*e.g.* small molecules) and genetic (*e.g.* RNAi, CRISPR) tools can be

used to investigate the influence of different intracellular barriers on the eventual transfection efficiency. We will further elaborate on the studies that reported an increased intracellular delivery upon (non-)genetic modulation of several intracellular barriers such as endosomal escape, exocytosis, autophagy *etc.*. In particular, given that small molecules have been (widely) applied for such purposes, this chapter also serves as an introduction for the use of low molecular weight adjuvants to improve NA delivery.

Based on our previous findings, a small selection of CADs can be repurposed to increase the gene silencing potential of siRNA-loaded nanogels. Despite the undoubtful promising profile of these molecules, multiple questions remain on the broader applicability of such an adjuvant strategy. For instance, only a limited number of CADs has been evaluated to date, raising the question if also other CADs share this adjuvant effect. Hence, in **Chapter 2**, we will perform a drug repurposing screen by applying the ‘National Institutes of Health Clinical Collection’ compound library (NIHCC) on the previously reported NSCLC cell model. This chapter will provide evidence that plenty more CADs, but not all CADs, phenocopy these delivery effects in the (low) micromolar range (*i.e.* siRNA delivery-promoting compounds or ‘hits’). Hence, to validate this finding, the contrasting effects of two CADs (a ‘hit’ and a ‘no hit’) on both the endo(lyso)somal compartment and the cytosolic siRNA delivery will be further investigated.

As the delivery effect of CADs is a relatively recent finding, its impact on other types of nanoparticles and other non-lung related cancer cell types has not been thoroughly investigated yet. Hence, this will be addressed in **Chapter 3**. Our previous work suggested that the CAD-induced pores in the lysosomal membrane are relatively small, only allowing the passage of siRNA but not substantially larger NA therapeutics such as mRNA. Hence, we will additionally investigate whether CADs can also improve the cytosolic delivery of other small NAs such as antisense oligonucleotides (ASOs). Most importantly, this chapter will establish that the CAD adjuvant effect is clearly dependent on the type of nanocarrier. Consequently, we will aim to understand which requirements a therapeutic siRNA-loaded nanoparticle should have to be compatible with the proposed CAD adjuvant approach.

Interestingly, several ‘hits’ from the compound screen (**Chapter 2**), do not comply with the applied CAD definition. We will discuss the potential mechanism of action of these unrelated compounds in **Chapter 4** and we will further focus on the effects of the number one ‘hit’ compound prazosin. We will combine siRNA transfection experiments with confocal

microscopy to provide a first indication on the mode of action and applicability of prazosin as a delivery-promoting compound. Importantly, based on our preliminary data and recent literature reports, we will propose that prazosin can potentially be used in a unique cancer treatment combination therapy to promote cancer cell death, intracellular siRNA delivery and cross-presentation of tumor-associated antigens.

Finally, in **Chapter 5** we will put the aims and obtained data of this dissertation in a broader international context and we will discuss how significant advances in delivery approaches have marked the development of the current generation of (si)RNA-based therapeutics. We will outline the outstanding (delivery) challenges to fully unlock the enormous therapeutic potential of RNA therapeutics. In addition, given that the majority of the investigated adjuvants in this thesis are (approved) small molecular drugs, we will elaborate on the concept of drug repurposing. Finally, we will formulate our recommendations on how research on the (CAD) adjuvant topic could be continued.

Chapter 1

Modulating intracellular pathways to improve the non-viral delivery of RNA therapeutics

An adapted version of this chapter is being prepared for publication.

Thijs Van de Vyver[†], Stefaan C. De Smedt[†], Koen Raemdonck[†]

[†] Ghent Research Group on Nanomedicines, Laboratory of General Biochemistry and Physical Pharmacy, Faculty of Pharmaceutical Sciences, Department of Pharmaceutics, Ghent University, Ottergemsesteenweg 460, 9000 Ghent, Belgium

Author contributions

Chapter 1 was written through contributions of all authors.

TABLE OF CONTENTS

1. INTRODUCTION	15
1.1. RNA therapies	15
1.2. RNA therapies in the clinic: where are we?	16
1.3. Extracellular barriers for nucleic acids and their delivery systems	17
1.4. Intracellular barriers	20
1.5. Going beyond novel materials	22
2. TOOLBOX TO INVESTIGATE INTRACELLULAR PROCESSING OF NAs/NPs.....	23
2.1. Non-genetic tools.....	23
2.2. Genetic perturbation	24
2.3. Transcriptomics.....	27
2.4. Knockout mice, alternative models and emerging technologies	29
3. INTRACELLULAR BARRIERS AND HOW TO MANIPULATE THEM	31
3.1. Cellular targeting and intracellular uptake	31
3.2. Intracellular trafficking.....	34
3.3. Endo(lyso)somal escape.....	45
3.4. Autophagy/cell metabolism.....	50
3.5. Translocation to the nucleus	53
3.6. Non-delivery aspects: modulate silencing, splicing or translation	53
4. CONCLUSION AND PERSPECTIVES	58

ABSTRACT

Ribonucleic acid (RNA) therapeutics show great potential for the treatment of a myriad of diseases. However, to reach their site of action in the cytosol or nucleus of target cells, a plethora of intra- and extracellular barriers have to be surmounted. Several non-viral delivery systems, such as nanoparticles and conjugates, have been successfully developed to meet this task. Unfortunately, despite these clear advances, state-of-the-art delivery agents still suffer from relatively low intracellular delivery efficiencies. Notably, our current understanding of the intracellular delivery process is largely oversimplified. Hence, increasing the understanding of the interaction of these delivery systems with the intracellular barriers can boost the development of the next generation of delivery strategies. In this review, we highlight how several modulators (small molecules, but also genetic perturbation technologies) can boost (ribo)nucleic acid delivery by intervening at differing stages of the intracellular delivery pathway (*e.g.* uptake, trafficking, endosomal escape, autophagy and exocytosis).

1. INTRODUCTION

1.1. RNA therapies

Ribonucleic acid (RNA) therapeutics have gathered a lot of attention the past three decades as promising tools to modulate gene expression levels, both by academia and pharmaceutical companies¹⁻⁵. In general, these therapeutics, which are based on DNA, RNA or hybrids/analogues thereof, can be divided into three categories: those targeting cellular RNA or DNA, those encoding for proteins and, to a lesser extent, those directly targeting proteins^{6,7}.

Indeed, as the majority (~80%) of the human genome is transcribed into RNA and as virtually any coding or non-coding RNA in the transcriptome can be considered as a therapeutic target, the introduction of exogenous RNA-targeting small nucleic acids (NAs) into cells has the potential to treat a myriad of disorders (*e.g.* cancer, viral infections, autoimmune diseases, cardiovascular disorders). Notably, also genes that were previously thought to be 'undruggable' by small molecules or proteins upon expression can be targeted^{1,4,8-10}. For example, antisense oligonucleotides (ASOs) and NAs triggering the RNA interference (RNAi) pathway, such as small interfering (si)RNA, short hairpin (sh)RNA and micro (mi)RNA mimics, can be used to induce post-transcriptional sequence-specific silencing of disease-promoting genes *via* mRNA degradation and/or translational repression¹¹⁻¹⁴. Notably, ASOs can also act as antagonists of endogenous miRNAs (antagomiRs), thereby controlling expression of miRNA-regulated genes^{15,16}. In turn, ASOs applied to modulate the splicing of pre-mRNA into mRNA in the nucleus (*i.e.* correcting aberrant splicing or inducing alternative splicing) are named splice switching oligonucleotides (SSOs) and can be used to repair protein function^{16,17}. In addition to SSOs, modulation of nonsense-mediated mRNA decay¹⁸ or mRNA translation¹⁹⁻²¹ by specifically designed ASOs has also shown to increase gene expression. Short activating RNA (saRNA), which has a similar structure as siRNA, can also boost gene expression, although this involves binding to promoter regions of genes in the nucleus to enhance transcription^{3,22}. Finally, short single-stranded RNA aptamers can also selectively bind and block proteins directly^{3,16}. Of note, as we mainly used siRNA in this dissertation, a brief description of the RNAi mechanism is provided in the supplementary information.

Next to the small non-coding NAs discussed above, also *in vitro* transcribed (IVT) messenger (m)RNA can be therapeutically exploited to transiently induce/restore protein expression,

providing a powerful alternative to conventional DNA-based gene therapy/vaccination (against cancer^{23–26} or infectious diseases^{26–29}) or traditional protein replacement strategies^{30–34}. On the one hand, the latter approach is generally unable to deliver intracellular proteins and is characterized by a very short half-life³⁰. Plasmid DNA (pDNA)-mediated gene transfer, on the other hand, requires nuclear translocation and is therefore most effective in dividing cells³⁵. In addition to the foregoing, mRNA can also be used in the field of regenerative medicine (cell reprogramming³⁶) or genome editing³⁷. Indeed, the components of the clustered regularly interspaced short palindromic repeats (CRISPR)-associated protein 9 (CRISPR-Cas9) nuclease system can be co-delivered as Cas9-encoding mRNA and single-guide RNA (sgRNA)^{38–41}, where the sgRNA recognizes specific target genomic loci, while the mRNA produces the Cas9 nuclease that cleaves the sgRNA-bound DNA sequence⁴². Alternatively, the sgRNA can also be delivered as a ribonucleoprotein complex with the Cas9 protein^{41,43}. Self-amplifying RNA (SAM or “replicon RNA”) is a special type of mRNA construct that, in addition to the protein of interest, also encodes a viral enzyme complex for self-amplification (*i.e.* replicase polyprotein)⁴⁴. Hence, upon transfection, the replicase is translated and *via* the generation of RNA intermediates multiple copies of the protein-encoding subgenomic mRNA are synthesized, producing very high levels of the encoded protein^{44–46}. Consequently, substantially lower amounts of SAM (compared to conventional IVT mRNA) need to be delivered intracellularly to enable effective protein production⁴⁴.

1.2. RNA therapies in the clinic: where are we?

Locally (*i.e.* intravitreal injection in the eye) administered ASO (Fomivirsen, 1998) or aptamer (Pegaptanib, 2004) therapies were the earliest small non-coding NA drugs to obtain FDA-approval, of which Fomivirsen is no longer marketed^{47,48}. Next, a subcutaneously injected ASO (Mipomersen, 2013)⁴⁹, a systemically applied SSO (Eteplirsen, 2016)⁵⁰ and a locally administered (*via* intrathecal injection) SSO (Nusinersen, 2016)⁵¹ were approved by the FDA and/or EMA and marketed with varying degree of success⁴⁷. In 2018, the FDA-approval of Patisiran, the first siRNA-based therapeutic, represented a crucial milestone for the field of NA-based drugs^{52–54}. This was shortly followed by the approval of Inotersen, an ASO developed for the same target and disease (*i.e.* transthyretin amyloidosis)⁵⁵. Since then, also Givosiran (siRNA)⁵⁶, Volanesorsen (ASO)⁵⁷, Golodirsen (SSO)⁵⁸ and Lumasiran (siRNA) have obtained approval by the FDA and/or EMA. Currently, many pharmaceutical companies have several RNA therapeutics in their pipelines^{2,59,60}, including potential mRNA vaccines^{61–65} and

siRNA therapeutics^{66–68} to support the fight against the COVID-19 pandemic. In this context, mRNAs encoding the spike protein^{61–65,69,70} or siRNAs targeting the SARS-CoV-2 genome^{69–7} are being explored.

Despite recent progress, the clinical translation of NA drugs is still relatively modest^{4,71}. This can largely be attributed to the numerous biological barriers encountered by NA therapeutics, both extra- and intracellular, which hinder their safe and effective delivery to the interior of target cells (as schematically shown in **Figure 1**)^{1,72–74}. Indeed, despite their distinct pharmacological effects, all classes of NA drugs share a few characteristics. For one, these molecules are relatively large compared to ‘classical’ small molecule drugs and they are typically polyanionic (except the charge-neutral morpholinos) and hydrophilic, altogether complicating their *in vitro* and *in vivo* delivery^{8,75}.

1.3. Extracellular barriers for nucleic acids and their delivery systems

In general, the extracellular barriers should be surmounted to convey NA drugs to the tissue and cells of interest, while minimizing delivery to off-target tissues. For naked (and/or unmodified) NAs that are administered systemically, these include degradation by serum nucleases, activation of the innate immune response, potentially disadvantageous interactions with blood components and, especially for small NAs, rapid clearance *via* renal elimination^{1,74–76}. Chemically modifying the NA strands (*e.g.* by introducing phosphorothioate (PS) backbones or modified nucleosides) could partially improve the nuclease resistance^{47,76}, reduce the immunostimulatory effects^{77–79} and, in the case of PS-containing single-stranded oligonucleotides (ONs), prolong the circulation half-life due to enhanced plasma protein binding^{47,76,80,81}. Hence, PS-containing ASOs (PS-ASOs) can be delivered *in vivo* to some tissues (mainly the liver) after formulation in simple saline solutions^{47,82–84}. However, double-stranded siRNA molecules have a much lower propensity for protein binding than single-stranded oligonucleotides, resulting in rapid renal clearance (short half-life of < 5 min for unstabilized, unformulated siRNA)^{85–88}. Therefore, siRNAs, but also the considerably larger mRNA molecules, need appropriate *in vivo* delivery systems to allow sufficient circulation, extravasation to target tissues and eventually cellular internalization^{1,16,74,89–91}. Exceptions to this rule are, for example, naked mRNA constructs that can be efficiently internalized by immature dendritic cells (DCs) in the case of local (*e.g.* intradermal, intranodal) mRNA vaccine applications^{5,59}. While both viral^{92,93} and non-viral¹ vectors are being evaluated simultaneously for DNA gene delivery, RNA therapeutics are predominantly delivered by non-

viral delivery systems. Such synthetic vectors are typically composed of polymeric^{94,95}, lipidic^{52,96–98} or inorganic⁹⁹ materials (or a combination thereof) that complex/encapsulate the negatively charged NAs to form nano-sized assemblies. Multiple types of nanoparticles (NPs) have been developed up till now for NA delivery⁸⁹, with lipid NPs (LNPs) being the state-of-the-art^{98,100,101} as they culminated in the first approval of a siRNA therapeutic (Patisiran)⁵². Another well-known approach to enhance the tissue-specific accumulation and uptake of siRNAs and other oligonucleotides is the use of receptor-targeted ligands that are covalently linked to the NA strands (*e.g.* N-acetylgalactosamine (GalNAc)-siRNA conjugates, such as Givosiran, which actively target the highly expressed asialoglycoprotein receptor (ASGPR) on hepatocytes)^{8,47,102–107}. Advances in the chemical stability of the siRNA duplex allowed these novel GalNAc-siRNA conjugates to show impressive pharmacodynamic properties in clinical trials, including sustained months-long knockdown of *e.g.* the proprotein convertase subtilisin/kexin type 9 (PCSK9) target^{108–110}. Next to GalNAc conjugates, there has also been a considerable interest in conjugation of small non-coding NAs with other components, including, but not limited to, lipophilic ligands^{111–116} (*e.g.* cholesterol that enhances association with blood lipoproteins and subsequent uptake by lipoprotein receptor-enriched tissues^{117–119}), cell-penetrating peptides (CPPs)¹²⁰, antibodies, antibody-peptide fragments¹²¹ (*e.g.* nanobodies^{122–125}), aptamers, small molecules¹²⁶ or combinations of different conjugations (*e.g.* dynamic polyconjugates^{127,128}). Ideally, targeting moieties bind cell-specific surface receptors that are rapidly internalized through receptor-mediated endocytosis (*e.g.* GalNAc-siRNA conjugates such as Givosiran), followed by rapid release of the ligand from the receptor and receptor recycling to the cell surface¹²⁶.

Nevertheless, despite the recent success of state-of-the-art NPs and conjugates for siRNA delivery in the liver and spleen^{52,56,129}, these delivery agents still suffer from relatively low delivery and transfection efficiencies in extrahepatic organs and tissues, including tumors^{8,74,130,131}. Indeed, as for naked NAs, also intravenously (I.V.) administered NPs face several extra- and intracellular obstacles^{72,73}. First, opsonization of plasma proteins on the NP surface creates a protein corona, which strongly influences their *in vivo* fate⁷². For example, macrophages of the mononuclear phagocyte system (MPS) quickly sequester and remove the NPs from the circulation *via* specific recognition of adsorbed proteins⁷². In addition, protein corona deposition has been shown to shield active targeting ligands on the NP surface and reduce, for example, tumor-specific delivery¹³². On the other hand, a protein corona can also promote endogenous active targeting, as binding of apolipoproteins (namely apolipoprotein

E, ApoE) on state-of-the-art ionizable LNPs has shown to facilitate the delivery to primarily hepatocytes by binding with the low density lipoprotein receptor (LDLR) and other ApoE-binding receptors^{100,133–135}. Next, unless circulating (*e.g.* leukocytes^{136–139}) or endothelial cells are targeted, the endothelial lining of the blood vessels imposes a second extracellular barrier, as circulating NPs need to extravasate to reach their target tissue. Liver/spleen sinusoidal capillaries have larger endothelial fenestrae (*i.e.* pores between adjacent endothelial cells)^{72,140}, with liver sinusoids also having a slower blood flow¹⁴⁰, which allows passive NP accumulation. Such passive targeting has also been demonstrated, albeit to a lesser extent, to other tissues that likewise show discontinuous endothelium (*e.g.* inflamed tissues and certain solid tumors). The latter phenomenon is called the enhanced permeability and retention (EPR) effect, which theoretically allows nanomedicines to accumulate more in solid tumor tissue than in normal healthy tissues. However, only a narrow subset of clinical tumors is amenable to the EPR-based targeting approach^{141,142}. Thirdly, if a NP successfully reaches its target site, it should be distributed throughout *e.g.* the tumor tissue, which might be complicated by a high interstitial pressure, high cell density and a dense extracellular matrix (ECM)⁷².

Multiple strategies have been developed to improve the biodistribution of systemic NA-loaded NPs and to overcome the different extracellular barriers. These include (a) the functionalization of NP surfaces or NA strands with polyethylene glycol (PEG) to hinder protein adsorption and MPS clearance or (b) the use of targeting agents (see 1.3). Other approaches carefully modulate the NP's (physico)chemical properties, such as NP size or surface charge^{41,129} by *e.g.* changing the lipid composition^{143–146}. In addition, pre-treatment with decoy NPs or chloroquine (CLQ) can prevent NP clearance by the MPS by saturating or actively blocking the phagocytic response^{147,148}. Altogether, despite these technological advances, systemic administration of NA-loaded NPs generally still results in a high non-specific accumulation in the spleen and liver^{147,149}. As a consequence, a recent meta-analysis of the literature (2006 – 2016) showed that less than 1% of administered spherical NPs is able to reach solid tumor tissue, regardless of the presence of active targeting tumor ligands¹⁵⁰. Nevertheless, such targeting moieties might still increase the residence time at the target site and could facilitate target cell recognition and subsequent uptake through receptor-mediated endocytosis⁷⁶. Hence, the improvement of biodistribution and extra-hepatic delivery of systemically applied NA drugs remains an active area of research^{151,152}. In this regard, local/topical administration (*e.g.* pulmonary⁹⁵, ocular^{153,154}, skin, oral, intrathecal¹⁵⁵ routes) is

also intensively explored, albeit these routes encompass their own specific extracellular barriers (*e.g.* enzymatic degradation, immobilization in mucus, *etc.*)⁷³.

1.4. Intracellular barriers

Upon arrival to the target cells, RNA therapeutics have to overcome multiple intracellular barriers, of which the first is the plasma membrane. Here, NAs and their carriers are typically internalized by endocytosis, localizing the cargo in early endosomes (EEs), which further mature *via* late endosomes (LEs) into endolysosomes, where both the cargo and the carrier face degradation due to the acidic pH and the presence of lysosomal hydrolases. However, as the NA molecules exert their function in the cytosol or nucleus, the cargo should escape the endosomal confinement¹⁵⁶. Consequently, numerous groups focused on methods that could enhance endosomal escape, including, but not limited to, (a) cationic polymers with endosomal buffering capacity that cause the inward flow of H⁺, Cl⁻, and water into the lysosomes (LYS), resulting in osmotic swelling and eventual rupture of the vesicles (the so-called proton-sponge effect¹⁵⁷), (b) pH-sensitive or fusogenic peptides/lipids/lipid-like materials (lipidoids) that interact with anionic endosomal membranes, and induce membrane fusion or (c) materials that induce pore formation such as certain CPPs. For a detailed description of each of these techniques, we refer the reader to the numerous comprehensive reviews on this topic^{156,158–161}. Unfortunately, despite years of extensive research, endosomal escape remains a major bottleneck as it has been shown that only 1–2% of the confined siRNA^{162,163} or mRNA¹⁶⁴ molecules are able to escape into the cytosol when delivered *via* state-of-the-art delivery systems. Furthermore, there are also additional intracellular barriers such as (a) the cellular excretion of NAs/NPs *via* exocytosis or recycling, (b) the degree and kinetics of vector unpacking or decomplexation^{165,166}, (c) the clearance of damaged endosomes or cytosolic residing NAs/NPs *via* autophagy and (d) the degradation of released NAs by cytoplasmic nucleases⁷³. Finally, for those NAs that require delivery into the nucleus, the nuclear envelope can be an important barrier as well^{1,73}.

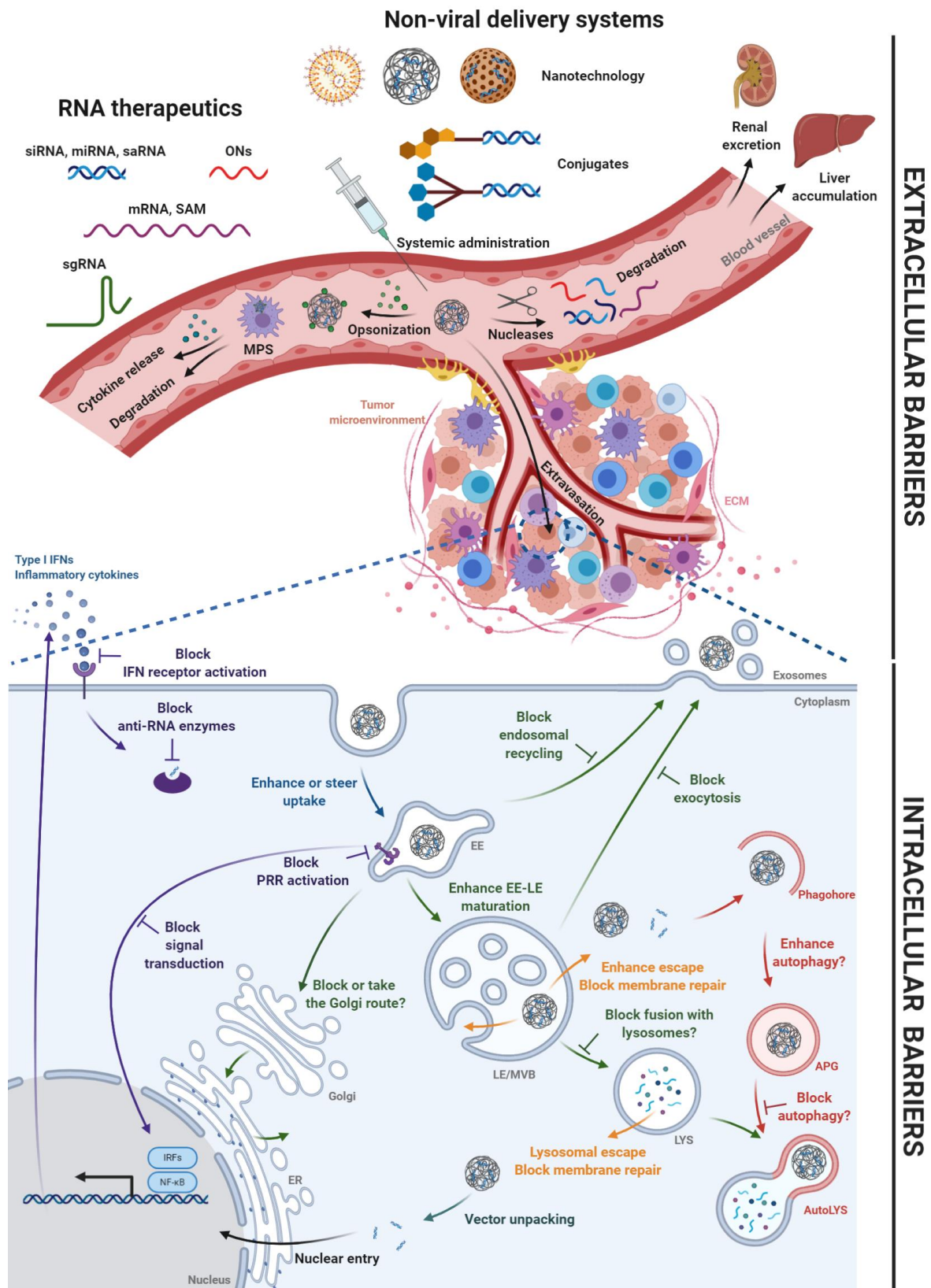


Figure 1. Overview of extracellular and intracellular barriers for RNA therapeutics systemically delivered *via* non-viral delivery systems. Nucleic acids (NAs, *e.g.* mRNA, siRNA, oligonucleotides (ONs)) are typically incorporated in nanoparticles (NPs), or alternatively, conjugated to (targeting) ligands, to overcome the plethora of extra- and intracellular barriers upon systemic administration. Extracellular barriers include (a) the degradation of NAs by serum nucleases, (b) the activation of innate

immune responses and subsequent cytokine release, (c) the opsonization of plasma proteins on the NP surface, which leads to removal of the NPs from the circulation by the mononuclear phagocyte system (MPS) and, especially for small NAs, (d) rapid clearance *via* renal excretion. Additionally, circulating NAs need to extravasate to reach their target cells. Upon arrival at the latter, several intracellular barriers have shown to limit the intracellular delivery. First, to overcome the plasma membrane, NAs/NPs are generally taken up by endocytosis. However, endocytic uptake results in sequestration of RNA therapeutics in the endolysosomal compartment, while these NA molecules exert their function in the cytosol (siRNA, mRNA, miRNA, SAM, ASOs) or nucleus (SSOs, saRNA, sgRNA). Hence, the NA cargo needs to gain access to the cytosol by escaping the endosomal pathway before lysosomal degradation occurs. Alternatively, lysosomal escape has also shown to contribute to functional RNA delivery. Additional intracellular barriers include (a) the removal of NAs/NPs to the extracellular environment *via* exocytosis or endocytic recycling, (b) the process of autophagy and (c) the recognition of NA molecules by pattern recognition receptors (PRRs) in the endosomal compartment or cytosol, which leads to an anti-RNA (anti-viral) state. Finally, RNA therapeutics that have a function in the nucleus need to cross the nuclear envelope. Interestingly, several small molecules have been shown to manipulate these intracellular barriers, hence increasing transfection¹²⁶. This figure was created with BioRender.com and was based on⁷³. (siRNA = small interfering RNA, miRNA = microRNA, ONs = oligonucleotides, SSO = splice-switching ON, ASO = antisense ON, sgRNA = single guide RNA, IFNs = interferons, NF- κ B = nuclear factor- κ B, IRFs = interferon regulatory factors, ER = endoplasmic reticulum, LYS = lysosomes, APG = autophagosome, AutoLYS = auto(phago)lysosomes, LE = late endosome, EE = early endosome, MVB = multivesicular body, PRR = pattern recognition receptor, MPS = mononuclear phagocyte system, ECM = extracellular matrix).

1.5. Going beyond novel materials

Numerous studies in the field of NA therapy have focused on the development of innovative delivery systems to overcome the abovementioned extra- and intracellular hurdles, which coincidentally led to an exponential growth of novel nanomaterials and increasingly sophisticated nanocarrier designs^{167,168}. Indeed, using the available technologies, it is possible to formulate billions of chemically distinct NA delivery vehicles¹⁶⁹. Although such complex delivery technologies significantly impacted advanced drug delivery, they also encompass major challenges from a manufacturing and regulatory point of view, which lowers their potential for clinical translation¹⁶⁸. In addition, successful delivery strategies from the past (*e.g.* enteric coating, PEGylation, controlled release) mainly rely on simple, but robust, physicochemical or biological principles¹⁶⁸. However, in the case of therapeutics with intracellular targets, the exact cellular biological pathways (and molecular regulators) that drive productive delivery are largely unknown and our current view on this process is usually oversimplified¹⁷⁰. Indeed, even for existing (and approved) nanomedicines, the most fundamental interactions within the body seem to be much more complex than previously anticipated¹⁶⁷. Likewise, even the mechanisms by which NA-loaded LNPs are formed, was

recently shown to be different than hitherto assumed¹⁷¹. Hence, albeit counterintuitive at first, expanding our fundamental knowledge of the ‘physicochemistry’ of existing NPs/NAs, the ‘biology’ of the target tissues/cells and the interaction between both, might fuel the rational development of less sophisticated, but more effective, delivery technologies that have a better chance of making it into the clinic^{167,168,170,172,173}. Intriguingly, important clues could be found in the way viruses and bacterial toxins exploit host trafficking machinery to gain access to intracellular targets, which are mechanisms that have been optimized by ‘Mother Nature’ for millions of years¹⁷⁰. Mimicking these virus-derived strategies by manipulation of key cellular processes or proteins may be a highly interesting approach to boost non-viral NA delivery as well.

In the present review, we provide a critical discussion of the established as well as emerging techniques that can be used to investigate the influence of different intracellular barriers on the eventual transfection efficiency. Next, we consider each intracellular barrier in more detail and provide an overview on how several molecular agents (small molecules, lipids, siRNAs, *etc.*) can boost transfection upon manipulation of the intracellular delivery process. Although it is still poorly understood which specific (set of) genes or cellular pathways eventually regulate the transfection process of RNA therapeutics, we describe a number of general processes that proved to be essential for successful delivery. It is important to note that the reports discussed in this last section of the review used both naked NAs (*e.g.* gymnotically delivered single-stranded oligonucleotides) and encapsulated NAs as their molecules of interest. Likewise, if relevant, we also highlight research that used naked NPs or carriers loaded with larger double-stranded NAs such as pDNA.

2. TOOLBOX TO INVESTIGATE INTRACELLULAR PROCESSING OF NAs/NPs

2.1. Non-genetic tools

2.1.1. Small molecules

Small molecules have been extensively used, both as chemical probes to dissect complex biological processes and as drugs to treat human disease¹⁷⁴. Hence, low molecular weight compounds were likewise applied as tools to elucidate endocytic uptake of NPs^{175,176} or as adjuvants to improve NA delivery¹²⁶. While the repurposing of the anti-malaria compound chloroquine is the best-known example of the latter (first reported to enhance pDNA

transfection *in vitro* in 1981¹⁷⁷), recent studies, including some large-scale compound screenings^{178–180}, were able to identify several novel small molecular NA delivery enhancers¹²⁶.

The use of small molecules, either as single compounds or embedded in a library screen, is relatively cheap and easy to use across various cellular assays. The latter is an advantage compared to complementary genetic perturbation technologies, such as RNAi or CRISPR, which have proven to be more challenging in more complex biological systems (*e.g.* primary cell types) that are recalcitrant to transfection-based protocols^{181,182}. In addition, small molecules can modulate specific protein–protein interactions or have an allosteric effect, modalities that cannot be explored with genetic perturbation¹⁸². Fundamental studies can also be more readily translated from bench to bedside *via* drug repurposing, especially if FDA-approved small molecules would be found effective in enhancing NA delivery¹⁸³. On the other hand, only a limited amount of small molecules has a specific and validated target with a known mode-of-action and few molecules are devoid of off-target effects at the relatively high concentrations typically used in high-throughput screenings (HTS)^{182,184}. For example, pharmacological inhibitors of endocytic pathways, used to clarify NP/NA cellular uptake (so-called exclusion studies), are characterized by a poor specificity and are highly cell type-dependent^{73,185}. In turn, large compound libraries might contain pan-assay interference compounds (PAINS), which are chemical agents that are known to often give false positive results in several HTS assays¹⁸⁶. Additionally, it has been shown that several compounds (*e.g.* cationic amphiphilic drugs or CADs) could have an adjuvant effect due to their general physicochemical properties, independent from their pharmacological mode-of-action (see below and **Chapter 2-3**)¹⁶⁶. Hence, identification of the precise molecular target of small molecule adjuvants is extremely difficult and requires time-consuming follow-up studies with proteomic or lipidomic techniques, albeit the use of chemogenomic libraries might improve the mechanistic and target deconvolution¹⁸².

2.2. Genetic perturbation

2.2.1. RNAi and CRISPR

Genome-wide RNA interference (RNAi) or CRISPR knockout screenings, in which > 20.000 cellular proteins are selectively depleted, have been previously used to investigate the genes/proteins associated with endocytosis^{187–189}, secretory pathways¹⁹⁰, lysosomal

function¹⁹¹ or autophagy¹⁹² in mammalian cells. Hence, such genetic perturbation technologies can also be used to gain understanding on or modulate the function of specific genes in NA delivery. However, to date only small-scale studies (either encompassing selected perturbation of a limited number of genes^{162,163,178,193–201} or relatively small targeted screenings^{202–206}) that investigated the endocytosis^{162,178,195}, intracellular trafficking^{193,205}, cytotoxicity¹⁹⁴ or effective delivery^{163,195–204,206} of NAs, have been reported²⁰⁷. Both RNAi and the diverse forms of CRISPR/Cas9 technology that either allows generation of gene knockouts (CRISPRko), or transcriptional modulation such as gene upregulation (CRISPR activation; CRISPRa) or gene downregulation (CRISPR interference; CRISPRi) have an advantage over small molecules^{208,209}. The results from such experiments enable scientist to directly correlate specific genes with the observed phenotype (*e.g.* improved NA delivery), while deconvoluting the exact target of a small molecule (hit) might be more challenging²¹⁰. Of note, when probing the impact of certain genes on the delivery of a siRNA therapeutic, a RNAi screening approach is considered less ideal as both siRNAs use the same intracellular machinery, thereby potentially interfering with each other²⁰³. On the one hand, CRISPR technology generally benefits from a lower tendency for off-target effects than RNAi^{211,212} and allows to probe genes that remain functional at low expression levels²⁰⁹. On the other hand, CRISPRko studies could overlook the involvement of essential genes (*e.g.* vital for maintaining cell viability) to the cellular phenotype of interest, favoring partial knockdown *via* RNAi or CRISPRi^{209,213}. Additionally, the displayed cellular phenotype might be substantially different upon knockout or knockdown as cellular signaling and gene regulation encompasses numerous feedback loops within highly interconnected networks²⁰⁹. Furthermore, transient knockdown phenotypes might be more compatible with pharmacological inhibition of the targets²¹⁴. For a more detailed comparison of the described techniques, we further refer the reader to comprehensive reviews on this topic^{208,209}.

When the described technologies are used in a large-scale screening format, two fundamentally different types of genetic library screens can be distinguished: the (a) ‘arrayed’ (‘plate’, ‘single well’) format where single (or a small pool of) siRNAs, shRNAs or sgRNAs are separately introduced into individual culture wells or (b) ‘pooled’ (‘barcode’) format, where a pool of sh/sgRNAs simultaneously infects numerous cells in one flask. While the latter is less time-consuming and expensive, the read-out requires next-generation sequencing (NGS) to determine the enrichment or depletion of the barcodes within the desired phenotype, thereby necessitating for a phenotype that could be selected with, for example, cell sorting

(e.g. fluorescence or cell surface markers) or selective cytotoxic agents (e.g. difference in barcodes between control and cytotoxic molecule treated groups)^{208–210}. This is in contrast to arrayed screens, where each well has a single known genetic perturbation, allowing to explore more complex cellular phenotypes (e.g. subcellular localization of NAs/NPs) using, for instance, fluorescent high-content imaging^{206,208}. In addition, these arrayed screens may be more suited to identify genes involved in intercellular communication and paracrine signalling (which might be of interest in NA delivery, given the anti-viral response triggered by several NAs and NPs) as the perturbed cells are surrounded by (equally) perturbed cells²⁰⁸.

As mentioned above, RNAi and CRISPR technologies have the potential to both increase our basic knowledge around the intracellular behaviour of NA (nano)carriers as well as to identify (novel) cellular targets involved in successful NA delivery. First, using a pooled shRNA screen (targeting ~5000 genes) Wagenaar *et al.* identified tumor susceptibility gene 101 (TSG101), a component of the endosomal sorting complex required for transport (ESCRT), as an important modulator of a miRNA-21 antagomiR activity, with TSG101 knockdown increasing antagomiR gymnotic delivery both *in vitro* and *in vivo*²⁰⁴. To the best of our knowledge, no pooled CRISPR screenings have been used to characterize the intracellular processing of NA-loaded NPs hitherto. Nevertheless, AstraZeneca recently reported on a CRISPR arrayed screen of the druggable genome (7795 genes) to identify novel targets that modulate productive delivery of mRNA encapsulated in a LNP *via* the ionizable lipid DLin-MC3-DMA²⁰⁶. Out of the 130 hits in the primary screen, the authors confirmed 37 and 17 genes that respectively increased or inhibited LNP-mediated mRNA delivery. The authors further focused on 2 of these genes that significantly increased (UDP-glucose ceramide glucosyltransferase or UGCG) or decreased (V-type proton ATPase or ATP6 V) mRNA delivery. Most importantly, the authors could recapitulate the enhanced delivery by *in vitro* co-treatment with a UGCG small molecule inhibitor. Hence, from a therapeutic perspective, co-dosing of LNP-formulated mRNA and UGCG small molecule inhibitors in patients could be envisioned to improve delivery.

2.2.2. Vectors expressing wild type or dominant negative proteins

Next to RNAi and CRISPR-mediated genetic perturbation, also other molecular techniques can be used to manipulate specific proteins and cellular pathways involved in the NA delivery process. For instance, expression of a mutated and dysfunctional dominant negative protein has been used to investigate e.g. the role of Rab11 in the internalization of cationic LNPs¹⁹⁵ or the effect of Rab5/Rab7 inhibition on the silencing potential of PS-ASOs²¹⁵ and siRNA-loaded

liposomes (LIPs)¹⁶³. In addition to dominant negative proteins, plasmid vectors have also been used to overexpress the functional wild type protein^{199,215}, thereby boosting PS-ASO delivery¹⁹⁹. As the delivered wild type or mutant proteins might also be engineered to co-express fluorescent report proteins, this technique allows direct visualization of the transfected cell population²¹⁶. Although this method appears to be highly specific for a particular protein of interest, the overexpression of the mutated or wild type proteins might possibly also result in non-specific interactions^{217–219}.

2.2.3. Cell lines with trafficking defects

A concern which might be raised for all the above-mentioned genetic perturbation techniques is that the transfection reagents, used for the cellular delivery of RNAi mediators or genes, could also impact intracellular trafficking²¹⁶. This problem can be tackled *via* the generation of stably transfected cell lines or the use of knockout cells derived from knockout animals. Examples of such knockout cells are caveolae-, Niemann-Pick type C protein 1 (NPC1)- or autophagy- deficient fibroblasts derived from caveolae^{-/-}, NPC1^{-/-} or ATG5^{-/-} mice^{195,220,221} or NPC1^{-/-} humans¹⁹⁵.

2.3. Transcriptomics

Advances in sequencing have led to so-called next-generation sequencing (NGS) technologies that enable scientists to sequence and quantify millions of DNA molecules at the same time. NGS enables to study the genome (DNA), the epigenome (DNA modifications) but also the transcriptome (RNA, after reverse transcription) in a pool of cells and even at the single cell level²²². Nowadays, the integrated single-cell sequencing (multiomics) of all these different biomolecules at the same time is possible^{223–225} and can even be correlated with protein mass spectrometry data (proteogenomics). Given that these technologies allow the characterization of complex cellular responses, the use of such (multi)omics approaches will likely increase in the field of NA delivery to study how cells respond to these materials^{222,226}. For example, Dowaidar *et al.* tested the adjuvant effect on CPP-mediated SSO delivery of a small set of autophagy-modulating compounds targeting previously identified autophagy-related genes that were dysregulated upon CPP/SSO transfection²²⁷. In addition, Linnane *et al.* investigated the intracellular delivery of an ASO in several cancer cell lines and found that the ASO-mediated knockdown significantly differed between the various cell types²⁰³. Next, the authors used publicly available RNA-sequencing data of the used cell panel to identify factors that may contribute to the observed differences in trafficking and subcellular

localization. Interestingly, two genes (KIF1A and KIF5C) that encode for components of kinesin motor protein complexes, *i.e.* kinesin-1 and kinesin-3, were significantly upregulated in cell lines with poor productive delivery.

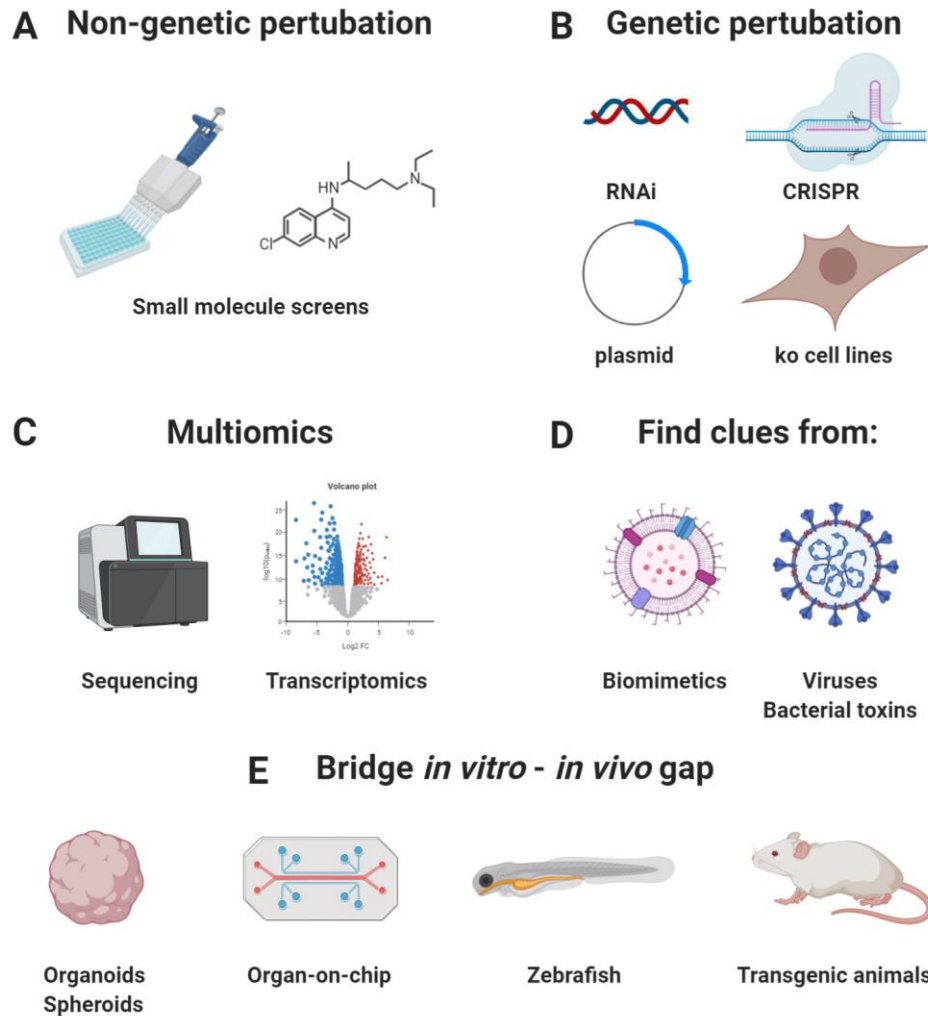


Figure 2. Overview of the experimental toolbox available to investigate the intracellular processing of RNA therapeutics. (A-B) Both non-genetic (*e.g.* small molecules) and genetic perturbation (*e.g.* RNAi, CRISPR) technologies can shed a light on the intracellular pathways involved in functional nucleic acid (NA) delivery. In addition, new targets or processes that boost NA delivery upon modulation can be identified. (C) (Multi)omics approaches (*e.g.* transcriptomics) can be used to study how cells respond to NA delivery systems. (D) Mimicking virus-derived intracellular delivery strategies by manipulation of key cellular processes or proteins may boost non-viral NA delivery as well. (E) Application of alternative *in vivo* and *in vitro* model systems may prove very valuable in bridging the *in vitro-in vivo* gap. This figure was created with BioRender.com. (ko = knockout, CRISPR = clustered regularly interspaced short palindromic repeats, RNAi = RNA interference).

2.4. Knockout mice, alternative models and emerging technologies

Development of new NA delivery methodologies usually starts with *in vitro* testing on easy to expand immortalized cell lines or isolated primary cells. A selection of *in vitro* optimized delivery systems is subsequently evaluated in an appropriate *in vivo* (typically rodent) model, as such *in vivo* experiments are extremely time and resource consuming, while there are also ethical constraints. Although the intracellular barriers are generally recapitulated in representative *in vitro* models, several extracellular barriers (*e.g.* formation of protein corona) can also affect downstream intracellular processing^{169,228}. In addition, such intracellular processes are carefully regulated²²⁹, and cellular homeostasis might be significantly altered in *in vitro* cultured cells relative to their *in vivo* counterparts^{228,230}. Consequently, it has been shown that the *in vitro* performance of NA carriers poorly correlates with *in vivo* NA delivery^{228,231}. Hence, more advanced *in vitro* (*e.g.* use of primary cells, transfection of cells in diseased conditions (*e.g.* hypoxia or hyperglycemia)²³², 3D spheroids, organoids, organ-on-chip models²³³, *etc.*) or less costly and more high-throughput *in vivo* models (*e.g.* zebrafish model) might be used to bridge this gap. For example, 3D spheroids consisting out of different cell types are able to more closely replicate some features of human solid tumors, including structural organization (cell-cell and cell-ECM interactions), oxygen/nutrients/pH gradients and drug resistance mechanisms^{234–236}. In addition, the spheroid can be used to test the penetration of NA carriers^{193,237–239}, even in a high-throughput manner¹⁹³. As such, several of the above-discussed technologies (*e.g.* small molecules^{238–240} or genetic perturbation¹⁹³), have already been used to manipulate the intracellular delivery process in 3D spheroids. In turn, the optical transparency, the availability of specific disease and transgenic models and the high degree of conservation of relevant biological features compared to mammals, make zebrafish (larvae) interesting *in vivo* models^{241,242}.

In addition to these promising models, the direct *in vivo* testing (*e.g.* in rodents) of new delivery approaches might be extremely valuable. Emerging new technologies such as DNA^{40,143–146,228,243–246}/RNA²⁴⁷ barcoding of NPs and transgenic animals engineered to express the Cre recombinase (Cre) reporter Lox-Stop-Lox tdTomato cassette^{39,40,146,243,245,248–250} or fluorescent reporter genes^{144,145} in (all) cells allows researchers to simultaneously test > 100 NPs *in vivo* in a high-throughput manner, generating data not only on the biodistribution of these NPs, but also on the successful intracellular delivery in an *in vivo* setting²⁵⁰. For example, Ai14 Cre-reporter mice (or similar reporter strains³⁹) contain a Lox-Stop-Lox-tdTomato

transgene under the control of a promoter. As a result, cells in these mice will only express tdTomato when Cre-encoding mRNA or sgRNA against LoxP/Stop site (together with a Cas9-encoding mRNA) are successfully delivered in the cytosol, translated into functional Cre or Cas9 proteins that subsequently translocate to the nucleus, where they excise the 'Stop' site from genomic DNA. Such a model allows to quantify *e.g.* functional mRNA delivery with a single-cell resolution, outperforming the use of mRNA encoding for reporter genes such as fluorescent proteins (low sensitivity) or *firefly* luciferase (no single-cell resolution) in wild type mice²⁴⁸. Another example is the eGFP654 transgenic mouse model that comprises a reporter gene of which the eGFP coding sequence is interrupted by an aberrantly spliced intron^{179,251–253}. Delivery of the proper SSO to nuclei of tissue cells will correct splicing leading to eGFP mRNA and protein expression. In turn, mice expressing the normal GFP reporter gene can be used to determine *in vivo* delivery of GFP-targeting siRNA/ASO¹⁴⁵. In addition to evaluating the extent of NA delivery, downstream next-generation sequencing (NGS) and digital droplet PCR on isolated cells can be used to quantify the intracellular DNA/RNA barcodes, originating from barcoded NPs, to assess the *in vivo* tropism and functionality of the screened NPs^{145,146,254}. Additionally, NGS could be used to analyze transcriptomic changes, yielding fundamental information on the off-target effects of NA formulations but also potentially on the genes and cellular pathways governing *in vivo* intracellular delivery^{222,255}.

In addition to engineering mice to encompass reporter genes, one can also generate transgenic mice with knockouts of specific genes involved in NA/NP delivery. Indeed, several reports have studied how plasma lipoproteins (*i.e.* ApoE), complement components (*i.e.* complement protein C3), glycoproteins (*i.e.* murine α -2-macroglobulin (M α 2M) and murinoglobulin-1 (MUG1)) and cell surface receptors (*e.g.* LDLR, very low DLR (vLDLR), ASGPR2 subunit of ASGPR) affect the *in vivo* pharmacokinetics and biodistribution of LNPs, polymeric NPs and GalNAc-conjugated siRNAs or free ASOs, by using the respective knockout mice^{94,133,144,256,257}. Another highly interesting study tested if manipulation of the endocytic gene CAV1 (caveolin-1^{-/-} mice), critical for caveolin-mediated endocytosis, could retarget LNPs *in vivo*. The authors found that CAV1 knockout did not alter LNP delivery to lung and kidney macrophages but substantially reduced LNP delivery to Kupffer cells, hence suggesting that the manipulation of intracellular endocytosis-related proteins could be a viable strategy to alter NA delivery²⁵⁴. In theory, knockout models of genes implicated in *e.g.* intracellular trafficking or endosomal release, provided they do not induce a lethal phenotype²⁵⁸, should allow to study the intracellular delivery process in an unprecedented way. Finally, approaches

such as pooled CRISPR/RNAi genetic screenings could also be used to investigate the genes involved in *in vivo* intracellular delivery, by xenografting the lentivirally-transduced cell pool in mice^{259,260}. Alternatively, a cell line with a single gene mutation could also be transplanted. For example, Wagenaar *et al.* tested if knockdown of TSG101 could also increase the delivery of a miR-21 antagomiR *in vivo*, by xenografting a cell line that stably expresses both a miR-21 luciferase reporter and a doxycycline-inducible shRNA targeting TSG101²⁰⁴.

Taken together, it is anticipated that advances in genetic engineering approaches and the application of alternative *in vivo* and *in vitro* model systems will prove very valuable to provide fundamental insights in the behavior of NA carrier systems, fueling the design of innovative formulations and delivery strategies (**Figure 2**)^{222,255}.

3. INTRACELLULAR BARRIERS AND HOW TO MANIPULATE THEM

3.1. Cellular targeting and intracellular uptake

Upon arrival at their target site, both ‘naked’ NAs as well as NA-conjugates and NA-loaded NPs need to traverse the plasma membrane to reach their site-of-action. Apart from some approaches that reported direct cytosolic delivery of the NA cargo^{261,262}, macromolecular materials are typically internalized by endocytosis and subsequently traffic through multiple membrane-bound vesicles^{76,216}. The general process of endocytosis can be subdivided in two broad categories, *i.e.* phagocytosis, a process of specialized antigen-presenting cells (APCs) such as macrophages and DCs that internalize large particles, and pinocytosis, which is present in all types of cells. The latter involves uptake of fluids or smaller particles through clathrin-dependent, clathrin-independent (*e.g.* macropinocytosis, caveolin-mediated endocytosis) or both clathrin-/caveolin-independent endocytic pathways (as excellently reviewed elsewhere^{176,216,255,263,264}). Both the type of endocytosis as well as its intrinsic efficiency and downstream intracellular trafficking influence transfection efficiency^{73,202,265–271}. For example, macropinocytosis and clathrin-mediated endocytosis are known to sequester NPs in acidified vesicles, a useful trait for pH-triggered NA release systems. On the other hand, caveolae-mediated endocytosis is believed to bypass lysosomes in certain cases, thus avoiding degradation by lysosomal hydrolases^{216,265,267,268,272–274}. Likewise, productive and non-productive internalization pathways have been described for gymnotically delivered oligonucleotides^{202,270}. Hence, increasing both total NA uptake and manipulating the

dominant endocytosis route are valuable approaches to increase intracellular NA delivery (**Figure 1**).

As discussed above, cellular uptake (and targeting) of NAs is generally improved by their encapsulation in NPs or the modification of the NA strands/NP surfaces with active targeting ligands. Despite efficient cellular targeting reported with, for example, the GalNAc moiety for delivery to hepatocytes, in many cases (*e.g.* solid tumor targeting) active targeting hardly showed a benefit over passive targeting^{150,152}. Hence, alternative or additional methods that manipulate the internalization process might be an interesting approach to improve NA delivery. Several small molecules have been documented in the literature to enhance NA internalization by actively modulating cellular processes¹²⁶. Indeed, in 2015 both Gilleron *et al.* and Osborn *et al.* reported on a screening of respectively 45.567 and 1280 compounds to identify intracellular delivery enhancers of cholesterol-conjugated siRNA (chol-siRNA) and/or siRNA-loaded LNPs^{178,180}. Among six hit compounds, Osborn *et al.* focused on Guanabenz acetate (Wytensin™), which improved chol-siRNA uptake and target gene silencing in HeLa cells likely by an interaction of its protonated guanidinium group with the negatively charged siRNA, although independent modulation of cellular pathways *via* an unknown mechanism could not be excluded¹⁸⁰. Similarly, Gilleron *et al.* discovered multiple small molecule compounds that boosted siRNA-induced silencing *via* either an improvement in cellular uptake or other mechanisms (*e.g.* blocking of endosomal maturation, destabilization of endosomal membranes). Strikingly, of the 25 and 28 hit compounds that improved delivery of chol-siRNAs or LNPs respectively, only 2 improved gene silencing with both delivery systems. Although several compounds were identified that likely increased uptake of LNPs by acting upon the cell *via* an unknown mechanism, the authors further focused on the application of Bisphenol A diglycidyl ether (BADGE). It was found that this compound, upon co-incubation with the LNPs prior to transfection, significantly reduces LNP size, thus facilitating cellular internalization both *in vitro* and *in vivo*¹⁷⁸. Also other groups have identified small molecules that directly interact with the NAs (*e.g.* aminoglycosides that bind SSOs²⁷⁵, synthesised small molecule carriers that bind siRNA^{276,277}) to improve delivery. In turn, Gustin *et al.* identified 3 small molecule drugs that upon co-incubation increased endocytosis and thus efficacy of a SSO complexed with a CPP (PepFect14), without interfering with the physicochemical properties of the formed particles. However, once again, the exact cellular target or mode-of-action of the increased uptake could not be unravelled²⁷⁸. Nevertheless,

some literature reports describe small molecule-based strategies that boost the NA uptake process *via* the modulation of a known cellular pathway as well.

A first example is the use of carbohydrates to stimulate endocytosis of NAs *via* an energy-dependent uptake mechanism. Han *et al.* showed that the intramuscular co-administration of several hexoses (*e.g.* 5% glucose, or the optimal combination of 2.5% glucose and 2.5% fructose) improved the exon-skipping activity of a SSO in muscle cells of a Duchenne muscular dystrophy (DMD) mouse model. Interestingly, also the uptake of other oligonucleotides and a siRNA could be increased in certain tissues upon I.V. injection in a carbohydrate solution, albeit to a significantly lower extent. The authors found that the generation of excess ATP by cellular metabolization of the administered hexoses enhanced the energy-dependent SSO uptake in energy-deficient muscle cells. Interestingly, as carbohydrate-based solutions are widely used in clinical practice for I.V. injections of NA therapeutics, this approach could be used more generally to stimulate NA uptake in differing energy-dependent tissues²⁷⁹. In two follow-up studies, the authors also showed the long-term clinical applicability of the SSO combination with glucose/fructose by treating DMD mice monthly for a period 1 year²⁸⁰ and the usefulness of this approach for enhancing peptide-SSO delivery to cardiac muscles²⁸¹.

Another interesting approach is the manipulation of ion channels that reside on the plasma membrane. For example, Choe *et al.* recently described a library screening of 2354 compounds in an effort to uncover small molecules that boost the potency of cholesterol-conjugated, cell-penetrating asymmetric siRNAs (cp-asiRNAs). Out of the 35 compounds that significantly enhanced cp-asiRNA silencing in HeLa cells, 3 were L-type calcium channel blockers (CCBs) with a common dihydropyridine (DHP) core²⁸². Further analysis revealed that DHP L-type CCBs (*e.g.* cilnidipine) increased the internalization (and subsequently silencing) of the cp-asiRNAs, not only *in vitro* but also *in vivo* when cilnidipine and cp-asiRNAs were co-injected intradermally in rat skin. In addition, also L-type CCBs without the DHP core (*e.g.* diltiazem) exhibited similar effects on the cp-asiRNA activity, albeit higher concentrations were required, while T-type CCBs did not improve cp-asiRNA delivery. Thus, the L-type CCB co-treatment likely improved cp-asiRNA internalization by inactivating L-type calcium channels²⁸³, as previous research suggested that the inactive state of the L-type calcium channel stimulates endocytosis^{284,285}. Interestingly, the above-mentioned study by Gilleron *et al.* also identified a L-type CCB, called tetrandrine (also a T-type CCB), as a chol-siRNA uptake booster¹⁷⁸. Of note, the delivery effects of DHP L-type CCBs could not be obtained in

combination with cationic lipid- (Lipofectamine 2000) or polymer-based (jetPRIME) siRNA delivery systems. Next, an earlier screening study by Tam *et al.* had identified seven candidate uptake enhancers of LNPs in HeLa cells, of which 3 were cardiac glycosides. It was hypothesized that the compound co-incubation increased the LNP uptake by enhancing the rate at which the plasma membrane was renewed. Indeed, cardiac glycosides bind the extracellular domain of the Na⁺/K⁺ ATPase pump, which induces its internalization. Consequently, the authors incorporated a PEG-lipid containing strophanthidin (a glycoside) into the LNP bilayer, which subsequently enhanced *in vitro* internalization and LNP-mediated silencing²⁸⁶. Although both studies noted that this strategy could theoretically boost respectively LNP and chol-siRNA uptake in a variety of tissues due to the widespread expression of both ion channels, the pharmacological effects and narrow therapeutic index of these drugs might limit their systemic *in vivo* use.

3.2. Intracellular trafficking

Following endocytosis, NAs/NPs are typically sequestered in the early endosomes (EEs), irrespective of the exploited endocytic pathway^{76,255}. Next, the cargo can progressively traffic towards the late endosomes (LEs, a process called “endosomal maturation”) and these LEs eventually fuse with lysosomes, where the cargo can be degraded. Alternatively, the EEs serve as sorting hubs that direct the payload to the endoplasmic reticulum (ER), the *trans*-Golgi network (TGN), or the endosomal recycling network^{76,255,287}. The latter directly recycles the internalized materials back to the extracellular environment¹²⁶. In addition, cargo excretion from the cell could also take place *via* late endosomal or lysosomal exocytosis⁷³. To escape this confinement in membrane-bound organelles, multiple fusion/fission events occasionally lead to discontinuities in the lipid bilayers^{288,289} (an endogenous process that can likewise be augmented by *e.g.* cationic lipids²⁹⁰), contributing to a partial release of NA cargo^{76,291}. However, in most cases cytosolic delivery is promoted by built-in endosomal release moieties in NA delivery carriers. The liberated NA fraction finally needs to navigate through the densely packed cytosol to reach its site of action in the cytosol or nucleus. Small NA therapeutics such as single-stranded oligonucleotides or double-stranded RNAi mediators are able to freely diffuse, while double-stranded DNA molecules larger than 2000 base pairs show little or no cytosolic diffusion and require active transport along the cytoskeleton by motor proteins^{292,293}. In case of cytosolic mRNA transport, the situation can be quite complex, as

some mRNAs predominantly diffuse, whereas other mRNAs are actively transported *via* cytoskeletal motors^{294–299}.

3.2.1. Fundamental molecular machinery of intracellular trafficking

The intracellular trafficking of endocytosed cargo is regulated by multiple protein(s) (complexes) and lipids and some are used as markers of specific organelles (*e.g.* Rab5 for EEs, Rab7 for LEs and LAMP1 for lysosomes)^{73,76,291}. This highly dynamic and complex process involves several basic steps^{300–303} (**Figure 3**), which are all guided by small GTPases, predominantly those of the ‘Ras-related in brain’ (Rab) family, which function as molecular switches that cycle between their inactive (GDP-bound) and active (GTP-bound) states^{304–308}.

First, invagination of the cell membrane (or the membrane from another intracellular donor compartment) is created by adaptor and coat proteins, and the formed pit subsequently pinches off to form a coated vesicle in the cytoplasm (**vesicle formation**)^{301,309,310}. For example, in clathrin-dependent endocytosis, adaptor proteins interact with membrane-bound proteins (and lipids) to deform the underlying membrane, followed by the dynamin GTPase-driven scission of clathrin protein-coated vesicles^{291,311}. Multiple other types of protein coats exist, of which the COP I and COP II proteins, involved in respectively Golgi to ER or the reverse transport are good examples³⁰⁹. Another trafficking event that merits attention is the retrograde trafficking between EEs and the TGN, a process in which tubulation of the early endosomal membrane results in the formation of vesicles that travel to the TGN^{312,313}. The key complex for this retrograde sorting is the retromer, which generates the tubulation of the early endosomal membrane^{312,314–316}. Second, once a vesicle is formed, it can move through the cell cytosol towards its target/recipient compartment (**vesicle movement**). For this transport, the vesicle will use motor proteins (*e.g.* kinesin, dynein, or myosin) that follow a track from the cytoskeleton (microtubules or actin)^{291,300,301}. Thirdly, before fusion can occur, the shuttle vesicle should be recognized by the target/recipient compartment⁷⁶. This process is facilitated by tethering proteins on the target membrane that recognize other tethers or Rab proteins on the vesicle membrane (**vesicle tethering**)^{317–319}. By doing so, the vesicle and the target membrane are now physically connected, which is followed by an additional recognition (**vesicle docking**) between transmembrane ‘Soluble N-methylmaleimide sensitive factor Attachment protein REceptors’ called v-SNAREs (located on vesicle) and t-SNAREs (located on target membrane)³¹⁷. Tethering factors, which contribute to the specificity and selectivity of the vesicle-target compartment interaction, can be broadly subdivided into two

major classes: long coiled-coil proteins (*e.g.* EEA1) and multisubunit complexes (*e.g.* HOPS)^{319–321}. **Vesicle fusion** is finally accomplished when the v-SNAREs and t-SNAREs wrap around each other to form a four-helix bundle, which induces membrane fusion and mixing of the two lipid bilayers^{317,322–324}. Lastly, next to the shuttling of vesicles between larger compartments, also the process in which one endomembrane compartment gradually acquires the characteristics of a second compartment (so-called **endosome maturation**) is extremely important for intracellular trafficking^{76,302,303}. The best known example is the maturation of EEs to LEs, which is characterized by the exchange of Rab5 by Rab7 (facilitated by the recruitment of several protein complexes such as the SAND-1/Mon1-Ccz1 complex and the HOPS complex^{302,325,326}) and a switch in lipid composition^{302,325,327,328}. Indeed, it appears that differing amounts of phosphoinositides regulate the binding of distinct effector proteins to the endosomal membranes³²⁹. As such, the FYVE domain-containing phosphatidylinositol 3-phosphate 5-kinase (PIKfyve) enzyme converts phosphatidylinositol-3-phosphate (PI3P, distinctive for EEs) into phosphatidylinositol-3,5-bisphosphate (PI(3,5)P₂, distinctive for LEs)³⁰². In addition, also other lipids are present in different amounts within the distinct endosomal compartments with, for example, lysobisphosphatidic acid (LBPA) that is enriched in the internal membranes of the LEs³²⁷. Other key aspects of the early-to-late endosomal maturation process is the luminal pH drop from pH ± 6.5 in EEs to pH ± 5 in the lysosomes (mediated by the proton pump V-ATPase) and the formation of multivesicular LEs (or multivesicular bodies, MVBs), of which the lumen is packed with intraluminal vesicles (ILVs) that originate from the MVB membrane by pinching off^{76,216}. The ILV formation process itself is regulated by both LBPA and the ESCRT machinery. The latter consists out of several distinct subcomplexes (ESCRT-0, ESCRT-I, ESCRT-II and ESCRT-III^{204,330}) and binds ubiquitinated cargo/proteins and sorts them into the ILVs⁷⁶.

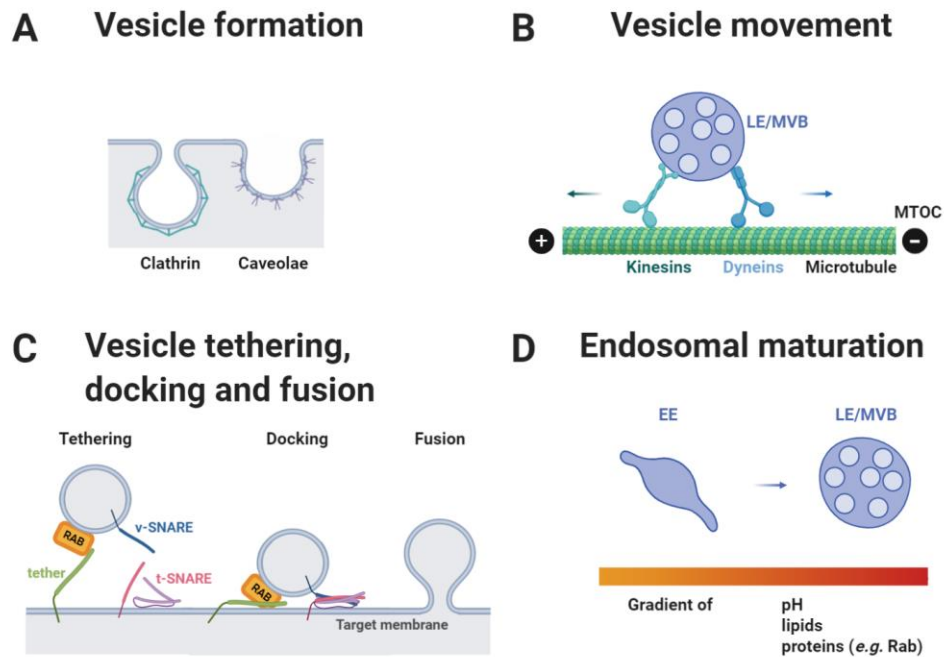


Figure 3. Overview of the basic steps in intracellular trafficking. (A) Following vesicle formation at *e.g.* the plasma membrane, (B) endomembrane compartments travel through the cytosol over the cytoskeleton (*e.g.* microtubules). (C) Endosomal vesicles can fuse with target compartments (*e.g.* lysosomes, TGN), mediated *via* tethering and fusion proteins. (D) The process in which an endomembrane compartment gradually acquires the characteristics of a second compartment (*e.g.* differences in pH and lipid/protein composition) is called endosomal maturation. This figure was created with BioRender.com. (LE = late endosome, MVB = multivesicular body, MTOC = microtubule-organizing center, Rab = Ras-related in brain, v-/t-SNARE = vesicle-/target- Soluble N-methylmaleimide sensitive factor attachment protein receptors, TGN = *trans*-Golgi network)

Given the extreme complexity of the trafficking pathways (as discussed above), and as relatively little is known regarding the exact molecular machineries used by the plethora of different RNA therapeutics and their respective delivery vehicles, we will focus on some general trafficking concepts that have been linked to an increased NA delivery (**Figure 1**).

3.2.2. Enhance early-to-late endosomal maturation, but delay accumulation in lysosomes?

Recent studies have shown that early-intermediate compartments (*i.e.* MVBs and LEs) are crucial for cytosolic release of both free oligonucleotides^{197,200,331,332}, CPPs³³³, conjugated siRNAs^{107,118} and NP-encapsulated NAs^{162,163,196}, before they reach the lysosomal compartment^{76,202,291,334–336}. For example, Wittrup *et al.* showed that Rab7 activity and endosomal maturation is crucial for the siRNA-mediated knockdown of both lipoplexes (LPXs, Lipofectamine 2000) and ionizable LNPs, with endosomal release occurring from respectively

EEA1⁻Rab5⁺Rab7⁺Rab9[±]LAMP1⁻ and EEA1⁻Rab5⁺Rab7[±]LAMP1⁻ maturing endosomes¹⁶³. The convergence on this early-intermediate stage of the intracellular trafficking as the key site for endosomal escape is quite remarkable given the plethora of used delivery systems, cell types and NAs²⁹¹. The reasons for this observation can be multifold. First, albeit a more simplistic explanation, the enhanced release from this hybrid organelles might be linked to the fact that there is just more NA or NP present in this compartment³³⁷, which increases the chance of successful 'random' escape rather than a selective release process²⁹¹. Second, despite the entire intracellular trafficking being a dynamic process, certain phases are especially active in terms of fusion and fission events, of which the ILV formation within MVBs is an important example²⁹¹. The continuous inward budding of the outer endosomal membrane and the subsequent back-fusion of ILVs at a later stage could induce discontinuities in the lipid bilayer, resulting in partial NA release. Finally, it has been reported that the Argonaute 2-RNA-induced silencing complexes (Ago2-RISCs) can be associated with membranes of LEs and even inside ILVs³³⁸⁻³⁴⁰, while LEs can form transient membrane contact sites *via* Rab7 with the ER³⁴¹, which is the active site of mRNA translation and siRNA silencing^{342,343}. Hence, even partial NA release from the intermediate endosomal compartments might directly be in close proximity to the translation- or silencing machinery. In addition, Patel *et al.* found that CRISPR-mediated depletion of Rab7, but not Rab4 or 5, abolished the expression of lipofected luciferase mRNA, which could not be overcome by electroporation of the non-formulated mRNA. It was subsequently hypothesized that late endosomal/lysosomal membranes, which serve as a host to the mammalian target of rapamycin (mTOR)-complex, may regulate multiple cellular processes such as translation of exogenously delivered mRNA and ribosomal biogenesis. Hence, inhibiting the formation of these key endomembrane structures by Rab7 deletion possibly prevented mTOR binding to the late endosomal/lysosomal membrane and the subsequent triggered mRNA translation¹⁹⁶.

Taken together, promoting the formation of these hybrid EE-LE-MVB compartments by enhancing early-to-late endosomal maturation or increasing the residence time in these vesicles by delaying further transport from LEs towards the degradative lysosomes, could increase the probability of endosomal escape. Indeed, Castanotto *et al.* found that the α isoform of protein kinase C (PKC- α), an enzyme known to **promote maturation of EEs to LEs/MVBs**^{344,345}, proved to be an essential protein for gymnotic ASO- and lipofected siRNA-mediated gene silencing in mammalian cells³³¹. In this study, downregulation of PKC- α expression by RNAi or pre-inhibition of PKC- α activity with a PKC classical isoform inhibitor

blocked ASO activity, while PKC- α overexpression or increased PKC- α activity by (a) incubation in high glucose-medium³⁴⁶ or (b) treatment with oleic acid (a well-known activator of PKC- α ^{347,348}) boosted ASO-mediated gymnotic gene silencing. The latter findings corroborate other studies by the same group that demonstrated oleic acid-enhanced ASO/SSO activity^{349–351}. Also other kinases have shown to regulate the activity of NA drugs^{240,274}. For instance, *via* a small molecule HTS, Zhang *et al.* identified the indirubin-derivate 6-bromo-indirubin-30-oxime (6BIO), a glycogen synthase kinase 3 α/β (GSK-3 α/β) inhibitor, as a gymnotic transfection enhancer of several ASOs/SSOs, albeit the underlying mechanism remains obscure²⁴⁰. Nevertheless, it is conceivable that these kinases do not directly act at the endosomal level, but affect the function of downstream effectors through phosphorylation³³¹.

Next, as mentioned above, **delaying or inhibiting the further fusion of LEs with lysosomes** can enhance the NA delivery process, as the degradative environment of the lysosomal lumen is usually seen as a dead end for NA therapeutics. One possibility to avoid endo-lysosomal fusion is preventing lysosomal acidification *via* alkalinizing agents (*e.g.* buffering agents such as chloroquine and ammonium chloride or ionophores³⁵² such as monensin or nigericin) or vacuolar-type (V-type) proton-pump ATPase inhibitors³⁵³ such as bafilomycins or concanamycins. Consequently, increasing lysosomal pH also impedes the degradation of cargo as lysosomal hydrolases (*e.g.* nucleases, etc.) generally require an acidic pH for proper functioning³⁵⁴. Chloroquine and analogues are probably the best-studied examples of small molecular endolysosomal buffering agents, with several reports showing increased pDNA^{177,354–367}, mRNA³⁶⁸, peptide nucleic acid^{369–371}, miRNA³⁷², antagomiR³⁷³ and siRNA^{154,359,374–379} transfection when applied as a free compound or incorporated in/conjugated to NPs. However, also other buffering agents have shown to increase NA transfection. Indeed, Zhang *et al.* showed that ASO and SSO gymnotic delivery could be increased by co-treatment with ammonium chloride (NH₄Cl) in several adherent or suspension cell types. Interestingly, ambroxol and cyclohexylamine, two other inhibitors of endosomal maturation/fusion, could also boost SSO delivery. Additionally, the above-mentioned high-throughput screening of Gilleron *et al.* identified several hit compounds that improved the transfection efficiency of LNP-encapsulated siRNA by most likely interfering with endosomal acidification and/or maturation¹⁷⁸. In turn, Rangasamy *et al.* and Orellana *et al.* showed that the transfection of folate-siRNA³⁸⁰ or folate-miRNA³⁷² conjugates could be boosted by coupling the ionophore nigericin to the conjugates with a disulfide linkage, which allows intra-endosomal dissociation of nigericin from the carrier³⁸¹. Likewise, the ionophore

monensin has shown to (moderately) increase the transfection efficiency of CPP:siRNA complexes³⁸² and cationic CPP:pDNA lipoplexes³⁸³.

However, next to preventing progression of cargo along the degradative pathway, alkalinizing agents might also work by enhancing endosomal escape *via* the proton sponge effect¹⁵⁷. In addition, chloroquine is also a cationic amphiphilic drug (CAD), which are known to induce phospholipidosis (PLD) and lysosomal swelling, as discussed in detail below. Hence, the induction of PLD can likewise result in trafficking defects (*e.g.* a hampered fusion between LEs and lysosomes) or an increased endolysosomal escape *via* the induction of membrane permeabilization. Moreover, Rangasamy *et al.* hypothesized that nigericin in their conjugates facilitates the selective transport of K⁺ from the K⁺-rich cytosol to the endosomes in exchange for a H⁺ (but not Na⁺), thus promoting osmotic swelling and bursting^{372,380}. Which process preferentially takes place overall depends on the timing of compound application (pre-, co- or post-transfection) and the type of delivery system. On the one hand, Tusup *et al.* showed an increased expression of lipofected mRNA *in vitro* and *in vivo* when chloroquine was applied 2 hours after transfection or injection, while pre- or co- treatment could not enhance the delivery³⁶⁸. However, postponing the chloroquine treatment too long after transfection might also impede the adjuvant effect, as Wang *et al.* showed that only chloroquine treatment 8 h post-transfection (but not 36 h after transfection) could enhance (non-stabilized) siRNA-mediated silencing by polyethylenimine (PEI)-coated mesoporous silica NPs (MSNPs). In contrast, the use of nuclease-stabilized siRNA could overcome this hurdle, emphasizing that lysosomal sequestration and subsequent NA degradation is an important barrier for RNA therapeutics³⁸⁴. On the other hand, some carriers (*e.g.* polymeric NPs with buffering capacity, LNPs with ionizable lipids, cationic liposomes with the pH-dependent fusogenic helper lipid DOPE^{385,386}, ...) are not perfectly compatible with alkalinizing agents, as they require an acidic endosomal pH to allow endosomal escape^{163,195,206,375,387,388}.

Interestingly, next to modulating the luminal pH, there are also other possibilities to block late endosomal-lysosomal fusion. For example, HPS4, a gene that is linked to the rare autosomal recessive disease Hermansky–Pudlak Syndrome 4, is known to be required for fusion of MVBs with lysosomes^{338,389}. Cuellar *et al.* found that silencing the tethering factor HPS4 doubled the efficiency of an antibody-siRNA conjugate²⁰¹, which corroborated earlier findings that loss of HPS4 likewise enhances Lipofectamine[®]-mediated siRNA silencing³⁴⁰. Similarly, it was suggested that the depletion of ESCRT-I proteins (TSG101 and VPS28) avoided

shuttling of antagomiRs to the lysosomes and thus enhanced their activity^{204,331}. On the other hand, Wang *et al.* could not reproduce this effect of TSG101 depletion on the silencing activity of other PS-ASOs¹⁹⁷.

3.2.3. Alter the dynamics and organization of the cytoskeleton

As mentioned above, cytosolic movement of both vesicles containing NA cargo and larger NAs such as pDNA and certain mRNA molecules occurs *via* motor proteins that ‘walk’ along the cytoskeleton. Consequently, it was hypothesized that altering the dynamics and organization of the cytoskeleton by (de)stabilizing these ‘trafficking highways’ could boost intracellular delivery *via* increasing the residence time, preventing lysosomal degradation, altering the intracellular destination *etc.*¹²⁶. Multiple studies have investigated the application of microtubule disrupting (*e.g.* colchicine^{383,390,391}, nocodazole^{383,392–394}, vinblastine³⁸³, vincristine³⁸³, podophyllotoxin³⁸³) or stabilizing (*e.g.* paclitaxel (PTX)^{293,390,394–397}, histone deacetylase 6 (HDAC6) inhibitors such as NCT-10b³⁹⁵, tubacin³⁹⁸, tubastatin A³⁹⁷ or siRNA against HDAC6³⁹⁵, general HDAC inhibitor trichostatin A^{395,397,398}) agents to boost pDNA transfection. Additionally, dynein inhibitors (*e.g.* ciliobrevin D³⁹³) and actin disrupting (*e.g.* cytochalasin B^{383,396}) compounds have been explored for the same purpose. In general, inhibition of actin polymerization with cytochalasin B did not affect transfection efficiency of both pDNA:polyplexes (PPXs)³⁹⁶ or lipoplexes³⁸³, highlighting that pDNA molecules and vesicles mainly move along microtubules. However, as actin is also a key protein in several endocytic pathways³⁹⁹, actin depolymerization might have lowered NP internalization, mitigating any downstream effects on delivery. In turn, the effects of microtubule (de)stabilizing compounds were clearly dependent on the applied cell types, delivery vehicles, compounds and timing of the compound application relative to the transfection¹²⁶. For example, PEI:pDNA polyplexes benefited from microtubule stabilization (*via* PTX), but not from microtubule disruption, which lowered delivery efficiency³⁹⁶, while lipoplex:pDNA transfection can be improved by both³⁹⁴ or only the latter^{390,392}. An explanation for this discrepancy could be the fact that PEI-based carriers need at least some endosomal acidification to allow endosomal escape *via* the proton-sponge effect. Of note, similar to the actin disrupting compounds, also microtubule modulating agents can negatively impact cellular uptake as *e.g.* nocodazole is widely used as an endocytosis inhibitor^{400,401}. However, in contrast to the delivery of pDNA, little to no such studies with cytoskeleton-modulating compounds exist for RNA therapeutics. One study demonstrated that, next to pDNA

transfection, post-incubation of transfected cells with vorinostat (SAHA, an inhibitor of several HDACs) could modestly enhance polymer-based (Turbofect) mRNA transfection³⁹⁷. Interestingly, Patel *et al.* identified the same compound as a hit from a bio-active lipid screen to discover lipid(-like) molecules that can boost the transfection of mRNA lipoplexes¹⁹⁶. In turn, pre-treatment with PTX improved the gene silencing of siRNA-loaded liposomes in tumor bearing mice^{402,403}, albeit this effect was linked to the concept of tumor priming, in which apoptosis-inducing compounds decrease tumor cell density, resulting in an expanded and more porous interstitial space that allows more NPs to deeper penetrate tumors⁴⁰⁴. Interestingly, Wang *et al.* also showed that co-treatment of PTX with siRNA lipoplexes could promote cytosolic release of a fluorescent siRNA, underscoring that microtubule modulating compounds could also boost the intracellular delivery of small RNAs⁴⁰³. In addition, a large amount of studies reported on the combination of PTX and siRNA, where siRNA is used to boost the therapeutic potential of the anti-cancer drug, instead of PTX promoting the siRNA silencing potential^{375,405-413}. Indeed, siRNAs can silence multidrug resistance proteins (*e.g.* multidrug resistance protein 1 (MDR-1)), anti-apoptotic proteins (*e.g.* B-cell lymphoma 2 protein (Bcl-2)) or proteins involved in cell cycle regulation/proliferation (*e.g.* Polo-like kinase 1 (PLK1)), hence increasing PTX concentration at the tumor site or obtaining a (synergistic) apoptotic effect⁴⁰⁵. Consequently, a combination approach can be envisioned, in which the extra- and intracellular siRNA delivery is boosted by the anti-cancer drug, while the siRNA-mediated silencing effect on its part promotes the drug-induced cell death.

3.2.4. Endosome – TGN retrograde trafficking and further trafficking towards ER?

Up to now, we have mainly described the intracellular trafficking as a one-way linear pathway towards the degradative lysosomes. It should however be noted that there are several detours and branches within these trafficking events. One process, the retrograde trafficking between the endosomal compartment and the TGN deserves special attention, as multiple (bacterial) toxins and viruses hijack this route to gain cytosolic access^{313,414-419}. Likewise, interfering with this pathway has shown to influence the trafficking and activity of small NAs^{199,420}. Retro-1, a small molecule that reduces the cytotoxic effect of bacterial toxins by blocking the retrograde endosome-TGN trafficking⁴¹⁵, improved ASO and SSO release *in vitro* by mainly destabilizing the LEs⁴²⁰. No adjuvant effect was seen in combination with 'naked' siRNA, possibly due to the limited uptake of the applied siRNA⁴²⁰. In addition, Retro-1 could also enhance the activity of SSO in mice⁴²⁰. However, conjugating this compound to a SSO did

not improve delivery⁴²¹. Up to now, neither the exact mechanism, nor the specific molecular target by which Retro-1 exerts this effect could be identified. Another study by the Juliano group did indicate that Retro-1's fundamental activity on toxin trafficking and ON delivery involve distinct molecular targets, potentially disconnecting the retrograde trafficking block from the ON delivery-enhancing effects⁴²². Next, Liang *et al.* showed that reducing shuttling of the mannose 6-phosphate receptor (M6PR) from the endosomes to the TGN (a process mediated by the *trans*-Golgi tether protein 'GRIP and coiled-coil domain-containing protein 2' (GCC2)) impaired PS-ASO endosomal escape and activity *in vitro* and *in vivo*¹⁹⁹. Normally, the M6PR binds mannose-6-phosphate (M6P)-tagged newly synthesized hydrolases in the TGN and shuttles them to LEs. Subsequently, the low pH of the late endosomal lumen causes the hydrolases to dissociate from the M6PR and the former is transported to the lysosomes. The latter returns to the TGN by vesicular transport, with the GCC2 tethers incoming M6PR vesicles to TGN membranes¹⁹⁹. As silencing of one these proteins impaired ASO-activity, the authors hypothesized that M6PR binds the PS-ASOs and facilitates their endosomal egress by vesicular escape and/or back-fusion-mediated processes. Hence, overexpression of M6PR could enhance PS-ASO activity in HeLa cells⁴²³. The inhibitory effect of M6PR/GCC2 downregulation on ON activity could not be reproduced for phosphodiester (PO)-ASOs or PS-ASO:lipoplexes, which was explained by the lower binding affinity of PO-ASOs for cellular proteins^{334,424,425} and the different trafficking pathways used by lipid-based nanocarriers¹⁹⁹. In addition, several other studies have shown that further trafficking towards the ER (passively or *via* active targeting peptides) can be beneficial for both siRNA^{426,427} or pDNA^{267,268,428,429}-loaded NPs. Indeed, while the cytoplasmic face of the rough ER membrane is the central nucleation site for siRNA-mediated gene silencing³⁴², the close relationship between the ER membrane and nuclear envelope suggests that transport to the nucleus *via* the ER can be an alternative approach to increase the local concentration of NAs that have an intranuclear function (*e.g.* SSOs)⁴²⁹.

3.2.5. Blocking exocytosis

The natural process of exocytosis is used by cells for a myriad of functions such as intercellular communication, the delivery of lipids and proteins from the Golgi network to the cell membrane or to remove membrane proteins (*e.g.* ion channels)^{430,431}. However, for NAs and NPs, this process is yet another major barrier for successful intracellular delivery⁴³⁰⁻⁴³³. Indeed, in case of LNP-mediated siRNA transfection, it has been reported that within 24 hours

70-80% of the initially internalized siRNA dose is exported back to the surrounding medium¹⁹⁵. Unfortunately, despite a pioneering study by Sahay *et al.*¹⁹⁵, relatively little is known about the cellular excretion mechanisms of RNA therapeutics⁷³. Different exocytosis pathways exist within cells and theoretically NAs and NPs can be routed for excretion by almost all of these processes.

First, fusion of EEs with recycling endosomes can immediately direct cargo towards the cell membrane. Several Rab GTPases (*e.g.* Rab4, Rab11, Rab35) are involved in this **endocytic recycling**, of which Rab11 is the best-known example^{434,435}. Indeed, siRNA-loaded C12-200 LNPs have shown to co-localize with Rab11-positive recycling endosomes within 30-60 min after application. However, depletion of Rab11 lowered LNP uptake instead of increasing the cellular retention¹⁹⁵. Second, **MVBs/lysosomes can also fuse with the plasma membrane**, thereby releasing their luminal content in the extracellular environment. The latter includes the secretion of ILVs as a specific type of extracellular vesicles (EVs), termed exosomes. Contrary to Rab11, silencing of Rab27b, which regulates the process of MVB/lysosomal exocytosis, did enhance cellular LNP retention and improved silencing. Interestingly, increased retention and silencing was also observed when LNPs were applied to NPC1-deficient cells¹⁹⁵. This transmembrane glycoprotein is located on the surface of MVBs and plays a role in the export of lipids (*e.g.* cholesterol) from LEs/lysosomes towards the extracellular milieu. A follow-up study by another group confirmed the major role of NPC1 in the cellular retention of siRNA:LNPs as the small molecule NPC1-inhibitor NP3.47 reduced recycling, increased late endosomal/lysosomal accumulation of LNPs and boosted siRNA silencing 2- to 4-fold in several cell lines⁴³⁶. On the contrary, the effect of the NPC1 transporter seems to be highly dependent on the type of NA and/or carrier, as NPC1 deficiency has shown to block both the delivery of gymnotic PS-ASOs¹⁹⁷ and pDNA:poly(β -amino ester) polyplexes⁴³⁷. Consequently, overexpressing NPC1 *in vitro* could enhance the uptake and transfection of the latter by respectively 3- and 10-fold⁴³⁷. Third, NAs/NPs that enter the TGN or ER upon intracellular redistribution can exit the cells *via* vesicles of the “**conventional secretion system**”. Exo-1 and Brefeldin A, two agents known to impede protein exocytosis by inducing a collapse of the Golgi apparatus, have shown to increase the retention of siRNA-loaded polyplexes in hepatic stellate cells⁴³⁸. Likewise, blocking Golgi/ER secretion by depletion of Rab8a by Sahay *et al.* led to a 5-fold increase in LNP cellular retention¹⁹⁵. Still, the latter did not result in a substantial improvement of LNP-mediated gene silencing, while the former study did not quantify the effect on silencing. Fourth, if endosomal escape happened,

the budding of another type of EVs at the cell membrane, called **ectosomes**, can also pick up NAs or NPs from the cytosol⁷³, albeit the involvement of this process has not been studied yet for RNA therapeutics.

Although the abovementioned studies describe exocytosis as a process that limits the activity of RNA therapeutics, it should be noted that secretion of EVs containing functional RNA molecules may still be beneficial in an *in vivo* setting as these EVs might mediate intercellular transport⁴³⁸. Indeed, Maugari *et al.* showed that LNP components (mRNA and ionizable lipids) are partly incorporated into EVs upon LNP *in vitro* transfection and that these EVs can subsequently transfect other cells both *in vitro* and *in vivo*¹⁶⁴.

3.3. Endo(lyso)somal escape

As mentioned previously, endocytic internalization results in cargo sequestration in the endosomes^{76,255}. Unfortunately, only a very limited amount of NAs is able to effectively overcome the endosomal limiting membrane and the majority of internalized NAs and carriers either undergo enzymatic degradation in the lysosomes or are recycled out of the cell⁷³. Therefore, various delivery systems have been designed to promote endosomal escape (*e.g. via* pore formation, endosomal membrane fusion, proton-sponge mechanism, CPPs *etc.*^{156,158}, see **Figure 4**). Still, despite the extensive research on this formidable intracellular barrier in the past decades, most state-of-the-art endosomal escape mechanisms are largely inefficient, as typically < 2% of the internalized NA dose escapes the endosomes^{162–164} and only ~ 10% of the NP-containing vesicles efficiently releases their cargo into the cytosol^{163,439}. Hence, improving our understanding of this barrier by elucidating the exact endosomal release mechanisms of existing RNA therapeutics might in turn converge into the design of more effective methods or improved carriers.

One can distinguish **3 different phases** or time-periods within in the endosomal escape process (*i.e.* (1) escape from intermediate compartments, (2) escape from lysosomes and (3) repair of damaged membranes). First, as described earlier, several RNA therapeutics seem to escape from an **intermediate endosomal compartment**²⁹¹. The formation of ILVs and their back-fusion with the MVB-limiting membrane are processes that can be hijacked by several toxins and viruses^{197,440,441}. This route is regulated by lysobisphosphatidic acid (LBPA, also known as bis(monoacylglycero)phosphate (BMP)), an unsaturated anionic isoform of phosphatidylglycerol that is enriched in the inner leaflet of MVB/late endosomal membranes

and in the membranes of the ILVs^{442–444}. In turn, Alix, an ESCRT-associated protein, controls the LBPA levels in LEs by binding to LBPA-containing bilayers^{197,200,444}. Interestingly, LBPA (and/or Alix) have shown to facilitate the escape of PS-ASOs¹⁹⁷ and peptides^{333,445} from the late endosomal compartment. In addition, it was demonstrated that co-incubation of PS-ASOs with a lipid precursor of LBPA (docosahexaenoic acid (DHA)) could moderately increase PS-ASO activity²¹⁵. The exact mechanism behind ILV back-fusion, how it results in cytosolic ON delivery and if LBPA (and/or Alix) could also be involved in endosomal release of other RNA therapeutics (*e.g.* NP-loaded) remains to be elucidated²⁹¹. Interestingly, recent research from our group indicated that surfactant protein B (SP-B), a protein that enhances endosomal escape when present in a proteolipid shell around siRNA-loaded dextran nanogels, exerts its function *via* interaction with the negatively charged endogenous LE-enriched lipids (*e.g.* LBPA). Hence, similarly to fusion events described for several viruses or CPPs, this direct interaction enhanced cytosolic siRNA release, either *via* fusion with the limiting membrane or, alternatively, *via* fusion with ILVs, followed by the back-fusion process (Guagliardo *et al.*, submitted). Sparked by the impact of LBPA, the group of Stanley T. Croke further evaluated the effects of other lipidic species on PS-ASO escape from LEs⁴⁴⁶. Membrane destabilization induced by pre- or post-treatment with free fatty acids (predominantly palmitic and oleic acid), cholesterol and ceramide indeed enhanced late endosomal release of PS-ASOs, which, in turn, increased silencing activity. Of note, total cellular PS-ASO uptake or intracellular trafficking processes were not significantly altered by the application of the lipids. In a follow-up study, the authors made conjugates of the lipids with PS-ASOs, which released more rapidly from the endosomes than parental PS-ASOs⁴⁴⁷. Interestingly, by utilizing a small library of 212 bioactive lipids (or lipid-like molecules), Patel *et al.* also discovered several lipids that enhanced the activity of lipofected mRNA¹⁹⁶. It was hypothesized that the bioactive lipids, which are either enriched in vesicular compartments or serve as signalling molecules³²⁸, could enhance the activity of the mRNA-loaded lipoplexes by altering intracellular trafficking⁴⁴³, endosomal escape or cell signalling. However, the exact mode of action remains unknown. The authors focused on one transfection-enhancing compound, MK-571 (a leukotriene inhibitor), which resulted in 2-fold increase in LNP-mediated mRNA expression *in vitro*. Two additional clinically-approved leukotriene receptor antagonists (pranlukast and zafirlukast) had a comparable efficacy. Notably, MK-571 could be readily incorporated into an ionizable LNP containing mRNA, which led to enhanced intracellular mRNA delivery both *in vitro* and *in vivo* in the liver and spleen of BALB/c mice.

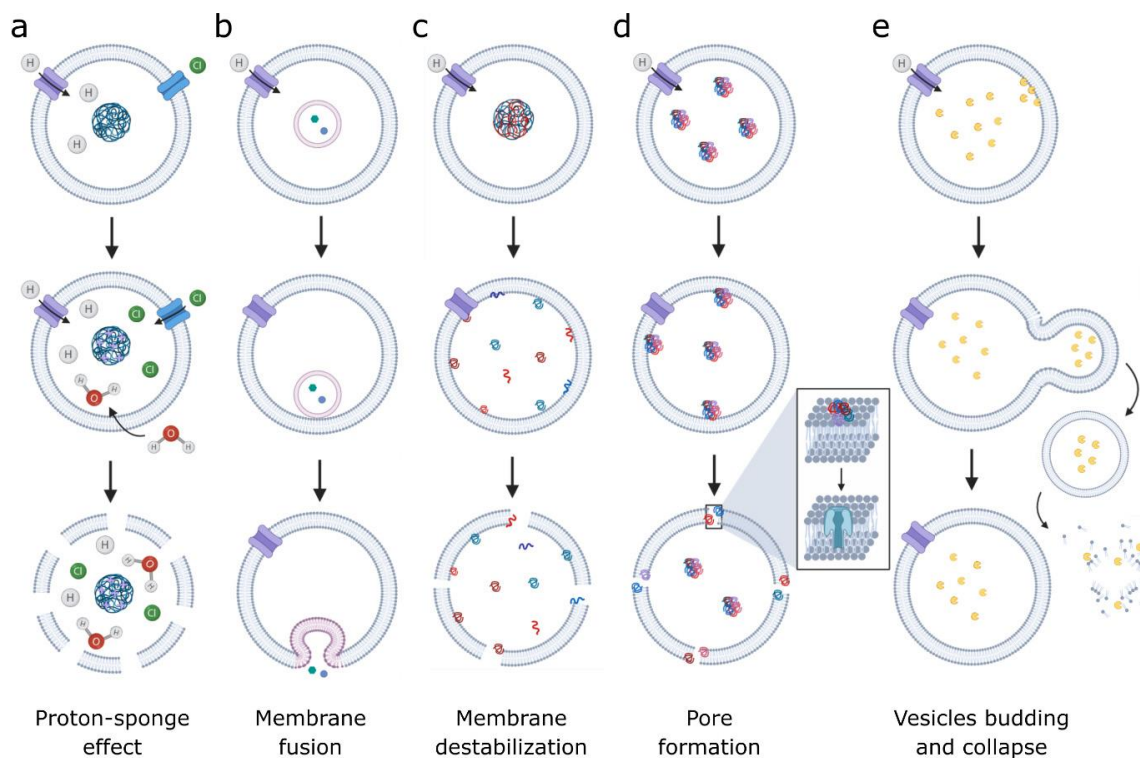


Figure 4. Endosomal escape strategies. (A) The proton-sponge effect: buffering polymers cause an increased influx of protons and chloride counterions into the endosomes, which leads to an enhanced osmotic pressure and endosomal rupture. (B) Lipid-based nanoparticles (NPs) which contain fusogenic lipids interact and fuse with the endosomal membrane, hence releasing their payload into the cytosol. (C) Polymers containing pH-sensitive groups are able to induce membrane destabilization following disassembly in monomers and interaction with the anionic endosomal membrane. (D) Certain cell-penetrating peptides (CPPs) are able to form pores in the endosomal limiting membrane, which subsequently allow passage of the NA cargo. (E) Vesicle budding and collapse mechanism suggested for cyclic CPPs. This figure is adapted from Guagliardo R. Beyond the surface: unraveling the intracellular mechanism behind surfactant protein B (SP-B) mediated siRNA delivery. 2020, thesis. This figure was created with BioRender.com.

Several interesting small molecules have been described that dramatically enhance release of small NAs from LEs *via* yet unknown mechanisms. A high throughput screening of > 100.000 compounds revealed several hits that improved the activity of SSOs¹⁷⁹. Here, the authors initially pursued a series of 3-deazapteridine analogs (*e.g.* UNC7938) that improved the activity of both SSO(s)-conjugates, ASOs and chol-siRNAs *in vitro*, with a higher efficacy than Retro-1 (see 3.2.1). Importantly, UNC7938 could also enhance the *in vivo* effects of a SSO and other groups have shown improved endosomal release of larger macromolecules (*e.g.* pDNA) with this compound⁴⁴⁸. In follow-up work, a number of UNC7938 analogs³³⁶ were synthesized or a second family of compounds²⁵³, derived from another hit (UNC2383) that emerged from their initial HTS, were described. For the UNC7938 analogs a detailed structure activity

relationship (SAR) was performed, which revealed that the lipophilic aromatic groups and the tertiary amino group were essential for activity³³⁶. Still, no compounds were identified that have a major advantage in terms of potency and toxicity over the respective parental compounds^{253,336}. Taken together, the described compounds mainly affected the LEs, in a similar way as Retro-1, to enable release of the NAs into the cytosol^{179,253,336}, although UNC2383 and its analogs affected the permeability of lysosomes to a certain extent²⁵³. Hence, the authors claimed that these compounds are quite distinct from typical lysosomotropic compounds such as chloroquine, albeit their precise molecular targets could not yet be determined^{179,253,336}.

In addition to Retro-1 and the UNC compounds, also other small molecule delivery enhancers have been identified that could (in)directly destabilize endosomal membranes. Examples are (a) certain hit compounds from the screening of Gilleron *et al.*¹⁷⁸, (b) the antifungal compound amphotericin B^{388,449} of which the proposed mode-of-action includes pore formation through interaction with the endosomal membrane, in accordance with its reported antifungal activity⁴⁵⁰, (c) the plant glycoside SO1861 that showed to improve siRNA delivery by lipid- and peptide-based carriers or (d) a solution called 'iTOP', which stands for induced Transduction by Osmocytosis and Propanebetaine. The latter strategy enhances both the uptake (*via* NaCl hypertonicity-induced macropinocytosis) and subsequent release of small RNAs/proteins from macropinosomes (*via* several non-detergent sulfobetaines (NDSBs) or the neurotransmitter gamma-amino- butyric acid (GABA)) in several primary cells^{449,451}.

In contrast to the general paradigm that lysosomes are a dead end for NA therapeutics, our group recently proposed to **stimulate NA release from the lysosomes**. Hereto, an initial selection of four lysosomotropic CADs, with diverging pharmacological activity, were applied to transfected non-small cell lung cancer cells, markedly improving the gene silencing potential of siRNA-loaded nanogels⁴⁵². In a follow-up study, it was found that many more physicochemical related compounds phenocopy this adjuvant effect (**Chapter 2**). Moreover, this effect was shown to be highly dependent on the type of nanocarrier (**Chapter 3**), with NPs that generate an appropriate pool of decomplexed siRNA in the endolysosomal compartment being most susceptible to CAD-promoted gene silencing. Hence, state-of-the-art DLin-MC3-DMA-containing LNPs that tightly complex the siRNA are resistant to CAD exposure¹⁶⁶. It was suggested that CADs improved the siRNA delivery through the functional inhibition of the lysosomal acid sphingomyelinase (ASM) enzyme and the subsequent

induction of a PLD phenotype. The phenotype conversion was accompanied by a transient minor lysosomal membrane permeabilization (LMP), which allowed the decomplexed siRNA/ASOs to diffuse towards the cytosol, while substantially larger molecules (*e.g.* mRNA) could not pass through these pores^{166,452}. Interestingly, an independent study by Du Rietz *et al.* showed that CADs could likewise boost the release of chol-siRNAs from LAMP1⁺ vesicles²³⁸. Given that *in vivo* applicability of the well-known delivery enhancer chloroquine, which is also a CAD, is hampered by its systemic dose-limiting toxicity⁴⁵³, other CADs such as antihistamines (*e.g.* desloratadine) may provide a safer alternative^{166,452}. In correspondence with data from Yang *et al.* and Du Rietz *et al.*, a single CAD treatment did not release the entire lysosomal siRNA content^{179,238}. Consequently, the lysosomes could be applied as an intracellular reservoir for prolonged and controlled siRNA release upon multiple CAD treatments⁴⁵². In addition, a recent study by Alnylam Pharmaceuticals showed that the remarkable silencing durability of novel GalNAc-conjugated siRNAs (up to months in preclinical tests and in humans) is linked to their accumulation and stability in highly acidic intracellular vesicles, which release functional siRNAs weeks after dosing¹⁰⁷.

In the event of endo(lyso)somal escape, a (transient) perturbation of the endo(lyso)somal membrane integrity occurs. As release of luminal contents (*e.g.* acid hydrolases in case of lysosomes) into the cytosol may be harmful to the cell, cells can either remove impaired organelles by selective macroautophagy (as discussed in section 3.4) or they are able to **repair the damaged membranes**^{454–456}. Which process will be deployed depends mainly on the extent of membrane damage and the timing following the initial rupture. Large membrane disruptions will expose the β -galactosides on the luminal side of vesicular membranes. These exposed sugar moieties will be bound by cytosolic β -galactoside-binding lectins (*i.e.* galectins such as galectin-3 and galectin-8), which subsequently recruit the autophagy machinery (a rather slow process with a timescale of ± 1 h)^{330,457,458}. Hence, galectin puncta assays, in which fluorescently-labeled galectins are imaged *via* confocal microscopy, are increasingly being used as endosomal escape assays^{163,238,459,460}. In case of smaller disruptions, (members of) the ESCRT (*e.g.* charged multivesicular body protein 1B (CHMP1B)^{448,456}) or the annexin A2/S100A10 complex may be recruited to the cytosolic side of the damaged vesicular membranes, where they mediate the membrane repair through supposedly sealing the damaged location or patching the bilayer by recruiting nearby vesicles^{457,461–463}. ESCRT recruitment is typically considered to be a rapid response to damage (*i.e.* first level of defense), but multiple repair pathways may occur in parallel^{330,461}. In addition, an overlap

between membrane repair and autophagic removal has recently been suggested as galectin-3 could also recruit ESCRT components to damaged lysosomes⁴⁶⁴. Finally, replacement of damaged organelles can also occur *via de novo* biogenesis, which is regulated by the transcription factor EB (TFEB)⁴⁵⁶. Considering that the described processes continually counteract the induced membrane damage, they could also inhibit endosomal NA release. Hence, inhibition of the involved proteins might extend vesicle permeability. For example, the previously mentioned study by Wagenaar *et al.*, where silencing of TSG101 enhanced antagomiR delivery both *in vitro* and *in vivo*²⁰⁴, could possibly be linked to this process as TSG101 is required for ESCRT-III-mediated repair of endolysosomal membranes^{461,465,466}. Of note, other reports have likewise demonstrated increased endolysosomal escape of antigens (enhanced cross-presentation)⁴⁶⁷ or tau proteins⁴⁶⁸ following TSG101 knockdown. However, the exact mechanism behind the delivery enhancing effect could not be clarified yet. As the ESCRTs are endosomal-associated proteins with a myriad of other functions in addition to endomembrane repair (*e.g.* nuclear envelope repair, ILV biogenesis (see above), autophagosome sealing³³⁰), it is difficult to assess which particular intracellular barrier is affected by this modulation. On the other hand, independently of its partner protein S100A10, annexin A2 knockdown has shown to block PS-ASO activity in several cell lines, which was linked to a delayed endocytic trafficking to LEs²⁰⁰. Interestingly, Ochaba *et al.* showed that the reduction or overexpression of TFEB could respectively slightly enhance or decrease ASO-mediated knockdown⁴⁶⁹.

3.4. Autophagy/cell metabolism

Autophagy (Greek for 'self-eating') is an evolutionary conserved catabolic process that removes damaged organelles and foreign materials (*e.g.* intracellular pathogens) from the cell's cytoplasm by delivering them to the degradative lysosomes^{470–472}. In this way, autophagy plays an important role in a plethora of physiological functions such as cell conservation, adaptation to starvation, tumor suppression, antigen presentation and cell cycle regulation^{73,470}. However, in the case of NA delivery, autophagy presents an additional intracellular barrier as it could sequester both individual NAs/NPs, which have escaped the endo(lyso)somal compartment, as well as engulf entire endosomes containing the endocytosed cargo^{73,471}. This process can be either non-selective (random sequestration of cytoplasmic material) or selective (*e.g. via* galectin recruitment as described above)^{163,330,473}. Of note, several NPs have shown to induce autophagy^{163,221,474–479} or rather cause its

malfunction⁴⁸⁰, altogether highlighting the potential of modulating this biological pathway to improve NA delivery^{469,481}.

Autophagy can be generally classified in 3 types: macroautophagy, microautophagy and chaperone-mediated autophagy (CMA). The term 'autophagy' usually refers to macroautophagy, a process of which the molecular mechanism is well-known⁴⁷⁰. Macroautophagy (hereafter referred to as autophagy) is initiated by the formation of an isolation membrane (*i.e.* phagophore) that subsequently engulfs a part of the cytoplasm and closes on itself, forming a double-membraned autophagosome (APG). Next, these organelles can fuse with endosomes, forming amphisomes, prior to fusion with the lysosomes or they can directly fuse with the latter, forming auto(phago)lysosomes (AutoLYS) where the sequestered cargo will undergo non-selective degradation^{439,470,471}. The molecular machinery that controls the membrane rearrangements, needed for APG formation, consists out of at least 30 tightly coordinated AuTophagy-related (ATG) proteins, which are regulated by the nutrient-sensing kinase mTOR^{221,470,482,483}.

As entrapment of NA cargo inside APGs would reduce the NA dose at their site of action^{471,484}, it was hypothesized that inhibiting autophagy by down-regulating one of its molecular factors, could increase NA activity. Indeed, when comparing pDNA:lipoplexes/polyplexes delivery in autophagy-competent (ATG5^{+/+}) and autophagy-deficient (ATG5^{-/-}) mouse embryonic fibroblasts, Roberts *et al.* showed an 8-fold increase in gene expression efficiency in the ATG5 knockout cells²²¹. This result was corroborated, albeit to a much lower extent, by Song *et al.* for lipoplex- and polyplex-delivery of siRNA⁴⁸⁵. In contrast, ATG5 was seemingly not involved in C12-200-based LNP-mediated gene silencing¹⁹⁵. Likewise, Wittrup *et al.* found that, despite siRNA-loaded liposomes activating autophagy, autophagic inhibition (by knockdown of galectin-8 or its adaptor NDP52) did not enhance target gene silencing. Hence, the authors hypothesized that siRNA and pDNA delivery might be differentially affected by an autophagic response, possibly due to the large difference in diffusion kinetics between both NAs¹⁶³. Additionally, a set of small molecules that suppress the autophagy process *via* distinct mechanisms have also been used by Dowaidar *et al.* to improve the transfection efficiency of CPP:SSOs, while pharmacological induction of autophagy downregulated the splice correction activity²²⁷.

Differently to the findings of Roberts *et al.* and Dowaidar *et al.*, several groups showed that also activating autophagy could promote NP-mediated NA delivery. For example, Zhong *et al.*

demonstrated that rapamycin, a small molecule autophagy inducer that inhibits mTOR, increased the transfection efficiency of PEI:pDNA polyplexes, while treatment with the early autophagy inhibitor 3-methyladenine (3-MA) decreased transgene expression in mouse fibroblasts⁴⁸⁶. Similar effects of rapamycin and 3-MA on the delivery of siRNA with lipoplexes (lipofectamine 2000) or polyplexes (chitosan NPs) were reported by Song *et al.* in H1299 cells⁴⁸⁵. Interestingly, the authors also showed that inducing autophagy through a mTOR-independent (mTOR-i) pathway (using LiBr) in fact lowered the silencing efficacy, while the mTOR-i autophagy inhibitor thapsigargin increased siRNA knockdown. The latter data emphasize the dual effect of autophagy on NA delivery, as the up- and downregulation of different autophagy pathways appears to generate divergent functional outcomes. Next to the modulation of NP-mediated NA delivery, autophagy can also influence the systemic delivery of ASOs. Ochaba *et al.* found that activating autophagy through small molecule mTOR inhibition (rapamycin or AZD8055) or physiological activation (serum starvation or a ketogenic diet), could increase ASO-mediated knockdown both *in vitro* and *in vivo*, while inhibiting autophagy had the opposite effect⁴⁶⁹. The enhanced knockdown activity could also be seen for GalNAc-conjugated ASOs and the effect was not limited to mTOR-dependent autophagy induction, as mTOR-i stimulation of autophagy by trehalose (through AMPK and activation of ULK1) also enhanced the silencing efficiency. Although the exact membrane origin of APGs remains ambiguous, it has been described that the *de novo* formation of phagophores uses various endosomes, the ER and/or Golgi as membrane sources. Hence, it was suggested that the NAs present in these organelles may potentially leak into the cytosol during the autophagy induction process⁴⁶⁹.

Finally, it should be noted that RNA therapeutics will *de facto* be delivered to patients that have illnesses characterized by strong metabolic phenotypes, including cancer^{487–489}. For example, activation of the mTOR signaling is involved in some of the cancer hallmarks and certain cancers (*e.g.* tuberous sclerosis complex (TSC)) are characterized by mutations in the mTOR gene that lead to constitutive activation of mTOR signaling^{490,491}. As described above, Patel *et al.* showed that activating mTOR (through knockout of the upstream effector TSC2) could enhance electroporation-delivered mRNA expression¹⁹⁶. Based upon this study, Paunovska *et al.* consequently hypothesized that modulating cell metabolism with the bioactive lipid phosphatidylinositol-3,4,5-triphosphate (PI(3,4,5)P₃), which plays a role in the upstream activation of the PI3K (phosphatidylinositol 3-kinase)/AKT/mTOR pathway, would transiently increase the translation of LNP-delivered mRNA once it reached the cytoplasm²⁵⁰.

Unexpectedly, their data showed the opposite as co- or pre-treatment with PI(3,4,5)P₃ blocked mRNA delivery both *in vitro* and *in vivo*, an effect which could not be linked to differences in toxicity, cell uptake or endosomal escape. The authors subsequently suggested, that the PI(3,4,5)P₃-driven reduction in mRNA-LNP delivery might be related to an increased basal metabolic rate.

3.5. Translocation to the nucleus

For those NAs that function in the nucleus, nuclear entry can be a final barrier. The nuclear envelope consists of a nuclear lamina with an inner and outer nuclear membrane on top, embedded with nuclear pore complexes that tightly control all transport between the nucleus and the cytoplasm^{73,492}. As passive diffusion through the nuclear pore complexes is limited to molecules < 40 kDa⁴⁹², mainly pDNA entry is hampered, while small NA therapeutics (*e.g.* SSO, saRNA) can readily enter the nucleus^{73,76}. Interestingly, recent research showed that cytoplasmic/nuclear shuttling of SSOs can still be increased by co-incubation with arsenic trioxide (As₂O₃), which induces cellular stress and the formation of a oligonucleotide-binding stress-induced response complex (SIRC)^{351,493}. This SIRC, which consists out of Argonaute proteins, transcription factors (TFs) and splicing regulators, binds the SSOs and transports them to the nucleus⁴⁹³. Of note, the combination of NH₄Cl and As₂O₃ produced a synergistic effect on SSO activity³⁵¹.

3.6. Non-delivery aspects: modulate silencing, splicing or translation

Finally, several approaches have been reported that can improve the intrinsic activity of RNAi-mediators, SSOs or mRNAs by affecting the fundamental molecular machinery involved in RNAi, SSO-mediated splicing or the innate immune response, while not altering the delivery of these NAs^{494–498}.

3.6.1. RNAi and SSO-mediated silencing

As a first example, certain fluoroquinolone antibiotics such as enoxacin have shown to increase RNAi efficiency by supposedly enhancing RISC loading or inhibiting RNA helicases^{495–497}. Similarly, overexpressing the human Argonaute 2 (Ago2), the key protein in RNAi silencing, could boost siRNA-mediated mRNA degradation⁴⁹⁸. Next, Kendall *et al.* performed a small compound screen (300 molecules) to identify compounds that improve SSO-mediated exon skipping in DMD. The hit group was enriched in compounds known to modulate the intracellular calcium level, with 2 out of 15 top hits that targeted the ryanodine receptor

(RyR)⁴⁹⁹. Although the precise mechanism remains obscure, this report and two follow-up studies showed that several structurally diverse RyR antagonists, known to act through a distinct molecular mechanism, share this function by presumably affecting the amount of nuclear calcium, an ion known to regulate splicing^{499–501}. Notably, one of these adjuvants, dantrolene, was also tested *in vivo*, thereby enhancing exon skipping and reducing muscle pathology in mdx mice over the course of both short- (1–3 weeks)⁴⁹⁹ and long-term (6-month chronic treatment)⁵⁰⁰ systemic SSO treatment. Interestingly, in the latter report the compound was dosed orally⁵⁰⁰. In addition to RyR antagonists, also others have reported skip boosting of SSOs in DMD *in vitro* (and/or *in vivo*) models using both small molecule and genetic modulators *via* distinct or unknown mechanisms^{502,503}.

3.6.2. Blocking anti-RNA immune response

RNA therapeutics and their delivery vehicles can be potent activators of the innate immune response in eukaryotic cells *via* the stimulation of so-called pattern recognition receptors (PRRs), which are located both on the cell/endolysosomal membranes and in the cytosol^{77–79,504–506}. Even though such an immune-stimulatory effect (or ‘anti-viral state’) can be beneficial in the context of immunotherapeutic vaccines (*e.g.* mRNA/SAM-based vaccines) by activating APCs, it presents a major barrier in non-vaccine applications^{79,507}. Hence, multiple studies focused on the passive evasion of the PRRs by encapsulating the RNA molecules in NPs and/or chemically modifying the RNA strands, which are widely adopted strategies nowadays⁵⁰⁸. Active inhibition of key immune-related proteins involved in the NA detection or downstream signaling pathways has likewise been postulated as an alternative approach to increase transfection efficiency as this would mimic the immune-evasion strategies used by RNA viruses^{79,509}. However, successfully reducing the innate immune response does not always result in more effective RNA transfection as recently shown by *Liu et al.*¹⁸³. Here, we will discuss a selection of immune-inhibiting modulators that up till now showed to clearly enhance the duration and/or extent of the RNA effect, which was mainly demonstrated for (un)modified IVT mRNA/SAM delivery.

The intracellular RNA sensing pathways are highly complex and they are extensively reviewed elsewhere⁷⁹. In short, three families of PRRs, the membrane-bound Toll-like receptors (TLRs), the cytosolic retinoic acid-inducible gene I (RIG-I)-like receptors (RLRs) and the cytosolic NOD-like receptors (NLRs) are believed to recognize the RNA cargo. Double-stranded and single-stranded RNAs activate different PRRs (*e.g.* single-stranded RNAs activate

TLR7/8, while TLR3 interacts with double-stranded RNA (dsRNA)) and the stimulated PRRs (TLRs and RLRs) transmit downstream signaling *via* specific cytosolic adaptor proteins such as the myeloid differentiation primary response gene 88 (MyD88, in case of TLR7/8) or the Toll/interleukin (IL)-1 receptor (TIR) domain-containing adaptor inducing IFN- β (TRIF, in case of TLR3). On the contrary, NLRs such as the NLR pyrin domain containing 3 (NLRP3) play a role in the formation of the inflammasome, a multi-protein complex responsible for the proteolytic maturation of the IL-1 β and IL-18 pro-inflammatory cytokines⁷⁹. Bell *et al.* showed that interfering with the PRR-mediated mRNA detection by using small molecule **TLR inhibitors** (E6446 and (hydroxy)chloroquine) could indeed enhance the expression of CPP-delivered mRNA *in vitro*⁵¹⁰. The TLR suppression effect of the used compounds has been previously ascribed to the direct interaction with the NAs, causing a block of NA recognition due to steric hindrance^{511,512}. Alternatively, the documented endolysosomal buffering for (hydroxy)chloroquine could also play a role in the TLR inhibitory effect, as an acidic pH is considered to be essential for TLR-mediated signal transduction⁷⁹. However, no evidence of decreased immune activation was provided and it should be noted that chloroquine has pleiotropic effects on NA delivery (as discussed above)¹²⁶.

Next, the adaptor molecules further initiate a complex signaling cascade, which eventually converges in the phosphorylation (by *e.g.* I κ B kinase (IKK) complex or IKK-related kinases TBK1 and IKK ϵ) of several cytosolic located transcription factors (TFs) such as the nuclear factor- κ B (NF- κ B), interferon regulatory factor 3 (IRF3) or IRF7. A similar process occurs after RLR activation. The activated TFs subsequently translocate to the nucleus where they induce expression of type I interferons (mainly IFN- α and IFN- β) and additionally pro-inflammatory cytokines in the case of NF- κ B (*e.g.* tumor necrosis factor- α (TNF- α)). Interestingly, Awe *et al.* demonstrated that co- and post-treatment with **kinase inhibitors** BX795 (inhibits TBK1 and IKK ϵ) or BAY11 (inhibits IKK complex) enhanced expression of lipofectamine-encapsulated mRNA in human skin cells, which was linked to a reduction in NF- κ B activation in the mRNA-transfected cells⁵¹³. Next, **targeting the TFs itself** has also shown to enhance mRNA-mediated protein expression. The best known example of a NF- κ B antagonist is the steroidal anti-inflammatory drug dexamethasone, which has shown to upregulate NF- κ B's cytoplasmic inhibitor I κ B, thereby reducing NF- κ B nuclear translocation. Hence, the presence of dexamethasone during transfection of LNP:mRNA complexes could increase luciferase expression *in vitro*, while inclusion of dexamethasone-palmitate in the LNP could also boost *in vivo* hepatic mRNA transfection efficiency after I.V. administration in two mouse models⁵¹⁴.

These results, corroborated earlier reports showing increased transgene expression when dexamethasone was combined with distinct pDNA nanocarriers^{515–519}. Notably, dexamethasone can also improve the therapeutic potential of RNA therapeutics by increasing the *in vivo* therapeutic window. Indeed, siRNA/mRNA/pDNA-loaded LNPs are immunogenic at high doses and dexamethasone pre-/co-treatment^{504,520} or incorporation of hydrophobic dexamethasone prodrugs in LNPs⁵⁰⁴ can suppress pro-inflammatory cytokine levels and gene expression in mice, thereby avoiding the immunostimulatory consequences of systemic LNP administration.

Finally, type I IFNs are secreted in the extracellular environment that stimulate the autocrine/paracrine transcription of more than 300 IFN-stimulated genes (ISGs), which encode proteins involved in signaling (*e.g.* PRRs or TFs) or proteins with strong anti-RNA activities (*e.g.* dsRNA-dependent protein kinase (PKR), 2'-5'-oligoadenylate synthetases (OASs) and RNA-specific adenosine deaminase (ADAR)). The latter proteins eventually lower the efficiency of mRNA translation, cause RNA degradation and induce cytotoxicity. It should be noted that PKRs, OASs and ADARs are not only effector proteins, but they also function as cytosolic PRRs, since they require the presence of dsRNA to initiate their activation^{79,521}. While the abovementioned approaches mainly focused on preventing the initial type I IFN production, also inhibition of the IFN-induced effects can boost mRNA transfection. For example, enhanced expression levels have been noted following application of the Vaccinia Virus-derived B18R^{522–525}, an IFN binding decoy receptor that captures the secreted IFNs and hence **blocks the cellular IFN receptor activation**. Another strategy is to **interfere with the IFN-induced anti-RNA response** by blocking proteins such as PKR^{79,508}. Indeed, Lokugamage *et al.* showed that C16, a potent small molecule inhibitor of PKR, could improve the translation of ionizable LNP-formulated mRNA *in vitro* in RAW macrophages⁵²⁶. In turn, Ohto *et al.* demonstrated that the Integrated Stress Response Inhibitor (ISRIB), also a PKR inhibitor, could likewise boost ionizable LNP-formulated mRNA delivery in mouse embryonic fibroblasts *in vitro*⁵¹⁴. Similarly, Kirschman *et al.* found higher protein expression levels of lipofected (un)modified mRNA in PKR-knockout mouse embryonic fibroblasts⁵²⁷. Also viral immune evasion proteins have been employed that act on this last step, such as the Vaccinia Virus-derived E3^{44,522,524} and K3^{508,522,524}, the swinepox virus derived C8L^{508,528} and the influenza A virus derived non-structural protein 1 (NS1)^{524,529–531}. While E3 and K3 inhibit PKR activation, NS1 is believed to block PKR, OAS, IRF3, NF- κ B and a non-immune related protein such as cleavage and polyadenylation factor 30 (CPSF30)⁵²⁴. Of interest, Beissert *et al.* showed that

co-injection of a SAM with a combination of 3 mRNAs encoding for E3, K3 and B18R, could enhance SAM expression *in vivo*, which suggests that supplementation with immune-inhibiting molecules could also be a valuable approach in an *in vivo* setting⁴⁴.

Taken together, targeting the (regulatory) mechanisms involved in RNAi-/ON-mediated silencing/splicing or innate immune activation might be a feasible strategy to enhance NA activity, albeit such modulators should be highly specific towards the NA of interest (and/or tissue of interest) to avoid serious off-target effects.

4. CONCLUSION AND PERSPECTIVES

The key obstacle to the development of more potent, more widely-applicable and safer RNA therapeutics is the limited mechanistic understanding of the interaction of NA molecules and their delivery systems, both extra- and intracellular, with target cells. Albeit multiple well-conducted studies, using *e.g.* state-of-the-art microscopic technologies, have undisputable contributed to our current understanding of intracellular NA delivery, this process is generally presented in an oversimplified way (uptake-trafficking-release happens somewhere) and detailed knowledge of the genes, pathways and molecular factors (*e.g.* lipids, proteins, sugars, ...) involved in productive delivery is scarce. To address this gap, we provided in the first part of this review an overview of tools available to the scientific community to investigate the mechanistic link between the intracellular delivery process and the eventual pharmacological effect of NA molecules. These tools consist largely out of non-genetic perturbation techniques (*e.g.* small molecule(s) screenings), genetic perturbation techniques (*e.g.* RNAi and CRISPR (screenings)) and alternative strategies (*e.g.* transcriptomics, learning from viruses, *etc.*). In addition, we show that contemporary advances in technologies (*e.g.* 3D cell cultures, organ-on-chips, new mouse models, *etc.*) could allow drug scientists to investigate the intracellular delivery pathways in an unprecedented way. Most importantly, the data obtained by the discussed tools could not only shed light on the fundamental understanding of the biological mechanisms impacting the therapeutic activity of NA molecules, it could also identify (novel) cellular targets/processes that could be modulated to increase the pharmacological effects and therapeutic window of existing RNA therapeutics. Consequently, in the second part of this review, we discussed how several modulators (predominantly small molecules, but also lipids, siRNAs, *etc.*) can boost RNA delivery by manipulating a plethora of intracellular processes such as uptake, trafficking, endosomal escape, autophagy, immune response *etc.* Nevertheless, it should be noted that much remains to be understood and that the provided summary is a non-exhaustive list. Consequently, there are undoubtedly multiple, currently unknown, intracellular pathways that positively or negatively affect RNA delivery. It is however exciting to know that with the current knowledge and the ever advancing technologies, answers to these questions are now within reach.

Table 1: (non-)genetic modulators shown to improve intracellular delivery of RNA therapeutics, grouped according to their mechanism of action.

Target?	Mechanism of improved delivery	Used tool	Moment of treatment	In vitro	In vivo	Carrier/NA type	Ref
<i>Alter cellular internalization</i>							
N.A.	Metabolization of hexoses produces ATP that is needed for energy-dependent NA uptake.	Hexoses (e.g. glucose and fructose)	co	X	X	SSO	279–281
L-type calcium channel	Binding to L-type calcium channels enhances endocytosis.	L-type CCBs with (cilnidipine, nifedipine, nicardipine and amlodipine) and without DHP core (diltiazem and verapamil)	co	X	X	cp-siRNAs	282
Na ⁺ /K ⁺ ATPase pump	Binding to Na ⁺ /K ⁺ ATPase pump enhances endocytosis.	Cardiac glycosides	co in carrier	X		LNP:siRNA	286
<i>Alter intracellular trafficking</i>							
Protein Kinase C- α	Increase PKC- α -dependent early-to-late endosomal maturation.	Oleic acid	pre	X		PS-ASO (gymnotic) LPX:siRNA	331
			co	X		SSO (gymnotic)	351
		High glucose or PKC- α expressing plasmid	pre	X		PS-ASO (gymnotic) LPX:siRNA	331
pH modulation	Inhibiting endosomal acidification blocks fusion of LEs with lysosomes and lysosomal degradation (or alternative mechanisms enhance endosomal escape).	Chloroquine (or analogues such as hydroxychloroquine, primaquine or trifluoromethylquinoline)	post	X		exosome:siRNA chol-siRNA	374
			post	X		micelle:siRNA	375
			post	X		MSNP-PEI:siRNA	384

			in carrier	X		MSNP-PEG-PDMAEMA:CLQ:siRNA	359
			co conjugated to carrier	X	X	CPP:siRNA	154
			co conjugated to carrier	X		siRNA-PEG-gold NP	376
			co conjugated to carrier	X	X	CPP:siRNA	377,378
			co	X		peptide-branched PEI:siRNA	379
			conjugated to carrier	X		PPX:antagomiR	373
			post	X		miRNA conjugate	372
			post	X	X	mRNA:Lipofectamine MessengerMAX or TransIT®	368
		NH ₄ ⁺ Ambroxol Cyclohexylamine	co	X		SSO (gymnotic) ASO (gymnotic)	351
		Hit compounds	co	X		chol-siRNA LNP:siRNA	178
		Nigericin	in carrier	X		siRNA conjugate	380
						miRNA conjugate	372
		Monensin	pre/co	X		CPP:siRNA	382

Hermansky–Pudlak syndrome 4 protein (HPS4) endosomal sorting complex required for transport (ESCRT)	Downregulation improves delivery by potentially inhibiting endosomal maturation or blocking fusion of MVBs with lysosomes.	RNAi-mediated downregulation	pre/co	X		Lipofectamine: siRNA	340
			pre	X		antibody-siRNA conjugate	201
			pre	X	X	antagomiR (gymnotic)	204
Microtubules	Microtubule stabilization to prevent fusion of LEs - lysosomes.	Paclitaxel	co	X		LPX:siRNA	403
Histone deacetylases (HDACs)	HDAC inhibitors that stabilize microtubules by acetylation.	Vorinostat (SAHA)	post	X		PPX:mRNA	397
			pre	X		Stemfect LIP:mRNA	196
mannose 6-phosphate receptor (M6PR)	Endosome-Golgi transport mediated by M6PR facilitates release from endosomes.	pDNA overexpression	pre	X		PS-ASO (gymnotic)	199
Rab27b	Inhibition blocks fusion of MVBs with plasma membrane.	siRab27b	pre	X		LNP:siRNA	195
Niemann-Pick type C protein 1 (NPC1)	NPC1 inhibition prevents recycling and increases intracellular residence time.	siNPC1 NPC1 ^{-/-} cells	pre	X		LNP:siRNA	195
		NP3.47 (inhibitor)	co	X		LNP:siRNA	436
<i>Improve endosomal escape</i>							
N.A.	Enhance back-fusion?	DHA (precursor of LBPA)	co	X		PS-ASO (gymnotic)	215
N.A.	Destabilization of (LE) membrane.	Free fatty acids (mainly palmitic and oleic acid) Cholesterol Ceramide	pre post	X		PS-ASO (gymnotic)	446

Unknown.	Block of retrograde trafficking from endosomes to TGN?	Retro-1	post	X	X	ASO (gymnotic) SSO (gymnotic)	420
Unknown.	Potential mechanism: destabilize late endosomal membrane?	Hit compounds	post	X	X	SSO (gymnotic) ASO (gymnotic) chol-siRNA	179
		UNC7938 and analogs	post	X		ASO (gymnotic) SSO (gymnotic)	336
		UNC2383 and analogs	post	X	X	ASO (gymnotic) SSO (gymnotic)	253
Unknown.	Different mechanisms proposed for hits: (i) block acidification/maturation (ii) interfere with intracellular trafficking and (iii) destabilize membranes of endosomes	Hit compounds	co	X		chol-siRNA LNP:siRNA	178
N.A.	Create pores in LE membrane.	Amphotericin B	in carrier	X		micelle:siRNA	388
N.A.	Direct interaction with endosomal membrane.	Plant glycoside (SO1681)	co post in carrier	X		peptide-based carrier:siRNA LNP:siRNA	532
Unknown.	Enhance uptake by macropinocytosis (NaCl) and enhance release from macropinosomes (NDSBs/GABA).	iTOP solution	co	X		siRNA and Cas9 protein/sgRNA	451
N.A.	Cause minor LMP upon phospholipidosis induction.	Cationic amphiphilic drugs (CADs)	post	X		NGs:siRNA MSNPs:siRNA	166,452
			co/post	X		chol-siRNA	238
<i>Autophagy modulation</i>							
mTOR	mTOR activation suppresses autophagy.	MHY1485 (mTOR activator)	pre	X		CPP:SSO	227

	mTOR inhibition triggers autophagy induction.	Rapamycin (allosterically inhibits mTORC1)	pre/co	X	X	ASO (gymnotic)	469
			co	X		LPX:siRNA PPX:siRNA	485
		AZD8055 (potent catalytic inhibitor of mTORC1 and mTORC2)	pre/co/post	X	X	ASO (gymnotic) and GalNAc-conjugated ASO (only <i>in vitro</i>)	469
		- fasting (<i>in vivo</i>) - serum-starvation (<i>in vitro</i>) - ketogenic diet (<i>in vivo</i>)	co/post	X	X	ASO (gymnotic)	469
SLC2A (GLUT) transporters	It was suggested that inhibition of glucose and fructose import into cells through SLC2A transporters produces a starvation-like (low ATP) state in cells that subsequently triggers mTOR-independent autophagy induction and APG production through AMPK and activation of ULK1.	Trehalose	pre	X		ASO (gymnotic)	469
TFEB	Inhibition of TFEB-mediated autophagy activation.	siTFEB	pre	X		ASO (gymnotic)	469
ATG5	Inhibition of autophagy.	siATG5	pre	X		LPX:siRNA PPX:siRNA	485
sarco/ER Ca ²⁺ ATPase	mTOR-independent autophagy inhibition.	Thapsigargin	co	X		LPX:siRNA PPX:siRNA	485
Heat shock protein 70 (HSP70)	It was suggested that blocking HSP70 inhibits autophagy (cytosolic chaperone HSP70 plays a role in CMA that uses lysosomal receptors and chaperone proteins to transfer target proteins immediately to lysosomal lumen).	Pifithrin- μ (selective inhibitor of HSP70)	pre	X		CPP:SSO	227

β2-adrenergic receptor (ADRB2)	Possibly: antagonism of ADRB2, a major activator of autophagy.	Alprenolol hydrochloride (β-adrenoceptor antagonist)					
Aryl hydrocarbon receptor (AHR)	Possibly: antagonism of AHR lowers cell surface levels of tissue factors, which leads to sterol synthesis inhibition, which could influence autophagy.	CH-223191 (AHR antagonist)					
TLR4	Possibly: inhibition of TLRs reduces the non-canonical recruitment of ATG proteins to phagophore formation process.	TLR-4-IN-C34 (TLR4 inhibitor)					
Nuclear transport receptor importin-β	Possibly: SSO functions in nucleus and nuclear pore complex participates in nuclear autophagy.	Importazole (nuclear transport receptor importin-β inhibitor)					
<i>Immune response modulation</i>							
Toll-like receptors (TLRs)	Inhibition of PRR-mediated mRNA recognition by endosomal TLR inhibitors.	E6446 and (hydroxy)chloroquine	co		X	CPP:mRNA (modified, non-specified)	510
TBK1 and IKKε	Inhibition of signal transduction.	BX795	co post		X	RNAiMAX:mRNA (m5C, Ψ)	513
IKK complex		BAY11					
NF-κβ		Dexamethasone	co in carrier	X	X	LNP:mRNA (non-modified)	514
Interferons (IFNs)	Capture secreted IFNs.	B18R mRNA	co		X	Lipofectamine 2000:mRNA (m5C, Ψ)	525
			co		X	Lipofectamine 2000:SAM (non-modified)	523
			pre		X	Stemfect:mRNA (non-modified)	524

dsRNA-dependent protein kinase (PKR)	Inhibition of IFN-induced anti-RNA response.	C16, 2-AP	pre	X		LNP:mRNA (modified)	526
		ISRIB	co	X		LNP:mRNA (non-modified)	514
		PKR ^{-/-}	pre	X		Lipofectamine 2000:mRNA (non-modified and m5C, Ψ)	527
		E3 mRNA (and + K3/B18R mRNA for <i>in vivo</i> in Beissert <i>et al.</i> ⁴⁴)	co	X	X	- RNAiMAX/MessengerMAX: SAM (<i>in vitro</i>) - naked (<i>in vivo</i>) (non-modified)	44
			co	X		RNAiMAX:mRNA (non-modified)	522
		E3 or K3 alone	pre	X		Stemfect:mRNA (non-modified)	524
PKR, OAS, IRF3, NF- κ B, CPSF30	Inhibition of several processes, which leads to a blockage of both type I IFN production and IFN-induced effects.	NS1 mRNA	co	X	X	- Stemfect:mRNA (<i>in vitro</i>) (non-modified + m5C and/or Ψ) - naked (<i>in vivo</i>)	529
			co	X		Stemfect:mRNA (non-modified)	530
			co	X		MessengerMAX:mRNA (non-modified)	531
			pre/co	X		Stemfect:mRNA (non-modified)	524
<i>Modulation of RNAi/ON intrinsic activity</i>							
Transactivating response RNA-binding protein (TRBP)	Enhancing RISC loading (possibly by enhancing the interaction between TRBP and RNAs) or inhibiting RNA helicases.	Enoxacin and analogs	co/post	X	X	Lipofectamine 2000:siRNA/miRNA and lentivirus producing shRNA	495–497

Argonaute 2 (Ago2)	Ago2 is a part of RISC and thus a central factor in RNAi silencing.	Overexpression <i>via</i> plasmid transfection or viral vector	pre	X		Lipofectamine 2000:siRNA	498
Ryanodine receptor (RyR)	Modulation of RyR-mediated calcium homeostasis in nucleus presumably leads to a greater exon-skipping frequency.	Dantrolene Ryanodine Rycal S107 Rycal ARM210	post	X	X	FuGENE/ Oligofectamine: SSO (<i>in vitro</i>) SSO saline solution (<i>in vivo</i>)	499–501,533
<i>Modulate nuclear shuttling</i>							
N.A.	A cellular stressor induces a stress-induced response complex (SIRC) that transports miRNAs, siRNAs and ONs to the nucleus.	As ₂ O ₃	co	X		LPX:splicing switching siRNA	493
						SSO (gymnotic)	351,493
<i>Pleiotropic adjuvants</i>							
Unknown.	Unknown mechanism, but likely linked to the role of bioactive lipids in intracellular trafficking, cell signalling, endosomal release, <i>etc.</i>	Leukotriene antagonists (MK-571, pranlukast and zafirlukast) and other hit compounds	pre in carrier	X	X	Stemfect LPX:mRNA LNP:mRNA	196
Glycogen synthase kinase 3 α and β isoforms (GSK-3 α and GSK-3 β)	GSK-3 α/β inhibition enhances ASO/SSO activity <i>via</i> unknown mechanism.	6BIO CHIR99021	co	X		ASO SSO (gymnotic)	240
UGCG (and other hits from CRISPRko screen)	UGCG inhibition enhances mRNA functional delivery <i>via</i> unknown mechanism.	CRISPRko(UGCG) siUGCG	pre	X		LNP:mRNA	206
		UGCG small molecule inhibitor (U1)	co				

UGCG = UDP-glucose ceramide glucosyltransferase, siUGCG = siRNA targeting UGCG, CRISPRko = CRISPR knockout, RNAi = RNA interference, NA = nucleic acid, LNP = lipid nanoparticle, LPX = lipoplex, PPX = polyplex, siRNA = small interfering RNA, mRNA = messenger RNA, SAM = self-amplifying RNA, shRNA = short hairpin RNA, pDNA = plasmid DNA, SSO = splice switching oligonucleotide, ASO = antisense oligonucleotide, miRNA = microRNA, CPP = cell-penetrating peptide, ON = oligonucleotide, GalNAc = N-acetylgalactosamine, chol-siRNA = cholesterol-conjugated siRNA, NG = nanogel, MSNP = mesoporous silica NP, NP = nanoparticle,

sgRNA = single-guide RNA, PS-ASO = phosphorothioate-containing ASO, PEI = polyethylenimine, PEG = polyethylene glycol, PDMAEMA = poly(2-(dimethylamino)ethyl methacrylate), LIP = liposome, cp-asiRNA = cell-penetrating asymmetric siRNA, GSK = glycogen synthase kinase, SIRC = stress-induced response complex, RyR= ryanodine receptor, Ago2 = argonaute 2, TRBP = transactivating response RNA-binding protein, RISC = RNA-induced silencing complex, PKR = dsRNA-dependent protein kinase, OAS = 2'-5'-oligoadenylate synthetase, IRF = interferon regulatory factor, NF- κ B = nuclear factor- κ B, CPSF30 = cleavage and polyadenylation factor 30, IFN = interferon, NS1 = non-structural protein 1, ISRIB = integrated stress response inhibitor, TLR = Toll-like receptor, PRR = pattern recognition receptor, IKK = I κ B kinase, IKK ϵ = inhibitor of nuclear factor kappa B kinase subunit epsilon, TBK1 = TANK-binding kinase 1, siTFEB = siRNA targeting TFEB, TFEB = transcription factor EB, ATG = autophagy-related, siATG5 = siRNA targeting ATG5, AHR = aryl hydrocarbon receptor, ADRB2 = β 2-adrenergic receptor, HSP70 = heat shock protein 70, HPS4 = Hermansky-Pudlak Syndrome 4 (protein), ESCRT = endosomal sorting complex required for transport, CMA = chaperone-mediated autophagy, APG = autophagosome, AMPK = adenosine monophosphate-activated protein kinase, ULK1 = Unc-51 like autophagy activating kinase 1, GLUT = glucose transporter, ATP = adenosine triphosphate, mTOR = mammalian target of rapamycin, mTORC1 = mTOR complex 1, mTORC2 = mTOR complex 2, LMP = lysosomal membrane permeabilization, CADs = cationic amphiphilic drugs, NDSB = non-detergent sulfobetaine, GABA = gamma-amino-butyric acid, LE = late endosome, TGN = *trans*-Golgi network, DHA = docosahexaenoic acid, LBPA = lysobisphosphatidic acid, NPC1 = Niemann-Pick type C protein 1, siNPC1 = siRNA targeting NPC1, M6PR = mannose 6-phosphate receptor, HDAC = histone deacetylase, MVBs = multivesicular bodies, PKC = protein kinase C, CCBs = calcium channel blockers, DHP = dihydropyridine, CLQ = chloroquine, Ψ = pseudouridine, m5C = 5-methylcytosine

REFERENCES

1. Yin, H. *et al.* Non-Viral Vectors for Gene-Based Therapy. *Nat. Rev. Genet.* **2014**, *15*, 541–555.
2. Wang, F.; Zuroske, T.; Watts, J. K. RNA Therapeutics on the Rise. *Nat. Rev. Drug Discov.* **2020**.
3. Dammes, N.; Peer, D. Paving the Road for RNA Therapeutics. *Trends Pharmacol. Sci.* **2020**, *41*, 755–775.
4. Delivering the Promise of RNA Therapeutics. *Nat. Med.* **2019**, *25*, 1321.
5. Sahin, U.; Karikó, K.; Türeci, Ö. mRNA-Based Therapeutics-Developing a New Class of Drugs. *Nat. Rev. Drug Discov.* **2014**, *13*, 759–780.
6. DeWeerd, S. RNA Therapies Explained. *Nature* **2019**, *574*, S2–S3.
7. Lieberman, J. Tapping the RNA World for Therapeutics. *Nat. Struct. Mol. Biol.* **2018**, *25*, 357–364.
8. Lorenzer, C.; Dirin, M.; Winkler, A. M.; Baumann, V.; Winkler, J. Going beyond the Liver: Progress and Challenges of Targeted Delivery of siRNA Therapeutics. *J. Control. Release* **2015**, *203*, 1–15.
9. Dixon, S. J.; Stockwell, B. R. Identifying Druggable Disease-Modifying Gene Products. *Curr. Opin. Chem. Biol.* **2009**, *13*, 549–555.
10. Dunham, I. *et al.* An Integrated Encyclopedia of DNA Elements in the Human Genome. *Nature* **2012**, *489*, 57–74.
11. Fire, A. *et al.* Potent and Specific Genetic Interference by Double-Stranded RNA in *Caenorhabditis Elegans*. *Nature* **1998**, *391*, 806–811.
12. Tuschl, T.; Zamore, P. D.; Lehmann, R.; Bartel, D. P.; Sharp, P. A. Targeted mRNA Degradation by Double-Stranded RNA in Vitro. *Genes Dev.* **1999**, *13*, 3191–3197.
13. Elbashir, S. M. *et al.* Duplexes of 21-Nucleotide RNAs Mediate RNA Interference in Cultured Mammalian Cells. *Nature* **2001**, *411*, 494–498.
14. Liang, X. H.; Nichols, J. G.; Hsu, C. W.; Vickers, T. A.; Crooke, S. T. mRNA Levels Can Be Reduced by Antisense Oligonucleotides *via* No-Go Decay Pathway. *Nucleic Acids Res.* **2019**, *47*, 6900–6916.
15. Bonneau, E.; Neveu, B.; Kostantin, E.; Tsongalis, G. J.; De Guire, V. How Close Are miRNAs from Clinical Practice? A Perspective on the Diagnostic and Therapeutic Market. *Electron. J. Int. Fed. Clin. Chem. Lab. Med.* **2019**, *30*, 114–127.
16. Roberts, T. C.; Langer, R.; Wood, M. J. A. Advances in Oligonucleotide Drug Delivery. *Nat. Rev. Drug Discov.* **2020**, *19*, 673–694.
17. Havens, M. A.; Hastings, M. L. Splice-Switching Antisense Oligonucleotides as Therapeutic Drugs. *Nucleic Acids Res.* **2016**, *44*, 6549–6563.
18. Nomakuchi, T. T.; Rigo, F.; Aznarez, I.; Krainer, A. R. Antisense Oligonucleotide-Directed Inhibition of Nonsense-Mediated mRNA Decay. *Nat. Biotechnol.* **2016**, *34*, 164–166.
19. Liang, X. H. *et al.* Translation Efficiency of mRNAs Is Increased by Antisense Oligonucleotides Targeting Upstream Open Reading Frames. *Nat. Biotechnol.* **2016**, *34*, 875–880.
20. Liang, X. H.; Shen, W.; Crooke, S. T. Specific Increase of Protein Levels by Enhancing Translation Using Antisense Oligonucleotides Targeting Upstream Open Frames. *Adv. Exp. Med. Biol.* **2017**, *983*, 129–146.
21. Liang, X. H. *et al.* Antisense Oligonucleotides Targeting Translation Inhibitory Elements in 5' UTRs Can Selectively Increase Protein Levels. *Nucleic Acids Res.* **2017**, *45*, 9528–9546.
22. Kwok, A.; Raulf, N.; Habib, N. Developing Small Activating RNA as a Therapeutic: Current Challenges and Promises. *Ther. Deliv.* **2019**, *10*, 151–164.
23. Phua, K. K. L.; Staats, H. F.; Leong, K. W.; Nair, S. K. Intranasal mRNA Nanoparticle Vaccination Induces Prophylactic and Therapeutic Anti-Tumor Immunity. *Sci. Rep.* **2014**, *4*, 1–7.
24. Sahin, U. *et al.* Personalized RNA Mutanome Vaccines Mobilize Poly-Specific Therapeutic Immunity against Cancer. *Nature* **2017**, *547*, 222–226.
25. Verbeke, R. *et al.* Broadening the Message: A Nanovaccine Co-Loaded with Messenger RNA

- and α -GalCer Induces Antitumor Immunity through Conventional and Natural Killer T Cells. *ACS Nano* **2019**, *13*, 1655–1669.
26. Pardi, N.; Hogan, M. J.; Porter, F. W.; Weissman, D. mRNA Vaccines—a New Era in Vaccinology. *Nat. Rev. Drug Discov.* **2018**, *17*, 261–279.
 27. Bahl, K. *et al.* Preclinical and Clinical Demonstration of Immunogenicity by mRNA Vaccines against H10N8 and H7N9 Influenza Viruses. *Mol. Ther.* **2017**, *25*, 1316–1327.
 28. Pardi, N. *et al.* Nucleoside-Modified mRNA Immunization Elicits Influenza Virus Hemagglutinin Stalk-Specific Antibodies. *Nat. Commun.* **2018**, *9*, 1–12.
 29. Richner, J. M. *et al.* Modified mRNA Vaccines Protect against Zika Virus Infection. *Cell* **2017**, *168*, 1114–1125.e10.
 30. Magadum, A.; Kaur, K.; Zangi, L. mRNA-Based Protein Replacement Therapy for the Heart. *Mol. Ther.* **2019**, *27*, 785–793.
 31. Zhu, X. *et al.* Systemic mRNA Therapy for the Treatment of Fabry Disease: Preclinical Studies in Wild-Type Mice, Fabry Mouse Model, and Wild-Type Non-Human Primates. *Am. J. Hum. Genet.* **2019**, *104*, 625–637.
 32. Nabhan, J. F. *et al.* Intrathecal Delivery of Frataxin mRNA Encapsulated in Lipid Nanoparticles to Dorsal Root Ganglia as a Potential Therapeutic for Friedreich’s Ataxia. *Sci. Rep.* **2016**, *6*, 1–10.
 33. An, D. *et al.* Systemic Messenger RNA Therapy as a Treatment for Methylmalonic Acidemia. *Cell Rep.* **2017**, *21*, 3548–3558.
 34. Cao, J. *et al.* mRNA Therapy Improves Metabolic and Behavioral Abnormalities in a Murine Model of Citrin Deficiency. *Mol. Ther.* **2019**, *27*, 1242–1251.
 35. Youn, H.; Chung, J. K. Modified mRNA as an Alternative to Plasmid DNA (pDNA) for Transcript Replacement and Vaccination Therapy. *Expert Opin. Biol. Ther.* **2015**, *15*, 1337–1348.
 36. Warren, L. *et al.* Highly Efficient Reprogramming to Pluripotency and Directed Differentiation of Human Cells with Synthetic Modified mRNA. *Cell Stem Cell* **2010**, *7*, 618–630.
 37. Shen, B. *et al.* Efficient Genome Modification by CRISPR-Cas9 Nickase with Minimal off-Target Effects. *Nat. Methods* **2014**, *11*, 399–402.
 38. Finn, J. D. *et al.* A Single Administration of CRISPR/Cas9 Lipid Nanoparticles Achieves Robust and Persistent *In Vivo* Genome Editing. *Cell Rep.* **2018**, *22*, 2227–2235.
 39. Miller, J. B. *et al.* Non-Viral CRISPR/Cas Gene Editing *In Vitro* and *In Vivo* Enabled by Synthetic Nanoparticle Co-Delivery of Cas9 mRNA and SgRNA. *Angew. Chemie - Int. Ed.* **2017**, *56*, 1059–1063.
 40. Sago, C. D. *et al.* High-Throughput *in Vivo* Screen of Functional mRNA Delivery Identifies Nanoparticles for Endothelial Cell Gene Editing. *Proc. Natl. Acad. Sci. U. S. A.* **2018**, *115*, E9944–E9952.
 41. Cheng, Q. *et al.* Selective Organ Targeting (SORT) Nanoparticles for Tissue-Specific mRNA Delivery and CRISPR–Cas Gene Editing. *Nat. Nanotechnol.* **2020**, 1–8.
 42. Wang, H. X. *et al.* CRISPR/Cas9-Based Genome Editing for Disease Modeling and Therapy: Challenges and Opportunities for Nonviral Delivery. *Chem. Rev.* **2017**, *117*, 9874–9906.
 43. Wei, T.; Cheng, Q.; Min, Y. L.; Olson, E. N.; Siegwart, D. J. Systemic Nanoparticle Delivery of CRISPR-Cas9 Ribonucleoproteins for Effective Tissue Specific Genome Editing. *Nat. Commun.* **2020**, *11*, 1–12.
 44. Beissert, T. *et al.* Improvement of *in Vivo* Expression of Genes Delivered by Self-Amplifying RNA Using Vaccinia Virus Immune Evasion Proteins. *Hum. Gene Ther.* **2017**, *28*, 1138–1146.
 45. Maruggi, G.; Zhang, C.; Li, J.; Ulmer, J. B.; Yu, D. mRNA as a Transformative Technology for Vaccine Development to Control Infectious Diseases. *Mol. Ther.* **2019**, *27*, 757–772.
 46. Fuller, D. H.; Berglund, P. Amplifying RNA Vaccine Development. *N. Engl. J. Med.* **2020**, *382*, 2469–2471.
 47. Shen, X.; Corey, D. R. Chemistry, Mechanism and Clinical Status of Antisense Oligonucleotides and Duplex RNAs. *Nucleic Acids Res.* **2018**, *46*, 1584–1600.
 48. Fine, S. L.; Martin, D. F.; Kirkpatrick, P. Pegaptanib Sodium. *Nat. Rev. Drug Discov.* **2005**, *4*,

- 187–188.
49. Hair, P.; Cameron, F.; McKeage, K. Mipomersen Sodium: First Global Approval. *Drugs* **2013**, *73*, 487–493.
 50. Syed, Y. Y. Eteplirsen: First Global Approval. *Drugs* **2016**, *76*, 1699–1704.
 51. Hoy, S. M. Nusinersen: First Global Approval. *Drugs* **2017**, *77*, 473–479.
 52. Akinc, A. *et al.* The Onpattro Story and the Clinical Translation of Nanomedicines Containing Nucleic Acid-Based Drugs. *Nat. Nanotechnol.* **2019**, *14*, 1084–1087.
 53. Ledford, H. Gene-Silencing Technology Gets First Drug Approval after 20-Year Wait. *Nature* **2018**, *560*, 291–292.
 54. Hoy, S. M. Patisiran: First Global Approval. *Drugs* **2018**, *78*, 1625–1631.
 55. Keam, S. J. Inotersen: First Global Approval. *Drugs* **2018**, *78*, 1371–1376.
 56. Balwani, M. *et al.* Phase 3 Trial of RNAi Therapeutic Givosiran for Acute Intermittent Porphyria. *N. Engl. J. Med.* **2020**, *382*, 2289–2301.
 57. Paik, J.; Duggan, S. Volanesorsen: First Global Approval. *Drugs* **2019**, *79*, 1349–1354.
 58. Heo, Y. A. Golodirsen: First Approval. *Drugs* **2020**, *80*, 329–333.
 59. Weng, Y. *et al.* The Challenge and Prospect of mRNA Therapeutics Landscape. *Biotechnol. Adv.* **2020**, *40*, 107534.
 60. Weng, Y.; Xiao, H.; Zhang, J.; Liang, X. J.; Huang, Y. RNAi Therapeutic and Its Innovative Biotechnological Evolution. *Biotechnol. Adv.* **2019**, *37*, 801–825.
 61. Jackson, L. A. *et al.* An mRNA Vaccine against SARS-CoV-2 — Preliminary Report. *N. Engl. J. Med.* **2020**.
 62. Zhang, N. N. *et al.* A Thermostable mRNA Vaccine against COVID-19. *Cell* **2020**, *182*, 1271–1283.e16.
 63. Mulligan, M. J. *et al.* Phase 1/2 Study of COVID-19 RNA Vaccine BNT162b1 in Adults. *Nature* **2020**, 1–8.
 64. McKay, P. F. *et al.* Self-Amplifying RNA SARS-CoV-2 Lipid Nanoparticle Vaccine Candidate Induces High Neutralizing Antibody Titers in Mice. *Nat. Commun.* **2020**, *11*, 1–7.
 65. Martin, C.; Lowery, D. mRNA Vaccines: Intellectual Property Landscape. *Nat. Rev. Drug Discov.* **2020**, *19*, 578.
 66. Hodgson, J. The Pandemic Pipeline. *Nat. Biotechnol.* **2020**, *38*, 523–532.
 67. Ghosh, S.; Firdous, S. M.; Nath, A. Sirna Could Be a Potential Therapy for Covid-19. *EXCLI J.* **2020**, *19*, 528–531.
 68. Uludağ, H.; Parent, K.; Aliabadi, H. M.; Haddadi, A. Prospects for RNAi Therapy of COVID-19. *Front. Bioeng. Biotechnol.* **2020**, *8*, 916.
 69. Rauch, S. *et al.* mRNA Based SARS-CoV-2 Vaccine Candidate CVnCoV Induces High Levels of Virus Neutralizing Antibodies and Mediates Protection in Rodents. *bioRxiv* **2020**, 2020.10.23.351775.
 70. Corbett, K. S. *et al.* Evaluation of the mRNA-1273 Vaccine against SARS-CoV-2 in Nonhuman Primates. *N. Engl. J. Med.* **2020**, *383*, 1544–1555.
 71. Sridharan, K.; Gogtay, N. J. Therapeutic Nucleic Acids: Current Clinical Status. *Br. J. Clin. Pharmacol.* **2016**, *82*, 659–672.
 72. Blanco, E.; Shen, H.; Ferrari, M. Principles of Nanoparticle Design for Overcoming Biological Barriers to Drug Delivery. *Nat. Biotechnol.* **2015**, *33*, 941–951.
 73. Vermeulen, L. M. P.; Brans, T.; De Smedt, S. C.; Remaut, K.; Braeckmans, K. Methodologies to Investigate Intracellular Barriers for Nucleic Acid Delivery in Non-Viral Gene Therapy. *Nano Today* **2018**, *21*, 74–90.
 74. Wittrup, A.; Lieberman, J. Knocking down Disease: A Progress Report on siRNA Therapeutics. *Nat. Rev. Genet.* **2015**, *16*, 543–552.
 75. Dowdy, S. F. Overcoming Cellular Barriers for RNA Therapeutics. *Nat. Biotechnol.* **2017**, *35*, 222–229.
 76. Juliano, R. L. The Delivery of Therapeutic Oligonucleotides. *Nucleic Acids Res.* **2016**, *44*, 6518–6548.

77. Morrissey, D. V. *et al.* Potent and Persistent *in Vivo* Anti-HBV Activity of Chemically Modified siRNAs. *Nat. Biotechnol.* **2005**, *23*, 1002–1007.
78. Judge, A. D. *et al.* Sequence-Dependent Stimulation of the Mammalian Innate Immune Response by Synthetic siRNA. *Nat. Biotechnol.* **2005**, *23*, 457–462.
79. Devoldere, J.; Dewitte, H.; De Smedt, S. C.; Remaut, K. Evading Innate Immunity in Nonviral mRNA Delivery: Don't Shoot the Messenger. *Drug Discov. Today* **2016**, *21*, 11–25.
80. Crooke, S. T.; Vickers, T. A.; Liang, X. H. Phosphorothioate Modified Oligonucleotide-Protein Interactions. *Nucleic Acids Res.* **2020**, *48*, 5235–5253.
81. Khvorova, A.; Watts, J. K. The Chemical Evolution of Oligonucleotide Therapies of Clinical Utility. *Nat. Biotechnol.* **2017**, *35*, 238–248.
82. Eckstein, F. Phosphorothioates, Essential Components of Therapeutic Oligonucleotides. *Nucleic Acid Ther.* **2014**, *24*, 374–387.
83. Zhang, Y. *et al.* Down-Modulation of Cancer Targets Using Locked Nucleic Acid (LNA)-Based Antisense Oligonucleotides without Transfection. *Gene Ther.* **2011**, *18*, 326–333.
84. Geary, R. S.; Norris, D.; Yu, R.; Bennett, C. F. Pharmacokinetics, Biodistribution and Cell Uptake of Antisense Oligonucleotides. *Adv. Drug Deliv. Rev.* **2015**, *87*, 46–51.
85. Fluiter, K.; Mook, O. R. F.; Baas, F. The Therapeutic Potential of LNA-Modified siRNAs: Reduction of off-Target Effects by Chemical Modification of the siRNA Sequence. *Methods Mol. Biol.* **2009**, *487*, 189–203.
86. Moschos, S. A. *et al.* Uptake, Efficacy, and Systemic Distribution of Naked, Inhaled Short Interfering RNA (siRNA) and Locked Nucleic Acid (LNA) Antisense. *Mol. Ther.* **2011**, *19*, 2163–2168.
87. Gao, S. *et al.* The Effect of Chemical Modification and Nanoparticle Formulation on Stability and Biodistribution of siRNA in Mice. *Mol. Ther.* **2009**, *17*, 1225–1233.
88. Andersson, P.; den Besten, C. Preclinical and Clinical Drug-Metabolism, Pharmacokinetics and Safety of Therapeutic Oligonucleotides. In *Advances in Nucleic Acid Therapeutics*; Gait, M. J., Agrawal, S., Eds.; Royal Society of Chemistry, **2019**; p 480.
89. Kanasty, R.; Dorkin, J. R.; Vegas, A.; Anderson, D. Delivery Materials for siRNA Therapeutics. *Nat. Mater.* **2013**, *12*, 967–977.
90. Uchida, S.; Perche, F.; Pichon, C.; Cabral, H. Nanomedicine-Based Approaches for mRNA Delivery. *Mol. Pharm.* **2020**, *17*, 3684.
91. Kowalski, P. S.; Rudra, A.; Miao, L.; Anderson, D. G. Delivering the Messenger: Advances in Technologies for Therapeutic mRNA Delivery. *Mol. Ther.* **2019**, *27*, 710–728.
92. Kotterman, M. A.; Chalberg, T. W.; Schaffer, D. V. Viral Vectors for Gene Therapy: Translational and Clinical Outlook. *Annu. Rev. Biomed. Eng.* **2015**, *17*, 63–89.
93. Wen, A. M.; Steinmetz, N. F. Design of Virus-Based Nanomaterials for Medicine, Biotechnology, and Energy. *Chem. Soc. Rev.* **2016**, *45*, 4074–4126.
94. Bertrand, N. *et al.* Mechanistic Understanding of *in Vivo* Protein Corona Formation on Polymeric Nanoparticles and Impact on Pharmacokinetics. *Nat. Commun.* **2017**, *8*, 1–8.
95. Merckx, P. *et al.* Surfactant Protein B (SP-B) Enhances the Cellular siRNA Delivery of Proteolipid Coated Nanogels for Inhalation Therapy. *Acta Biomater.* **2018**, *78*, 236–246.
96. Patel, S. *et al.* Naturally-Occurring Cholesterol Analogues in Lipid Nanoparticles Induce Polymorphic Shape and Enhance Intracellular Delivery of mRNA. *Nat. Commun.* **2020**, *11*, 983.
97. Ball, R. L.; Hajj, K. A.; Vizelman, J.; Bajaj, P.; Whitehead, K. A. Lipid Nanoparticle Formulations for Enhanced Co-Delivery of siRNA and mRNA. *Nano Lett.* **2018**, *18*, 3814–3822.
98. Rietwyk, S.; Peer, D. Next-Generation Lipids in RNA Interference Therapeutics. *ACS Nano* **2017**, *11*, 7572–7586.
99. Varshosaz, J.; Taymouri, S. Hollow Inorganic Nanoparticles as Efficient Carriers for siRNA Delivery: A Comprehensive Review. *Curr. Pharm. Des.* **2015**, *21*, 4310–4328.
100. Jayaraman, M. *et al.* Maximizing the Potency of siRNA Lipid Nanoparticles for Hepatic Gene Silencing *In Vivo*. *Angew. Chemie Int. Ed.* **2012**, *51*, 8529–8533.
101. Sabnis, S. *et al.* A Novel Amino Lipid Series for mRNA Delivery: Improved Endosomal Escape

- and Sustained Pharmacology and Safety in Non-Human Primates. *Mol. Ther.* **2018**, *26*, 1509–1519.
102. Nair, J. K. *et al.* Multivalent N -Acetylgalactosamine-Conjugated SiRNA Localizes in Hepatocytes and Elicits Robust RNAi-Mediated Gene Silencing. *J. Am. Chem. Soc.* **2014**, *136*, 16958–16961.
 103. Nair, J. K. *et al.* Impact of Enhanced Metabolic Stability on Pharmacokinetics and Pharmacodynamics of GalNAc-SiRNA Conjugates. *Nucleic Acids Res.* **2017**, *45*, 10969–10977.
 104. Matsuda, S. *et al.* SiRNA Conjugates Carrying Sequentially Assembled Trivalent N-Acetylgalactosamine Linked Through Nucleosides Elicit Robust Gene Silencing *In Vivo* in Hepatocytes. *ACS Chem. Biol.* **2015**, *10*, 1181–1187.
 105. Zimmermann, T. S. *et al.* Clinical Proof of Concept for a Novel Hepatocyte-Targeting GalNAc-SiRNA Conjugate. *Mol. Ther.* **2017**, *25*, 71–78.
 106. Foster, D. J. *et al.* Advanced SiRNA Designs Further Improve *In Vivo* Performance of GalNAc-SiRNA Conjugates. *Mol. Ther.* **2018**, *26*, 708–717.
 107. Brown, C. R. *et al.* Investigating the Pharmacodynamic Durability of GalNAc-SiRNA Conjugates. *Nucleic Acids Res.* **2020**, gkaa670.
 108. Ray, K. K. *et al.* Inclisiran in Patients at High Cardiovascular Risk with Elevated LDL Cholesterol. *N. Engl. J. Med.* **2017**, *376*, 1430–1440.
 109. Fitzgerald, K. *et al.* A Highly Durable RNAi Therapeutic Inhibitor of PCSK9. *N. Engl. J. Med.* **2017**, *376*, 41–51.
 110. Ray, K. K. *et al.* Two Phase 3 Trials of Inclisiran in Patients with Elevated LDL Cholesterol. *N. Engl. J. Med.* **2020**, *382*, 1507–1519.
 111. Hassler, M. R. *et al.* Comparison of Partially and Fully Chemically-Modified SiRNA in Conjugate-Mediated Delivery *in Vivo*. *Nucleic Acids Res.* **2018**, *46*, 2185–2196.
 112. Haraszti, R. A. *et al.* 5'-Vinylphosphonate Improves Tissue Accumulation and Efficacy of Conjugated SiRNAs *in Vivo*. *Nucleic Acids Res.* **2017**, *45*, 7581–7592.
 113. Nishina, K. *et al.* Efficient *in Vivo* Delivery of SiRNA to the Liver by Conjugation of α -Tocopherol. *Mol. Ther.* **2008**, *16*, 734–740.
 114. Osborn, M. F. *et al.* Hydrophobicity Drives the Systemic Distribution of Lipid-Conjugated SiRNAs *via* Lipid Transport Pathways. *Nucleic Acids Res.* **2019**, *47*, 1070–1081.
 115. Sarett, S. M. *et al.* Lipophilic SiRNA Targets Albumin *In Situ* and Promotes Bioavailability, Tumor Penetration, and Carrier-Free Gene Silencing. *Proc. Natl. Acad. Sci. U. S. A.* **2017**, *114*, E6490–E6497.
 116. Wolfrum, C. *et al.* Mechanisms and Optimization of *in Vivo* Delivery of Lipophilic SiRNAs. *Nat. Biotechnol.* **2007**, *25*, 1149–1157.
 117. Bennett, C. F.; Baker, B. F.; Pham, N.; Swayze, E.; Geary, R. S. Pharmacology of Antisense Drugs. *Annu. Rev. Pharmacol. Toxicol.* **2017**, *57*, 81–105.
 118. Ly, S. *et al.* Visualization of Self-Delivering Hydrophobically Modified SiRNA Cellular Internalization. *Nucleic Acids Res.* **2017**, *45*, 15–25.
 119. Østergaard, M. E. *et al.* Conjugation of Hydrophobic Moieties Enhances Potency of Antisense Oligonucleotides in the Muscle of Rodents and Non-Human Primates. *Nucleic Acids Res.* **2019**.
 120. Tai, W.; Gao, X. Functional Peptides for SiRNA Delivery. *Adv. Drug Deliv. Rev.* **2017**, *110–111*, 157–168.
 121. Chen, F. *et al.* Ultrasmall Targeted Nanoparticles with Engineered Antibody Fragments for Imaging Detection of HER2-Overexpressing Breast Cancer. *Nat. Commun.* **2018**, *9*, 1–11.
 122. Kijanka, M.; Dorresteyn, B.; Oliveira, S.; Van Bergen En Henegouwen, P. M. P. Nanobody-Based Cancer Therapy of Solid Tumors. *Nanomedicine* **2015**, *10*, 161–174.
 123. Arias, J. L. *et al.* Nanobody Conjugated PLGA Nanoparticles for Active Targeting of African Trypanosomiasis. *J. Control. Release* **2015**, *197*, 190–198.
 124. Hu, Y.; Liu, C.; Muyldermans, S. Nanobody-Based Delivery Systems for Diagnosis and Targeted Tumor Therapy. *Front. Immunol.* **2017**, *8*, 1442.
 125. Van Audenhove, I.; Gettemans, J. Nanobodies as Versatile Tools to Understand, Diagnose,

- Visualize and Treat Cancer. *EBioMedicine* **2016**, *8*, 40–48.
126. Joris, F.; De Smedt, S. C.; Raemdonck, K. Small Molecules Convey Big Messages: Boosting Non-Viral Nucleic Acid Delivery with Low Molecular Weight Drugs. *Nano Today* **2017**, *16*, 14–29.
 127. Rozema, D. B. *et al.* Dynamic PolyConjugates for Targeted *in Vivo* Delivery of siRNA to Hepatocytes. *Proc. Natl. Acad. Sci. U. S. A.* **2007**, *104*, 12982–12987.
 128. Wong, S. C. *et al.* Co-Injection of a Targeted, Reversibly Masked Endosomolytic Polymer Dramatically Improves the Efficacy of Cholesterol-Conjugated Small Interfering RNAs *In Vivo*. *Nucleic Acid Ther.* **2012**, *22*, 380–390.
 129. Kranz, L. M. *et al.* Systemic RNA Delivery to Dendritic Cells Exploits Antiviral Defence for Cancer Immunotherapy. *Nature* **2016**, *534*, 396–401.
 130. Zhi, D.; Zhao, Y.; Cui, S.; Chen, H.; Zhang, S. Conjugates of Small Targeting Molecules to Non-Viral Vectors for the Mediation of siRNA. *Acta Biomater.* **2016**, *36*, 21–41.
 131. Winkler, J. Oligonucleotide Conjugates for Therapeutic Applications. *Ther. Deliv.* **2013**, *4*, 791–809.
 132. Salvati, A. *et al.* Transferrin-Functionalized Nanoparticles Lose Their Targeting Capabilities When a Biomolecule Corona Adsorbs on the Surface. *Nat. Nanotechnol.* **2013**, *8*, 137–143.
 133. Akinc, A. *et al.* Targeted Delivery of RNAi Therapeutics with Endogenous and Exogenous Ligand-Based Mechanisms. *Mol. Ther.* **2010**, *18*, 1357–1364.
 134. Semple, S. C. *et al.* Rational Design of Cationic Lipids for siRNA Delivery. *Nat. Biotechnol.* **2010**, *28*, 172–176.
 135. Sato, Y.; Kinami, Y.; Hashiba, K.; Harashima, H. Different Kinetics for the Hepatic Uptake of Lipid Nanoparticles between the Apolipoprotein E/Low Density Lipoprotein Receptor and the N-Acetyl-D-Galactosamine/Asialoglycoprotein Receptor Pathway. *J. Control. Release* **2020**, *322*, 217–226.
 136. Ramishetti, S. *et al.* Systemic Gene Silencing in Primary T Lymphocytes Using Targeted Lipid Nanoparticles. *ACS Nano* **2015**, *9*, 6706–6716.
 137. Veiga, N.; Diesendruck, Y.; Peer, D. Targeted Lipid Nanoparticles for RNA Therapeutics and Immunomodulation in Leukocytes. *Adv. Drug Deliv. Rev.* **2020**.
 138. Ramishetti, S. *et al.* A Combinatorial Library of Lipid Nanoparticles for RNA Delivery to Leukocytes. *Adv. Mater.* **2020**, *32*, 1906128.
 139. Kon, E. *et al.* Resveratrol Enhances mRNA and siRNA Lipid Nanoparticles Primary CLL Cell Transfection. *Pharmaceutics* **2020**, *12*, 520.
 140. Tsoi, K. M. *et al.* Mechanism of Hard-Nanomaterial Clearance by the Liver. *Nat. Mater.* **2016**, *15*, 1212–1221.
 141. Jain, R. K.; Stylianopoulos, T. Delivering Nanomedicine to Solid Tumors. *Nat. Rev. Clin. Oncol.* **2010**, *7*, 653–664.
 142. Dhaliwal, A.; Zheng, G. Improving Accessibility of EPR-Insensitive Tumor Phenotypes Using EPR-Adaptive Strategies: Designing a New Perspective in Nanomedicine Delivery. *Theranostics* **2019**, *9*, 8091–8108.
 143. Sago, C. D. *et al.* Nanoparticles That Deliver RNA to Bone Marrow Identified by *in Vivo* Directed Evolution. *J. Am. Chem. Soc.* **2018**, *140*, 17095–17105.
 144. Paunovska, K. *et al.* Analyzing 2000 *in Vivo* Drug Delivery Data Points Reveals Cholesterol Structure Impacts Nanoparticle Delivery. *ACS Nano* **2018**, *12*, 8341–8349.
 145. Lokugamage, M. P.; Sago, C. D.; Gan, Z.; Krupczak, B. R.; Dahlman, J. E. Constrained Nanoparticles Deliver siRNA and SgRNA to T Cells *In Vivo* without Targeting Ligands. *Adv. Mater.* **2019**, *31*, 1902251.
 146. Gan, Z. *et al.* Nanoparticles Containing Constrained Phospholipids Deliver mRNA to Liver Immune Cells *in Vivo* without Targeting Ligands. *Bioeng. Transl. Med.* **2020**.
 147. Zhang, Y. N.; Poon, W.; Tavares, A. J.; McGilvray, I. D.; Chan, W. C. W. Nanoparticle–Liver Interactions: Cellular Uptake and Hepatobiliary Elimination. *J. Control. Release* **2016**, *240*, 332–348.
 148. Wolfram, J. *et al.* A Chloroquine-Induced Macrophage-Preconditioning Strategy for Improved

- Nanodelivery. *Sci. Rep.* **2017**, *7*.
149. Tavares, A. J. *et al.* Effect of Removing Kupffer Cells on Nanoparticle Tumor Delivery. *Proc. Natl. Acad. Sci. U. S. A.* **2017**, *114*, E10871–E10880.
 150. Wilhelm, S. *et al.* Analysis of Nanoparticle Delivery to Tumours. *Nat. Rev. Mater.* **2016**, *1*, 1–12.
 151. Poon, W.; Kingston, B. R.; Ouyang, B.; Ngo, W.; Chan, W. C. W. A Framework for Designing Delivery Systems. *Nat. Nanotechnol.* **2020**, *15*, 819–829.
 152. Ouyang, B. *et al.* The Dose Threshold for Nanoparticle Tumour Delivery. *Nat. Mater.* **2020**, 1–10.
 153. Cursiefen, C. *et al.* Aganirsen Antisense Oligonucleotide Eye Drops Inhibit Keratitis-Induced Corneal Neovascularization and Reduce Need for Transplantation: The I-CAN Study. *Ophthalmology* **2014**, *121*, 1683–1692.
 154. Schirotti, D. *et al.* Effective *In Vivo* Topical Delivery of siRNA and Gene Silencing in Intact Corneal Epithelium Using a Modified Cell Penetrating Peptide. *Mol. Ther. - Nucleic Acids* **2019**, *17*, 891–906.
 155. Evers, M. M.; Toonen, L. J. A.; van Roon-Mom, W. M. C. Antisense Oligonucleotides in Therapy for Neurodegenerative Disorders. *Adv. Drug Deliv. Rev.* **2015**, *87*, 90–103.
 156. Martens, T. F.; Remaut, K.; Demeester, J.; De Smedt, S. C.; Braeckmans, K. Intracellular Delivery of Nanomaterials: How to Catch Endosomal Escape in the Act. *Nano Today* **2014**, *9*, 344–364.
 157. Vermeulen, L. M. P.; De Smedt, S. C.; Remaut, K.; Braeckmans, K. The Proton Sponge Hypothesis: Fable or Fact? *Eur. J. Pharm. Biopharm.* **2018**, *129*, 184–190.
 158. Stewart, M. P.; Langer, R.; Jensen, K. F. Intracellular Delivery by Membrane Disruption: Mechanisms, Strategies, and Concepts. **2018**.
 159. Ma, D. Enhancing Endosomal Escape for Nanoparticle Mediated siRNA Delivery. *Nanoscale* **2014**, *6*, 6415.
 160. Smith, S. A.; Selby, L. I.; Johnston, A. P. R.; Such, G. K. The Endosomal Escape of Nanoparticles: Toward More Efficient Cellular Delivery. *Bioconjug. Chem.* **2019**, *30*, 263–272.
 161. Pei, D.; Buyanova, M. Overcoming Endosomal Entrapment in Drug Delivery. *Bioconjug. Chem.* **2019**, *30*, 273–283.
 162. Gilleron, J. *et al.* Image-Based Analysis of Lipid Nanoparticle–Mediated siRNA Delivery, Intracellular Trafficking and Endosomal Escape. *Nat. Biotechnol.* **2013**, *31*, 638–646.
 163. Wittrup, A. *et al.* Visualizing Lipid-Formulated siRNA Release from Endosomes and Target Gene Knockdown. *Nat. Biotechnol.* **2015**, *33*, 870–876.
 164. Maugeri, M. *et al.* Linkage between Endosomal Escape of LNP-mRNA and Loading into EVs for Transport to Other Cells. *Nat. Commun.* **2019**, *10*.
 165. Wojnilowicz, M.; Glab, A.; Bertucci, A.; Caruso, F.; Cavalieri, F. Super-Resolution Imaging of Proton Sponge-Triggered Rupture of Endosomes and Cytosolic Release of Small Interfering RNA. *ACS Nano* **2019**, acsnano.8b05151.
 166. Van de Vyver, T. *et al.* Cationic Amphiphilic Drugs Boost the Lysosomal Escape of Small Nucleic Acid Therapeutics in a Nanocarrier-Dependent Manner. *ACS Nano* **2020**, *14*, 4774–4791.
 167. Witzigmann, D.; Hak, S.; van der Meel, R. Translating Nanomedicines: Thinking beyond Materials? A Young Investigator’s Reply to ‘The Novelty Bubble.’ *J. Control. Release* **2018**, *290*, 138–140.
 168. Raemdonck, K.; De Smedt, S. C. Lessons in Simplicity That Should Shape the Future of Drug Delivery. *Nat. Biotechnol.* **2015**, *33*, 1026–1027.
 169. Lokugamage, M. P.; Sago, C. D.; Dahlman, J. E. Testing Thousands of Nanoparticles *in Vivo* Using DNA Barcodes. *Curr. Opin. Biomed. Eng.* **2018**, *7*, 1–8.
 170. Time to Deliver. *Nat. Biotechnol.* **2014**, *32*, 961.
 171. Kulkarni, J. A. *et al.* On the Formation and Morphology of Lipid Nanoparticles Containing Ionizable Cationic Lipids and siRNA. *ACS Nano* **2018**, *12*, 4787–4795.
 172. Leroux, J.-C. Editorial: Drug Delivery: Too Much Complexity, Not Enough Reproducibility?

- Angew. Chemie Int. Ed.* **2017**, *56*, 15170–15171.
173. Chan, W. C. W. Nanomedicine 2.0. *Acc. Chem. Res.* **2017**, *50*, 627–632.
174. Skuta, C. *et al.* Probes & Drugs Portal: An Interactive, Open Data Resource for Chemical Biology. *Nat. Methods* **2017**, *14*, 759–760.
175. Dutta, D.; Donaldson, J. G. Search for Inhibitors of Endocytosis. *Cell. Logist.* **2012**, *2*, 203–208.
176. Zaki, N. M.; Tirelli, N. Gateways for the Intracellular Access of Nanocarriers: A Review of Receptor-Mediated Endocytosis Mechanisms and of Strategies in Receptor Targeting. *Expert Opin. Drug Deliv.* **2010**, *7*, 895–913.
177. Fraley, R.; Straubinger, R. M.; Louise Springer, E.; Papahadjopoulos, D.; Rule, G. Liposome-Mediated Delivery of Deoxyribonucleic Acid to Cells: Enhanced Efficiency of Delivery Related to Lipid Composition and Incubation Conditions. *Biochemistry* **1981**, *20*, 6978–6987.
178. Gilleron, J. *et al.* Identification of siRNA Delivery Enhancers by a Chemical Library Screen. *Nucleic Acids Res.* **2015**, *43*, 7984–8001.
179. Yang, B. *et al.* High-Throughput Screening Identifies Small Molecules That Enhance the Pharmacological Effects of Oligonucleotides. *Nucleic Acids Res.* **2015**, *43*, 1987–1996.
180. Osborn, M. F. *et al.* Guanabenz (Wytensin™) Selectively Enhances Uptake and Efficacy of Hydrophobically Modified siRNAs. *Nucleic Acids Res.* **2015**, *43*, 8664–8672.
181. Ovcharenko, D.; Jarvis, R.; Hunnicke-Smith, S.; Kelnar, K.; Brown, D. High-Throughput RNAi Screening *in Vitro*: From Cell Lines to Primary Cells. *RNA* **2005**, *11*, 985–993.
182. Jones, L. H.; Bunnage, M. E. Applications of Chemogenomic Library Screening in Drug Discovery. *Nat. Rev. Drug Discov.* **2017**, *16*, 285–296.
183. Liu, Y.; Krishnan, M. N.; Phua, K. K. L. Suppression of mRNA Nanoparticle Transfection in Human Fibroblasts by Selected Interferon Inhibiting Small Molecule Compounds. *Biomolecules* **2017**, *7*, 56.
184. Wassermann, A. M.; Camargo, L. M.; Auld, D. S. Composition and Applications of Focus Libraries to Phenotypic Assays. *Front. Pharmacol.* **2014**, *24*, 164.
185. Vercauteren, D. *et al.* The Use of Inhibitors to Study Endocytic Pathways of Gene Carriers: Optimization and Pitfalls. *Mol. Ther.* **2010**, *18*, 561–569.
186. Baell, J.; Walters, M. A. Chemistry: Chemical Con Artists Foil Drug Discovery. *Nature* **2014**, *513*, 481–483.
187. Collinet, C. *et al.* Systems Survey of Endocytosis by Multiparametric Image Analysis. *Nature* **2010**, *464*, 243–249.
188. Liberali, P.; Snijder, B.; Pelkmans, L. A Hierarchical Map of Regulatory Genetic Interactions in Membrane Trafficking. *Cell* **2014**, *157*, 1473–1487.
189. Kozik, P. *et al.* A Human Genome-Wide Screen for Regulators of Clathrin-Coated Vesicle Formation Reveals an Unexpected Role for the V-ATPase. *Nat. Cell Biol.* **2013**, *15*, 50–60.
190. Simpson, J. C. *et al.* Genome-Wide RNAi Screening Identifies Human Proteins with a Regulatory Function in the Early Secretory Pathway. *Nat. Cell Biol.* **2012**, *14*, 764–774.
191. Lenk, G. M. *et al.* CRISPR Knockout Screen Implicates Three Genes in Lysosome Function. *Sci. Rep.* **2019**, *9*, 1–10.
192. Shoemaker, C. J. *et al.* CRISPR Screening Using an Expanded Toolkit of Autophagy Reporters Identifies TMEM41B as a Novel Autophagy Factor. *PLoS Biol.* **2019**, *17*, e2007044.
193. Cutrona, M. B.; Simpson, J. C. A High-Throughput Automated Confocal Microscopy Platform for Quantitative Phenotyping of Nanoparticle Uptake and Transport in Spheroids. *Small* **2019**, *15*, 1902033.
194. Bexiga, M. G.; Kelly, C.; Dawson, K. A.; Simpson, J. C. RNAi-Mediated Inhibition of Apoptosis Fails to Prevent Cationic Nanoparticle-Induced Cell Death in Cultured Cells. *Nanomedicine* **2014**, *9*, 1651–1664.
195. Sahay, G. *et al.* Efficiency of siRNA Delivery by Lipid Nanoparticles Is Limited by Endocytic Recycling. *Nat. Biotechnol.* **2013**, *31*, 653–658.
196. Patel, S. *et al.* Boosting Intracellular Delivery of Lipid Nanoparticle-Encapsulated mRNA. *Nano Lett.* **2017**, *17*, 5711–5718.

197. Wang, S.; Sun, H.; Tanowitz, M.; Liang, X.; Crooke, S. T. Intra-Endosomal Trafficking Mediated by Lysobisphosphatidic Acid Contributes to Intracellular Release of Phosphorothioate-Modified Antisense Oligonucleotides. *Nucleic Acids Res.* **2017**, *45*, 5309–5322.
198. Liang, X. hai *et al.* COPII Vesicles Can Affect the Activity of Antisense Oligonucleotides by Facilitating the Release of Oligonucleotides from Endocytic Pathways. *Nucleic Acids Res.* **2018**, *46*, 10225–10245.
199. Liang, X. H. *et al.* Golgi-Endosome Transport Mediated by M6PR Facilitates Release of Antisense Oligonucleotides from Endosomes. *Nucleic Acids Res.* **2020**, *48*, 1372–1391.
200. Shiyu Wang, Hong Sun, Michael Tanowitz, Xue-hai Liang, S. T. C. Annexin A2 Facilitates Endocytic Trafficking of Antisense Oligonucleotides. *Nucleic Acids Res.* **2016**, *44*, 7314–7330.
201. Cuellar, T. L. *et al.* Systematic Evaluation of Antibody-Mediated siRNA Delivery Using an Industrial Platform of THIOMAB-siRNA Conjugates. *Nucleic Acids Res.* **2015**, *43*, 1189–1203.
202. Koller, E. *et al.* Mechanisms of Single-Stranded Phosphorothioate Modified Antisense Oligonucleotide Accumulation in Hepatocytes. *Nucleic Acids Res.* **2011**, *39*, 4795–4807.
203. Linnane, E. *et al.* Differential Uptake, Kinetics and Mechanisms of Intracellular Trafficking of next-Generation Antisense Oligonucleotides across Human Cancer Cell Lines. *Nucleic Acids Res.* **2019**, *47*, 4375–4392.
204. Wagenaar, T. R. *et al.* Identification of the Endosomal Sorting Complex Required for Transport-I (ESCRT-I) as an Important Modulator of Anti-MiR Uptake by Cancer Cells. *Nucleic Acids Res.* **2015**, *43*, 1204–1215.
205. Panarella, A. *et al.* A Systematic High-Content Screening Microscopy Approach Reveals Key Roles for Rab33b, OATL1 and Myo6 in Nanoparticle Trafficking in HeLa Cells. *Sci. Rep.* **2016**, *6*, 1–11.
206. Ross-Thriepland, D. *et al.* Arrayed CRISPR Screening Identifies Novel Targets That Enhance the Productive Delivery of mRNA by MC3-Based Lipid Nanoparticles. *SLAS Discov.* **2020**, *25*, 605–617.
207. Brayden, D. J.; Cryan, S. A.; Dawson, K. A.; O’Brien, P. J.; Simpson, J. C. High-Content Analysis for Drug Delivery and Nanoparticle Applications. *Drug Discov. Today* **2015**, *20*, 942–957.
208. Schuster, A. *et al.* RNAi/CRISPR Screens: From a Pool to a Valid Hit. *Trends Biotechnol.* **2019**, *37*, 38–55.
209. Shalem, O.; Sanjana, N. E.; Zhang, F. High-Throughput Functional Genomics Using CRISPR-Cas9. *Nat. Rev. Genet.* **2015**, *16*, 299–311.
210. Gianni, D.; Farrow, S. Functional Genomics for Target Identification. *SLAS Discov.* **2020**, *25*, 531–534.
211. Evers, B. *et al.* CRISPR Knockout Screening Outperforms ShRNA and CRISPRi in Identifying Essential Genes. *Nat. Biotechnol.* **2016**, *34*, 631–633.
212. Smith, I. *et al.* Evaluation of RNAi and CRISPR Technologies by Large-Scale Gene Expression Profiling in the Connectivity Map. *PLoS Biol.* **2017**, *15*.
213. Yuan, F.; Sun, M.; Liu, H.; Qian, F. Albumin-Conjugated Drug Is Irresistible by Single Gene Mutation of Endocytic System: Verification by Genome-Wide CRISPR-Cas9 Loss-of-Function Screens. *J. Control. Release* **2020**, *323*, 311–320.
214. Kampmann, M. CRISPRi and CRISPRa Screens in Mammalian Cells for Precision Biology and Medicine. *ACS Chem. Biol.* **2018**, *13*, 406–416.
215. Miller, C. M.; Wan, W. B.; Seth, P. P.; Harris, E. N. Endosomal Escape of Antisense Oligonucleotides Internalized by Stabilin Receptors Is Regulated by Rab5C and EEA1 during Endosomal Maturation. *Nucleic Acid Ther.* **2018**, *28*, 86–96.
216. Sahay, G.; Alakhova, D. Y.; Kabanov, A. V. Endocytosis of Nanomedicines. *J. Control. Release* **2010**, *145*, 182–195.
217. Iversen, T. G.; Skotland, T.; Sandvig, K. Endocytosis and Intracellular Transport of Nanoparticles: Present Knowledge and Need for Future Studies. *Nano Today* **2011**, *6*, 176–185.
218. Vercauteren, D. *et al.* On the Cellular Processing of Non-Viral Nanomedicines for Nucleic Acid

- Delivery: Mechanisms and Methods. *J. Control. Release* **2012**, *161*, 566–581.
219. Sandvig, K.; Pust, S.; Skotland, T.; van Deurs, B. Clathrin-Independent Endocytosis: Mechanisms and Function. *Curr. Opin. Cell Biol.* **2011**, *23*, 413–420.
 220. Damm, E. M. *et al.* Clathrin- and Caveolin-1-Independent Endocytosis: Entry of Simian Virus 40 into Cells Devoid of Caveolae. *J. Cell Biol.* **2005**, *168*, 477–488.
 221. Roberts, R. *et al.* Autophagy and Formation of Tubulovesicular Autophagosomes Provide a Barrier against Nonviral Gene Delivery. *Autophagy* **2013**, *9*, 667–682.
 222. Paunovska, K.; Loughrey, D.; Sago, C. D.; Langer, R.; Dahlman, J. E. Using Large Datasets to Understand Nanotechnology. *Adv. Mater.* **2019**, *31*, 1902798.
 223. Dey, S. S.; Kester, L.; Spanjaard, B.; Bienko, M.; Van Oudenaarden, A. Integrated Genome and Transcriptome Sequencing of the Same Cell. *Nat. Biotechnol.* **2015**, *33*, 285–289.
 224. Angermueller, C. *et al.* Parallel Single-Cell Sequencing Links Transcriptional and Epigenetic Heterogeneity. *Nat. Methods* **2016**, *13*, 229–232.
 225. Cheow, L. F. *et al.* Single-Cell Multimodal Profiling Reveals Cellular Epigenetic Heterogeneity. *Nat. Methods* **2016**, *13*, 833–836.
 226. Hebels, D. G. A. J.; Carlier, A.; Coonen, M. L. J.; Theunissen, D. H.; de Boer, J. CBIT: A Transcriptomics Database for Innovative Biomaterial Engineering. *Biomaterials* **2017**, *149*, 88–97.
 227. Dowaidar, M. *et al.* Role of Autophagy in Cell-Penetrating Peptide Transfection Model. *Sci. Rep.* **2017**, *7*, 1–14.
 228. Paunovska, K. *et al.* A Direct Comparison of *in Vitro* and *in Vivo* Nucleic Acid Delivery Mediated by Hundreds of Nanoparticles Reveals a Weak Correlation. *Nano Lett.* **2018**, *18*, 2148–2157.
 229. Sigismund, S. *et al.* Endocytosis and Signaling: Cell Logistics Shape the Eukaryotic Cell Plan. *Physiol. Rev.* **2012**, *92*, 273–366.
 230. Zhang, Y. *et al.* Purification and Characterization of Progenitor and Mature Human Astrocytes Reveals Transcriptional and Functional Differences with Mouse. *Neuron* **2016**, *89*, 37–53.
 231. Whitehead, K. A. *et al.* *In Vitro* - *In Vivo* Translation of Lipid Nanoparticles for Hepatocellular siRNA Delivery. *ACS Nano* **2012**, *6*, 6922–6929.
 232. Peynshaert, K. *et al.* Influence of Pathogenic Stimuli on Müller Cell Transfection by Lipoplexes. *Eur. J. Pharm. Biopharm.* **2020**, *150*, 87–95.
 233. Bhatia, S. N.; Ingber, D. E. Microfluidic Organs-on-Chips. *Nat. Biotechnol.* **2014**, *32*, 760–772.
 234. Lazzari, G.; Couvreur, P.; Mura, S. Multicellular Tumor Spheroids: A Relevant 3D Model for the: *In Vitro* Preclinical Investigation of Polymer Nanomedicines. *Polym. Chem.* **2017**, *8*, 4947–4969.
 235. Costa, E. C. *et al.* 3D Tumor Spheroids: An Overview on the Tools and Techniques Used for Their Analysis. *Biotechnol. Adv.* **2016**, *34*, 1427–1441.
 236. Nunes, A. S.; Barros, A. S.; Costa, E. C.; Moreira, A. F.; Correia, I. J. 3D Tumor Spheroids as *in Vitro* Models to Mimic *in Vivo* Human Solid Tumors Resistance to Therapeutic Drugs. *Biotechnol. Bioeng.* **2019**, *116*, 206–226.
 237. Tchoryk, A. *et al.* Penetration and Uptake of Nanoparticles in 3D Tumor Spheroids. *Bioconjug. Chem.* **2019**, *30*, 1371–1384.
 238. Du Rietz, H.; Hedlund, H.; Wilhelmson, S.; Nordenfelt, P.; Wittrup, A. Imaging Small Molecule-Induced Endosomal Escape of siRNA. *Nat. Commun.* **2020**, *11*, 1809.
 239. Carver, K.; Ming, X.; Juliano, R. L. Multicellular Tumor Spheroids as a Model for Assessing Delivery of Oligonucleotides in Three Dimensions. *Mol. Ther. - Nucleic Acids* **2014**, *3*, e153.
 240. Zhang, X.; Castanotto, D.; Nam, S.; Horne, D.; Stein, C. 6BIO Enhances Oligonucleotide Activity in Cells: A Potential Combinatorial Anti-Androgen Receptor Therapy in Prostate Cancer Cells. *Mol. Ther.* **2017**, *25*, 79–91.
 241. Jia, H.-R.; Zhu, Y.-X.; Duan, Q.-Y.; Chen, Z.; Wu, F.-G. Nanomaterials Meet Zebrafish: Toxicity Evaluation and Drug Delivery Applications. *J. Control. Release* **2019**.
 242. Sieber, S. *et al.* Zebrafish as a Preclinical *in Vivo* Screening Model for Nanomedicines. *Adv. Drug Deliv. Rev.* **2019**, *151–152*, 152–168.

243. Sago, C. D.; Krupczak, B. R.; Lokugamage, M. P.; Gan, Z.; Dahlman, J. E. Cell Subtypes Within the Liver Microenvironment Differentially Interact with Lipid Nanoparticles. *Cell. Mol. Bioeng.* **2019**, *12*, 389–397.
244. Sago, C. D. *et al.* Barcoding Chemical Modifications into Nucleic Acids Improves Drug Stability *in Vivo*. *J. Mater. Chem. B* **2018**, *6*, 7197–7203.
245. Paunovska, K. *et al.* Nanoparticles Containing Oxidized Cholesterol Deliver mRNA to the Liver Microenvironment at Clinically Relevant Doses. *Adv. Mater.* **2019**, *31*, 1807748.
246. Dahlman, J. E. *et al.* Barcoded Nanoparticles for High Throughput *in Vivo* Discovery of Targeted Therapeutics. *Proc. Natl. Acad. Sci. U. S. A.* **2017**, *114*, 2060–2065.
247. Guimaraes, P. P. G. *et al.* Ionizable Lipid Nanoparticles Encapsulating Barcoded mRNA for Accelerated *in Vivo* Delivery Screening. *J. Control. Release* **2019**, *316*, 404–417.
248. Kauffman, K. J. *et al.* Rapid, Single-Cell Analysis and Discovery of Vectors of MRNA Transfection *In Vivo* with a LoxP-Flanked TdTomato Reporter Mouse. *Mol. Ther. - Nucleic Acids* **2018**, *10*, 55–63.
249. Li, Y. *et al.* Protein and MRNA Delivery Enabled by Cholesteryl-Based Biodegradable Lipidoid Nanoparticles. *Angew. Chemie Int. Ed.* **2020**, *59*, 14957–14964.
250. Paunovska, K. *et al.* Increased PIP3 Activity Blocks Nanoparticle MRNA Delivery. *Sci. Adv.* **2020**, *6*, eaba5672.
251. Sazani, P. *et al.* Systemically Delivered Antisense Oligomers Upregulate Gene Expression in Mouse Tissues. *Nat. Biotechnol.* **2002**, *20*, 1228–1233.
252. Roberts, J. *et al.* Efficient and Persistent Splice Switching by Systemically Delivered LNA Oligonucleotides in Mice. *Mol. Ther.* **2006**, *14*, 471–475.
253. Wang, L. *et al.* A Novel Family of Small Molecules That Enhance the Intracellular Delivery and Pharmacological Effectiveness of Antisense and Splice Switching Oligonucleotides. *ACS Chem. Biol.* **2017**, *12*, 1999–2007.
254. Sago, C. D. *et al.* Modifying a Commonly Expressed Endocytic Receptor Retargets Nanoparticles *in Vivo*. *Nano Lett.* **2018**, *18*, 7590–7600.
255. Patel, S. *et al.* Brief Update on Endocytosis of Nanomedicines. *Adv. Drug Deliv. Rev.* **2019**, *144*, 90–111.
256. Willoughby, J. L. S. *et al.* Evaluation of GalNAc-SiRNA Conjugate Activity in Pre-Clinical Animal Models with Reduced Asialoglycoprotein Receptor Expression. *Mol. Ther.* **2018**, *26*, 105–114.
257. Shemesh, C. S. *et al.* Pharmacokinetic and Pharmacodynamic Investigations of ION-353382, a Model Antisense Oligonucleotide: Using Alpha-2-Macroglobulin and Murinoglobulin Double-Knockout Mice. *Nucleic Acid Ther.* **2016**, *26*, 223–235.
258. Wu, Y. *et al.* Generating Viable Mice with Heritable Embryonically Lethal Mutations Using the CRISPR-Cas9 System in Two-Cell Embryos. *Nat. Commun.* **2019**, *10*, 1–13.
259. Manguso, R. T. *et al.* *In Vivo* CRISPR Screening Identifies Ptpn2 as a Cancer Immunotherapy Target. *Nature* **2017**, *547*, 413–418.
260. Li, F. *et al.* *In Vivo* Epigenetic Crispr Screen Identifies Asf1a as an Immunotherapeutic Target in Kras-Mutant Lung Adenocarcinoma. *Cancer Discov.* **2020**, *10*, 270–287.
261. Ding, Y. *et al.* Direct Cytosolic siRNA Delivery by Reconstituted High Density Lipoprotein for Target-Specific Therapy of Tumor Angiogenesis. *Biomaterials* **2014**, *35*, 7214–7227.
262. Jiang, Y. *et al.* Direct Cytosolic Delivery of siRNA Using Nanoparticle-Stabilized Nanocapsules. *Angew. Chemie* **2015**, *127*, 516–520.
263. Doherty, G. J.; McMahon, H. T. Mechanisms of Endocytosis. *Annu. Rev. Biochem.* **2009**, *78*, 857–902.
264. Khalil, I. A.; Kogure, K.; Akita, H.; Harashima, H. Uptake Pathways and Subsequent Intracellular Trafficking in Nonviral Gene Delivery. *Pharmacol. Rev.* **2006**, *58*, 32–45.
265. Gabrielson, N. P.; Pack, D. W. Efficient Polyethylenimine-Mediated Gene Delivery Proceeds via a Caveolar Pathway in HeLa Cells. *J. Control. Release* **2009**, *136*, 54–61.
266. Rejman, J.; Bragonzi, A.; Conese, M. Role of Clathrin- and Caveolae-Mediated Endocytosis in Gene Transfer Mediated by Lipo- and Polyplexes. *Mol. Ther.* **2005**, *12*, 468–474.

267. Fichter, K. M.; Ingle, N. P.; McLendon, P. M.; Reineke, T. M. Polymeric Nucleic Acid Vehicles Exploit Active Interorganellar Trafficking Mechanisms. *ACS Nano* **2013**, *7*, 347–364.
268. Reilly, M. J.; Larsen, J. D.; Sullivan, M. O. Polyplexes Traffic through Caveolae to the Golgi and Endoplasmic Reticulum En Route to the Nucleus. *Mol. Pharm.* **2012**, *9*, 1280–1290.
269. Alam, R. *et al.* Intracellular Delivery of an Anionic Antisense Oligonucleotide *via* Receptor-Mediated Endocytosis. *Nucleic Acids Res.* **2008**, *36*, 2764–2776.
270. Alam, M. R. *et al.* The Biological Effect of an Antisense Oligonucleotide Depends on Its Route of Endocytosis and Trafficking. *Oligonucleotides* **2010**, *20*, 103–109.
271. Ming, X. *et al.* Intracellular Delivery of an Antisense Oligonucleotide *via* Endocytosis of a G Protein-Coupled Receptor. *Nucleic Acids Res.* **2010**, *38*, 6567–6576.
272. Kim, A. J.; Boylan, N. J.; Suk, J. S.; Lai, S. K.; Hanes, J. Non-Degradative Intracellular Trafficking of Highly Compacted Polymeric DNA Nanoparticles. *J. Control. Release* **2012**, *158*, 102–107.
273. McLendon, P. M.; Fichter, K. M.; Reineke, T. M. Poly(Glycoamidoamine) Vehicles Promote PDNA Uptake through Multiple Routes and Efficient Gene Expression *via* Caveolae-Mediated Endocytosis. *Mol. Pharm.* **2010**, *7*, 738–750.
274. Rehman, Z. U.; Hoekstra, D.; Zuhorn, I. S. Protein Kinase A Inhibition Modulates the Intracellular Routing of Gene Delivery Vehicles in HeLa Cells, Leading to Productive Transfection. *J. Control. Release* **2011**, *156*, 76–84.
275. Wang, M.; Wu, B.; Shah, S. N.; Lu, P.; Lu, Q. Aminoglycoside Enhances the Delivery of Antisense Morpholino Oligonucleotides *In Vitro* and in Mdx Mice. *Mol. Ther. - Nucleic Acids* **2019**, *16*, 663–674.
276. Gooding, M. *et al.* Exploring the Interaction Between siRNA and the SMOc Biomolecule Transporters: Implications for Small Molecule-Mediated Delivery of siRNA. *Chem. Biol. Drug Des.* **2012**, *79*, 9–21.
277. Gooding, M. *et al.* A Bifurcated Proteoglycan Binding Small Molecule Carrier for siRNA Delivery. *Chem. Biol. Drug Des.* **2014**, *84*, 24–35.
278. Gestin, M. *et al.* Effect of Small Molecule Signaling in PepFect14 Transfection. *PLoS One* **2020**, *15*, e0228189.
279. Han, G. *et al.* Hexose Enhances Oligonucleotide Delivery and Exon Skipping in Dystrophin-Deficient Mdx Mice. *Nat. Commun.* **2016**, *7*, 1–11.
280. Han, G.; Lin, C.; Ning, H.; Gao, X.; Yin, H. F. Long-Term Morpholino Oligomers in Hexose Elicits Long-Lasting Therapeutic Improvements in Mdx Mice. *Mol. Ther. - Nucleic Acids* **2018**, *12*, 478–489.
281. Han, G. *et al.* Hexose Potentiates Peptide-Conjugated Morpholino Oligomer Efficacy in Cardiac Muscles of Dystrophic Mice in an Age-Dependent Manner. *Mol. Ther. - Nucleic Acids* **2019**, *18*, 341–350.
282. Choe, J. Y. *et al.* L-Type Calcium Channel Blocker Enhances Cellular Delivery and Gene Silencing Potency of Cell-Penetrating Asymmetric siRNAs. *Mol. Pharm.* **2020**, *17*, 777–786.
283. Striessnig, J.; Ortner, N.; Pinggera, A. Pharmacology of L-Type Calcium Channels: Novel Drugs for Old Targets? *Curr. Mol. Pharmacol.* **2015**, *8*, 110–122.
284. Rosa, J. M. *et al.* Calcium Entry through Slow-Inactivating L-Type Calcium Channels Preferentially Triggers Endocytosis Rather than Exocytosis in Bovine Chromaffin Cells. *Am. J. Physiol. Physiol.* **2011**, *301*, C86–C98.
285. Rosa, J. M. *et al.* Regulation by L-Type Calcium Channels of Endocytosis: An Overview. In *Journal of Molecular Neuroscience*; Springer, **2012**; Vol. 48, pp 360–367.
286. Tam, Y. Y. C. *et al.* Small Molecule Ligands for Enhanced Intracellular Delivery of Lipid Nanoparticle Formulations of siRNA. *Nanomedicine Nanotechnology, Biol. Med.* **2013**, *9*, 665–674.
287. Naslavsky, N.; Caplan, S. The Enigmatic Endosome - Sorting the Ins and Outs of Endocytic Trafficking. *J. Cell Sci.* **2018**, *131*.
288. Bennett, W. F. D.; Tieleman, D. P. The Importance of Membrane Defect-Lessons from Simulations. *Acc. Chem. Res.* **2014**, *47*, 2244–2251.

289. Cullis, P. R.; Hope, M. J.; Tilcock, C. P. S. Lipid Polymorphism and the Roles of Lipids in Membranes. *Chem. Phys. Lipids* **1986**, *40*, 127–144.
290. Zelphati, O.; Szoka, F. C. Mechanism of Oligonucleotide Release from Cationic Liposomes. *Proc. Natl. Acad. Sci. U. S. A.* **1996**, *93*, 11493–11498.
291. Juliano, R. L. Intracellular Trafficking and Endosomal Release of Oligonucleotides: What We Know and What We Do Not. *Nucleic Acid Ther.* **2018**, nat.2018.0727.
292. Lukacs, G. L. *et al.* Size-Dependent DNA Mobility in Cytoplasm and Nucleus. *J. Biol. Chem.* **2000**, *275*, 1625–1629.
293. Vaughan, E. E.; Dean, D. A. Intracellular Trafficking of Plasmids during Transfection Is Mediated by Microtubules. *Mol. Ther.* **2006**, *13*, 422–428.
294. Fusco, D. *et al.* Single mRNA Molecules Demonstrate Probabilistic Movement in Living Mammalian Cells. *Curr. Biol.* **2003**, *13*, 161–167.
295. Chen, J. *et al.* Cytoplasmic HIV-1 RNA Is Mainly Transported by Diffusion in the Presence or Absence of Gag Protein. *Proc. Natl. Acad. Sci. U. S. A.* **2014**, *111*, E5205–E5213.
296. Lifland, A. W.; Zurla, C.; Yu, J.; Santangelo, P. J. Dynamics of Native β -Actin mRNA Transport in the Cytoplasm. *Traffic* **2011**, *12*, 1000–1011.
297. Wu, B.; Chao, J. A.; Singer, R. H. Fluorescence Fluctuation Spectroscopy Enables Quantitative Imaging of Single MRNAs in Living Cells. *Biophys. J.* **2012**, *102*, 2936–2944.
298. Yamagishi, M.; Ishihama, Y.; Shirasaki, Y.; Kurama, H.; Funatsu, T. Single-Molecule Imaging of β -Actin MRNAs in the Cytoplasm of a Living Cell. *Exp. Cell Res.* **2009**, *315*, 1142–1147.
299. Ben-Ari, Y. *et al.* The Life of an mRNA in Space and Time. *J. Cell Sci.* **2010**, *123*, 1761–1774.
300. Barlan, K.; Rossow, M. J.; Gelfand, V. I. The Journey of the Organelle: Teamwork and Regulation in Intracellular Transport. *Curr. Opin. Cell Biol.* **2013**, *25*, 483–488.
301. Cai, H.; Reinisch, K.; Ferro-Novick, S. Coats, Tethers, Rabs, and SNAREs Work Together to Mediate the Intracellular Destination of a Transport Vesicle. *Dev. Cell* **2007**, *12*, 671–682.
302. Huotari, J.; Helenius, A. Endosome Maturation. *EMBO J.* **2011**, *30*, 3481–3500.
303. Scott, C. C.; Vacca, F.; Gruenberg, J. Endosome Maturation, Transport and Functions. *Seminars in Cell and Developmental Biology*. Elsevier Ltd July 1, 2014, pp 2–10.
304. Zerial, M.; McBride, H. Rab Proteins as Membrane Organizers. *Nat. Rev. Mol. Cell Biol.* **2001**, *2*, 107–117.
305. Stenmark, H. Rab GTPases as Coordinators of Vesicle Traffic. *Nat. Rev. Mol. Cell Biol.* **2009**, *10*, 513–525.
306. Stenmark, H.; Olkkonen, V. M. The Rab GTPase Family. *Genome Biol.* **2001**, *2*, reviews3007.1–reviews3007.7.
307. Hutagalung, A. H.; Novick, P. J. Role of Rab GTPases in Membrane Traffic and Cell Physiology. *Physiol. Rev.* **2011**, *91*, 119–149.
308. Pfeffer, S. R. Rab GTPases: Master Regulators That Establish the Secretory and Endocytic Pathways. *Mol. Biol. Cell* **2017**, *28*, 712–715.
309. Bonifacino, J. S.; Lippincott-Schwartz, J. Coat Proteins: Shaping Membrane Transport. *Nat. Rev. Mol. Cell Biol.* **2003**, *4*, 409–414.
310. Brandizzi, F.; Barlowe, C. Organization of the ER-Golgi Interface for Membrane Traffic Control. *Nat. Rev. Mol. Cell Biol.* **2013**, *14*, 382–392.
311. Mayor, S.; Parton, R. G.; Donaldson, J. G. Clathrin-Independent Pathways of Endocytosis. *Cold Spring Harb. Perspect. Biol.* **2014**, *6*.
312. Johannes, L.; Wunder, C. Retrograde Transport: Two (or More) Roads Diverged in an Endosomal Tree? *Traffic* **2011**, *12*, 956–962.
313. Sandvig, K. *et al.* Retrograde Transport of Endocytosed Shiga Toxin to the Endoplasmic Reticulum. *Nature* **1992**, *358*, 510–512.
314. Attar, N.; Cullen, P. J. The Retromer Complex. *Adv. Enzyme Regul.* **2010**, *50*, 216–236.
315. Seaman, M. N. J. The Retromer Complex-Endosomal Protein Recycling and Beyond. *J. Cell Sci.* **2012**, *125*, 4693–4702.
316. Burd, C.; Cullen, P. J. Retromer: A Master Conductor of Endosome Sorting. *Cold Spring Harb.*

- Perspect. Biol.* **2014**, *6*.
317. Kümmel, D.; Ungermann, C. Principles of Membrane Tethering and Fusion in Endosome and Lysosome Biogenesis. *Curr. Opin. Cell Biol.* **2014**, *29*, 61–66.
 318. Ungermann, C.; Kümmel, D. Structure of Membrane Tethers and Their Role in Fusion. *Traffic* **2019**, *20*, 479–490.
 319. Chia, P. Z. C.; Gleeson, P. A. Membrane Tethering. *F1000Prime Rep.* **2014**, *6*, 74.
 320. Bröcker, C.; Engelbrecht-Vandré, S.; Ungermann, C. Multisubunit Tethering Complexes and Their Role in Membrane Fusion. *Curr. Biol.* **2010**, *20*, R943–R952.
 321. Toh, W. H.; Gleeson, P. A. Emerging Insights into the Roles of Membrane Tethers from Analysis of Whole Organisms: The Tip of an Iceberg? *Front. Cell Dev. Biol.* **2016**, *4*, 12.
 322. Han, J.; Pluhackova, K.; Böckmann, R. A. The Multifaceted Role of SNARE Proteins in Membrane Fusion. *Front. Physiol.* **2017**, *8*, 5.
 323. Ungar, D.; Hughson, F. M. SNARE Protein Structure and Function. *Annu. Rev. Cell Dev. Biol.* **2003**, *19*, 493–517.
 324. Malsam, J.; Kreye, S.; Söllner, T. H. Membrane Traffic in the Secretory Pathway: Membrane Fusion: SNAREs and Regulation. *Cell. Mol. Life Sci.* **2008**, *65*, 2814–2832.
 325. Poteryaev, D.; Datta, S.; Ackema, K.; Zerial, M.; Spang, A. Identification of the Switch in Early-to-Late Endosome Transition. *Cell* **2010**, *141*, 497–508.
 326. Kinchen, J. M.; Ravichandran, K. S. Identification of Two Evolutionarily Conserved Genes Regulating Processing of Engulfed Apoptotic Cells. *Nature* **2010**, *464*, 778–782.
 327. Hullin-Matsuda, F.; Taguchi, T.; Greimel, P.; Kobayashi, T. Lipid Compartmentalization in the Endosome System. *Semin. Cell Dev. Biol.* **2014**, *31*, 48–56.
 328. Bissig, C.; Johnson, S.; Gruenberg, J. Studying Lipids Involved in the Endosomal Pathway. *Methods Cell Biol.* **2012**, *108*, 19–46.
 329. Vicinanza, M.; D’Angelo, G.; Di Campli, A.; De Matteis, M. A. Function and Dysfunction of the PI System in Membrane Trafficking. *EMBO J.* **2008**, *27*, 2457–2470.
 330. Vietri, M.; Radulovic, M.; Stenmark, H. The Many Functions of ESCRTs. *Nat. Rev. Mol. Cell Biol.* **2020**, *21*, 25–42.
 331. Castanotto, D. *et al.* Protein Kinase C- α Is a Critical Protein for Antisense Oligonucleotide-Mediated Silencing in Mammalian Cells. *Mol. Ther.* **2016**, *24*, 1117–1125.
 332. Castanotto, D. *et al.* A Cytoplasmic Pathway for Gapmer Antisense Oligonucleotide-Mediated Gene Silencing in Mammalian Cells. *Nucleic Acids Res.* **2015**, *43*, 9350–9361.
 333. Erazo-Oliveras, A. *et al.* The Late Endosome and Its Lipid BMP Act as Gateways for Efficient Cytosolic Access of the Delivery Agent DfTAT and Its Macromolecular Cargos. *Cell Chem. Biol.* **2016**, *23*, 598–607.
 334. Croke, S. T.; Wang, S.; Vickers, T. A.; Shen, W.; Liang, X. Cellular Uptake and Trafficking of Antisense Oligonucleotides. *Nat. Biotechnol.* **2017**, *35*, 230–237.
 335. Juliano, R. L.; Ming, X.; Carver, K.; Laing, B. Cellular Uptake and Intracellular Trafficking of Oligonucleotides: Implications for Oligonucleotide Pharmacology. *Nucleic Acid Ther.* **2014**, *24*, 101–113.
 336. Juliano, R. L. *et al.* Structure-Activity Relationships and Cellular Mechanism of Action of Small Molecules That Enhance the Delivery of Oligonucleotides. *Nucleic Acids Res.* **2018**, *46*, 1601–1613.
 337. Van de Vyver, T. *et al.* Cationic Amphiphilic Drugs Boost the Lysosomal Escape of Small Nucleic Acid Therapeutics in a Nanocarrier-Dependent Manner. *ACS Nano* **2020**, *14*, 4774–4791.
 338. Siomi, H.; Siomi, M. C. RISC Hitches onto Endosome Trafficking. *Nat. Cell Biol.* **2009**, *11*, 1049–1051.
 339. Gibbings, D. J.; Ciaudo, C.; Erhardt, M.; Voinnet, O. Multivesicular Bodies Associate with Components of MiRNA Effector Complexes and Modulate MiRNA Activity. *Nat. Cell Biol.* **2009**, *11*, 1143–1149.
 340. Lee, Y. S. *et al.* Silencing by Small RNAs Is Linked to Endosomal Trafficking. *Nat. Cell Biol.* **2009**, *11*, 1150–1156.

341. Raiborg, C.; Wenzel, E. M.; Stenmark, H. ER–Endosome Contact Sites: Molecular Compositions and Functions. *EMBO J.* **2015**, *34*, 1848–1858.
342. Stalder, L. *et al.* The Rough Endoplasmatic Reticulum Is a Central Nucleation Site of SiRNA-Mediated RNA Silencing. *EMBO J.* **2013**, *32*, 1115–1127.
343. Nechaev, S. *et al.* Intracellular Processing of Immunostimulatory CpG-SiRNA: Toll-like Receptor 9 Facilitates SiRNA Dicing and Endosomal Escape. *J. Control. Release* **2013**, *170*, 307–315.
344. Tamari, F.; Chen, F. W.; Li, C.; Chaudhari, J.; Ioannou, Y. A. PKC Activation in Niemann Pick C1 Cells Restores Subcellular Cholesterol Transport. *PLoS One* **2013**, *8*, e74169.
345. Ng Yan Hing, J. D.; Desjardins, M.; Descoteaux, A. Proteomic Analysis Reveals a Role for Protein Kinase C- α in Phagosome Maturation. *Biochem. Biophys. Res. Commun.* **2004**, *319*, 810–816.
346. Hempel, A. *et al.* High Glucose Concentrations Increase Endothelial Cell Permeability *via* Activation of Protein Kinase C α . *Circ. Res.* **1997**, *81*, 363–371.
347. Khan, W. A.; Blobbe, G. C.; Hannunt, Y. A. Activation of Protein Kinase C by Oleic Acid. *J. Biol. Chem.* **1992**, *267*, 3605–3612.
348. W A Khan, G Blobbe, A Halpern, W Taylor, W C Wetsel, D Burns, C. L. and Y. A. H. Selective Regulation of Protein Kinase C Isoenzymes by Oleic Acid in Human Platelets. *J. Biol. Chem.* **1993**, *268*, 5063–5068.
349. Souleimanian, N. *et al.* Antisense 2'-Deoxy, 2'-Fluoroarabino Nucleic Acid (2'F-ANA) Oligonucleotides: *In Vitro* Gymnotic Silencers of Gene Expression Whose Potency Is Enhanced by Fatty Acids. *Mol. Ther. - Nucleic Acids* **2012**, *1*, e43.
350. Khaled, Z.; Ho, Y. Y.; Benimetskaya, L.; Deckelbaum, R. J.; Stein, C. A. ω -6 Polyunsaturated Fatty Acid-Stimulated Cellular Internalization of Phosphorothioate Oligodeoxynucleotides. Evidence for Protein Kinase C- ζ Dependency. *Biochem. Pharmacol.* **1999**, *58*, 411–423.
351. Zhang, X.; Castanotto, D.; Liu, X.; Shemi, A.; Stein, C. A. Ammonium and Arsenic Trioxide Are Potent Facilitators of Oligonucleotide Function When Delivered by Gymnosis. *Nucleic Acids Res.* **2018**, *46*, 3612–3624.
352. Jacquin, E. *et al.* Pharmacological Modulators of Autophagy Activate a Parallel Noncanonical Pathway Driving Unconventional LC3 Lipidation. *Autophagy* **2017**, *13*, 854–867.
353. Dröse, S.; Altendorf, K. Bafilomycins and Concanamycins as Inhibitors of V-ATPases and P-ATPases. *J. Exp. Biol.* **1997**, *200*.
354. Ciftci, K.; Levy, R. J. Enhanced Plasmid DNA Transfection with Lysosomotropic Agents in Cultured Fibroblasts. *Int. J. Pharm.* **2001**, *218*, 81–92.
355. Shewring, L. *et al.* A Nonviral Vector System for Efficient Gene Transfer to Corneal Endothelial Cells *via* Membrane Integrins. *Transplantation* **1997**, *64*, 763–769.
356. Collins, L.; Asuni, A. A.; Anderton, B. H.; Fabre, J. W. Efficient Gene Delivery to Primary Neuron Cultures Using a Synthetic Peptide Vector System. *J. Neurosci. Methods* **2003**, *125*, 113–120.
357. Collins, L.; Fabre, J. W. A Synthetic Peptide Vector System for Optimal Gene Delivery to Corneal Endothelium. *J. Gene Med.* **2004**, *6*, 185–194.
358. Zhang, X. *et al.* *In Vivo* Gene Delivery *via* Portal Vein and Bile Duct to Individual Lobes of the Rat Liver Using a Polylysine-Based Nonviral DNA Vector in Combination with Chloroquine. *Hum. Gene Ther.* **2001**, *12*, 2179–2190.
359. Bhattarai, S. R. *et al.* Enhanced Gene and SiRNA Delivery by Polycation-Modified Mesoporous Silica Nanoparticles Loaded with Chloroquine. *Pharm. Res.* **2010**, *27*, 2556–2568.
360. Soundara Manickam, D.; Bisht, H. S.; Wan, L.; Mao, G.; Oupicky, D. Influence of TAT-Peptide Polymerization on Properties and Transfection Activity of TAT/DNA Polyplexes. *J. Control. Release* **2005**, *102*, 293–306.
361. Kilk, K. *et al.* Evaluation of Transportan 10 in PEI Mediated Plasmid Delivery Assay. *J. Control. Release* **2005**, *103*, 511–523.
362. Wang, J. *et al.* Autophagy-Inhibiting Polymer as an Effective Nonviral Cancer Gene Therapy Vector with Inherent Apoptosis-Sensitizing Ability. *Biomaterials* **2020**, *255*, 120156.
363. Erbacher, P.; Roche, A. C.; Monsigny, M.; Midoux, P. Putative Role of Chloroquine in Gene

- Transfer into a Human Hepatoma Cell Line by DNA/Lactosylated Polylysine Complexes. *Exp. Cell Res.* **1996**, *225*, 186–194.
364. Jeon, E.; Kim, H.-D.; Kim, J.-S. Pluronic-Grafted Poly-(L)-Lysine as a New Synthetic Gene Carrier. *J. Biomed. Mater. Res.* **2003**, *66A*, 854–859.
365. Katav, T. *et al.* Modified Pectin-Based Carrier for Gene Delivery: Cellular Barriers in Gene Delivery Course. *J. Control. Release* **2008**, *130*, 183–191.
366. Forrest, M. L.; Pack, D. W. On the Kinetics of Polyplex Endocytic Trafficking: Implications for Gene Delivery Vector Design. *Mol. Ther.* **2002**, *6*, 57–66.
367. Wadhwa, M. S.; Rice, K. G.; Knoell, D. L.; Young, A. P. Targeted Gene Delivery with a Low Molecular Weight Glycopeptide Carrier. *Bioconjug. Chem.* **1995**, *6*, 283–291.
368. Tusup, Marina, French, Lars E, Guenova, Emmanuella, Kundig, Thomas, Pascolo, S. Chloroquine Enhances Expression of Lipofected lvt-MRNA. *J. Pharmacol. Clin. Toxicol.* **2018**, *6*, 1117.
369. El-Andaloussi, S.; Johansson, H. J.; Lundberg, P.; Langel, Ü. Induction of Splice Correction by Cell-Penetrating Peptide Nucleic Acids. *J. Gene Med.* **2006**, *8*, 1262–1273.
370. Abes, S. *et al.* Endosome Trapping Limits the Efficiency of Splicing Correction by PNA-Oligolysine Conjugates. *J. Control. Release* **2006**, *110*, 595–604.
371. Turner, J. J. *et al.* Cell-Penetrating Peptide Conjugates of Peptide Nucleic Acids (PNA) as Inhibitors of HIV-1 Tat-Dependent Trans-Activation in Cells. *Nucleic Acids Res.* **2005**, *33*, 6837–6849.
372. Orellana, E. A. *et al.* Enhancing MicroRNA Activity through Increased Endosomal Release Mediated by Nigericin. *Mol. Ther. - Nucleic Acids* **2019**, *16*, 505–518.
373. Xie, Y. *et al.* Synthesis and Evaluation of Chloroquine-Containing DMAEMA Copolymers as Efficient Anti-MiRNA Delivery Vectors with Improved Endosomal Escape and Antimigratory Activity in Cancer Cells. *Macromol. Biosci.* **2018**, *18*, 1700194.
374. Stremersch, S. *et al.* Comparing Exosome-like Vesicles with Liposomes for the Functional Cellular Delivery of Small RNAs. *J. Control. Release* **2016**, *232*, 51–61.
375. Yu, H. *et al.* Reversal of Lung Cancer Multidrug Resistance by PH-Responsive Micelleplexes Mediating Co-Delivery of SiRNA and Paclitaxel. *Macromol. Biosci.* **2014**, *14*, 100–109.
376. Perche, F. *et al.* Hydroxychloroquine-Conjugated Gold Nanoparticles for Improved SiRNA Activity. *Biomaterials* **2016**, *90*, 62–71.
377. El Andaloussi, S. *et al.* Design of a Peptide-Based Vector, PepFect6, for Efficient Delivery of SiRNA in Cell Culture and Systemically *in Vivo*. *Nucleic Acids Res.* **2011**, *39*, 3972–3987.
378. Pärnaste, L.; Arukuusk, P.; Langel, K.; Tenson, T.; Langel, Ü. The Formation of Nanoparticles between Small Interfering RNA and Amphipathic Cell-Penetrating Peptides. *Mol. Ther. - Nucleic Acids* **2017**, *7*, 1–10.
379. Xie, Y.; Killinger, B.; Moszczynska, A.; Merkel, O. M. Targeted Delivery of SiRNA to Transferrin Receptor Overexpressing Tumor Cells *via* Peptide Modified Polyethylenimine. *Molecules* **2016**, *21*, 1334.
380. Rangasamy, L. *et al.* New Mechanism for Release of Endosomal Contents: Osmotic Lysis *via* Nigericin-Mediated K⁺/H⁺ Exchange. *Bioconjug. Chem.* **2018**, *29*, 1047–1059.
381. Yang, J.; Chen, H.; Vlahov, I. R.; Cheng, J. X.; Low, P. S. Evaluation of Disulfide Reduction during Receptor-Mediated Endocytosis by Using FRET Imaging. *Proc. Natl. Acad. Sci. U. S. A.* **2006**, *103*, 13872–13877.
382. Veldhoen, S.; Laufer, S. D.; Trampe, A.; Restle, T. Cellular Delivery of Small Interfering RNA by a Non-Covalently Attached Cell-Penetrating Peptide: Quantitative Analysis of Uptake and Biological Effect. *Nucleic Acids Res.* **2006**, *34*, 6561–6573.
383. Wang, L.; MacDonald, R. C. Effects of Microtubule-Depolymerizing Agents on the Transfection of Cultured Vascular Smooth Muscle Cells: Enhanced Expression with Free Drug and Especially with Drug-Gene Lipoplexes. *Mol. Ther.* **2004**, *9*, 729–737.
384. Wang, M.; Li, X.; Ma, Y.; Gu, H. Endosomal Escape Kinetics of Mesoporous Silica-Based System for Efficient SiRNA Delivery. *Int. J. Pharm.* **2013**, *448*, 51–57.

385. Mochizuki, S. *et al.* The Role of the Helper Lipid Dioleoylphosphatidylethanolamine (DOPE) for DNA Transfection Cooperating with a Cationic Lipid Bearing Ethylenediamine. *Biochim. Biophys. Acta - Biomembr.* **2013**, *1828*, 412–418.
386. Yongliang Chu, Malek Masoud, G. G. US7479573B2 Transfection Reagents, January 20, 2009.
387. Chen, Q. R.; Zhang, L.; Stass, S. A.; Mixson, A. J. Branched Co-Polymers of Histidine and Lysine Are Efficient Carriers of Plasmids. *Nucleic Acids Res.* **2001**, *29*, 1334–1340.
388. Yu, H. *et al.* Overcoming Endosomal Barrier by Amphotericin B-Loaded Dual PH-Responsive PDMA- b-PDPA Micelleplexes for siRNA Delivery. *ACS Nano* **2011**, *5*, 9246–9255.
389. Li, W. *et al.* Murine Hermansky-Pudlak Syndrome Genes: Regulators of Lysosome-Related Organelles. *BioEssays* **2004**, *26*, 616–628.
390. Nair, R. R.; Rodgers, J. R.; Schwarz, L. A. Enhancement of Transgene Expression by Combining Glucocorticoids and Anti-Mitotic Agents during Transient Transfection Using DNA-Cationic Liposomes. *Mol. Ther.* **2002**, *5*, 455–462.
391. Chowdhury, N. R. *et al.* Microtubular Disruption Prolongs the Expression of Human Bilirubin-Uridinediphosphoglucuronate-Glucuronosyltransferase-1 Gene Transferred into Gunn Rat Livers. *J. Biol. Chem.* **1996**, *271*, 2341–2346.
392. Lindberg, J.; Fernandez, M. A. M.; Ropp, J. D.; Hamm-Alvarez, S. F. Nocodazole Treatment of CV-1 Cells Enhances Nuclear/Perinuclear Accumulation of Lipid-DNA Complexes and Increases Gene Expression. *Pharm. Res.* **2001**, *18*, 246–249.
393. Cardarelli, F. *et al.* The Intracellular Trafficking Mechanism of Lipofectamine-Based Transfection Reagents and Its Implication for Gene Delivery. *Sci. Rep.* **2016**, *6*, 25879.
394. Hasegawa, S.; Hirashima, N.; Nakanishi, M. Microtubule Involvement in the Intracellular Dynamics for Gene Transfection Mediated by Cationic Liposomes. *Gene Ther.* **2001**, *8*, 1669–1673.
395. Vaughan, E. E. *et al.* Microtubule Acetylation through HDAC6 Inhibition Results in Increased Transfection Efficiency. *Mol. Ther.* **2008**, *16*, 1841–1847.
396. Drake, D. M.; Pack, D. W. Biochemical Investigation of Active Intracellular Transport of Polymeric Gene-Delivery Vectors. *J. Pharm. Sci.* **2008**, *97*, 1399–1413.
397. Ho, Y. K.; Zhou, L. H.; Tam, K. C.; Too, H. P. Enhanced Non-Viral Gene Delivery by Coordinated Endosomal Release and Inhibition of β -Tubulin Deacetylase. *Nucleic Acids Res.* **2017**, *45*, e38–e38.
398. Barua, S.; Rege, K. The Influence of Mediators of Intracellular Trafficking on Transgene Expression Efficacy of Polymer-Plasmid DNA Complexes. *Biomaterials* **2010**, *31*, 5894–5902.
399. Mooren, O. L.; Galletta, B. J.; Cooper, J. A. Roles for Actin Assembly in Endocytosis. *Annu. Rev. Biochem.* **2012**, *81*, 661–686.
400. dos Santos, T.; Varela, J.; Lynch, I.; Salvati, A.; Dawson, K. A. Effects of Transport Inhibitors on the Cellular Uptake of Carboxylated Polystyrene Nanoparticles in Different Cell Lines. *PLoS One* **2011**, *6*, e24438.
401. Francia, V. *et al.* Corona Composition Can Affect the Mechanisms Cells Use to Internalize Nanoparticles. *ACS Nano* **2019**, *13*, 11107–11121.
402. Wang, J. *et al.* Tumor Priming Enhances siRNA Delivery and Transfection in Intraperitoneal Tumors. *J. Control. Release* **2014**, *178*, 79–85.
403. Wang, J. *et al.* Paclitaxel Tumor Priming Promotes Delivery and Transfection of Intravenous Lipid-siRNA in Pancreatic Tumors. *J. Control. Release* **2015**, *216*, 103–110.
404. Lu, D.; Wientjes, M. G.; Lu, Z.; Au, J. L. S. Tumor Priming Enhances Delivery and Efficacy of Nanomedicines. *J. Pharmacol. Exp. Ther.* **2007**, *322*, 80–88.
405. Saraswathy, M.; Gong, S. Recent Developments in the Co-Delivery of siRNA and Small Molecule Anticancer Drugs for Cancer Treatment. *Mater. Today* **2014**, *17*, 298–306.
406. Yin, T.; Wang, L.; Yin, L.; Zhou, J.; Huo, M. Co-Delivery of Hydrophobic Paclitaxel and Hydrophilic AURKA Specific siRNA by Redox-Sensitive Micelles for Effective Treatment of Breast Cancer. *Biomaterials* **2015**, *61*, 10–25.
407. Zhu, H. *et al.* Combined Modality Therapy Based on Hybrid Gold Nanostars Coated with

- Temperature Sensitive Liposomes to Overcome Paclitaxel-Resistance in Hepatic Carcinoma. *Pharmaceutics* **2019**, *11*, 683.
408. Sun, T. M. *et al.* Simultaneous Delivery of siRNA and Paclitaxel via a “Two-in-One” Micelleplex Promotes Synergistic Tumor Suppression. *ACS Nano* **2011**, *5*, 1483–1494.
409. Reddy, T. L. *et al.* Simultaneous Delivery of Paclitaxel and Bcl-2 siRNA via PH-Sensitive Liposomal Nanocarrier for the Synergistic Treatment of Melanoma. *Sci. Rep.* **2016**, *6*, 1–12.
410. Yang, X. *et al.* MDR1 siRNA Loaded Hyaluronic Acid-Based CD44 Targeted Nanoparticle Systems Circumvent Paclitaxel Resistance in Ovarian Cancer. *Sci. Rep.* **2015**, *5*, 1–9.
411. Yadav, S.; Van Vlerken, L. E.; Little, S. R.; Amiji, M. M. Evaluations of Combination MDR-1 Gene Silencing and Paclitaxel Administration in Biodegradable Polymeric Nanoparticle Formulations to Overcome Multidrug Resistance in Cancer Cells. *Cancer Chemother. Pharmacol.* **2009**, *63*, 711–722.
412. Liu, W. *et al.* CS-PEI/Beclin-siRNA Downregulate Multidrug Resistance Proteins and Increase Paclitaxel Therapeutic Efficacy against NSCLC. *Mol. Ther. - Nucleic Acids* **2019**, *17*, 477–490.
413. Lee, S. H.; Lee, J. Y.; Kim, J. S.; Park, T. G.; Mok, H. Amphiphilic siRNA Conjugates for Co-Delivery of Nucleic Acids and Hydrophobic Drugs. *Bioconjug. Chem.* **2017**, *28*, 2051–2061.
414. Alouf, J.; Ladant, D.; Popoff, M. *The Comprehensive Sourcebook of Bacterial Protein Toxins*; Elsevier Inc., **2015**.
415. Stechmann, B. *et al.* Inhibition of Retrograde Transport Protects Mice from Lethal Ricin Challenge. *Cell* **2010**, *141*, 231–242.
416. Sandvig, K.; Skotland, T.; Van Deurs, B.; Klok, T. I. Retrograde Transport of Protein Toxins through the Golgi Apparatus. *Histochem. Cell Biol.* **2013**, *140*, 317–326.
417. Sandvig, K.; Van Deurs, B. Endocytosis, Intracellular Transport, and Cytotoxic Action of Shiga Toxin and Ricin. *Physiol. Rev.* **1996**, *76*, 949–966.
418. Mallard, F. *et al.* Direct Pathway from Early/Recycling Endosomes to the Golgi Apparatus Revealed through the Study of Shiga Toxin B-Fragment Transport. *J. Cell Biol.* **1998**, *143*, 973–990.
419. Liu, X.; Tsai, B. Ubqln4 Facilitates Endoplasmic Reticulum-to-Cytosol Escape of a Nonenveloped Virus during Infection. *J. Virol.* **2020**, *94*, e00103-20.
420. Ming, X. *et al.* The Small Molecule Retro-1 Enhances the Pharmacological Actions of Antisense and Splice Switching Oligonucleotides. *Nucleic Acids Res.* **2013**, *41*, 3673–3687.
421. Agramunt, J.; Pedroso, E.; Kreda, S. M.; Juliano, R. L.; Grandas, A. Retro-1-Oligonucleotide Conjugates. Synthesis and Biological Evaluation. *Molecules* **2019**, *24*.
422. Yang, B. *et al.* Retro-1 Analogues Differentially Affect Oligonucleotide Delivery and Toxin Trafficking. *ChemMedChem* **2016**, *11*, 2506–2510.
423. Lartigue, J. de *et al.* PIKfyve Regulation of Endosome-Linked Pathways. *Traffic* **2009**, *10*, 883.
424. Vickers, T. A.; Crooke, S. T. Development of a Quantitative BRET Affinity Assay for Nucleic Acid-Protein Interactions. *PLoS One* **2016**, *11*, e0161930.
425. Liang, X. H.; Shen, W.; Sun, H.; Prakash, T. P.; Crooke, S. T. TCP1 Complex Proteins Interact with Phosphorothioate Oligonucleotides and Can Co-Localize in Oligonucleotide-Induced Nuclear Bodies in Mammalian Cells. *Nucleic Acids Res.* **2014**, *42*, 7819–7832.
426. Acharya, S.; Hill, R. A. High Efficacy Gold-KDEL Peptide-siRNA Nanoconstruct-Mediated Transfection in C2C12 Myoblasts and Myotubes. *Nanomedicine Nanotechnology, Biol. Med.* **2014**, *10*, 329–337.
427. Qiu, C. *et al.* Regulating Intracellular Fate of siRNA by Endoplasmic Reticulum Membrane-Decorated Hybrid Nanoplexes. *Nat. Commun.* **2019**, *10*, 1–14.
428. Ross, N. L.; Munsell, E. V.; Sabanayagam, C.; Sullivan, M. O. Histone-Targeted Polyplexes Avoid Endosomal Escape and Enter the Nucleus during Postmitotic Redistribution of ER Membranes. *Mol. Ther. - Nucleic Acids* **2015**, *4*, e226.
429. Qin, B. *et al.* Targeting DNA to Endoplasmic Reticulum Efficiently Enhances Gene Delivery and Therapy. *Nanoscale* **2020**, *12*, 18249.
430. Sakhtianchi, R. *et al.* Exocytosis of Nanoparticles from Cells: Role in Cellular Retention and

- Toxicity. *Adv. Colloid Interface Sci.* **2013**, 201–202, 18–29.
431. Dahiya, U. R.; Ganguli, M. Exocytosis - a Putative Road-Block in Nanoparticle and Nanocomplex Mediated Gene Delivery. *J. Control. Release* **2019**, 303, 67–76.
 432. Yanes, R. E. *et al.* Involvement of Lysosomal Exocytosis in the Excretion of Mesoporous Silica Nanoparticles and Enhancement of the Drug Delivery Effect by Exocytosis Inhibition. *Small* **2013**, 9, 697–704.
 433. Corvaglia, S.; Guarnieri, D.; Pompa, P. P. Boosting the Therapeutic Efficiency of Nanovectors: Exocytosis Engineering. *Nanoscale* **2017**, 9, 3757–3765.
 434. Takahashi, S. *et al.* Rab11 Regulates Exocytosis of Recycling Vesicles at the Plasma Membrane. *J. Cell Sci.* **2012**, 125, 4049–4057.
 435. Sandin, P.; Fitzpatrick, L. W.; Simpson, J. C.; Dawson, K. A. High-Speed Imaging of Rab Family Small GTPases Reveals Rare Events in Nanoparticle Trafficking in Living Cells. *ACS Nano* **2012**, 6, 1513–1521.
 436. Wang, H. *et al.* The Niemann-Pick C1 Inhibitor NP3.47 Enhances Gene Silencing Potency of Lipid Nanoparticles Containing siRNA. *Mol. Ther.* **2016**, 24, 2100–2108.
 437. Eltoukhy, A. A.; Sahay, G.; Cunningham, J. M.; Anderson, D. G. Niemann-Pick C1 Affects the Gene Delivery Efficacy of Degradable Polymeric Nanoparticles. *ACS Nano* **2014**, 8, 7905–7913.
 438. Shukla, R. S.; Jain, A.; Zhao, Z.; Cheng, K. Intracellular Trafficking and Exocytosis of a Multi-Component siRNA Nanocomplex. *Nanomedicine Nanotechnology, Biol. Med.* **2016**, 12, 1323–1334.
 439. Vermeulen, L. M. P. *et al.* Endosomal Size and Membrane Leakiness Influence Proton Sponge-Based Rupture of Endosomal Vesicles. *ACS Nano* **2018**, 12, 2332–2345.
 440. van der Goot, F. G.; Gruenberg, J. Intra-Endosomal Membrane Traffic. *Trends Cell Biol.* **2006**, 16, 514–521.
 441. Pasqual, G.; Rojek, J. M.; Masin, M.; Chatton, J.-Y.; Kunz, S. Old World Arenaviruses Enter the Host Cell *via* the Multivesicular Body and Depend on the Endosomal Sorting Complex Required for Transport. *PLoS Pathog.* **2011**, 7, e1002232.
 442. Kobayashi, T. *et al.* Separation and Characterization of Late Endosomal Membrane Domains. *J. Biol. Chem.* **2002**, 277, 32157–32164.
 443. Bissig, C.; Gruenberg, J. Lipid Sorting and Multivesicular Endosome Biogenesis. *Cold Spring Harb. Perspect. Biol.* **2013**, 5.
 444. Bissig, C.; Gruenberg, J. Special Issue: Membrane Trafficking ALIX and the Multivesicular Endosome: ALIX in Wonderland. *Trends Cell Biol.* **2014**, 24, 19–25.
 445. Brock, D. J. *et al.* Efficient Cell Delivery Mediated by Lipid-Specific Endosomal Escape of Supercharged Branched Peptides. *Traffic* **2018**, 19, 421–435.
 446. Wang, S.; Allen, N.; Liang, X.; Crooke, S. T. Membrane Destabilization Induced by Lipid Species Increases Activity of Phosphorothioate-Antisense Oligonucleotides. *Mol. Ther. - Nucleic Acids* **2018**, 13, 686–698.
 447. Wang, S.; Allen, N.; Prakash, T. P.; Liang, X. H.; Crooke, S. T. Lipid Conjugates Enhance Endosomal Release of Antisense Oligonucleotides into Cells. *Nucleic Acid Ther.* **2019**, 29, 245–255.
 448. Allen, J. *et al.* Cytosolic Delivery of Macromolecules in Live Human Cells Using the Combined Endosomal Escape Activities of a Small Molecule and Cell Penetrating Peptides. *ACS Chem. Biol.* **2019**, acschembio.9b00585.
 449. Heath, N. *et al.* Endosomal Escape Enhancing Compounds Facilitate Functional Delivery of Extracellular Vesicle Cargo. *Nanomedicine* **2019**, nnm-2019-0061.
 450. Andreoli, T. E. The Structure and Function of Amphotericin B-Cholesterol Pores in Lipid Bilayer Membranes. *Ann. N. Y. Acad. Sci.* **1974**, 235, 448–468.
 451. D’Astolfo, D. S. *et al.* Efficient Intracellular Delivery of Native Proteins. *Cell* **2015**, 161, 674–690.
 452. Joris, F. *et al.* Repurposing Cationic Amphiphilic Drugs as Adjuvants to Induce Lysosomal siRNA Escape in Nanogel Transfected Cells. *J. Control. Release* **2018**, 269, 266–276.

453. Zhang, X. *et al.* The *in Vivo* Use of Chloroquine to Promote Non-Viral Gene Delivery to the Liver *via* the Portal Vein and Bile Duct. *J. Gene Med.* **2003**, *5*, 209–218.
454. Daussy, C. F.; Wodrich, H. “Repair Me If You Can”: Membrane Damage, Response, and Control from the Viral Perspective. *Cells* **2020**, *9*, 2042.
455. Papadopoulos, C.; Kravic, B.; Meyer, H. Repair or Lysophagy: Dealing with Damaged Lysosomes. *J. Mol. Biol.* **2019**, *432*, 231–239.
456. Kondow-McConaghy, H. M. *et al.* Impact of the Endosomal Escape Activity of Cell-Penetrating Peptides on the Endocytic Pathway. *ACS Chem. Biol.* **2020**, *15*, 2355–2363.
457. Brock, D. J.; Kondow-McConaghy, H. M.; Hager, E. C.; Pellois, J. P. Endosomal Escape and Cytosolic Penetration of Macromolecules Mediated by Synthetic Delivery Agents. *Bioconjug. Chem.* **2019**, *30*, 293–304.
458. Papadopoulos, C.; Meyer, H. Detection and Clearance of Damaged Lysosomes by the Endo-Lysosomal Damage Response and Lysophagy. *Curr. Biol.* **2017**, *27*, R1330–R1341.
459. Kilchrist, K. V. *et al.* Gal8 Visualization of Endosome Disruption Predicts Carrier-Mediated Biologic Drug Intracellular Bioavailability. *ACS Nano* **2019**, *13*, 1136–1152.
460. Joshi, B. S.; de Beer, M. A.; Giepmans, B. N. G.; Zuhorn, I. S. Endocytosis of Extracellular Vesicles and Release of Their Cargo from Endosomes. *ACS Nano* **2020**, *14*, 4444–4455.
461. Skowyra, M. L.; Schlesinger, P. H.; Naismith, T. V.; Hanson, P. I. Triggered Recruitment of ESCRT Machinery Promotes Endolysosomal Repair. *Science (80-.)*. **2018**, *360*.
462. Scharf, B. *et al.* Annexin A2 Binds to Endosomes Following Organelle Destabilization by Particulate Wear Debris. *Nat. Commun.* **2012**, *3*, 1–10.
463. Scheffer, L. L. *et al.* Mechanism of Ca²⁺-Triggered ESCRT Assembly and Regulation of Cell Membrane Repair. *Nat. Commun.* **2014**, *5*, 5646.
464. Jia, J. *et al.* Galectin-3 Coordinates a Cellular System for Lysosomal Repair and Removal. *Dev. Cell* **2020**, *52*, 69-87.e8.
465. Radulovic, M. *et al.* ESCRT-mediated Lysosome Repair Precedes Lysophagy and Promotes Cell Survival. *EMBO J.* **2018**, *37*, e99753.
466. Gros, M.; Amigorena, S. Regulation of Antigen Export to the Cytosol during Cross-Presentation. *Front. Immunol.* **2019**, *10*, 41.
467. Zehner, M. *et al.* Mannose Receptor Polyubiquitination Regulates Endosomal Recruitment of P97 and Cytosolic Antigen Translocation for Cross-Presentation. *Proc. Natl. Acad. Sci. U. S. A.* **2011**, *108*, 9933–9938.
468. Chen, J. J. *et al.* Compromised Function of the ESCRT Pathway Promotes Endolysosomal Escape of Tau Seeds and Propagation of Tau Aggregation. *J. Biol. Chem.* **2019**, *294*, 18952–18966.
469. Joseph Ochaba, Andrew F. Powers, Kaitlyn A. Tremble, Sarah Greenlee, N. M. P.; John E. Matson, A. Robert MacLeod, S. G. and M. A. A Novel and Translational Role for Autophagy in Antisense Oligonucleotide Trafficking and Activity. *Nucleic Acids Res.* **2019**, *47*, 11284–11303.
470. Mizushima, N. Autophagy: Process and Function. *Genes Dev.* **2007**, *21*, 2861–2873.
471. Remaut, K.; Oorschot, V.; Braeckmans, K.; Klumperman, J.; De Smedt, S. C. Lysosomal Capturing of Cytoplasmic Injected Nanoparticles by Autophagy: An Additional Barrier to Non Viral Gene Delivery. *J. Control. Release* **2014**, *195*, 29–36.
472. Yu, L.; Chen, Y.; Tooze, S. A. Autophagy Pathway: Cellular and Molecular Mechanisms. *Autophagy* **2018**, *14*, 207–215.
473. Lahiri, V.; Hawkins, W. D.; Klionsky, D. J. What You (Self-) Eat: Autophagic Mechanisms That Modulate Metabolism. *Cell Metab.* **2019**, *29*, 803–826.
474. Ma, X. *et al.* Gold Nanoparticles Induce Autophagosome Accumulation through Size-Dependent Nanoparticle Uptake and Lysosome Impairment. *ACS Nano* **2011**, *5*, 8629–8639.
475. Chen, X. *et al.* Autophagy Induced by Calcium Phosphate Precipitates Targets Damaged Endosomes. *J. Biol. Chem.* **2014**, *289*, 11162–11174.
476. Man, N.; Chen, Y.; Zheng, F.; Zhou, W.; Wen, L. P. Induction of Genuine Autophagy by Cationic Lipids in Mammalian Cells. *Autophagy* **2010**, *6*, 449–454.

477. Gao, W. *et al.* Biochemical Isolation and Characterization of the Tubulovesicular LC3-Positive Autophagosomal Compartment. *J. Biol. Chem.* **2010**, *285*, 1371–1383.
478. Sarkar, S.; Korolchuk, V.; Renna, M.; Winslow, A.; Rubinsztein, D. C. Methodological Considerations for Assessing Autophagy Modulators: A Study with Calcium Phosphate Precipitates. *Autophagy* **2009**, *5*, 307–313.
479. Mo, R. H.; Zaro, J. L.; Ou, J. H. J.; Shen, W. C. Effects of Lipofectamine 2000/SiRNA Complexes on Autophagy in Hepatoma Cells. *Mol. Biotechnol.* **2012**, *51*, 1–8.
480. Wang, J. *et al.* Silica Nanoparticles Induce Autophagy Dysfunction *via* Lysosomal Impairment and Inhibition of Autophagosome Degradation in Hepatocytes. *Int. J. Nanomedicine* **2017**, *Volume 12*, 809–825.
481. Behzadi, S. *et al.* Cellular Uptake of Nanoparticles: Journey inside the Cell. *Chem. Soc. Rev.* **2017**, *46*, 4218–4244.
482. Xie, Z.; Klionsky, D. J. Autophagosome Formation: Core Machinery and Adaptations. *Nat. Cell Biol.* **2007**, *9*, 1102–1109.
483. Karaniasios, E.; Ktistakis, N. T.; Karaniasios, E.; Ktistakis, N. T. Autophagosome Formation. In *Autophagy at the Cell, Tissue and Organismal Level*; Springer International Publishing, **2016**; pp 35–50.
484. Vercauteren, D. *et al.* Dynamic Colocalization Microscopy to Characterize Intracellular Trafficking of Nanomedicines. *ACS Nano* **2011**, *5*, 7874–7884.
485. Song, W.; Ma, Z.; Zhang, Y.; Yang, C. Autophagy Plays a Dual Role during Intracellular SiRNA Delivery by Lipoplex and Polyplex Nanoparticles. *Acta Biomater.* **2017**, *58*, 196–204.
486. Zhong, X.; Panus, D.; Ji, W.; Wang, C. Modulating Polyplex-Mediated Gene Transfection by Small-Molecule Regulators of Autophagy. *Mol. Pharm.* **2015**, *12*, 932–940.
487. Anselmo, A. C.; Mitragotri, S. Nanoparticles in the Clinic: An Update. *Bioeng. Transl. Med.* **2019**, *4*.
488. Pavlova, N. N.; Thompson, C. B. The Emerging Hallmarks of Cancer Metabolism. *Cell Metab.* **2016**, *23*, 27–47.
489. Collier, H. A. Is Cancer a Metabolic Disease? *Am. J. Pathol.* **2014**, *184*, 4–17.
490. Hanahan, D.; Weinberg, R. A. Hallmarks of Cancer: The next Generation. *Cell* **2011**, *144*, 646–674.
491. Pópulo, H.; Lopes, J. M.; Soares, P. The MTOR Signalling Pathway in Human Cancer. *Int. J. Mol. Sci.* **2012**, *13*, 1886–1918.
492. Lange, A.; Corbett, A. H. Nuclear Pores and Nuclear Import/Export. In *Encyclopedia of Biological Chemistry: Second Edition*; Elsevier Inc., **2013**; pp 109–114.
493. Castanotto, D. *et al.* A Stress-Induced Response Complex (SIRC) Shuttles MiRNAs, SiRNAs, and Oligonucleotides to the Nucleus. *Proc. Natl. Acad. Sci. U. S. A.* **2018**, *115*, E5756–E5765.
494. Young, D. D.; Connelly, C. M.; Grohmann, C.; Deiters, A. Small Molecule Modifiers of MicroRNA MiR-122 Function for the Treatment of Hepatitis C Virus Infection and Hepatocellular Carcinoma. *J. Am. Chem. Soc.* **2010**, *132*, 7976–7981.
495. Shan, G. *et al.* A Small Molecule Enhances RNA Interference and Promotes MicroRNA Processing. *Nat. Biotechnol.* **2008**, *26*, 933–940.
496. Zhang, Q.; Zhang, C.; Xi, Z. Enhancement of RNAi by a Small Molecule Antibiotic Enoxacin. *Cell Res.* **2008**, *18*, 1077–1079.
497. Li, Y.; Ji, P.; Jin, P. Probing the MicroRNA Pathway with Small Molecules. *Bioorganic Med. Chem.* **2013**, *21*, 6119–6123.
498. Börner, K. *et al.* Robust RNAi Enhancement *via* Human Argonaute-2 Overexpression from Plasmids, Viral Vectors and Cell Lines. *Nucleic Acids Res.* **2013**, *41*, e199–e199.
499. Kendall, G. C. *et al.* Dantrolene Enhances Antisense-Mediated Exon Skipping in Human and Mouse Models of Duchenne Muscular Dystrophy. *Sci. Transl. Med.* **2012**, *4*, 164ra160-164ra160.
500. Wang, D. W. *et al.* Repurposing Dantrolene for Long-Term Combination Therapy to Potentiate Antisense-Mediated DMD Exon Skipping in the Mdx Mouse. *Mol. Ther. - Nucleic Acids* **2018**,

- 11, 180–191.
501. Barthélémy, F. *et al.* Targeting RyR Activity Boosts Antisense Exon 44 and 45 Skipping in Human DMD Skeletal or Cardiac Muscle Culture Models. *Mol. Ther. - Nucleic Acids* **2019**, *18*, 580–589.
 502. Hu, Y. *et al.* Guanine Analogues Enhance Antisense Oligonucleotide-Induced Exon Skipping in Dystrophin Gene *in Vitro* and *in Vivo*. *Mol. Ther.* **2010**, *18*, 812–818.
 503. O’Leary, D. A. *et al.* Identification of Small Molecule and Genetic Modulators of AON-Induced Dystrophin Exon Skipping by High-Throughput Screening. *PLoS One* **2009**, *4*, e8348.
 504. Chen, S. *et al.* Dexamethasone Prodrugs as Potent Suppressors of the Immunostimulatory Effects of Lipid Nanoparticle Formulations of Nucleic Acids. *J. Control. Release* **2018**, *286*, 46–54.
 505. Hornung, V. *et al.* Sequence-Specific Potent Induction of IFN- α by Short Interfering RNA in Plasmacytoid Dendritic Cells through TLR7. *Nat. Med.* **2005**, *11*, 263–270.
 506. Karikó, K.; Bhuyan, P.; Capodici, J.; Weissman, D. Small Interfering RNAs Mediate Sequence-Independent Gene Suppression and Induce Immune Activation by Signaling through Toll-Like Receptor 3. *J. Immunol.* **2004**, *172*, 6545–6549.
 507. Linares-Fernández, S.; Lacroix, C.; Exposito, J. Y.; Verrier, B. Tailoring mRNA Vaccine to Balance Innate/Adaptive Immune Response. *Trends Mol. Med.* **2020**, *26*, 311–323.
 508. Anderson, B. R. *et al.* Incorporation of Pseudouridine into mRNA Enhances Translation by Diminishing PKR Activation. *Nucleic Acids Res.* **2010**, *38*, 5884–5892.
 509. Zhong, Z. *et al.* mRNA Therapeutics Deliver a Hopeful Message. *Nano Today* **2018**, *23*, 16–39.
 510. Bell, G. D.; Yang, Y.; Leung, E.; Krissansen, G. W. mRNA Transfection by a Xentry-Protamine Cell-Penetrating Peptide Is Enhanced by TLR Antagonist E6446. *PLoS One* **2018**, *13*, e0201464.
 511. Kužnik, A. *et al.* Mechanism of Endosomal TLR Inhibition by Antimalarial Drugs and Imidazoquinolines. *J. Immunol.* **2011**, *186*, 4794–4804.
 512. Lamphier, M. *et al.* Novel Small Molecule Inhibitors of Tlr7 and Tlr9: Mechanism of Action and Efficacy *in Vivo*. *Mol. Pharmacol.* **2014**, *85*, 429–440.
 513. Awe, J. P.; Crespo, A. V.; Li, Y.; Kiledjian, M.; Byrne, J. A. BAY11 Enhances OCT4 Synthetic mRNA Expression in Adult Human Skin Cells. *Stem Cell Res. Ther.* **2013**, *4*, 15.
 514. Ohto, T. *et al.* Inhibition of the Inflammatory Pathway Enhances Both the *in Vitro* and *in Vivo* Transfection Activity of Exogenous *in Vitro*-Transcribed MRNAs Delivered by Lipid Nanoparticles. *Biol. Pharm. Bull.* **2019**, *42*, 299–302.
 515. Malone, R. W. *et al.* Dexamethasone Enhancement of Gene Expression after Direct Hepatic DNA Injection - PubMed. *J Biol Chem* . **1994**, *269*, 29903–29907.
 516. Tan, Y.; Li, S.; Pitt, B. R.; Huang, L. The Inhibitory Role of CpG Immunostimulatory Motifs in Cationic Lipid Vector-Mediated Transgene Expression *in Vivo*. *Hum. Gene Ther.* **1999**, *10*, 2153–2161.
 517. Togashi, R. *et al.* A Hepatic PDNA Delivery System Based on an Intracellular Environment Sensitive Vitamin E-Scaffold Lipid-like Material with the Aid of an Anti-Inflammatory Drug. *J. Control. Release* **2018**, *279*, 262–270.
 518. Braun, S. *et al.* *In Vitro* and *in Vivo* Effects of Glucocorticoids on Gene Transfer to Skeletal Muscle. *FEBS Lett.* **1999**, *454*, 277–282.
 519. Kelly, A. M.; Plautz, S. A.; Zempleni, J.; Pannier, A. K. Glucocorticoid Cell Priming Enhances Transfection Outcomes in Adult Human Mesenchymal Stem Cells. *Mol. Ther.* **2016**, *24*, 331–341.
 520. Abrams, M. T. *et al.* Evaluation of Efficacy, Biodistribution, and Inflammation for a Potent siRNA Nanoparticle: Effect of Dexamethasone Co-Treatment. *Mol. Ther.* **2010**, *18*, 171–180.
 521. Sadler, A. J.; Williams, B. R. G. Interferon-Inducible Antiviral Effectors. *Nat. Rev. Immunol.* **2008**, *8*, 559–568.
 522. Poleganov, M. A. *et al.* Efficient Reprogramming of Human Fibroblasts and Blood-Derived Endothelial Progenitor Cells Using Nonmodified RNA for Reprogramming and Immune Evasion. *Hum. Gene Ther.* **2015**, *26*, 751–766.

523. Yoshioka, N. *et al.* Efficient Generation of Human iPSCs by a Synthetic Self-Replicative RNA. *Cell Stem Cell* **2013**, *13*, 246–254.
524. Liu, Y.; Chin, J. M.; Choo, E. L.; Phua, K. K. L. Messenger RNA Translation Enhancement by Immune Evasion Proteins: A Comparative Study between EKB (Vaccinia Virus) and NS1 (Influenza A Virus). *Sci. Rep.* **2019**, *9*, 1–9.
525. Michel, T. *et al.* Efficient Reduction of Synthetic mRNA Induced Immune Activation by Simultaneous Delivery of B18R Encoding mRNA. *J. Biol. Eng.* **2019**, *13*, 40.
526. Lokugamage, M. P. *et al.* Mild Innate Immune Activation Overrides Efficient Nanoparticle-Mediated RNA Delivery. *Adv. Mater.* **2020**, *32*, 1904905.
527. Kirschman, J. L. *et al.* Characterizing Exogenous mRNA Delivery, Trafficking, Cytoplasmic Release and RNA–Protein Correlations at the Level of Single Cells. *Nucleic Acids Res.* **2017**, *45*, e113–e113.
528. Kawagishi-Kobayashi, M.; Cao, C.; Lu, J.; Ozato, K.; Dever, T. E. Pseudosubstrate Inhibition of Protein Kinase PKR by Swine Pox Virus C8L Gene Product. *Virology* **2000**, *276*, 424–434.
529. Phua, K. K. L.; Liu, Y.; Sim, S. H. Non-Linear Enhancement of mRNA Delivery Efficiencies by Influenza A Derived NS1 Protein Engendering Host Gene Inhibition Property. *Biomaterials* **2017**, *133*, 29–36.
530. Liu, Y.; Chia, Z. H.; Liew, J. N. M. H.; Or, S. M.; Phua, K. K. L. Modulation of mRNA Translation and Cell Viability by Influenza A Virus Derived Nonstructural Protein 1. *Nucleic Acid Ther.* **2018**, *28*, 200–208.
531. Wang, P. *et al.* Co-Delivery of NS1 and BMP2 MRNAs to Murine Pluripotent Stem Cells Leads to Enhanced BMP-2 Expression and Osteogenic Differentiation. *Acta Biomater.* **2020**, *108*, 337–346.
532. Weng, A. *et al.* Improved Intracellular Delivery of Peptide- and Lipid-Nanoplexes by Natural Glycosides. *J. Control. Release* **2015**, *206*, 75–90.
533. Barthelemy, F.; Wang, D.; Nelson, S. F.; Miceli, M. C. Validation and Detection of Exon Skipping Boosters in DMD Patient Cell Models and Mdx Mouse. In *Methods in Molecular Biology*; Humana Press Inc., **2018**; Vol. 1828, pp 309–326.

SUPPLEMENTARY INFORMATION

RNA interference (RNAi) is a highly evolutionary conserved cellular mechanism that allows the sequence-specific modulation of gene expression at the post-transcriptional level. By impeding messenger RNA (mRNA) translation, this endogenous process has an important function in *e.g.* the defense against viruses and/or foreign genetic material (*e.g.* transposons)¹. Although RNA gene silencing was first reported in plants in 1990 by Napoli *et al.*², it was only eight years later that Andrew Fire and Craig Mello unraveled the biological mechanism underlying RNAi (in *Caenorhabditis elegans*)³, for which they were jointly awarded the Nobel Prize in Physiology or Medicine in 2006⁴. The discovery in 2001 that such a gene silencing mechanism could also be triggered in mammalian cells by application of 21- and 22-nucleotide (nt) long double-stranded RNAs (dsRNAs, *i.e.* small interfering RNAs (siRNAs))^{5,6}, represented a crucial milestone for the development of RNAi-based therapeutics. Indeed, since then, multiple studies have explored the use of RNAi triggers both as a research lab tool and for therapeutic purposes⁷. Notably, in 2018, this resulted in the approval of the first siRNA-based therapeutic (Onpattro®) for the treatment of polyneuropathy in adult patients with hereditary transthyretin-mediated amyloidosis (hATTR)^{8,9}. For a detailed discussion on the crucial milestones and discoveries in the development of RNAi-based therapeutics, we refer the reader to **Chapter 5**.

The RNAi pathway can be activated by cytosolic located short dsRNA molecules such as microRNA (miRNA) and siRNA¹⁰. Although these RNAi triggers differ in their biogenesis and their mechanism of gene silencing, they both rely on common steps and enzymes involved in the pathway¹¹. While miRNAs originate from endogenously expressed transcripts, siRNAs are predominantly exogenous in origin. Indeed, in the early reports on RNAi or upon viral infection^{12,13}, large and exogenous dsRNA molecules are/were introduced in the cytosol, where a member of the RNase III family (the Dicer enzyme) cleaves the dsRNAs into duplexes of 21-23 nucleotides, called siRNAs. In this process, the transactivating response RNA-binding protein (TRBP) serves as a cofactor that binds the RNA substrate before processing by Dicer ('dicing') occurs. Next, these mature siRNA duplexes are integrated in the RNA-induced silencing complex (RISC). Following unwinding of the duplex in an ATP-dependent fashion, the sense strand is degraded, while the antisense strand guides the activated RISC towards complementary sequences in the target mRNA, enabling cleavage of the latter by the RISC-component Argonaute 2 (Ago2). The cleaved mRNA strands are then

further degraded by ribonucleases (RNases) in the cytosol^{7,14–16}. Notably, the activated RISC follows Michaelis-Menten kinetics¹⁷. Hence, a single siRNA-activated RISC has the ability to sequentially bind and cleave multiple mRNA targets, allowing potent gene silencing with only a few hundred siRNAs present in the cytosol¹⁵.

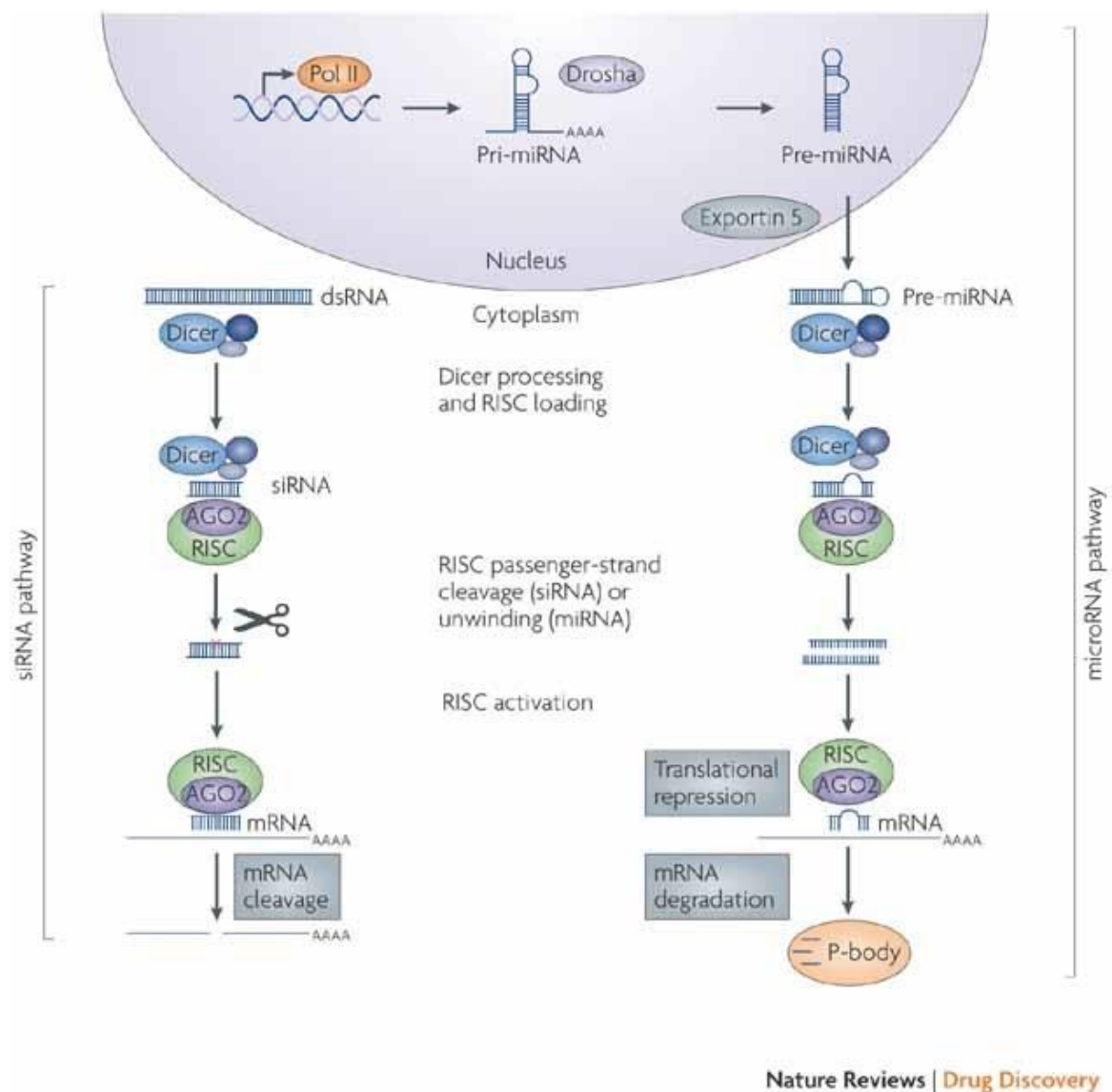


Figure S1. Mechanism of RNA interference (RNAi), by siRNAs and miRNAs, in mammalian cells. Both small interfering (si)RNAs and micro (mi)RNAs are able to induce post-transcriptional gene silencing *via* differing modes of action. Figure adapted from¹⁰.

In contrast to siRNAs, miRNAs are endogenously present in mammalian cells, as they are encoded in the genome¹⁸. Transcription *via* RNA polymerase II generates large RNA hairpins, termed primary miRNAs (pri-miRNAs). These pri-miRNAs are subsequently cropped by the microprocessor complex (a nuclear protein complex composed out of the RNase III-enzyme Droscha and the DiGeorge syndrome critical region gene 8 (DCGR8), which acts as a RNA-

binding cofactor) into 60-70 nt precursor miRNAs (pre-miRNAs). Following shuttling of the latter from the nucleus to the cytosol *via* Exportin-5, pre-miRNAs are diced into 18-25 nt miRNA duplexes. Similarly to siRNA, these miRNAs are loaded onto RISC, resulting in an activated RISC that binds its target mRNA. However, the mechanism to induce silencing differs between siRNAs and miRNAs. Indeed, while siRNAs require full complementarity with their target mRNA, miRNAs only require complementarity with the 'seed' region, which is a 6-8 nt long region at the 5' end of the guide strand^{19,20}. Only in the (rare) cases that miRNAs are fully complementary with the target mRNA, Ago2-directed cleavage will occur. In the case of semi-complementarity, mechanisms such as *e.g.* steric hindrance of ribosomes are believed to hamper mRNA translation. The mRNAs that undergo such a translational repression are finally targeted towards the cytoplasmic processing bodies (P-bodies) for degradation^{10,16,18,21,22}.

From a therapeutic perspective, multiple RNAi-based therapeutics have been explored. These include, next to synthetic (Dicer-substrate) siRNAs, also plasmid DNA (pDNA) encoding for short hairpin (sh)RNAs and miRNA mimics^{23,24}. Albeit the delivery of shRNA-encoding pDNA (*e.g. via* viral vectors) could result in prolonged and stable gene silencing^{25,26}, a useful trait in the treatment of chronic diseases, this approach also poses several concerns and challenges^{27,28}. First, pDNA has to cross the nuclear envelope to be functional, which remains one of the major bottlenecks during transfection²⁹. Secondly, the encoded shRNAs mimic the pre-miRNA intermediates, thus requiring further processing along the miRNA pathway^{27,28}. Hence, saturation of Exportin-5 or other downstream proteins/enzymes may disrupt the endogenous RNAi homeostasis, possibly resulting in adverse effects^{30,31}. Mimics of miRNAs, on the other hand, might be useful in *e.g.* multigenic diseases, since a single miRNA is able to affect the expression of multiple genes (see above). However, such an approach also increases the risk of off-target effects and, consequently, undesired gene knockdown^{11,32}. Taken together, as synthetic ~22 nt siRNA duplexes have a superior specificity compared to miRNAs, while not requiring extensive processing along the RNAi pathway (*e.g.* shRNA-encoding pDNA), these molecules constitute the most investigated type of RNAi-based therapeutics and the first to be finally approved in the clinic (see **Chapter 5**).

REFERENCES FOR SUPPORTING INFORMATION

1. Hannon, G. J. RNA Interference. *Nature* **2002**, *418*, 244–251.
2. Napoli, C.; Lemieux, C.; Jorgensen, R. Introduction of a Chimeric Chalcone Synthase Gene into Petunia Results in Reversible Co-Suppression of Homologous Genes in Trans. *Plant Cell* **1990**, *2*, 279–289.
3. Fire, A. *et al.* Potent and Specific Genetic Interference by Double-Stranded RNA in *Caenorhabditis Elegans*. *Nature* **1998**, *391*, 806–811.
4. Hopkin, M. RNAi Scoops Medical Nobel. *Nature* **2006**.
5. Caplen, N. J.; Parrish, S.; Imani, F.; Fire, A.; Morgan, R. A. Specific Inhibition of Gene Expression by Small Double-Stranded RNAs in Invertebrate and Vertebrate Systems. *Proc. Natl. Acad. Sci. U. S. A.* **2001**, *98*, 9742–9747.
6. Elbashir, S. M. *et al.* Duplexes of 21-Nucleotide RNAs Mediate RNA Interference in Cultured Mammalian Cells. *Nature* **2001**, *411*, 494–498.
7. Setten, R. L.; Rossi, J. J.; Han, S. ping. The Current State and Future Directions of RNAi-Based Therapeutics. *Nat. Rev. Drug Discov.* **2019**, *18*, 421–446.
8. Hoy, S. M. Patisiran: First Global Approval. *Drugs* **2018**, *78*, 1625–1631.
9. Akinc, A. *et al.* The Onpattro Story and the Clinical Translation of Nanomedicines Containing Nucleic Acid-Based Drugs. *Nat. Nanotechnol.* **2019**, *14*, 1084–1087.
10. de Fougères, A.; Vornlocher, H. P.; Maraganore, J.; Lieberman, J. Interfering with Disease: A Progress Report on siRNA-Based Therapeutics. *Nat. Rev. Drug Discov.* **2007**, *6*, 443–453.
11. Lam, J. K. W.; Chow, M. Y. T.; Zhang, Y.; Leung, S. W. S. siRNA versus miRNA as Therapeutics for Gene Silencing. *Mol. Ther. - Nucleic Acids* **2015**, *4*, e252.
12. Piatek, M. J.; Werner, A. Endogenous siRNAs: Regulators of Internal Affairs. *Biochem. Soc. Trans.* **2014**, *42*, 1174–1179.
13. Carthew, R. W.; Sontheimer, E. J. Origins and Mechanisms of miRNAs and siRNAs. *Cell* **2009**, *136*, 642–655.
14. Gavrillov, K.; Saltzman, W. M. Therapeutic siRNA: Principles, Challenges, and Strategies. *Yale J. Biol. Med.* **2012**, *85*, 187–200.
15. Wittrup, A.; Lieberman, J. Knocking down Disease: A Progress Report on siRNA Therapeutics. *Nat. Rev. Genet.* **2015**, *16*, 543–552.
16. Wilson, R. C.; Doudna, J. A. Molecular Mechanisms of RNA Interference. *Annu. Rev. Biophys.* **2013**, *42*, 217–239.
17. Haley, B.; Zamore, P. D. Kinetic Analysis of the RNAi Enzyme Complex. *Nat. Struct. Mol. Biol.* **2004**, *11*, 599–606.
18. O'Brien, J.; Hayder, H.; Zayed, Y.; Peng, C. Overview of MicroRNA Biogenesis, Mechanisms of Actions, and Circulation. *Front. Endocrinol. (Lausanne)*. **2018**, *9*, 402.
19. Ambros, V. The Functions of Animal MicroRNAs. *Nature* **2004**, *431*, 350–355.
20. Bartel, D. P. MicroRNAs: Genomics, Biogenesis, Mechanism, and Function. *Cell* **2004**, *116*, 281–297.
21. Ozcan, G.; Ozpolat, B.; Coleman, R. L.; Sood, A. K.; Lopez-Berestein, G. Preclinical and Clinical Development of siRNA-Based Therapeutics. *Adv. Drug Deliv. Rev.* **2015**, *87*, 108–119.
22. Liu, J.; Valencia-Sanchez, M. A.; Hannon, G. J.; Parker, R. MicroRNA-Dependent Localization of Targeted mRNAs to Mammalian P-Bodies. *Nat. Cell Biol.* **2005**, *7*, 719–723.
23. Kim, D. H.; Rossi, J. J. RNAi Mechanisms and Applications. *Biotechniques* **2008**, *44*, 613–616.
24. Weng, Y.; Xiao, H.; Zhang, J.; Liang, X. J.; Huang, Y. RNAi Therapeutic and Its Innovative Biotechnological Evolution. *Biotechnol. Adv.* **2019**, *37*, 801–825.
25. Vorhies, J. S.; Nemunaitis, J. Nonviral Delivery Vehicles for Use in Short Hairpin RNA-

- Based Cancer Therapies. *Expert Rev. Anticancer Ther.* **2007**, *7*, 373–382.
26. Manjunath, N.; Wu, H.; Subramanya, S.; Shankar, P. Lentiviral Delivery of Short Hairpin RNAs. *Adv. Drug Deliv. Rev.* **2009**, *61*, 732–745.
 27. Moore, C. B.; Guthrie, E. H.; Huang, M. T. H.; Taxman, D. J. Short Hairpin RNA (ShRNA): Design, Delivery, and Assessment of Gene Knockdown. *Methods Mol. Biol.* **2010**, *629*, 141–158.
 28. Rao, D. D.; Vorhies, J. S.; Senzer, N.; Nemunaitis, J. SiRNA vs. ShRNA: Similarities and Differences. *Adv. Drug Deliv. Rev.* **2009**, *61*, 746–759.
 29. Vermeulen, L. M. P.; Brans, T.; De Smedt, S. C.; Remaut, K.; Braeckmans, K. Methodologies to Investigate Intracellular Barriers for Nucleic Acid Delivery in Non-Viral Gene Therapy. *Nano Today* **2018**, *21*, 74–90.
 30. Grimm, D. *et al.* Fatality in Mice Due to Oversaturation of Cellular MicroRNA/Short Hairpin RNA Pathways. *Nature* **2006**, *441*, 537–541.
 31. Yi, R.; Qin, Y.; Macara, I. G.; Cullen, B. R. Exportin-5 Mediates the Nuclear Export of Pre-MicroRNAs and Short Hairpin RNAs. *Genes Dev.* **2003**, *17*, 3011–3016.
 32. Singh, S.; Narang, A. S.; Mahato, R. I. Subcellular Fate and Off-Target Effects of SiRNA, ShRNA, and MiRNA. *Pharm. Res.* **2011**, *28*, 2996–3015.

Chapter 2

Screening a drug repurposing library for adjuvants that induce lysosomal siRNA escape in nanogel transfected cells

This chapter is published as a part of:

Van de Vyver, T.[†]; Bogaert, B.[†]; De Backer, L.[†]; Joris, F.[†]; Guagliardo, R.[†]; Van Hoeck, J.[†]; Merckx, P.[†]; Van Calenbergh, S.[‡]; Ramishetti, S.^{§||⊥}; Peer, D.^{§||⊥}; Remaut, K.[†]; De Smedt, S.C.[†]; Raemdonck, K.[†] Cationic Amphiphilic Drugs Boost the Lysosomal Escape of Small Nucleic Acid Therapeutics in a Nanocarrier-Dependent Manner. *ACS Nano* **2020**, *14*, 4774–4791.

DOI: 10.1021/acsnano.0c00666

[†] Ghent Research Group on Nanomedicines, Laboratory of General Biochemistry and Physical Pharmacy, Faculty of Pharmaceutical Sciences, Ghent University, Ottergemsesteenweg 460, 9000 Ghent, Belgium

[‡] Laboratory for Medicinal Chemistry, Faculty of Pharmaceutical Sciences, Ghent University, Ottergemsesteenweg 460, 9000 Ghent, Belgium

[§] Laboratory of Precision NanoMedicine, School of Molecular Cell Biology and Biotechnology, George S.

Wise Faculty of Life Sciences; ^{||} Department of Materials Sciences and Engineering, Iby and Aladar

Fleischman Faculty of Engineering; [⊥] Center for Nanoscience and Nanotechnology, Cancer Biology Research Center, Tel Aviv University, Tel Aviv, 6997801, Israel

Author contributions

Conceptualization and study design: T.V.d.V., S.C.D.S., and K. Raemdonck. Experimental work and data analysis: T.V.d.V., L.D.B., R.G., F.J., and K. Raemdonck. S.V.C. contributed to the compound screen. Chapter 2 was written through contributions of all authors.

TABLE OF CONTENTS

1. INTRODUCTION	101
2. RESULTS AND DISCUSSION.....	104
2.1. Compound screen of NIH Clinical Collection on nanogel-transfected NSCLC cells	104
2.2. Secondary validation of the CADs ketotifen and loperamide	108
3. CONCLUSION	112
4. MATERIALS AND METHODS	113
4.1. siRNA duplexes.....	113
4.2. Nanogel (NG) synthesis, preparation and siRNA complexation	113
4.3. Cell lines and cell culture conditions	114
4.4. Compound library stock preparation and small molecules	114
4.5. NIHCC screening protocol	115
4.6. Hit identification procedure.....	116
4.7. Quantification of transfection efficiency/lysosomal volume of NG transfection and sequential adjuvant treatment by flow cytometry.....	116
4.8. Cell viability	117
4.9. Visualizing eGFP expression with confocal microscopy.....	117
4.10. Visualization and quantification of the cytosolic release of siCy5®	118
4.11. Phospholipidosis detection with LipidTOX™ Red	119
4.12. BODIPY™ FL C12-Sphingomyelin staining	119
4.13. Statistical analysis	120

ABSTRACT

Small nucleic acid (NA) therapeutics, such as small interfering RNA (siRNA), are generally formulated in nanoparticles (NPs) to overcome the multiple extra- and intracellular barriers upon *in vivo* administration. Interaction with target cells typically triggers endocytosis and sequesters the NPs in endosomes, thus hampering the pharmacological activity of the encapsulated siRNAs that occurs in the cytosol. Unfortunately, for most state-of-the-art NPs, endosomal escape is largely inefficient. As a result, the bulk of the endocytosed NA drug is rapidly trafficked towards the degradative lysosomes that are considered as a dead end for siRNA nanomedicines. Opposed to this paradigm, we recently reported that cationic amphiphilic drugs (CADs) could strongly promote functional siRNA delivery from the endolysosomal compartment *via* transient induction of lysosomal membrane permeabilization. However, only a limited number of CADs has been evaluated to date, raising the question if also other CADs share this delivery-promoting effect. In this chapter, we report on a drug repurposing screen (National Institutes of Health (NIH) Clinical Collection) that allowed identification of 56 CAD adjuvants that boost the intracellular delivery of polymeric nanogel-transfected siRNAs. However, not all CADs present in the primary screen were identified as delivery-enhancing compounds (*i.e* 'hits'). Hence, the contrasting effects of two CADs (a 'hit' and a 'no hit') on both the lysosomal phenotype and the cytosolic siRNA delivery were further validated. In conclusion, our study highlights that the observed adjuvant effect on siRNA delivery is not limited to the previously identified CAD molecules, but that many more CADs phenocopy these effects.

KEYWORDS: drug repurposing; cationic amphiphilic drugs; lysosomal membrane permeabilization; nucleic acid therapeutics; cellular delivery; endosomal escape

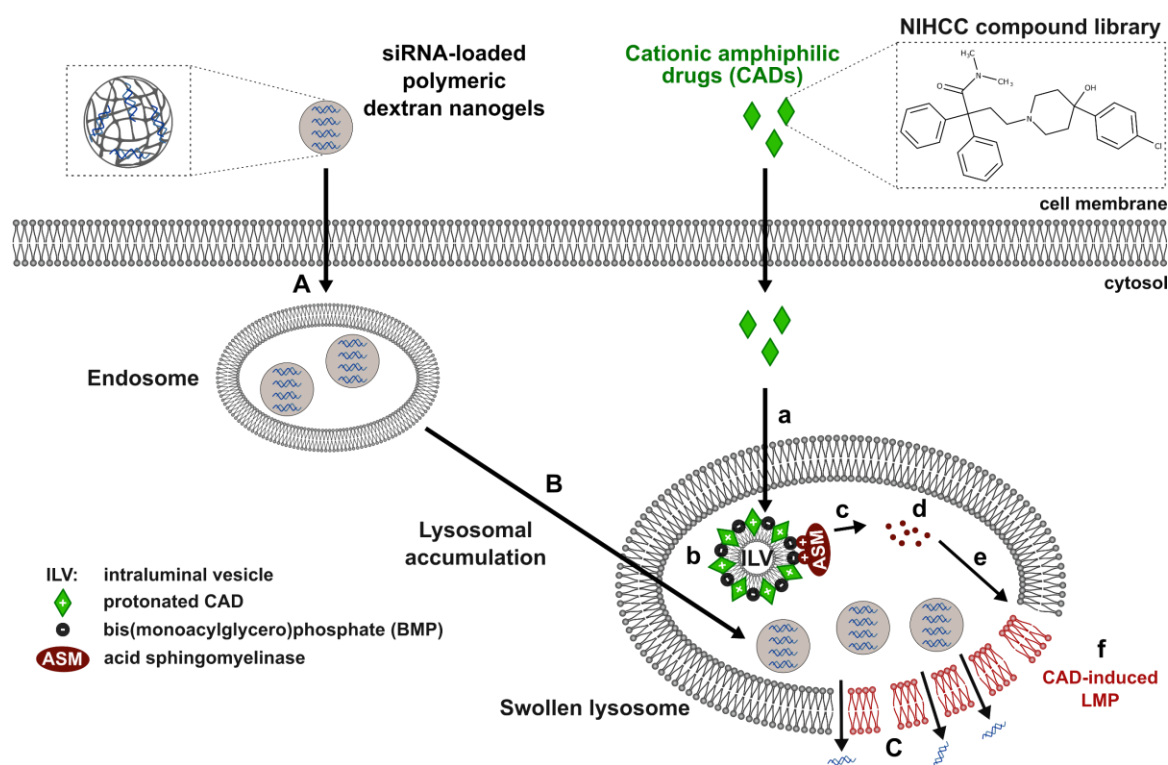
1. INTRODUCTION

Over the last two decades, the use of small interfering RNA (siRNA) therapeutics has gathered a lot of attention for the treatment of a plethora of diseases. SiRNAs activate the RNA interference (RNAi) machinery in the cytosol of target cells, enabling specific post-transcriptional knockdown of key disease-related genes¹⁻³. In theory, virtually all genes can be targeted, including those that were previously thought to be ‘undruggable’ by classical small molecule inhibitors or monoclonal antibodies upon expression⁴. Nevertheless, to reach their site of action in the cytosol, these nucleic acid (NA) drugs have to be formulated in suitable delivery systems (*e.g.* nanoparticles (NPs)) to overcome the numerous extra- and intracellular delivery barriers^{1,5,6}. Upon successful arrival at their target cells, NPs boost the intracellular uptake of NAs through endocytosis, resulting in endosomal sequestration of the NA cargo⁵⁻⁷. However, endosomal escape is necessary to achieve functional siRNA delivery^{1,7}. Unfortunately, this process remains one of the major bottlenecks, as recent studies have shown that only 1-2% of the endocytosed NA dose is typically released into the cytosol⁷⁻¹⁰. As a consequence, the vast majority of internalized NA drug accumulates in the lysosomes, where both NAs and NPs can be degraded^{8,9,11-14}.

Small molecular drugs have proven successful in facilitating (one or more steps) of the intracellular NA delivery process¹⁵⁻²⁵. Since the discovery of chloroquine as a small molecule endosomal escape enhancer in 1981, it was only in recent years that other NA delivery enhancers were identified^{15,17,24,25}. Recently, our group demonstrated that lysosomal sequestered siRNA can be released into the cytosol by exposing dextran nanogel-transfected non-small cell lung cancer (NSCLC) cells to selected cationic amphiphilic drugs (CADs)²¹. Due to their physicochemical properties, these drugs tend to accumulate inside the acidified lysosomal compartment where they functionally inhibit the acid sphingomyelinase (ASM) enzyme. ASM inhibition leads to a lysosomal storage disease phenotype characterized by phospholipidosis (PLD), lysosomal swelling and transient lysosomal membrane permeabilization (LMP), allowing the siRNA molecules to diffuse from the lysosomal lumen into the cytosol (**Scheme 1**)²¹. These data suggest that, in contrast to general belief, lysosomes should not be considered *per se* as a dead end for siRNA nanomedicines.

As many CADs are widely used (*e.g.* antihistamines, antidepressants,...) and have a well-documented safety profile, their repurposing as NA delivery enhancers could foster clinical translation of NA drugs. However, only a limited number of CADs has been evaluated to

date, raising the question if also other CADs share this adjuvant effect. Here, a drug repurposing screen was performed by applying the 'National Institutes of Health Clinical Collection' compound library (NIHCC) on the previously reported NSCLC cell model (with siRNA-loaded nanogels (siNGs) as model NPs)²¹. Our data revealed a strong enrichment of both CADs and PLD inducers in the hit group, correlating the lysosomotropic properties of CADs with the induction of an acquired lysosomal storage disease phenotype and improved cytosolic siRNA delivery. Although we identified 56 CADs that can promote intracellular delivery of dextran nanogel-transfected siRNAs, ~56% of the CADs in the primary screen were not identified as hits. Hence, the effects of both a 'CAD hit' and a 'CAD-no hit' were further investigated in secondary validation experiments. Interestingly, ~42% of the hit compounds did not comply to the applied CAD definition, which will be further investigated in **Chapter 4**.



Scheme 1. Cationic amphiphilic drugs (CADs) enhance the escape of siRNA from the lysosomes into the cytosol. (A) Most nanomedicines (*e.g.* dextran nanogels) are internalized by cells *via* an endocytic process and (B) are efficiently routed towards the lysosomal compartment. (C) A CAD-induced transient lysosomal membrane permeabilization (LMP) allows the siRNA molecules to diffuse from the lysosomal lumen into the cytosol (see **Chapter 3**). (a) CADs specifically accumulate in lysosomes due to their physicochemical (amphiphilic and weak basic) properties. (b) The cationic lysosomal membrane-associated enzyme acid sphingomyelinase (ASM) is electrostatically bound to the anionic bis(monoacylglycerol)phosphate (BMP) lipids of the intraluminal vesicles (ILVs). (c) Also the CADs become protonated inside the lysosomal lumen and they insert in intra-lysosomal membranes where they induce release of ASM into the lysosomal lumen, followed by (d) its degradation by cathepsins. As the ASM enzyme plays an important role in the lipid homeostasis, functional ASM inhibition leads to (e) lysosomal (phospho)lipidosis (PLD), lysosomal swelling and (f) a transient lysosomal membrane permeabilization (LMP)²¹.

2. RESULTS AND DISCUSSION

2.1. Compound screen of NIH Clinical Collection on nanogel-transfected

NSCLC cells

Our previous work disclosed four CADs with diverging chemical structure and pharmacology (*i.e.* nortriptyline, salmeterol, carvedilol and desloratadine) as siRNA delivery enhancers, when applied in a sequential manner to siRNA transfected cells²¹. To identify additional CADs with an adjuvant effect on the gene silencing potential of siRNA-loaded dex-HEMA nanogels (dex-HEMA siNGs) in NSCLC cells, we screened the NIH Clinical Collection compound library (NIHCC, 700 compounds) (**Figure 1A** and **Figure 1B**). A sequential (post-)treatment protocol with the compounds was used in these experiments, as pre-incubation was not able to promote gene knockdown (**Figure S1A**), despite clear indication that the applied CAD (*in casu* desloratadine (DES)) evoked the anticipated lysosomal swelling (**Figure S1B**). Applying desloratadine immediately after (post) or 20 h after transfection (20 h post) equally promoted the siNG-mediated enhanced green fluorescent protein (eGFP) knockdown. Given the lysosomal accumulation of siNGs demonstrated in earlier work and as CADs are described as lysosomotropic drugs, these results suggest that functional siRNA release mainly occurs from the lysosomal compartment^{11,26}. Although we previously showed that a 2 h desloratadine exposure is sufficient to promote siRNA delivery, a 20 h compound treatment was used in this screen, as the lysosomal accumulation kinetics are influenced by the compound's physicochemical properties^{21,27}. 'Minor' and 'major' hit compounds were defined as compounds that significantly promote siNG-mediated eGFP knockdown (*i.e.* a decrease in % eGFP expression of respectively more than 3 and 6 times the standard deviation (SD) on the percent of eGFP expression obtained with the siNG transfection alone, **Figure 1A** and **Figure S2A**). Using this protocol, 96 hit compounds that enhance the silencing potential of the siNGs were identified (58 'minor' and 38 'major' hits), with 56 compounds being CADs (calculated logP (clogP) > 3 and pKa1 > 6, **Table S1**)²⁸. The high hit rate of 13.7% indicates that physicochemical properties of the compounds may play an important role in the improved siRNA delivery, rather than the specific interaction of a compound with a molecular target²⁹. Interestingly, the 'hit' group was significantly enriched in CADs (**Figure 1C**, **Figure S2E**, **Table S1**), with diverging chemical structure and pharmacological activity. Many CADs are known as functional inhibitors of the lysosomal acid sphingomyelinase (FIASMAS) enzyme, which in part explains the concurrent enrichment in both documented

ASM inhibitors ('ASMi +', **Figure S2B**, **Figure S2E**) and phospholipidosis (PLD) inducers ('LipidTOX™ +', 'PLD +', **Figure S2C-E**)^{27,28,30,31}. Note that within the CAD group a clear positive correlation was found between the side scatter (SSC) signal, indicative of increased cellular granularity as a result of lysosomal swelling, and the siNG-mediated knockdown (**Figure 1D**)²¹. Moreover, the CADs in the hit group have a higher clogP (4.49 ± 1.08) compared to that of the CAD-no hit group (3.94 ± 0.73), whereas the pKa1 value was not significantly different (**Figure S2G**). This result suggests that the siRNA delivery-promoting effect is dependent on the degree of lysosomal accumulation and membrane insertion, which is facilitated by CAD lipophilicity^{27,32,33}. Although these data correlate CAD physicochemistry with the induction of an acquired lysosomal storage disease phenotype and improved siRNA delivery (**Figure 1D**), 72 of the 128 CADs (~56%) present in the screen were not identified as adjuvants at 20 μ M (**Figure S2E-F**), which corroborates earlier findings by us and others that not all CADs are FIASMAs, induce lysosomal membrane permeabilization (LMP) or are active in the same dose range^{21,27,34-37}. 'Cationic amphiphilic drugs' is considered an umbrella term for a class of pharmacologically and structurally very diverse compounds. As all compounds were added to the cells in serum-containing cell culture medium, differences in structure and physicochemical properties between the various CADs will affect protein binding and final endolysosomal concentration³⁸⁻⁴⁵. Previous compound screens have likewise shown that the presence of serum in the incubation medium can influence a molecule's cellular activity^{46,47}. In addition, it is conceivable that structural differences will also impact the efficiency with which the CADs insert in lysosomal membranes and induce an acquired lysosomal storage disease phenotype⁴⁸. Indeed, a recent study by Rhein *et al.* showed that subtle modifications of the structures of the CADs imipramine and desipramine (both 'CAD-hits' in our study, **Table S1**) could markedly change their ability to inhibit ASM and induce PLD⁴⁹. To investigate whether distinctive structural components could be unveiled in the various groups ('hits', 'no hits', 'CAD-hits', 'CAD-no hits'), the structures of all 700 NIHCC compounds were analyzed using a web-based principal component analysis (PCA)-tool that projects Morgan fingerprints, which are representations of the chemical structures of the compounds, into new sets of coordinates (PC1 and PC2; **Figure S2F**)⁵⁰. The 'CAD-hits' being randomly distributed across the PCA scatter plots, suggests that the chemical diversity of the 'CAD-hits' is not substantially different from the CADs that were not identified as hits. However, a more detailed structure-activity relationship falls beyond the scope of this manuscript. Although our data strongly suggests

that the CAD-induced LMP is a consequence of the functional inhibition of ASM, we cannot rule out the possibility that CADs might promote siRNA delivery *via* one or more alternative mechanisms. These could include proteolysis of other lysosomal lipases (*e.g.* acid ceramidase) and the ability of certain CADs to induce a direct detergent effect or to enhance reactive oxygen species (ROS) production^{35,51}. The extent to which these additional effects take place are likely different for each CAD, making an unambiguous correlation between CAD adjuvant effect and CAD-induced ASM inhibition especially difficult.

Most importantly, this compound screen highlights that the observed adjuvant effect on siRNA delivery is not limited to the previously identified CAD molecules (*i.e.* nortriptyline, carvedilol, salmeterol and desloratadine (DES)), but that many more physicochemical related compounds phenocopy these effects²¹.

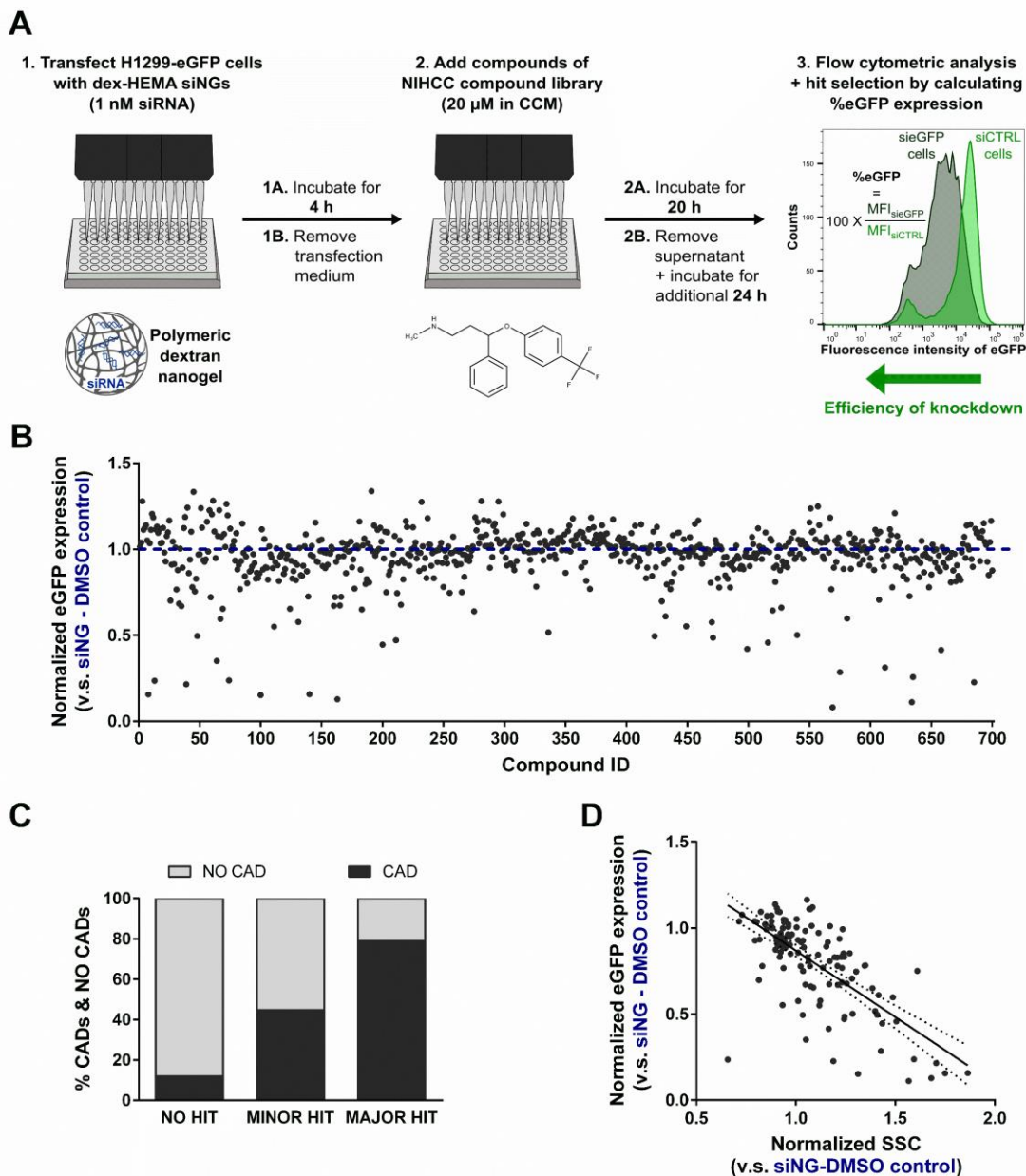


Figure 1. NIHCC compound library identifies multiple CADs as siRNA-delivery promoting compounds. (A) Schematic representation of the protocol used to classify NIHCC compounds as siRNA-delivery promoting compounds (*i.e.* 'hits'). The CAD fluoxetine is shown as an example of a hit. (B) NIHCC screen summary. The abscissa indicates the number of each compound screened. The ordinate indicates the sequential adjuvant effect of the screened compounds on the eGFP gene silencing potential of dex-HEMA siNGs (compound concentration = 20 μ M, 20 h incubation). The calculated % eGFP expression values of the individual compounds are normalized to the siNG transfection alone (siNG-DMSO control) of each plate. (C) The fraction of cationic amphiphilic drugs (CADs, $\text{clogP} > 3$ and $\text{pKa}1 > 6$) in the 'no hit', 'minor hit' and 'major hit' group, respectively. (D) Correlation between the SSC signal, normalized to the siNG-DMSO control of each plate, and the normalized eGFP expression (see above) in the group of CADs ($n = 128$). The dashed line represents the 95% confidence band of the regression line ($R^2 = 0.478$; $p < 0.0001$). (eGFP = enhanced green fluorescent protein, NG = dex-HEMA nanogels, siNG = siRNA-loaded NG, NIHCC = National Institutes of Health Clinical Collection, CAD = cationic amphiphilic drug, CCM = complete cell culture medium,

siNG-DMSO control = 'siNG transfection alone' with equal amount of DMSO, SSC = side scatter, MFI_{siCTRL} = mean fluorescence intensity of the H1299-eGFP cells transfected with siCTRL-loaded NGs, MFI_{sieGFP} = mean fluorescence intensity of the H1299-eGFP cells transfected with sieGFP-loaded NGs).

2.2. Secondary validation of the CADs ketotifen and loperamide

As mentioned above, not all CADs emerged as hits in our primary screen. To validate this finding, two CADs were selected for secondary testing. As shown in **Table S1**, loperamide (LOP, **Figure 2A**) is a 'CAD-hit', whereas ketotifen (KET, **Figure 2B**) has the physicochemical properties of a CAD but was not identified as a hit (not shown in **Table S1**). While loperamide evoked a concentration-dependent increase in (a) eGFP silencing (**Figure 2C**), (b) lysosomal volume (**Figure 2E**) and (c) cellular granularity (**Figure S3A**) compared to untreated and dex-HEMA siNG-transfected cells, exposure of the cells to mounting concentrations of ketotifen could not replicate these effects (**Figure 2D**, **Figure 2F**, **Figure S3B**). The contrasting effect of both compounds on dex-HEMA siNG-induced eGFP silencing was also visually confirmed with confocal microscopy (**Figure 3A**). In addition, staining of CAD-treated cells with the PLD detection reagent LipidTOX™ Red (**Figure 3B**, **Figure S4A**), revealed that 20 μ M loperamide treatment induced an accumulation of lipids in vesicular structures, while the same concentration of ketotifen did not. In line with previously documented data on the functional inhibition of ASM, loperamide-treated H1299-WT cells (as well as cells treated with 6 other 'CAD-hit' compounds) also showed a higher green fluorescent signal when stained overnight with BODIPY™ FL C12-Sphingomyelin, in contrast to 20 μ M ketotifen treatment (**Figure S4B**), which indicates reduced sphingomyelin (SM) degradation due to ASM inhibition⁵²⁻⁵⁵. Similarly, only loperamide exposure could visually increase the cytosolic delivery of Cy5®-labeled siRNA, as evident from **Figure 3C**. Upon treatment with 20 μ M loperamide, ~38% of the cells showed a diffuse cytosolic siRNA fluorescence in contrast to the untreated and ketotifen-exposed cells where a punctate pattern, indicative of lysosomal sequestration, was observed. Note that the percentage of cells that showed cytosolic delivery of fluorescent siRNA is lower than was expected based on the eGFP gene silencing results (**Figure 2C-D**, **Figure 3A**), which can be most likely attributed to the cytosolic dilution of the labeled siRNAs below the detection limit of a standard confocal microscope^{8,21}. Of note, the tested CADs were overall well tolerated in the applied concentrations (**Figure S4C**), in line with our previously reported data²¹. It should, however, be noted that not all 'CAD-hits' shown in **Table S1** have been routinely tested for

their impact on cell viability. In summary, the effects of the ‘CAD-hit’ loperamide and the ‘CAD-no hit’ ketotifen on gene knockdown and lysosomal phenotype could be validated.

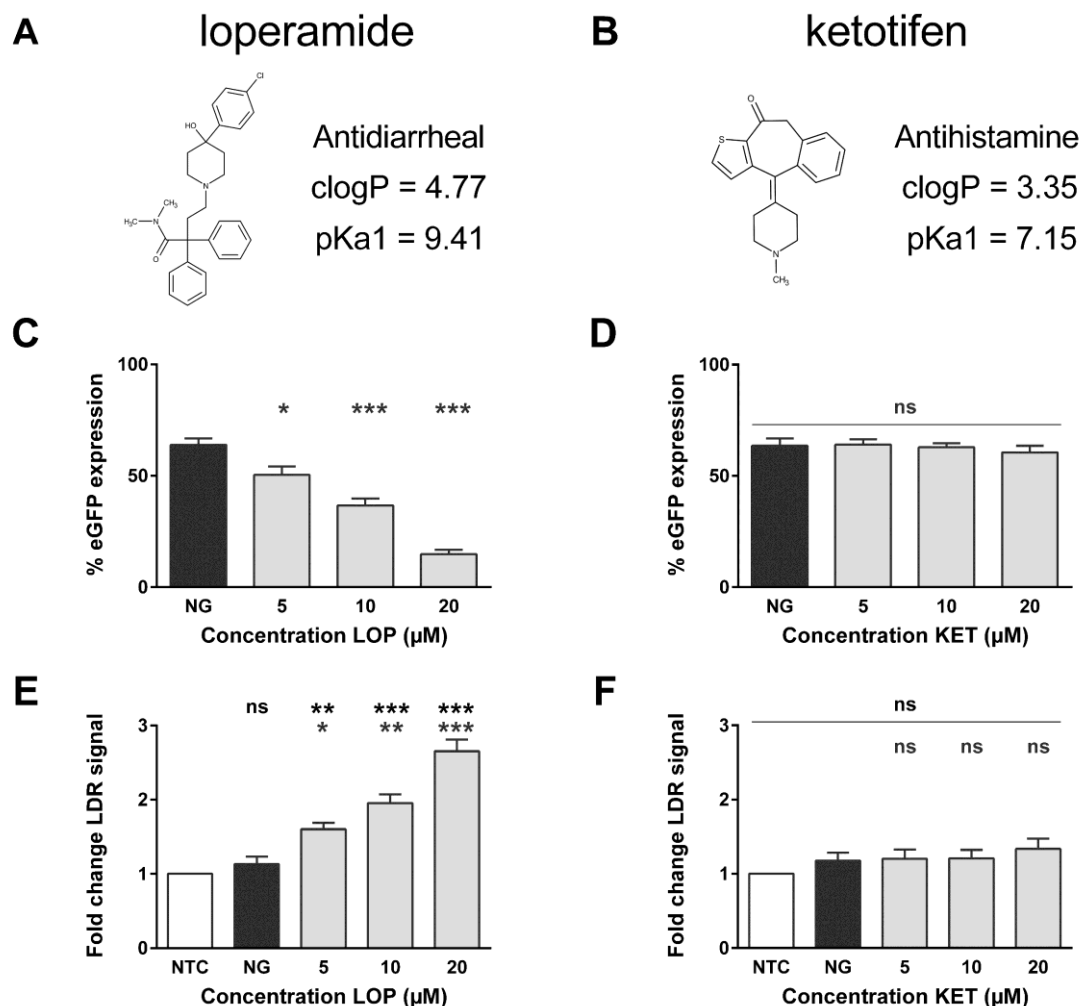


Figure 2. Loperamide but not ketotifen improves the eGFP silencing potential of dex-HEMA siNGs in NSCLC cells. (A-B) The drug class, clogP, pKa1 values and molecular structure of loperamide (LOP) and ketotifen (KET)⁵⁶. The pKa1 and clogP values of the compounds were predicted with JChem for Office (version 17.21.0.1797, ChemAxon Ltd., Budapest, Hungary)⁵⁶. (C-D) Sequential treatment of siNG-transfected H1299-eGFP cells (1 nM siRNA) with ‘CAD-hit’ LOP caused significant additional eGFP silencing in a concentration-dependent manner, while ‘CAD-no hit’ KET had no effect at all tested concentrations (20 h). (E-F) Fold change in LDR signal, measured *via* flow cytometry, for H1299-eGFP cells sequentially transfected with dex-HEMA siNGs and treated with mounting concentrations of LOP or KET. Data are represented as mean ± the standard error of the mean (SEM) for minimum three independent repeats. Statistical significance is indicated when appropriate, in black * when referring to the untreated control and in grey * when compared to dex-HEMA siNG transfection alone (ns p > 0.05, * p ≤ 0.05, ** p ≤ 0.01, *** p ≤ 0.001). (clogP = calculated logP, pKa1 = pKa of the most basic amine, eGFP = enhanced green fluorescent protein, NG = dex-HEMA siNG transfection without sequential CAD treatment, NTC = not treated control, KET = ketotifen, LOP = loperamide, ns = not significant, LDR = LysoTracker® Deep Red).

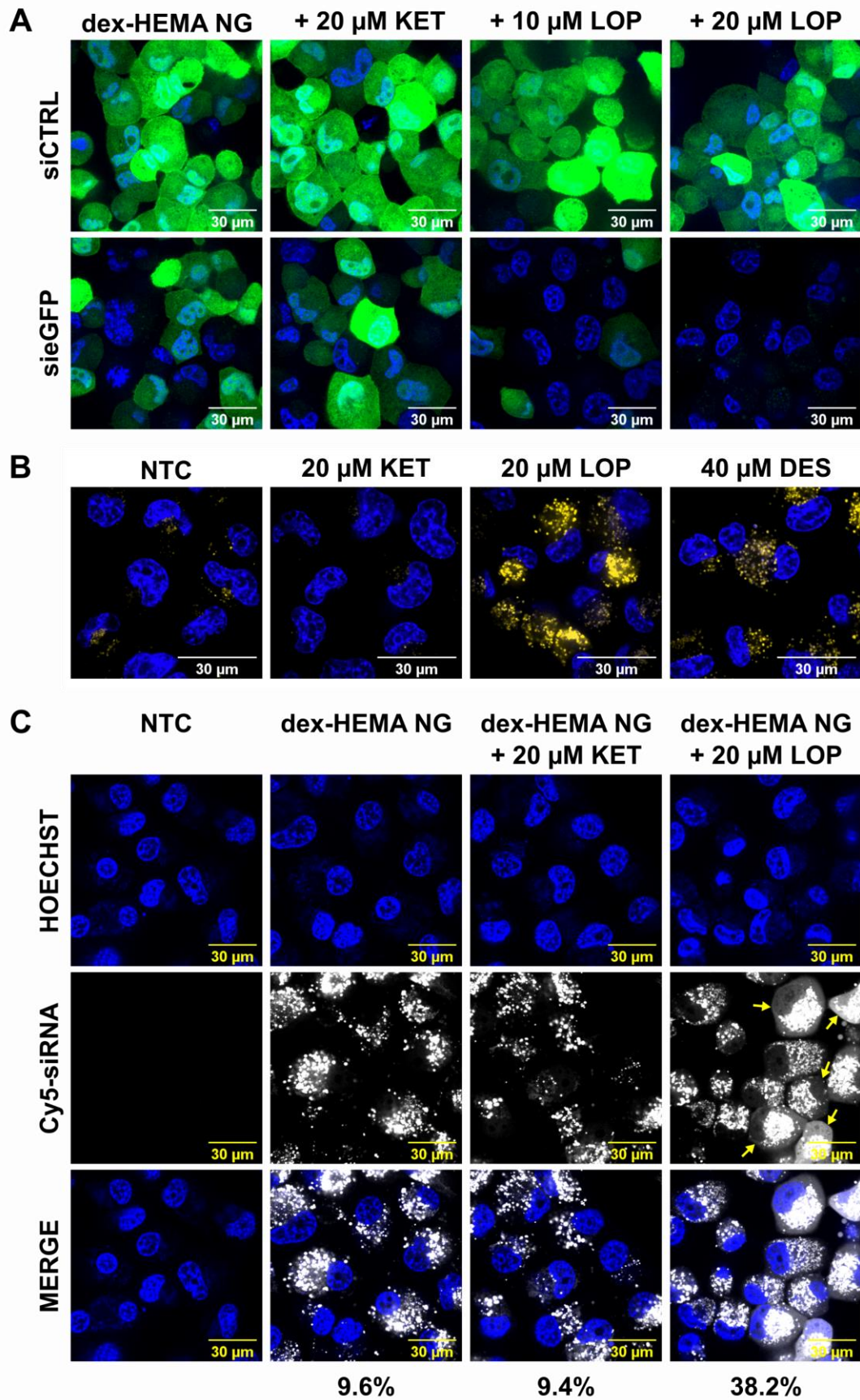


Figure 3. Loperamide, but not ketotifen, induces a phospholipidosis phenotype and promotes siRNA release into the cytosol. (A) Representative confocal images from the eGFP expression of

H1299-eGFP cells after transfection with dex-HEMA NGs loaded with a suboptimal amount of siCTRL or sieGFP (2 nM), whether or not followed by treatment with 20 μ M ketotifen (KET) or 10-20 μ M loperamide (LOP) for 20 h. (B) Representative confocal images from the phospholipid distribution in H1299-eGFP cells visualized with LipidTOX™ Red PLD detection reagent in untreated and 20 μ M ketotifen (KET)/20 μ M loperamide (LOP)/40 μ M desloratadine (DES) treated cells (20 h). (C) Representative confocal images from the intracellular siCy5® distribution in H1299-WT cells, only transfected with siCy5®-loaded dex-HEMA NGs, or cells subsequently incubated with 20 μ M ketotifen (KET) or loperamide (LOP) for 20 h. The values below the images correspond to the percentage of cells with a diffuse cytosolic siCy5® signal. Cells with a diffusive siCy5® signal are shown with yellow arrows. The scale bar corresponds to 30 μ m. (NTC = not treated control, NG = nanogels, siCTRL = siRNA scrambled control, sieGFP = siRNA targeting eGFP, eGFP = enhanced green fluorescent protein, KET = ketotifen, LOP = loperamide, DES = desloratadine).

3. CONCLUSION

The data presented here clearly demonstrate that multiple cationic amphiphilic drugs (CADs) can be repurposed as potent adjuvants to promote cytosolic siRNA delivery in non-small cell lung cancer (NSCLC) cells. In line with our previous work²¹, our data indicate that the CAD-induced lysosomal storage disease phenotype (characterized by phospholipidosis (PLD), lysosomal swelling and lysosomal membrane permeabilization (LMP)) is responsible for the observed adjuvant effect on siNG-transfected NSCLC cells. As inefficient cellular delivery to date remains the most important cellular barrier for NA therapeutics and many CADs are clinically approved drugs, this adjuvant strategy can be exploited as leverage for clinical translation. Moreover, as the identified nucleic acid (NA) delivery-promoting CADs have diverging pharmacological action, such a combination therapy can provide synergistic therapeutic effects. However, it should be further investigated if this promising approach can also be used for other siRNA-loaded nanoparticles (NPs), other cancer cells and other small NAs (**Chapter 3**). Finally, 40 out of the 96 hit compounds of the screen were not classified as CADs, which will be further discussed in **Chapter 4**.

ACKNOWLEDGMENTS

T. Van de Vyver is a doctoral fellow of the Research Foundation-Flanders (grant 1198719N, FWO, Belgium). B. Bogaert is a doctoral fellow of the FWO (grant 1S75019N). L. De Backer acknowledges the Special Research Fund of Ghent University (BOF12/GOA/014). F. Joris acknowledges the Agency for Innovation by Science and Technology in Flanders (IWT, Belgium). R. Guagliardo is an early stage researcher within the NANOMED project, which has received funding from the European Union's Horizon 2020 Research and Innovation Programme Marie Skłodowska Curie Innovative Training Networks (ITN) under grant number 676137. J. Van Hoeck is a doctoral fellow of the FWO (grant 1S62519N). P. Merckx is a doctoral fellow of the FWO (grant 1S30618N). Prof. K. Raemdonck acknowledges the FWO for a postdoctoral Research Grant (grant 1517516N). We thank Prof. T. Coenye and C. Rigauts from the Laboratory of Pharmaceutical Microbiology (UGent, Belgium) for the use of the Attune™ NxT flow cytometer.

4. MATERIALS AND METHODS

4.1. siRNA duplexes

The 21mer siRNA duplexes targeted against the enhanced green fluorescent protein (eGFP, sieGFP) and the negative control siRNA (siCTRL) were purchased from Eurogentec (Seraing, Belgium). The negative control siRNA consist of a sequence that has no relevant homology to any known eukaryotic gene sequences. Fluorescent siCTRL was labeled with a Cy5[®] dye at the 5' end of the (sense) strand (abbreviated as siCy5[®], Eurogentec, Seraing, Belgium). The concentration of the siRNA stock solutions in nuclease-free water (Ambion[®]-Life Technologies, Ghent, Belgium) was calculated from absorption measurements at 260 nm ($1 \text{ OD}_{260} = 40 \mu\text{g mL}^{-1}$) with a NanoDrop 2000c UV-Vis spectrophotometer (Thermo Fisher Scientific, Rockford, USA). The sequences and modifications of the applied siRNA duplexes are summarized in **Table 1**.

Table 1. Applied siRNA sequences and modifications.

siRNA	Modification	Manufacturer	Sequence ^a	
			(Sense) strand (5' > 3')	Antisense strand (5' > 3')
siCTRL ^b	/	Eurogentec	UGCGCUACGAUCGACGAUGtt	CAUCGUCGAUCGUAGCGCAtt
siCTRL ^b	Cy5 [®] -labeled ^c	Eurogentec	UGCGCUACGAUCGACGAUGtt	CAUCGUCGAUCGUAGCGCAtt
sieGFP ^d	/	Eurogentec	CAAGCUGACCCUGAAGUUCtt	GAACUUCAGGGUCAGCUUGtt

^a Capital and lower case letters respectively represent ribonucleotides and 2'-deoxyribonucleotides; ^b negative control siRNA duplex^{21,26,57,58}; ^c labeled with a Cy5[®] dye at the 5' end of the (sense) strand^{21,26,57,58}; ^d siRNA duplex targeting enhanced green fluorescent protein^{21,26,57,58}.

4.2. Nanogel (NG) synthesis, preparation and siRNA complexation

Dextran hydroxyethyl methacrylate or dextran methacrylate (dex-HEMA or dex-MA) was copolymerized with a cationic methacrylate monomer [2-(methacryloyloxy)ethyl]-trimethylammonium chloride (TMAEMA) to produce cationic dex-HEMA-co-TMAEMA (degree of substitution (DS) of 5.2) and dex-MA-co-TMAEMA (DS of 5.9) nanogels (hereafter abbreviated as respectively dex-HEMA NGs and dex-MA NGs), using an inverse miniemulsion photopolymerization method as reported previously^{11,26,57-59}. To assure long-term stability, the NGs were lyophilized and stored desiccated. To obtain siRNA-loaded NGs (siNGs) for *in vitro* experiments, a stock (2 mg/mL) was prepared by dispersing a weighed amount of particles in ice-cooled nuclease-free water (Ambion[®]-Life Technologies, Ghent, Belgium), followed by sonication (3 x 5 sec, amplitude 10%; Branson Digital Sonifier[®], Danbury, USA).

Subsequently, equal volumes of NG and siRNA dilutions in 4-(2-hydroxyethyl)-1-piperazineethanesulfonic acid (HEPES) buffer (pH 7.4, 20 mM) were mixed and incubated at 4 °C for 10 min to allow electrostatic complexation, prior to further dilution in Opti-MEM® (Invitrogen, Merelbeke, Belgium). This complexation procedure was applied for all cell-based experiments in a 96-well plate and resulted in a 30 µg/mL NG dispersion loaded with 1 nM siRNA (0.033 pmol siRNA/µg NGs or 0.1 pmol siRNA/well), unless indicated otherwise. In case 24-well plates (**Figure S1A-B**) or 35 mm diameter CELLview™ microscopy dishes with glass bottom (Greiner Bio-One GmbH, Vilvoorde, Belgium) were used, a NG dispersion of 30 µg/mL loaded with 2 nM siRNA (0.067 pmol siRNA/µg NGs or 0.6 pmol siRNA/well or 1.8 pmol siRNA/dish) was applied, unless indicated otherwise.

4.3. Cell lines and cell culture conditions

The human non-small cell lung epithelial carcinoma cell line (H1299) that stably expresses eGFP (H1299-eGFP) was obtained from the lab of Prof. Camilla Foged (Department of Pharmacy, University of Copenhagen, Denmark)^{21,57,60–62}. The wild type variant of the H1299 cells (H1299-WT, ATCC® CRL-5803™) was obtained from American Type Culture Collection (ATCC, Manassas, USA). H1299 cells (H1299-WT and H1299-eGFP) were maintained in Roswell Park Memorial Institute (RPMI) 1640 culture medium, supplemented with 10% fetal bovine serum (FBS, Hyclone™, GE Healthcare, Machelen, Belgium), 2 mM L-Glutamine and 100 U/mL penicillin/streptomycin (hereafter collectively called ‘complete cell culture medium’ or CCM). The cell lines were cultured in a humidified atmosphere containing 5% CO₂ at 37 °C and culture medium was renewed every other day unless the 80% confluence level was reached. In this case, the cells were split using 0.25% trypsin-ethylenediaminetetraacetic acid (EDTA). For eGFP transgene selection, H1299-eGFP cells were treated with medium containing 1 mg/mL Geneticin® once per month. All cells were regularly tested and found negative for mycoplasma. All products were purchased from Gibco®-Life Technologies (Grand Island, NY, USA) unless specifically mentioned otherwise.

4.4. Compound library stock preparation and small molecules

The National Institutes of Health Clinical Collection (NIHCC) library was acquired from Evotec (San Francisco, CA, USA), which supplied the DMSO-dissolved compounds at a concentration of 10 mM. Stock plates were made by transferring 2 µL of each compound to a new 96-well plate, followed by dilution to 10 µL with sterile-filtered BioPerformance Certified dimethyl sulfoxide (DMSO, Sigma-Aldrich, Overijse, Belgium), resulting in a concentration of 2 mM for

each compound. Two μL of the latter stock solutions were diluted with 198 μL serum-containing complete cell culture medium (CCM) directly before use to give a final concentration of 20 μM for each drug. The final DMSO concentration brought onto the cells (both compound-treated and DMSO control) was 1% (v/v). Note that apart from the NIHCC-compounds, all the small molecules were obtained from Sigma-Aldrich (Overijse, Belgium), except loperamide HCl (LKT Laboratories Inc., St. Paul, MN, USA), and the stock solutions were also prepared in sterile-filtered BioPerformance Certified dimethyl sulfoxide (DMSO, Sigma-Aldrich, Overijse, Belgium).

4.5. NIHCC screening protocol

H1299-eGFP cells were seeded in 96-well plates (SPL Lifesciences Co. Ltd., Naechon-Myeon Pocheon, South Korea) at a density of 7500 cells/well (100 μL /well) and were allowed to settle overnight. Next, the cells were transfected with dex-HEMA siNGs (0.1 pmol siRNA/well, prepared as described above) during 4 hours at 37 °C in a humidified atmosphere containing 5% CO₂. Note that for every sieGFP condition a siCTRL sample was included to account for potential off-target effects. Subsequently, the siNG dispersion was removed and the cells received 50 μL fresh (DMSO control) or compound-containing CCM (20 μM). Each 96-well plate contained a siNG-DMSO control (n = 4, 4 siCTRL and 4 sieGFP conditions) and 50 wells treated with 25 compounds (20 μM , n = 1, 1 siCTRL and 1 sieGFP condition). After 20 hours, the small molecule containing CCM (and DMSO control) was removed and cells were kept in 50 μL fresh CCM for an additional 24 hours until flow cytometry analysis. Sample preparation consisted of detachment with 30 μL 0.25% trypsin-EDTA, neutralization with 120 μL CCM and a transfer of the cell suspensions to an U-bottom 96-well plate (Greiner Bio-One GmbH, Vilvoorde, Belgium), which was centrifuged during 5 minutes at 500 g. After removal of 120 μL supernatant, the cells were resuspended in 80 μL flow buffer (phosphate buffered saline (PBS, no calcium, no magnesium) with 1% (v/v) FBS (Hyclone™, GE Healthcare, Machelen, Belgium) and 0.1% (w/v) sodium azide (Sigma Aldrich, Overijse, Belgium)) and kept on ice until analysis. For each sample the forward and side scatter (respectively FSC and SSC) as well as the green fluorescent signal of single cells were measured for 100 seconds at a flow rate of 25 μL /min. The samples were excited with the 488 nm laser line and the signal was detected with the 530/30 filter using the Attune™ NxT flow cytometer with the Attune™ auto sampler (Applied Biosystems™ by Life Technologies™, Foster City, CA, USA) and Attune™ NxT acquisition software. Finally, data analysis was

performed using the FlowJo software (Tree Star Inc., Ashland, OR, USA) and data were exported into Microsoft® Excel® (16th version, Microsoft Corp., Redmond, WA, USA) for hit classification. The detailed hit identification procedure is provided below.

4.6. Hit identification procedure

Within each 96-well plate, a % eGFP expression was calculated for all the compound-treated ($n = 1$) and DMSO control-treated ($n = 4$) cells. For every plate, ‘minor’ and ‘major’ hits were defined as compounds that caused a decrease in % eGFP expression of more than respectively 3 and 6 times the standard deviation (SD) on the % eGFP expression obtained with the DMSO control (*e.g.* values outside the 99.7% confidence interval (CI) of the siNG-DMSO control for the ‘minor’ hits). A schematic representation of the hit classification procedure is shown in **Figure S2A**. The SSC signal and the calculated % eGFP expression of each condition is normalized to the siNG-DMSO control of each plate (‘siNG transfection alone’ has a normalized SSC and eGFP expression of 1) for graphic representation. The pKa values of the most basic amines (macroscopic pKa of the conjugated acid, pKa1) and the clogP values of the compounds were predicted with JChem for Office (version 17.21.0.1797, ChemAxon Ltd., Budapest, Hungary)⁵⁶. The physiological charge (at pH 7.4) was calculated with the cxcalc calculator function (formal charge at pH 7.4, Marvin 17.21.0, 2017, ChemAxon Ltd., Budapest, Hungary)⁵⁶. CADs were defined as described previously (clogP > 3 and pKa1 > 6)²⁸.

4.7. Quantification of transfection efficiency/lysosomal volume of NG transfection and sequential adjuvant treatment by flow cytometry

Other transfection experiments with H1299-eGFP cells were performed similar to the abovementioned screening protocol. Following 20 h of CAD treatment (ketotifen fumarate (KET), loperamide HCl (LOP)) with the indicated concentrations (maximally 0.08% (v/v) residual DMSO), and an additional incubation with 50 μ L fresh CCM for 24 hours, the lysosomes were labeled with the LysoTracker® Deep Red (LDR) probe (Molecular Probes™, Eugene, OR, USA) through incubation with 50 μ L 75 nM LDR in CCM for 30 min at 37 °C. After removal of the LDR-containing CCM and a washing step with 30 μ L PBS, further sample preparations were carried out as described above. For each sample the FSC and SSC as well as the green and red fluorescent signal of single cells were measured. The samples were excited with the 488 and 638 nm laser lines and the signal was detected with the 525/40

and 660/20 filters using the CytoFLEX flow cytometer with plate loader for 96-well plates (Beckman Coulter, Krefeld, Germany) and CytExpert software. FlowJo software was used for data analysis as described above. The calculated percentages eGFP expression and fold changes in LDR signal intensity/SSC signal are presented as the mean \pm standard error of the mean (SEM) for minimum 3 independent repeats (biological replicates), unless otherwise indicated. In an additional experiment (**Figure S1A-B**), H1299-eGFP cells (seeded at 35000 cells/well) were transfected in 24-well plates with dex-HEMA siNGs for 4 h at 37 °C as described before.²¹ Note that in this experiment the indicated desloratadine (DES) concentrations (applied in pre-incubation (Pre), immediately after (Post) or 20 h after transfection (20 h Post)) were only applied on the cells for 2 h. LysoTracker® Deep Red (LDR) staining was performed similar to the aforementioned protocol.

4.8. Cell viability

H1299-eGFP cells were seeded, transfected with dex-HEMA siNGs and treated with the CADs similar to the silencing experiments. The cell viability was determined with the CellTiter GLO® assay (Promega, Belgium). According to manufacturer instructions, the culture plates and reconstituted assay buffer were placed at room temperature for 30 min, before initiating the assay. Subsequently, the CCM was replaced by 100 μ L fresh CCM and an equal amount of assay buffer was added. To induce complete cell lysis, the plates were shaken during 2 min and the signal was allowed to stabilize the following 10 min. Next, 100 μ L from each well was transferred to an opaque 96-well plate, which was measured with a GloMax® 96 Microplate Luminometer (Promega, Belgium). Data are presented as the mean cell viability (%; percentage of luminescent signal relative to non-treated cells (NTC) for each condition) \pm standard error of the mean (SEM) for minimum three independent repeats.

4.9. Visualizing eGFP expression with confocal microscopy

H1299-eGFP cells were seeded at 105000 cells/dish in 35 mm diameter CELLview™ microscopy dishes with glass bottom (Greiner Bio-One GmbH, Vilvoorde, Belgium) and were allowed to settle overnight. After removal of the complete cell culture medium (CCM), the cells were transfected with 900 μ L of a 30 μ g/mL NG dispersion loaded with 2 nM siRNA (= 0.067 pmol siRNA/ μ g NGs or 1.8 pmol siRNA/dish). Following incubation for 4 h (37 °C, 5% CO₂), the siNG dispersion was removed and the cells were washed once with phosphate buffered saline (PBS, Invitrogen, Merelbeke, Belgium). Next, the cells received 1.5 mL fresh CCM, containing different micromolar concentrations of LOP/KET or a DMSO control, for 20

h (37 °C, 5% CO₂). Subsequently, the CAD-containing CCM was removed and cells were kept in 1.5 mL fresh CCM for an additional 24 h. Before confocal imaging, the cells were fixed with 4% paraformaldehyde (PFA) during 15 minutes at room temperature. After a double washing step with PBS, the cells were finally stored at 4 °C until imaging in Vectashield antifade mounting medium containing DAPI (Vector Laboratories, Burlingame, USA). A spinning disk confocal (SDC) microscope (Nikon eclipse Ti, Japan), equipped with a MLC 400 B laser box (Agilent technologies, California, USA), a Yokogawa CSU-X confocal spinning disk device (Andor, Belfast, UK), an iXon ultra EMCCD camera (Andor Technology, Belfast, UK), a Plan Apo VC 60× 1.4 NA oil immersion objective lens (Nikon, Japan) and NIS Elements software (Nikon, Japan) was applied for imaging. The 408 nm and 488 nm laser lines were, respectively, used to excite the DAPI-labeled nuclei and the eGFP protein. A wait command of 0.2 seconds in between the image acquisition of the 2 channels was applied to avoid spectral overlap of the DAPI dye and the eGFP protein.

4.10. Visualization and quantification of the cytosolic release of siCy5®

H1299-WT cells were seeded at 105000 cells/dish in 35 mm diameter glass bottom microscopy dishes (Greiner Bio-One GmbH, Germany) and were allowed to settle overnight. To visualize the siCy5® release, dex-HEMA NGs were first loaded with 100 nM siCy5® and subsequently added to each dish as described above (3.35 pmol siCy5®/µg NGs, 4 h incubation). Further steps (*e.g.* CAD treatments, imaging) were done as described above for visualizing the eGFP expression with confocal microscopy, unless mentioned otherwise. No fixation step was applied, but an extra washing step with dextran sulfate sodium salt (Sigma-Aldrich, 1 mg/mL in PBS) was done after removal of the dex-HEMA siNG dispersion. After removal of the small molecule-containing CCM, the nuclei were labeled with Hoechst 33342 (Molecular Probes™, Belgium) in CCM (1 mg/mL in water, 1/1000 dilution) during 15 minutes at 37 °C. Finally, the Hoechst solution was removed, fresh CCM was added and cells were kept at 37 °C in a humidified atmosphere containing 5% CO₂ until imaging. The 408 nm and 633 nm laser lines were applied to, respectively, excite the Hoechst-labeled nuclei and the fluorescence resulting from siCy5®. To detect the faint cytosolic staining of siCy5®, a long exposure time of 500 ms was used for the red channel as described before⁹. During data analysis with ImageJ (FIJI) software, both the total cell number and amount of cells with a diffuse siCy5® labeling were counted. Data are represented as the percentage of cells with a diffuse siCy5® signal for minimum 278 cells per condition in minimum 42 images.

4.11. Phospholipidosis detection with LipidTOX™ Red

H1299-eGFP cells were seeded (200000 cells/dish) and allowed to settle overnight as specified for the siCy5[®] release experiment. Next, the cells were incubated with a mixture of a 1/1000 dilution of the LipidTOX™ Red Phospholipidosis Detection Reagent (Thermo Fisher Scientific, Rockford, USA) and the desired CAD in CCM. Upon 20 hours incubation, the nuclei were labeled with Hoechst 33342 (Molecular Probes™, Belgium) as detailed for the siCy5[®] release experiment. The 408 nm and 561 nm laser lines were applied to, respectively, excite the Hoechst-labeled nuclei and the fluorescence resulting from the LipidTOX™ Red Phospholipidosis dye. Imaging occurred with a Plan Apo VC 100× 1.4 NA oil immersion objective lens (Nikon, Japan) and a SDC microscope as described above for visualizing the eGFP expression with confocal microscopy. The LipidTOX™ Red Phospholipidosis signal area was determined with ImageJ (FIJI) in at least 432 cells from 62 images. To this end, all confocal images were processed by applying the same offset values for the LipidTOX™ Red Phospholipidosis signal. In each image, both the number of cells and signal area of the LipidTOX™ Red Phospholipidosis dye was determined to allow calculation of the normalized LipidTOX™ Red Phospholipidosis area (*i.e.* LipidTOX™ Red Phospholipidosis signal area/cell number) in each image. The fold change in LipidTOX™ Red Phospholipidosis signal area was calculated by dividing the normalized signal area in treated cells by the normalized signal area in untreated cells.

4.12. BODIPY™ FL C12-Sphingomyelin staining

H1299-WT cells were seeded at 7500 cells/well in 96-well plates (SPL Lifesciences Co. Ltd., Naechon-Myeon Pocheon, South Korea) and were allowed to settle overnight. After 20 h incubation with the CADs, the compound-containing CCM was removed and cells were incubated overnight with 0.2 µg/mL BODIPY™ FL C12-sphingomyelin (BODIPY™ FL C12-SM, Thermo Fisher Scientific, Rockford, USA) in CCM (37 °C, 5% CO₂)⁵⁴. Following a washing step with PBS and flow cytometry preparation (see above), the samples were excited with the 488 nm laser line and the signal was detected with the 525/40 filter using the CytoFLEX flow cytometer with plate loader for 96-well plates (Beckman Coulter, Krefeld, Germany) and CytExpert software. FlowJo software was used for data analysis. Cells without BODIPY™ FL C12-SM staining, but with the same treatments, were used as controls for non-specific changes in green fluorescence.

4.13. Statistical analysis

Statistical analysis was performed using the 6th version of the GraphPad Prism software. One-way ANOVA combined with the post-hoc Dunnett test was applied to compare multiple conditions, whereas the student *t*-test was used for direct comparison of 2 conditions. χ^2 likelihood ratio tests with Yates continuity correction were used to analyze 2 x 2 contingency tables to check statistical dependence of the two properties shown in the contingency tables. Multiple linear regression analysis was performed with normalized eGFP expression as a dependent variable. A *p* value ≤ 0.05 was considered *a priori* to be statistically significant.

Associated content

Supporting information consists out of 4 additional figures and 1 additional table. **Figure S1:** pre-incubation of desloratadine (DES), in H1299-eGFP cells. **Figure S2:** hit selection procedure, association of screened compounds ('hits' and 'no hits') with published drug characteristics and PCA-analysis. **Table S1:** hit adjuvant compounds that comply with the CAD definition. **Figure S3:** fold change in SSC signal for loperamide (LOP) and ketotifen (KET) treatment, in H1299-eGFP cells. **Figure S4:** fold change in LipidTOX™ signal area, cell viability and BODIPY™ FL C 12-SM signal for multiple CADs, in H1299-eGFP cells.

REFERENCES

1. Dowdy, S. F. Overcoming Cellular Barriers for RNA Therapeutics. *Nat. Biotechnol.* **2017**, *35*, 222–229.
2. Wittrup, A.; Lieberman, J. Knocking down Disease: A Progress Report on siRNA Therapeutics. *Nat. Rev. Genet.* **2015**, *16*, 543–552.
3. Shen, X.; Corey, D. R. Chemistry, Mechanism and Clinical Status of Antisense Oligonucleotides and Duplex RNAs. *Nucleic Acids Res.* **2018**, *46*, 1584–1600.
4. Setten, R. L.; Rossi, J. J.; Han, S. ping. The Current State and Future Directions of RNAi-Based Therapeutics. *Nat. Rev. Drug Discov.* **2019**, *18*, 421–446.
5. Kanasty, R.; Dorkin, J. R.; Vegas, A.; Anderson, D. Delivery Materials for siRNA Therapeutics. *Nat. Mater.* **2013**, *12*, 967–977.
6. Yin, H. *et al.* Non-Viral Vectors for Gene-Based Therapy. *Nat. Rev. Genet.* **2014**, *15*, 541–555.
7. Martens, T. F.; Remaut, K.; Demeester, J.; De Smedt, S. C.; Braeckmans, K. Intracellular Delivery of Nanomaterials: How to Catch Endosomal Escape in the Act. *Nano Today* **2014**, *9*, 344–364.
8. Gilleron, J. *et al.* Image-Based Analysis of Lipid Nanoparticle-Mediated siRNA Delivery, Intracellular Trafficking and Endosomal Escape. *Nat. Biotechnol.* **2013**, *31*, 638–646.
9. Wittrup, A. *et al.* Visualizing Lipid-Formulated siRNA Release from Endosomes and Target Gene Knockdown. *Nat. Biotechnol.* **2015**, *33*, 870–876.
10. Ma, D. Enhancing Endosomal Escape for Nanoparticle Mediated siRNA Delivery. *Nanoscale* **2014**, *6*, 6415.
11. Raemdonck, K. *et al.* Biodegradable Dextran Nanogels for RNA Interference: Focusing on Endosomal Escape and Intracellular siRNA Delivery. *Adv. Funct. Mater.* **2009**, *19*, 1406–1415.
12. Sahay, G. *et al.* Efficiency of siRNA Delivery by Lipid Nanoparticles Is Limited by Endocytic Recycling. *Nat. Biotechnol.* **2013**, *31*, 653–658.
13. Hirsch, M.; Helm, M. Live Cell Imaging of Duplex siRNA Intracellular Trafficking. *Nucleic Acids Res.* **2015**, *43*, 4650–4660.
14. Crooke, S. T.; Wang, S.; Vickers, T. A.; Shen, W.; Liang, X. Cellular Uptake and Trafficking of Antisense Oligonucleotides. *Nat. Biotechnol.* **2017**, *35*, 230–237.
15. Joris, F.; De Smedt, S. C.; Raemdonck, K. Small Molecules Convey Big Messages: Boosting Non-Viral Nucleic Acid Delivery with Low Molecular Weight Drugs. *Nano Today* **2017**, *16*, 14–29.
16. Patel, S. *et al.* Boosting Intracellular Delivery of Lipid Nanoparticle-Encapsulated mRNA. *Nano Lett.* **2017**, *17*, 5711–5718.
17. Yang, B. *et al.* High-Throughput Screening Identifies Small Molecules That Enhance the Pharmacological Effects of Oligonucleotides. *Nucleic Acids Res.* **2015**, *43*, 1987–1996.
18. Wang, L. *et al.* A Novel Family of Small Molecules That Enhance the Intracellular Delivery and Pharmacological Effectiveness of Antisense and Splice Switching Oligonucleotides. *ACS Chem. Biol.* **2017**, *12*, 1999–2007.
19. Juliano, R. L. *et al.* Structure-Activity Relationships and Cellular Mechanism of Action of Small Molecules That Enhance the Delivery of Oligonucleotides. *Nucleic Acids Res.* **2018**, *46*, 1601–1613.
20. Zhang, X.; Castanotto, D.; Liu, X.; Shemi, A.; Stein, C. A. Ammonium and Arsenic Trioxide Are Potent Facilitators of Oligonucleotide Function When Delivered by Gymnosis. *Nucleic Acids Res.* **2018**, *46*, 3612–3624.
21. Joris, F. *et al.* Repurposing Cationic Amphiphilic Drugs as Adjuvants to Induce Lysosomal siRNA Escape in Nanogel Transfected Cells. *J. Control. Release* **2018**, *269*, 266–276.
22. Castanotto, D. *et al.* A Stress-Induced Response Complex (SIRC) Shuttles miRNAs, siRNAs,

- and Oligonucleotides to the Nucleus. *Proc. Natl. Acad. Sci. U. S. A.* **2018**, *115*, E5756–E5765.
23. Zhou, X. *et al.* SAHA (Vorinostat) Facilitates Functional Polymer-Based Gene Transfection via Upregulation of ROS and Synergizes with TRAIL Gene Delivery for Cancer Therapy. *J. Drug Target.* **2018**, 1–9.
 24. Gilleron, J. *et al.* Identification of SiRNA Delivery Enhancers by a Chemical Library Screen. *Nucleic Acids Res.* **2015**, *43*, 7984–8001.
 25. Osborn, M. F. *et al.* Guanabenz (Wytensin™) Selectively Enhances Uptake and Efficacy of Hydrophobically Modified SiRNAs. *Nucleic Acids Res.* **2015**, *43*, 8664–8672.
 26. De Backer, L. *et al.* Bio-Inspired Pulmonary Surfactant-Modified Nanogels: A Promising SiRNA Delivery System. *J. Control. Release* **2015**, *206*, 177–186.
 27. Kornhuber, J. *et al.* Identification of Novel Functional Inhibitors of Acid Sphingomyelinase. *PLoS One* **2011**, *6*, e23852.
 28. Lepri, S. *et al.* Synthesis and Phospholipidosis Effect of a Series of Cationic Amphiphilic Compounds: A Case Study to Evaluate *In Silico* and *In Vitro* Assays. *Med. Chem. Res.* **2018**, *27*, 679–692.
 29. Devlin, J. P. Assay Technologies and Detection Methods. In *High Throughput Screening: The Discovery of Bioactive Substances*; Devlin, J. P., Ed.; Marcel Dekker: New York, **1997**; pp 273–328.
 30. Muehlbacher, M.; Tripal, P.; Roas, F.; Kornhuber, J. Identification of Drugs Inducing Phospholipidosis by Novel *In Vitro* Data. *ChemMedChem* **2012**, *7*, 1925–1934.
 31. Goracci, L.; Ceccarelli, M.; Bonelli, D.; Cruciani, G. Modeling Phospholipidosis Induction: Reliability and Warnings. *J. Chem. Inf. Model.* **2013**, *53*, 1436–1446.
 32. Lemieux, B.; Percival, M. D.; Falguyret, J.-P. Quantitation of the Lysosomotropic Character of Cationic Amphiphilic Drugs Using the Fluorescent Basic Amine Red DND-99. *Anal. Biochem.* **2004**, *327*, 247–251.
 33. Ishizaki, J.; Yokogawa, K.; Ichimura, F.; Ohkuma, S. Uptake of Imipramine in Rat Liver Lysosomes *In Vitro* and Its Inhibition by Basic Drugs. *J. Pharmacol. Exp. Ther.* **2000**, *294*, 1088–1098.
 34. Ellegaard, A.-M. *et al.* Repurposing Cationic Amphiphilic Antihistamines for Cancer Treatment. *EBioMedicine* **2016**, *9*, 130–139.
 35. Petersen, N. H. T. *et al.* Transformation-Associated Changes in Sphingolipid Metabolism Sensitize Cells to Lysosomal Cell Death Induced by Inhibitors of Acid Sphingomyelinase. *Cancer Cell* **2013**, *24*, 379–393.
 36. Shahane, S. A. *et al.* Detection of Phospholipidosis Induction: A Cell-Based Assay in High-Throughput and High-Content Format. *J. Biomol. Screen.* **2014**, *19*, 66–76.
 37. Kornhuber, J. *et al.* Identification of New Functional Inhibitors of Acid Sphingomyelinase Using a Structure-Property-Activity Relation Model. *J. Med. Chem.* **2008**, *51*, 219–237.
 38. Wishart, D. S. *et al.* DrugBank: A Comprehensive Resource for *In Silico* Drug Discovery and Exploration. *Nucleic Acids Res.* **2006**, *34*, D668–72.
 39. Kessel, M.; Gieseler, F.; Woodcock, B. G. Influence of Serum Protein Binding on the Uptake and Retention of Idarubicin by Sensitive and Multidrug Resistant Human Leukemic Cells. *Eur. J. Clin. Pharmacol.* **1999**, *55*, 369–373.
 40. Trainor, G. L. The Importance of Plasma Protein Binding in Drug Discovery. *Expert Opin. Drug Discov.* **2007**, *2*, 51–64.
 41. Schmidt, S. *et al.* Effect of Protein Binding on the Pharmacological Activity of Highly Bound Antibiotics. *Antimicrob. Agents Chemother.* **2008**, *52*, 3994–4000.
 42. Kramer, N. I.; Krismartina, M.; Rico-Rico, Á.; Blaauboer, B. J.; Hermens, J. L. M. Quantifying Processes Determining the Free Concentration of Phenanthrene in Basal Cytotoxicity Assays. *Chem. Res. Toxicol.* **2012**, *25*, 436–445.
 43. Ghafourian, T.; Amin, Z. QSAR Models for the Prediction of Plasma Protein Binding.

- Bioimpacts* **2013**, *3*, 21–27.
44. Trapp, S.; Rosania, G. R.; Horobin, R. W.; Kornhuber, J. Quantitative Modeling of Selective Lysosomal Targeting for Drug Design. *Eur. Biophys. J.* **2008**, *37*, 1317–1328.
 45. Ufuk, A.; Somers, G.; Houston, J. B.; Galetin, A. *In Vitro* Assessment of Uptake and Lysosomal Sequestration of Respiratory Drugs in Alveolar Macrophage Cell Line NR8383. *Pharm. Res.* **2015**, *32*, 3937–3951.
 46. van Rensburg, J. J. *et al.* Development and Validation of a High-Throughput Cell-Based Screen to Identify Activators of a Bacterial Two-Component Signal Transduction System. *Antimicrob. Agents Chemother.* **2015**, *59*, 3789–3799.
 47. Tsai, C. M.; Perng, R. P.; Chang, K. T.; Venzon, D.; Gazdar, A. F. Evaluation of the Relative Cytotoxic Effects of Anticancer Agents in Serum-Supplemented *versus* Serum-Free Media Using a Tetrazolium Colorimetric Assay. *Jpn. J. Cancer Res.* **1996**, *87*, 91–97.
 48. Schreier, S.; Malheiros, S. V. P.; de Paula, E. Surface Active Drugs: Self-Association and Interaction with Membranes and Surfactants. Physicochemical and Biological Aspects. *Biochim. Biophys. Acta - Biomembr.* **2000**, *1508*, 210–234.
 49. Rhein, C. *et al.* Derivatization of Common Antidepressant Drugs Increases Inhibition of Acid Sphingomyelinase and Reduces Induction of Phospholipidosis. *J. Neural Transm.* **2018**, 1–9.
 50. Skuta, C. *et al.* Probes & Drugs Portal: An Interactive, Open Data Resource for Chemical Biology. *Nat. Methods* **2017**, *14*, 759–760.
 51. Kornhuber, J. *et al.* Functional Inhibitors of Acid Sphingomyelinase (FIASMA)s: A Novel Pharmacological Group of Drugs with Broad Clinical Applications. *Cell Physiol Biochem* **2010**, *26*, 9–20.
 52. Erlich, S. *et al.* Fluorescence-Based Selection of Gene-Corrected Hematopoietic Stem and Progenitor Cells from Acid Sphingomyelinase-Deficient Mice: Implications for Niemann-Pick Disease Gene Therapy and the Development of Improved Stem Cell Gene Transfer Procedures. *Blood* **1999**, *93*, 80–86.
 53. Butler, A.; He, X.; Gordon, R. E.; Gatt, S.; Schuchman, E. H. Reproductive Pathology and Sperm Physiology in Acid Sphingomyelinase-Deficient Mice. *Am. J. Pathol.* **2002**, *161*, 1061–1075.
 54. Manthe, R. L. *et al.* δ -Tocopherol Effect on Endocytosis and Its Combination with Enzyme Replacement Therapy for Lysosomal Disorders: A New Type of Drug Interaction? *J. Pharmacol. Exp. Ther.* **2019**, *370*, 823–833.
 55. Klutzny, S. *et al.* Functional Inhibition of Acid Sphingomyelinase by Fluphenazine Triggers Hypoxia-Specific Tumor Cell Death. *Cell Death Dis.* **2017**, *8*, e2709.
 56. *JChem for Office (Excel)*, Version 17.21.0.1797; Software Was Used for Chemical Database Access, Structure Based Property Calculation, Search and Reporting; ChemAxon: Budapest, Hungary, 2017. [Http://www.chemaxon.com](http://www.chemaxon.com).
 57. Merckx, P. *et al.* Surfactant Protein B (SP-B) Enhances the Cellular siRNA Delivery of Proteolipid Coated Nanogels for Inhalation Therapy. *Acta Biomater.* **2018**, *78*, 236–246.
 58. De Backer, L.; Braeckmans, K.; Demeester, J.; De Smedt, S. C.; Raemdonck, K. The Influence of Natural Pulmonary Surfactant on the Efficacy of siRNA-Loaded Dextran Nanogels. *Nanomedicine* **2013**, *8*, 1625–1638.
 59. Raemdonck, K.; Naeye, B.; Høgset, A.; Demeester, J.; De Smedt, S. C. Prolonged Gene Silencing by Combining siRNA Nanogels and Photochemical Internalization. *J. Control. Release* **2010**, *145*, 281–288.
 60. Ragelle, H. *et al.* Intracellular siRNA Delivery Dynamics of Integrin-Targeted, PEGylated Chitosan–Poly(Ethylene Imine) Hybrid Nanoparticles: A Mechanistic Insight. *J. Control. Release* **2015**, *211*, 1–9.
 61. Bramsen, J. B. *et al.* Improved Silencing Properties Using Small Internally Segmented Interfering RNAs. *Nucleic Acids Res.* **2007**, *35*, 5886–5897.

62. Fraire, J. C. *et al.* Vapor Nanobubble Is the More Reliable Photothermal Mechanism for Inducing Endosomal Escape of SiRNA without Disturbing Cell Homeostasis. *J. Control. Release* **2020**, *319*, 262–275.

SUPPLEMENTARY FIGURES AND TABLES

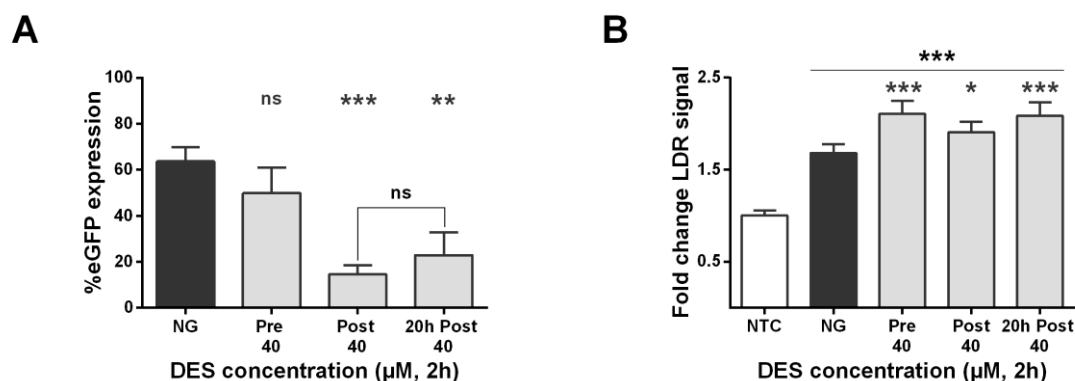
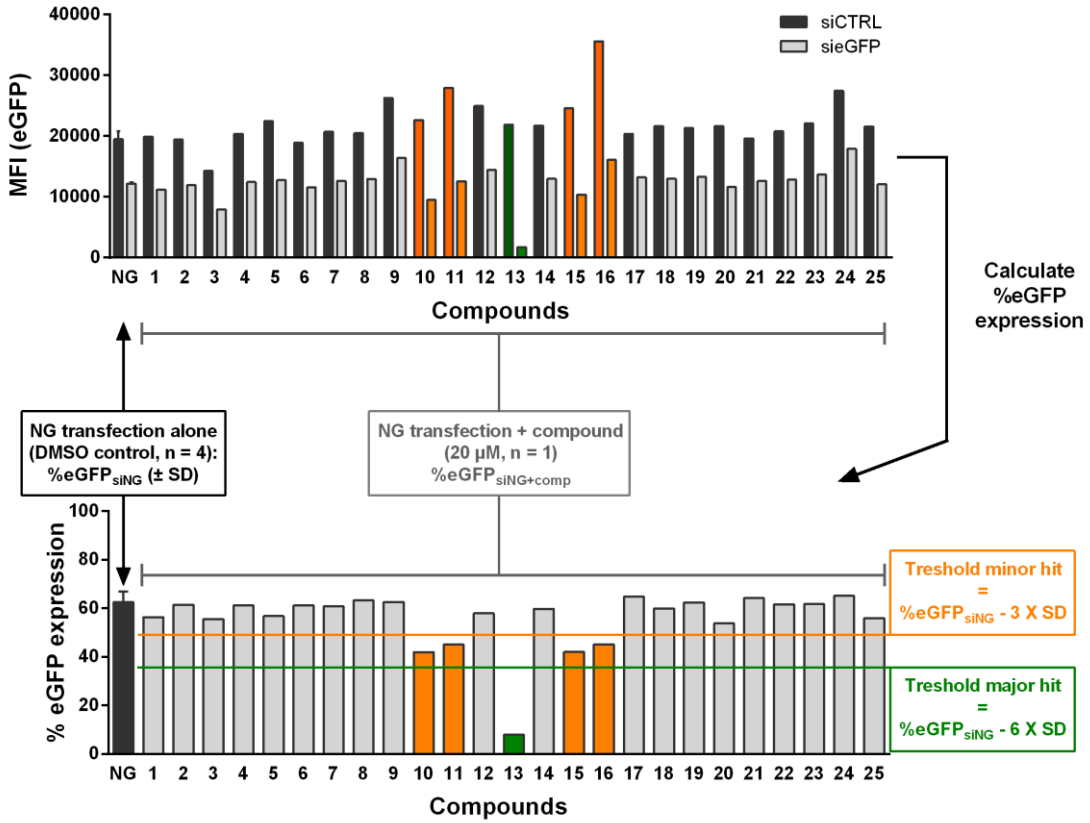
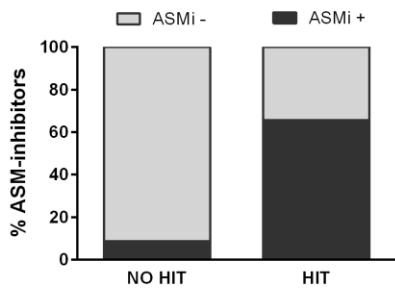


Figure S1. Desloratadine (DES) treatment significantly improves the silencing potential of dex-HEMA siNGs in NSCLC cells when applied post-incubation, but not in a pre-incubation step. (A) Impact on dex-HEMA siNG (2 nM siRNA) mediated eGFP silencing of a 2 h DES pre-incubation (Pre), 2 h DES treatment immediately after (Post) or 2 h DES treatment 20 h after transfection (20 h Post). (B) Fold change in LDR signal, measured *via* flow cytometry, for H1299-eGFP cells transfected with dex-HEMA siNGs and exposed to DES (2 h) on different time points. Data are represented as mean \pm the standard error of the mean (SEM) for minimum three independent repeats (**Figure S1A**) or mean \pm SD (n = 3, technical replicates, **Figure S1B**). Statistical significance is indicated when appropriate, in black * when referring to the untreated control and in grey * when compared to dex-HEMA siNG transfection alone (ns p > 0.05, * p \leq 0.05, ** p \leq 0.01, *** p \leq 0.001). (siNG = siRNA-loaded nanogel, NTC = not treated control, NG = dex-HEMA siNG transfection without CAD treatment, DES = desloratadine, eGFP = enhanced green fluorescent protein, ns = not significant, LDR = LysoTracker[®] Deep Red, NSCLC = non-small cell lung cancer).

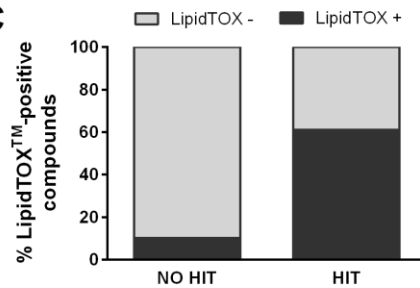
A



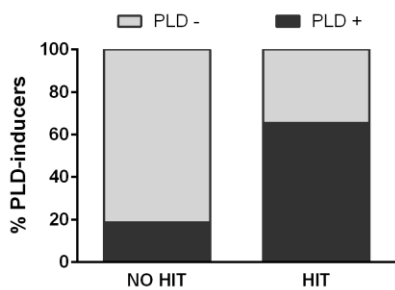
B



C



D



E

	NO CAD	CAD	Total		ASMi -	ASMi +	Total
NO HIT	532	72	604	NO HIT	73	8	81
HIT	40	56	96	HIT	12	23	35
Total	572	128	700	Total	85	31	116

	LT -	LT +	Total		PLD -	PLD +	Total
NO HIT	83	6	89	NO HIT	105	24	129
HIT	15	22	37	HIT	10	19	29
Total	98	28	126	Total	115	43	158

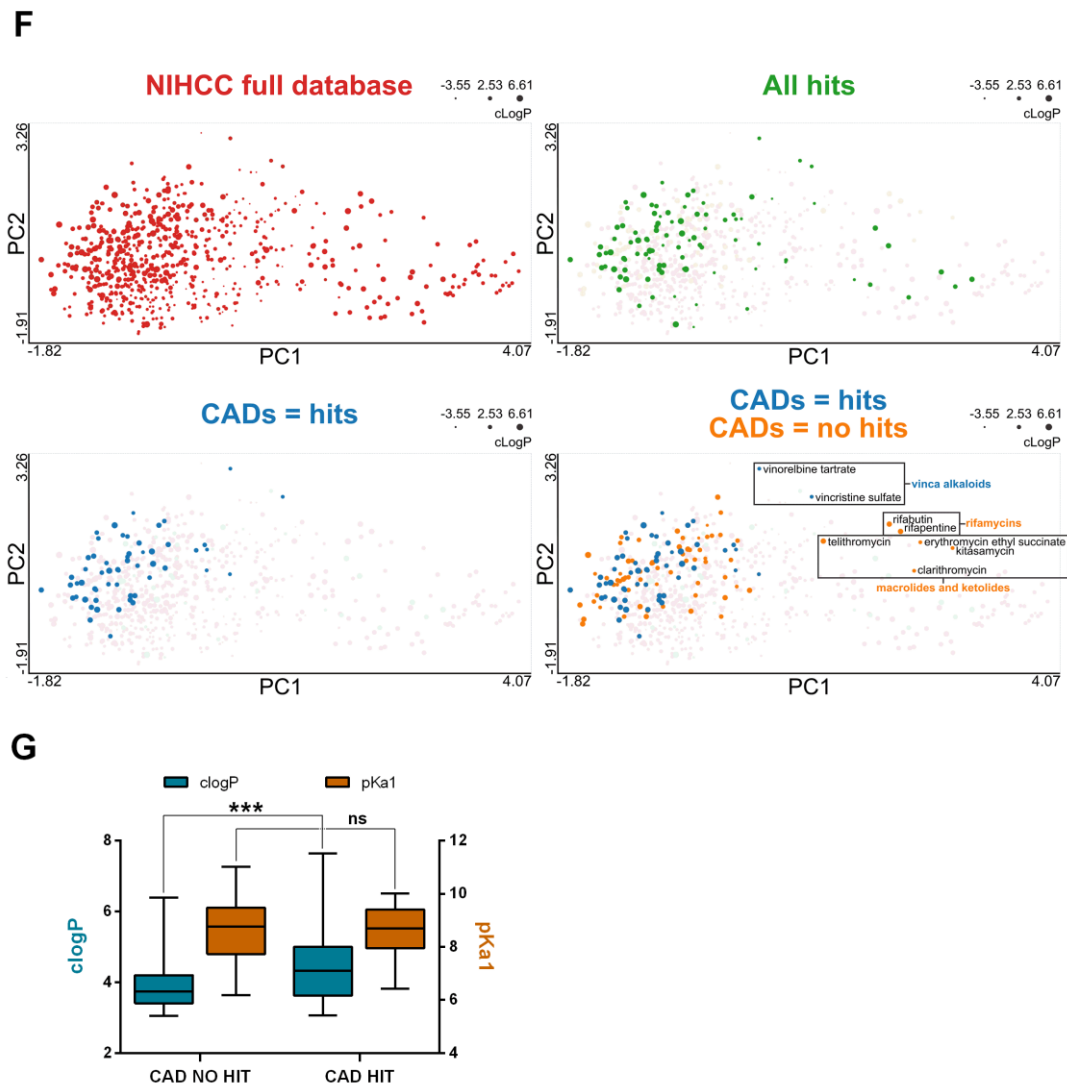
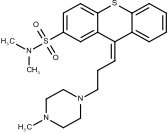
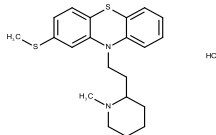
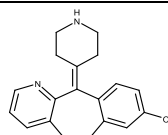
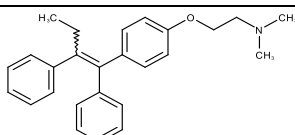
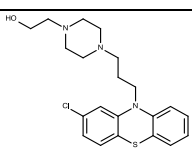
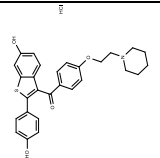
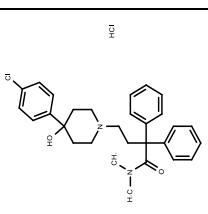
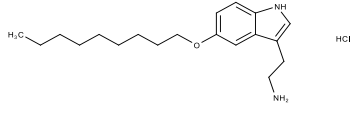
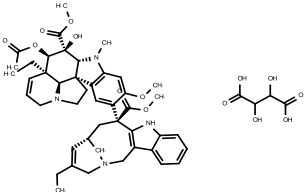
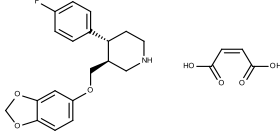
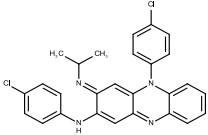
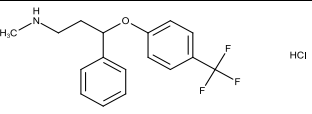
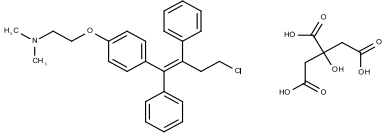
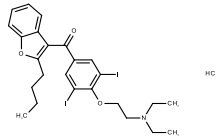
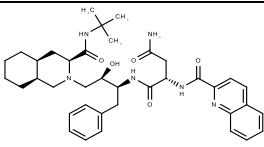
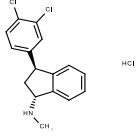
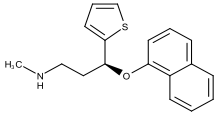


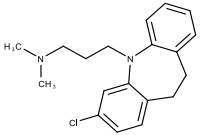
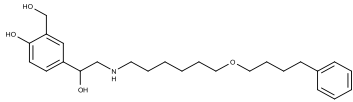
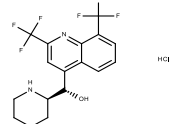
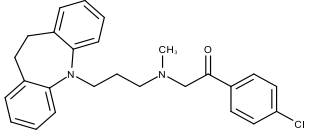
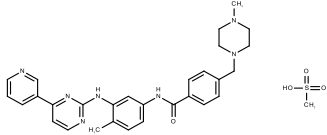
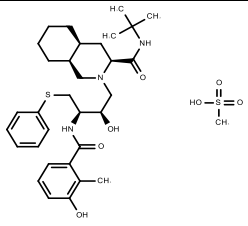
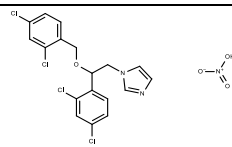
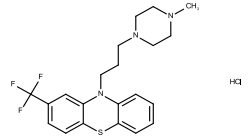
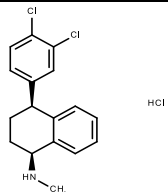
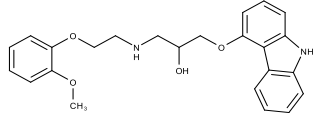
Figure S2. Hit selection procedure, association of screened compounds ('hits' and 'no hits') with published drug characteristics and PCA-analysis of the structures of the NIHCC compounds. (A) Hit selection procedure. After calculation of a % eGFP expression for all the 'siNG transfection + compound'-treated ($n = 1$) and 'siNG transfection alone'-treated ($n = 4$) cells, hits are identified within each 96-well plate (28 plates in total). For every plate, hits are defined as compounds that cause a decrease in % eGFP expression of respectively more than 3 and 6 times the standard deviation (SD) on the % eGFP expression obtained with the siNG-DMSO control ('siNG transfection alone' with equal amount of DMSO, *i.e.* 1% v/v) for the 'minor' and 'major' hits. The data analysis of one 96-well plate is shown as an example. (B) The relative amount of acid sphingomyelinase inhibitors (ASMi +) increases from 8.6% in the 'no hit' group to 65.7% in the 'hit' group (both 'minor' and 'major' hits). Compounds were considered 'ASMi +' if they were classified as ASM-inhibitors by Kornhuber *et al.* (residual activity of ASM of $\leq 50\%$ at $10 \mu\text{M}$ in Human brain neuroglioma H4-cells)¹. (C) The relative amount of LipidTOX™ accumulation inducing compounds (LipidTOX™ +) increases from 10.1% in the 'no hit' group to 61.1% in the 'hit' group. Compounds were considered 'LipidTOX™ +' if they were classified as LipidTOX™ positive compounds by Muehlbacher *et al.* (cellular LipidTOX™ fluorescence (normalized to % of respective control) $> 200\%$ at $5 \mu\text{M}$ in Human brain neuroglioma H4-cells)². (D) The relative amount of phospholipidosis (PLD) inducers (PLD +) increases from 18.6% in the 'no hit' group to 65.5% in the 'hit' group. Compounds were considered 'PLD +' if they were

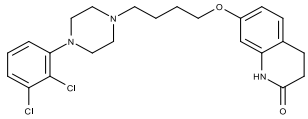
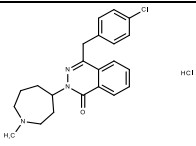
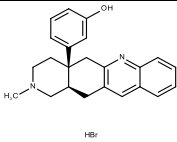
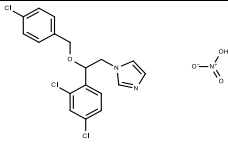
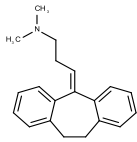
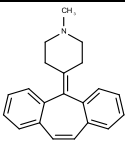
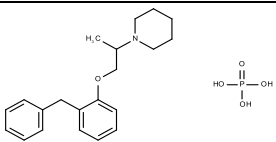
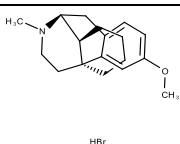
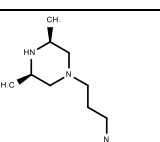
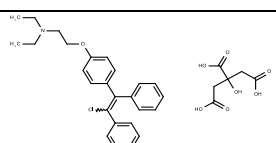
classified as PLD inducers by Goracci *et al.* (compiled a new database of 331 compounds with 'PLD +' and 'PLD -' assignments, by comparing 7 previously published databases (based upon 'in vitro', 'in vivo' and 'in silico' data) with 'PLD + or -' annotations, after removal of identified inconsistencies between the databases)³. (E) Contingency tables. CADs ($\chi^2 = 116$, $df = 1$, $p < 0.0001$), ASM-inhibitors ($\chi^2 = 36.1$, $df = 1$, $p < 0.0001$), LipidTOX™ positive compounds ($\chi^2 = 39$, $df = 1$, $p < 0.0001$) and PLD inducers ($\chi^2 = 24$, $df = 1$, $p < 0.0001$) are enriched in the 'hit' group, which is supported by χ^2 likelihood ratio tests with Yates continuity correction ($p < 0.05$ indicates an association between the two properties, being either (NO) CADs/(NO) ASMi/(NO) LipidTOX™ positive compounds/(NO) PLD inducers vs. (NO) hits)². (F) Chemical space of NIHCC compounds, hits and CADs. The structural similarities of all the NIHCC compounds were analyzed using a web-based principal component analysis (PCA)-tool that projects circular molecular fingerprints (512bits long Morgan fingerprints (extended-connectivity fingerprint 4, ECFP4) with the radius of 2), which are representations of the structures of the compounds, into new sets of coordinates (PC1 and PC2)⁴. The distance between, the size of and the color of the data points (each dot represents 1 compound) in the scatter plot correspond respectively to their structural resemblance, the clogP of the compound and the annotation of the compound to a certain group (NIHCC full database = red, all hits = green, CAD-hits = blue, CAD-no hits = orange). (G) Box and whisker plot of the clogP and pKa1 values of the 'CAD-no hit' and 'CAD-hit group'. (MFI (eGFP) = mean fluorescence intensity of the H1299-eGFP cells transfected with siCTRL- or sieGFP-loaded NGs, NG = nanogels, SD = standard deviation, NIHCC = National Institutes of Health Clinical Collection, CAD = cationic amphiphilic drug, ASM = acid sphingomyelinase, ASMi + = ASM inhibitor, PLD = phospholipidosis, PCA = principal component analysis, PC1 = principal component 1, PC2 = principal component 2, LT = LipidTOX™, clogP = calculated logP, pKa1 = macroscopic pKa of the conjugated acid of the most basic amine).

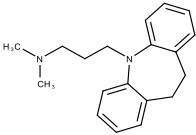
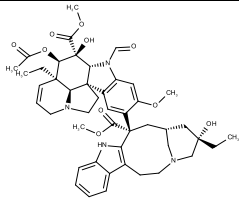
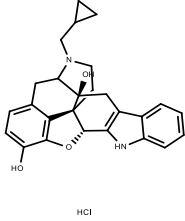
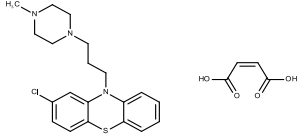
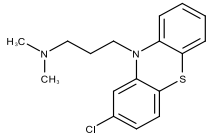
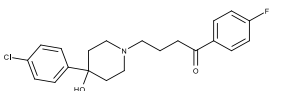
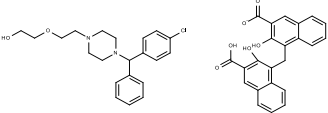
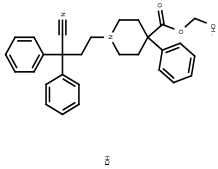
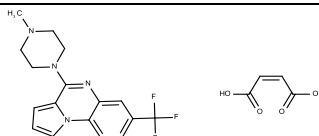
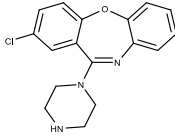
Table S1. Hit adjuvant compounds that comply with the CAD definition ($\text{clogP} > 3$, $\text{pKa1} > 6$), and having a molecular weight (MW) of less than 1000 g/mol. (pKa1 = macroscopic pKa of the conjugated acid of the most basic amine, Norm EE = normalized eGFP expression vs. siNG-DMSO control). The pKa values of the most basic amines (macroscopic pKa of the conjugated acid, pKa1) and the clogP (calculated $\log\text{P}$) values of the compounds were predicted with JChem for Office (version 17.21.0.1797, ChemAxon Ltd., Budapest, Hungary)⁵. The physiological charge (at pH 7.4) was calculated with the cxcalc calculator function (formal charge at pH 7.4, Marvin 17.21.0, 2017, ChemAxon Ltd., Budapest, Hungary)⁵. Structures were obtained from JChem for Office (version 17.21.0.1797, ChemAxon Ltd., Budapest, Hungary)⁵.

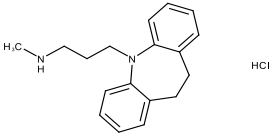
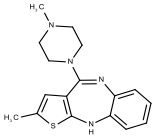
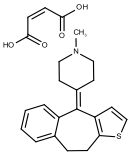
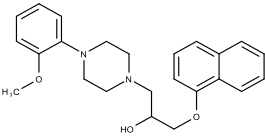
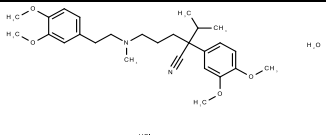
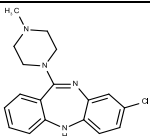
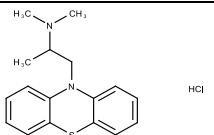
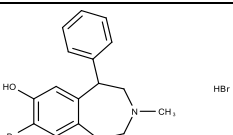
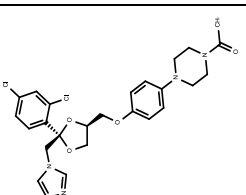
Compound Number & Name	Structure	MW (g/mol)	clogP	pKa1	Physiological charge (at pH 7.4)	Norm EE
(1) Thiothixene		443.62	3.36	8.16	1	0.11
(2) Thioridazine hydrochloride		407.03	5.47	8.93	1	0.13
(3) Desloratadine		310.83	3.97	9.73	1	0.15
(4) Tamoxifen		371.52	6.35	8.76	1	0.16
(5) Perphenazine		403.97	3.69	7.81	1	0.16
(6) Raloxifene hydrochloride		510.05	5.69	7.95	1	0.21
(7) Loperamide hydrochloride		513.5	4.77	9.41	1	0.23

(8) 5-Nonyloxytryptamine hydrochloride		338.92	4.88	9.76	1	0.24
(9) Vinorelbine tartrate		929.03	4.65	8.66	2	0.24
(10) Paroxetine maleate		445.44	3.15	9.77	1	0.29
(11) Clofazimine		473.4	7.30	6.63	0	0.35
(12) Fluoxetine hydrochloride		345.79	4.17	9.80	1	0.41
(13) Toremifene citrate		598.09	6.27	8.76	1	0.45
(14) Amiodarone hydrochloride		681.78	7.64	8.47	1	0.46
(15) Saquinavir mesylate		766.96	3.16	8.47	1	0.47
(16) Indatraline hydrochloride		328.66	4.70	9.50	1	0.49
(17) Duloxetine hydrochloride		333.87	4.20	9.70	1	0.49

(18) Clomipramine hydrochloride		351.32	4.88	9.20	1	0.49
(19) Salmeterol		415.57	3.61	9.40	1	0.50
(20) Mefloquine hydrochloride		414.78	4.11	9.46	1	0.52
(21) Lofepramine		418.97	6.11	6.53	0	0.55
(22) Imatinib mesylate		589.72	4.38	7.84	1	0.55
(23) Nelfinavir mesylate		663.89	4.72	8.18	1	0.57
(24) Miconazole nitrate		479.14	5.96	6.48	0	0.58
(25) Trifluoperazine hydrochloride		443.96	4.66	7.99	1	0.60
(26) Sertraline hydrochloride		342.69	5.15	9.56	1	0.61
(27) Carvedilol		406.48	3.42	8.74	1	0.65

(28) Aripiprazole		448.39	4.90	7.46	1	0.65
(29) Azelastine hydrochloride		418.36	4.04	8.88	1	0.66
(30) SB 205607 dihydrobromide		443.39	3.92	8.28	1	0.67
(31) Econazole nitrate		444.69	5.35	6.48	0	0.67
(32) Amitriptyline hydrochloride		313.87	4.81	9.76	1	0.67
(33) Cyproheptadine hydrochloride		323.86	4.38	8.05	1	0.68
(34) Benproperine phosphate		407.45	5.19	9.05	1	0.68
(35) Dextromethorphan hydrobromide, monohydrate		370.33	3.49	9.85	1	0.70
(36) Rimcazole dihydrochloride		375.94	3.69	9.81	1	0.71
(37) Clomifene citrate		598.09	6.47	9.31	1	0.75

(38) Imipramine hydrochloride		316.87	4.28	9.20	1	0.75
(39) Vincristine sulfate		923.04	3.13	8.66	2	0.75
(40) Naltrindole hydrochloride hydrate		468.98	3.07	8.64	1	0.77
(41) Prochlorperazine maleate		490.02	4.38	7.99	1	0.77
(42) Chlorpromazine hydrochloride		355.32	4.54	9.20	1	0.77
(43) Haloperidol hydrochloride		412.33	3.66	8.05	1	0.78
(44) Hydroxyzine pamoate		762.28	3.41	7.45	1	0.78
(45) Diphenoxylate hydrochloride		489.06	5.88	8.50	1	0.78
(46) CGS 12066B dimaleate		450.42	3.22	7.61	1	0.78
(47) Amoxapine		313.79	3.08	8.83	1	0.78

(48) Desipramine hydrochloride		302.85	3.90	10.02	1	0.81
(49) Olanzapine		312.44	3.39	7.24	1	0.83
(50) Pizotyline maleate		411.52	4.49	7.98	1	0.83
(51) Naftopidil		392.50	3.77	7.35	1	0.83
(52) Verapamil hydrochloride		509.08	5.04	9.68	1	0.83
(53) Clozapine		326.83	3.40	7.35	1	0.85
(54) Promethazine hydrochloride		320.88	4.29	9.05	1	0.85
(55) SKF 83566 hydrobromide		413.15	3.60	8.77	1	0.88
(56) Ketoconazole		531.43	4.19	6.42	0	0.89

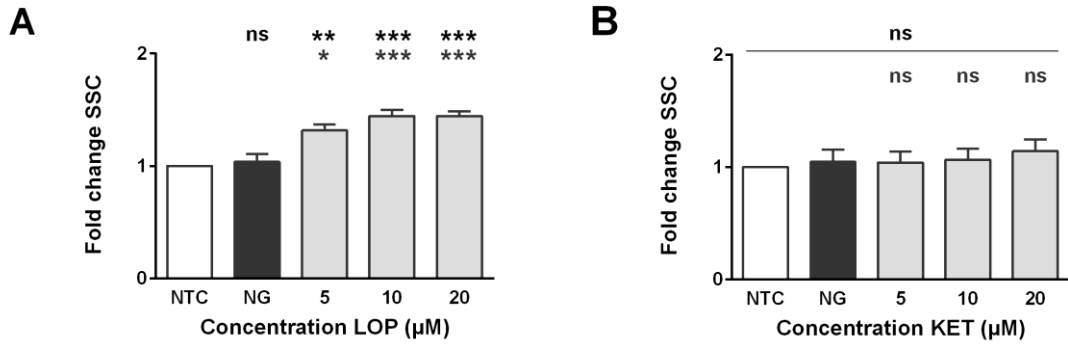


Figure S3. Loperamide, but not ketotifen, induces a concentration-dependent increase in cellular granularity of NSCLC cells. (A-B) Fold change in side scatter (SSC) signal for H1299-eGFP cells treated with the sequential combination of siNG transfection and treatment with 3 different μM concentrations of ketotifen (KET) or loperamide (LOP). Data are represented as the mean \pm the standard error of the mean (SEM) for minimum three independent repeats. Statistical significance is indicated when appropriate, in black * when referring to the untreated control and in grey * when compared to siNG transfection alone (ns $p > 0.05$, * $p \leq 0.05$, ** $p \leq 0.01$, *** $p \leq 0.001$). (NTC = not treated control, NG = dex-HEMA siNG transfection without sequential CAD treatment, KET = ketotifen, LOP = loperamide, ns = not significant, SSC = side scatter).

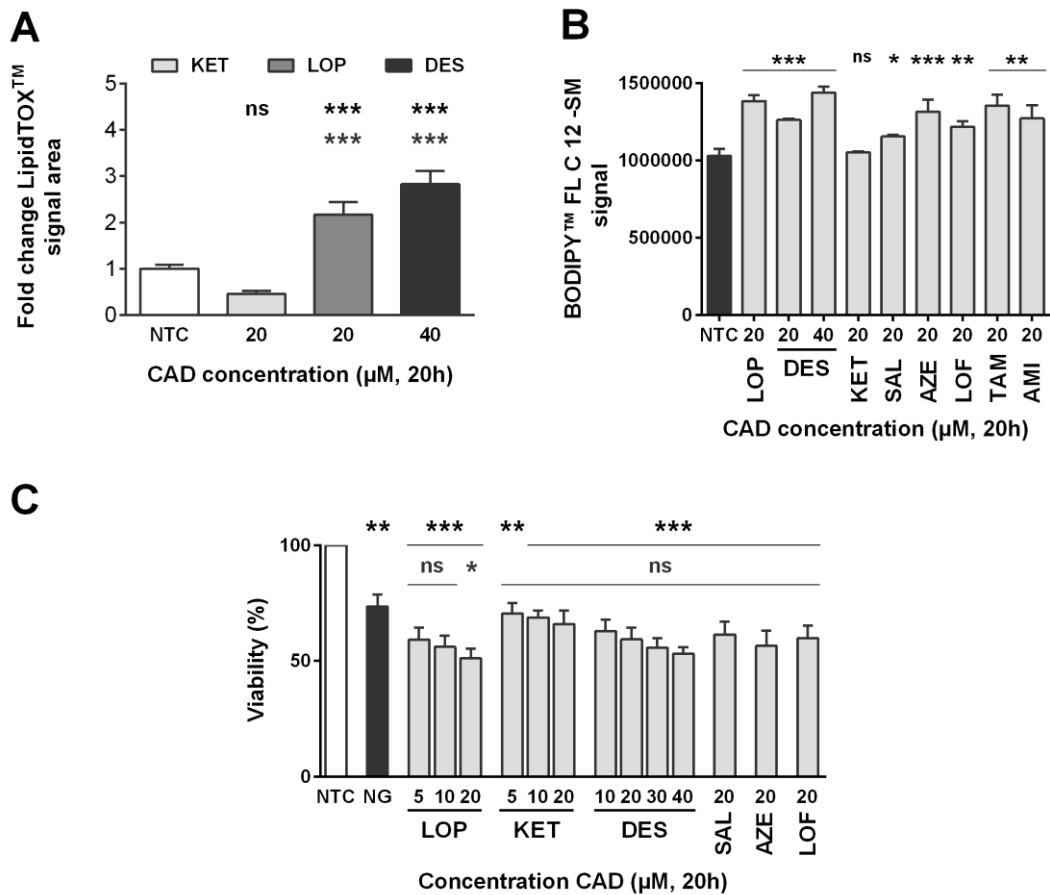


Figure S4. Loperamide and desloratadine, but not ketotifen, induce a phospholipidosis phenotype in NSCLC cells while inducing limited cytotoxicity. (A) Fold increase in LipidTOX™ Red phospholipidosis signal area relative to the untreated control quantified from the confocal images in **Figure 3B**. The data are represented as mean ± SD. Statistical significance with respect to the NTC (black *) or 20 μM KET treated cells (grey *) is indicated when appropriate (ns p > 0.05, *** p ≤ 0.001). (B) Increase in BODIPY™ FL C12-SM signal compared to the untreated control. The data are represented as mean ± SD (n = 3, technical replicates). Statistical significance with respect to the NTC (black *) is indicated when appropriate (ns p > 0.05, * p ≤ 0.05, ** p ≤ 0.01, *** p ≤ 0.001). (C) Cell viability of H1299-eGFP cells following sequential dex-HEMA siNG transfection (1 nM siCTRL) and CAD addition. Data are represented as mean ± the standard error of the mean (SEM) for minimum three independent repeats. Statistical significance is indicated when appropriate, in black * when referring to the untreated control and in grey * when compared to dex-HEMA siNG transfection alone (ns p > 0.05, * p ≤ 0.05, ** p ≤ 0.01, *** p ≤ 0.001). (NTC = not treated control, NG = dex-HEMA siNG transfection without sequential CAD treatment, CAD = cationic amphiphilic drug, KET = ketotifen, LOP = loperamide, DES = desloratadine, SAL = salmeterol, AZE = azelastine, LOF = lofepramine, TAM = tamoxifen, AMI = amitriptyline, BODIPY™ FL C12-SM = BODIPY™ FL C12-sphingomyelin, ns = not significant).

REFERENCES FOR SUPPORTING INFORMATION

1. Kornhuber, J. *et al.* Identification of Novel Functional Inhibitors of Acid Sphingomyelinase. *PLoS One* **2011**, *6*, e23852.
2. Muehlbacher, M.; Tripal, P.; Roas, F.; Kornhuber, J. Identification of Drugs Inducing Phospholipidosis by Novel *In Vitro* Data. *ChemMedChem* **2012**, *7*, 1925–1934.
3. Goracci, L.; Ceccarelli, M.; Bonelli, D.; Cruciani, G. Modeling Phospholipidosis Induction: Reliability and Warnings. *J. Chem. Inf. Model.* **2013**, *53*, 1436–1446.
4. Skuta, C. *et al.* Probes & Drugs Portal: An Interactive, Open Data Resource for Chemical Biology. *Nat. Methods* **2017**, *14*, 759–760.
5. *JChem for Office (Excel)*, Version 17.21.0.1797; Software Was Used for Chemical Database Access, Structure Based Property Calculation, Search and Reporting; ChemAxon: Budapest, Hungary, 2017. [Http://www.chemaxon.com](http://www.chemaxon.com).

Chapter 3

Cationic amphiphilic drugs boost the lysosomal escape of small nucleic acid therapeutics in a nanocarrier-dependent manner

This chapter is published as a part of:

Van de Vyver, T.[†]; Bogaert, B.[†]; De Backer, L.[†]; Joris, F.[†]; Guagliardo, R.[†]; Van Hoeck, J.[†]; Merckx, P.[†]; Van Calenbergh, S.[‡]; Ramishetti, S.[§]; Peer, D.[§]; Remaut, K.[†]; De Smedt, S.C.[†]; Raemdonck, K.[†] Cationic Amphiphilic Drugs Boost the Lysosomal Escape of Small Nucleic Acid Therapeutics in a Nanocarrier-Dependent Manner. *ACS Nano* **2020**, *14*, 4774–4791.

DOI: 10.1021/acsnano.0c00666

Joris, F.[†]; De Backer, L.[†]; Van de Vyver, T.[†]; Bastiancich, C.^{||}; De Smedt, S. C.[†]; Raemdonck, K.[†] Repurposing Cationic Amphiphilic Drugs as Adjuvants to Induce Lysosomal siRNA Escape in Nanogel Transfected Cells. *J. Control. Release* **2018**, *269*, 266–276.

DOI: 10.1016/j.jconrel.2017.11.019

[†] Ghent Research Group on Nanomedicines, Laboratory of General Biochemistry and Physical Pharmacy, Faculty of Pharmaceutical Sciences, Ghent University, Ottergemsesteenweg 460, 9000 Ghent, Belgium

[‡] Laboratory for Medicinal Chemistry, Faculty of Pharmaceutical Sciences, Ghent University, Ottergemsesteenweg 460, 9000 Ghent, Belgium

[§] Laboratory of Precision NanoMedicine, School of Molecular Cell Biology and Biotechnology, George S. Wise Faculty of Life Sciences, Tel Aviv University, Tel Aviv, 6997801, Israel

^{||} Louvain Drug Research Institute, Advanced Drug Delivery and Biomaterials, Université Catholique de Louvain, 1200 Brussels, Belgium

Author contributions

Conceptualization and study design: T.V.d.V., S.C.D.S., and K. Raemdonck. Experimental work and data analysis: T.V.d.V., B.B., L.D.B., R.G., P.M., F.J., J.V.H., K. Remaut, and K. Raemdonck. S.R. and D.P. assisted with the design and evaluation of the ionizable lipid nanoparticles. Chapter 3 was written through contributions of all authors.

TABLE OF CONTENTS

1. INTRODUCTION	141
2. RESULTS AND DISCUSSION.....	144
2.1. Confirmation of the CAD adjuvant effect on a different cargo and cell model....	144
2.2. Evaluation of CAD adjuvant effect on different siRNA-loaded nanocarriers	147
2.3. Decomplexation efficiency and intracellular siRNA dose define successful CAD-nanocarrier combinations.....	150
3. CONCLUSION	157
4. MATERIALS AND METHODS	158
4.1. siRNA duplexes and oligonucleotides	158
4.2. Nanoparticle (NP) synthesis, preparation and siRNA complexation	159
4.3. Cell lines and cell culture conditions	161
4.4. Fluorescence fluctuation spectroscopy (FFS) on siRNA-loaded NPs	162
4.5. Quantification of transfection efficiency/lysosomal volume of NP transfection and sequential adjuvant treatment by flow cytometry.....	162
4.6. Quantification of <i>in vitro</i> cellular ASO or siRNA internalization in H1299-eGFP and SKOV-3-LUC+ cells by flow cytometry	164
4.7. Visualization and quantification of the cytosolic release of AF647 ONs	164
4.8. Visualization of the cytosolic release of FITC-dextran	165
4.9. Statistical analysis	165

ABSTRACT

In **Chapter 2**, we reported on a drug repurposing screen that identified multiple cationic amphiphilic drugs (CADs) as potent siRNA delivery enhancers. These results corroborated our earlier findings that a selection of CADs could promote cytosolic release of siRNA from the endolysosomal compartment *via* transient induction of lysosomal membrane permeabilization. However, many questions still remain regarding the broader applicability of such a CAD adjuvant effect on nucleic acid (NA) delivery. Here, we demonstrate that the CAD adjuvant effect is dependent on the type of nanocarrier, with nanoparticles (NPs) that generate an appropriate pool of decomplexed siRNA in the endolysosomal compartment being most susceptible to CAD-promoted gene silencing. Additionally, the CAD adjuvant effect was verified on other cancer cell types (*i.e.* SKOV-3 and HeLa cells) and for other small NAs (antisense oligonucleotides and Dicer-substrate siRNAs). In conclusion, this study strongly expands our current knowledge on how CADs increase the cytosolic release of small NAs, providing relevant insights to more rationally combine CAD adjuvants with NA-loaded NPs for future therapeutic applications.

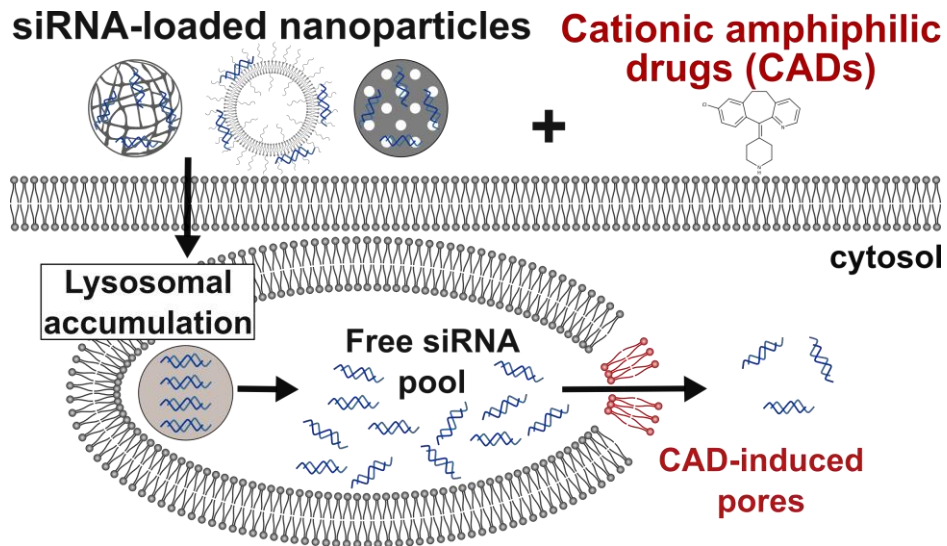
KEYWORDS: drug repurposing; cationic amphiphilic drugs; lysosomal membrane permeabilization; nucleic acid therapeutics; cellular delivery; endosomal escape; lipid nanoparticles

1. INTRODUCTION

Small non-coding RNAs, such as small interfering RNA (siRNA), show great potential for the treatment of a myriad of diseases for which no suitable cure exists to date. Their main mode-of-action involves post-transcriptional sequence-specific gene silencing, permitting to address virtually any human pathology with a recognized (over)expression of a disease-causing protein¹⁻³. To overcome the multiple extra- and intracellular barriers upon *in vivo* administration, nucleic acid (NA) drugs are generally encapsulated into nanoparticles (NPs)^{1,4,5}. At the cellular level, NPs foster intracellular uptake of NAs by target cells through endocytosis, sequestering them in endosomes⁴⁻⁶. However, to exert their gene silencing function, NAs have to be released from the endosomal lumen into the cytosol^{1,6}. Unfortunately, despite the development of multiple endosomal escape strategies (*e.g.* based on endosomal membrane fusion or disruption), this process remains largely inefficient, with the vast majority of endocytosed drug being unintentionally routed towards lysosomes for degradation⁷⁻¹². As a result, typically less than 1% of the internalized NA dose is released into the cytosol^{6-8,13}.

Notably, several small molecular drugs have shown to improve the delivery of NAs by modulating (one or more) of the extra- and/or intracellular barriers (**Chapter 1**)¹⁴⁻²⁴. In this context, we recently demonstrated that a selection of cationic amphiphilic drugs (CADs) can enhance the release of nanogel-transfected siRNAs from the lysosomal compartment into the cytosol of non-small cell lung cancer (NSCLC) cells²⁰. Mechanistically, these CADs are known to accumulate inside the acidified lysosomes *via* pH-dependent ion trapping, leading to phospholipidosis (PLD) induction, lysosomal swelling and a transient lysosomal membrane permeabilization (LMP), most probably as a result of functional inhibition of the acid sphingomyelinase (ASM) enzyme. Subsequently, the destabilized lysosomal membrane allows lysosomal sequestered siRNA molecules to diffuse into the cytosol²⁰. Hence, in contrast to the current paradigm, that states that lysosomal entrapment is a non-functional dead end for siRNA therapeutics, these data indicated that the lysosomes can be exploited as depots for triggered siRNA release by CAD treatments. In **Chapter 2**, our compound screening furthermore showed that the observed adjuvant effect on siRNA delivery is not limited to the previously identified CAD molecules, but that many more CADs phenocopy these effects. However, many questions still remain regarding the broader applicability of CADs as adjuvants for NA delivery. For instance, our previous study indicated that CADs

were unable to boost the delivery efficiency of larger NA therapeutics such as enhanced green fluorescent protein (eGFP)-encoding messenger (m)RNA (~350 kDa), suggesting that the CAD-induced pores are relatively small and only permit passage of small NAs²⁰. Hence, we here evaluated if the CADs, besides 21mer siRNA molecules (~14 kDa), could also improve the cytosolic delivery of chemically modified antisense oligonucleotides (ASOs, ~6 kDa) and 25-27mer Dicer-substrate siRNAs (DsiRNA, ~18 kDa) in NSCLC cancer cells. In addition, given that we solely used a single NSCLC cell line up till now, we confirmed the adjuvant effect of the CADs on a human ovarian SKOV-3 and cervical HeLa cancer cell line. Finally, the siRNA-loaded dextran nanogels were used as model NPs in our earlier studies (Joris *et al.*²⁰ and **Chapter 2**), as they have previously shown both a high loading capacity for siRNA as well as feasible cellular uptake, lysosomal accumulation and gene silencing efficiency in various cancer cells^{9,20,25–28}. However to probe the broader applicability of our approach, it was investigated if the CAD adjuvant effect can also be extended to other nanocarrier types, including cationic mesoporous silica nanoparticles (MSNPs), (PEGylated) cationic liposomes (LIPs) and lipid nanoparticles (LNPs) containing the ionizable lipid DLin-MC3-DMA²⁹. Our data indicate that a multitude of CADs can promote cellular delivery of both siRNAs and ASOs. Importantly, we discovered that the extent of NP internalization by target cells as well as the efficiency of NA decomplexation dictate the success of CAD-promoted endolysosomal escape. Indeed, our data suggest that a sufficient amount of free siRNA is needed inside the lysosomal lumen (*i.e.* lysosomal pool of free siRNA) to allow diffusion through the CAD-created lysosomal pores into the cytosol (**Scheme 1**).



Scheme 1. Transfection with siRNA-loaded nanoparticles needs to result in a lysosomal pool of free (decomplexed) siRNA, in order to be compatible with the CAD adjuvant approach. Multiple siRNA-loaded nanoparticles (siNPs) are internalized by cells *via* an endocytic process and efficiently routed towards the lysosomal compartment. Cationic amphiphilic drugs (CADs) accumulate in the lysosomal compartment *via* pH-driven ion trapping, where they can strongly promote functional siRNA delivery by the transient induction of lysosomal membrane permeabilization (LMP). However, the CAD adjuvant effect is only observed for siNPs that result in a sufficient amount of free siRNA inside the lysosomal lumen to allow diffusion through the CAD-created lysosomal pores into the cytosol.

2. RESULTS AND DISCUSSION

2.1. Confirmation of the CAD adjuvant effect on a different cargo and cell model

Although chemically stabilized gapmer antisense oligonucleotides (ASOs, ~6 kDa) are single stranded NAs with a different mode-of-action for mRNA cleavage compared to double-stranded siRNAs, they face similar intracellular delivery challenges^{1,30,31}. Hence, the effect of the previously identified CAD adjuvant desloratadine (DES) on the eGFP gene silencing potential of dex-HEMA nanogels (dex-HEMA NGs) loaded with an eGFP-targeting ASO (eGFP-ASO) was examined²⁰. Note that desloratadine, the main compound tested in our earlier work, was confirmed in the NIHCC screen as one of the most promising hits (**Chapter 2**). Keeping clinical translation in mind, antihistamines like desloratadine may provide a safer alternative compared to *e.g.* antipsychotics or compounds targeting opioid receptors. Hence, we mainly used desloratadine to assess the broader applicability of the CAD adjuvant approach in this chapter. The ASO-loaded dex-HEMA NGs (ASO-NGs) were efficiently internalized by the H1299-eGFP cells (**Figure 1A**) and both tested ASO concentrations induced a suboptimal eGFP knockdown (**Figure 1B**). Sequential treatment with 40 μ M desloratadine, the most effective concentration for this compound²⁰, clearly promoted ASO-NG gene silencing (**Figure 1B**), which coincided with a marked enlargement of the total lysosomal volume (**Figure 1C**). Visual microscopic confirmation of the enhanced cytosolic oligonucleotide delivery by desloratadine and loperamide (LOP) adjuvant treatment was obtained with Alexa Fluor® 647-labeled oligonucleotides (AF647 ONs), which upon endosomal egress migrate to the cell nucleus (**Figure 1D**). A punctate pattern was observed for the majority of untreated and 20 μ M ketotifen (KET)-treated cells, indicating lysosomal sequestration, whereas 20 μ M loperamide and 30 μ M desloratadine clearly increased the amount of stained nuclei (**Figure 1D**). The percentage of cells that showed cytosolic ON delivery is relatively low, which likely can be attributed to the cytosolic dilution of the labeled ONs^{7,20}. While gapmer ASOs induce RNase H1 cleavage of the target mRNA, siRNAs make use of the endogenous RNAi machinery^{3,12}. The enhanced ASO-mediated eGFP knockdown upon desloratadine exposure thus proves that the enhanced silencing effect is independent of the RNAi pathway, but likely results from improved cytosolic delivery. Of note, in addition to ASOs/ONs and 21mer siRNA duplexes (~14 kDa), sequential desloratadine treatment could also promote the delivery efficiency of dex-HEMA NGs

loaded with the slightly larger 25-27mer Dicer-substrate siRNAs (DsiRNAs, ~18 kDa) (**Figure S1**).

Next, we also quantified the effect of two CAD adjuvants (*i.e.* desloratadine and salmeterol (SAL), see **Chapter 2**) on the luciferase silencing potential of siRNA-loaded dex-HEMA NGs (dex-HEMA siNGs) in a SKOV-3-LUC+ cell line that stably expresses the *firefly* luciferase protein (**Figure S2**). Similar to the experiments with the H1299-eGFP cells, the siNGs were efficiently internalized (**Figure S2A**), and a sequential 20 h drug treatment with salmeterol or desloratadine strongly enhanced the luciferase silencing in a concentration-dependent manner (**Figure S2B-D**). Comparable results were seen for the SKOV-3-LUC2 IP2 (20 h incubation) and HeLa NLS-GFP (2 h incubation) cell line (**Figure S4H-I**). Finally, enhanced endolysosomal escape of AF647 ONs could be visualized in SKOV-3-LUC2 IP2 cells for 30 μ M desloratadine, 30 μ M salmeterol and 20 μ M loperamide, but not 20 μ M ketotifen (**Figure S3, Figure S4A-G**). In conclusion, next to the NSCLC cell model we could confirm the CAD adjuvant effect for (D)siRNA and/or oligonucleotide delivery on a luciferase expressing SKOV-3 cell line and a HeLa cell line.

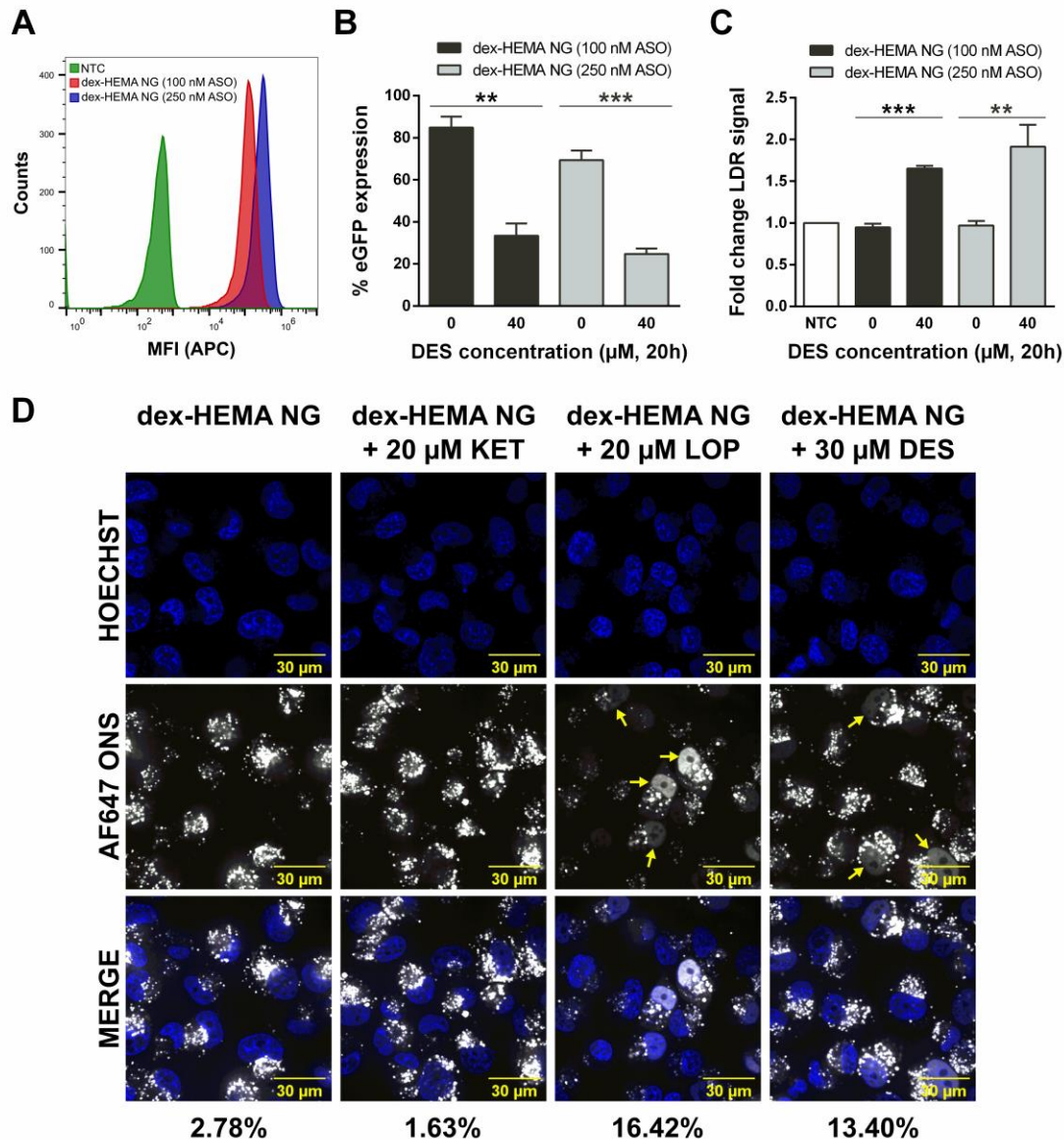


Figure 1. CADs enhance the delivery of ASOs/ONs in NSCLC cells. (A) Evaluation of cellular uptake of dex-HEMA ASO-NGs, loaded with suboptimal amounts of Cy5[®]-labeled ASOs, in H1299-eGFP cells determined *via* flow cytometry. (B) eGFP silencing in H1299-eGFP cells with dex-HEMA ASO-NGs could be significantly improved through sequential treatment with 40 μM desloratadine (DES) for 20 h. (C) Fold change in LDR signal, measured *via* flow cytometry, for H1299-eGFP cells sequentially transfected with dex-HEMA ASO-NGs and treated with 40 μM DES for 20 h. (D) Representative confocal images from the intracellular AF647 ON distribution in H1299-eGFP cells, only transfected with AF647 ON-loaded dex-HEMA NGs, or cells subsequently incubated with 20 μM ketotifen (KET)/20 μM loperamide (LOP)/30 μM desloratadine (DES) for 20 h. Nuclei can be seen in blue, while cells in which escape happened show nuclear fluorescence in the red channel (red fluorescence is depicted white) due to the release of AF647 ONs in the cytosol. The values below the images correspond to the percentage of cells with white nuclei (yellow arrows). The scale bar corresponds to 30 μm . Data are represented as mean \pm the standard error of the mean (SEM) for minimum three independent repeats. Statistical significance is indicated when appropriate, in black * when referring to ASO-NG transfection alone (100 nM ASO) and in grey * when compared to ASO-NG transfection alone (250 nM ASO) (** $p \leq 0.01$, *** $p \leq 0.001$). (CADs = cationic amphiphilic drugs, ASO =

phosphorothioate gapmer antisense oligonucleotide, NTC = not treated control, NG = nanogels, DES = desloratadine, KET = ketotifen, LOP = loperamide, LDR = LysoTracker® Deep Red, MFI = mean fluorescence intensity, APC = allophycocyanin (red channel), ON = oligonucleotide, AF647 = Alexa Fluor® 647 dye).

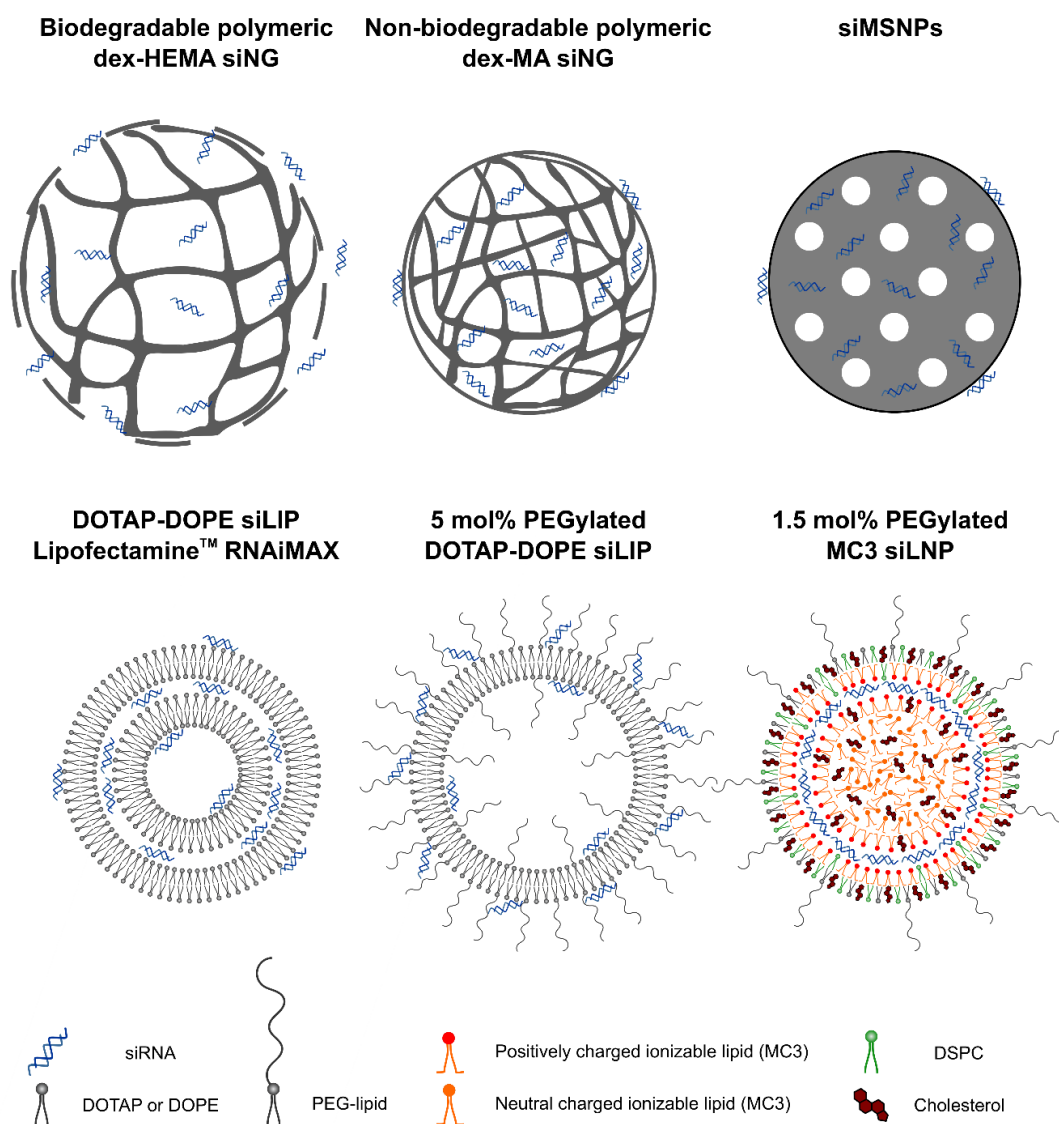
2.2. Evaluation of CAD adjuvant effect on different siRNA-loaded nanocarriers

Next to the biodegradable dex-HEMA siNGs used above and in **Chapter 2**, also many other nanoparticles (NPs) are internalized by cells *via* an endocytic process and efficiently routed towards the lysosomal compartment^{7–11,32–35}. Here, we evaluated if the CAD adjuvant approach could similarly improve the cytosolic siRNA delivery of a panel of siRNA-loaded NPs (siNPs): *i.e.* non-biodegradable polymeric dextran NGs (dex-MA)^{9,26}, inorganic propylamine functionalized mesoporous silica NPs (MSNPs), cationic lipid NPs (LNPs) such as (PEGylated) DOTAP-DOPE liposomes (LIPs), the lipofection reagent Lipofectamine® RNAiMAX and lipid nanoparticles containing the ionizable lipid DLin-MC3-DMA (MC3 LNPs) in H1299-eGFP cells (**Scheme 2**). The physicochemical properties of the (PEGylated) DOTAP-DOPE liposomes and the MC3 siRNA-loaded LNPs (siLNPs) are shown in **Figures S7-8**. A sequential 20 h incubation with 40 µM desloratadine, a previously identified adjuvant that also emerged as a major CAD-hit in the NIHCC screen (**Chapter 2**), was used as CAD treatment to ensure clear induction of the anticipated lysosomal phenotype²⁰.

Although lower eGFP silencing was observed for the stable dex-MA siNGs compared to their degradable dex-HEMA counterparts, sequential desloratadine treatment achieved >90% eGFP knockdown for both particles (**Figure 2A**). A comparable result was obtained with siRNA-loaded MSNPs (siMSNPs) (**Figure 2B**). Hence, these data indicate that the CAD adjuvant effect is independent of the intrinsic degradability of the used NGs and can also be effective on inorganic nanocarriers.

In contrast, this CAD adjuvant effect on siRNA delivery could not be observed for the cells transfected with siRNA-loaded cationic lipid nanoparticles (LNPs) such as DOTAP-DOPE liposomes or Lipofectamine® RNAiMAX (**Figure 2C, Figure S6A**), despite clear indication that the applied desloratadine evoked lysosomal swelling (**Figure S5A, Figure S6B**). Previous studies by our group and others, evaluating the effect of photochemical internalization (PCI) on siRNA-loaded Lipofectamine® RNAiMAX or Lipofectamine® 2000, showed comparable

results. PCI is a technique that destabilizes endosomal membranes by the application of amphiphilic photosensitizers, which upon photoactivation evoke oxidative endolysosomal membrane damage through the production of reactive oxygen species (ROS)^{9,26,36}. In line with the observations on CADs, the silencing potential of siRNA-loaded cationic LNPs was unaffected by PCI, whereas the cellular siRNA delivery *via* dex-(HE)MA siNGs was strongly enhanced^{9,26}.



Scheme 2. Schematic representation of the tested siRNA-loaded NPs. The structure of siLNPs with an ionizable lipid (*e.g.* MC3) is shown as recently proposed by Kulkarni *et al.*³⁷. (siNPs = siRNA-loaded nanoparticles, siNG = siRNA-loaded nanogel, siMSNPs = inorganic propylamine functionalized mesoporous silica siNPs, siLIP = siRNA-loaded liposome, siLNP(s) = siRNA-loaded lipid nanoparticle(s), MC3 = DLin-MC3-DMA).

As state-of-the-art LNPs are generally PEGylated, also the influence of including a PEGylated lipid (DSPE-PEG₂₀₀₀) in the formulation was probed. Although higher siRNA and liposome (LIP) concentrations were needed to achieve target gene knockdown compared to the non-PEGylated counterpart, a clear adjuvant effect of desloratadine on the siRNA delivery efficiency could be seen when the DOTAP-DOPE liposomes were modified with 5 mol% of the PEGylated lipid (**Figure 2D, Figure S5B**). In contrast, desloratadine was not able to improve siRNA delivery mediated by ionizable MC3 siLNPs (**Figure S9A-B**), despite being PEGylated (1.5 mol% DMG-PEG₂₀₀₀) and neutrally charged at physiological pH. Given the clear dependency on the type of nanocarrier, we next sought to investigate in more detail which requirements a therapeutic siNP should have to be compatible with the proposed CAD adjuvant approach.

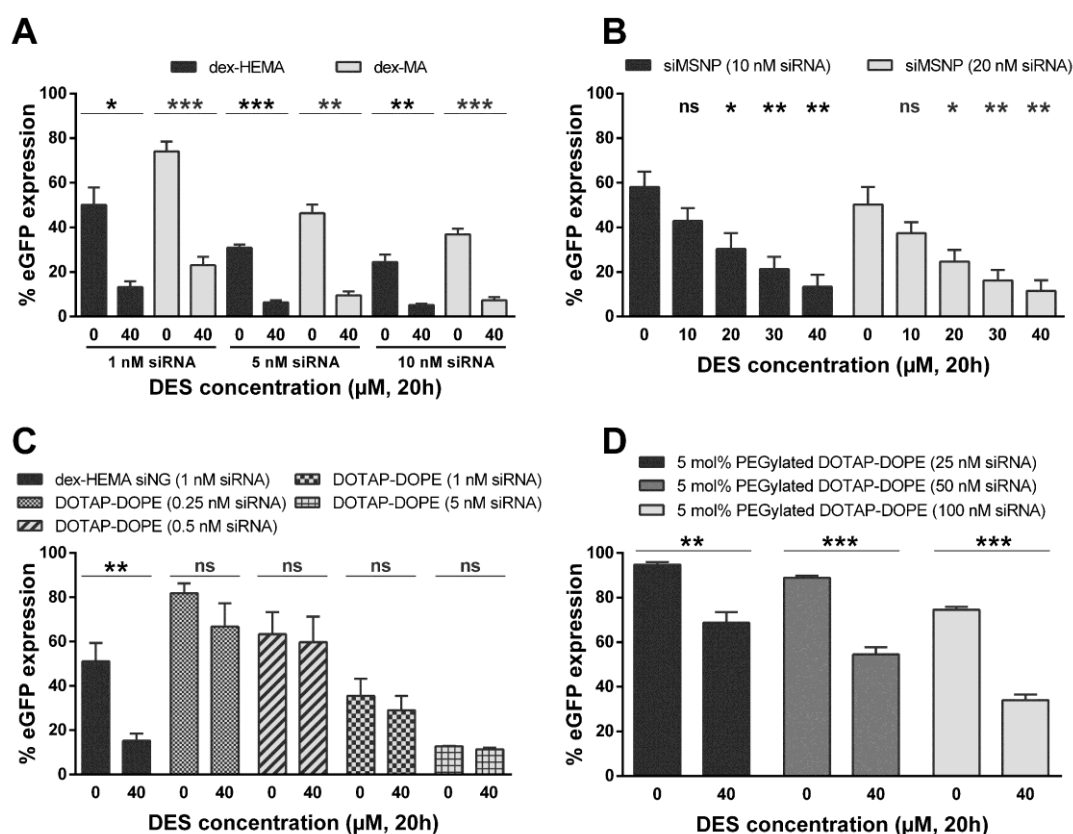


Figure 2. Adjuvant effect of desloratadine on eGFP silencing in H1299-eGFP cells is nanocarrier-dependent. (A-D) The influence of 20 h sequential adjuvant treatment with desloratadine (DES) on the transfection efficiency of dex-(HE)MA siNGs, siMSNPs or (PEGylated) DOTAP-DOPE siLIPs. Data are represented as mean \pm the standard error of the mean (SEM) for minimum three independent repeats. Statistical significance is indicated when appropriate, in black * when referring to dex-HEMA siNG, PEGylated DOTAP-DOPE siLIP or siMSNP (10 nM siRNA) transfection alone and in grey * when

compared to dex-MA siNG, DOTAP-DOPE siLIP or siMSNP (20 nM siRNA) transfection alone (ns $p > 0.05$, * $p \leq 0.05$, ** $p \leq 0.01$, *** $p \leq 0.001$). (siNG = siRNA-loaded nanogel, siLIP = siRNA-loaded liposome, DES = desloratadine, ns = not significant, siMSNP = siRNA-loaded propylamine functionalized mesoporous silica nanoparticle).

2.3. Decomplexation efficiency and intracellular siRNA dose define successful CAD-nanocarrier combinations

Previous work from our group suggested that the CAD-induced pores in the lysosomal membrane are relatively small, only allowing the passage of decomplexed siRNA but not substantially larger NA therapeutics, *e.g.* mRNA²⁰. To probe the size of the CAD-induced pores, we examined the ability of 40 μM desloratadine to improve the cytosolic delivery of FITC-labeled dextrans (FDs) of different molecular weight, which were co-incubated with the MSNPs for 4 h. The confocal images (**Figure 3**) clearly indicate that the combination of a CAD-responsive NP (MSNPs) and 40 μM desloratadine can release FDs up to 150 kDa in the cytosol, judging from the diffuse cellular FD signal. Of note, the used FD solutions are rather polydisperse mixtures (as indicated by the manufacturer and as previously shown by our group), with the 150 kDa dispersion having a size range of approximately 10 nm - 40 nm³⁸. As such, these data imply that the actual pore size might be lower than the average 150 kDa size. Although such a pore size is larger than the size of most cell death-evoking cathepsins (20-30 kDa), no extensive reduction in cell viability is observed (**Chapter 2**). These results suggest that CADs only trigger minor and non-lethal LMP. Extensive LMP involves a substantial release of lysosomal cathepsins and cytosolic acidification, which would cause uncontrolled cell death. On the contrary, partial LMP might release a limited amount of cathepsins, which are subsequently deactivated by the neutral pH of the cytosol or by the action of endogenous cathepsin inhibitors³⁹⁻⁴¹. In addition, components of the endosomal sorting complex required for transport (ESCRT) machinery, such as the ESCRT-III complex, are able to repair permeabilized lysosomal membranes or damaged lysosomes can be routed into the lysophagy pathway^{42,43}. Altogether, these data indicate that the desloratadine-created pores exceed the size of a single siRNA duplex (~14 kDa), but not that of siRNA-loaded NPs used in this chapter (60 nm – 200 nm), thus only allowing passive diffusion of the decomplexed fraction of siRNA. We postulate that differences in this free siRNA fraction, which is determined by both the total intracellular dose as well as the siRNA

release efficiency from the nanocarrier, could explain why the delivery efficiency of some nanocarriers can be stimulated with CADs, while not of others.

Therefore, we first quantified the nanocarrier's susceptibility to siRNA decomplexation with a competing polyanion (10 kDa dextran sulphate (DEXS)) of which the size approximates that of a siRNA duplex^{35,44}. Exposure of the different siNPs to DEXS resulted in marked differences in the extent of siRNA decomplexation, with the siNGs and siMSNPs being most and least susceptible to siRNA release, respectively (**Figure 4A**, **Figure S9C**). Importantly, also PEGylation of the DOTAP-DOPE liposomes led to a higher fraction of free siRNA in the presence of DEXS. A possible explanation for this discrepancy can be found in the impact of PEGylation on the liposome nanoarchitecture. Indeed, siRNA complexation by non-PEGylated cationic liposomes leads to a multilamellar formulation with the majority of the siRNA molecules packed between opposing bilayers. In contrast, the presence of a PEG layer on the liposomal surface prior to siRNA complexation precludes this multilayer buildup, thus leaving the siRNA mostly associated to the liposomal surface (as schematically shown in **Figure S7B**). This PEG-induced difference in nanoarchitecture could lead to an easier decomplexation (**Figure 4A**) of the nucleic acid payload in extracellular biofluids as well as inside the cell, as previously shown by our group and others for siRNA, oligonucleotides and/or pDNA⁴⁵⁻⁵². One could expect that a facilitated decomplexation in the endolysosomal compartment increases the likelihood of successful cytosolic influx of siRNA through CAD-induced pores in the limiting endolysosomal membrane. This model is further supported by the data obtained with the MC3 siLNPs. A MC3 formulation prepared *via* microfluidic mixing leads to stable siRNA encapsulation in the LNP core and precludes siRNA decomplexation in the presence of competing polyanions, even at higher DEXS concentrations (**Figure S9C**)^{37,53,54}. This suggests that the fraction of siRNA that is not released into the cytosol *via* fusion of the LNP with the limiting endosomal membrane, remains tightly complexed and is not available for CAD-induced lysosomal escape.

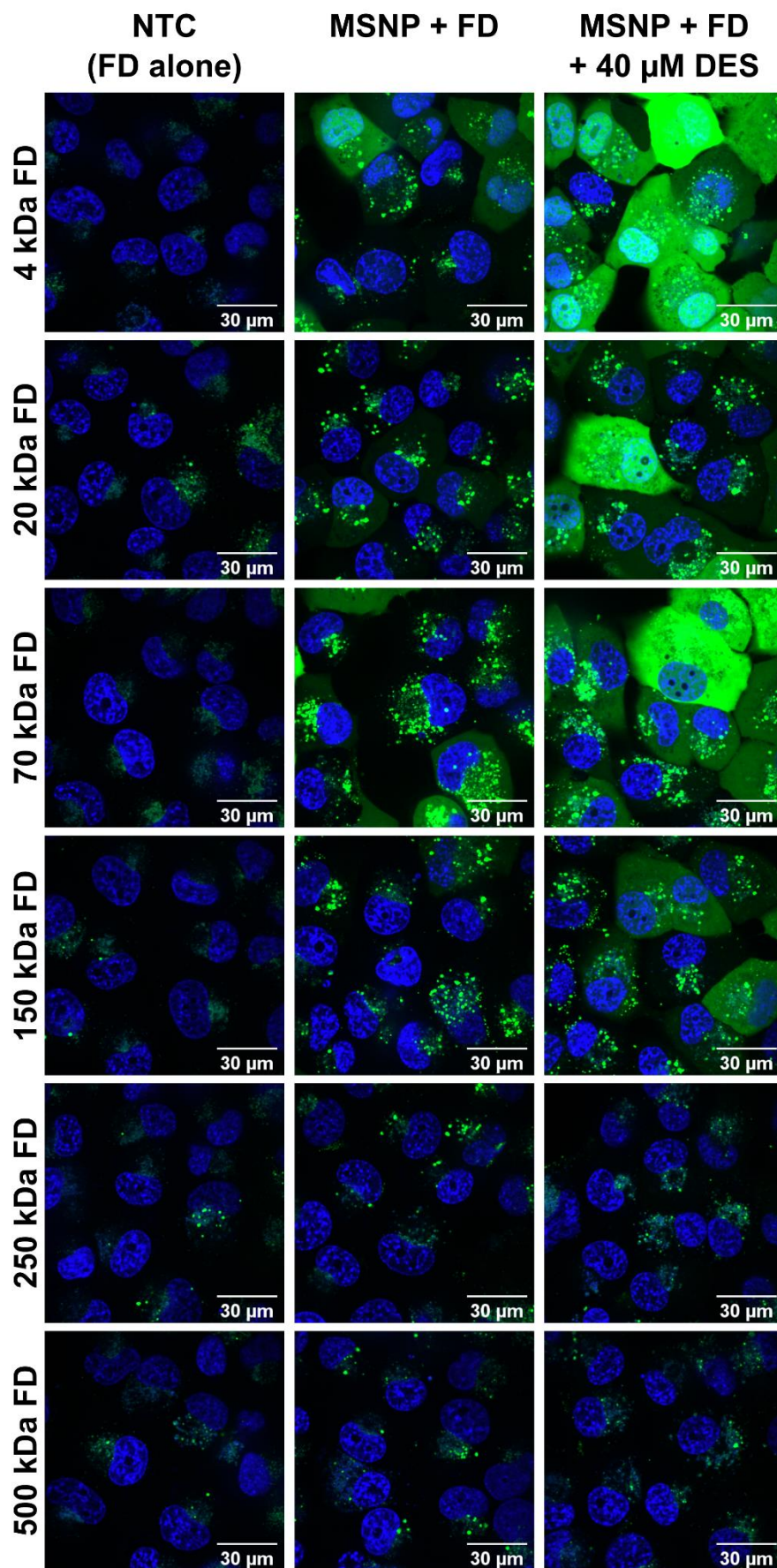


Figure 3. CADs improve cytosolic release of FITC-dextran up to 150 kDa in H1299-WT cells. Representative confocal images from the intracellular FITC-dextran (FD) distribution in H1299-WT cells, only co-incubated with propylamine functionalized mesoporous silica NPs (MSNPs), or cells subsequently incubated with 40 μ M desloratadine (DES) for 20 h. Nuclei can be seen in blue, while cells in which endolysosomal escape occurred show a diffuse cellular FD signal. The scale bar corresponds to 30 μ m. (NTC = not treated control, MSNPs = inorganic propylamine functionalized mesoporous silica NPs, DES = desloratadine, FD = FITC-dextran).

Secondly, the cellular uptake of the siNPs was investigated at the siRNA concentrations used for the silencing experiments, which gives an indication of the intracellular siRNA dose at the time of CAD exposure. As evident from **Figure 4B**, DOTAP-DOPE liposomes and dex-HEMA NGs are the most efficient siRNA carriers in contrast to the MSNPs, the latter which require markedly higher intracellular siRNA doses to achieve significant knockdown. As expected, PEGylation decreases the siRNA delivery performance of the DOTAP-DOPE liposomes⁵⁰. PEGylated MC3 siLNPs, on the other hand, show a similar uptake behavior as the non-PEGylated DOTAP-DOPE liposomes, albeit with a marginally lower siRNA delivery efficiency (**Figure S9A** and **Figure S9D**).

In summary, the straightforward siRNA decomplexation observed for the dex-HEMA NGs, in line with previous observations^{35,44}, likely correlates with the improved siRNA delivery following CAD exposure (**Figure 4A**), as we envisioned only the transfer of decomplexed siRNA/ASO molecules to the cytosol. On the other hand, the siMSNPs have a low decomplexation efficiency (**Figure 4A**), similar to the DOTAP-DOPE siRNA-loaded liposomes (siLIPs), while the delivery efficiency of the former can still be promoted with sequential CAD treatment (**Figure 2B**). The explanation for this observation lies in the much higher intracellular siRNA dose introduced by the MSNPs (~80-162 fold), compared to the DOTAP-DOPE liposomes (~1.2-1.9 fold) (**Figure 4B**). Likewise, the much higher intracellular siRNA doses required by PEGylated DOTAP-DOPE liposomes to achieve target gene knockdown (**Figure 4B**), will, in part, account for their CAD responsiveness. MC3 siLNPs obtained *via* rapid microfluidic mixing behave similarly as the DOTAP-DOPE siLIPs (**Figure S9**), as the very stable siRNA encapsulation in the LNP core precludes the observation of a CAD adjuvant effect.

Based on the present results, it is suggested that a lysosomal pool of free (decomplexed) siRNA is needed to obtain a CAD adjuvant effect. This is achieved either by a sufficient siRNA

decomplexation, a high extent of NP endocytosis or a combination of both (*i.e.* dex-HEMA NGs, PEGylated DOTAP-DOPE liposomes and MSNPs), altogether contributing to the intracellular fraction of decomplexed siRNA (**Scheme 3**).

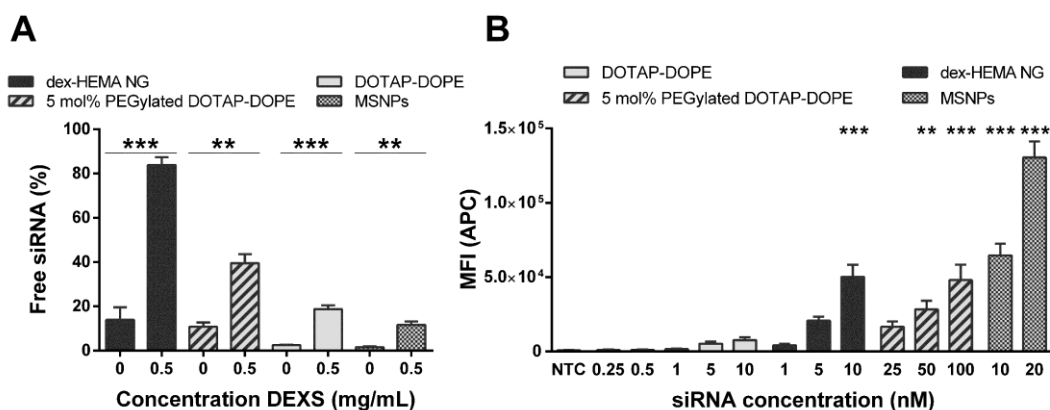
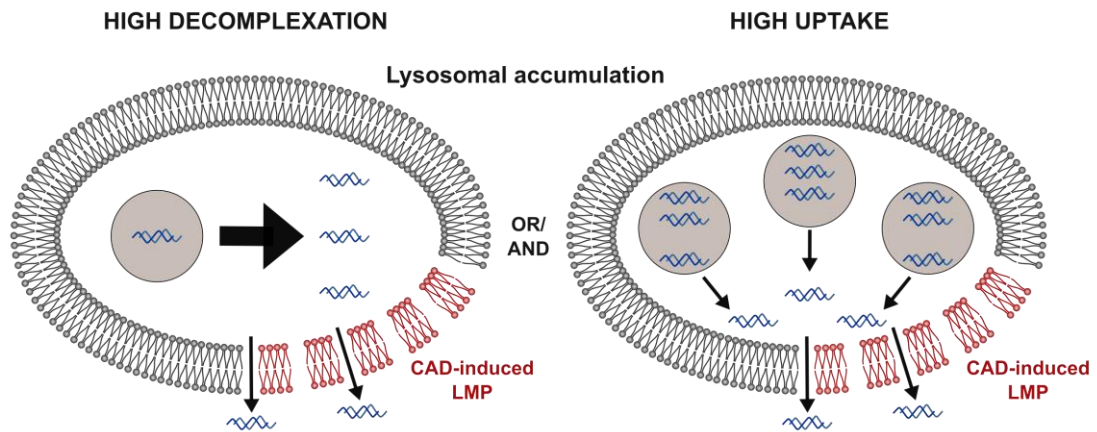


Figure 4. siRNA nanocarrier decomplexation and intracellular siRNA amount. (A) DEXS-induced siRNA release from the indicated siNPs in HEPES buffer (pH 7.4, 20 mM), as measured by fluorescence fluctuation spectroscopy (FFS). The concentration of fluorescent siRNA (siCy5[®]) equaled 25 nM in all samples. Data are represented as mean \pm the standard error of the mean (SEM) for minimum three independent repeats. Statistical significance with respect to the 0 mg/mL DEXS condition (black *) is indicated when appropriate (** $p \leq 0.01$, *** $p \leq 0.001$). (B) Quantification of cellular uptake of dex-HEMA NGs, MSNPs and (PEGylated) DOTAP-DOPE liposomes (at varying siRNA concentrations), in H1299-eGFP cells determined *via* flow cytometry. Data are represented as mean \pm the standard error of the mean (SEM) for minimum three independent repeats. Statistical significance with respect to the NTC (black *) is indicated when appropriate (** $p \leq 0.01$, *** $p \leq 0.001$). (FFS = fluorescence fluctuation spectroscopy, DEXS = 10 kDa dextran sulphate, NG = nanogel, MSNP = propylamine functionalized mesoporous silica nanoparticle, NP = nanoparticle, NTC = not treated control, MFI = mean fluorescence intensity, APC = allophycocyanin (red channel)).



Scheme 3. siRNA-loaded nanoparticle (siNP) transfection needs to result in a lysosomal pool of free (decomplexed) siRNA, in order to be responsive to CAD adjuvant treatment. At the used siRNA and NP concentrations, the cellular internalization of the dex-(HE)MA siNGs remains low, but the siRNA is easily decomplexed from the NGs. On the contrary, the siMSNPs are taken up very efficiently, but the siRNA decomplexation remains low. The 5 mol% PEGylated DOTAP-DOPE siLIPs combine features of both the latter NPs (decomplexation and cellular internalization in between the siNGs and the siMSNPs). All these types of NPs subsequently result in a lysosomal pool of free (decomplexed) siRNA and the CAD molecules can induce extra siRNA release by the formation of small and transient pores in the lysosomal membranes. DOTAP-DOPE siLIPs, Lipofectamine[®] RNAiMAX and MC3 siLNPs are however incompatible with the CAD adjuvants, as the siLIP/siLNP uptake remains low while the lysosomally accumulated lipoplexes are also not easily decomplexed. (CAD = cationic amphiphilic drug, siLIPs = siRNA-loaded liposomes, siNG = siRNA-loaded nanogel, siMSNP = siRNA-loaded propylamine functionalized mesoporous silica nanoparticle, MC3 siLNPs = siRNA-loaded lipid nanoparticles containing the ionizable lipid DLin-MC3-DMA, NP = nanoparticle, LMP = lysosomal membrane permeabilization).

The data shown in this chapter strongly contribute to our knowledge about the prerequisites a therapeutic siRNA-loaded nanoparticle (siNP) should have to be compatible with the proposed CAD adjuvant approach. More specifically, the nanocarrier should be stable in extracellular media, such as the bloodstream, but should easily release the encapsulated siRNA following endocytosis. State-of-the-art MC3 LNPs have demonstrated excellent *in vivo* siRNA delivery performance, but studies have shown that the majority of LNPs also accumulates in the lysosomal compartment, with only a small fraction (1–2%) of siRNAs being able to escape to the cytosol^{7,8,55}. Our data indicate that this lysosomal fraction cannot be additionally released by CAD-induced LMP, likely due to too stable siRNA incorporation. Hence, *in vivo* evaluation of CAD-promoted siRNA delivery would require dedicated NP design taking into account the above mentioned criteria^{44,47,56,57}. Also other challenges (*e.g.* identification of suitable CAD doses) should be taken into account. It has

been observed in the literature that CADs, even after oral administration and in therapeutic doses, can block ASM activity and induce LMP *in vivo* in cancer cells⁵⁸⁻⁶¹. CADs typically have high distribution volumes (*e.g.* > 100 L/kg for desloratadine), facilitating efficient distribution to tissues where *in vivo* PLD induction has been documented, while the lower pH in tumors may lead to more efficient accumulation of the weak basic CADs^{60,62}. Moreover, transformed cells have a significantly altered sphingolipid metabolism (*i.e.* lower intrinsic ASM activity), which sensitizes cancer cells to the CAD-induced LMP^{58,59,63}. As we show that non-lethal LMP is sufficient to considerably promote small NA delivery *in vitro*, we anticipate that CADs could reach target cancer cells in appropriate concentrations to enable their use as small NA delivery-enhancing compounds^{20,60}. Of note, antidepressant CADs (*e.g.* amitriptyline, fluoxetine) were also shown to decrease ASM activity *in vivo* in non-cancerous tissues, such as the hippocampus (oral administration) or lungs (inhalation or intraperitoneal injection) of mice⁶⁴⁻⁶⁷. Likewise, the CAD-induced cellular phenotypes (*e.g.* functional inhibition of ASM, PLD induction, lysosomal swelling) have also been described in endothelial cells and macrophages, which are generally the first cells encountered by nanocarriers upon systemic administration⁶⁸⁻⁷³. Altogether, these data indicate that the concept of CAD repurposing to promote small NA delivery could be practicable *in vivo* as well. Nonetheless, as CADs and NPs need to be present in the same intracellular compartment to enable the adjuvant effect, co-encapsulation of the CAD and the small NA in the same NP and/or local application (*e.g.* topical, pulmonary) should improve control over extra-and intracellular distribution, thus contributing to a successful *in vivo* translation^{14,74}.

3. CONCLUSION

The data presented in this chapter clearly demonstrate that CAD adjuvants can be repurposed to promote cytosolic (D)siRNA and oligonucleotide delivery in distinct cancer cell lines. Importantly, our data also indicate that the CAD adjuvant approach is carrier-specific, likely providing benefit mainly for nanomedicines that entail a substantial endolysosomal pool of decomplexed NAs to diffuse through the CAD-induced pores in the limiting endolysosomal membrane²⁰. In contrast to the governing nanomedicine model, stating that cytosolic release of siRNA should ideally occur prior to fusion of endosomes with the degradative lysosomes, these data support the rational design of nanocarriers that release their NA payload in the lysosomal lumen with the aim to maximize the CAD adjuvant effect.

ACKNOWLEDGMENTS

T. Van de Vyver is a doctoral fellow of the Research Foundation-Flanders (grant 1198719N, FWO, Belgium). B. Bogaert is a doctoral fellow of the FWO (grant 1S75019N). L. De Backer acknowledges the Special Research Fund of Ghent University (BOF12/GOA/014). F. Joris acknowledges the Agency for Innovation by Science and Technology in Flanders (IWT, Belgium). R. Guagliardo is an early stage researcher within the NANOMED project, which has received funding from the European Union's Horizon 2020 Research and Innovation Programme Marie Skłodowska Curie Innovative Training Networks (ITN) under grant number 676137. J. Van Hoeck is a doctoral fellow of the FWO (grant 1S62519N). P. Merckx is a doctoral fellow of the FWO (grant 1S30618N). Prof. K. Raemdonck acknowledges the FWO for a postdoctoral Research Grant (grant 1517516N). We thank Prof. R. Vandenbroucke from the VIB-UGent Center for Inflammation Research (Ghent, Belgium) for the use of the microfluidic NanoAssemblr[®] Benchtop mixing device.

4. MATERIALS AND METHODS

4.1. siRNA duplexes and oligonucleotides

The 21mer siRNA duplexes targeted against the enhanced green fluorescent protein (eGFP, sieGFP), the pGL3 (luc+ gene) and pGL4 (luc2 gene) *firefly* luciferase (siLUC+ and siLUC2) and the negative control siRNA (siCTRL) were purchased from Eurogentec (Seraing, Belgium). Dicer substrate asymmetric 25/27mer siRNA duplexes targeting eGFP (DsieGFP) or luciferase (DsiFLuc) were provided by Integrated DNA Technologies BVBA (IDT, Leuven, Belgium). The 16mer phosphorothioate gapmer antisense oligonucleotides (ASOs) with locked nucleic acid (LNA) modifications targeting eGFP (ASO-eGFP) were also purchased from Eurogentec (Seraing, Belgium).⁷⁵ A phosphorothioate negative control gapmer ASO with LNA-modifications (Antisense LNATM GapmeR Control, Negative control A, ASO-CTRL) was from Qiagen (Germantown, USA). Both negative controls (siRNA and ASO) consist of a sequence that has no relevant homology to any known eukaryotic gene sequences. Fluorescent siCTRL and ASO-eGFP were labeled with a Cy5[®] dye at the 5' end of the (sense) strand (respectively abbreviated siCy5[®] and ASO-Cy5[®] (Eurogentec, Seraing, Belgium)). Alexa Fluor[®] 647 labeled 21mer oligonucleotides (AF647 ONs) were from Eurogentec (Seraing, Belgium) as well. The concentration of the siRNA/ASO/ON stock solutions in nuclease-free water (Ambion[®]-Life Technologies, Ghent, Belgium) was calculated from absorption measurements at 260 nm ($1 \text{ OD}_{260} = 40 \mu\text{g mL}^{-1}$) with a NanoDrop 2000c UV-Vis spectrophotometer (Thermo Fisher Scientific, Rockford, USA). The sequences and modifications of the applied siRNA duplexes/ASOs/ONs are summarized in **Table 1**. The sequences of the applied Dicer substrate asymmetric 25/27mer siRNA duplexes (DsiRNAs) are provided in **Figure S1**.

Table 1. Applied siRNA/ASO/ON sequences and modifications.

siRNA/ ASO/ON	Modification	Manufacturer	Sequence ^a	
			(Sense) strand (5' > 3')	Antisense strand (5' > 3')
siCTRL ^b	/	Eurogentec	UGCGCUACGAUCGACGAUGtt	CAUCGUCGAUCGUAGCGCAtt
siCTRL ^b	Cy5 [®] -labeled ^c	Eurogentec	UGCGCUACGAUCGACGAUGtt	CAUCGUCGAUCGUAGCGCAtt
siEGFP ^d	/	Eurogentec	CAAGCUGACCCUGAAGUUCtt	GAACUUCAGGGUCAGCUUGtt
siLUC ^{+e}	/	Eurogentec	CUUACGCUGAGUACUUCGAtt	UCGAAGUACUCAGCGUAAGtt
siLUC2 ^e	/	Eurogentec	GGACGAGGACGAGCACUUCUU	GAAGUGCUCGUCCUCGUCCUU
ASOeGFP ^f	LNA-modified ^g Phosphorothioate -linked	Eurogentec	GAActtcagggtcAGC	N/A
ASOeGFP ^f	Cy5 [®] -labeled ^c LNA-modified ^g Phosphorothioate -linked	Eurogentec	GAActtcagggtcAGC	N/A
ASOCTRL ^h	LNA-modified Phosphorothioate -linked	Qiagen	AACacgtctataCGC	N/A
AF647 ON	Alexa Fluor [®] 647- labeled ⁱ Phosphorothioate -linked	Eurogentec	gaacttcagggtcagcttgg	N/A

^a Capital and lower case letters respectively represent ribonucleotides and 2'-deoxyribonucleotides; ^b negative control siRNA duplex^{20,25,28,35}; ^c labeled with a Cy5[®] dye at the 5' end of the (sense) strand^{20,25,28,35}; ^d siRNA duplex targeting enhanced green fluorescent protein^{20,25,28,35}; ^e siRNA duplex targeting pGL3 (siLUC+) or pGL4 (siLUC2) firefly luciferase⁷⁶⁻⁸⁰; ^f ASO single strand targeting enhanced green fluorescent protein⁷⁵; ^g the phosphorothioate gapmer ASOs contain three locked nucleic acid (LNA) modifications at each end; ^h negative control ASO⁸¹; ⁱ labeled with an Alexa Fluor[®] 647 dye at the 5' end⁸².

4.2. Nanoparticle (NP) synthesis, preparation and siRNA complexation

Dextran hydroxyethyl methacrylate or dextran methacrylate (dex-HEMA, degree of substitution (DS) of 5.2 or dex-MA, DS of 5.9) was copolymerized with a cationic methacrylate monomer [2-(methacryloyloxy)ethyl]-trimethyl-ammonium chloride (TMAEMA) to produce cationic dex-HEMA-co-TMAEMA and dex-MA-co-TMAEMA nanogels (hereafter abbreviated as respectively dex-HEMA NGs and dex-MA NGs), using an inverse miniemulsion photopolymerization method as reported previously^{9,25,26,28,35}. To assure long-term stability, the NGs were lyophilized and stored desiccated. Propylamine functionalized mesoporous silica nanoparticles (MSNPs, particle size of 200 nm as documented by manufacturer, pore size = 4 nm) were obtained from Sigma-Aldrich (Overijse, Belgium). To obtain ASO/siRNA-loaded NGs or MSNPs (ASO-/siNGs or siMSNPs) for *in vitro* experiments, a stock (2 mg/mL) was prepared by dispersing a weighed amount of particles in ice-cooled nuclease-free water (Ambion[®]-Life Technologies, Ghent, Belgium), followed by sonication (3 x 5 sec, amplitude 10% for NGs; 1 x 3 min, amplitude 15%, 10 sec on/10 sec off for MSNPs;

Branson Digital Sonifier[®], Danbury, USA). Subsequently, equal volumes of NG/MSNP and siRNA/ASO dilutions in 4-(2-hydroxyethyl)-1-piperazineethanesulfonic acid (HEPES) buffer (pH 7.4, 20 mM) were mixed and incubated at 4 °C for 10 min to allow electrostatic complexation, prior to further dilution in Opti-MEM[®] (Invitrogen, Merelbeke, Belgium). This complexation procedure was applied for all cell-based experiments in a 96-well plate and resulted in a 30 µg/mL NG dispersion loaded with 1 nM siRNA (0.033 pmol siRNA/µg NGs or 0.1 pmol siRNA/well) or 100-250 nM ASO (3.3-8.3 pmol ASO/µg NGs or 10-25 pmol ASO/well) for the H1299-eGFP cells, unless indicated otherwise. SKOV-3-LUC+, SKOV-3-LUC2 IP2 and HeLa NLS-GFP cells were transfected in 96-well plates with a 25 µg/mL NG dispersion loaded with, respectively, 2 nM and 10 nM (the latter two) siRNA (0.080 and 0.4 pmol siRNA/µg NGs or 0.2 and 1 pmol siRNA/well), unless indicated otherwise. In case of the siMSNPs, a dispersion of 30 µg/mL loaded with 10 or 20 nM siRNA (0.334-0.667 pmol siRNA/µg MSNP or 1-2 pmol siRNA/well) was applied in 96-well plates.

Lipofectamine[®] RNAiMAX (LF RNAiMAX) (Thermo Fisher Scientific, Rockford, USA) was applied as prescribed by the manufacturer. In short, equal volumes of LF RNAiMAX and siRNA dilutions in Opti-MEM[®] were mixed and allowed to complex during 5 minutes at room temperature. The subsequent cell transfection occurred in Opti-MEM[®] for 4 h at 37 °C. According to the guidelines, 1 pmol siRNA/well (10 nM siRNA) and 0.25 µL LF RNAiMAX/well were applied to obtain optimal transfection efficiencies in 96-well plates. Additionally, the LF RNAiMAX lipoplexes were further diluted to 0.5, 0.1, 0.05 and 0.025 pmol siRNA/well.

DOTAP ((2,3-dioleoyloxy-propyl)-trimethylammonium) - DOPE (1,2-dioleoyl-*sn*-glycero-3-phosphoethanolamine) liposomes (LIPs) were prepared *via* the lipid film hydration method. All lipids were obtained from Avanti Polar Lipids, Inc. (Alabaster, AL, USA) as solutions in chloroform. Appropriate volumes of the lipid solutions were mixed in a round bottom flask to obtain a 1:1 molar ratio. For the preparation of PEGylated LIPs, the desired amounts of DSPE-PEG₂₀₀₀ (1,2-distearoyl-*sn*-glycero-3-phosphoethanolamine-N-[methoxy(polyethylene glycol)-2000]) dissolved in chloroform (corresponding to 5 mol% of the total lipids) were added to the lipids in the round-bottomed flask. Through rotary evaporation under vacuum at 40 °C, a lipid film was created and subsequently hydrated using 1 mL HEPES buffer (pH 7.4, 20 mM). The obtained mixture was vortexed and sonicated for 1 minute at 10% amplitude to obtain a monodisperse 2 mM liposome dispersion (total lipid concentration). Hydrodynamic diameter and zeta-potential of these (PEGylated) DOTAP-DOPE LIPs were

determined *via* Dynamic Light Scattering (DLS, **Figure S7A**) (Zetasizer Nano, Malvern Instruments, Worcestershire, United Kingdom). Subsequently, siRNA was complexed with the (PEGylated) DOTAP-DOPE LIPs at an optimal charge ratio equal to eight⁴⁷. Hereto, equal volumes of LIPs and siRNA in HEPES buffer were mixed and allowed to complex at room temperature for 30 minutes prior to further dilution in Opti-MEM[®] and transfection.

Preparation of lipid nanoparticles, containing the ionizable lipid MC3 (MC3 siLNPs), is described in supplementary information.

4.3. Cell lines and cell culture conditions

The human non-small cell lung epithelial carcinoma cell line (H1299) that stably expresses eGFP (H1299-eGFP), the human ovarian cancer cell line (SKOV-3) that stably expresses the pGL3 *firefly* luciferase (SKOV-3-LUC+), the *in vivo* selected SKOV-3 IP2 cell line that stably expresses the pGL4 *firefly* luciferase (SKOV-3-LUC2 IP2) and the HeLa cells stably transfected with a nuclear-localized signaling expressing GFP (HeLa NLS-GFP) were, respectively, obtained from the lab of Prof. Camilla Foged (Department of Pharmacy, University of Copenhagen, Denmark), the lab of Prof. Achim Aigner (Institute of Pharmacology, Pharmacy and Toxicology, University of Leipzig, Germany), the lab of Prof. Olivier De Wever (Laboratory of Experimental Cancer Research, Ghent University, Belgium) and the lab of Prof. Winnok H. De Vos (Laboratory of Cell Biology and Histology, University of Antwerp, Belgium)^{20,28,83-88}. The wild type variant of the H1299 cells (H1299-WT, ATCC[®] CRL-5803[™]) was obtained from American Type Culture Collection (ATCC, Manassas, USA). H1299 cells (H1299-WT and H1299-eGFP), SKOV-3 cells and HeLa NLS-GFP cells were, respectively, maintained in Roswell Park Memorial Institute (RPMI) 1640 culture medium, McCoy's 5A culture medium and Dulbecco's Modified Eagle Medium (supplemented with growth factor F12; DMEM/F-12) culture medium, all supplemented with 10% fetal bovine serum (FBS, Hyclone[™], GE Healthcare, Machelen, Belgium), 2 mM L-Glutamine and 100 U/mL penicillin/streptomycin (hereafter collectively called 'complete cell culture medium' or CCM). The cell lines were cultured in a humidified atmosphere containing 5% CO₂ at 37 °C and culture medium was renewed every other day unless the 80% confluence level was reached. In this case, the cells were split using 0.25% trypsin-ethylenediaminetetraacetic acid (EDTA). For eGFP transgene selection, H1299-eGFP cells were treated with medium containing 1 mg/mL Geneticin[®] once per month. All cells were regularly tested and found

negative for mycoplasma. All products were purchased from Gibco®-Life Technologies (Grand Island, NY, USA) unless specifically mentioned otherwise.

4.4. Fluorescence fluctuation spectroscopy (FFS) on siRNA-loaded NPs

Fluorescence fluctuation spectroscopy (FFS) is a microscopy-based technique that monitors the fluorescence intensity fluctuations of fluorescent molecules diffusing in and out of the focal volume (a fixed excitation volume) of a confocal microscope^{25,35,48}. Previous work by our group used FFS to quantify the complexation of fluorescently labeled siRNA to various nanocarriers^{9,25,35,44,47,48}. In this study, FFS experiments were carried out on dex-HEMA NGs, (PEGylated) DOTAP-DOPE LIPs and MSNPs, loaded with siCy5® (0.033 pmol siRNA/μg NGs, 0.667 pmol siRNA/μg MSNP and a charge ratio of 8 for the (PEGylated) DOTAP-DOPE LIPs). Next, the release of siRNA from the NPs was evaluated in the presence of competing polyanions, *i.e.* dextran sulfate sodium salt (DEXS, 10 kDa, Sigma-Aldrich). Equal volumes of DEXS and siRNA-loaded NPs in HEPES buffer were mixed, resulting in a final siRNA concentration of 25 nM. After 10 min incubation at room temperature, the samples were transferred to a glass bottom 96-well plate (Greiner Bio-One GmbH, Frickenhausen, Germany) and the focal volume of the microscope was positioned in the sample, followed by the recording of the fluorescence fluctuations during a 60 s time interval. Samples were measured in triplicate for 3 independent experiments. The average fluorescence intensity of freely diffusing and complexed siRNA in the fluorescence fluctuation profile was determined as described previously^{25,35,48}. FFS measurements were performed with a laser scanning confocal microscope (C2si, Nikon, Japan) equipped with a water immersion objective lens (Plan Apo 60×, NA 1.2, collar rim correction, Nikon, NY, USA), using a 633 nm laser line for the excitation of fluorescent siRNA (siCy5®). Fluorescence was detected with the detection channels of the fluorescence correlation spectrometer MicroTime 200 (Picoquant GmbH, Berlin, Germany) that was equipped with SymPhoTime software (Picoquant GmbH, Germany).

4.5. Quantification of transfection efficiency/lysosomal volume of NP

transfection and sequential adjuvant treatment by flow cytometry

H1299-eGFP cells were seeded in 96-well plates (SPL Lifesciences Co. Ltd., Naechon-Myeon Pocheon, South Korea) at a density of 7500 cells/well (100 μL/well) and were allowed to settle overnight. Next, the cells were transfected with siRNA-/ASO-loaded NPs (si-/ASO-NPs,

prepared as described above) during 4 hours at 37 °C in a humidified atmosphere containing 5% CO₂. Note that for every siGFP condition a siCTRL sample was included to account for potential off-target effects (similar for ASOs). Subsequently, the si-/ASO-NP dispersion was removed and the cells received 50 µL fresh (DMSO control) or compound-containing CCM (maximally 0.08% (v/v) residual DMSO). After 20 hours, the small molecule containing CCM (and DMSO control) was removed and cells were kept in 50 µL fresh CCM for an additional 24 hours. Before flow cytometry analysis, lysosomes were labeled with the LysoTracker® Deep Red (LDR) probe (Molecular Probes™, Eugene, OR, USA) through incubation with 50 µL 75 nM LDR in CCM for 30 min at 37 °C. After removal of the LDR-containing CCM and a washing step with 30 µL PBS, further sample preparation consisted of detachment with 30 µL 0.25% trypsin-EDTA, neutralization with 120 µL CCM and a transfer of the cell suspensions to an U-bottom 96-well plate (Greiner Bio-One GmbH, Vilvoorde, Belgium), which was centrifuged during 5 minutes at 500 g. After removal of 120 µL supernatant, the cells were resuspended in 80 µL flow buffer (phosphate buffered saline (PBS, no calcium, no magnesium) with 1% (v/v) FBS (Hyclone™, GE Healthcare, Machelen, Belgium) and 0.1% (w/v) sodium azide (Sigma Aldrich, Overijse, Belgium)) and kept on ice until analysis. For each sample the forward and side scatter (respectively FSC and SSC) as well as the green and red fluorescent signal of single cells were measured. The samples were excited with the 488 and 638 nm laser lines and the signal was detected with the 525/40 and 660/20 filters using the CytoFLEX flow cytometer with plate loader for 96-well plates (Beckman Coulter, Krefeld, Germany) and CytExpert software. Finally, data analysis was performed using the FlowJo software (Tree Star Inc., Ashland, OR, USA) and data were exported into Microsoft® Excel® (16th version, Microsoft Corp., Redmond, WA, USA). The calculated percentages eGFP expression and fold changes in LDR signal intensity/SSC signal are presented as the mean ± standard error of the mean (SEM) for minimum 3 independent repeats (biological replicates), unless otherwise indicated. In an additional experiment (**Figure S1**), H1299-eGFP cells (seeded at 35000 cells/well) were transfected in 24-well plates with dex-HEMA NGs (NG dispersion of 30 µg/mL loaded with 5 nM siRNA or DsiRNA) for 4 h at 37 °C as described before²⁰. Transfection procedure and transfection efficiency determination of SKOV-3-LUC+/2 (IP2) and HeLa NLS-GFP cells is detailed described in supporting information.

4.6. Quantification of *in vitro* cellular ASO or siRNA internalization in H1299-eGFP and SKOV-3-LUC+ cells by flow cytometry

To quantify the cellular uptake of ASO or siRNA by flow cytometry, H1299-eGFP and SKOV-3-LUC+ cells were seeded in 96-well plates at a density of 7500 cells/well and left to settle overnight. NPs were loaded with different amounts of siCTRL:siCy5[®] or ASO-CTRL:ASO-Cy5[®] (90:10 mol%). Following dilution in Opti-MEM[®] (final NP concentrations are described above), the particles were incubated with the cells for 3 h (SKOV-3-LUC+ cells) or 4 h (H1299-eGFP) (37 °C, 5% CO₂). Next, the cells were washed with dextran sulfate sodium salt (1 mg/mL in PBS) to remove cell surface-bound fluorescence. Further sample preparations were carried out as previously described for the silencing experiments.

4.7. Visualization and quantification of the cytosolic release of AF647 ONs

H1299-eGFP and SKOV-3-LUC2 IP2 cells were seeded at 200000 cells/dish in 35 mm diameter glass bottom microscopy dishes (Greiner Bio-One GmbH, Germany) and were allowed to settle overnight. After removal of the CCM, the cells were transfected with 900 µL of a dex-HEMA NG dispersion loaded with 25 nM AF647 ONs (0.833 pmol AF647 ONs/µg NGs, 4 h incubation for H1299-eGFP cells and 1 pmol AF647 ONs/µg NGs, 3 h incubation for SKOV-3-LUC2 IP2 cells). Following incubation at 37 °C in a humidified atmosphere containing 5% CO₂, the ON-NG dispersion was removed and the cells were washed once with dextran sulfate sodium salt (1 mg/mL in PBS) and once with phosphate buffered saline (PBS, Invitrogen, Merelbeke, Belgium). Next, the cells received 1.5 mL fresh CCM, containing different µM concentrations of the described compounds or a DMSO control, for 20 h (37 °C, 5% CO₂). After removal of the small molecule-containing CCM, the nuclei were labeled with Hoechst 33342 (Molecular Probes™, Belgium) in CCM (1 mg/mL in water, 1/1000 dilution) during 15 minutes at 37 °C. Finally, the Hoechst solution was removed, fresh CCM was added and cells were kept at 37 °C in a humidified atmosphere containing 5% CO₂ until imaging. A spinning disk confocal (SDC) microscope (Nikon eclipse Ti, Japan), equipped with a MLC 400 B laser box (Agilent technologies, California, USA), a Yokogawa CSU-X confocal spinning disk device (Andor, Belfast, UK), an iXon ultra EMCCD camera (Andor Technology, Belfast, UK), a Plan Apo VC 60× 1.4 NA oil immersion objective lens (Nikon, Japan) and NIS Elements software (Nikon, Japan) was applied for imaging. The 408 nm and 633 nm laser lines were applied to, respectively, excite the Hoechst-labeled nuclei and the fluorescence resulting from the AF647 ONs. If endolysosomal escape of the AF647 ONs occurs, the

labeled ONs will spread towards the cytosol, dequench and finally accumulate into the nucleus^{82,89}. During data analysis with ImageJ (FIJI) software, both the total cell number and amount of cells with AF647 ON-positive nuclei were counted. Nuclei were detected in the blue channel by thresholding (applying the same offset values for every image) and intensity analysis (mean grey value), of the nuclear fluorescence signal in the red channel, was done. Using the 6th version of the GraphPad Prism software, these intensity values were plotted in frequency distributions and based on these histograms, a percentage of cells with AF647 ON-positive nuclei was determined. Data are represented the percentage of cells with AF647 ON-positive nuclei for at least 545 cells in minimum 53 images.

4.8. Visualization of the cytosolic release of FITC-dextran

H1299-WT cells were seeded at 75000 cells/compartiment in 35 mm diameter glass bottom microscopy dishes with 4 compartments (Greiner Bio-One GmbH, Germany) and were allowed to settle overnight. To visualize the FITC-dextran (FD) release, MSNPs (30 µg/mL) were co-incubated with FDs (2 mg/mL, Sigma-Aldrich, Overijse, Belgium) of different molecular weight (4, 20, 70, 150, 250 and 500 kDa) for 4 h in Opti-MEM[®]. Further steps (*e.g.* CAD treatments, confocal imaging) were done as described for the AF647 ON release experiments, unless mentioned otherwise. No fixation step was applied and confocal imaging was done immediately after removal of the CAD-containing CCM. The nuclei were labeled with Hoechst 33342 (Molecular Probes[™], Belgium) in CCM (1 mg/mL in water, 1/1000 dilution) during 15 min at 37 °C. Finally, the Hoechst solution was removed, fresh CCM was added and cells were kept at 37 °C in a humidified atmosphere containing 5% CO₂ until imaging (see above). Representative images are shown from at least 454 cells per condition in minimum 79 images.

4.9. Statistical analysis

Statistical analysis was performed using the 6th version of the GraphPad Prism software. One-way ANOVA combined with the post-hoc Dunnett test was applied to compare multiple conditions, whereas the student *t*-test was used for direct comparison of 2 conditions. A *p* value ≤ 0.05 was considered *a priori* to be statistically significant.

Associated content

Supporting information consists out of 9 additional figures. **Figure S1**: effect of sequential 40 μ M desloratadine (DES) treatment on the gene silencing potential of NGs loaded with 25-27 mer Dicer-substrate siRNAs in H1299-eGFP cells. **Figure S2-4**: CADs increase small NA release to the cytosol, leading to an enhanced dex-HEMA siNG LUC/GFP silencing potential in SKOV-3-LUC and HeLa NLS-GFP cells. **Figure S5**: effect of sequential DES treatment on LDR signal in combination with (PEGylated) DOTAP-DOPE siLIPs, in H1299-eGFP cells. **Figure S6**: effect of sequential DES treatment on the silencing potential of siRNA-loaded RNAiMAX LIPs and the LDR signal, in H1299-eGFP cells. **Figure S7**: physicochemical properties of the (PEGylated) DOTAP-DOPE LIPs and the visual representation of lipoplex formation. **Figure S8**: physicochemical properties of MC3 siLNPs. **Figure S9**: effect of sequential DES treatment on the silencing potential of MC3 siLNPs and the LDR signal, in H1299-eGFP cells. Decomplexation efficiency and uptake of MC3 siLNPs. Supplementary materials and methods: information about (a) the quantification of siNG transfection efficiency in SKOV-3-LUC/HeLa NLS-GFP cells and (b) MC3 siLNPs (synthesis, DLS, transfection, uptake, agarose gel electrophoresis, Quant-iT™ RiboGreen® RNA assay).

REFERENCES

1. Dowdy, S. F. Overcoming Cellular Barriers for RNA Therapeutics. *Nat. Biotechnol.* **2017**, *35*, 222–229.
2. Wittrup, A.; Lieberman, J. Knocking down Disease: A Progress Report on siRNA Therapeutics. *Nat. Rev. Genet.* **2015**, *16*, 543–552.
3. Shen, X.; Corey, D. R. Chemistry, Mechanism and Clinical Status of Antisense Oligonucleotides and Duplex RNAs. *Nucleic Acids Res.* **2018**, *46*, 1584–1600.
4. Kanasty, R.; Dorkin, J. R.; Vegas, A.; Anderson, D. Delivery Materials for siRNA Therapeutics. *Nat. Mater.* **2013**, *12*, 967–977.
5. Yin, H. *et al.* Non-Viral Vectors for Gene-Based Therapy. *Nat. Rev. Genet.* **2014**, *15*, 541–555.
6. Martens, T. F.; Remaut, K.; Demeester, J.; De Smedt, S. C.; Braeckmans, K. Intracellular Delivery of Nanomaterials: How to Catch Endosomal Escape in the Act. *Nano Today* **2014**, *9*, 344–364.
7. Gilleron, J. *et al.* Image-Based Analysis of Lipid Nanoparticle-Mediated siRNA Delivery, Intracellular Trafficking and Endosomal Escape. *Nat. Biotechnol.* **2013**, *31*, 638–646.
8. Wittrup, A. *et al.* Visualizing Lipid-Formulated siRNA Release from Endosomes and Target Gene Knockdown. *Nat. Biotechnol.* **2015**, *33*, 870–876.
9. Raemdonck, K. *et al.* Biodegradable Dextran Nanogels for RNA Interference: Focusing on Endosomal Escape and Intracellular siRNA Delivery. *Adv. Funct. Mater.* **2009**, *19*, 1406–1415.
10. Sahay, G. *et al.* Efficiency of siRNA Delivery by Lipid Nanoparticles Is Limited by Endocytic Recycling. *Nat. Biotechnol.* **2013**, *31*, 653–658.
11. Hirsch, M.; Helm, M. Live Cell Imaging of Duplex siRNA Intracellular Trafficking. *Nucleic Acids Res.* **2015**, *43*, 4650–4660.
12. Crooke, S. T.; Wang, S.; Vickers, T. A.; Shen, W.; Liang, X. Cellular Uptake and Trafficking of Antisense Oligonucleotides. *Nat. Biotechnol.* **2017**, *35*, 230–237.
13. Ma, D. Enhancing Endosomal Escape for Nanoparticle Mediated siRNA Delivery. *Nanoscale* **2014**, *6*, 6415.
14. Joris, F.; De Smedt, S. C.; Raemdonck, K. Small Molecules Convey Big Messages: Boosting Non-Viral Nucleic Acid Delivery with Low Molecular Weight Drugs. *Nano Today* **2017**, *16*, 14–29.
15. Patel, S. *et al.* Boosting Intracellular Delivery of Lipid Nanoparticle-Encapsulated mRNA. *Nano Lett.* **2017**, *17*, 5711–5718.
16. Yang, B. *et al.* High-Throughput Screening Identifies Small Molecules That Enhance the Pharmacological Effects of Oligonucleotides. *Nucleic Acids Res.* **2015**, *43*, 1987–1996.
17. Wang, L. *et al.* A Novel Family of Small Molecules That Enhance the Intracellular Delivery and Pharmacological Effectiveness of Antisense and Splice Switching Oligonucleotides. *ACS Chem. Biol.* **2017**, *12*, 1999–2007.
18. Juliano, R. L. *et al.* Structure-Activity Relationships and Cellular Mechanism of Action of Small Molecules That Enhance the Delivery of Oligonucleotides. *Nucleic Acids Res.* **2018**, *46*, 1601–1613.
19. Zhang, X.; Castanotto, D.; Liu, X.; Shemi, A.; Stein, C. A. Ammonium and Arsenic Trioxide Are Potent Facilitators of Oligonucleotide Function When Delivered by Gymnosis. *Nucleic Acids Res.* **2018**, *46*, 3612–3624.
20. Joris, F. *et al.* Repurposing Cationic Amphiphilic Drugs as Adjuvants to Induce Lysosomal siRNA Escape in Nanogel Transfected Cells. *J. Control. Release* **2018**, *269*, 266–276.
21. Castanotto, D. *et al.* A Stress-Induced Response Complex (SIRC) Shuttles miRNAs, siRNAs, and Oligonucleotides to the Nucleus. *Proc. Natl. Acad. Sci. U. S. A.* **2018**, *115*, E5756–E5765.

22. Zhou, X. *et al.* SAHA (Vorinostat) Facilitates Functional Polymer-Based Gene Transfection via Upregulation of ROS and Synergizes with TRAIL Gene Delivery for Cancer Therapy. *J. Drug Target.* **2018**, 1–9.
23. Gilleron, J. *et al.* Identification of SiRNA Delivery Enhancers by a Chemical Library Screen. *Nucleic Acids Res.* **2015**, *43*, 7984–8001.
24. Osborn, M. F. *et al.* Guanabenz (Wytensin™) Selectively Enhances Uptake and Efficacy of Hydrophobically Modified SiRNAs. *Nucleic Acids Res.* **2015**, *43*, 8664–8672.
25. De Backer, L.; Braeckmans, K.; Demeester, J.; De Smedt, S. C.; Raemdonck, K. The Influence of Natural Pulmonary Surfactant on the Efficacy of SiRNA-Loaded Dextran Nanogels. *Nanomedicine* **2013**, *8*, 1625–1638.
26. Raemdonck, K.; Naeye, B.; Høgset, A.; Demeester, J.; De Smedt, S. C. Prolonged Gene Silencing by Combining SiRNA Nanogels and Photochemical Internalization. *J. Control. Release* **2010**, *145*, 281–288.
27. Naeye, B. *et al.* PEGylation of Biodegradable Dextran Nanogels for SiRNA Delivery. *Eur. J. Pharm. Sci.* **2010**, *40*, 342–351.
28. Merckx, P. *et al.* Surfactant Protein B (SP-B) Enhances the Cellular SiRNA Delivery of Proteolipid Coated Nanogels for Inhalation Therapy. *Acta Biomater.* **2018**, *78*, 236–246.
29. Jayaraman, M. *et al.* Maximizing the Potency of SiRNA Lipid Nanoparticles for Hepatic Gene Silencing *In Vivo*. *Angew. Chemie Int. Ed.* **2012**, *51*, 8529–8533.
30. Evers, M. M.; Toonen, L. J. A.; van Roon-Mom, W. M. C. Antisense Oligonucleotides in Therapy for Neurodegenerative Disorders. *Adv. Drug Deliv. Rev.* **2015**, *87*, 90–103.
31. Lieberman, J. Tapping the RNA World for Therapeutics. *Nat. Struct. Mol. Biol.* **2018**, *25*, 357–364.
32. Schütz, I. *et al.* Lysosomal Dysfunction Caused by Cellular Accumulation of Silica Nanoparticles. *J. Biol. Chem.* **2016**, *291*, 14170–14184.
33. Shen, J. *et al.* Cyclodextrin and Polyethylenimine Functionalized Mesoporous Silica Nanoparticles for Delivery of SiRNA Cancer Therapeutics. *Theranostics* **2014**, *4*, 487–497.
34. Wang, M.; Li, X.; Ma, Y.; Gu, H. Endosomal Escape Kinetics of Mesoporous Silica-Based System for Efficient SiRNA Delivery. *Int. J. Pharm.* **2013**, *448*, 51–57.
35. De Backer, L. *et al.* Bio-Inspired Pulmonary Surfactant-Modified Nanogels: A Promising SiRNA Delivery System. *J. Control. Release* **2015**, *206*, 177–186.
36. Bøe, S.; Longva, A. S.; Hovig, E. Photochemically Induced Gene Silencing Using Small Interfering RNA Molecules in Combination with Lipid Carriers. *Oligonucleotides* **2007**, *17*, 166–173.
37. Kulkarni, J. A. *et al.* On the Formation and Morphology of Lipid Nanoparticles Containing Ionizable Cationic Lipids and SiRNA. *ACS Nano* **2018**, *12*, 4787–4795.
38. Xiong, R. *et al.* Sizing Nanomaterials in Bio-Fluids by CFRAP Enables Protein Aggregation Measurements and Diagnosis of Bio-Barrier Permeability. *Nat. Commun.* **2016**, *7*, 12982.
39. Aits, S.; Jäätelä, M. Lysosomal Cell Death at a Glance. *J. Cell Sci.* **2013**, *126*, 1905–1912.
40. Gómez-Sintes, R.; Ledesma, M. D.; Boya, P. Lysosomal Cell Death Mechanisms in Aging. *Ageing Res. Rev.* **2016**, *32*, 150–168.
41. Stoka, V.; Turk, V.; Turk, B. Lysosomal Cathepsins and Their Regulation in Aging and Neurodegeneration. *Ageing Res. Rev.* **2016**, *32*, 22–37.
42. Papadopoulos, C.; Kravic, B.; Meyer, H. Repair or Lysophagy: Dealing with Damaged Lysosomes. *J. Mol. Biol.* **2019**, *432*, 231–239.
43. Radulovic, M. *et al.* ESCRT-mediated Lysosome Repair Precedes Lysophagy and Promotes Cell Survival. *EMBO J.* **2018**, *37*, e99753.
44. Naeye, B. *et al.* Hemocompatibility of SiRNA Loaded Dextran Nanogels. *Biomaterials* **2011**, *32*, 9120–9127.
45. Remaut, K. *et al.* Protection of Oligonucleotides against Nucleases by Pegylated and Non-Pegylated Liposomes as Studied by Fluorescence Correlation Spectroscopy. *J. Control.*

- Release* **2005**, *110*, 212–226.
46. Buyens, K.; Demeester, J.; De Smedt, S. S.; Sanders, N. N. Elucidating the Encapsulation of Short Interfering RNA in PEGylated Cationic Liposomes. *Langmuir* **2009**, *25*, 4886–4891.
 47. Dakwar, G. R. *et al.* Colloidal Stability of Nano-Sized Particles in the Peritoneal Fluid: Towards Optimizing Drug Delivery Systems for Intraperitoneal Therapy. *Acta Biomater.* **2014**, *10*, 2965–2975.
 48. Buyens, K. *et al.* A Fast and Sensitive Method for Measuring the Integrity of SiRNA-Carrier Complexes in Full Human Serum. *J. Control. Release* **2008**, *126*, 67–76.
 49. Shi, F. *et al.* Interference of Poly(Ethylene Glycol)-Lipid Analogues with Cationic-Lipid-Mediated Delivery of Oligonucleotides; Role of Lipid Exchangeability and Non-Lamellar Transitions. *Biochem. J.* **2002**, *366*, 333–341.
 50. Remaut, K.; Lucas, B.; Braeckmans, K.; Demeester, J.; De Smedt, S. C. Pegylation of Liposomes Favours the Endosomal Degradation of the Delivered Phosphodiester Oligonucleotides. *J. Control. Release* **2007**, *117*, 256–266.
 51. Pedrosa de Lima, M. C.; Simões, S.; Pires, P.; Faneca, H.; Düzgüneş, N. Cationic Lipid–DNA Complexes in Gene Delivery: From Biophysics to Biological Applications. *Adv. Drug Deliv. Rev.* **2001**, *47*, 277–294.
 52. Zelphati, O.; Szoka, F. C. Cationic Liposomes as an Oligonucleotide Carrier: Mechanism of Action. *J. Liposome Res.* **1997**, *7*, 31–49.
 53. Jyotsana, N. *et al.* Lipid Nanoparticle-Mediated SiRNA Delivery for Safe Targeting of Human CML *In Vivo*. *Ann. Hematol.* **2019**, *98*, 1905–1918.
 54. Leung, A. K. K.; Tam, Y. Y. C.; Chen, S.; Hafez, I. M.; Cullis, P. R. Microfluidic Mixing: A General Method for Encapsulating Macromolecules in Lipid Nanoparticle Systems. *J. Phys. Chem. B* **2015**, *119*, 8698–8706.
 55. Wood, H. FDA Approves Patisiran to Treat Hereditary Transthyretin Amyloidosis. *Nat. Rev. Neurol.* **2018**, *14*, 570.
 56. Gould, S. E.; Junttila, M. R.; De Sauvage, F. J. Translational Value of Mouse Models in Oncology Drug Development. *Nat. Med.* **2015**, *21*, 431–439.
 57. Dakwar, G. R. *et al.* Disregarded Effect of Biological Fluids in SiRNA Delivery: Human Ascites Fluid Severely Restricts Cellular Uptake of Nanoparticles. *ACS Appl. Mater. Interfaces* **2015**, *7*, 24322–24329.
 58. Petersen, N. H. T. *et al.* Transformation-Associated Changes in Sphingolipid Metabolism Sensitize Cells to Lysosomal Cell Death Induced by Inhibitors of Acid Sphingomyelinase. *Cancer Cell* **2013**, *24*, 379–393.
 59. Gulbins, E.; Kolesnick, R. N. It Takes a CAD to Kill a Tumor Cell with a LMP. *Cancer Cell* **2013**, *24*, 279–281.
 60. Ellegaard, A.-M. *et al.* Repurposing Cationic Amphiphilic Antihistamines for Cancer Treatment. *EBioMedicine* **2016**, *9*, 130–139.
 61. Verdoodt, F. *et al.* Antihistamines and Ovarian Cancer Survival: Nationwide Cohort Study and *In Vitro* Cell Viability Assay. *JNCI J. Natl. Cancer Inst.* **2020**, *112*, djz217.
 62. Goracci, L.; Ceccarelli, M.; Bonelli, D.; Cruciani, G. Modeling Phospholipidosis Induction: Reliability and Warnings. *J. Chem. Inf. Model.* **2013**, *53*, 1436–1446.
 63. Boya, P.; Kroemer, G. Lysosomal Membrane Permeabilization in Cell Death. *Oncogene* **2008**, *27*, 6434–6451.
 64. Gulbins, E. *et al.* Acid Sphingomyelinase-Ceramide System Mediates Effects of Antidepressant Drugs. *Nat. Med.* **2013**, *19*, 934–938.
 65. Teichgräber, V. *et al.* Ceramide Accumulation Mediates Inflammation, Cell Death and Infection Susceptibility in Cystic Fibrosis. *Nat. Med.* **2008**, *14*, 382–391.
 66. Becker, K. A. *et al.* Acid Sphingomyelinase Inhibitors Normalize Pulmonary Ceramide and Inflammation in Cystic Fibrosis. *Am. J. Respir. Cell Mol. Biol.* **2010**, *42*, 716–724.
 67. Becker, K. A. *et al.* Sphingolipids as Targets for Inhalation Treatment of Cystic Fibrosis.

- Adv. Drug Deliv. Rev.* **2018**, *133*, 66–75.
68. Campbell, F. *et al.* Directing Nanoparticle Biodistribution through Evasion and Exploitation of Stab2-Dependent Nanoparticle Uptake. *ACS Nano* **2018**, *12*, 2138–2150.
 69. Hayashi, Y. *et al.* Differential Nanoparticle Sequestration by Macrophages and Scavenger Endothelial Cells Visualized *In Vivo* in Real-Time and at Ultrastructural Resolution. *ACS Nano* **2020**, *14*, 1665–1681.
 70. Kannan, R.; Sarma, J. S. M.; Guha, M.; Venkataraman, K. Amiodarone Toxicity: II. Desethylamiodarone-Induced Phospholipidosis and Ultrastructural Changes during Repeated Administration in Rats. *Fundam. Appl. Toxicol.* **1991**, *16*, 103–109.
 71. Hostetler, K. Y.; Reasor, M.; Yazaki, P. J. Chloroquine-Induced Phospholipid Fatty Liver, Measurement of Drug and Lipid Concentrations in Rat Liver. *J. Biol. Chem.* **1985**, *260*, 215–219.
 72. Jiang, M.; Huang, S.; Duan, W.; Liu, Q.; Lei, M. Inhibition of Acid Sphingomyelinase Activity Ameliorates Endothelial Dysfunction in Db/Db Mice. *Biosci. Rep.* **2019**, *39*, BSR20182144.
 73. Li, X.; Jin, S. J.; Su, J.; Li, X. X.; Xu, M. Acid Sphingomyelinase Down-Regulation Alleviates Vascular Endothelial Insulin Resistance in Diabetic Rats. *Basic Clin. Pharmacol. Toxicol.* **2018**, *123*, 645–659.
 74. Schirotti, D. *et al.* Effective *In Vivo* Topical Delivery of siRNA and Gene Silencing in Intact Corneal Epithelium Using a Modified Cell Penetrating Peptide. *Mol. Ther. - Nucleic Acids* **2019**, *17*, 891–906.
 75. Castanotto, D. *et al.* A Cytoplasmic Pathway for Gapmer Antisense Oligonucleotide-Mediated Gene Silencing in Mammalian Cells. *Nucleic Acids Res.* **2015**, *43*, 9350–9361.
 76. Ragelle, H. *et al.* Chitosan Nanoparticles for siRNA Delivery: Optimizing Formulation to Increase Stability and Efficiency. *J. Control. Release* **2014**, *176*, 54–63.
 77. Xue, L.; Ingle, N. P.; Reineke, T. M. Highlighting the Role of Polymer Length, Carbohydrate Size, and Nucleic Acid Type in Potency of Glycopolycation Agents for PDNA and siRNA Delivery. *Biomacromolecules* **2013**, *14*, 3903–3915.
 78. Pitchiaya, S.; Heinicke, L. A.; Park, J. I.; Cameron, E. L.; Walter, N. G. Resolving Subcellular miRNA Trafficking and Turnover at Single-Molecule Resolution. *Cell Rep.* **2017**, *19*, 630–642.
 79. Pitchiaya, S.; Krishnan, V.; Custer, T. C.; Walter, N. G. Dissecting Non-Coding RNA Mechanisms *In Cellulo* by Single-Molecule High-Resolution Localization and Counting. *Methods* **2013**, *63*, 188–199.
 80. Pärnaste, L.; Arukuusk, P.; Langel, K.; Tenson, T.; Langel, Ü. The Formation of Nanoparticles between Small Interfering RNA and Amphipathic Cell-Penetrating Peptides. *Mol. Ther. - Nucleic Acids* **2017**, *7*, 1–10.
 81. Sutaria, D. S. *et al.* Expression Profiling Identifies the Noncoding Processed Transcript of HNRNPU with Proliferative Properties in Pancreatic Ductal Adenocarcinoma. *Non-Coding RNA* **2017**, *3*, 24.
 82. Vermeulen, L. M. P. *et al.* Endosomal Size and Membrane Leakiness Influence Proton Sponge-Based Rupture of Endosomal Vesicles. *ACS Nano* **2018**, *12*, 2332–2345.
 83. Ragelle, H. *et al.* Intracellular siRNA Delivery Dynamics of Integrin-Targeted, PEGylated Chitosan–Poly(Ethylene Imine) Hybrid Nanoparticles: A Mechanistic Insight. *J. Control. Release* **2015**, *211*, 1–9.
 84. Bramsen, J. B. *et al.* Improved Silencing Properties Using Small Internally Segmented Interfering RNAs. *Nucleic Acids Res.* **2007**, *35*, 5886–5897.
 85. Schwabe, K. *et al.* Sustained Delivery of siRNA Poly- and Lipopolyplexes from Porous Macromer-Crosslinked Gelatin Gels. *Int. J. Pharm.* **2017**, *526*, 178–187.
 86. De Vlieghere, E.; Carlier, C.; Ceelen, W.; Bracke, M.; De Wever, O. Data on *In Vivo* Selection of SK-OV-3 Luc Ovarian Cancer Cells and Intraperitoneal Tumor Formation with Low Inoculation Numbers. *Data Br.* **2016**, *6*, 542–549.

87. Houthaeve, G. *et al.* Targeted Perturbation of Nuclear Envelope Integrity with Vapor Nanobubble-Mediated Photoporation. *ACS Nano* **2018**, *12*, 7791–7802.
88. Fraire, J. C. *et al.* Vapor Nanobubble Is the More Reliable Photothermal Mechanism for Inducing Endosomal Escape of siRNA without Disturbing Cell Homeostasis. *J. Control. Release* **2020**, *319*, 262–275.
89. Rehman, Z. ur; Hoekstra, D.; Zuhorn, I. S. Mechanism of Polyplex- and Lipoplex-Mediated Delivery of Nucleic Acids: Real-Time Visualization of Transient Membrane Destabilization without Endosomal Lysis. *ACS Nano* **2013**, *7*, 3767–3777.

SUPPLEMENTARY FIGURES AND TABLES

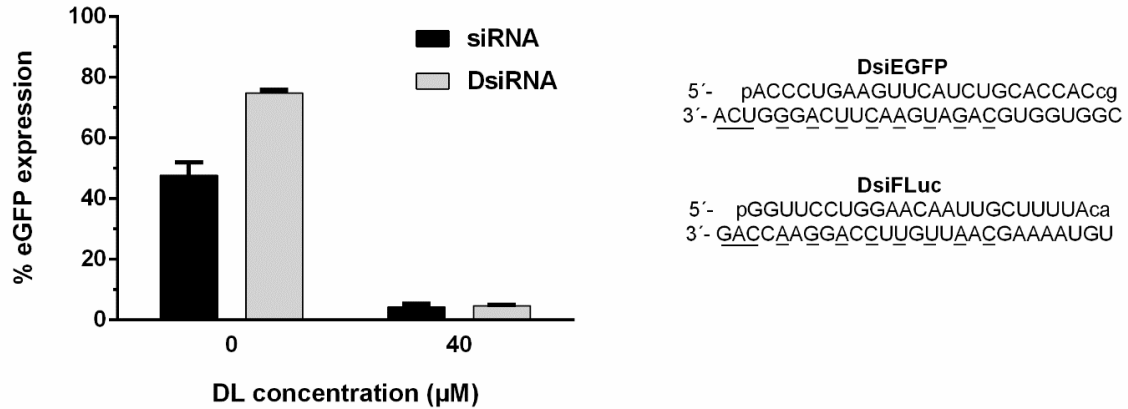


Figure S1. Evaluation of gene silencing potential of NGs loaded with siRNA (black) or 25-27mer Dicer-substrate siRNA (DsiRNA; grey) in H1299-eGFP cells upon sequential treatment with 40 µM desloratadine (DL) during 20 hours. The experiments were performed with a fixed NG concentration (30 µg/mL) and siRNA/DsiRNA concentration (5 nM). The eGFP expression of the cells treated with eGFP-targeting siRNA or DsiRNA was normalized to the expression of cells treated with control siRNA or DsiRNA. siRNA targeting eGFP (siEGFP) and negative control siRNA (siCTRL) were purchased from Eurogentec. Sequences are illustrated in the section Materials and Methods. DsiRNA targeting eGFP (DsiEGFP) or targeting firefly luciferase (DsiFLuc; used as negative control), were obtained from IDT (Leuven, Belgium). The sequence is illustrated in the figure, whereby p denotes a phosphate residue, lower case letters are 2'-deoxyribonucleotides, capital letters are ribonucleotides and underlined capital letters are 2'-O-methylribonucleotides. The data are represented as mean ± SD (n = 3, technical replicates). (DL = desloratadine, DsiRNA = Dicer-substrate siRNA, DsieGFP = eGFP-targeting DsiRNA, DsiFluc = DsiRNA targeting firefly luciferase).

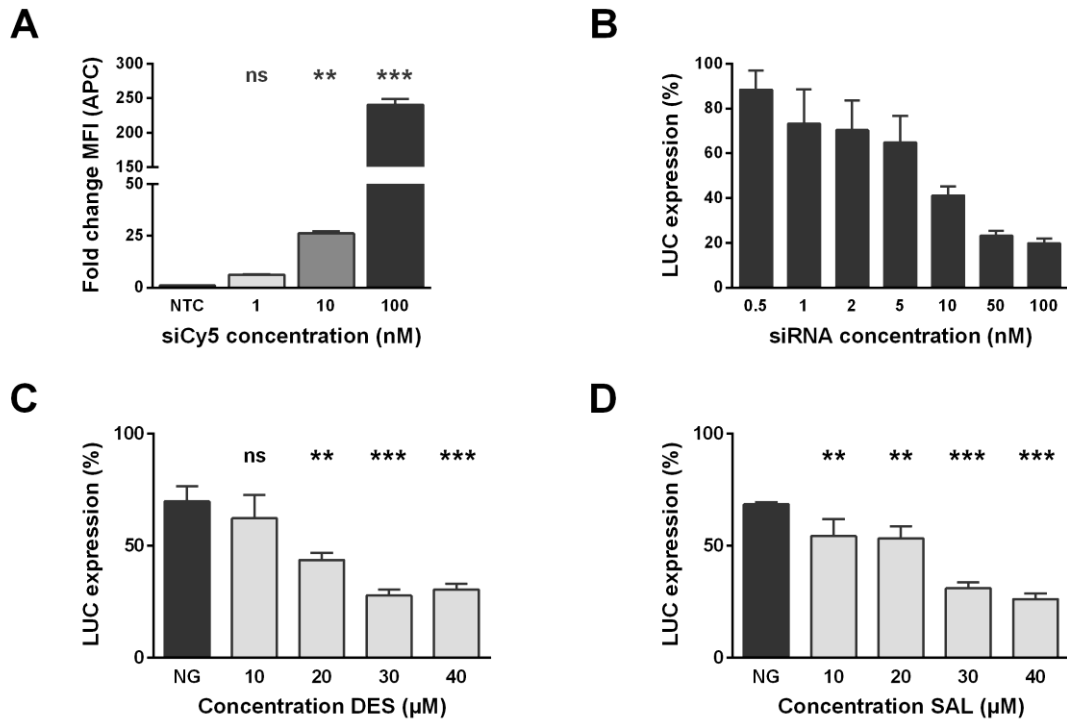


Figure S2. Desloratadine and salmeterol increase the luciferase gene silencing potential of dex-HEMA siNGs in SKOV-3-LUC+ cells. (A) Evaluation of cellular uptake of dex-HEMA siNGs, loaded with different amounts of Cy5[®]-labeled siRNA, in SKOV-3-LUC+ cells determined *via* flow cytometry. (B) Transfection of SKOV-3-LUC+ cells with dex-HEMA siNGs, loaded with different amounts of siRNA. (C-D) Transfection of SKOV-3-LUC+ cells with dex-HEMA siNGs loaded with 2 nM siRNA resulted in ~30% eGFP silencing. Sequential treatment (20 h) with ‘CAD-hits’ (**Chapter 2**) desloratadine (DES) and salmeterol (SAL) caused significant additional LUC silencing in a concentration-dependent manner. The data are represented as mean ± SD (n = 3, technical replicates). Statistical significance with respect to the NG-transfected cells (black *) or NTC (grey *) is indicated when appropriate (ns p > 0.05, ** p ≤ 0.01, *** p ≤ 0.001). (siNG = siRNA-loaded nanogel, NTC = not treated control, NG = dex-HEMA siNG transfection without sequential CAD treatment, LUC = luciferase, DES = desloratadine, SAL = salmeterol, ns = not significant, MFI = mean fluorescence intensity, APC = allophycocyanin (red channel)).

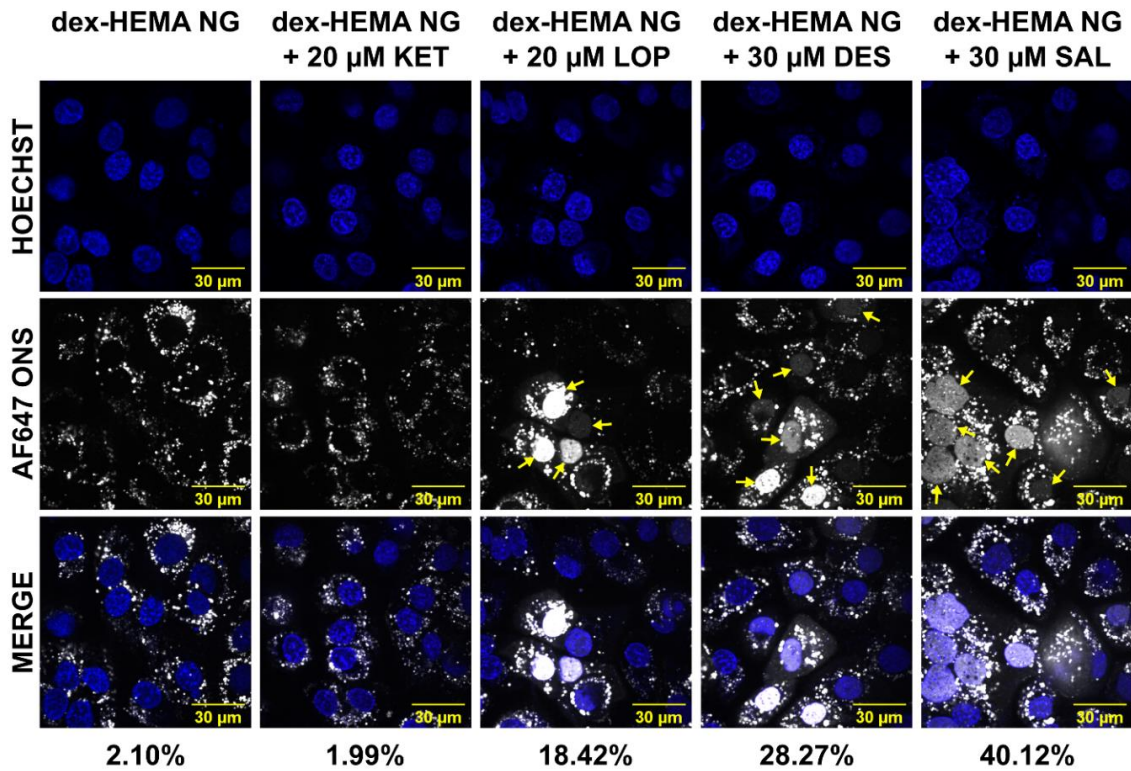
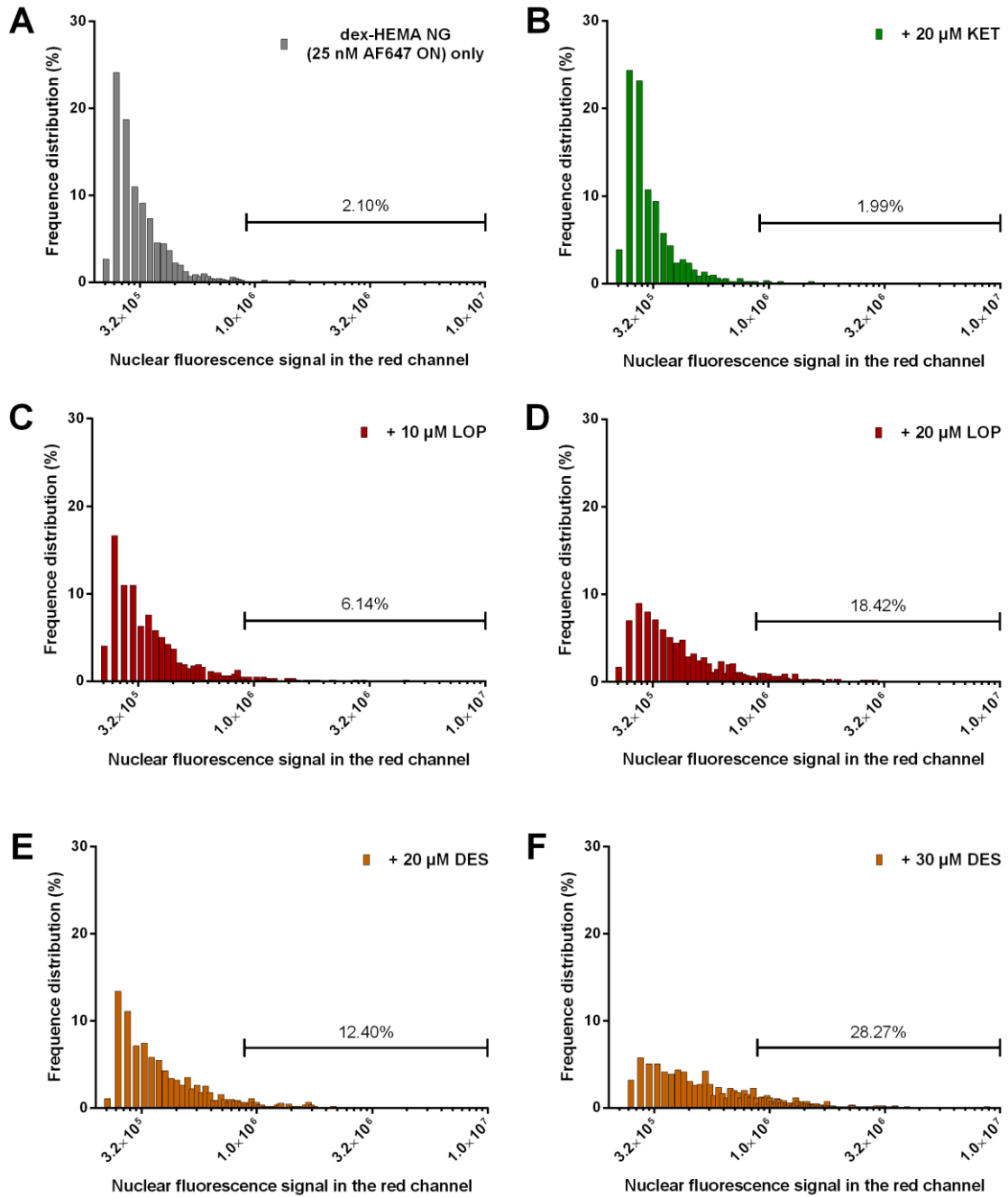


Figure S3. CADs improve cytosolic oligonucleotide (ON) release in SKOV-3 cells. Representative confocal images from the intracellular AF647 ON distribution in SKOV-3-LUC2 IP2 cells, only transfected with AF647 ON-loaded dex-HEMA NGs, or cells subsequently incubated with 20 μ M ketotifen (KET)/20 μ M loperamide (LOP)/30 μ M desloratadine (DES)/30 μ M salmeterol (SAL) for 20 h. Nuclei can be seen in blue, while cells in which endolysosomal escape happened show nuclear fluorescence in the red channel (red fluorescence is depicted white). The values below the images correspond to the percentage of cells with white nuclei (yellow arrows). The scale bar corresponds to 30 μ m. (NTC = not treated control, NG = nanogels, LOP = loperamide, KET = ketotifen, DES = desloratadine, SAL = salmeterol, ON = oligonucleotide, AF647 = Alexa Fluor® 647 dye).



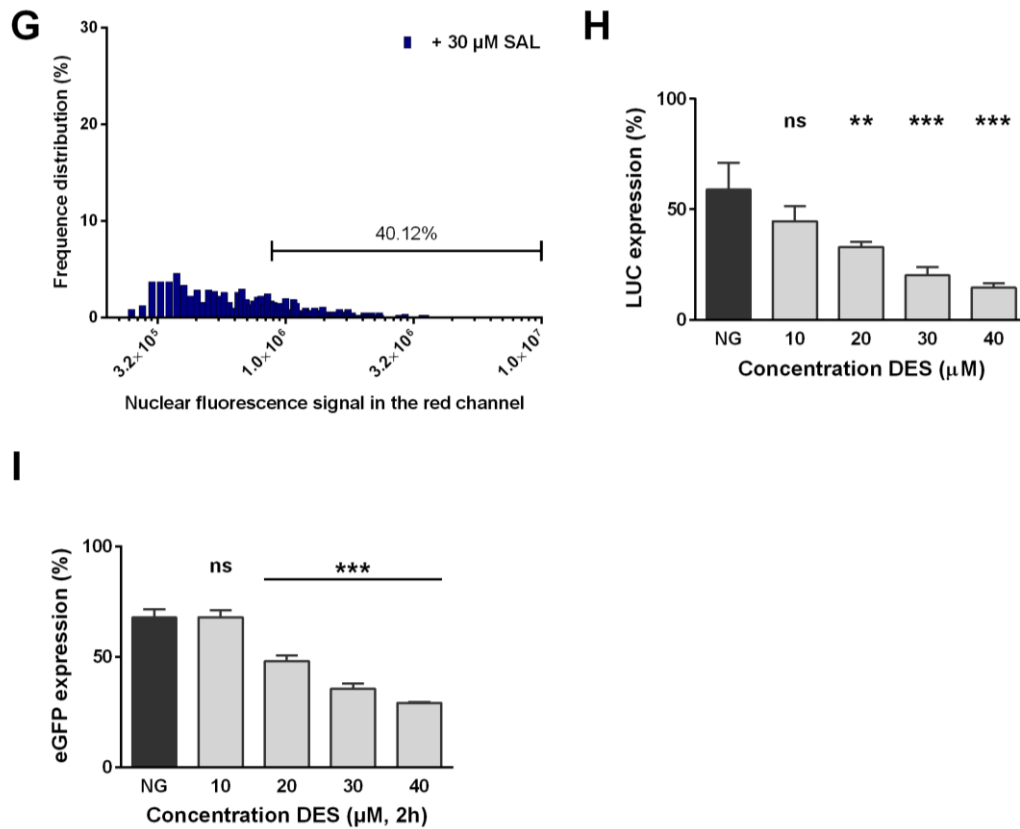


Figure S4. CADs increase small NA release to the cytosol, leading to an enhanced dex-HEMA siNG LUC/GFP silencing potential in SKOV-3-LUC2 IP2 and HeLa NLS-GFP cells. (A-G) Frequency distributions of the nuclear fluorescence signal in the red channel of all SKOV-3-LUC2 IP2 cells per condition, quantified from the confocal images in **Figure S3** (+ data not shown for 10 μM LOP and 20 μM DES). The percentages, determined on the histograms, correspond to the percentage of cells with red nuclei (red fluorescence is depicted white in **Figure S3**) in which escape has happened. (H) Transfection of SKOV-3-LUC2 IP2 cells with dex-HEMA siNGs loaded with 10 nM siRNA resulted in ~40% eGFP silencing. Sequential treatment with ‘CAD-hit’ (**Chapter 2**) desloratadine (DES, 20 h) caused significant additional LUC silencing in a concentration-dependent manner. (I) Transfection of HeLa NLS-GFP cells with dex-HEMA siNGs loaded with 10 nM siRNA resulted in ~30% GFP silencing. Sequential treatment with ‘CAD-hit’ desloratadine (DES, 2 h) caused significant additional GFP silencing in a concentration-dependent manner. The data (**Figure S4H-I**) are represented as mean \pm SD ($n = 3$, technical replicates). Statistical significance with respect to the NG-transfected cells is indicated when appropriate (ns $p > 0.05$, ** $p \leq 0.01$, *** $p \leq 0.001$). (CAD = cationic amphiphilic drug, NA = nucleic acid, NTC = not treated control, siNG = siRNA-loaded nanogel, NG = dex-HEMA siNG transfection without sequential CAD treatment, LUC = luciferase, NLS-GFP = nuclear-localized signaling expressing GFP, DES = desloratadine, SAL = salmeterol, LOP = loperamide, KET = ketotifen, ON = oligonucleotide, AF647 = Alexa Fluor[®] 647 dye, ns = not significant).

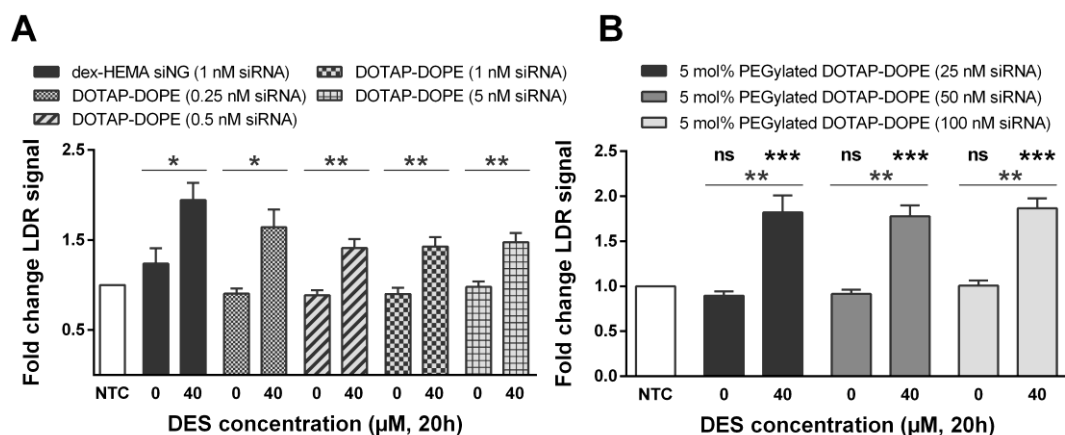


Figure S5. Desloratadine induces a marked enlargement of the total lysosomal volume in combination with (PEGylated) DOTAP-DOPE siRNA-loaded liposomes (siLIPs). (A-B) Fold change in LDR signal, measured *via* flow cytometry, for H1299-eGFP cells sequentially transfected with (PEGylated) DOTAP-DOPE siLIPs and treated with different concentrations of desloratadine (DES) for 20 h. Data are represented as mean \pm the standard error of the mean (SEM) for minimum three independent repeats. Statistical significance is indicated when appropriate, in black * when referring to the untreated control and in grey * when compared to siRNA-loaded NP transfection alone (ns $p > 0.05$, * $p \leq 0.05$, ** $p \leq 0.01$, *** $p \leq 0.001$). (NP = nanoparticle, siNG = siRNA-loaded nanogel, siLIPs = siRNA-loaded liposomes, NTC = not treated control, DES = desloratadine, ns = not significant, LDR = LysoTracker® Deep Red).

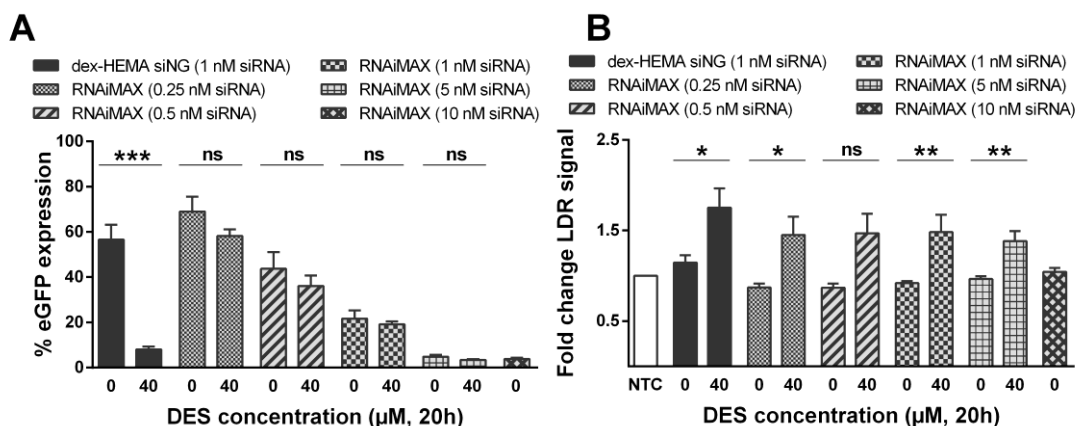


Figure S6. Sequential desloratadine (DES) treatment significantly improves the silencing potential of siRNA-loaded dex-HEMA NGs, but not of siRNA-loaded RNAiMAX liposomes, in H1299-eGFP cells. (A) The influence of 20 h sequential adjuvant treatment with 40 μ M desloratadine (DES) on the transfection efficiency of siNGs (dex-HEMA, complexing 1 nM siRNA) or Lipofectamine® RNAiMAX liposomes (at varying siRNA concentrations). (B) Fold change in LDR signal, measured *via* flow cytometry, for H1299-eGFP cells sequentially transfected with siRNA-loaded dex-HEMA NGs or Lipofectamine® RNAiMAX liposomes and treated with 40 μ M DES for 20 h. Data are represented as mean \pm the standard error of the mean (SEM) for minimum three independent repeats. Statistical

significance is indicated when appropriate, in black * when compared to siNP transfection alone (ns $p > 0.05$, * $p \leq 0.05$, ** $p \leq 0.01$, *** $p \leq 0.001$). (siNG = siRNA-loaded nanogel, RNAiMAX = Lipofectamine[®] RNAiMAX, siLIPs = siRNA-loaded liposomes, siNP = siRNA-loaded nanoparticle, NTC = not treated control, DES = desloratadine, ns = not significant, LDR = LysoTracker[®] Deep Red).

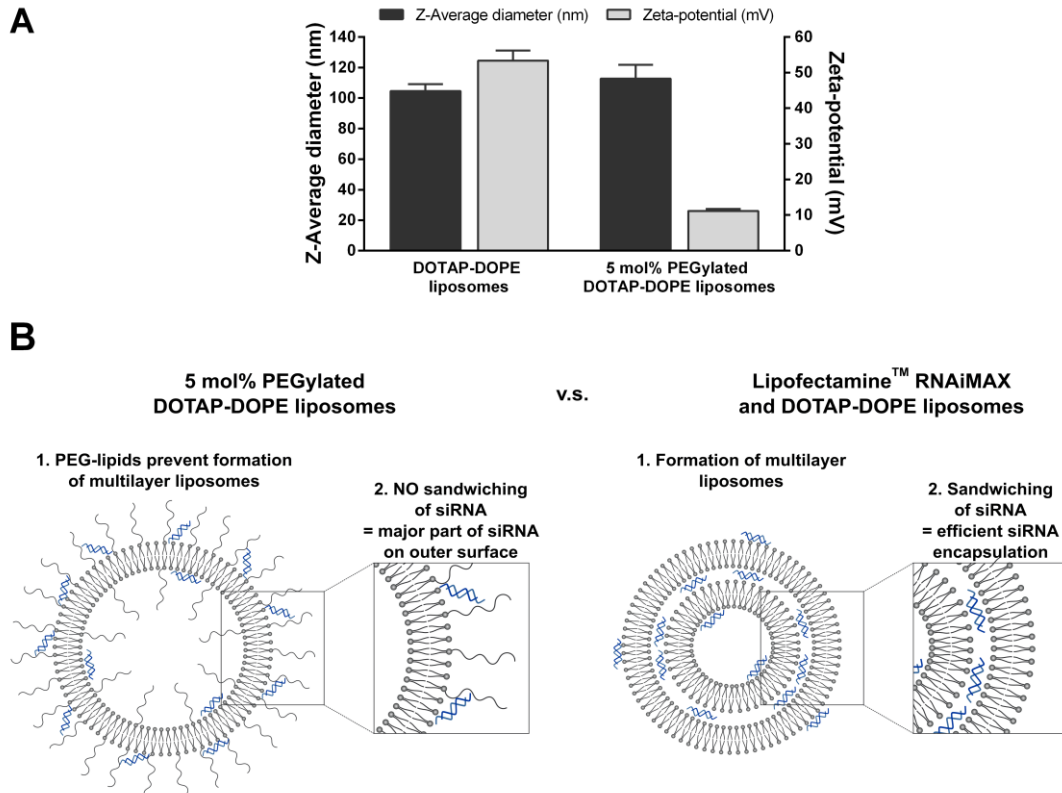


Figure S7. Physicochemical properties of the (PEGylated) DOTAP-DOPE liposomes and the visual representation of lipoplex formation. (A) Hydrodynamic diameter (Z-Average diameter) and zeta-potential of unloaded DOTAP-DOPE liposomes, with or without 5 mol% DSPE-PEG₂₀₀₀, determined by DLS (from at least 3 independent repeats). (B) Graphical representation of the different mechanisms of lipoplex formation, when mixed with siRNA, for DOTAP-DOPE liposomes vs. 5 mol% PEGylated DOTAP-DOPE liposomes. (DLS = dynamic light scattering).

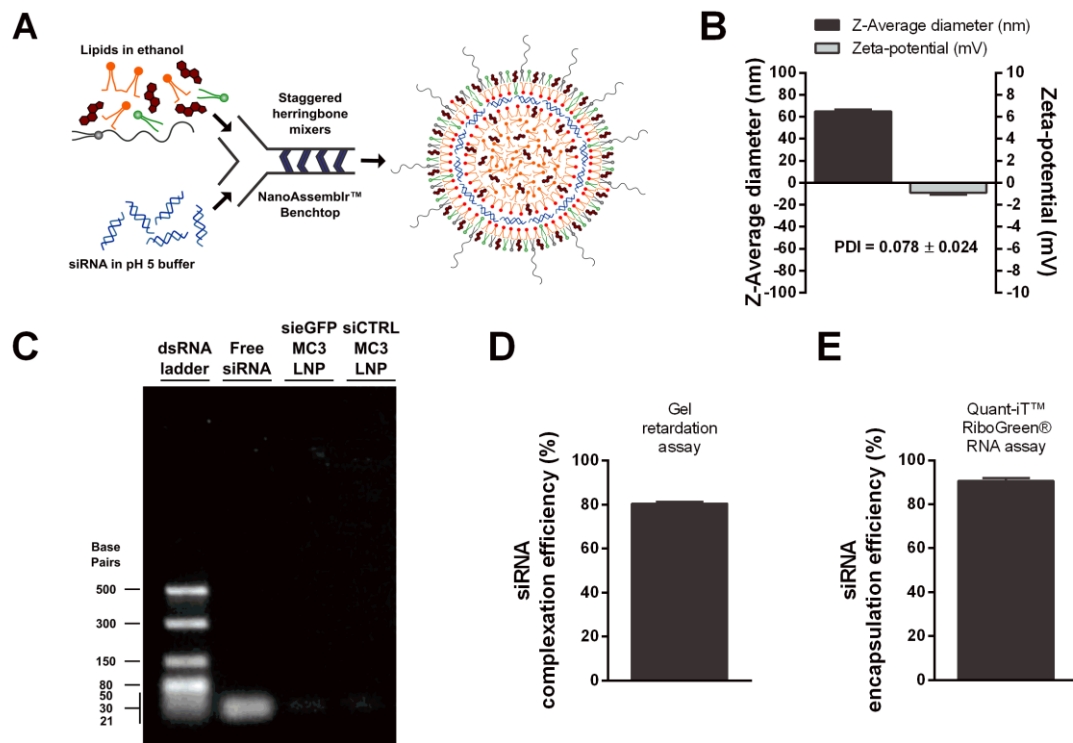


Figure S8. Physicochemical properties of the siRNA-loaded MC3 lipid nanoparticles. (A) Graphical representation of the formulation scheme for the MC3 siRNA-loaded lipid nanoparticles (siLNPs). In short, lipid components dissolved in ethanol were mixed with siRNA dissolved in acetate buffer (pH 5, 10 mM) in a microfluidic chip using the NanoAssemblr™ Benchtop instrument (Precision Nanosystems). The explanation of the differently coloured lipids is shown in **Scheme 2**. (B) Hydrodynamic diameter (Z-Average diameter), zeta-potential and PDI of siRNA-loaded MC3 LNPs (optimal molar N/P charge ratio of 4.7), determined by DLS (n = 2, two technical triplicates per independent repeat of the same formulation). (C) Gel (2% agarose) retardation assay of MC3 siLNPs and (D) quantification of siRNA complexation efficiency in the MC3 siLNPs, based upon the intensity of the gel bands in panel C. Data are represented as mean ± the standard deviation (SD) for 2 repeats. (E) Encapsulation efficiency of siRNA in MC3 siLNPs, measured by the Invitrogen™ Quant-iT™ RiboGreen™ RNA assay. Data are represented as mean ± the standard deviation (SD) for minimum three independent repeats of the same formulation. (MC3 siLNPs = siRNA-loaded lipid nanoparticles containing the ionizable lipid DLin-MC3-DMA, DLS = dynamic light scattering, PDI = polydispersity index, dsRNA = double-stranded RNA).

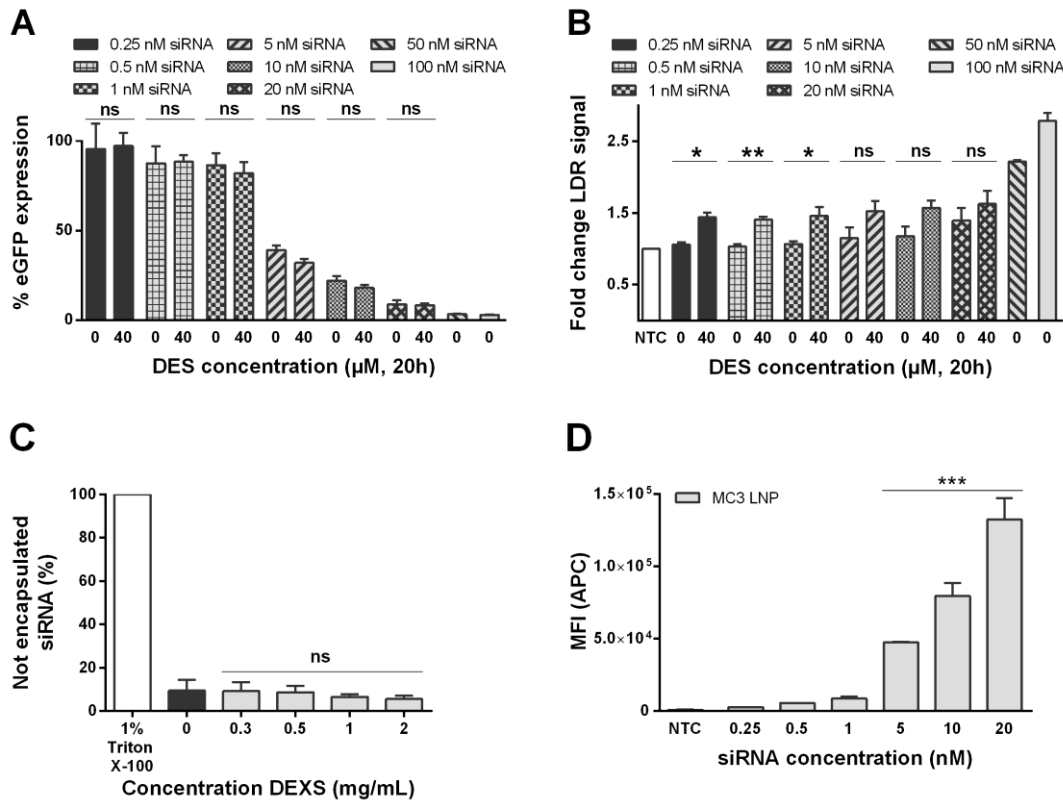


Figure S9. Sequential desloratadine treatment does not improve the silencing potential of siRNA-loaded MC3 LNPs in H1299-eGFP cells. (A) The influence of 20 h sequential adjuvant treatment with desloratadine (DES) on the transfection efficiency of MC3 siLNPs. Data are represented as mean \pm the standard deviation (SD) for two independent repeats. Statistical significance with respect to the MC3 siLNP transfection alone is indicated when appropriate (ns $p > 0.05$). (B) Fold change in LDR signal, measured *via* flow cytometry, for H1299-eGFP cells sequentially transfected with siRNA-loaded MC3 LNPs and treated with 40 μ M DES for 20 h. Data are represented as mean \pm the standard deviation (SD) for two independent repeats. Statistical significance with respect to the MC3 siLNP transfection alone is indicated when appropriate (ns $p > 0.05$, * $p \leq 0.05$, ** $p \leq 0.01$). (C) The influence of different concentrations of the competing polyanion DEXS on the siRNA encapsulation of MC3 siLNPs, as measured by the Quant-iTTM RiboGreen[®] RNA assay. Data are represented as mean \pm the standard deviation (SD) for minimum three independent repeats. Statistical significance with respect to the control (0 mg/mL DEXS) is indicated when appropriate (ns $p > 0.05$). (D) Quantification of cellular uptake of MC3 siLNPs, in H1299-eGFP cells determined *via* flow cytometry. Data are represented as mean \pm the standard deviation (SD) for two independent repeats. Statistical significance with respect to the NTC (black *) is indicated when appropriate (***) $p \leq 0.001$. (siNPs = siRNA-loaded nanoparticles, MC3 siLNPs = siRNA-loaded lipid nanoparticles containing the ionizable lipid DLin-MC3-DMA, LDR = LysoTracker[®] Deep Red, DEXS = 10 kDa dextran sulphate, DES = desloratadine, ns = not significant, NTC = not treated control, MFI = mean fluorescence intensity, APC = allophycocyanin (red channel)).

SUPPLEMENTARY MATERIALS AND METHODS

NG transfection, sequential adjuvant treatment and quantification of transfection efficiency with a luciferase assay in SKOV-3-LUC cells

SKOV-3-LUC+ and SKOV-3-LUC2 IP2 cells were seeded in 96-well plates (SPL Lifesciences Co. Ltd., Naechon-Myeon Pocheon, South Korea) at a density of 7500 cells/well in 100 μ L of serum-containing complete cell culture medium (CCM) 24 h prior to transfection. The edge wells were filled with 100 μ L CCM to reduce evaporation in the cell-containing wells. Next, the cells were transfected with dex-HEMA siNGs (prepared as described in main text) during 3 hours at 37 °C in a humidified atmosphere containing 5% CO₂. Note that for every siLUC+/2 condition a siCTRL sample was included to account for potential off-target effects. Subsequently, the siNG dispersion was removed, and after a washing step with 50 μ L CCM, the cells received 50 μ L fresh (DMSO control) or CAD-containing CCM (DES or salmeterol (SAL), maximally 0.08% (v/v) residual DMSO) at the indicated concentrations. After 20 hours, the small molecule containing CCM (and DMSO control) was removed and the cells were lysed with 50 μ L of a 1X dilution of the Luciferase Cell Culture Lysis 5X Reagent (Promega, Leiden, The Netherlands) to analyze the *firefly* luciferase expression using the Luciferase Assay System (Promega, Leiden, The Netherlands). This was done according to the manufacturer's instructions. The bioluminescence (relative light units, RLU) was measured using a GloMax Luminometer (Promega, Leiden, The Netherlands). The percentage of luciferase knockdown (mean \pm SD, n = 3 technical replicates) was determined by the following equation: % LUC expression = 100 x RLU-LUC/RLU-CTRL, where RLU-CTRL is the mean RLU for siCTRL and RLU-LUC is the mean RLU for siLUC+/2.

NG transfection and sequential adjuvant treatment in HeLa NLS-GFP cells

HeLa NLS-GFP cells were seeded in 96-well plates (SPL Lifesciences Co. Ltd., Naechon-Myeon Pocheon, South Korea) at a density of 10000 cells/well in 100 μ L of CCM 24 h prior to transfection. The edge wells were filled with 100 μ L CCM to reduce evaporation in the cell-containing wells. Next, the cells were transfected with dex-HEMA siNGs (prepared as described in main text) during 3 hours at 37 °C in a humidified atmosphere containing 5% CO₂. Note that for every sieGFP condition a siCTRL sample was included to account for potential off-target effects. Subsequently, the siNG dispersion was removed and the cells received 50 μ L fresh (DMSO control) or DES-containing CCM (maximally 0.08% (v/v) residual

DMSO) at the indicated concentrations. After 2 hours, the small molecule containing CCM (and DMSO control) was removed and the cells were analysed with flow cytometry 42 h later as described in main text.

siRNA-loaded MC3 lipid nanoparticles (MC3 siLNPs): synthesis, DLS, transfection and uptake

MC3 siLNPs were synthesized by injecting one volume of lipid mixture of DLin-MC3-DMA (heptatriaconta-6,9,28,31-tetraen-19-yl 4-(dimethylamino)butanoate, abbreviated as MC3), DSPC (1,2-distearoyl-*sn*-glycero-3-phosphocholine), cholesterol and DMG-PEG₂₀₀₀ (1,2-dimyristoyl-*rac*-glycero-3-methoxypolyethylene glycol-2000) (50:10:38.5:1.5 mol ratio, as previously described) in ethanol and three volumes of siRNA (optimal molar N/P charge ratio of 4.7) in acetate buffer (pH 5, 10 mM) in the microfluidic NanoAssemblr[®] Benchtop mixing device (Precision Nanosystems, Vancouver BC, Canada) at a total flow rate of 12 mL/min (3 mL/min for ethanol and 9 mL/min for aqueous buffer, flow rate ratio of 3:1 (aqueous to ethanol)). The resultant mixture (5.8 mg/mL total lipid concentration) was dialyzed (Pur-A-Lyzer[™] Maxi 12000 Dialysis Kit) overnight against phosphate buffered saline (PBS) to remove residual ethanol and to raise the pH to 7.4. MC3 was obtained from Prof. Dan Peer (Laboratory of Precision NanoMedicine, Tel Aviv University, Israel). All other lipids were purchased from Avanti Polar Lipids, Inc. (Alabaster, AL, USA). Samples were stored at 4 °C until use. Hydrodynamic diameter, zeta-potential and polydispersity index (PDI) of the MC3 siLNPs (after dialysis) were determined in HEPES buffer (pH 7.4, 20 mM) *via* Dynamic Light Scattering (DLS) (Zetasizer Nano, Malvern Instruments Ltd., Worcestershire, UK). siRNA complexation and encapsulation efficiency were respectively determined by agarose gel electrophoresis and a Quant-iT[™] RiboGreen[®] RNA assay, as described below. Transfection (including LysoTracker[®] Deep Red staining and compound treatment) and uptake experiments were performed similar to the protocol described in the manuscript main text (MC3 siLNPs formulated with siCTRL:siCy5[®] (90:10 mol%)). MC3 siLNPs were diluted in CCM and incubated with the cells overnight (24 h) at 37 °C in a humidified atmosphere containing 5% CO₂, followed by CAD treatment for 20 h. Flow cytometry acquisition (silencing) was done 20 h after CAD removal.

Agarose gel electrophoresis

MC3 siLNPs (in PBS) were equilibrated at 37°C and mixed with 10 µL Ambion loading buffer (Thermo Fisher Scientific, Rockford, USA) prior to loading on a 2% agarose gel in GelRed™ (Biotium, Hayward, CA, USA) supplemented TRIS/Borate/EDTA (TBE) buffer. After running the gel for 40 min at 100 V, the gel was photographed under UV illumination. A sample containing free siRNA in PBS was run as control. Additionally, a 21 - 500 base pairs dsRNA (double-stranded RNA) ladder (New England Biolabs Ltd., Hitchin, UK) was included. The complexation efficiency was determined by quantifying the intensity of the gel bands for every condition, relative to the intensity of free siRNA (intensity calculated as area under the curve (AUC) of intensity plot for every band), using ImageJ software (FIJI).

Quant-iT™ RiboGreen® RNA assay

To determine the capacity of the MC3 LNPs to encapsulate siRNA, 2 µL of the MC3 siLNPs was diluted in a final volume of 100 µL TE buffer (10 mM Tris-HCl, 20 mM EDTA) with or without 1% Triton™ X-100 (Sigma-Aldrich, Overijse, Belgium) in a black 96-well fluorescent plate (Greiner Bio-One GmbH, Vilvoorde, Belgium). After incubating the plate for 10 min at 40 °C, 100 µL of a 200-fold dilution of the RiboGreen® reagent (Molecular Probes™, Eugene, OR, USA) in TE buffer was added to each well. Plates were shaken at room temperature for 5 min and fluorescence (ex –485 nm, em –535 nm) was measured using a 1420 Multilabel Counter Victor3™ plate reader (PerkinElmer, Waltham, MA, USA). Encapsulation efficiencies for siRNA were calculated by $(F_{\text{total siRNA}} - F_{\text{ne siRNA}})/F_{\text{total siRNA}} \times 100$, with $F_{\text{ne siRNA}}$ = the amount of not encapsulated siRNA (measured by the fluorescence upon the addition of RiboGreen® reagent to the MC3 siLNP formulation) and $F_{\text{total siRNA}}$ = the total siRNA content (obtained with lysis of the MC3 siLNP formulation by 1% Triton™ X-100)¹.

In an additional experiment, the release of siRNA from the MC3 siLNPs was evaluated in the presence of a competing polyanion, *i.e.* dextran sulfate sodium salt (DEXS, 10 kDa, Sigma-Aldrich). In short, 2 µL of the MC3 siLNPs was diluted in a final volume of 100 µL TE buffer (10 mM Tris-HCl, 20 mM EDTA) with or without different concentrations of DEXS (0.3, 0.5, 1, 2 mg/mL) in a black 96-well fluorescent plate (Greiner Bio-One GmbH, Vilvoorde, Belgium). After 10 min incubation at room temperature (incubation with 1% Triton™ X-100 as a control), the samples were analysed with the Quant-iT™ RiboGreen® RNA assay, as described above.

REFERENCES FOR SUPPORTING INFORMATION

1. Leung, A. K. K.; Tam, Y. Y. C.; Chen, S.; Hafez, I. M.; Cullis, P. R. Microfluidic Mixing: A General Method for Encapsulating Macromolecules in Lipid Nanoparticle Systems. *J. Phys. Chem. B* **2015**, *119*, 8698–8706.

Chapter 4

Repurposing prazosin as a cell death inducer and lysosomal escape enhancer of siRNA

An adapted version of this chapter is in preparation as:

Van de Vyver, T.[†]; Muntean, C.[†]; Efimova, L.^{‡§}; De Backer, L.[†]; Krysko, D. V.^{‡§||}; De Smedt, S.C.[†]; Raemdonck, K.[†] Repurposing prazosin as a cell death inducer and lysosomal escape enhancer of siRNA.

[†] Ghent Research Group on Nanomedicines, Laboratory of General Biochemistry and Physical Pharmacy, Faculty of Pharmaceutical Sciences, Ghent University, Ottergemsesteenweg 460, 9000 Ghent, Belgium

[‡] Cell Death Investigation and Therapy Laboratory, Department of Human Structure and Repair, Ghent University, 9000 Ghent, Belgium; [§] Cancer Research Institute Ghent, 9000 Ghent, Belgium

^{||} Department of Pathophysiology, Sechenov First Moscow State Medical University, 119146 Moscow, Russia

Author contributions

Conceptualization and study design: T.V.d.V., S.C.D.S., and K. Raemdonck. Experimental work and data analysis: T.V.d.V., C.M., L.E., L.D.B., and K. Raemdonck. D.K. contributed to the cell death experiments. Chapter 4 was written through contributions of all authors.

TABLE OF CONTENTS

1. INTRODUCTION	189
2. RESULTS AND DISCUSSION.....	191
2.1. NIHCC compound screen reveals several non-CAD siRNA delivery enhancers....	191
2.2. Secondary validation of quinazoline derivatives	194
2.3. PIKfyve inhibitors induce pronounced vacuolization with limited adjuvant effect....	199
2.4. Prazosin improves silencing of cholesterol-siRNA conjugates	203
2.5. Mapping the cell death pathways induced by prazosin	205
3. CONCLUSION.....	211
4. MATERIALS AND METHODS	212
4.1. siRNA duplexes and oligonucleotides	212
4.2. Nanoparticle (NP) synthesis, preparation and siRNA complexation	212
4.3. Cell lines and cell culture conditions.....	213
4.4. Quantification of transfection efficiency/lysosomal volume of NP transfection and sequential adjuvant treatment by flow cytometry.....	214
4.5. Cell viability	215
4.6. Quantification of cell death mechanism.....	216
4.7. Visualization and quantification of the cytosolic release of AF647 ONs	216
4.8. Phospholipidosis detection with LipidTOX™ Red	217
4.9. Visualizing lysosomes.....	218
4.10. Statistical analysis	218

ABSTRACT

The widespread use of small interfering RNA (siRNA) is limited by the multiple extra- and intracellular barriers upon *in vivo* administration. Hence, suitable delivery systems, based upon encapsulation in nanoparticles or conjugation to targeting ligands, have been developed, which recently cumulated in the approval of the first RNA interference (RNAi)-based treatments for liver-related diseases. Nevertheless, at the intracellular level, most of these state-of-the-art delivery systems suffer from a low endosomal escape efficiency, thus hindering the pharmacological activity of siRNA molecules in the cytosol. Consequently, the bulk of the endocytosed siRNA drug rapidly accumulates in the lysosomal compartment, which is thought to be a dead end for siRNA (nano)medicines. In contrast to this general belief, we recently reported that a wide variety of cationic amphiphilic drugs (CADs) can strongly boost small nucleic acid delivery from the endolysosomal compartment *via* transient induction of lysosomal membrane permeabilization (**Chapter 2**). Here, we report on the compounds that were additionally identified as siRNA delivery enhancers in our drug repurposing screen (**Chapter 2**), but do not have the typical physicochemical properties of CADs. We further focused on the major hit prazosin, which improved endolysosomal escape of cholesterol-conjugated and polymer-transfected siRNA molecules, despite inducing a clearly different cellular phenotype compared to typical CAD adjuvants. As it has been described that prazosin also induces cancer cell apoptosis and promotes antigen cross-presentation in dendritic cells, the proof-of-concept data illustrated in this chapter represent a starting point to further study the effects of prazosin in an anti-cancer combination strategy.

KEYWORDS: drug repurposing; prazosin; apoptosis; cationic amphiphilic drugs; lysosomal membrane permeabilization; siRNA; endosomal escape; lysosomal escape

1. INTRODUCTION

Post-transcriptional gene silencing by small interfering RNA (siRNA) shows great therapeutic promise for the treatment of any type of human disease with a recognized (over)expression of one or more disease-causing genes¹⁻³. Since the discovery of the RNA interference (RNAi) mechanism more than 2 decades ago⁴, considerable efforts have been made to identify suitable delivery systems that can effectively and safely deliver siRNA drugs to target cells^{1,2}. Indeed, as discussed in **Chapter 1**, siRNAs are negatively charged macromolecular drugs that encounter multiple extra- and intracellular hurdles upon *in vivo* administration^{1,5,6}. At the intracellular level, siRNAs need to access the cytosol to activate the RNAi machinery and induce sequence-specific mRNA degradation^{1,7}. While multiple delivery strategies are under investigation, lipid nanoparticles (LNPs) and conjugates are the most advanced siRNA delivery technologies to date, as exemplified by the recent approval of patisiran (siRNA-loaded LNPs) and givosiran/lumasiran (N-acetylgalactosamine (GalNAc)-siRNA conjugates)⁸⁻¹¹. Unfortunately, despite their clinical approval, cytosolic delivery remains relatively inefficient. Indeed, upon arrival at the target cells, endocytic uptake of LNPs and conjugates *via* receptor-mediated endocytosis results in endosomal sequestration^{5-7,12} and the majority of the endocytosed drug is routed towards the lysosomal compartment, where both carrier and cargo face degradation¹³⁻¹⁸. Since recent studies showed that only a minor fraction (*i.e.* 1-2% in case of LNPs^{13,14} and estimated < 0.01% in case of GalNAc-siRNA conjugates^{1,12,19}) of the internalized siRNA dose escapes into the cytosol during this rapid trafficking process, endosomal escape remains a major bottleneck^{7,13,14,20}.

Interestingly, growing evidence suggests that both the extra- and intracellular barriers for nucleic acid (NA) delivery can in part be overcome by the application of distinct classes of small molecule(s) (drugs) (**Chapter 1**)²¹⁻³⁰. We recently reported that structurally and pharmacologically diverse cationic amphiphilic drugs (CADs) can be repurposed as siRNA delivery enhancers when applied in a sequential manner to siRNA-transfected cells^{26,31}. CADs are known to mainly accumulate in lysosomes upon exposure to cells *via* a well-known pH-dependent ion trapping mechanism, leading to functional inhibition of the lysosomal acid sphingomyelinase (ASM)^{32,33}, phospholipidosis (PLD)^{34,35}, lysosomal swelling^{36,37} and lysosomal membrane permeabilization (LMP)^{38,39}. CAD-induced LMP is actively being explored as a means to selectively kill cancer cells *via* so-called lysosomal cell death (LCD)^{38,39}. However, it was demonstrated by Joris *et al.* that some CADs (*e.g.* the anti-histaminic compound desloratadine (DES)) can induce a transient and non-lethal LMP

phenotype in non-small cell lung cancer (NSCLC) cells, which allowed dextran nanogel-encapsulated siRNA molecules to diffuse from the lysosomal compartment into the cytosol²⁶. Hence, in contrast to governing endosomal escape models, these data suggest that lysosomes are not necessarily a dead end for siRNA nanomedicines. In follow-up work (**Chapter 3**), we established the broader applicability of CADs as adjuvants for the delivery of both siRNA and antisense oligonucleotides (ASOs) in distinct cancer cell lines. Additionally, we found that the CAD adjuvant approach is carrier-specific, as only nanomedicines that resulted in a sufficient amount of free siRNA inside the lysosomal lumen allowed diffusion of siRNA molecules through the CAD-induced pores in the limiting lysosomal membrane³¹. In an attempt to identify additional small molecules that could similarly enhance the gene-silencing potential of siRNA-loaded nanogels in NSCLC cells, a drug repurposing screen was performed, exposing the transfected cells to the 'National Institutes of Health Clinical Collection' compound library (NIHCC, 700 compounds)³¹. This screen revealed a strong enrichment of both CADs and PLD inducers in the hit group, correlating the lysosomotropic properties of CADs with the induction of an acquired lysosomal storage disease phenotype and improved cytosolic siRNA delivery²⁶. However, several hits from this compound screen did not comply with the applied CAD definition (calculated logP (clogP) > 3 and pKa1 > 6). In this work, we further describe these unrelated hit compounds and investigated the adjuvant activity of the α 1-adrenergic receptor antagonist prazosin (PRA), the number one ranked hit compound of the screen, in more detail. Our data revealed that PRA, but not the structural quinazoline-analogues doxazosin (DOX) or terazosin (TER), can strongly promote the cytosolic delivery of cholesterol-conjugated or polymer-transfected siRNA in NSCLC cells. Importantly, PRA treatment leads to lysosomal swelling and the appearance of cytoplasmic vacuoles while PLD induction was not observed, highlighting that PRA induces a distinct cellular phenotype than CADs^{26,40}. Additionally, we showed that several PIKfyve inhibitors, likewise known to generate vacuoles and enlarged lysosomes, could promote siRNA delivery, although to a much lower extent compared to PRA and CADs. It is therefore hypothesized that besides lysosomal swelling and vacuolization, other yet unidentified cellular processes might contribute to PRA-induced cytosolic siRNA delivery. Notably, previous work has shown that PRA is able to induce apoptotic cell death in several cancer cell types, both *in vitro* and *in vivo*^{41–50}. In line with these reports, our preliminary data using well-known inhibitors of various cell death modalities indicates that PRA likewise induces apoptosis in our NSCLC cell model. In addition, recent research demonstrated that PRA can

also be repurposed to increase, both *in vitro* and *in vivo*, dendritic cell (DC) cross-presentation of antigenic peptides to naïve CD8⁺ T-cells⁵¹, which is one of the main driving forces of anti-tumor immunity⁵¹⁻⁵³. Consequently, building on the clear potential of PRA to strongly promote siRNA delivery as well as its various described anti-tumor effects, we here propose a unique triple combination cancer treatment exploiting PRA to concurrently promote cancer cell death, intracellular siRNA delivery (*e.g.* targeting specific oncogenes) and cross-presentation of tumor-associated antigens.

2. RESULTS AND DISCUSSION

2.1. NIHCC compound screen reveals several non-CAD siRNA delivery enhancers

Screening of the NIHCC compound library identified 96 compounds that significantly enhance the gene silencing potential of siRNA-loaded dex-HEMA nanogels (siNGs) in H1299 cells stably expressing the enhanced green fluorescent protein (eGFP)³¹ (**Chapter 2**). The cells were transfected with siNGs, loaded with eGFP targeting siRNA (sieGFP) or a negative control sequence (siCTRL) respectively, and subsequently incubated with the compounds (20 μ M) for 20 h in complete cell culture medium. In the hit group, 56 compounds (~58%) adhered to the applied CAD definition ($\text{clogP} > 3$ and $\text{pKa1} > 6$)⁵⁴, which have been described in detail in **Chapter 2**. However, 40 hit compounds (~42%) with diverging chemical structures and pharmacology could not be classified as CADs ('non-CAD hits', **Table S1**). Hence, the observed siRNA delivery-promoting effect of these compounds cannot readily be correlated to the induction of a phospholipidosis (PLD) phenotype and lysosomal membrane permeabilization (LMP), as has been extensively described in the literature for CADs^{26,31,34,35,38,39}.

To shed light on the potential mode of action of these non-CAD delivery enhancers, we first screened for enriched annotated molecular targets of the latter compounds in **Figure 1A**. Here, a series of common targets and/or drug classes could be distinguished. First, three L-type calcium channel blockers (CCBs) that share a dihydropyridine (DHP) structure (amlodipine, lacidipine and felodipine) were identified as hits. As discussed in **Chapter 1**, L-type CCBs with and without a DHP core have previously shown to boost the potency of cholesterol-conjugated, cell-penetrating asymmetric siRNAs (cp-asiRNAs) when used in a co-

incubation protocol, albeit this effect was linked to the stimulation of endocytosis instead of cytosolic delivery⁵⁵. Hence, as the compounds in our screen were added after siNG transfection and given that five other L-type CCBs (isradipine, nifedipine, nimodipine, nitrendipine, nisoldipine and diltiazem) were not identified as hits, the involvement of this process in our screen seems unlikely. Interestingly, publicly available transcriptomics data (Connectivity Map or CMap data set of the Broad Institute⁵⁶) suggest that CCBs can induce a transcriptional response similar to PLD inducers, which may be linked to the role of calcium signalling in lysosomal function⁵⁷. Moreover, amlodipine contains a side chain with a basic amino group (pKa1 = 9.45) and has lysosomotropic properties, albeit the clogP < 3. As such, amlodipine is a known functional inhibitor of the ASM enzyme (FIASMA)³³ and PLD inducer³⁵ and might thus have a similar mode-of-action as the previously discussed CADs. Secondly, a set of tubulin polymerization inhibitors (vindesine, podophyllotoxin and the anthelmintics albendazole, mebendazole and flubendazole) and four steroids (19-norethindrone acetate, medroxyprogesterone 17-acetate, tibolone and megestrol acetate) were defined as hits. As endo(lyso)somal vesicles move through the cytosol *via* microtubules, disrupting this network might increase the intracellular residence time and the likelihood of endosomal escape⁵⁸⁻⁶³. On the other hand, several steroids have shown to promote the activity of nucleic acid drugs with a pleiotropic mode-of-action (*e.g.* enhance cellular uptake, *etc.*)²¹. Next, some antineoplastic drugs (triptolide, mitoxantrone, dactinomycin and the thymidylate synthase inhibitors carmofur and 5-fluorouracil) emerged as hits, albeit their supporting effects on siRNA delivery were overall rather limited and could potentially be linked to their toxic effects. Only four non-CAD compounds (*i.e.* 10%) improved siRNA-mediated eGFP knockdown to > 50% relative to control, compared to almost 32% of CADs (**Figure 1B**). Hexachlorophene and oligomycin A, respectively an antiseptic⁶⁴ and a potent inhibitor of the mitochondrial ATP synthase⁶⁵, have not yet been described as drug repurposing candidates. On the other hand, the antifungal itraconazole has recently been shown to enhance liposomal pDNA and siRNA delivery⁶⁶. The latter was suggested to occur *via* the known binding of itraconazole to the Niemann-Pick C1 (NPC1) protein^{67,68} in the late endosomal/lysosomal membrane, which leads to a blocked intracellular cholesterol trafficking and hyper-accumulation of cholesterol in the late endosomes and lysosomes. In accordance to other studies that inhibited NPC1 *via* genetic¹⁶ or pharmacological⁶⁹ means, the enhanced transfection could potentially be linked to an increased cellular retention of pDNA/siRNA as a consequence of reduced recycling of endocytosed NAs out of the cell.

Finally, although the adjuvant effect is generally lower in the non-CAD hit group, compared to the CAD hits (**Figure 1B**), the most effective hit prazosin (PRA), a quinazoline-based α 1-adrenergic antagonist, is not a typical CAD. Although PRA did strongly increase the cellular granularity, as indicated by the augmented side scatter (SSC) signal, in contrast to the CADs (see **Chapter 2**) no correlation was found here between the SSC signal and improved knockdown within the total non-CAD group (**Figure 1C**). Nevertheless, the mean SSC signal in the ‘non-CAD hit group’ was still significantly higher compared to the ‘non-CAD no hit group’ (**Figure S1**). Interestingly, 2 structural analogues of PRA, *i.e.* doxazosin (DOX) and terazosin (TER), were respectively a minor hit (27% additional eGFP silencing) and a no hit. Given that the strongest adjuvant effect in this screen was obtained with PRA, we next aimed to investigate the cellular phenotype of this compound in more detail.

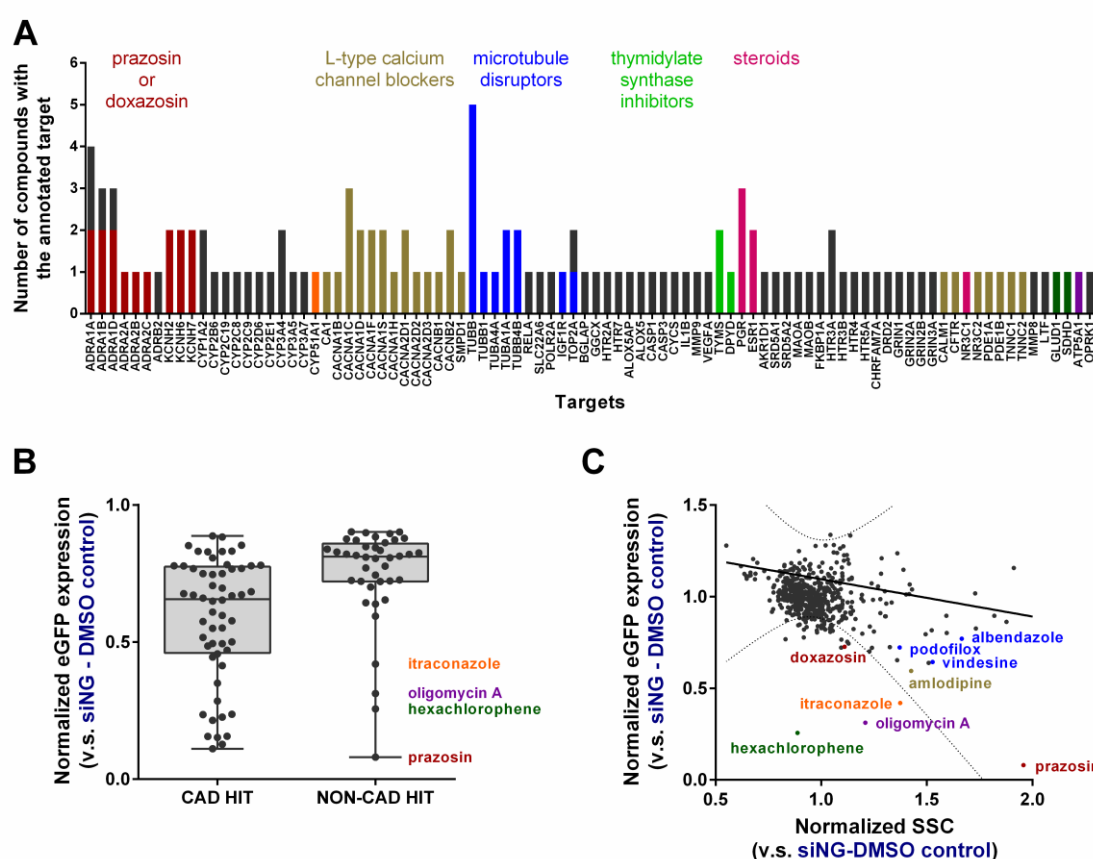
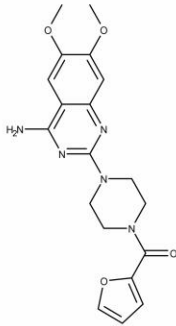
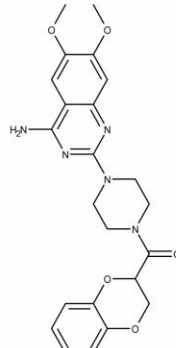
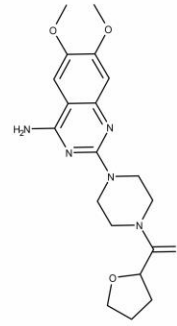
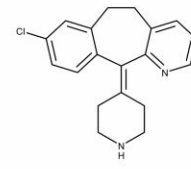


Figure 1. Next to CADs ($\text{clogP} > 3$ and $\text{pKa}1 > 6$), also non-CAD compounds were identified as siRNA delivery-promoting hits in the NIHCC library screen (**Chapter 2**). (A) Summary of annotated targets for the siRNA delivery-promoting non-CAD compounds (*i.e.* ‘non-CAD hits’). The abscissa indicates the documented protein targets of the non-CAD hits. The ordinate indicates the number of non-CAD hits that have each of the depicted proteins as a validated target according to the Drug Repurposing

Hub database⁷⁰. A summary of the annotated targets for each compound is provided in **Table S1**. (B) Box and whisker plot of the normalized eGFP expression (calculated % eGFP expression values of the individual compounds (20 μ M, 20 h) were normalized to the siNG transfection alone (siNG-DMSO control) of each plate) of the 'CAD hit' (n = 56) and 'non-CAD hit' (n = 40) group. (C) Correlation between the SSC signal, normalized to the siNG-DMSO control of each plate, and the normalized eGFP expression (see above) in the group of all non-CADs (n = 572). The dashed line represents the 95% confidence band of the regression line ($R^2 = 0.000207$; ns). In both (A), (B) and (C), discussed compounds or drug classes are highlighted in associated colors. (eGFP = enhanced green fluorescent protein, NG = dex-HEMA nanogels, siNG = siRNA-loaded NG, NIHCC = National Institutes of Health Clinical Collection, CAD = cationic amphiphilic drug, siNG-DMSO control = siNG transfection in the absence of compound with equal amount of DMSO, SSC = side scatter).

2.2. Secondary validation of quinazolinamine derivatives

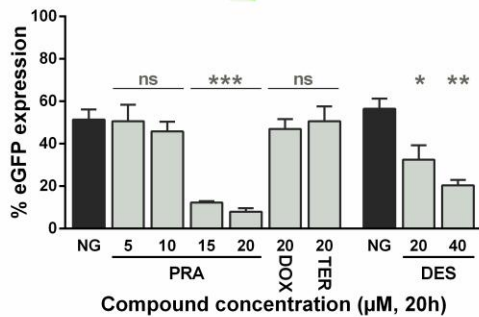
To validate PRA as a potent siRNA delivery enhancer, PRA and its structural analogues DOX and TER were subjected to secondary testing. Additionally, the previously identified CAD adjuvant desloratadine (DES)^{31,71} is included as a comparison (**Figure 2A**). Both PRA and DES evoked a clear concentration-dependent increase in (a) eGFP silencing (**Figure 2B**), (b) total lysosomal volume (**Figure 2C, Figure S2D**) and (c) cellular granularity (**Figure 2D, Figure S2C**) compared to untreated and siNG-transfected cells. In contrast, exposure of the cells to 20 μ M DOX or TER could not phenocopy these effects, despite only minor structural differences relative to PRA (**Figure 2A-D**). Of note, the relative mean fluorescence intensity (rMFI) in the siCTRL sample increased markedly upon treatment with 10-20 μ M PRA (**Figure S2A-B**), which is indicative of cell stress⁷². In addition to dextran NGs, a series of other siRNA nanocarriers was screened. Similar results were obtained for PRA in combination with the commercially available polymeric transfection reagent *in vivo*-jetPEI® (JP) when used in serum-containing (10% FBS) cell medium (**Figure S3A-E**). In contrast, even 40 μ M DES did not have a substantial adjuvant effect on these NPs with only moderate improvement in knockdown observed at 250 nM siRNA, **Figure S3A**), despite clear indication that the applied DES evoked the anticipated lysosomal swelling in all conditions tested (**Figure S3B**). Likewise, PRA outperformed DES in boosting the siRNA delivery of PEGylated DOTAP-DOPE liposomes (**Figure S4A, Figure S4C**) and only PRA was able to moderately improve eGFP knockdown obtained with state-of-the-art lipid nanoparticles containing the ionizable lipid DLin-MC3-DMA (MC3 LNPs, **Figure S4B, Figure S4D**). From these data it is clear that PRA has more outspoken effects on lysosomal swelling and siRNA delivery than DES. However, PRA also has a greater impact on cell viability than DES (**Figure 2E**).

A	prazosin	doxazosin	terazosin	desloratadine
drug class	α 1-adrenergic receptor antagonists, used for benign prostatic hyperplasia or hypertension			antihistamine
clogP	1.65	2.14	1.18	3.97
pKa1	7.24	7.24	7.24	9.73
				

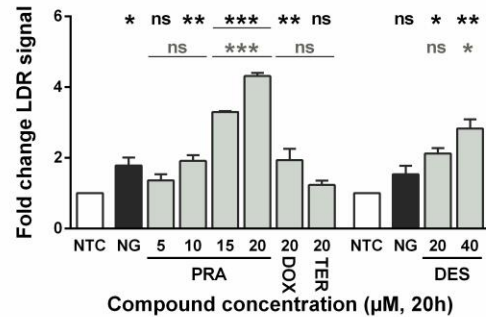


Polymeric dextran nanogel

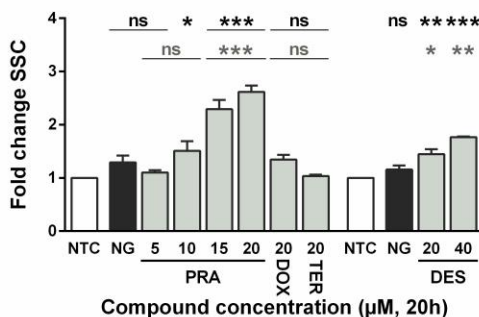
B silencing



C lysosomes



D cellular granularity



E viability

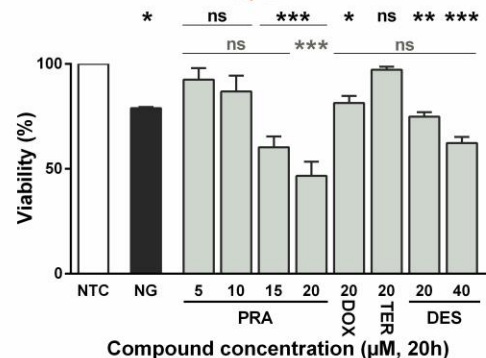


Figure 2. Prazosin and desloratadine, but not doxazosin or terazosin, improve the eGFP silencing potential of dex-HEMA siNGs in NSCLC cells, while increasing the lysosomal volume and cellular granularity. (A) The drug class, clogP, pKa1 values and molecular structure of prazosin (PRA), doxazosin (DOX), terazosin (TER) and desloratadine (DES)⁷³. The pKa1 and clogP values of the

compounds were predicted with JChem for Office (version 17.21.0.1797, ChemAxon Ltd., Budapest, Hungary)⁷³. (B) Sequential treatment of siNG-transfected H1299-eGFP cells (1 nM siRNA) with the quinazoline-based 'non-CAD hit' PRA or the CAD DES caused significant additional eGFP silencing in a concentration-dependent manner, while the quinazolines DOX and TER had no effect at 20 μ M. (C-D) Fold change in LDR signal and side scatter (SSC) signal, measured *via* flow cytometry, for H1299-eGFP cells sequentially transfected with dex-HEMA siNGs and treated with several concentrations of PRA/DOX/TER/DES for 20 h. (E) Cell viability of H1299-eGFP cells following sequential dex-HEMA siNG transfection and PRA/DOX/TER/DES addition for 20 h. Data are represented as mean \pm the standard error of the mean (SEM) for three independent repeats. Statistical significance is indicated when appropriate, in black * when referring to the untreated control and in grey * when compared to dex-HEMA siNG transfection alone (ns $p > 0.05$, * $p \leq 0.05$, ** $p \leq 0.01$, *** $p \leq 0.001$). (clogP = calculated logP, pKa1 = pKa of the most basic amine, eGFP = enhanced green fluorescent protein, NG = dex-HEMA siNG transfection without sequential compound treatment, NTC = not treated control, PRA = prazosin, DOX = doxazosin, TER = terazosin, DES = desloratadine, ns = not significant, LDR = LysoTracker[®] Deep Red, SSC = side scatter).

Next, we used confocal fluorescence microscopy to visualize and quantify cytosolic delivery of Alexa Fluor[®] 647-labeled oligonucleotides (AF647 ONs), which upon endosomal escape migrate to the cell nucleus^{31,74,75}. Hence, quantification of the AF647 ON fluorescence in the nuclear region of each individual cell can be used as a measure of endosomal escape efficiency. A punctate pattern was observed for most untreated cells and cells exposed to 20 μ M DOX or TER (< 5% of labeled nuclei), indicating lysosomal sequestration of AF647 ON-loaded dextran NGs. In contrast, incubation with 15 or 20 μ M PRA and 40 μ M DES increased the amount of stained nuclei up to ~52-72% and ~31%, respectively (**Figure 3A**, **Figure S5A**, **Figure S6A-I**). Additionally, PRA induced the formation of intracellular galectin-3 foci in H1299-WT cells expressing mCherry-galectin-3, while such foci were scarce in untreated cells. Galectin-3 is a cytosolic protein that acts as a membrane damage sensor, since it is able to bind carbohydrates on the luminal side of endolysosomes, which are exposed upon membrane damage^{51,76}. These data indicate that the enhanced cytosolic delivery upon PRA treatment is likely the result of an increased endolysosomal membrane permeability (**Figure S5B**).

Interestingly, in contrast to DES, PRA treatment also led to the rapid (< 1 hour, data not shown) formation of large vacuoles (indicated with red arrows in **Figure 3** and **Figure S5A,C**), which has been reported previously for this compound^{41,45}. Notably, both LysoTracker[®] Deep Red (LDR) positive (indicated with white circles in **Figure S2D**) and negative vacuoles (indicated with yellow circles in **Figure S2D**) could be observed, which corroborates earlier findings and indicates that not all vacuoles are acidic⁴⁵. In addition, staining of compound-

treated cells with the PLD detection reagent LipidTOX™ Red (Figure 3B, Figure S5C, Figure S6J) revealed that 40 μM DES treatment, in line with our previously obtained data^{26,31}, induced the accumulation of phospholipids in vesicular structures, while none of the applied PRA concentrations could replicate this. Hence, these data altogether clearly indicate that PRA treatment results in a different cellular phenotype compared to the previously identified CAD adjuvants^{26,31}.

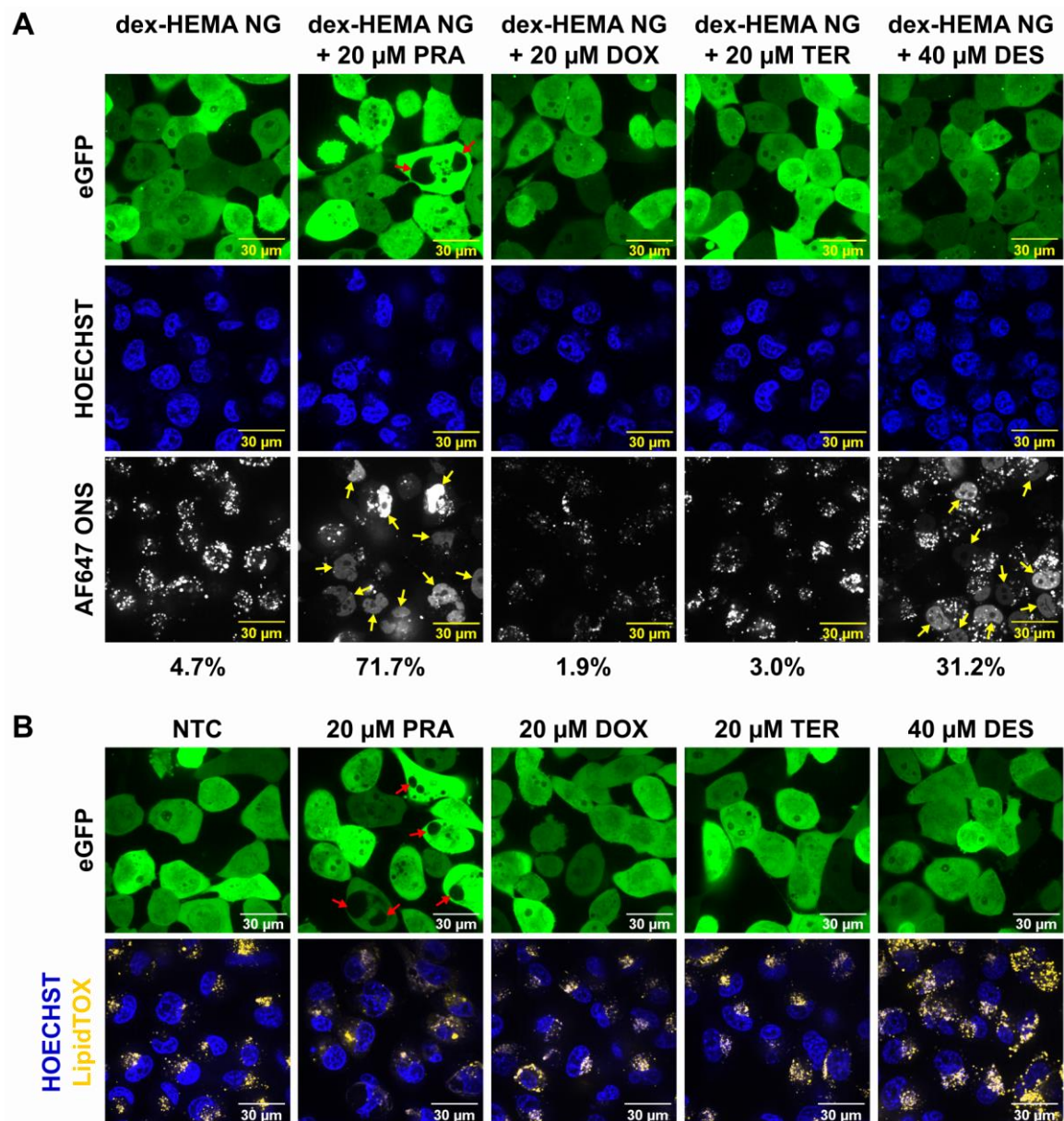


Figure 3. Both desloratadine and prazosin, but not doxazosin or terazosin, promote ON release into the cytosol, while only DES induces a phospholipidosis phenotype in NSCLC cells. (A) Representative confocal images from the intracellular AF647 ON distribution in H1299-eGFP cells, only transfected with AF647 ON-loaded dex-HEMA NGs, or cells subsequently incubated with 20 μM PRA/20 μM

DOX/20 μ M TER/40 μ M DES for 20 h. Nuclei can be seen in blue, while cells in which endolysosomal escape happened show nuclear fluorescence in the red channel (red fluorescence is depicted white). The values below the images correspond to the percentage of cells with white nuclei (yellow arrows). The red arrows highlight the presence of vacuoles. (B) Representative confocal images from the phospholipid distribution in H1299-eGFP cells visualized with LipidTOX Red PLD detection reagent in 20 μ M PRA/20 μ M DOX/20 μ M TER/40 μ M DES treated cells (20 h). The scale bar corresponds to 30 μ m. (eGFP = enhanced green fluorescent protein, NTC = not treated control, NG = nanogels, PRA = prazosin, DOX = doxazosin, TER = terazosin, DES = desloratadine, ON = oligonucleotide, AF647 = Alexa Fluor® 647 dye).

In summary, the (lack of) adjuvant effect of the ‘non-CAD hit’ prazosin (PRA) and the inactive structural analogue terazosin (TER) could be validated, albeit PRA clearly induced cell toxicity. However, we could not confirm the enhanced siRNA delivery of doxazosin (DOX), a minor hit in the primary screen at 20 μ M, although an effect at higher concentrations cannot be ruled out. Most likely PRA exerts its adjuvant effect *via* an off-target perturbation independently of its pharmacological action at the documented clinical target (α 1-adrenergic receptor)⁷⁷. First, micromolar PRA concentrations are needed to be effective as a delivery-promoting compound⁵¹ or cell death inducer^{41–50}, while nanomolar concentrations are sufficient to block the adrenergic receptor⁴⁵. Second, the structurally very similar quinazolamines TER and DOX (**Figure 2A**) did not have such an adjuvant effect, although they antagonize the same receptor. It is anticipated that the adjuvant effect of PRA on siRNA delivery could be the result of its lysosomal accumulation. Despite a relatively low clogP value (**Figure 2A**), the presence of a protonatable amino group within the PRA structure can still result in some degree of lysosomotropic behaviour. Indeed, studies have shown that a fluorescent derivative of PRA (BODIPY™ FL PRA) co-localizes with the lysosomal compartment^{41,45,51}. On the other hand, PRA has also shown to enter cells *via* an endocytic mechanism⁴¹ and, in this way, finally end up in the lysosomes. Notably, the described lysosomal localization of PRA and the lysosomal accumulation of siNGs demonstrated in earlier work^{15,78}, suggests that the majority of siRNAs are released from the lysosomal compartment. A recent report similarly identified PRA as a compound that can boost the import of soluble and cell-associated antigens from endolysosomal compartments into the cytosol and subsequently enhance cross-presentation in dendritic cells (DCs)⁵¹. Nevertheless, to the best of our knowledge, the presented study is the first to show that PRA can boost siRNA delivery in cancer cells by increasing endolysosomal escape. Notably, also other studies revealed damaging effects of PRA on the endolysosomal system in a

similar concentration range, *e.g.* inhibition of endocytic sorting⁷⁹ and tubulation of endosomes/lysosomes^{41,45,79,80}, which subsequently led to inhibition of cytokinesis^{43,45,79}. PRA induced a remarkably different phenotype (*i.e.* vacuolization, absence of PLD, higher cytotoxicity) compared to our typical lysosomotropic CAD adjuvant DES. Hence, in conjunction with the absence of a similar lysosomal phenotype for the physicochemically equivalent TER and DOX, these data suggest that the siRNA delivery-promoting effect of PRA is not solely linked to simple lysosomal accumulation and PLD induction as proposed for CAD molecules (calculated logP (clogP) > 3 and pKa1 > 6)⁵⁴. Interestingly, similar differences in other cellular activities (*e.g.* cell death induction^{46,49,81}, inhibition of endocytic sorting⁷⁹ or increase in DC cross-presentation⁵¹) of the three tested quinazolamines have been reported in the literature, with TER and PRA being inactive or most effective, respectively.

2.3. PIKfyve inhibitors induce pronounced vacuolization with limited adjuvant effect

Our data clearly indicate that PRA induces a distinct cellular phenotype than typical CAD adjuvants^{26,31,37,40}. Indeed, PRA-treated cells are, in contrast to DES-treated cells, characterized by large cytoplasmic vacuoles, while PLD induction was not observed. Consequently, these findings prompted us to investigate if other physicochemical, structural and pharmacological non-related (drug) compounds that are known to induce marked vacuolization can also have an adjuvant effect on siRNA delivery. Hence, we here evaluated if post-incubation (20 h) with four well-known chemical PIKfyve inhibitors (apilimod (API)^{82,83}, vacuolin-1 (VAC-1)⁸⁴, YM-201636 (YM)^{83–85} and APY-0201 (APY)^{83,86}) (**Figure 4A**) could improve the gene-silencing potential of dex-HEMA siNGs in NSCLC cells.

As discussed in **Chapter 1**, the various subcompartments of the endolysosomal system contain distinct (amounts of) phosphoinositide lipids⁸⁷. A very low-abundance (~0.04% – 0.1% of the total phosphoinositide pool) but particularly important phosphoinositide for maintaining endomembrane homeostasis is phosphatidylinositol-3,5-bisphosphate (PI(3,5)P₂)^{88–91}. The latter is formed by the phosphorylation of phosphatidylinositol-3-phosphate (PI3P) *via* the phosphatidyl 3-phosphate 5-kinase (PIKfyve)^{82,92–96}. PIKfyve inhibition *via* genetic^{82,85,96–104} or small molecule^{82,85,96,101,103,105–116} perturbation has shown to cause swelling and vacuolization of early endosomes, late endosomes and lysosomes, which is thought to occur *via* decreased membrane fission and/or increased (homotypic)

fusion^{105,117,118}. Additionally, since PI(3,5)P₂ is a known activator of the lysosomal cation channel ‘transient receptor potential mucolipin 1’ (TRPML1/MCOLN1) and inactivation of this channel is characterized by a similar vacuolization phenotype as PIKfyve-deficient cells^{119,120}, it has been suggested that the interplay of PI(3,5)P₂ and TRPML1 contributes to the vacuole formation upon PIKfyve inhibition^{119,121}.

Albeit lower concentrations of these compounds (nM range) have previously shown to induce vacuolization in other cell types^{85,96,112–114,122}, the appearance of large translucent cytoplasmic vacuoles in H1299-eGFP cells (**Figure S7**) was only observed in the low micromolar range. While the tested compounds were overall well tolerated (except for 10 μM APY, **Figure 4E**), all PIKfyve inhibitors induced an increase in (a) eGFP silencing (**Figure 4B**), (b) lysosomal volume (**Figure 4C**) and (c) cellular granularity (**Figure 4D**) compared to untreated and siNG-transfected cells. The formation of cytoplasmic vacuoles (as can be seen in the eGFP channel) and the marked enlargement of LysoTracker Deep Red (LDR)-labeled vesicles upon PIKfyve inhibitor treatment were also visually confirmed with confocal microscopy (**Figure 5A**). Note that the majority of the large vacuoles were LDR positive, suggesting that these large, swollen vesicles are of late endosomal or lysosomal origin in our cell model. In addition, staining of the PIKfyve inhibitor-treated cells with the PLD detection reagent LipidTOX™ Red (**Figure 5B, Figure S8**), revealed that there was also an accumulation of phospholipids in these vacuoles, albeit not to the same extent for all compounds. This PLD phenotype is clearly different from DES treatment, where phospholipids seem to accumulate in much smaller vesicular structures (**Figure 5B**). Interestingly, the PIKfyve inhibitor that induced the most apparent lysosomal swelling (**Figure 4C**) and vacuolization (**Figure S7**), but the least PLD induction (**Figure 5B, Figure S8**) (*i.e.* APY) also had the greatest effect on eGFP silencing. However, as PIKfyve inhibition has also shown to inhibit autophagy^{84,106,122,123}, exocytosis¹⁰⁵, endosomal maturation¹¹⁵ and endosome-to-*trans*-Golgi network retrograde transport¹⁰², it cannot be excluded that these effects might likewise contribute to the adjuvant effect (see **Chapter 1**). Of note, despite the extensive vacuolization in these cells, the eGFP knockdown enhancement was inferior to that observed following PRA treatment, suggesting that also for PRA other cellular mechanisms than mere vacuolization are involved in improved siRNA delivery.

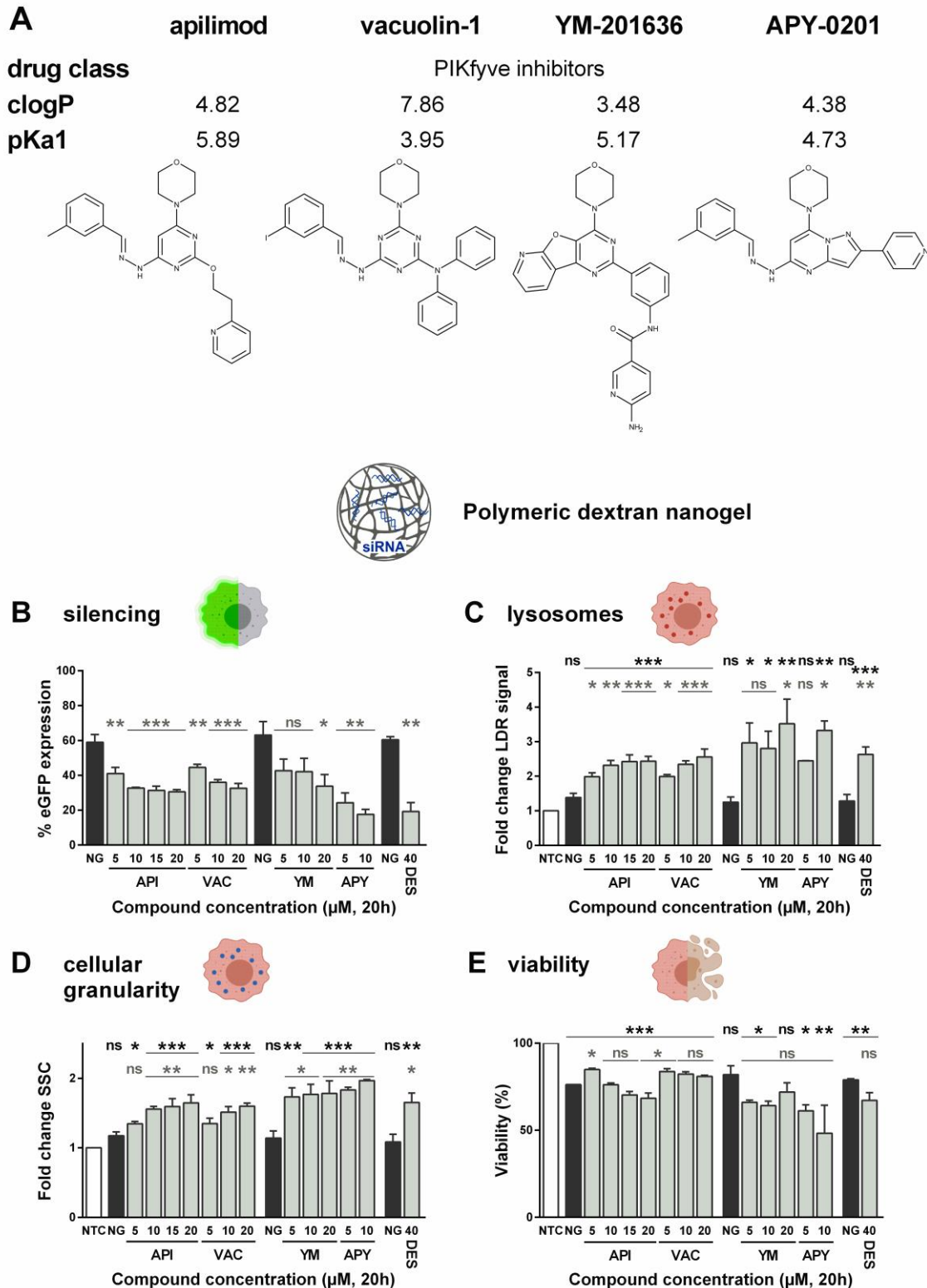


Figure 4. PIKfyve inhibitors improve the eGFP silencing potential of dex-HEMA siNGs in NSCLC cells to a limited extent, while increasing the lysosomal volume and cellular granularity. (A) The drug class, clogP, pKa1 values and molecular structure of apilimod (API), vacuolin-1 (VAC), YM-201636 (YM) and APY-0201 (APY)⁷³. The pKa1 and clogP values of the compounds were predicted with JChem for Office (version 17.21.0.1797, ChemAxon Ltd., Budapest, Hungary)⁷³. (B) Sequential treatment of siNG-transfected H1299-eGFP cells (1 nM siRNA) with PIKfyve inhibitors caused significant additional

eGFP silencing, albeit the effect was generally lower than the CAD desloratadine (DES). (C-D) Fold change in LDR signal and side scatter (SSC) signal, measured *via* flow cytometry, for H1299-eGFP cells sequentially transfected with dex-HEMA siNGs and treated with different μM concentrations of API/VAC/YM/APY/DES for 20 h. (E) Cell viability of H1299-eGFP cells following sequential dex-HEMA siNG transfection and API/VAC/YM/APY/DES addition for 20 h. Data are represented as mean \pm the standard error of the mean (SEM) for three independent repeats (except viability, which is done in two independent repeats). Statistical significance is indicated when appropriate, in black * when referring to the untreated control and in grey * when compared to dex-HEMA siNG transfection alone (ns $p > 0.05$, * $p \leq 0.05$, ** $p \leq 0.01$, *** $p \leq 0.001$). (clogP = calculated logP, pKa1 = pKa of the most basic amine, eGFP = enhanced green fluorescent protein, NG = dex-HEMA siNG transfection without sequential compound treatment, NTC = not treated control, API = apilimod, VAC = vacuolin-1, YM = YM-201636, APY = APY-0201, ns = not significant, LDR = LysoTracker® Deep Red, SSC = side scatter).

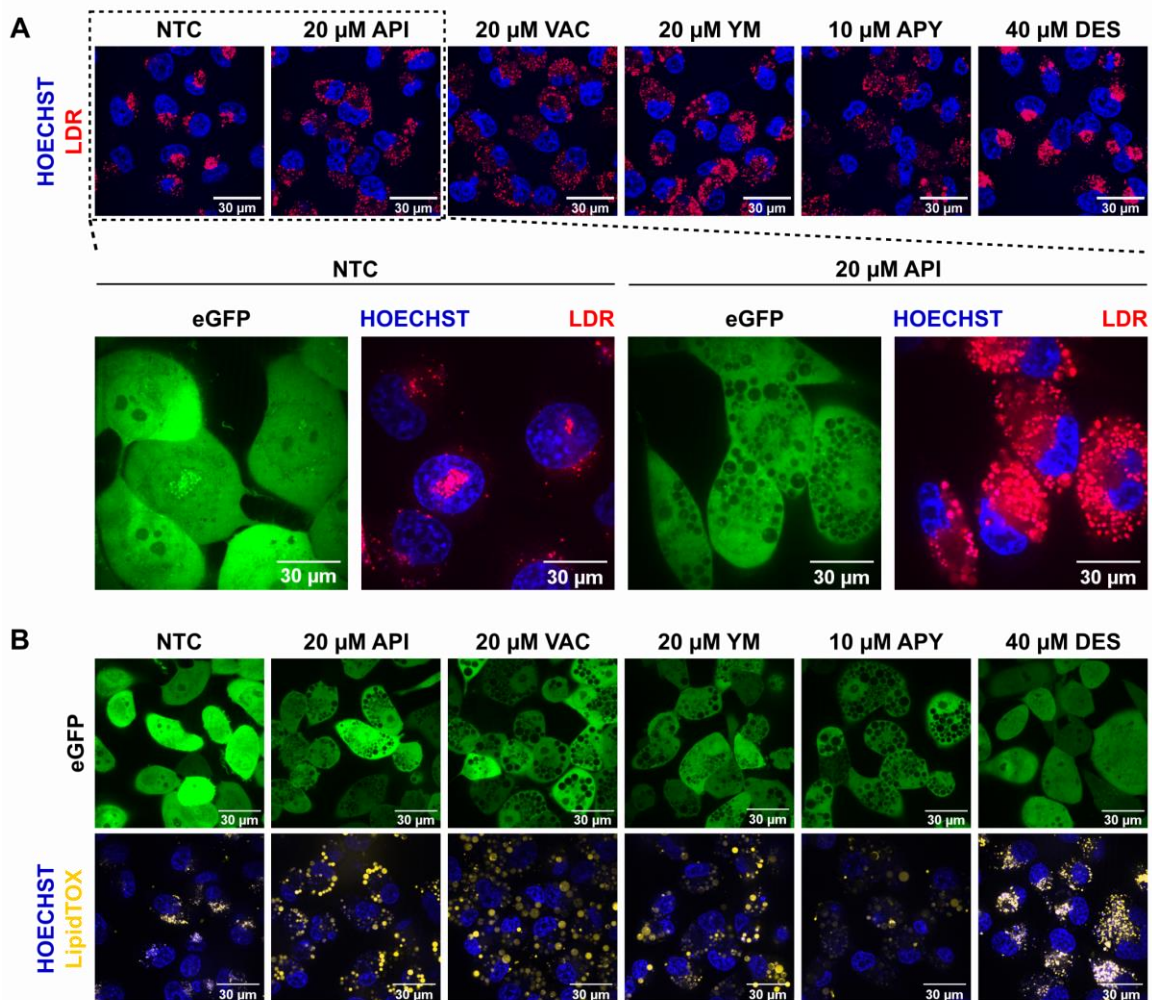


Figure 5. Several PIKfyve inhibitors and desloratadine (DES) induce varying degrees of lysosomal swelling and phospholipidosis in NSCLC cells. (A) Representative confocal images showing the lysosomal compartment (red) following LysoTracker® Deep Red (LDR) labeling for untreated and 20 μM apilimod (API)/20 μM vacuolin-1 (VAC)/20 μM YM-201636 (YM)/10 μM APY0201 (APY)/40 μM DES treated H1299-eGFP cells (20 h). (B) Representative confocal images from the phospholipid

distribution in H1299-eGFP cells visualized with LipidTOX Red PLD detection reagent in 20 μ M API/20 μ M VAC/20 μ M YM/10 μ M APY/40 μ M DES treated cells (20 h). The scale bar corresponds to 30 μ m. (eGFP = enhanced green fluorescent protein, NTC = not treated control, DES = desloratadine, API = apilimod, VAC = vacuolin-1, YM = YM-201636, APY = APY0201, LDR = LysoTracker® Deep Red).

2.4. Prazosin improves silencing of cholesterol-siRNA conjugates

As discussed in **Chapter 1**, covalent conjugation of (targeting) ligands to the siRNA strands can be an effective and simple alternative to NP-based delivery. While N-acetylgalactosamine (GalNAc)-siRNA conjugates, which target the asialoglycoprotein receptor (ASGPR) on hepatocytes, are now clinically validated drugs (*e.g.* givosiran, lumasiran)¹⁰, their use is largely restricted to liver-related diseases. Hence, other self-deliverable siRNAs that are able to reach tissues or tumors are highly sought after^{76,124}. In this context, siRNAs modified with lipids such as cholesterol-linked siRNAs (chol-siRNAs) are one of the most reported conjugates^{124–129} that have shown *in vivo* accumulation and gene silencing in solid tumors^{128,130,131}. However, despite adequate accumulation and endocytic internalization, high conjugate concentrations are still needed, both *in vitro* and *in vivo*, to achieve significant knockdown due to inefficient endosomal escape^{1,12,19,76}. Hence, we evaluated here if PRA and DES could similarly improve the cytosolic delivery of two cholesterol-conjugated eGFP-targeting siRNAs with different sequences in H1299-eGFP cancer cells. As shown in **Figure 6A** and **Figure S9A**, the intrinsic silencing potential of both chol-siRNAs was low, with chol-siRNA 1 inducing less than 10% eGFP silencing at 250 nM, while chol-siRNA 2 was slightly more potent (~30% eGFP silencing at 250 nM). Whereas sequential treatment for 20 h with 40 μ M DES had little impact on the silencing efficiency, the application of 20 μ M PRA achieved 80 - 90% eGFP knockdown, despite clear indication that both compounds evoked lysosomal swelling (**Figure 6B-C** and **Figure S9B-C**). Notably, 20 μ M PRA induced a significant drop in cell viability (**Figure 6D**), in line with the aforementioned data on dex-HEMA siNGs (**Figure 2E**). Other CADs (*e.g.* amitriptyline, siramesine, loperamide and chloroquine) have recently shown to facilitate endosomal escape of chol-siRNAs in other cancer cells (*e.g.* HeLa)⁷⁶. Here it was demonstrated that the fraction of damaged endocytic vesicles that also contain chol-siRNA was highly dependent on the type of CAD, leading to differences in target gene knockdown⁷⁶. Hence, this might explain the absence of an adjuvant effect for DES in our experiments. In summary, next to

polymeric NPs, we could confirm the significantly larger adjuvant effect of PRA, compared to DES, on gene knockdown *via* chol-siRNAs.

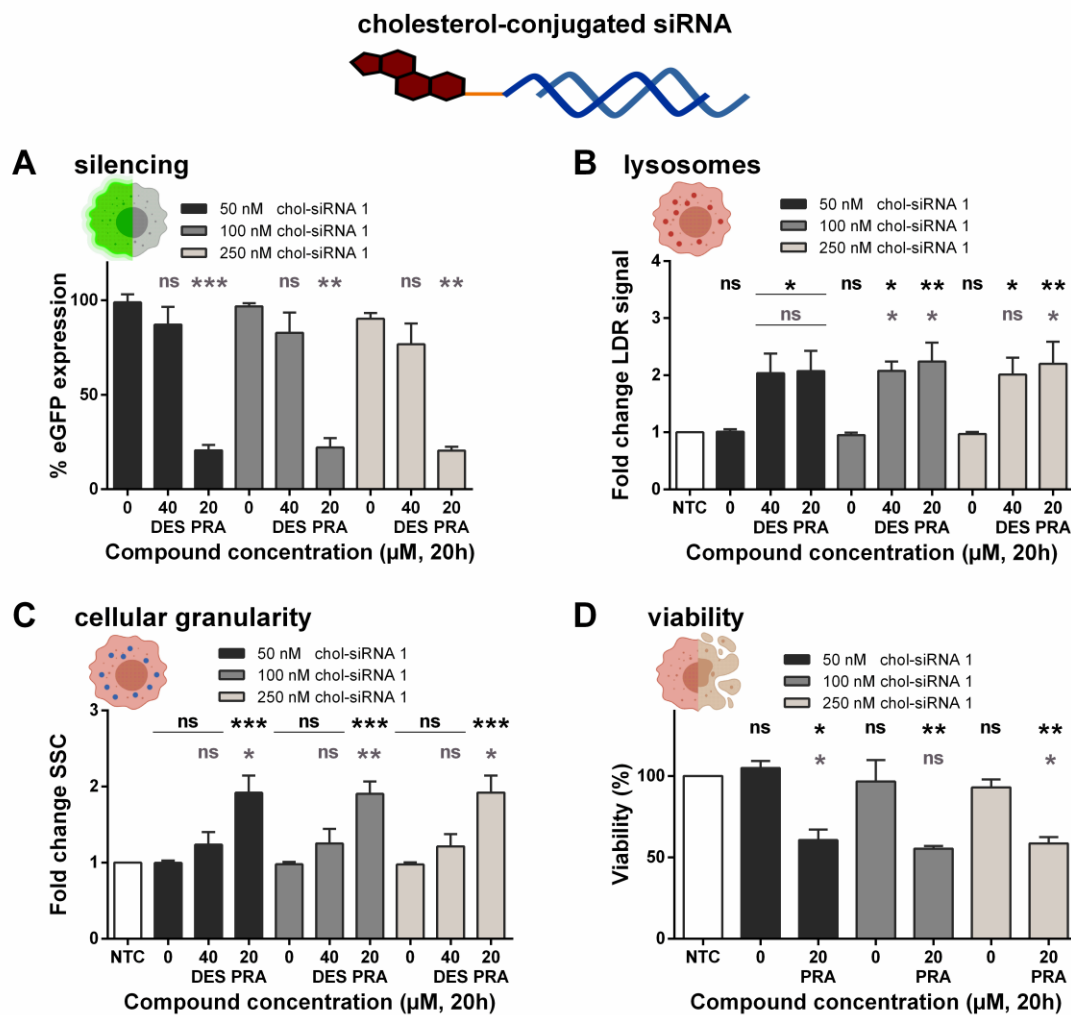


Figure 6. Prazosin, but not desloratadine, enhances eGFP silencing potential of chol-siRNAs in NSCLC cells. (A) Sequential treatment of chol-siRNAs (different concentrations) with 20 μ M prazosin (PRA) caused a significant additional eGFP silencing, while 40 μ M desloratadine (DES) had no effect. (B-C) Fold change in LDR and SSC signal, measured *via* flow cytometry, for H1299-eGFP cells sequentially transfected with chol-siRNAs and treated with 40 μ M DES or 20 μ M PRA for 20 h. (D) Cell viability of H1299-eGFP cells following sequential chol-siRNA transfection and 20 μ M PRA addition. Data are represented as mean \pm the standard error of the mean (SEM) for two independent repeats. Statistical significance is indicated when appropriate, in black * when referring to the untreated control and in grey * when compared to chol-siRNA transfection alone (ns $p > 0.05$, * $p \leq 0.05$, ** $p \leq 0.01$, *** $p \leq 0.001$). (eGFP = enhanced green fluorescent protein, NTC = not treated control, DES = desloratadine, PRA = prazosin, ns = not significant, LDR = LysoTracker[®] Deep Red, chol-siRNA = cholesterol-conjugated siRNA).

2.5. Mapping the cell death pathways induced by prazosin

Several literature reports have shown that PRA is able to induce apoptosis in malignant cells in micromolar concentrations, both *in vitro*^{41–43,45,46,48,50,132} and *in vivo* in xenograft models⁴⁶, while PRA is less (or not) toxic to healthy cells⁴⁶. Given the clear induction of cell death by 20 μ M PRA treatment in the H1299 cell line (**Figure 2E**, **Figure 6D**), we aimed to further investigate the type of cell death triggered by PRA in our particular cell model. Next to the well-known apoptosis and necrosis pathways, several additional cell death mechanisms such as lysosomal cell death, necroptosis, ferroptosis, pyroptosis and autophagic cell death have more recently been described^{133–137}. To characterize the PRA-induced cell death modality, we applied 20 μ M PRA and the cell-impermeable membrane exclusion dye SYTOX™ Blue for 24 h on H1299-eGFP cells in the absence or presence of several well established cell death inhibitors (zVAD-fmk for apoptosis, necrostatin-1s (NEC-1) for necroptosis and ferrostatin-1 (FER-1), deferoxamine (DFO) and α -tocopherol (α -TOC) for ferroptosis)^{138,139} at previously used fixed concentrations¹⁴⁰. As evident from **Figure 7**, only 10 μ M zVAD-fmk, a pan-caspase inhibitor, had an inhibitory effect on the PRA-induced toxicity, albeit only moderate. These results were confirmed in an additional experiment with increasing concentrations of the applied inhibitors (data not shown). However, in further confirmatory experiments, also cathepsin inhibitors could be applied to investigate the role of leaked lysosomal proteases in lysosomal cell death (LCD). In addition, detection of phosphatidylserine externalization with labeled Annexin V might also be used to verify the induction of apoptotic cell death⁴⁶. Nevertheless, our preliminary data at least suggest that PRA also induces caspase-dependent apoptosis in H1299 cells, in line with existing literature.

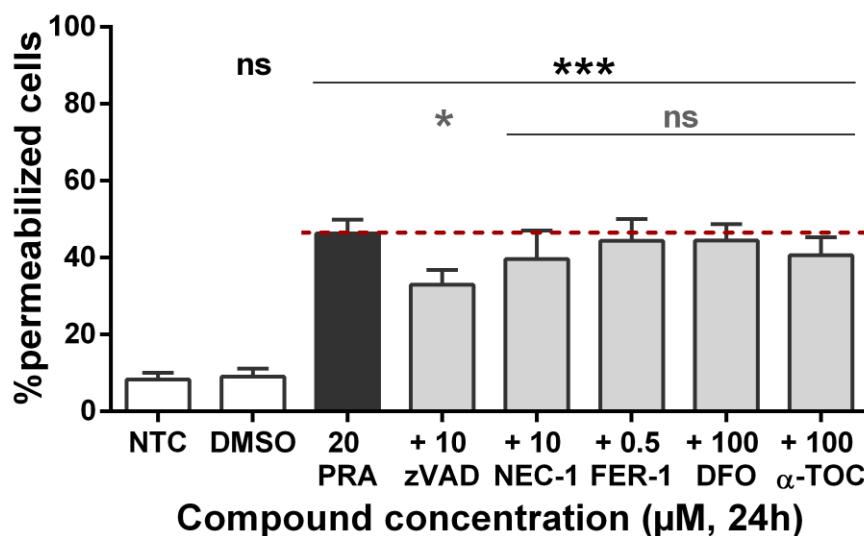


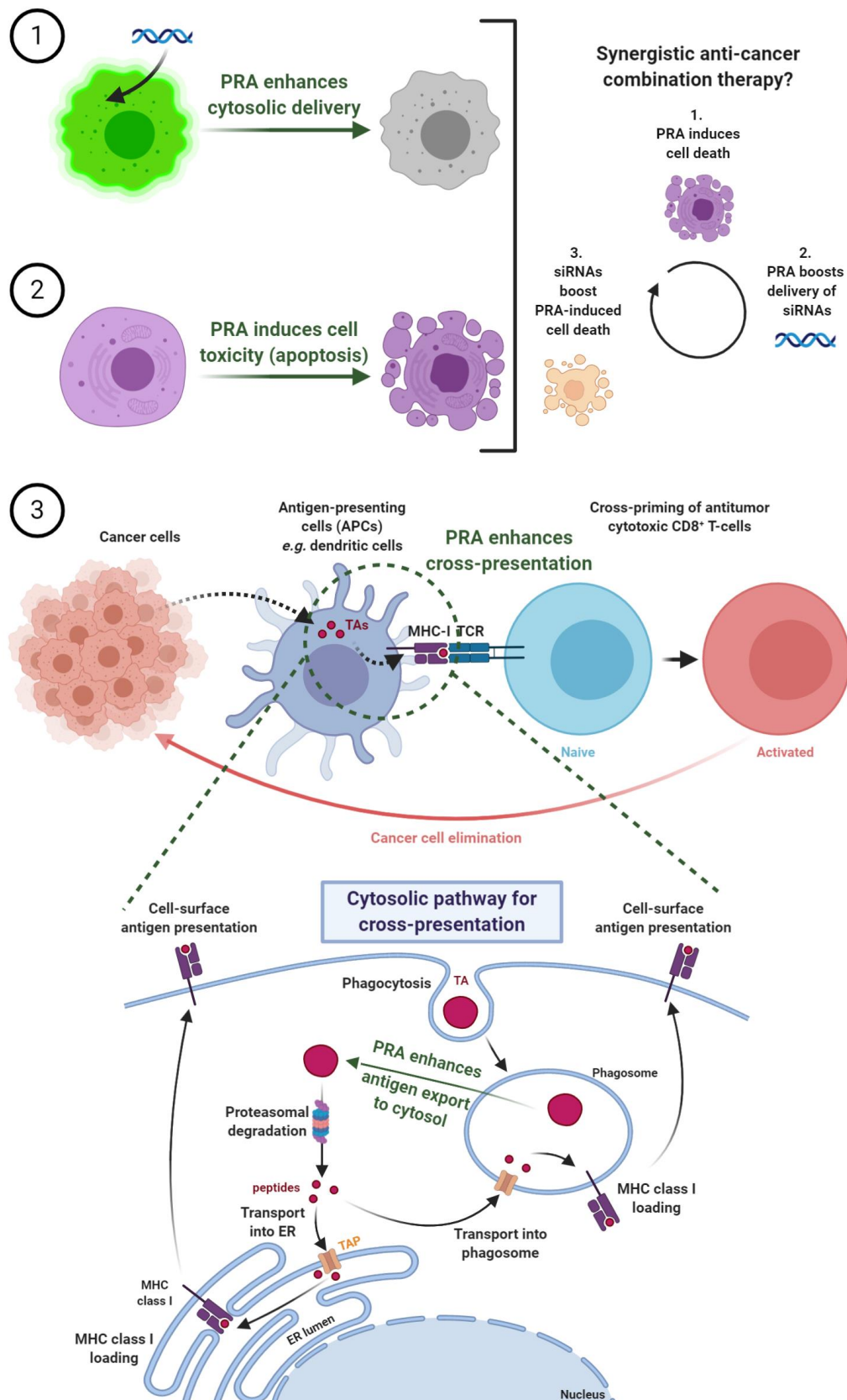
Figure 7. Prazosin induces apoptosis in NSCLC cells. Quantification of cell death, determined *via* a cell-impermeable membrane exclusion dye SYTOX™ Blue, for H1299-eGFP cells treated with 20 μM prazosin (PRA) for 24 h, in the presence of absence of different inhibitors of cell death modalities. The data are represented as mean ± SD (n = 3, technical replicates). Statistical significance is indicated when appropriate, in black * when referring to the untreated control and in grey * when compared to 20 μM PRA treatment alone (ns p > 0.05, * p ≤ 0.05, *** p ≤ 0.001). (NTC = not treated control, DMSO = NTC with equal amount of DMSO as treated conditions, PRA = prazosin, zVAD = zVAD-fmk, NEC-1 = necrostatin-1s, FER-1 = ferrostatin-1, DFO = deferoxamine, α-TOC = α-tocopherol, ns = not significant).

Given that PRA can boost the cytosolic delivery of siRNA, while also having a direct pro-apoptotic activity (as suggested by our preliminary data and as shown by others^{41–43,45,46,48,50,132}), the combination of PRA and siRNA can open up avenues for synergistic anti-cancer therapy. Indeed, siRNAs are often studied to enhance the tumor killing efficacy of low molecular weight anti-cancer drugs *e.g. via* silencing of efflux multidrug resistance proteins (*e.g.* multidrug resistance protein 1 (MDR-1)^{141–143}) to increase the drug concentration in the target cells. In this work, as PRA strongly improves siRNA delivery, a synergistic tumor killing effect could be obtained when selecting a siRNA that triggers a complementary cell death pathway (**Scheme 1.1-1.2**). Here, the silencing of (a) anti-apoptotic proteins (*e.g.* B-cell lymphoma 2 protein (Bcl-2)^{144–146}), (b) other cell death regulators (*e.g.* the key regulator of ferroptosis, glutathione peroxidase 4 (GPX4)¹⁴⁷, which upon inhibition induces immunogenic ferroptosis that can activate anti-tumor immunity) or (c) cell cycle regulators (*e.g.* polo-like kinase 1 (PLK1)¹⁴⁸) could be envisioned¹⁴⁹. However, this hypothesis requires additional experimental validation *in vitro* and in a relevant *in vivo* model. Importantly, it can be

rationalized from the literature that PRA holds the potential to enhance siRNA delivery to (cancer) cells *in vivo*. Indeed, systemic administration of non-toxic PRA concentrations could specifically reduce xenograft tumor growth (and/or mice survival) *via* a direct anti-proliferative effect⁴⁶ or by enhancing cross-presentation⁵¹, both independently of its anti-adrenergic activity. In addition, local administration (*e.g.* intratumoral injection) of the PRA adjuvant in combination with chol-siRNAs might be a valuable option to induce synergistic tumor cell killing, while avoiding systemic exposure to high drug concentrations. For example, modified chol-siRNAs have shown to widely distribute throughout xenografted glioblastoma tumors upon intratumoral injection and subsequently produce functional knockdown¹⁵⁰. Furthermore, co-encapsulation of PRA and siRNA in a (polymeric) nanocarrier could allow spatiotemporally controlled delivery of both drugs at the cellular level²¹, which could facilitate *in vivo* translation.

The documented *in vitro* and *in vivo* anti-tumor activity of quinazolines includes, besides apoptosis induction^{41–43,45–49,132}, the activation of the metastasis-protective anoikis effect¹⁵¹, the inhibition of tumor-angiogenesis¹⁵² and the abovementioned enhancement of cross-presentation in DCs by PRA, both *in vitro* and *in vivo*⁵¹. The process of cross-presentation (**Scheme 1.3**) involves the internalization of exogenous proteins (*e.g.* cell-associated antigens released by dying cancer cells) by antigen-presenting cells (APCs), which are subsequently broken down into short peptides that can be loaded onto Major Histocompatibility Complex class I (MHC I) molecules. In this way, tumor antigens (TAs) are presented to naive antigen-specific CD8⁺ T-cells, which require this activation step to proliferate and differentiate into effector cytotoxic T lymphocytes (CTLs)^{51,153}. Two main cross-presentation pathways have been described. In the vacuolar pathway, antigens are processed by endolysosomal proteases and directly loaded on MHC I molecules within the endocytic compartment. In contrast, the cytosolic pathway (**Scheme 1.3**) involves endosome-to-cytosol antigen import, where proteasomal degradation produces peptides that are delivered to the lumen of MHC I-containing compartments (*e.g.* endoplasmic reticulum, ER) *via* the transporter for antigen presentation (TAP)^{51,153,154}. Interestingly, albeit the relative involvement of both models in *in vivo* cross-presentation remains unclear, the endolysosomal escape of antigens into the cytosol has shown to be a crucial and rate-limiting step in the cytosolic pathway^{51,154}. Similarly to our results with siRNA, PRA has shown to enhance the efficiency of this TA endosome-to-cytosol transport in DCs, leading to a synergistic effect with checkpoint anti-tumor immunotherapy in a melanoma xenograft

mouse model⁵¹. As combination therapies are the mainstay of clinical cancer care, it has been previously postulated to increasingly allow nanomedicines to synergize with pharmacological and physical co-treatments¹⁵⁵. This recently published study together with our own data suggest that a multifaceted anti-cancer combination strategy could potentially be pursued with PRA.



Scheme 1. Schematic illustration of the main anti-tumor actions of prazosin. (1-2) As prazosin (PRA) can boost the cytosolic delivery of siRNA, while also having a direct pro-apoptotic activity, the combination of PRA and a therapeutic siRNA (*e.g.* against efflux multidrug resistance proteins, anti-apoptotic proteins, *etc.*) can open up avenues for synergistic treatment in the context of anti-cancer

therapy. Ideally, PRA would improve the functional delivery of these siRNAs, which in turn may boost the PRA-induced cell death. (3) Interestingly, similar to the observed boost in endolysosomal escape of siRNA molecules, PRA has also been described as a molecule that can improve the import of tumor antigens (TAs) from the endolysosomes into the cytosol of dendritic cells, thus improving cross-presentation (*i.e.* presentation of TAs on Major Histocompatibility Complex class I molecules) and -priming, which is necessary for cytotoxic T lymphocyte-mediated anti-tumor immune responses. (PRA = prazosin, MHC class I = Major Histocompatibility Complex class I molecules, TA = tumor antigen, ER = endoplasmic reticulum, TAP = transporter for antigen presentation, TCR = T-cell receptor).

3. CONCLUSION

Inefficient intracellular delivery remains one of the most important barriers for nucleic acid therapeutics. We recently discovered that multiple cationic amphiphilic drugs (CADs) can be repurposed as cytosolic delivery-promoting adjuvants of siRNA and ASO molecules in distinct cancer cell lines. In this chapter, we demonstrated that other small molecular drugs, which do not have the typical physicochemical properties of CADs⁵⁴, can likewise be repurposed as siRNA delivery enhancers. Most importantly, our data indicate that prazosin (PRA), a quinazoline-based α 1-adrenergic antagonist, can both induce apoptosis and increase the permeability of endolysosomes for small nucleic acid cargo. Consequently, we anticipate that the gained insights will fuel further experiments in which the PRA adjuvant approach is used in a combination therapy that could potentially provide synergistic anti-cancer effects.

ACKNOWLEDGMENTS

T. Van de Vyver is a doctoral fellow of the Research Foundation-Flanders (grant 1198719N, FWO, Belgium). L. De Backer acknowledges the Special Research Fund of Ghent University (BOF12/GOA/014). Prof. K. Raemdonck acknowledges the FWO for a postdoctoral Research Grant (grant 1517516N). Scheme 1 was created with BioRender.com. We thank Prof. R. Vandenbroucke from the VIB-UGent Center for Inflammation Research (Ghent, Belgium) for the use of the microfluidic NanoAssemblr® Benchtop mixing device.

4. MATERIALS AND METHODS

4.1. siRNA duplexes and oligonucleotides

The 21mer siRNA duplexes targeted against the enhanced green fluorescent protein (eGFP, sieGFP) and the negative control siRNA (siCTRL) were purchased from Eurogentec (Seraing, Belgium). The 19mer chol-conjugated siRNAs (Accell, chol-siRNA 2) were purchased from Dharmacon (Lafayette, CO, USA). The other chol-conjugated siRNAs (chol-siRNA 1) with siSTABLE modifications were also purchased from Dharmacon (Lafayette, CO, USA). Dicer substrate asymmetric 25/27mer siRNA duplexes targeting eGFP (DsieGFP) or *firefly* luciferase (DsiFLuc) were provided by Integrated DNA Technologies BVBA (IDT, Leuven, Belgium). The used negative controls consist of a sequence that has no relevant homology to any known eukaryotic gene sequences. Alexa Fluor® 647 labeled 21mer oligonucleotides (AF647 ONs) were from Eurogentec (Seraing, Belgium). The concentration of the siRNA/ON stock solutions in nuclease-free water (Ambion®-Life Technologies, Ghent, Belgium) was calculated from absorption measurements at 260 nm ($1 \text{ OD}_{260} = 40 \mu\text{g mL}^{-1}$) with a NanoDrop 2000c UV-Vis spectrophotometer (Thermo Fisher Scientific, Rockford, USA). The sequences and modifications of the applied (chol-conjugated) siRNA duplexes/ONs are summarized in **Table S2**.

4.2. Nanoparticle (NP) synthesis, preparation and siRNA complexation

Using an inverse miniemulsion photopolymerization method as previously reported, dextran hydroxyethyl methacrylate or dextran methacrylate (dex-HEMA, degree of substitution (DS) of 5.2 or dex-MA, DS of 5.9) was copolymerized with a cationic methacrylate monomer [2-(methacryloyloxy)ethyl]-trimethyl-ammonium chloride (TMAEMA) to produce cationic dex-HEMA-co-TMAEMA and dex-MA-co-TMAEMA nanogels (hereafter abbreviated as respectively dex-HEMA NGs and dex-MA NGs)^{15,78,156–158}. The synthesized NGs were lyophilized and stored desiccated to ensure long-term stability. To produce siRNA-loaded NGs (siNGs) for *in vitro* experiments, a NG stock (2 mg/mL) was prepared by dispersing a weighed amount of nanoparticles (NPs) in ice-cooled nuclease-free water (Ambion®-Life Technologies, Ghent, Belgium), followed by brief sonication (3 x 5 sec, amplitude 10%; Branson Ultrasonics Digital Sonifier®, Danbury, USA). Next, equal volumes of NGs and siRNA in 4-(2-hydroxyethyl)-1-piperazineethanesulfonic acid (HEPES) buffer (20 mM, pH 7.4) were mixed and allowed to incubate on ice for 10 min, prior to further dilution in Opti-MEM®

(Invitrogen, Merelbeke, Belgium). This complexation procedure was applied for all cell-based experiments in a 96-well plate and resulted in a 30 µg/mL NG dispersion loaded with 1 nM siRNA (0.033 pmol siRNA/µg NGs or 0.1 pmol siRNA/well), unless indicated otherwise.

To obtain PEGylated cationic liposomes (LIPs), (2,3-dioleoyloxy-propyl)-trimethylammonium (DOTAP), 1,2-dioleoyl-*sn*-glycero-3-phosphoethanolamine (DOPE) and 1,2-distearoyl-*sn*-glycero-3-phosphoethanolamine-N-[methoxy(polyethylene glycol)-2000] (DSPE-PEG₂₀₀₀) were purchased from Avanti Polar Lipids, Inc. (Alabaster, AL, USA) as solutions in chloroform. PEGylated (corresponding to 5 mol% of the total lipids) DOTAP-DOPE (1:1 molar ratio) LIPs were prepared *via* the lipid film hydration method by mixing appropriate amounts of the mentioned lipids in a round bottom flask. Rotary evaporation under vacuum at 40 °C resulted in a lipid film, which was subsequently hydrated using 1 mL HEPES buffer (pH 7.4, 20 mM). The lipid dispersion was vortexed and sonicated using a probe sonicator (1 min, amplitude 10%; Branson Ultrasonics Digital Sonifier®, Danbury, USA) to obtain a monodisperse 2 mM liposome dispersion (total lipid concentration). Next, PEGylated DOTAP-DOPE LIPs were complexed with siRNA at an optimal charge ratio (nitrogen/phosphate ratio) equal to eight.¹⁵⁹ Hereto, equal volumes of LIPs and siRNA in HEPES buffer were mixed and allowed to complex at room temperature for 30 minutes prior to further dilution in Opti-MEM® and transfection.

Preparation of DsiRNA-loaded ionizable lipid (MC3)-based lipid NPs (MC3 DsiLNPs) and siRNA-*in vivo*-jetPEI® polyplexes (PPXs) is described in supplementary information.

4.3. Cell lines and cell culture conditions

Cell culture experiments were performed using a human non-small cell lung epithelial carcinoma cell line (H1299) stably expressing eGFP (H1299-eGFP) or the wild type variant (H1299-WT, ATCC® CRL-5803™), respectively obtained from the lab of Prof. Camilla Foged (Department of Pharmacy, University of Copenhagen, Denmark) and the American Type Culture Collection (ATCC, Manassas, USA)^{26,31,158,160–162}. H1299 cells (H1299-WT and H1299-eGFP) were cultured in Roswell Park Memorial Institute (RPMI) 1640 culture medium, supplemented with 10% fetal bovine serum (FBS, Hyclone™, GE Healthcare, Machelen, Belgium), 2 mM L-Glutamine and 100 U/mL penicillin/streptomycin (hereafter collectively called 'complete cell culture medium' or CCM). Cells were cultured at 37 °C in a humidified atmosphere containing 5% CO₂ and were passed every 3 days using a 0.25% trypsin-

ethylenediaminetetraacetic acid (EDTA) solution to maintain subconfluency. H1299-eGFP cells were treated with CCM containing 1 mg/mL Geneticin® once per month to allow eGFP transgene selection. All cells were regularly tested and found negative for mycoplasma. All cell culture products were purchased from Gibco®-Life Technologies (Grand Island, NY, USA) unless specifically mentioned otherwise.

4.4. Quantification of transfection efficiency/lysosomal volume of NP

transfection and sequential adjuvant treatment by flow cytometry

To quantify gene silencing efficiency and lysosomal volume, H1299-eGFP cells were seeded in 96-well plates (VWR, Radnor, USA) at a density of 7500 cells/well (100 µL/well) and were allowed to settle overnight. Next, the cells were transfected with dex-HEMA siNGs (0.1 pmol siRNA/well, prepared as described above) or PEGylated DOTAP-DOPE siRNA-loaded LIPs (siLIPs) (50 nM siRNA, prepared as discussed above) during 4 hours at 37 °C in a humidified atmosphere containing 5% CO₂. For chol-siRNA experiments, cells were transfected for 6 hours in Opti-MEM® as previously described⁷⁶. Note that for every sieGFP condition a siCTRL sample was included to account for potential off-target effects. Subsequently, the transfection dispersion was removed and the cells were washed with phosphate buffered saline (PBS, no calcium, no magnesium) and subsequently received 50 µL fresh (DMSO control) or compound-containing CCM at the indicated concentrations (maximally 0.08% (v/v) residual DMSO). Note that apart from the NIHCC-compounds (described in our previous work³¹), all small molecules were obtained from Cayman Chemicals (Michigan, USA), except terazosin HCl dihydrate (TER) and YM-201636 (YM) which were from LKT Laboratories Inc. (St. Paul, USA) and Invivogen (San Diego, CA), respectively. Stock solutions were prepared in sterile-filtered BioPerformance Certified dimethyl sulfoxide (DMSO, Sigma-Aldrich, Overijse, Belgium). After 20 hours, the small molecule containing CCM (and DMSO control) was removed and cells were kept in 50 µL fresh CCM for an additional 24 hours. Following labeling of lysosomes with the LysoTracker® Deep Red (LDR) probe (Molecular Probes™, Eugene, OR, USA) through incubation with 50 µL 75 nM LDR in CCM for 30 min at 37 °C, flow cytometry analysis was performed. Sample preparation consisted of detachment with 30 µL 0.25% trypsin-EDTA, neutralization with 120 µL CCM and a transfer of the cell suspensions to an U-bottom 96-well plate (Greiner Bio-One GmbH, Vilvoorde, Belgium), which was centrifuged during 5 minutes at 500 g. After removal of 120 µL supernatant, the cells were resuspended in 80 µL flow buffer (PBS (no calcium, no magnesium) with 1% (v/v)

FBS (Hyclone™, GE Healthcare, Machelen, Belgium) and 0.1% (w/v) sodium azide (Sigma Aldrich, Overijse, Belgium)) and kept on ice until analysis. For each sample the forward and side scatter (respectively FSC and SSC) as well as the green and red fluorescent signal of single cells were measured. The samples were excited with the 488 and 638 nm laser lines and the signal was detected with the 525/40 and 660/20 filters using the CytoFLEX flow cytometer with plate loader for 96-well plates (Beckman Coulter, Krefeld, Germany) and CytExpert software. FlowJo software (Tree Star Inc., Ashland, OR, USA) was used for data analysis. The calculated percentages eGFP expression (*i.e.* the eGFP expression of cells treated with sieGFP was normalized to the expression of cells treated with a siCTRL under the same conditions) and fold changes in LDR signal intensity/SSC signal are presented as the mean \pm standard error of the mean (SEM) for minimum 3 independent repeats (biological replicates), unless otherwise indicated.

In an additional experiment (**Figure S7A-B**), H1299-eGFP cells (seeded at 35000 cells/well) were transfected in 24-well plates with dex-HEMA siNGs for 4 h at 37 °C and subsequently treated with compounds as described before²⁶. Transfection procedure and transfection efficiency determination for *in vivo*-jetPEI® and MC3 DsiLNPs is described in supporting information.

4.5. Cell viability

H1299-eGFP cells were seeded, transfected with dex-HEMA siNGs/chol-siRNAs and treated with the compounds similar to the silencing experiments. The cell viability was determined with the CellTiter GLO® assay (Promega, Belgium), according to the manufacturer guidelines. Before initiating the assay, the culture plates and reconstituted assay buffer were placed at room temperature for 30 min. Next, the CCM was replaced by 100 μ L fresh CCM and an equal volume of assay buffer was added. To induce complete cell lysis, the plates were shaken during 2 min and the signal was allowed to stabilize the following 10 min. Next, 100 μ L from each well was transferred to an opaque 96-well plate, which was measured with a GloMax® 96 Microplate Luminometer (Promega, Belgium). Data are presented as the mean cell viability (%; percentage of luminescent signal relative to non-treated cells (NTC) for each condition) \pm standard error of the mean (SEM) for three independent repeats (or a biological duplicate in **Figure 4E** and **Figure 6D**).

4.6. Quantification of cell death mechanism

Similar to the gene silencing experiments, H1299-eGFP cells were seeded in 96-well plates (VWR, Radnor, USA) at a density of 7500 cells/well (100 μ L/well) and were allowed to settle overnight. Next, cells were stained with 5 μ M SYTOX™ Blue nucleic acid stain (Molecular Probes™, Eugene, OR, USA) in a volume of 20 μ L added to the medium. SYTOX™ dyes are cell-impermeable dyes that intercalate with double-stranded DNA with a high affinity¹⁶³. When permeabilization of the plasma membrane occurs at the end of any cell death process, SYTOX™ dyes enter the cell and bind to the DNA, causing a large increase in fluorescence signal that can be correlated to the percentage of cell death^{138,140}. An apoptosis inhibitor (zVAD-fmk, BACHEM, Budendorf, Switzerland), necroptosis inhibitor (NEC-1s, Abcam, Cambridge, UK) and several ferroptosis inhibitors (FER-1, DFO and α -TOC, Sigma, Saint Louis, MO, USA) were added at the indicated concentrations (20 μ L added to the medium) 30 min before cell death induction with 20 μ M PRA (30 μ L added to the medium). After 24 h, SYTOX™ Blue intensity was measured using the Tecan Spark® (Tecan, Männedorf, Switzerland) 20M microplate fluorescence reader (SYTOX™ Blue: λ_{ex} = 430 nm, λ_{em} = 460 nm). Afterwards, cells were permeabilized with Triton X-100 (0.8% v/v, MERCK, Darmstadt, Germany), in a volume of 10 μ L added to the medium, to obtain 100% of cell death. After 2 h of incubation, SYTOX™ Blue intensity was measured again. The cell death percentage was calculated by the following equation: % permeabilized cells = 100 x (average_{SYTOX™ Blue}[sample] – average_{SYTOX™ Blue}[background]) / (average_{SYTOX™ Blue}[Triton X-100] – average_{SYTOX™ Blue}[background]).

4.7. Visualization and quantification of the cytosolic release of AF647 ONs

H1299-eGFP cells were seeded at 75000 cells/compartiment in 35mm diameter glass bottom microscopy dishes with 4 compartments (Greiner Bio-One GmbH, Germany) and were allowed to settle overnight. After removal of the complete cell culture medium (CCM), the cells were transfected with 300 μ L of a 30 μ g/mL NG dispersion loaded with 50 nM AF647 ONs (= 1.667 pmol AF647 ONs/ μ g NGs). Following incubation for 4 h (37 °C, 5% CO₂), the ON-NG dispersion was removed and the cells were washed once with dextran sulfate sodium salt (Sigma-Aldrich, Overijse, Belgium, 1 mg/mL in PBS) and once with phosphate buffered saline (PBS, Invitrogen, Merelbeke, Belgium). Next, the cells received 500 μ L fresh CCM, containing different μ M concentrations of PRA/DOX/TER/DES or a DMSO control, for 20 h (37 °C, 5% CO₂). After removal of the small molecule-containing CCM, the nuclei were

labeled with Hoechst 33342 (Molecular Probes™, Belgium) in CCM (1 mg/mL in water, 1/1000 dilution) during 15 minutes at 37 °C. Finally, the Hoechst solution was removed, fresh CCM was added and cells were kept at 37 °C in a humidified atmosphere containing 5% CO₂ until imaging. A spinning disk confocal (SDC) microscope (Nikon eclipse Ti, Japan), equipped with a MLC 400 B laser box (Agilent technologies, California, USA), a Yokogawa CSU-X confocal spinning disk device (Andor, Belfast, UK), an iXon ultra EMCCD camera (Andor Technology, Belfast, UK), a Plan Apo VC 60× 1.4 NA oil immersion objective lens (Nikon, Japan) and NIS Elements software (Nikon, Japan) was applied for imaging. The 408 nm, 488 nm and 663 nm laser lines were, respectively, used to excite the DAPI-labeled nuclei, the eGFP protein and the fluorescence resulting from AF647 ONs. A wait command of 0.2 seconds in between the image acquisition of the 3 channels was applied to avoid spectral overlap of the DAPI dye and the eGFP protein. If endolysosomal escape occurs, the labeled ONs will spread towards the cytosol, dequench and finally accumulate into the nucleus^{31,75,164}. During data analysis with ImageJ (FIJI) software, both the total cell number and amount of cells with AF647 ON-positive nuclei were counted. Nuclei were detected in the blue channel by thresholding (applying the same offset values for every image) and intensity analysis (mean grey value), of the nuclear fluorescence signal in the red channel, was done. Using the 6th version of the GraphPad Prism software, these intensity values were plotted in frequency distributions and based on these histograms, a percentage of cells with AF647 ON-positive nuclei was determined. Data are represented as the percentage of cells with AF647 ON-positive nuclei for at least 496 cells in minimum 54 images.

4.8. Phospholipidosis detection with LipidTOX™ Red

H1299-eGFP cells were seeded (75000 cells/compartiment) and were allowed to settle overnight as specified for the AF647 ON release experiment. Next, the cells were incubated with a mixture of a 1/1000 dilution of the LipidTOX™ Red Phospholipidosis Detection Reagent (Thermo Fisher Scientific, Rockford, USA) and the desired compounds in CCM. Upon 20 hours incubation, the nuclei were labeled with Hoechst 33342 as detailed for the AF647 ON release experiment. The 408 nm, 488 nm and 561 nm laser lines were applied to, respectively, excite the Hoechst labeled nuclei, the eGFP protein and the fluorescence resulting from the LipidTOX™ Red Phospholipidosis dye. Imaging occurred with a SDC microscope as described above for visualizing the cytosolic release of AF647 ONs with confocal microscopy. The LipidTOX™ Red Phospholipidosis signal area was determined with

ImageJ (FIJI) in at least 175 cells from minimum 41 images. To this end, all confocal images were processed by applying the same offset values for the LipidTOX™ Red Phospholipidosis signal. In each image, both the number of cells and signal area of the LipidTOX™ Red Phospholipidosis dye was determined to allow calculation of the normalized LipidTOX™ Red Phospholipidosis area (*i.e.* LipidTOX™ Red Phospholipidosis signal area/cell number) in each image. The fold change in LipidTOX™ Red Phospholipidosis signal area was calculated by dividing the normalized signal area in treated cells by the normalized signal area in untreated cells.

4.9. Visualizing lysosomes

H1299-eGFP cells were seeded as specified for the AF647 ON release and LipidTOX™ experiment and subsequently treated with the indicated compound concentrations for 20 hours. Next, after removal of the compound-containing CCM, lysosomes and nuclei were labeled with, respectively, 75 nM LysoTracker® Deep Red (LDR) and Hoechst 33342 in CCM (1 mg/mL in water, 1/1000 dilution) during 30 minutes at 37 °C. Finally, following dye removal, fresh CCM was added and cells were kept at 37 °C in a humidified atmosphere containing 5% CO₂ until imaging (no fixation step was applied). A laser scanning confocal microscope (Nikon A1R HD confocal, Nikon, Japan), equipped with a Plan Apo VC 60× 1.4 NA oil immersion objective lens (Nikon, Japan), a resonant scanner and NIS Elements software (Nikon, Japan) was applied for imaging. The 405 nm, 488 nm and 640 nm laser lines were applied to, respectively, excite the Hoechst labeled nuclei, the eGFP protein and the fluorescence resulting from the LDR-stained lysosomes.

4.10. Statistical analysis

Statistical analysis was performed using the 6th version of the GraphPad Prism software. One-way ANOVA combined with the post-hoc Dunnett test was applied to compare multiple conditions, whereas the student *t*-test was used for direct comparison of 2 conditions. Multiple linear regression analysis was performed with normalized eGFP expression as a dependent variable. A *p* value ≤ 0.05 was considered *a priori* to be statistically significant.

Associated content

Supporting information consists out of 9 additional figures, 2 additional tables and a supplementary materials and methods section.

REFERENCES

1. Dowdy, S. F. Overcoming Cellular Barriers for RNA Therapeutics. *Nat. Biotechnol.* **2017**, *35*, 222–229.
2. Wittrup, A.; Lieberman, J. Knocking down Disease: A Progress Report on siRNA Therapeutics. *Nat. Rev. Genet.* **2015**, *16*, 543–552.
3. Shen, X.; Corey, D. R. Chemistry, Mechanism and Clinical Status of Antisense Oligonucleotides and Duplex RNAs. *Nucleic Acids Res.* **2018**, *46*, 1584–1600.
4. Fire, A. *et al.* Potent and Specific Genetic Interference by Double-Stranded RNA in *Caenorhabditis Elegans*. *Nature* **1998**, *391*, 806–811.
5. Kanasty, R.; Dorkin, J. R.; Vegas, A.; Anderson, D. Delivery Materials for siRNA Therapeutics. *Nat. Mater.* **2013**, *12*, 967–977.
6. Yin, H. *et al.* Non-Viral Vectors for Gene-Based Therapy. *Nat. Rev. Genet.* **2014**, *15*, 541–555.
7. Martens, T. F.; Remaut, K.; Demeester, J.; De Smedt, S. C.; Braeckmans, K. Intracellular Delivery of Nanomaterials: How to Catch Endosomal Escape in the Act. *Nano Today* **2014**, *9*, 344–364.
8. Hoy, S. M. Patisiran: First Global Approval. *Drugs* **2018**, *78*, 1625–1631.
9. Akinc, A. *et al.* The Onpattro Story and the Clinical Translation of Nanomedicines Containing Nucleic Acid-Based Drugs. *Nat. Nanotechnol.* **2019**, *14*, 1084–1087.
10. Balwani, M. *et al.* Phase 3 Trial of RNAi Therapeutic Givosiran for Acute Intermittent Porphyria. *N. Engl. J. Med.* **2020**, *382*, 2289–2301.
11. Garrelfs, S. *et al.* LB002ILLUMINATE-A, A PHASE 3 STUDY OF LUMASIRAN, AN INVESTIGATIONAL RNAI THERAPEUTIC, IN CHILDREN AND ADULTS WITH PRIMARY HYPEROXALURIA TYPE 1 (PH1). *Nephrol. Dial. Transplant.* **2020**, *35*, gfaa146.LB002.
12. Brown, C. R. *et al.* Investigating the Pharmacodynamic Durability of GalNAc–siRNA Conjugates. *Nucleic Acids Res.* **2020**, gkaa670.
13. Gilleron, J. *et al.* Image-Based Analysis of Lipid Nanoparticle–Mediated siRNA Delivery, Intracellular Trafficking and Endosomal Escape. *Nat. Biotechnol.* **2013**, *31*, 638–646.
14. Wittrup, A. *et al.* Visualizing Lipid-Formulated siRNA Release from Endosomes and Target Gene Knockdown. *Nat. Biotechnol.* **2015**, *33*, 870–876.
15. Raemdonck, K. *et al.* Biodegradable Dextran Nanogels for RNA Interference: Focusing on Endosomal Escape and Intracellular siRNA Delivery. *Adv. Funct. Mater.* **2009**, *19*, 1406–1415.
16. Sahay, G. *et al.* Efficiency of siRNA Delivery by Lipid Nanoparticles Is Limited by Endocytic Recycling. *Nat. Biotechnol.* **2013**, *31*, 653–658.
17. Hirsch, M.; Helm, M. Live Cell Imaging of Duplex siRNA Intracellular Trafficking. *Nucleic Acids Res.* **2015**, *43*, 4650–4660.
18. Crooke, S. T.; Wang, S.; Vickers, T. A.; Shen, W.; Liang, X. Cellular Uptake and Trafficking of Antisense Oligonucleotides. *Nat. Biotechnol.* **2017**, *35*, 230–237.
19. Springer, A. D.; Dowdy, S. F. GalNAc–siRNA Conjugates: Leading the Way for Delivery of RNAi Therapeutics. *Nucleic Acid Ther.* **2018**, *28*, 109–118.
20. Ma, D. Enhancing Endosomal Escape for Nanoparticle Mediated siRNA Delivery. *Nanoscale* **2014**, *6*, 6415.
21. Joris, F.; De Smedt, S. C.; Raemdonck, K. Small Molecules Convey Big Messages: Boosting Non-Viral Nucleic Acid Delivery with Low Molecular Weight Drugs. *Nano Today* **2017**, *16*, 14–29.
22. Patel, S. *et al.* Boosting Intracellular Delivery of Lipid Nanoparticle-Encapsulated mRNA. *Nano Lett.* **2017**, *17*, 5711–5718.
23. Wang, L. *et al.* A Novel Family of Small Molecules That Enhance the Intracellular Delivery and Pharmacological Effectiveness of Antisense and Splice Switching Oligonucleotides.

- ACS Chem. Biol.* **2017**, *12*, 1999–2007.
24. Juliano, R. L. *et al.* Structure-Activity Relationships and Cellular Mechanism of Action of Small Molecules That Enhance the Delivery of Oligonucleotides. *Nucleic Acids Res.* **2018**, *46*, 1601–1613.
 25. Zhang, X.; Castanotto, D.; Liu, X.; Shemi, A.; Stein, C. A. Ammonium and Arsenic Trioxide Are Potent Facilitators of Oligonucleotide Function When Delivered by Gymnosis. *Nucleic Acids Res.* **2018**, *46*, 3612–3624.
 26. Joris, F. *et al.* Repurposing Cationic Amphiphilic Drugs as Adjuvants to Induce Lysosomal SiRNA Escape in Nanogel Transfected Cells. *J. Control. Release* **2018**, *269*, 266–276.
 27. Castanotto, D. *et al.* A Stress-Induced Response Complex (SIRC) Shuttles MiRNAs, SiRNAs, and Oligonucleotides to the Nucleus. *Proc. Natl. Acad. Sci. U. S. A.* **2018**, *115*, E5756–E5765.
 28. Gilleron, J. *et al.* Identification of SiRNA Delivery Enhancers by a Chemical Library Screen. *Nucleic Acids Res.* **2015**, *43*, 7984–8001.
 29. Osborn, M. F. *et al.* Guanabenz (Wytensin™) Selectively Enhances Uptake and Efficacy of Hydrophobically Modified SiRNAs. *Nucleic Acids Res.* **2015**, *43*, 8664–8672.
 30. Yang, B. *et al.* High-Throughput Screening Identifies Small Molecules That Enhance the Pharmacological Effects of Oligonucleotides. *Nucleic Acids Res.* **2015**, *43*, 1987–1996.
 31. Van de Vyver, T. *et al.* Cationic Amphiphilic Drugs Boost the Lysosomal Escape of Small Nucleic Acid Therapeutics in a Nanocarrier-Dependent Manner. *ACS Nano* **2020**, *14*, 4774–4791.
 32. Kornhuber, J. *et al.* Identification of New Functional Inhibitors of Acid Sphingomyelinase Using a Structure-Property-Activity Relation Model. *J. Med. Chem.* **2008**, *51*, 219–237.
 33. Kornhuber, J. *et al.* Identification of Novel Functional Inhibitors of Acid Sphingomyelinase. *PLoS One* **2011**, *6*, e23852.
 34. Goracci, L.; Ceccarelli, M.; Bonelli, D.; Cruciani, G. Modeling Phospholipidosis Induction: Reliability and Warnings. *J. Chem. Inf. Model.* **2013**, *53*, 1436–1446.
 35. Muehlbacher, M.; Tripal, P.; Roas, F.; Kornhuber, J. Identification of Drugs Inducing Phospholipidosis by Novel *In Vitro* Data. *ChemMedChem* **2012**, *7*, 1925–1934.
 36. Funk, R. S.; Krise, J. P. Cationic Amphiphilic Drugs Cause a Marked Expansion of Apparent Lysosomal Volume: Implications for an Intracellular Distribution-Based Drug Interaction. *Mol. Pharm.* **2012**, *9*, 1384–1395.
 37. Logan, R.; Kong, A. C.; Axcell, E.; Krise, J. P. Amine-Containing Molecules and the Induction of an Expanded Lysosomal Volume Phenotype: A Structure-Activity Relationship Study. *J. Pharm. Sci.* **2014**, *103*, 1572–1580.
 38. Petersen, N. H. T. *et al.* Transformation-Associated Changes in Sphingolipid Metabolism Sensitize Cells to Lysosomal Cell Death Induced by Inhibitors of Acid Sphingomyelinase. *Cancer Cell* **2013**, *24*, 379–393.
 39. Gulbins, E.; Kolesnick, R. N. It Takes a CAD to Kill a Tumor Cell with a LMP. *Cancer Cell* **2013**, *24*, 279–281.
 40. Van de Vyver, T. *et al.* Cationic Amphiphilic Drugs Boost the Lysosomal Escape of Small Nucleic Acid Therapeutics in a Nanocarrier-Dependent Manner. *ACS Nano* **2020**, *14*, 4774–4791.
 41. Fuchs, R. *et al.* The Cytotoxicity of the A1-Adrenoceptor Antagonist Prazosin Is Linked to an Endocytotic Mechanism Equivalent to Transport-P. *Toxicology* **2015**, *338*, 17–29.
 42. Lin, S. C. *et al.* Prazosin Displays Anticancer Activity against Human Prostate Cancers: Targeting DNA and Cell Cycle. *Neoplasia* **2007**, *9*, 830–839.
 43. Fuchs, R. *et al.* The A1-Adrenergic Receptor Antagonists, Benoxathian and Prazosin, Induce Apoptosis and a Switch towards Megakaryocytic Differentiation in Human Erythroleukemia Cells. *Ann. Hematol.* **2009**, *88*, 989–997.
 44. Fuchs, R. *et al.* The Anti-Hypertensive Drug Prazosin Induces Apoptosis in the Medullary

- Thyroid Carcinoma Cell Line TT. *Anticancer Res.* **2015**, *35*, 31–38.
45. Fuchs, R. *et al.* Prazosin Induced Lysosomal Tubulation Interferes with Cytokinesis and the Endocytic Sorting of the Tumour Antigen CD98hc. *Biochim. Biophys. Acta - Mol. Cell Res.* **2018**, *1865*, 1211–1229.
 46. Assad Kahn, S. *et al.* The Anti-hypertensive Drug Prazosin Inhibits Glioblastoma Growth via the PKC δ -dependent Inhibition of the AKT Pathway. *EMBO Mol. Med.* **2016**, *8*, 511–526.
 47. Zhang, J.; Fan, J. Prazosin Inhibits the Proliferation, Migration and Invasion, but Promotes the Apoptosis of U251 and U87 Cells via the PI3K/AKT/MTOR Signaling Pathway. *Exp. Ther. Med.* **2020**, *20*, 1145–1152.
 48. Fuchs, R. *et al.* A1-Adrenergic Drugs Modulate Differentiation and Cell Death of Human Erythroleukemia Cells through Non Adrenergic Mechanism. *Exp. Cell Res.* **2011**, *317*, 2239–2251.
 49. Forbes, A.; Anoopkumar-Dukie, S.; Chess-Williams, R.; McDermott, C. Relative Cytotoxic Potencies and Cell Death Mechanisms of α_1 -Adrenoceptor Antagonists in Prostate Cancer Cell Lines. *Prostate* **2016**, *76*, 757–766.
 50. Sun, X.; Yang, S.; Song, W. Prazosin Inhibits the Proliferation and Survival of Acute Myeloid Leukaemia Cells through Down-Regulating TNS1. *Biomed. Pharmacother.* **2020**, *124*, 109731.
 51. Kozik, P. *et al.* Small Molecule Enhancers of Endosome-to-Cytosol Import Augment Anti-Tumor Immunity. *Cell Rep.* **2020**, *32*, 107905.
 52. Turubanova, V. D. *et al.* Immunogenic Cell Death Induced by a New Photodynamic Therapy Based on Photosens and Photodithazine. *J. Immunother. Cancer* **2019**, *7*, 350.
 53. Yatim, N.; Cullen, S.; Albert, M. L. Dying Cells Actively Regulate Adaptive Immune Responses. *Nat. Rev. Immunol.* **2017**, *17*, 262–275.
 54. Lepri, S. *et al.* Synthesis and Phospholipidosis Effect of a Series of Cationic Amphiphilic Compounds: A Case Study to Evaluate *In Silico* and *In Vitro* Assays. *Med. Chem. Res.* **2018**, *27*, 679–692.
 55. Choe, J. Y. *et al.* L-Type Calcium Channel Blocker Enhances Cellular Delivery and Gene Silencing Potency of Cell-Penetrating Asymmetric siRNAs. *Mol. Pharm.* **2020**, *17*, 777–786.
 56. Lamb, J. *et al.* The Connectivity Map: Using Gene-Expression Signatures to Connect Small Molecules, Genes, and Disease. *Science (80-.)*. **2006**, *313*, 1929–1935.
 57. Sirci, F. *et al.* Comparing Structural and Transcriptional Drug Networks Reveals Signatures of Drug Activity and Toxicity in Transcriptional Responses. *npj Syst. Biol. Appl.* **2017**, *3*, 23.
 58. Wang, L.; MacDonald, R. C. Effects of Microtubule-Depolymerizing Agents on the Transfection of Cultured Vascular Smooth Muscle Cells: Enhanced Expression with Free Drug and Especially with Drug-Gene Lipoplexes. *Mol. Ther.* **2004**, *9*, 729–737.
 59. Nair, R. R.; Rodgers, J. R.; Schwarz, L. A. Enhancement of Transgene Expression by Combining Glucocorticoids and Anti-Mitotic Agents during Transient Transfection Using DNA-Cationic Liposomes. *Mol. Ther.* **2002**, *5*, 455–462.
 60. Chowdhury, N. R. *et al.* Microtubular Disruption Prolongs the Expression of Human Bilirubin-Uridinediphosphoglucuronate-Glucuronosyltransferase-1 Gene Transferred into Gunn Rat Livers. *J. Biol. Chem.* **1996**, *271*, 2341–2346.
 61. Lindberg, J.; Fernandez, M. A. M.; Ropp, J. D.; Hamm-Alvarez, S. F. Nocodazole Treatment of CV-1 Cells Enhances Nuclear/Perinuclear Accumulation of Lipid-DNA Complexes and Increases Gene Expression. *Pharm. Res.* **2001**, *18*, 246–249.
 62. Cardarelli, F. *et al.* The Intracellular Trafficking Mechanism of Lipofectamine-Based Transfection Reagents and Its Implication for Gene Delivery. *Sci. Rep.* **2016**, *6*, 25879.
 63. Hasegawa, S.; Hirashima, N.; Nakanishi, M. Microtubule Involvement in the Intracellular Dynamics for Gene Transfection Mediated by Cationic Liposomes. *Gene Ther.* **2001**, *8*,

- 1669–1673.
64. Wishart, D. S. *et al.* DrugBank: A Comprehensive Resource for *In Silico* Drug Discovery and Exploration. *Nucleic Acids Res.* **2006**, *34*, D668-72.
 65. Symersky, J.; Osowski, D.; Walters, D. E.; Mueller, D. M. Oligomycin Frames a Common Drug-Binding Site in the ATP Synthase. *Proc. Natl. Acad. Sci. U. S. A.* **2012**, *109*, 13961–13965.
 66. Shrestha, I.; Choi, J. S.; Bae, Y. U.; Doh, K. O. Enhancement of Liposomal Plasmid DNA and siRNA Delivery by Itraconazole through Intracellular Cholesterol Accumulation. *Pharm. Res.* **2020**, *37*, 1–9.
 67. Trinha, M. N. *et al.* Triazoles Inhibit Cholesterol Export from Lysosomes by Binding to NPC1. *Proc. Natl. Acad. Sci. U. S. A.* **2017**, *114*, 89–94.
 68. Head, S. A. *et al.* Simultaneous Targeting of NPC1 and VDAC1 by Itraconazole Leads to Synergistic Inhibition of mTOR Signaling and Angiogenesis. *ACS Chem. Biol.* **2017**, *12*, 174–182.
 69. Wang, H. *et al.* The Niemann-Pick C1 Inhibitor NP3.47 Enhances Gene Silencing Potency of Lipid Nanoparticles Containing siRNA. *Mol. Ther.* **2016**, *24*, 2100–2108.
 70. Corsello, S. M. *et al.* The Drug Repurposing Hub: A next-Generation Drug Library and Information Resource. *Nat. Med.* **2017**, *23*, 405–408.
 71. Joris, F. *et al.* Repurposing Cationic Amphiphilic Drugs as Adjuvants to Induce Lysosomal siRNA Escape in Nanogel Transfected Cells. *J. Control. Release* **2018**, *269*, 266–276.
 72. Surre, J. *et al.* Strong Increase in the Autofluorescence of Cells Signals Struggle for Survival. *Sci. Rep.* **2018**, *8*, 12088.
 73. *JChem for Office (Excel)*, Version 17.21.0.1797; Software Was Used for Chemical Database Access, Structure Based Property Calculation, Search and Reporting; ChemAxon: Budapest, Hungary, 2017. <http://www.chemaxon.com>.
 74. Rehman, Z. ur; Hoekstra, D.; Zuhorn, I. S. Mechanism of Polyplex- and Lipoplex-Mediated Delivery of Nucleic Acids: Real-Time Visualization of Transient Membrane Destabilization without Endosomal Lysis. *ACS Nano* **2013**, *7*, 3767–3777.
 75. Vermeulen, L. M. P. *et al.* Endosomal Size and Membrane Leakiness Influence Proton Sponge-Based Rupture of Endosomal Vesicles. *ACS Nano* **2018**, *12*, 2332–2345.
 76. Du Rietz, H.; Hedlund, H.; Wilhelmson, S.; Nordenfelt, P.; Wittrup, A. Imaging Small Molecule-Induced Endosomal Escape of siRNA. *Nat. Commun.* **2020**, *11*, 1809.
 77. MacDonald, M. L. *et al.* Identifying Off-Target Effects and Hidden Phenotypes of Drugs in Human Cells. *Nat. Chem. Biol.* **2006**, *2*, 329–337.
 78. De Backer, L. *et al.* Bio-Inspired Pulmonary Surfactant-Modified Nanogels: A Promising siRNA Delivery System. *J. Control. Release* **2015**, *206*, 177–186.
 79. Zhang, X. *et al.* Dopamine Receptor D3 Regulates Endocytic Sorting by a Prazosin-Sensitive Interaction with the Coatamer COPI. *Proc. Natl. Acad. Sci. U. S. A.* **2012**, *109*, 12485–12490.
 80. Fuchs, R. *et al.* A1-Adrenergic Drugs Exhibit Affinity to a Thapsigargin-Sensitive Binding Site and Interfere with the Intracellular Ca²⁺ Homeostasis in Human Erythroleukemia Cells. *Exp. Cell Res.* **2011**, *317*, 2969–2980.
 81. González-Juanatey, J. R.; Iglesias, M. J.; Alcaide, C.; Piñeiro, R.; Lago, F. Doxazosin Induces Apoptosis in Cardiomyocytes Cultured *in Vitro* by a Mechanism That Is Independent of A1-Adrenergic Blockade. *Circulation* **2003**, *107*, 127–131.
 82. Cai, X. *et al.* PIKfyve, a Class III PI Kinase, Is the Target of the Small Molecular IL-12/IL-23 Inhibitor Apilimod and a Player in Toll-like Receptor Signaling. *Chem. Biol.* **2013**, *20*, 912–921.
 83. Fogarty, K. *et al.* Development of Three Orthogonal Assays Suitable for the Identification and Qualification of PIKfyve Inhibitors. *Assay Drug Dev. Technol.* **2017**, *15*, 210–219.
 84. Sano, O. *et al.* Vacuolin-1 Inhibits Autophagy by Impairing Lysosomal Maturation *via*

- PIKfyve Inhibition. *FEBS Lett.* **2016**, *590*, 1576–1585.
85. Jefferies, H. B. J. *et al.* A Selective PIKfyve Inhibitor Blocks PtdIns(3,5)P₂ Production and Disrupts Endomembrane Transport and Retroviral Budding. *EMBO Rep.* **2008**, *9*, 164–170.
 86. Hayakawa, N. *et al.* Structure–Activity Relationship Study, Target Identification, and Pharmacological Characterization of a Small Molecular IL-12/23 Inhibitor, APY0201. *Bioorg. Med. Chem.* **2014**, *22*, 3021–3029.
 87. Carlton, J. G.; Cullen, P. J. Coincidence Detection in Phosphoinositide Signaling. *Trends Cell Biol.* **2005**, *15*, 540–547.
 88. Ho, C. Y.; Alghamdi, T. A.; Botelho, R. J. Phosphatidylinositol-3,5-Bisphosphate: No Longer the Poor PIP₂. *Traffic* **2012**, *13*, 1–8.
 89. Jin, N.; Lang, M. J.; Weisman, L. S. Phosphatidylinositol 3,5-Bisphosphate: Regulation of Cellular Events in Space and Time. *Biochem. Soc. Trans.* **2016**, *44*, 177–184.
 90. Dove, S. K.; Dong, K.; Kobayashi, T.; Williams, F. K.; Michell, R. H. Phosphatidylinositol 3,5-Bisphosphate and Fab1p/PIKfyve UnderPPI_n Endo-Lysosome Function. *Biochem. J.* **2009**, *419*, 1–13.
 91. McCartney, A. J.; Zhang, Y.; Weisman, L. S. Phosphatidylinositol 3,5-Bisphosphate: Low Abundance, High Significance. *BioEssays* **2014**, *36*, 52–64.
 92. Sbrissa, D. *et al.* A Mammalian Ortholog of *Saccharomyces Cerevisiae* Vac14 That Associates with and Up-Regulates PIKfyve Phosphoinositide 5-Kinase Activity. *Mol. Cell. Biol.* **2004**, *24*, 10437–10447.
 93. Sbrissa, D. *et al.* Core Protein Machinery for Mammalian Phosphatidylinositol 3,5-Bisphosphate Synthesis and Turnover That Regulates the Progression of Endosomal Transport: Novel Sac Phosphatase Joins the ArPIKfyve-PIKfyve Complex. *J. Biol. Chem.* **2007**, *282*, 23878–23891.
 94. Sbrissa, D.; Ikononov, O. C.; Shisheva, A. Phosphatidylinositol 3-Phosphate-Interacting Domains in PIKfyve. Binding Specificity and Role in PIKfyve Endomembrane Localization. *J. Biol. Chem.* **2002**, *277*, 6073–6079.
 95. Shisheva, A. PIKfyve: Partners, Significance, Debates and Paradoxes. *Cell Biol. Int.* **2008**, *32*, 591–604.
 96. Baranov, M. V. *et al.* The Phosphoinositide Kinase PIKfyve Promotes Cathepsin-S-Mediated Major Histocompatibility Complex Class II Antigen Presentation. *iScience* **2019**, *11*, 160–177.
 97. Compton, L. M.; Ikononov, O. C.; Sbrissa, D.; Garg, P.; Shisheva, A. Active Vacuolar H⁺ ATPase and Functional Cycle of Rab5 Are Required for the Vacuolation Defect Triggered by PtdIns(3,5)P₂ Loss under PIKfyve or Vps34 Deficiency. *Am. J. Physiol. Physiol.* **2016**, *311*, C366–C377.
 98. Ikononov, O. C.; Sbrissa, D.; Shisheva, A. Mammalian Cell Morphology and Endocytic Membrane Homeostasis Require Enzymatically Active Phosphoinositide 5-Kinase PIKfyve. *J. Biol. Chem.* **2001**, *276*, 26141–26147.
 99. Ikononov, O. C.; Sbrissa, D.; Yoshimori, T.; Cover, T. L.; Shisheva, A. PIKfyve Kinase and SKD1 AAA ATPase Define Distinct Endocytic Compartments: Only PIKfyve Expression Inhibits the Cell-Vacuolating Activity of *Helicobacter Pylori* VacA Toxin. *J. Biol. Chem.* **2002**, *277*, 46785–46790.
 100. Ikononov, O. C. *et al.* Functional Dissection of Lipid and Protein Kinase Signals of PIKfyve Reveals the Role of PtdIns 3,5-P₂ Production for Endomembrane Integrity. *J. Biol. Chem.* **2002**, *277*, 9206–9211.
 101. de Lartigue, J. *et al.* PIKfyve Regulation of Endosome-Linked Pathways. *Traffic* **2009**, *10*, 883–893.
 102. Rutherford, A. C. *et al.* The Mammalian Phosphatidylinositol 3-Phosphate 5-Kinase (PIKfyve) Regulates Endosome-to-TGN Retrograde Transport. *J. Cell Sci.* **2006**, *119*, 3944–3957.

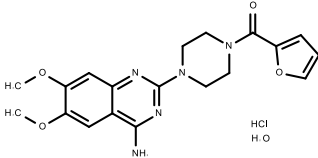
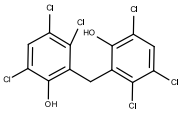
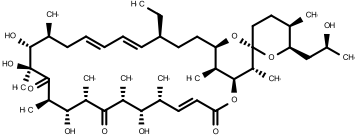
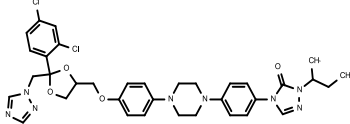
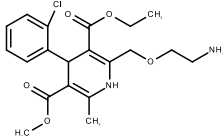
103. Hazeki, K.; Uehara, M.; Nigorikawa, K.; Hazeki, O. PIKfyve Regulates the Endosomal Localization of CpG Oligodeoxynucleotides to Elicit TLR9-Dependent Cellular Responses. *PLoS One* **2013**, *8*, e73894.
104. Min, S. H. *et al.* Loss of PIKfyve in Platelets Causes a Lysosomal Disease Leading to Inflammation and Thrombosis in Mice. *Nat. Commun.* **2014**, *5*, 1–12.
105. Cerny, J. *et al.* The Small Chemical Vacuolin-1 Inhibits Ca²⁺-Dependent Lysosomal Exocytosis but Not Cell Resealing. *EMBO Rep.* **2004**, *5*, 883–888.
106. Lu, Y. *et al.* Vacuolin-1 Potently and Reversibly Inhibits Autophagosome-Lysosome Fusion by Activating RAB5A. *Autophagy* **2014**, *10*, 1895–1905.
107. Huynh, C.; Andrews, N. W. The Small Chemical Vacuolin-1 Alters the Morphology of Lysosomes without Inhibiting Ca²⁺-Regulated Exocytosis. *EMBO Rep.* **2005**, *6*, 843–847.
108. Shaik, G. M.; Dráberová, L.; Heneberg, P.; Dráber, P. Vacuolin-1-Modulated Exocytosis and Cell Resealing in Mast Cells. *Cell. Signal.* **2009**, *21*, 1337–1345.
109. Isobe, Y. *et al.* PIKfyve Accelerates Phagosome Acidification through Activation of TRPML1 While Arrests Aberrant Vacuolation Independent of the Ca²⁺ Channel. *J. Biochem.* **2019**, *165*, 75–84.
110. Goodridge, J. P. *et al.* Remodeling of Secretory Lysosomes during Education Tunes Functional Potential in NK Cells. *Nat. Commun.* **2019**, *10*, 514.
111. Martin, S. *et al.* Inhibition of PIKfyve by YM-201636 Dysregulates Autophagy and Leads to Apoptosis-Independent Neuronal Cell Death. *PLoS One* **2013**, *8*, e60152.
112. Kang, Y. L. *et al.* Inhibition of PIKfyve Kinase Prevents Infection by Zaire Ebolavirus and SARS-CoV-2. *Proc. Natl. Acad. Sci. U. S. A.* **2020**, *117*, 20803–20813.
113. Sbrissa, D.; Naisan, G.; Ikononov, O. C.; Shisheva, A. Apilimod, a Candidate Anticancer Therapeutic, Arrests Not Only PtdIns(3,5)P₂ but Also PtdIns5P Synthesis by PIKfyve and Induces Bafilomycin A1-Reversible Aberrant Endomembrane Dilation. *PLoS One* **2018**, *13*, e0204532.
114. Dayam, R. M. *et al.* The Lipid Kinase PIKfyve Coordinates the Neutrophil Immune Response through the Activation of the Rac GTPase. *J. Immunol.* **2017**, *199*, 2096–2105.
115. Kim, G. H. E.; Dayam, R. M.; Prashar, A.; Terebiznik, M.; Botelho, R. J. PIKfyve Inhibition Interferes with Phagosome and Endosome Maturation in Macrophages. *Traffic* **2014**, *15*, 1143–1163.
116. Sbrissa, D.; Ikononov, O. C.; Filios, C.; Delvecchio, K.; Shisheva, A. Functional Dissociation between PIKfyve-Synthesized PtdIns5P and PtdIns(3,5)P₂ by Means of the PIKfyve Inhibitor YM201636. *Am. J. Physiol. Physiol.* **2012**, *303*, C436–C446.
117. Sharma, G. *et al.* A Family of PIKfyve Inhibitors with Therapeutic Potential against Autophagy-Dependent Cancer Cells Disrupt Multiple Events in Lysosome Homeostasis. *Autophagy* **2019**, 1–25.
118. Choy, C. H. *et al.* Lysosome Enlargement during Inhibition of the Lipid Kinase PIKfyve Proceeds through Lysosome Coalescence. *J. Cell Sci.* **2018**, jcs.213587.
119. Dong, X. P. *et al.* PI(3,5)P₂ Controls Membrane Trafficking by Direct Activation of Mucolipin Ca²⁺ Release Channels in the Endolysosome. *Nat. Commun.* **2010**, *1*, 1–11.
120. Dong, X. P. *et al.* The Type IV Mucopolidosis-Associated Protein TRPML1 Is an Endolysosomal Iron Release Channel. *Nature* **2008**, *455*, 992–996.
121. Currinn, H.; Guscott, B.; Balklava, Z.; Rothnie, A.; Wassmer, T. APP Controls the Formation of PI(3,5)P₂ Vesicles through Its Binding of the PIKfyve Complex. *Cell. Mol. Life Sci.* **2016**, *73*, 393–408.
122. Gayle, S. *et al.* Identification of Apilimod as a First-in-Class PIKfyve Kinase Inhibitor for Treatment of B-Cell Non-Hodgkin Lymphoma. *Blood* **2017**, *129*, 1768–1778.
123. Chen, C. *et al.* Identification of Novel Vacuolin-1 Analogues as Autophagy Inhibitors by Virtual Drug Screening and Chemical Synthesis. *Molecules* **2017**, *22*, 891.
124. Osborn, M. F. *et al.* Hydrophobicity Drives the Systemic Distribution of Lipid-Conjugated

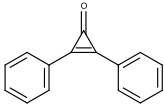
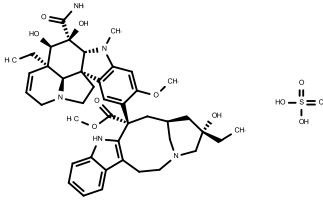
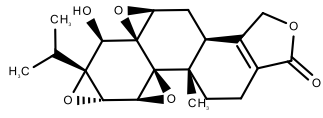
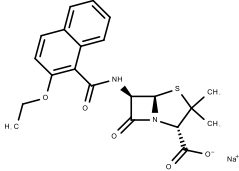
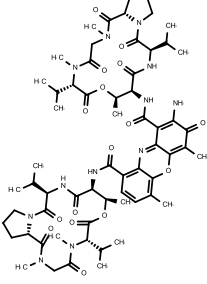
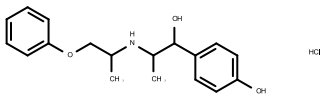
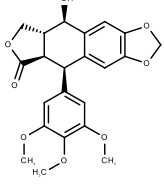
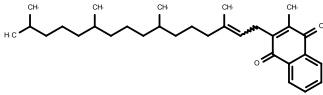
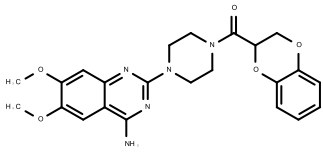
- SiRNAs via Lipid Transport Pathways. *Nucleic Acids Res.* **2019**, *47*, 1070–1081.
125. Hassler, M. R. *et al.* Comparison of Partially and Fully Chemically-Modified SiRNA in Conjugate-Mediated Delivery *in Vivo*. *Nucleic Acids Res.* **2018**, *46*, 2185–2196.
 126. Haraszti, R. A. *et al.* 5'-Vinylphosphonate Improves Tissue Accumulation and Efficacy of Conjugated SiRNAs *in Vivo*. *Nucleic Acids Res.* **2017**, *45*, 7581–7592.
 127. Nishina, K. *et al.* Efficient *in Vivo* Delivery of SiRNA to the Liver by Conjugation of α -Tocopherol. *Mol. Ther.* **2008**, *16*, 734–740.
 128. Sarett, S. M. *et al.* Lipophilic SiRNA Targets Albumin *in Situ* and Promotes Bioavailability, Tumor Penetration, and Carrier-Free Gene Silencing. *Proc. Natl. Acad. Sci. U. S. A.* **2017**, *114*, E6490–E6497.
 129. Wolfrum, C. *et al.* Mechanisms and Optimization of *in Vivo* Delivery of Lipophilic SiRNAs. *Nat. Biotechnol.* **2007**, *25*, 1149–1157.
 130. Chernikov, I. V. *et al.* Trimeric Small Interfering RNAs and Their Cholesterol-Containing Conjugates Exhibit Improved Accumulation in Tumors, but Dramatically Reduced Silencing Activity. *Molecules* **2020**, *25*, 1877.
 131. Chernikov, I. V. *et al.* Cholesterol-Containing Nuclease-Resistant SiRNA Accumulates in Tumors in a Carrier-Free Mode and Silences MDR1 Gene. *Mol. Ther. - Nucleic Acids* **2017**, *6*, 209–220.
 132. Fuchs, R. *et al.* The Anti-Hypertensive Drug Prazosin Induces Apoptosis in the Medullary Thyroid Carcinoma Cell Line TT. *Anticancer Res.* **2015**, *35*, 31–38.
 133. Tait, S. W. G.; Ichim, G.; Green, D. R. Die Another Way - Non-Apoptotic Mechanisms of Cell Death. *J. Cell Sci.* **2014**, *127*, 2135–2144.
 134. Nirmala, J. G.; Lopus, M. Cell Death Mechanisms in Eukaryotes. *Cell Biol. Toxicol.* **2020**, *36*, 145–164.
 135. Bedoui, S.; Herold, M. J.; Strasser, A. Emerging Connectivity of Programmed Cell Death Pathways and Its Physiological Implications. *Nat. Rev. Mol. Cell Biol.* **2020**, *21*, 678–695.
 136. Tang, D.; Kang, R.; Berghe, T. Vanden; Vandenabeele, P.; Kroemer, G. The Molecular Machinery of Regulated Cell Death. *Cell Res.* **2019**, *29*, 347–364.
 137. Galluzzi, L. *et al.* Molecular Mechanisms of Cell Death: Recommendations of the Nomenclature Committee on Cell Death 2018. *Cell Death Differ.* **2018**, *25*, 486–541.
 138. Grootjans, S. *et al.* A Real-Time Fluorometric Method for the Simultaneous Detection of Cell Death Type and Rate. *Nat. Protoc.* **2016**, *11*, 1444–1454.
 139. Vanden Berghe, T. *et al.* Determination of Apoptotic and Necrotic Cell Death *in Vitro* and *in Vivo*. *Methods* **2013**, *61*, 117–129.
 140. Demuyne, R.; Efimova, I.; Lin, A.; Declercq, H.; Krysko, D. V. A 3D Cell Death Assay to Quantitatively Determine Ferroptosis in Spheroids. *Cells* **2020**, *9*, 703.
 141. Yang, X. *et al.* MDR1 SiRNA Loaded Hyaluronic Acid-Based CD44 Targeted Nanoparticle Systems Circumvent Paclitaxel Resistance in Ovarian Cancer. *Sci. Rep.* **2015**, *5*, 1–9.
 142. Yadav, S.; Van Vlerken, L. E.; Little, S. R.; Amiji, M. M. Evaluations of Combination MDR-1 Gene Silencing and Paclitaxel Administration in Biodegradable Polymeric Nanoparticle Formulations to Overcome Multidrug Resistance in Cancer Cells. *Cancer Chemother. Pharmacol.* **2009**, *63*, 711–722.
 143. Liu, W. *et al.* CS-PEI/Beclin-SiRNA Downregulate Multidrug Resistance Proteins and Increase Paclitaxel Therapeutic Efficacy against NSCLC. *Mol. Ther. - Nucleic Acids* **2019**, *17*, 477–490.
 144. Reddy, T. L. *et al.* Simultaneous Delivery of Paclitaxel and Bcl-2 SiRNA via PH-Sensitive Liposomal Nanocarrier for the Synergistic Treatment of Melanoma. *Sci. Rep.* **2016**, *6*, 1–12.
 145. Yu, H. *et al.* Reversal of Lung Cancer Multidrug Resistance by PH-Responsive Micelleplexes Mediating Co-Delivery of SiRNA and Paclitaxel. *Macromol. Biosci.* **2014**, *14*, 100–109.

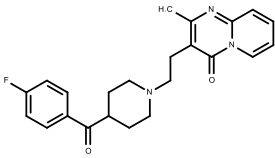
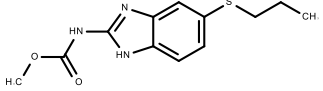
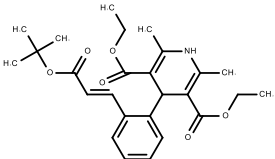
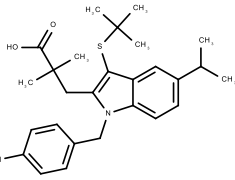
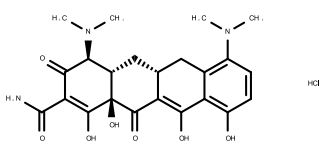
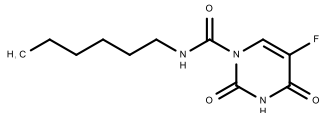
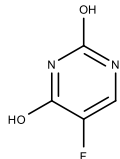
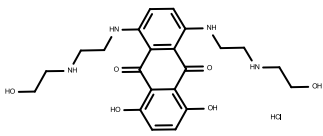
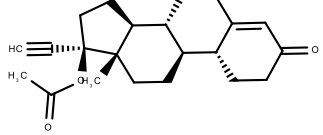
146. Lee, S. H.; Lee, J. Y.; Kim, J. S.; Park, T. G.; Mok, H. Amphiphilic siRNA Conjugates for Co-Delivery of Nucleic Acids and Hydrophobic Drugs. *Bioconjug. Chem.* **2017**, *28*, 2051–2061.
147. Zhang, Y. *et al.* Glioblastoma Therapy Using Codelivery of Cisplatin and Glutathione Peroxidase Targeting siRNA from Iron Oxide Nanoparticles. *ACS Appl. Mater. Interfaces* **2020**, *12*, 43408–43421.
148. Sun, T. M. *et al.* Simultaneous Delivery of siRNA and Paclitaxel via a “Two-in-One” Micelleplex Promotes Synergistic Tumor Suppression. *ACS Nano* **2011**, *5*, 1483–1494.
149. Saraswathy, M.; Gong, S. Recent Developments in the Co-Delivery of siRNA and Small Molecule Anticancer Drugs for Cancer Treatment. *Mater. Today* **2014**, *17*, 298–306.
150. Osborn, M. F. *et al.* Efficient Gene Silencing in Brain Tumors with Hydrophobically Modified siRNAs. *Mol. Cancer Ther.* **2018**, *17*, 1251–1258.
151. Sakamoto, S.; Schwarze, S.; Kyprianou, N. Anoikis Disruption of Focal Adhesion-Akt Signaling Impairs Renal Cell Carcinoma. *Eur. Urol.* **2011**, *59*, 734–744.
152. Park, M. S. *et al.* The Antihypertension Drug Doxazosin Inhibits Tumor Growth and Angiogenesis by Decreasing VEGFR-2/Akt/MTOR Signaling and VEGF and HIF-1 α Expression. *Oncotarget* **2014**, *5*, 4935–4944.
153. Joffre, O. P.; Segura, E.; Savina, A.; Amigorena, S. Cross-Presentation by Dendritic Cells. *Nat. Rev. Immunol.* **2012**, *12*, 557–569.
154. Gros, M.; Amigorena, S. Regulation of Antigen Export to the Cytosol during Cross-Presentation. *Front. Immunol.* **2019**, *10*, 41.
155. van der Meel, R. *et al.* Smart Cancer Nanomedicine. *Nat. Nanotechnol.* **2019**, *14*, 1007–1017.
156. Raemdonck, K.; Naeye, B.; Høgset, A.; Demeester, J.; De Smedt, S. C. Prolonged Gene Silencing by Combining siRNA Nanogels and Photochemical Internalization. *J. Control. Release* **2010**, *145*, 281–288.
157. De Backer, L.; Braeckmans, K.; Demeester, J.; De Smedt, S. C.; Raemdonck, K. The Influence of Natural Pulmonary Surfactant on the Efficacy of siRNA-Loaded Dextran Nanogels. *Nanomedicine* **2013**, *8*, 1625–1638.
158. Merckx, P. *et al.* Surfactant Protein B (SP-B) Enhances the Cellular siRNA Delivery of Proteolipid Coated Nanogels for Inhalation Therapy. *Acta Biomater.* **2018**, *78*, 236–246.
159. Dakwar, G. R. *et al.* Colloidal Stability of Nano-Sized Particles in the Peritoneal Fluid: Towards Optimizing Drug Delivery Systems for Intraperitoneal Therapy. *Acta Biomater.* **2014**, *10*, 2965–2975.
160. Ragelle, H. *et al.* Intracellular siRNA Delivery Dynamics of Integrin-Targeted, PEGylated Chitosan–Poly(Ethylene Imine) Hybrid Nanoparticles: A Mechanistic Insight. *J. Control. Release* **2015**, *211*, 1–9.
161. Bramsen, J. B. *et al.* Improved Silencing Properties Using Small Internally Segmented Interfering RNAs. *Nucleic Acids Res.* **2007**, *35*, 5886–5897.
162. Fraire, J. C. *et al.* Vapor Nanobubble Is the More Reliable Photothermal Mechanism for Inducing Endosomal Escape of siRNA without Disturbing Cell Homeostasis. *J. Control. Release* **2020**, *319*, 262–275.
163. Thakur, S.; Cattoni, D. I.; Nöllmann, M. The Fluorescence Properties and Binding Mechanism of SYTOX Green, a Bright, Low Photo-Damage DNA Intercalating Agent. *Eur. Biophys. J.* **2015**, *44*, 337–348.
164. Rehman, Z. ur; Hoekstra, D.; Zuhorn, I. S. Mechanism of Polyplex- and Lipoplex-Mediated Delivery of Nucleic Acids: Real-Time Visualization of Transient Membrane Destabilization without Endosomal Lysis. *ACS Nano* **2013**, *7*, 3767–3777.

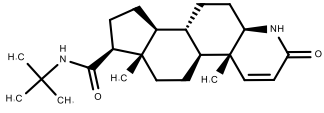
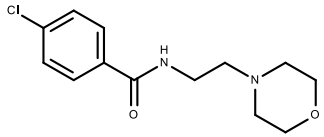
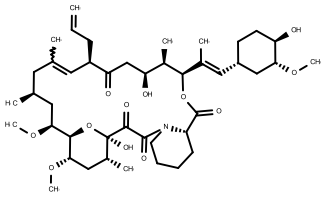
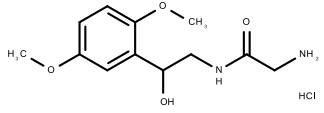
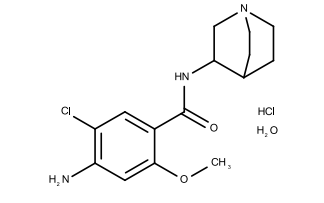
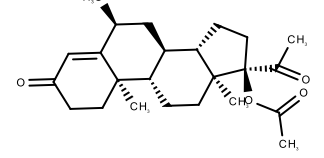
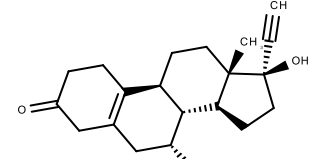
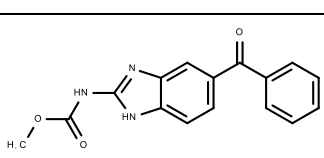
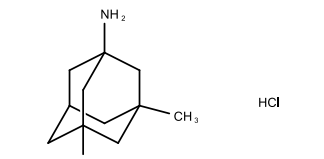
SUPPLEMENTARY FIGURES AND TABLES

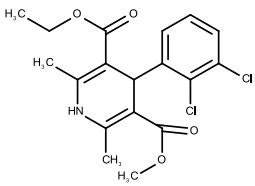
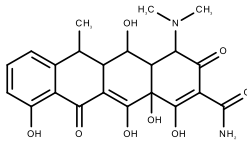
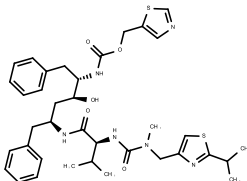
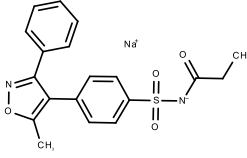
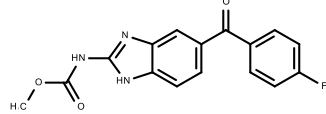
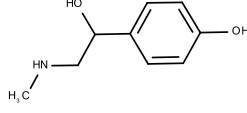
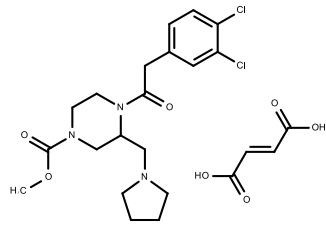
Table S1. Hit adjuvant compounds that do not comply with the applied CAD definition ($\text{clogP} > 3$, $\text{pKa1} > 6$)¹. (pKa1 = macroscopic pKa of the conjugated acid of the most basic amine, Norm EE = normalized eGFP expression vs. siNG-DMSO control). The pKa values of the most basic amines (macroscopic pKa of the conjugated acid, pKa1) and the clogP (calculated $\log\text{P}$) values of the compounds were predicted with JChem for Office (version 17.21.0.1797, ChemAxon Ltd., Budapest, Hungary)². The physiological charge (at pH 7.4) was calculated with the cxcalc calculator function (formal charge at pH 7.4, Marvin 17.21.0, 2017, ChemAxon Ltd., Budapest, Hungary)². Structures were obtained from JChem for Office (version 17.21.0.1797, ChemAxon Ltd., Budapest, Hungary)². Annotated targets were obtained from the Drug Repurposing Hub database³.

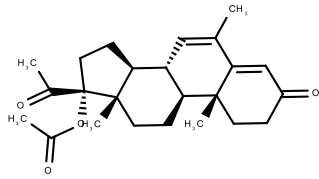
Compound Name & Documented Pharmacological Effect	Structure	Annotated Targets ^a	clogP	pKa1	Physiological charge (at pH 7.4)	Norm EE
(1) Prazosin hydrochloride hydrate <i>adrenergic receptor antagonist</i>		ADRA1A ADRA1B ADRA1D ADRA2A ADRA2B ADRA2C KCNH2 KCNH6 KCNH7	1.65	7.24	1	0.08
(2) Hexachlorophene <i>antiseptic</i>		GLUD1 SDHD	7.08	N.A.	-1	0.26
(3) Oligomycin A <i>ATP synthase inhibitor</i>		ATP5A1	7.45	N.A.	0	0.31
(4) Itraconazole <i>antifungal</i>		CYP51A1	7.31	3.91	0	0.42
(5) Amlodipine <i>calcium channel blocker</i>		CA1, CACNA1B CACNA1C CACNA1D CACNA1F CACNA1S CACNA2D1 CACNA2D3 CACNB1 CACNB2 SMPD1	1.64	9.45	1	0.59

(6) Diphenylcyclopropenone <i>immunostimulant</i>		N.A.	3.85	N.A.	0	0.64
(7) Vindesine sulfate <i>tubulin polymerization inhibitor</i>		TUBB TUBB1	2.79	8.68	2	0.64
(8) Triptolide <i>RNA polymerase inhibitor</i>		RELA	1.33	N.A.	0	0.65
(9) Nafcillin sodium <i>bacterial cell wall synthesis inhibitor</i>		CYP1A2 CYP3A4 SLC22A6	2.29	N.A.	-1	0.70
(10) Dactinomycin <i>RNA polymerase inhibitor</i>		POLR2A	-0.10	-12.9	0	0.72
(11) Duvadilan (Isoxsuprine hydrochloride) <i>adrenergic receptor agonist</i>		ADRB2	2.56	9.00	1	0.72
(12) Podofilox <i>tubulin polymerization inhibitor</i>		IGF1R TOP2A TUBA4A TUBB	1.62	N.A.	0	0.72
(13) Phylloquinone <i>vitamin K1</i>		BGLAP GGCX	9.70	N.A.	0	0.72
(14) Doxazosin <i>adrenergic receptor antagonist</i>		ADRA1A ADRA1B ADRA1D KCNH2 KCNH6 KCNH7	2.14	7.24	1	0.73

<p>(15) Pirenperone <i>serotonin receptor antagonist</i></p>		<p>HTR2A HTR7</p>	<p>2.82</p>	<p>8.02</p>	<p>1</p>	<p>0.74</p>
<p>(16) Albendazole <i>tubulin polymerization inhibitor (anthelmintic)</i></p>		<p>TUBA1A TUBB TUBB4B</p>	<p>3.20</p>	<p>4.21</p>	<p>0</p>	<p>0.77</p>
<p>(17) Lacidipine <i>calcium channel blocker</i></p>		<p>CACNA1C</p>	<p>4.19</p>	<p>N.A.</p>	<p>0</p>	<p>0.78</p>
<p>(18) MK-886 <i>lipoygenase inhibitor</i></p>		<p>ALOX5AP</p>	<p>8.19</p>	<p>N.A.</p>	<p>-1</p>	<p>0.80</p>
<p>(19) Minocycline hydrochloride <i>bacterial 30S ribosomal subunit inhibitor</i></p>		<p>ALOX5 CASP1 CASP3 CYCS IL1B MMP9 VEGFA</p>	<p>-3.31</p>	<p>6.68</p>	<p>-2</p>	<p>0.81</p>
<p>(20) Carmofur <i>thymidylate synthase inhibitor</i></p>		<p>TYMS</p>	<p>1.44</p>	<p>N.A.</p>	<p>-1</p>	<p>0.81</p>
<p>(21) 5-Fluorouracil <i>thymidylate synthase inhibitor</i></p>		<p>DPYD TYMS</p>	<p>0.86</p>	<p>N.A.</p>	<p>0</p>	<p>0.81</p>
<p>(22) Mitoxantrone hydrochloride <i>topoisomerase inhibitor</i></p>		<p>TOP2A</p>	<p>0.75</p>	<p>9.22</p>	<p>2</p>	<p>0.82</p>
<p>(23) 19-Norethindrone acetate <i>progesterone receptor agonist</i></p>		<p>PGR</p>	<p>3.66</p>	<p>N.A.</p>	<p>0</p>	<p>0.82</p>

(24) Finasteride <i>5 alpha reductase inhibitor</i>		AKR1D1 SRD5A1 SRD5A2	3.07	N.A.	0	0.82
(25) Moclobemide <i>monoamine oxidase inhibitor</i>		MAOA MAOB	1.45	6.02	0	0.82
(26) Tacrolimus <i>calcineurin inhibitor</i>		FKBP1A	5.59	N.A.	0	0.83
(27) Midodrine hydrochloride <i>adrenergic receptor agonist</i>		ADRA1A ADRA1B ADRA1D	-0.95	8.14	1	0.83
(28) Zacopride hydrochloride hydrate <i>serotonin receptor antagonist</i>		HTR3A HTR3B HTR4 HTR5A	1.04	7.79	1	0.84
(29) Medroxyprogesterone 17-acetate <i>progesterone receptor agonist</i>		ESR1 PGR	4.13	N.A.	0	0.84
(30) Tibolone <i>androgen/estrogen/ progesterone receptor agonist</i>		ESR1	3.10	N.A.	0	0.85
(31) Mebendazole <i>tubulin polymerization inhibitor (anthelmintic)</i>		TUBA1A TUBB TUBB4B	3.26	3.42	0	0.86
(32) Memantine hydrochloride <i>glutamate receptor antagonist</i>		CHRFAM7A DRD2 GRIN1 GRIN2A GRIN2B GRIN3A HTR3A	2.07	10.70	1	0.87

<p>(33) Felodipine <i>calcium channel blocker</i></p>		<p>CACNA1C CACNA1D CACNA1F CACNA1H CACNA1S CACNA2D1 CACNA2D2 CACNB2 CALM1 CFTR NR3C2 PDE1A PDE1B TNNC1 TNNC2</p>	3.44	N.A.	0	0.87
<p>(34) Doxycycline <i>metalloproteinase inhibitor</i></p>		MMP8	-3.37	5.77	-1	0.88
<p>(35) Ritonavir <i>HIV protease inhibitor</i></p>		<p>CYP1A2 CYP2B6 CYP2C19 CYP2C8 CYP2C9 CYP2D6 CYP2E1 CYP3A4 CYP3A5 CYP3A7</p>	5.22	2.84	0	0.88
<p>(36) Parecoxib sodium <i>cyclooxygenase inhibitor</i></p>		LTF	3.51	0.42	-1	0.88
<p>(37) Flubendazole <i>tubulin polymerization inhibitor (anthelmintic)</i></p>		TUBB	3.40	3.42	0	0.90
<p>(38) Syneprine <i>adrenergic receptor agonist</i></p>		ADRA1A	-0.07	9.15	1	0.90
<p>(39) GR 89696 fumarate <i>k-opioid agonist</i></p>		OPRK1	2.64	8.33	1	0.90

<p>(40) Megestrol acetate <i>progesterone receptor agonist</i></p>		<p>NR3C1 PGR</p>	<p>3.72</p>	<p>N.A.</p>	<p>0</p>	<p>0.90</p>
---	---	----------------------	-------------	-------------	----------	-------------

^a ADRA1A = Adrenoceptor Alpha 1A, ADRA1B = Adrenoceptor Alpha 1B, ADRA1D = Adrenoceptor Alpha 1D, ADRA2A = Adrenoceptor Alpha 2A, ADRA2B = Adrenoceptor Alpha 2B, ADRA2C = Adrenoceptor Alpha 2C, ADRB2 = Adrenoceptor Beta 2, KCNH2 = Potassium Voltage-Gated Channel Subfamily H Member 2, KCNH6 = Potassium Voltage-Gated Channel Subfamily H Member 6, KCNH7 = Potassium Voltage-Gated Channel Subfamily H Member 7, CYP1A2 = Cytochrome P450 Family 1 Subfamily A Member 2, CYP2B6 = CYP Family 2 Subfamily B Member 6, CYP2C19 = CYP Family 2 Subfamily C Member 19, CYP2C8 = CYP Family 2 Subfamily C Member 8, CYP2C9 = CYP Family 2 Subfamily C Member 9, CYP2D6 = CYP Family 2 Subfamily D Member 6, CYP2E1 = CYP Family 2 Subfamily E Member 1, CYP3A4 = CYP Family 3 Subfamily A Member 4, CYP3A5 = CYP Family 3 Subfamily A Member 5, CYP3A7 = CYP Family 3 Subfamily A Member 7, CYP51A1 = CYP Family 51 Subfamily A Member 1, CA1 = Carbonic Anhydrase 1, CACNA1B = Calcium Voltage-Gated Channel Subunit Alpha1 B, CACNA1C = Calcium Voltage-Gated Channel Subunit Alpha1 C, CACNA1D = Calcium Voltage-Gated Channel Subunit Alpha1 D, CACNA1F = Calcium Voltage-Gated Channel Subunit Alpha1 F, CACNA1S = Calcium Voltage-Gated Channel Subunit Alpha1 S, CACNA1H = Calcium Voltage-Gated Channel Subunit Alpha1 H, CACNA2D1 = Calcium Voltage-Gated Channel Auxiliary Subunit Alpha2delta 1, CACNA2D2 = Calcium Voltage-Gated Channel Auxiliary Subunit Alpha2delta 2, CACNA2D3 = Calcium Voltage-Gated Channel Auxiliary Subunit Alpha2delta 3, CACNB1 = Calcium Voltage-Gated Channel Auxiliary Subunit Beta 1, CACNB2 = Calcium Voltage-Gated Channel Auxiliary Subunit Beta 2, SMPD1 = Sphingomyelin Phosphodiesterase 1, TUBB = Tubulin Beta, TUBB1 = Tubulin Beta 1 Class VI, TUBA4A = Tubulin Alpha 4a, TUBA1A = Tubulin Alpha 1a, TUBB4B = Tubulin Beta 4B Class IVb, RELA = RELA Proto-Oncogene, NF-KB Subunit, SLC22A6 = Solute Carrier Family 22 Member 6, POLR2A = RNA Polymerase II Subunit A, IGF1R = Insulin Like Growth Factor 1 Receptor, TOP2A = DNA Topoisomerase II Alpha, BGLAP = Bone Gamma-Carboxyglutamate Protein, GGCX = Gamma-Glutamyl Carboxylase, HTR2A = 5-Hydroxytryptamine Receptor 2A, HTR7 = 5-Hydroxytryptamine Receptor 7, ALOX5AP = Arachidonate 5-Lipoxygenase Activating Protein, ALOX5 = Arachidonate 5-Lipoxygenase, CASP1 = Caspase 1, CASP3 = Caspase 3, CYCS = Cytochrome C Somatic, IL1B = Interleukin 1 Beta, MMP9 = Matrix Metalloproteinase 9, MMP8 = Matrix Metalloproteinase 8, VEGFA = Vascular Endothelial Growth Factor A, TYMS = Thymidylate Synthetase, DPYD = Dihydropyrimidine Dehydrogenase, PGR = Progesterone Receptor, AKR1D1 = Aldo-Keto Reductase Family 1 Member D1, SRD5A1 = Steroid 5 Alpha-Reductase 1, SRD5A2 = Steroid 5 Alpha-Reductase 2, MAOA = Monoamine Oxidase A, MAOB = Monoamine Oxidase B, FKBP1A = FKBP Prolyl Isomerase 1A, HTR3A = 5-Hydroxytryptamine Receptor 3A, HTR3B = 5-Hydroxytryptamine Receptor 3B, HTR4 = 5-Hydroxytryptamine Receptor 4, HTR5A = 5-Hydroxytryptamine Receptor 5A, ESR1 = Estrogen Receptor 1, CHRFAM7A = CHRNA7 (Exons 5-10) And FAM7A (Exons A-E) Fusion, DRD2 = Dopamine Receptor D2, GRIN1 = Glutamate Ionotropic Receptor NMDA Type Subunit 1, GRIN2A = GRIN Type Subunit 2A, GRIN2B = GRIN Type Subunit 2B, GRIN3A = GRIN Type Subunit 3A, CALM1 = Calmodulin 1, CFTR = CF Transmembrane Conductance Regulator, NR3C1 = Nuclear Receptor Subfamily 3 Group C Member 1, NR3C2 = NR Subfamily 3 Group C Member 2, PDE1A = Phosphodiesterase 1A, PDE1B = Phosphodiesterase 1B, TNNC1 = Troponin C1, TNNC2 = Troponin C2, LTF = Lactotransferrin, GLUD1 = Glutamate Dehydrogenase 1, SDHD = Succinate Dehydrogenase Complex Subunit D, ATP5A1 = ATP Synthase F1 Subunit Alpha, OPRK1 = Opioid Receptor Kappa 1.

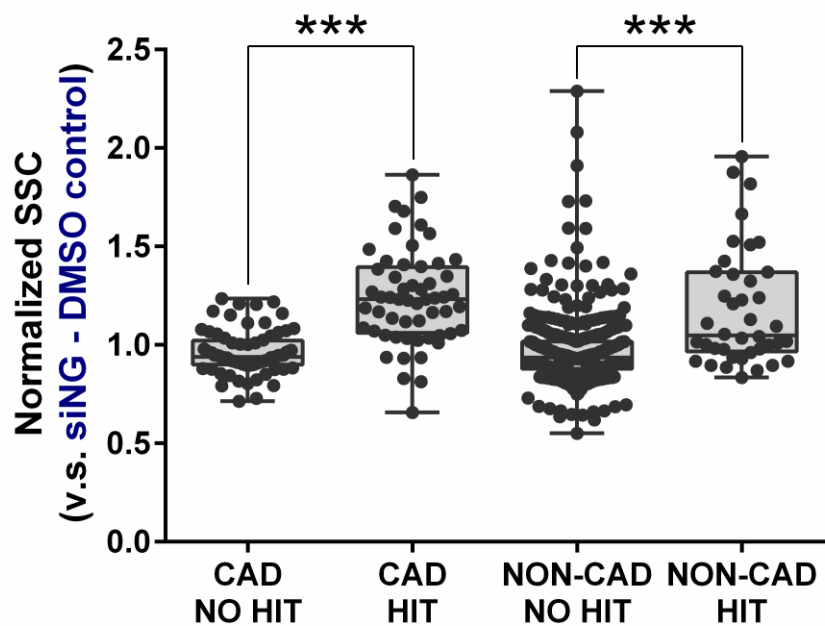


Figure S1. Box and whisker plot of the SSC values, normalized to the siNG-DMSO control of each plate, in the group of 'CAD no hits' (n = 72), 'CAD hits' (n = 56), 'non-CAD no hits' (n = 532) and 'non-CAD hits' (n = 40). Statistical significance is indicated when appropriate (***) $p \leq 0.001$. (CAD = cationic amphiphilic drug, siNG-DMSO control = siNG transfection in the absence of compound with equal amount of DMSO, SSC = side scatter).

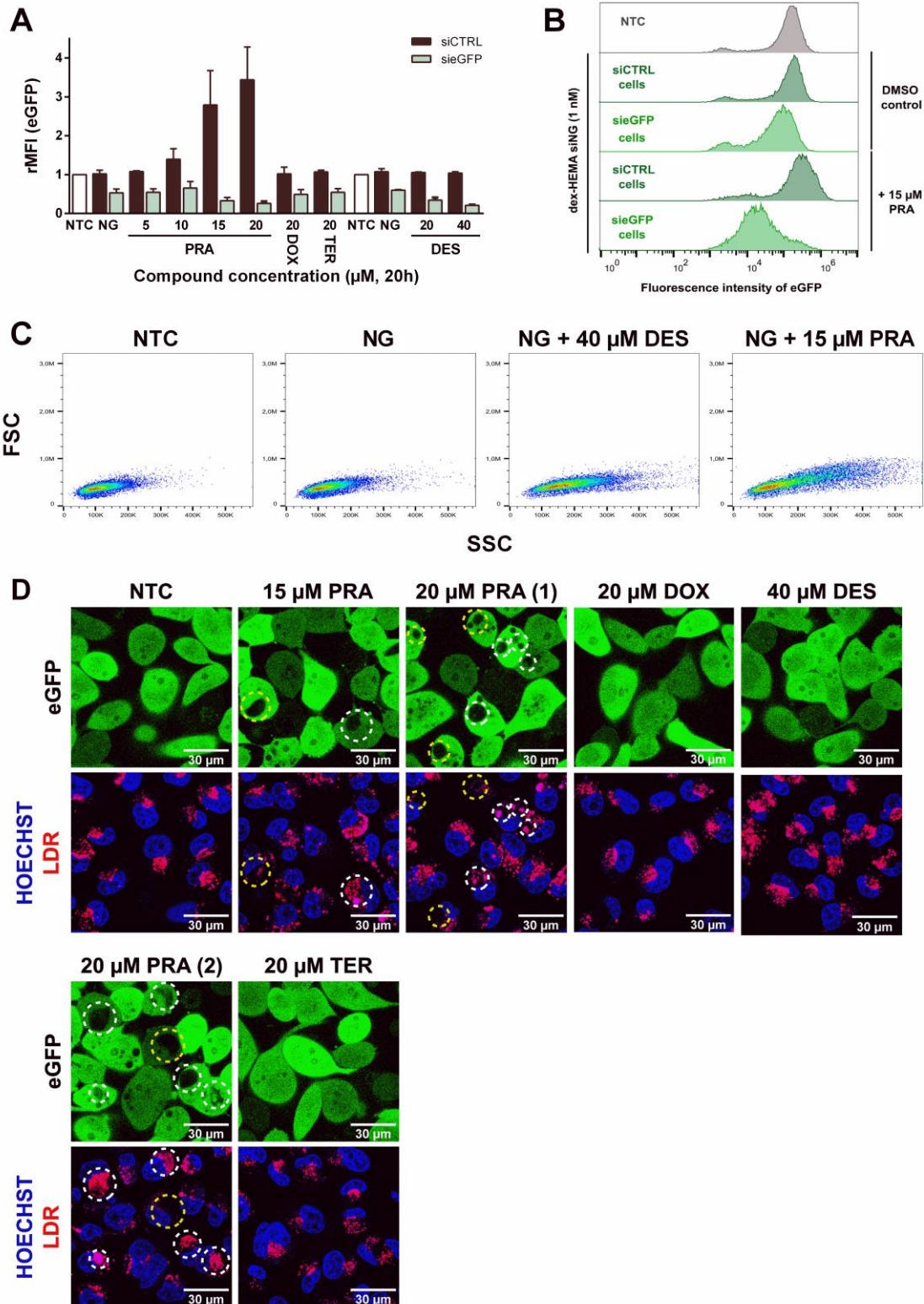


Figure S2. Prazosin and desloratadine, but not doxazosin or terazosin, improve the eGFP silencing potential of dex-HEMA siNGs in NSCLC cells, while increasing the lysosomal volume and cellular granularity. (A) The relative mean fluorescence intensity (rMFI) for the H1299-eGFP cells transfected with siCTRL-loaded NGs (black) and sieGFP-loaded NGs (grey) followed by adjuvant treatment with 5-20 μM prazosin (PRA)/20 μM doxazosin (DOX)/20 μM terazosin (TER)/20-40 μM desloratadine (DES)

(20 h). Data are represented as mean \pm the standard error of the mean (SEM) for three independent repeats. (B) EGFP gene silencing in H1299-eGFP cells, following dex-HEMA siNG transfection and 15 μ M PRA treatment (20 h), demonstrated by flow cytometry histograms. (C) Representative scatter plots for untreated cells, dex-HEMA siNG transfected cells or cells transfected with siNGs followed by 40 μ M DES or 15 μ M PRA treatment for 20 h. (D) Representative confocal images showing the lysosomal compartment (red) following LysoTracker[®] Deep Red (LDR) labeling for untreated and 15-20 μ M PRA-/20 μ M DOX-/20 μ M TER-/40 μ M DES-treated H1299-eGFP cells (20 h). LDR-positive vacuoles are highlighted with a white circle, while LDR-negative vacuoles are highlighted with a yellow circle. The scale bar corresponds to 30 μ m. (eGFP = enhanced green fluorescent protein, rMFI (eGFP) = relative mean fluorescence intensity of the H1299-eGFP cells transfected with siCTRL-or siGFP loaded NGs, NTC = not treated control, NG = dex-HEMA siNG transfection without compound treatment, siNGs = siRNA-loaded nanogels, PRA = prazosin, DOX = doxazosin, TER = terazosin, DES = desloratadine, LDR = LysoTracker[®] Deep Red, FSC = forward scatter, SSC = side scatter).

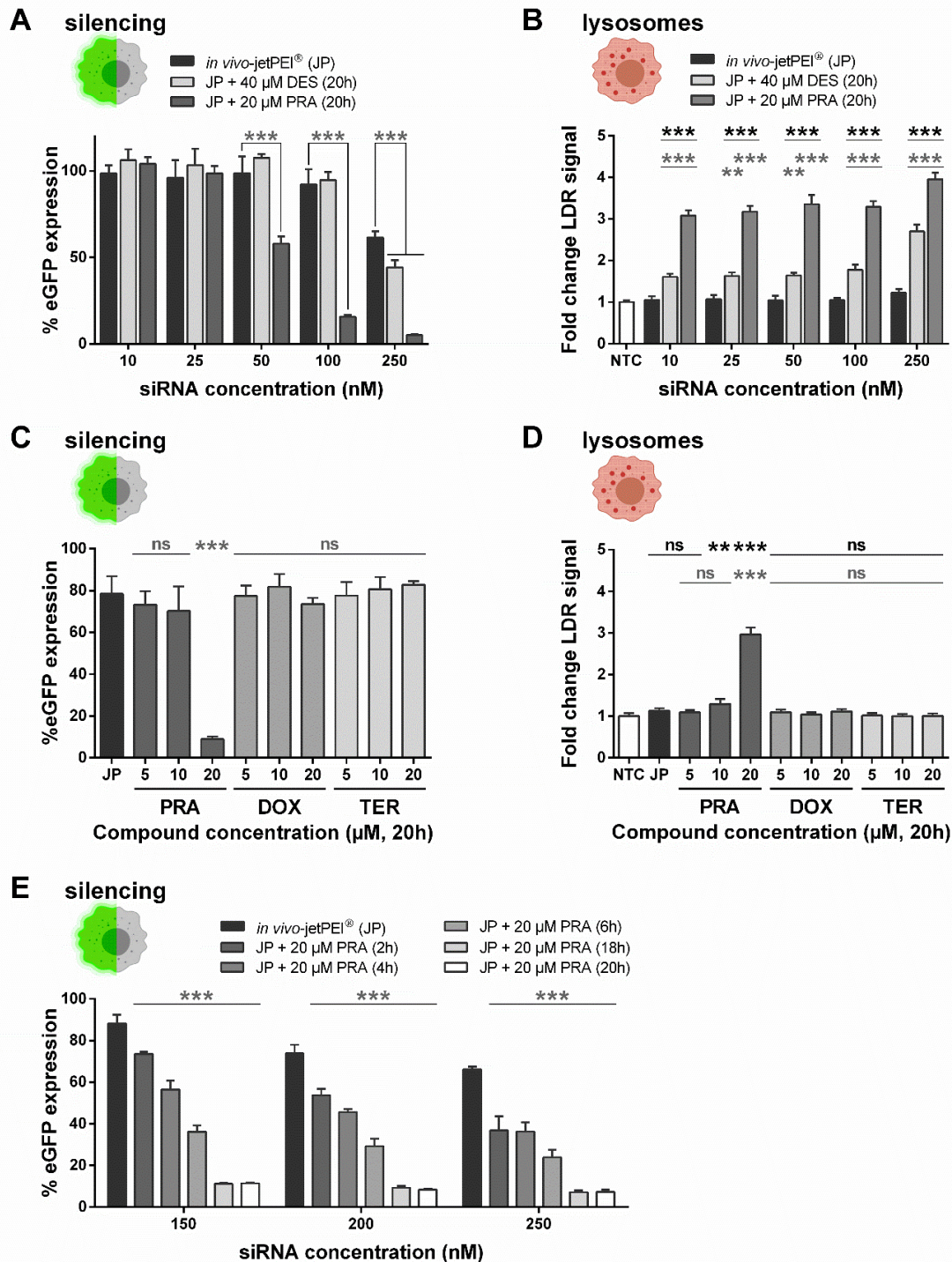


Figure S3. Prazosin, but not desloratadine, doxazosin or terazosin, enhance eGFP silencing potential of *in vivo*-jetPEI® transfected siRNA in full cell culture medium. (A,C,E) Sequential transfection of siRNA in different concentrations (with the commercial polymeric transfection reagent *in vivo*-jetPEI® (JP) for 4 h in serum-containing medium (10% FBS)) and treatment with 20 μM prazosin (PRA, at the indicated incubation times) caused significant additional eGFP silencing, while 20 μM doxazosin (DOX)/20 μM terazosin (TER) and 40 μM desloratadine (DES) had (almost) no effect. In **Figure S3C-D**, 200 nM siRNA was used. (B, D) Fold change in LDR signal, measured *via* flow cytometry, for H1299-eGFP cells sequentially transfected with siRNA-complexed JP and treated with 40 μM DES/20 μM PRA/20 μM DOX/20 μM TER for 20 h. The data are represented as mean ± SD (n =

3, technical replicates). Statistical significance is indicated when appropriate, in black * when referring to the untreated control and in grey * when compared to siRNA:JP transfection alone (ns $p > 0.05$, ** $p \leq 0.01$, *** $p \leq 0.001$). (eGFP = enhanced green fluorescent protein, NTC = not treated control, DES = desloratadine, PRA = prazosin, doxazosin = DOX, TER = terazosin, JP = *in vivo*-jetPEI®, ns = not significant, LDR = LysoTracker® Deep Red).

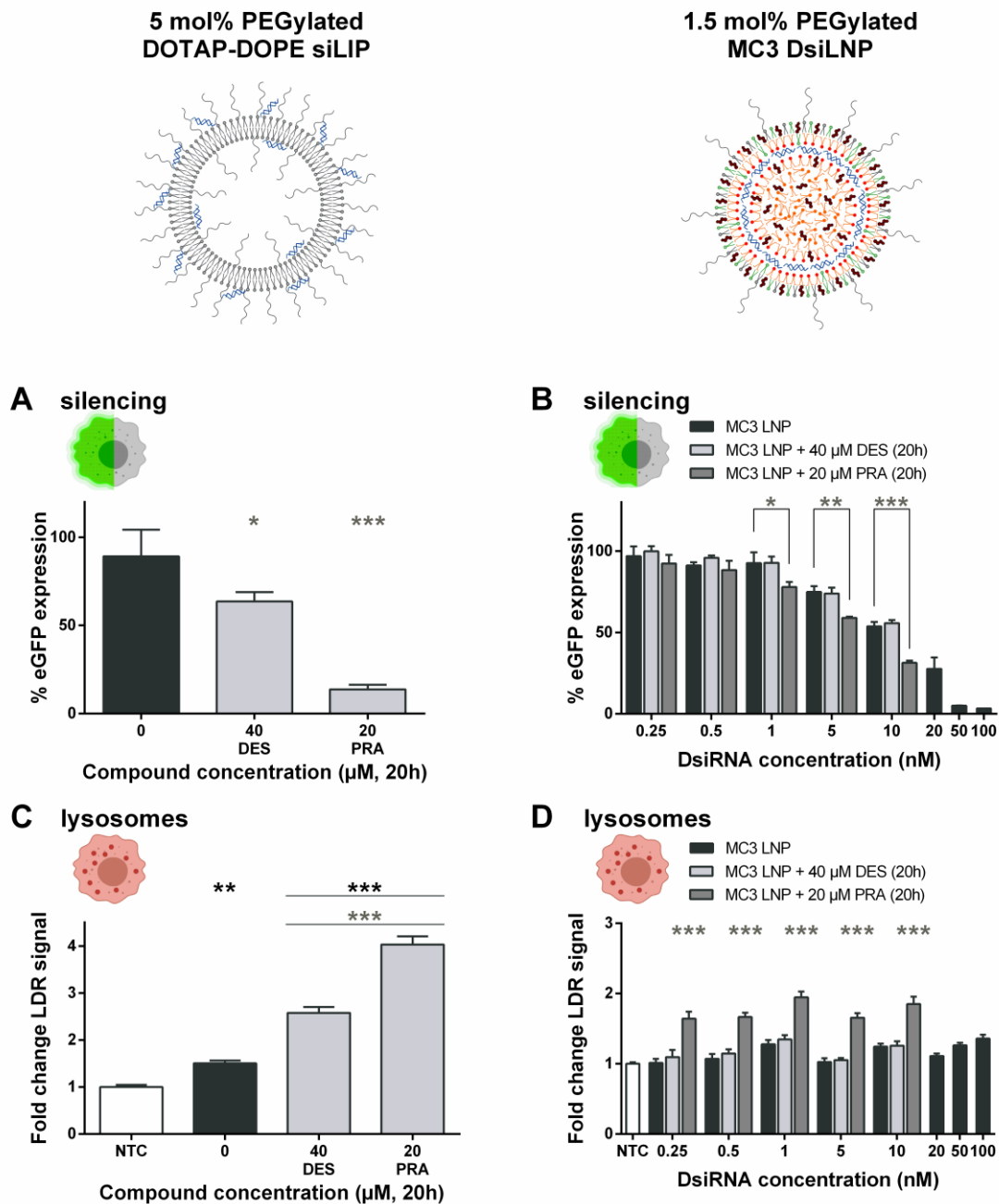


Figure S4. Prazosin outperforms desloratadine in enhancing the eGFP silencing potential of siRNA-loaded PEGylated DOTAP-DOPE liposomes (siLIPs) and siRNA-loaded MC3 LNPs in H1299-eGFP cells. (A-B) The influence of 20 h sequential adjuvant treatment with prazosin (PRA) or desloratadine (DES) on the transfection efficiency of 5 mol% PEGylated DOTAP-DOPE siLIPs (transfection in Opti-MEM®, 50 nM siRNA) or MC3 DsiLNPs (transfection in CCM). (C-D) Fold change in LDR signal, measured *via* flow cytometry, for H1299-eGFP cells sequentially transfected with 5 mol% PEGylated DOTAP-DOPE siLIPs (transfection in Opti-MEM®) or MC3 DsiLNPs (transfection in CCM) and treated with 40 µM DES or 20 µM PRA for 20 h. The data are represented as mean ± SD (n = 3, technical replicates). Statistical significance is indicated when appropriate, in black * when referring to the untreated control and in grey * when compared to transfection alone (* p ≤ 0.05, ** p ≤ 0.01, *** p ≤ 0.001). (eGFP = enhanced green fluorescent protein, NTC = not treated control, siLIPs = siRNA-loaded

liposomes, MC3 DsiLNPs = Dicer substrate siRNA-loaded lipid nanoparticles containing the ionizable lipid DLin-MC3-DMA, DES = desloratadine, PRA = prazosin, LDR = LysoTracker® Deep Red).

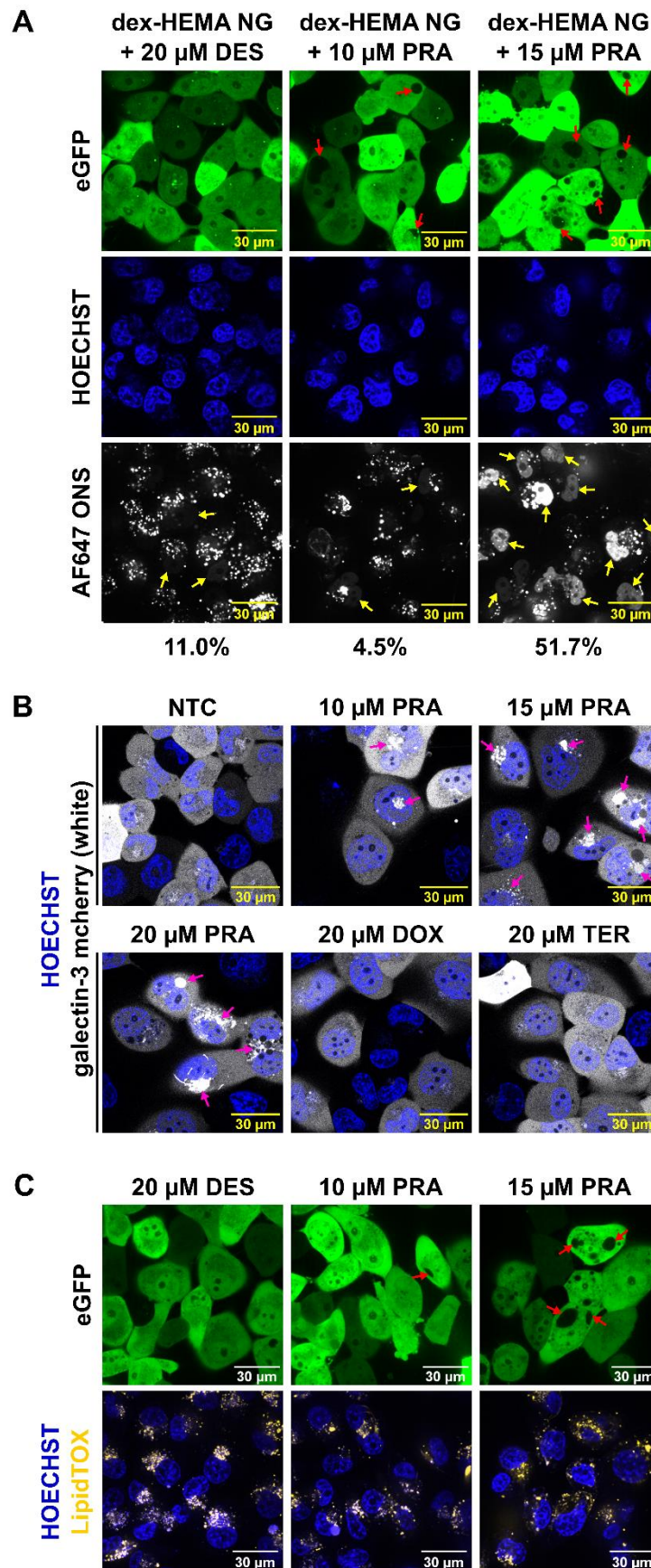
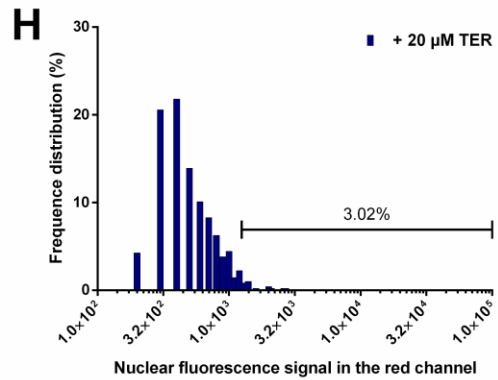
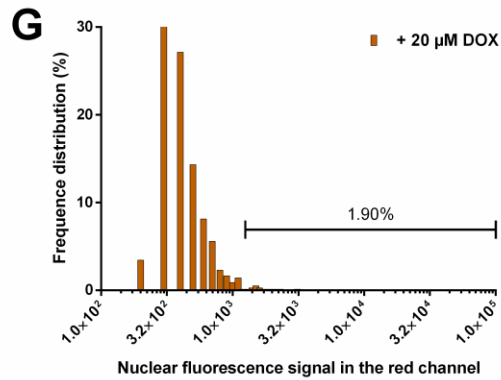
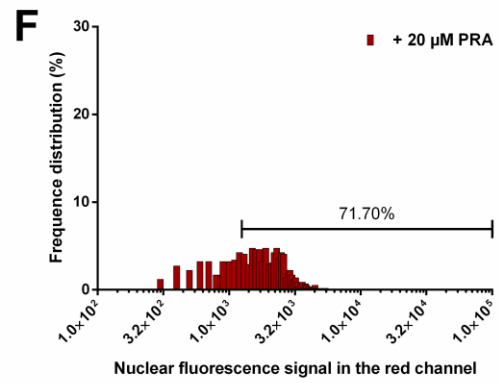
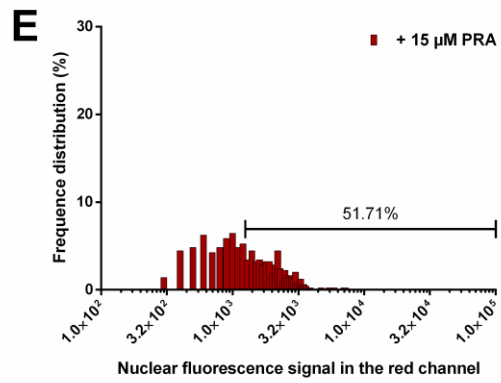
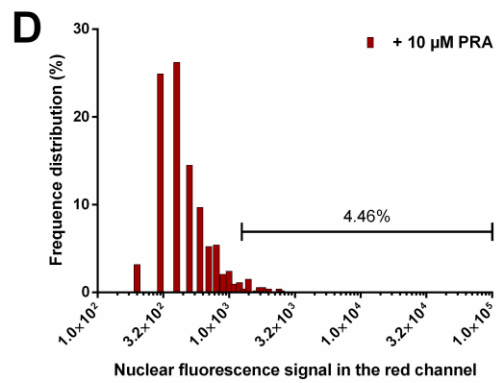
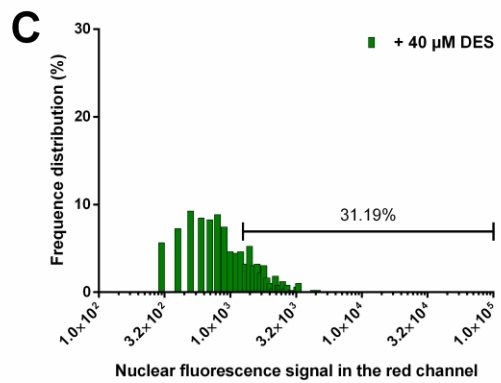
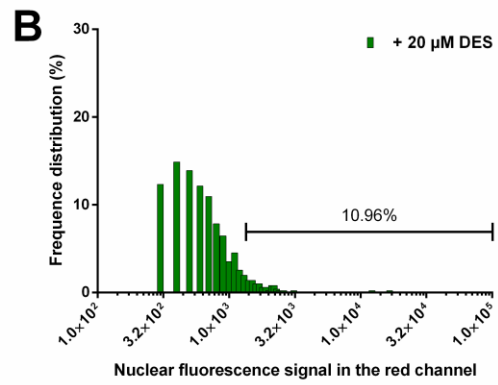
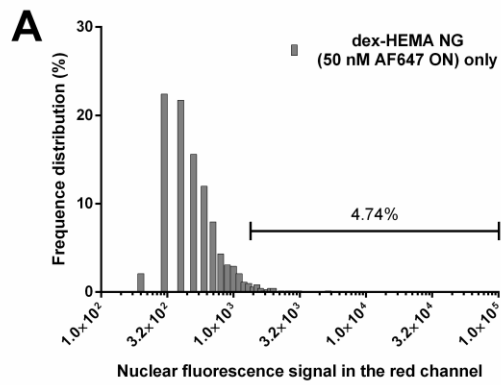


Figure S5. Desloratadine, but not prazosin, doxazosin or terazosin, induces a phospholipidosis phenotype while both desloratadine and prazosin promote oligonucleotide (ON) release from the

endolysosomal compartment in NSCLC cells. (A) Representative confocal images from the intracellular AF647 ON distribution in H1299-eGFP cells, transfected with AF647 ON-loaded dex-HEMA NGs and subsequently incubated with 20 μ M desloratadine (DES)/10-15 μ M prazosin (PRA) for 20 h. Nuclei can be seen in blue, while cells in which endolysosomal escape happened show nuclear fluorescence in the red channel (red fluorescence is depicted white). The values below the images correspond to the percentage of cells with white nuclei (yellow arrows). The red arrows highlight the presence of vacuoles. (B) H1299-WT cells expressing mCherry-galectin-3 were imaged with confocal microscopy after treatment with 10-20 μ M PRA/20 μ M doxazosin (DOX)/20 μ M terazosin (TER) for 20 h. The purple arrows highlight the presence of galectin puncta. (C) Representative confocal images from the phospholipid distribution in H1299-eGFP cells visualized with LipidTOX Red PLD detection reagent in 20 μ M DES/10-15 μ M PRA treated cells (20 h). The scale bar corresponds to 30 μ m. (eGFP = enhanced green fluorescent protein, NTC = not treated control, NG = nanogels, PRA = prazosin, DOX = doxazosin, TER = terazosin, DES = desloratadine, ON = oligonucleotide, AF647 = Alexa Fluor® 647 dye).



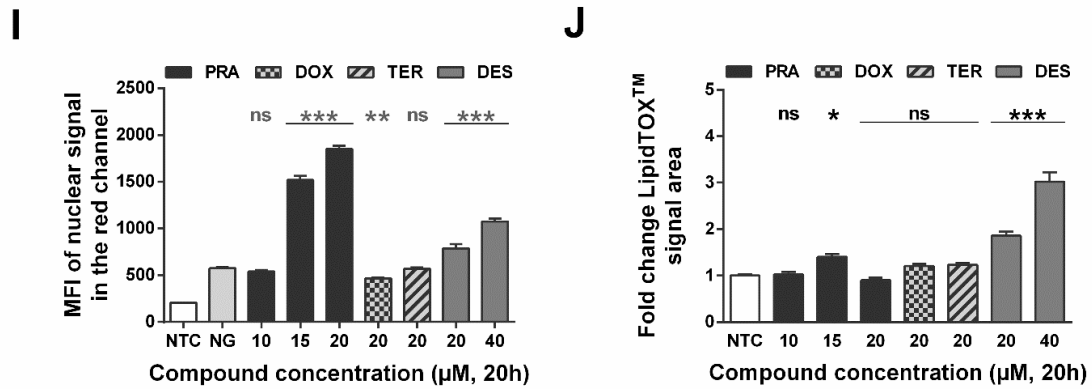


Figure S6. Desloratadine, but not prazosin, doxazosin or terazosin, induces a phospholipidosis phenotype while both desloratadine and prazosin promote cytosolic oligonucleotide (ON) release in NSCLC cells. (A-H) Frequency distributions of the nuclear fluorescence signal in the red channel of all H1299-eGFP cells per condition, quantified from the confocal images in **Figure 3A** and **Figure S5A**. The percentages, determined on the histograms, correspond to the percentage of cells with red nuclei (red fluorescence is depicted white in **Figure 3A** and **Figure S5A**) in which escape has happened. (I) The mean fluorescence intensity (MFI) of the nuclear AF647 ON fluorescence signal in the red channel of all H1299-eGFP cells per condition, quantified from the confocal images in **Figure 3A** and **Figure S5A**. The data are represented as mean \pm the standard error of the mean (SEM). Statistical significance with respect to the dex-HEMA ON-NG transfection alone (grey *) is indicated when appropriate (ns $p > 0.05$, ** $p \leq 0.01$, *** $p \leq 0.001$). (J) Fold increase in LipidTOX™ Red phospholipidosis signal area relative to the untreated control, quantified from the confocal images in **Figure 3B** and **Figure S5C**. The data are represented as mean \pm the standard error of the mean (SEM). Statistical significance with respect to the untreated control (black *) is indicated when appropriate (ns $p > 0.05$, * $p \leq 0.05$, *** $p \leq 0.001$). (MFI = mean fluorescence intensity, NTC = not treated control, NG = dex-HEMA ON-NG transfection without sequential compound treatment, PRA = prazosin, DOX = doxazosin, TER = terazosin, DES = desloratadine, ns = not significant, ON = oligonucleotide, AF647 = Alexa Fluor® 647 dye).

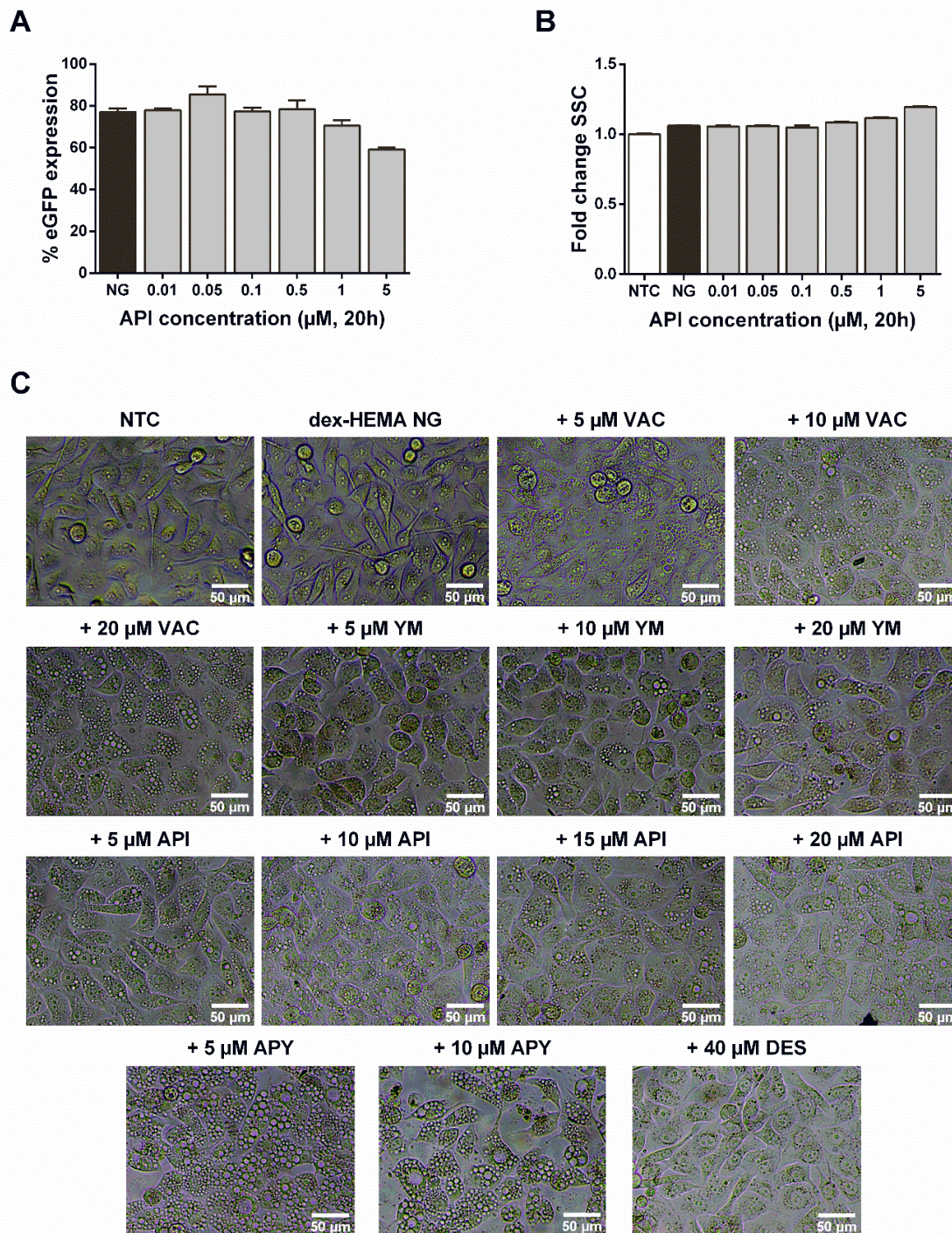


Figure S7. PIKfyve inhibitors induce vacuolization of H1299-eGFP cells in the micromolar range. (A) Sequential treatment of dex-HEMA siNG-transfected H1299-eGFP cells (2 nM siRNA) with the PIKfyve inhibitor apilimod (API) caused additional eGFP silencing starting from 5 μM (20 h incubation). The data are represented as mean ± SD (n = 3, technical replicates). (B) Fold change in side scatter (SSC) signal for H1299-eGFP cells treated with the sequential combination of dex-HEMA siNG transfection and treatment with different nM and μM concentrations of API for 20 h. The data are represented as mean ± SD (n = 3, technical replicates). (C) Representative phase contrast light microscopy images from H1299-eGFP cells, only transfected with dex-HEMA siNGs, or cells subsequently incubated with different micromolar concentrations of the shown compounds for 20 h. Images were taken with a Nikon Eclipse TS100-F inverted microscope, equipped with a digital camera and a 20× objective lens.

The scale bar corresponds to 50 μm . (NTC = not treated control, NG = dex-HEMA siNG transfection without sequential compound treatment, eGFP = enhanced green fluorescent protein, SSC = side scatter, API = apilimod, VAC = vacuolin-1, YM = YM-201636, APY = APY0201, DES = desloratadine).

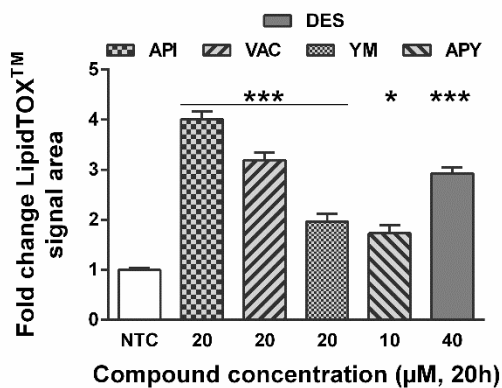
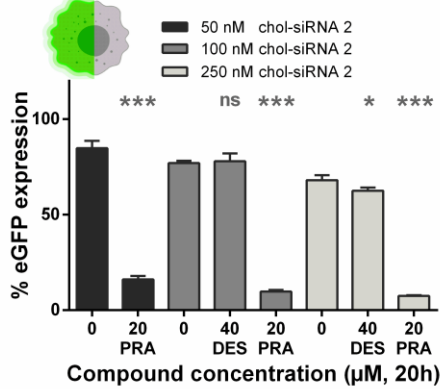


Figure S8. PIKfyve inhibitors induce varying degrees of phospholipidosis. Fold increase in LipidTOX™ Red phospholipidosis signal area relative to the untreated control, quantified from the confocal images in **Figure 5B**. The data are represented as mean \pm the standard error of the mean (SEM). Statistical significance with respect to the untreated control (black *) is indicated when appropriate (* $p \leq 0.05$, *** $p \leq 0.001$). (NTC = not treated control, API = apilimod, VAC = vacuolin-1, YM = YM-201636, APY = APY0201, DES = desloratadine).

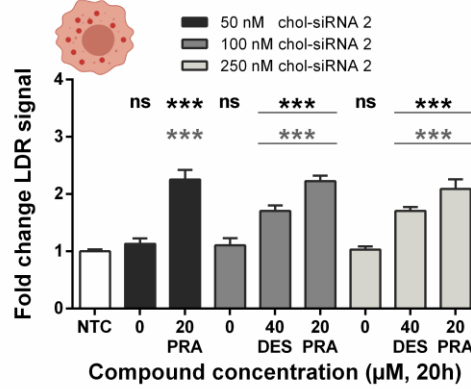
cholesterol-conjugated siRNA



A silencing



B lysosomes



C cellular granularity

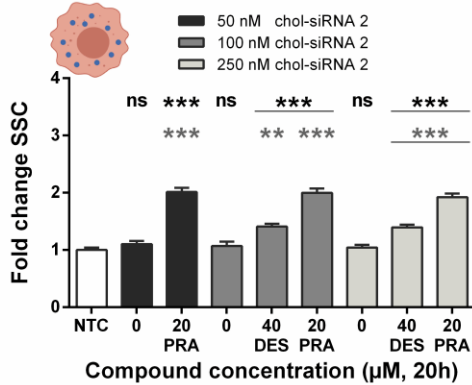


Figure S9. Prazosin, but not desloratadine, enhances eGFP silencing potential of chol-siRNAs in NSCLC cells. (A) Sequential treatment of chol-siRNAs (different concentrations) with 20 μ M prazosin (PRA) caused a significant additional eGFP silencing, while 40 μ M desloratadine (DES) had no effect. (B-C) Fold change in LDR and SSC signal, measured *via* flow cytometry, for H1299-eGFP cells sequentially transfected with chol-siRNAs and treated with 40 μ M DES or 20 μ M PRA for 20 h. The data are represented as mean \pm SD ($n = 3$, technical replicates). Statistical significance is indicated when appropriate, in black * when referring to the untreated control and in grey * when compared to chol-siRNA transfection alone (ns $p > 0.05$, * $p \leq 0.05$, *** $p \leq 0.001$). (eGFP = enhanced green fluorescent protein, NTC = not treated control, DES = desloratadine, PRA = prazosin, ns = not significant, LDR = LysoTracker[®] Deep Red, SSC = side scatter).

SUPPLEMENTARY MATERIALS AND METHODS

Table S2. Applied siRNA/ASO/ON sequences and modifications.

siRNA/ ON	Modification	Manu- facturer	Sequence ^a	
			(Sense) strand (5' > 3')	Antisense strand (5' > 3')
siCTRL ^b	/	Eurogentec	UGCGCUACGAUCGACGAUGtt	CAUCGUCGAUCGUAGCGCAtt
sieGFP ^c	/	Eurogentec	CAAGCUGACCCUGAAGUUCtt	GAACUUCAGGGUCAGCUUGtt
chol- siCTRL 1 ^b	Cholesterol- linked ^d Stabilized ^e	Dharmacon	Not provided	Not provided
chol- siCTRL 2 ^b	Cholesterol- linked Stabilized ^h	Dharmacon	UGGUUUACAUGUCGACUAA non-targeting #1	Not provided
chol- sieGFP 1 ^c	Cholesterol- linked ^d Stabilized ^e	Dharmacon	GCAAGCUGACCCUGAAGUUCUU	GAACUUCAGGGUCAGCUUGCUU
chol- sieGFP 2 ^c	Cholesterol- linked Stabilized ^h	Dharmacon	GCCACAACGUCUAUAUCAU	Not provided
DsieGFP ^c	Not provided	IDT	pACCCUGAAGUUAUCUGCACCCacg	<u>CGGUGGUGCAGAUGAACUUCAGGGUCA</u>
DsiFLuc ^g	Not provided	IDT	pGGUUCUGGAACAAUUGCUUUUAca	<u>UGUAAAAGCAUUGUUCAGGAACCAG</u>
AF647 ON	Alexa Fluor® 647- labeled ^f Phosphorothioate -linked	Eurogentec	gaacttcagggtcagcttggt	N/A

^a p denotes a phosphate residue, lower case letters are 2'-deoxyribonucleotides, capital letters are ribonucleotides and underlined capital letters are 2'-O-methylribonucleotides; ^b negative control siRNA duplex⁴⁻⁷; ^c 21mer siRNA duplex⁴⁻⁷, Dicer substrate asymmetric 25/27mer siRNA duplex⁸⁻¹¹ or chol-siRNA¹²⁻¹⁴ targeting enhanced green fluorescent protein; ^d 5' end of the sense strand modified with a cholesteryl-tetraethyleneglycol linker; ^e siSTABLE modification (Dharmacon); ^f labeled with an Alexa Fluor® 647 dye at the 5' end¹⁵; ^g Dicer substrate asymmetric 25/27mer siRNA duplex targeting luciferase¹⁶⁻¹⁸; ^h Accell modification (Dharmacon).

Galectin-3 puncta assay

H1299-WT cells were seeded at 75000 cells/compartiment in 35mm diameter glass bottom microscopy dishes with 4 compartments (Greiner Bio-One GmbH, Germany) and were allowed to settle overnight. Next, a plasmid encoding mCherry-tagged galectin-3 (pmCherry-Gal3 was a gift from Hemmo Meyer, Addgene plasmid # 85662) was transfected with Lipofectamine[®] 2000 (LF 2000) (Thermo Fisher Scientific, Rockford, USA) according to the manufacturer's guidelines. In brief, LF 2000 and pmCherry-Gal3 dilutions in Opti-MEM[®] were mixed in equal volumes and incubated for 5 minutes at room temperature to allow complexation. Subsequently, the obtained lipoplexes (LPXs) were transfected in Opti-MEM[®] for 4 h at 37 °C. Per compartment, 0.5 µL LF 2000 and 0.25 µg pmCherry-Gal3 was applied. Next, the transfection medium was removed and cells were kept in 0.5 mL fresh CCM. After 20 h, the cells received 0.5 mL fresh CCM, containing different µM concentrations of PRA/DOX/TER or a DMSO control, for 20 h (37 °C, 5% CO₂). After removal of the small molecule-containing CCM, the nuclei were labeled with Hoechst 33342 (Molecular Probes[™], Belgium) in CCM (1 mg/mL in water, 1/1000 dilution) during 15 minutes at 37 °C. Finally, the Hoechst solution was removed, fresh CCM was added and cells were kept at 37 °C in a humidified atmosphere containing 5% CO₂ until imaging (no fixation step was applied). A laser scanning confocal microscope (Nikon A1R HD confocal, Nikon, Japan), equipped with a Plan Apo VC 60× 1.4 NA oil immersion objective lens (Nikon, Japan), a galvoscaner and NIS Elements software (Nikon, Japan) was applied for imaging. The 405 nm and 561 nm laser lines were applied to, respectively, excite the Hoechst labeled nuclei and the fluorescence resulting from the mCherry-tagged galectin-3. Control cells show a diffuse cytosolic fluorescence of the mCherry-tagged galectin-3 protein. If endolysosomal membranes become permeable, the cytosolic galectin-3 protein associates with the carbohydrates on the luminal side of the endolysosomes and a punctate pattern can be observed¹⁹.

***In vivo*-jetPEI[®]-mediated siRNA transfection and sequential adjuvant treatment in H1299-eGFP cells**

In vivo-jetPEI[®] (Polyplus Transfection[®] SA, Illkirch-Graffenstaden, France) is a commercially available linear polyethylenimine (PEI)-based cationic transfection reagent. SiRNA transfection was done according to the manufacturer's guidelines. In brief, *in vivo*-jetPEI[®] (JP) and siRNA (21mer) dilutions in RNase free water with 5% (w/v) glucose were mixed in equal volumes and incubated for 15 minutes at room temperature to allow complexation

(optimal charge ratio of 6²⁰). Subsequently, the obtained polyplexes (PPXs) were transfected in full cell culture medium containing 10% FBS (CCM) as described below. The PPXs were diluted to a concentration corresponding to 250, 200, 100, 50, 25 or 10 nM siRNA.

H1299-eGFP cells were seeded in 96-well plates (VWR, Radnor, USA) at a density of 7500 cells/well in 100 μ L of CCM 24 h prior to transfection. The edge wells were filled with 100 μ L CCM to reduce evaporation in the cell-containing wells. Next, the cells were transfected with JP PPXs (prepared as described above) during 4 hours at 37 °C in a humidified atmosphere containing 5% CO₂. Note that for every sieGFP condition a siCTRL sample was included to account for potential off-target effects. Subsequently, the JP PPX dispersion was removed and the cells received 50 μ L fresh (DMSO control) or compound-containing CCM (maximally 0.08% (v/v) residual DMSO) at the indicated concentrations. After 20 hours, the small molecule containing CCM (and DMSO control) was replaced by fresh CCM and following an additional 24 h incubation, the cells were analysed with flow cytometry as described in main text.

DsiRNA-loaded MC3 lipid nanoparticles (MC3 DsiLNPs): synthesis and transfection

MC3 DsiLNPs were synthesized by injecting one volume of lipid mixture of DLin-MC3-DMA (heptatriaconta-6,9,28,31-tetraen-19-yl 4-(dimethylamino)butanoate, abbreviated as MC3), DSPC (1,2-distearoyl-*sn*-glycero-3-phosphocholine), cholesterol and DMG-PEG₂₀₀₀ (1,2-dimyristoyl-*rac*-glycero-3-methoxypolyethylene glycol-2000) (50:10:38.5:1.5 mol ratio, as previously described) in ethanol and three volumes of DsiRNA (optimal molar N/P charge ratio of 4.7) in acetate buffer (pH 5, 10 mM) in the microfluidic NanoAssemblr[®] Benchtop mixing device (Precision Nanosystems, Vancouver BC, Canada) at a total flow rate of 12 mL/min (3 mL/min for ethanol and 9 mL/min for aqueous buffer, flow rate ratio of 3:1 (aqueous to ethanol)). The resultant mixture (5.8 mg/mL total lipid concentration) was dialyzed (Pur-A-Lyzer[™] Maxi 12000 Dialysis Kit) overnight against phosphate buffered saline (PBS) to remove residual ethanol and to raise the pH to 7.4. MC3 was obtained from Prof. Dan Peer (Laboratory of Precision NanoMedicine, Tel Aviv University, Israel). All other lipids were purchased from Avanti Polar Lipids, Inc. (Alabaster, AL, USA). Samples were stored at 4 °C until use. Transfection (including Lyotracker[®] Deep Red staining and compound treatment) was performed similar to the protocol described in the manuscript main text. In short, MC3 DsiLNPs were diluted in CCM and incubated with the cells overnight (24 h) at 37

°C in a humidified atmosphere containing 5% CO₂, followed by CAD treatment for 20 h. Flow cytometry acquisition was done 20 h after CAD removal.

REFERENCES FOR SUPPORTING INFORMATION

1. Lepri, S. *et al.* Synthesis and Phospholipidosis Effect of a Series of Cationic Amphiphilic Compounds: A Case Study to Evaluate *In Silico* and *In Vitro* Assays. *Med. Chem. Res.* **2018**, *27*, 679–692.
2. *JChem for Office (Excel)*, Version 17.21.0.1797; Software Was Used for Chemical Database Access, Structure Based Property Calculation, Search and Reporting; ChemAxon: Budapest, Hungary, 2017. [Http://www.chemaxon.com](http://www.chemaxon.com).
3. Corsello, S. M. *et al.* The Drug Repurposing Hub: A next-Generation Drug Library and Information Resource. *Nat. Med.* **2017**, *23*, 405–408.
4. Joris, F. *et al.* Repurposing Cationic Amphiphilic Drugs as Adjuvants to Induce Lysosomal SiRNA Escape in Nanogel Transfected Cells. *J. Control. Release* **2018**, *269*, 266–276.
5. Merckx, P. *et al.* Surfactant Protein B (SP-B) Enhances the Cellular SiRNA Delivery of Proteolipid Coated Nanogels for Inhalation Therapy. *Acta Biomater.* **2018**, *78*, 236–246.
6. De Backer, L.; Braeckmans, K.; Demeester, J.; De Smedt, S. C.; Raemdonck, K. The Influence of Natural Pulmonary Surfactant on the Efficacy of SiRNA-Loaded Dextran Nanogels. *Nanomedicine* **2013**, *8*, 1625–1638.
7. De Backer, L. *et al.* Bio-Inspired Pulmonary Surfactant-Modified Nanogels: A Promising SiRNA Delivery System. *J. Control. Release* **2015**, *206*, 177–186.
8. Xie, Y.; Killinger, B.; Moszczynska, A.; Merkel, O. M. Targeted Delivery of SiRNA to Transferrin Receptor Overexpressing Tumor Cells *via* Peptide Modified Polyethylenimine. *Molecules* **2016**, *21*, 1334.
9. Gupta, K. *et al.* Oxime Ether Lipids Containing Hydroxylated Head Groups Are More Superior SiRNA Delivery Agents than Their Nonhydroxylated Counterparts. *Nanomedicine* **2015**, *10*, 2805–2818.
10. Marques, J. T. *et al.* A Structural Basis for Discriminating between Self and Nonspecific Double-Stranded RNAs in Mammalian Cells. *Nat. Biotechnol.* **2006**, *24*, 559–565.
11. Naeye, B. *et al.* PEGylation of Biodegradable Dextran Nanogels for SiRNA Delivery. *Eur. J. Pharm. Sci.* **2010**, *40*, 342–351.
12. Du Rietz, H.; Hedlund, H.; Wilhelmson, S.; Nordenfelt, P.; Wittrup, A. Imaging Small Molecule-Induced Endosomal Escape of SiRNA. *Nat. Commun.* **2020**, *11*, 1809.
13. Castanotto, D. *et al.* Protein Kinase C- α Is a Critical Protein for Antisense Oligonucleotide-Mediated Silencing in Mammalian Cells. *Mol. Ther.* **2016**, *24*, 1117–1125.
14. Yang, B. *et al.* High-Throughput Screening Identifies Small Molecules That Enhance the Pharmacological Effects of Oligonucleotides. *Nucleic Acids Res.* **2015**, *43*, 1987–1996.
15. Vermeulen, L. M. P. *et al.* Endosomal Size and Membrane Leakiness Influence Proton Sponge-Based Rupture of Endosomal Vesicles. *ACS Nano* **2018**, *12*, 2332–2345.
16. Zeng, X. *et al.* Surface Coating of SiRNA-Peptidomimetic Nano-Self-Assemblies with Anionic Lipid Bilayers: Enhanced Gene Silencing and Reduced Adverse Effects *in Vitro*. *Nanoscale* **2015**, *7*, 19687–19698.
17. Jensen, D. M. K. *et al.* Spray Drying of SiRNA-Containing PLGA Nanoparticles Intended for Inhalation. *J. Control. Release* **2010**, *142*, 138–145.
18. Bohr, A. *et al.* Anti-Inflammatory Effect of Anti-TNF- α SiRNA Cationic Phosphorus Dendrimer Nanocomplexes Administered Intranasally in a Murine Acute Lung Injury Model. *Biomacromolecules* **2017**, *18*, 2379–2388.
19. Thurston, T. L. M.; Wandel, M. P.; Von Muhlinen, N.; Foeglein, Á.; Randow, F. Galectin 8 Targets Damaged Vesicles for Autophagy to Defend Cells against Bacterial Invasion. *Nature* **2012**, *482*, 414–418.
20. Zhang, T.; Bai, X.; Mao, X. Systemic Delivery of Small Interfering RNA Targeting the Interleukin-2/15 Receptor β Chain Prevents Disease Progression in Experimental Arthritis. *PLoS One* **2013**, *8*, e78619.

Chapter 5

Broader international context, relevance and future perspectives

Thijs Van de Vyver[†], Stefaan C. De Smedt[†], Koen Raemdonck[†]

[†] Ghent Research Group on Nanomedicines, Laboratory of General Biochemistry and Physical Pharmacy, Faculty of Pharmaceutical Sciences, Department of Pharmaceutics, Ghent University, Ottergemsesteenweg 460, 9000 Ghent, Belgium

Author contributions

Chapter 5 was written by T.V.d.V. and K. Raemdonck.

TABLE OF CONTENTS

1. RNAi THERAPEUTICS AND THE INDUSTRY: THE OBSTACLE IS THE WAY.....	257
2. DELIVERY IS KEY.....	261
2.1. Going beyond the liver, where are we?.....	261
2.2. Addressing the ongoing challenges	264
3. DRUG REPURPOSING: OLD DRUGS, NEW TRICKS	265
4. HOW TO PROCEED WITH (CAD) ADJUVANT EFFECT?	269
4.1. Recommendations for future (repurposing library) screenings.....	269
4.2. Exact mechanism and general effects on cells	270
4.3. Broader applicability	271
4.3.1. Cell types	271
4.3.2. Compatible nanocarriers and drug payloads?.....	272
4.4. Bridging <i>in vitro-in vivo</i> gap.....	273
5. CONCLUSION.....	276

ABSTRACT

In this thesis, we have described a drug repurposing screen to identify small molecules that enhance the intracellular delivery potential of siRNA-loaded polymeric nanogels in a non-small cell lung cancer (NSCLC) cell model (**Chapter 2**). Given that the majority of the hits are physicochemical related compounds called cationic amphiphilic drugs (CADs), we further evaluated the broader applicability of this CAD-induced adjuvant effect in **Chapter 3**. Most importantly, we highlighted that the CAD adjuvant effect on siRNA delivery is dependent on the type of nanocarrier, with nanoparticles (NPs) that generate an appropriate pool of decomplexed siRNA in the endolysosomal compartment being most susceptible to CAD-promoted gene silencing. Finally, in **Chapter 4**, we described the effect of the α 1-adrenergic antagonist prazosin on intracellular siRNA delivery in more detail. Prazosin, which does not have the typical characteristics of a CAD, was previously identified as the most potent hit compound in the screen (**Chapter 2**). In this final chapter, we aim to discuss the broader international context of the RNA interference (RNAi) field of research, the relevance of our findings and the current prospects for the described small molecule adjuvant concept. Hereto, we first look into the history and clinical development of siRNA-based therapeutics, underscoring the multiple obstacles that had to be overcome to bring these products to the market. We further focus on the remaining “delivery problem”. Indeed, although the regulatory approval of the first siRNA-based drugs paves the way for other formulations, the need for extrahepatic applications becomes increasingly clear. In addition, we also discuss the concept of drug repurposing. Finally, we identify the outstanding questions regarding our work and we suggest how research on the adjuvant concept could be continued, with a focus on bridging the gap between fundamental (*in vitro*) and applied (*in vivo*) research.

1. RNAi THERAPEUTICS AND THE INDUSTRY: THE OBSTACLE IS THE WAY

Despite the recent approval of several siRNA-based therapeutics, the pharmaceutical development of these drugs went through several ups and downs¹, which is graphically represented in **Figure 1** by the stock curve of Alnylam Pharmaceuticals, the current leading RNAi company². Indeed, this curve and several crucial milestones in the development of RNAi therapeutics can be easily mapped to the Gartner Hype Cycle, which shows that the RNAi technology passed through several phases (*e.g.* 'technology trigger', 'peak of inflated expectations', 'trough of disillusionment' and 'slope of enlightenment') before approaching a 'plateau of productivity' today^{2,3}. We will discuss each of these key events in more detail and highlight how this turbulent history has impacted the current RNAi drug pipelines¹.

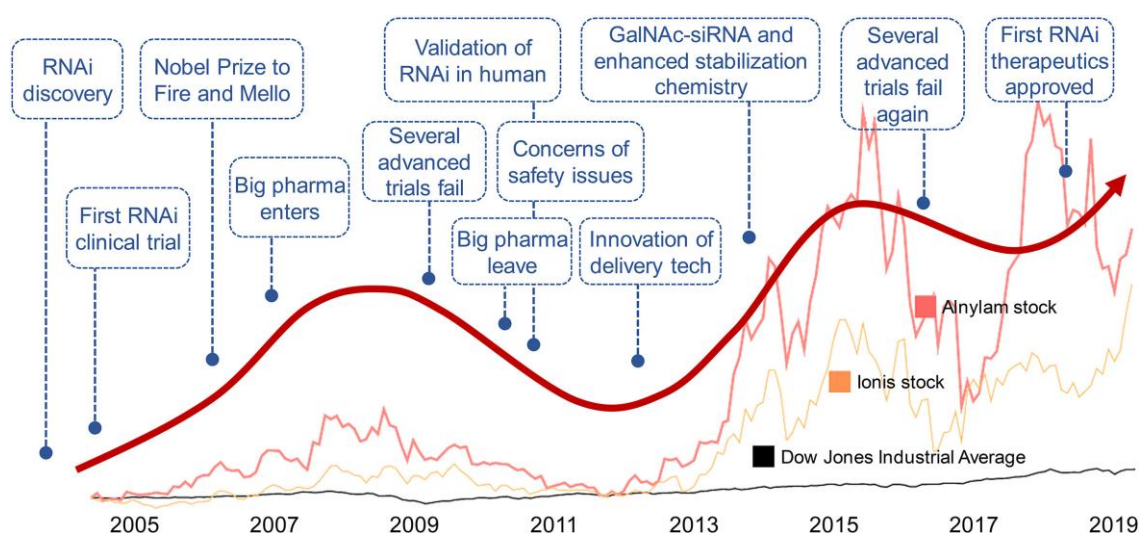


Figure 1. Key events in the development history of RNAi therapeutics, mapped to Alnylam's (light red) stock curves and a fitted Gartner Hype Cycle. The stock curve of Ionis (orange), a leading company in the development of antisense oligonucleotides is shown as a comparison. Adapted from².

In 1998, Andrew Fire and Craig Mello reported in *Nature* that double-stranded RNAs (dsRNAs) could induce transient post-transcriptional silencing of target genes after injection in the nematode *Caenorhabditis elegans*⁴. Three years later, both Elbashir *et al.*⁵ and Caplen *et al.*⁶ provided evidence that the application of 21- to 22-nucleotide siRNAs could replicate the observed gene knockdown phenomenon in mammalian and human cells. These findings were soon followed by an abundance of studies that investigated the molecular mechanism

involved in RNAi and how differing RNAi triggers could harness this pathway for both functional genomics and therapeutic applications^{2,7}. Indeed, a first milestone was the successful *in vivo* use of the RNAi technology in mice⁸, and afterwards non-human primates⁹, highlighting the potential of siRNAs as therapeutic agents. The prospect that siRNA drugs could specifically and safely silence virtually any disease-causing gene, fostered the investment of several (newly founded) biotech companies (*e.g.* SiRNA Therapeutics, Alnylam Pharmaceuticals) in advancing RNAi into the clinic⁷.

In 2006, both Fire and Mello were granted the Nobel Prize in Physiology and Medicine¹⁰, which, in conjunction with the growing *in vitro* and *in vivo* evidence^{9,11,12}, attracted several 'Big Pharma' companies to invest in the field in various ways. Merck & Co. bought SiRNA Therapeutics for over US\$1.1 billion and Takeda, Roche and Novartis partnered with Alnylam by paying billions of dollars (~ US\$2.5 - 3.5 billion) for non-exclusive rights on their intellectual property^{1,2}. In addition, Pfizer and Abbott started their own independent RNAi units¹. In this early enthusiasm, the big pharmaceutical companies anticipated that the RNAi technology could rapidly amplify their drug pipelines and lower the ever-growing costs and timelines required for the discovery and development of new (small molecule) drugs^{1,13}.

However, a series of events between 2008 and 2012 soon shattered the high expectations of the industry². First, Kleinman *et al.* questioned the efficacy of Bevasiranib (the first siRNA therapeutic that entered clinical trials in 2004) and AGN211745, two intravitreally injected naked siRNAs that respectively targeted vascular endothelial growth factor-A or its receptor VEGFR1 for the potential treatment of age-related macular degeneration¹⁴. The authors demonstrated that the anti-angiogenic effects of the siRNAs in question were caused by a non-specific activation of the innate immune system, rather than sequence-specific silencing of the intended target. In addition, the first clinical trials of systemically administered siRNA formulations likewise raised significant concerns about dose-limiting toxicities, insufficient efficacy and immune activation^{2,7}.

"Is RNAi Dead?"

Arthur M. Krieg in an editorial of *Molecular Therapy* (2011)¹³

As a result of such findings, and in the aftermath of the economic recession in 2008, the major pharmaceutical companies realized that a quick return on investment was not within

reach^{2,7}. They had overestimated the druggability of siRNA molecules and without a proper delivery technology, which was not available at the time, RNAi was doomed to fail as a clinical tool¹⁵. Investors lost their confidence in the technology and in 2010 both Roche and Novartis terminated their partnerships with Alnylam¹⁶. Pfizer and Abbott closed down their in-house RNAi units the next year and Merck finally sold their RNAi activities to Alnylam in 2014¹. Notably, Alnylam paid less than 20% of the price Merck had paid in 2006 to acquire SiRNA Therapeutics¹⁷.

On the contrary, academia and smaller RNAi-focused biotechnology companies, such as Alnylam, Arbutus (formerly known as Tekmira), Arrowhead, Dicerna, Silence, *etc.*, did not abandon their hope in RNAi as a therapeutic tool^{1,2,7}. Guided by the lessons learned from the early clinical failures, researchers persisted to overcome the inherent barriers of the technology⁷. By introducing chemical modifications of the RNA strands, the stability, target specificity and immunogenicity of the siRNA molecules was significantly improved². Further advances in sequence selection led to reduced off-target effects. Additionally, the growing awareness that the poor *in vivo* delivery was the main bottleneck in the realization of therapeutic RNAi-based products, stimulated the development of safer and more effective delivery systems⁷. Finally, the finding that the majority of intravenously administered siRNA-based drugs accumulates in the liver, shifted the attention of the RNAi biotech to hepatic disease indications aiming to increase the chances of therapeutic success^{7,18}.

In 2010, phase I and/or II clinical trials with RNAi drug candidates such as ALN-RSV01¹⁹ (Alnylam) and CALAA01²⁰ (Arrowhead) confidently showed that siRNA molecules produced their therapeutic effect *via* the sequence-specific RNAi silencing mechanism instead of the previously ascribed off-target immune activation². Meanwhile, Tekmira Pharmaceuticals (currently Arbutus Biopharma) completed their phase I clinical trial for the treatment of hypercholesterolemia with an anti-apolipoprotein B siRNA that was formulated in a stable nucleic acid-lipid nanoparticle (SNALP)²¹. Following licensing of this SNALP technology²², also Alnylam started phase I clinical trials with ALN-TTR01 and ALN-TTR02 (Patisiran) for the treatment of hATTR amyloidosis²³. Overall, ALN-TTR02, which contained a second-generation ionizable lipid (DLin-MC3-DMA), had a better safety profile and was more potent than ALN-TTR01, a first-generation siRNA-loaded lipid nanoparticle (LNP)^{2,7}. Hence, Alnylam terminated the development of ALN-TTR01 and Patisiran was further developed and finally tested in the phase III, double-blind, placebo-controlled APOLLO clinical trial that

demonstrated impressive safety and efficacy in patients with hATTR²⁴. Consequently, Patisiran gained regulatory FDA and EMA approval as Onpattro[®] in 2018^{22,25,26}.

Despite the considerable advances made with LNP-based siRNA therapies, those drugs require intravenous (I.V.) administration and pre-treatment with corticosteroids to attenuate infusion reactions^{7,27}. Hence, Alnylam, Dicerna and Arrowhead invested early on in the research of N-acetylgalactosamine (GalNAc)-conjugated ‘naked’ RNAi triggers, which have a much more convenient dosing and delivery regimen²⁷, given that they are injected subcutaneously (S.C.)⁷. As the GalNAc ligands bind to the asialoglycoprotein receptor (ASGPR), which is highly expressed on hepatocytes, these conjugates also mainly function in the liver, which explains the current liver disease-related RNAi drug pipelines^{28,29}. However, in 2016, Alnylam terminated its phase III trial of Revusiran, a first-generation GalNAc-conjugated siRNA for the same indication as Patisiran, due to an excess mortality in the treatment group¹⁶. To make matters worse, also Arrowhead discontinued the development of their RNAi therapeutic candidates relying on the dynamic polyconjugate (DPC)iv[™] delivery system². These events once again led to disillusionment in the field. Nevertheless, these products relied on chemical modifications and delivery systems of the first generation^{2,30}. Further improvements such as the ‘enhanced stability chemistries’ (ESCs) allowed the follow-on GalNAc-siRNA formulations to be administered at dramatically lower doses³⁰, which finally resulted in the approvals of Givlaari[®] and Oxlumo[™] in 2020^{31,32}.

Taken together, the companies (*e.g.* Alnylam) that stayed on the RNAi train when the ‘Big Pharma’ lost its faith in RNAi in the beginning of the 2010s, are now harvesting the fruits of their hard work^{22,33}. Although current clinical drug (candidates) mainly target rare diseases, Alnylam/Novartis’s PCSK9 inhibitor Inclisiran, for the treatment of hypercholesterolemia, has very recently obtained EMA approval (still awaiting FDA approval)³⁴ and will impact significantly larger patient populations⁷. Interestingly, Inclisiran requires administration only twice a year, while existing anti-PCSK9 monoclonal antibodies should be injected 12-26 times per year to maintain low low-density lipoprotein cholesterol (LDL-C) levels³⁵. In addition, it will be interesting to see how siRNA drugs will compete clinically with gapmer antisense oligonucleotides (ASO), as both technologies rely on gene knockdown *via* sequence-specific mRNA degradation (*e.g.* Ionis Pharmaceuticals’ inotersen (an ASO) vs. Patisiran)^{22,36}. Finally, the gained experience from siRNA drug development will likely accelerate the progression of newly emerging technologies such mRNA therapeutics and

clustered regularly interspaced short palindromic repeats (CRISPR)-based products²⁷. Indeed, the first nucleic acid (NA)-based lipid nanoparticle (NP) drug Patisiran undoubtedly contributed to the LNP-based COVID-19 mRNA vaccines of BioNTech/Pfizer and Moderna that are waiting to get regulatory approval at the time of writing³⁷.

2. DELIVERY IS KEY

2.1. Going beyond the liver, where are we?

The siRNA drugs that are approved or currently in a phase III clinical trial (**Table 1**) mostly target either the liver, upon systemic administration, or the eye by local application (topical or intravitreal injection)^{2,38}. Indeed, given the preferential hepatic accumulation of (L)NPs and GalNAC-conjugates *via* respectively passive and active mechanisms (see **Chapter 1** and above), it is not surprisingly that the industry exploited this ‘limitation’ to select liver-related diseases as the number one targets for I.V. or S.C. administrated RNAi therapeutics⁷. Notably, only one systemically applied phase III-advanced siRNA drug (QPI-1002, a naked modified siRNA) does not target hepatic cells but is clinically tested for the treatment of acute kidney injury or delayed graft function².

Table 1. Overview of siRNA therapeutics that are approved or in phase III clinical development^{2,38}.

Name	Condition(s)	Target	Product & administration	Sponsor	Current status
Patisiran (ALN-TTR02)	hATTR amyloidosis	TTR	LNP containing siRNA I.V.	Alnylam Pharmaceuticals	Approved in 2018 by FDA and EMA; Marketed as Onpattro®
Givosiran (ALN-AS1)	Acute hepatic porphyria	ALAS1	GalNAC-conjugate siRNA S.C.	Alnylam Pharmaceuticals	Approved in 2019/2020 by FDA and EMA; Marketed as Givlaari®
Lumasiran (ALN-GO1)	Primary hyperoxaluria type 1 (PH1)	HAO1	GalNAC-conjugate siRNA S.C.	Alnylam Pharmaceuticals	Approved in 2020 by FDA and EMA; Marketed as Oxlumo™
Inclisiran (ALN-PCSSc)	Primary hypercholesterolemia or mixed dyslipidaemia	PCSK9	GalNAC-conjugate siRNA S.C.	Alnylam Pharmaceuticals - Novartis partnership	Approved in 2020 by EMA; Marketed as Leqvio®
Vutrisiran (ALN-TTRSC02)	hATTR amyloidosis	TTR	GalNAC-conjugate siRNA S.C.	Alnylam Pharmaceuticals	Phase III

Fitusiran (ALN-AT3SC)	Hemophilia A and B	AT	GalNAc- conjugate siRNA S.C.	Alnylam Pharmaceuticals – Sanofi Genzyme partnership	Phase III
Nedosiran (DCR-PHXC)	Primary hyperoxaluria	LDHA	GalNAc- conjugate siRNA S.C.	Dicerna	Phase III
ARO-AAT	Alpha-1 antitrypsin deficiency	AAT	GalNAc- conjugate siRNA S.C.	Arrowhead Takeda	Phase III
QPI-1002 (I5NP or Teprasiran)	Delayed graft function and other complications of kidney transplant	p53	Naked siRNA I.V.	Quark Pharmaceuticals	Phase III
QPI-1007	Non-arteritic anterior ischemic optic neuropathy (NAION)	Caspase-2	Naked siRNA Intravitreal	Quark Pharmaceuticals	Phase III terminated
Tivanisiran (SYL1001)	Dry eye syndrome	TRVP1	Naked siRNA Eye drops	Sylentis, S.A.	Phase III completed

hATTR = hereditary transthyretin, TTR = transthyretin, ALAS1 = delta-aminolevulinic acid synthase 1, HAO1 = hydroxyacid oxidase 1, PCSK9 = proprotein convertase subtilisin/kexin type 9, AT = antithrombin, TRVP1 = transient receptor potential cation channel subfamily V member 1, LDHA = lactate dehydrogenase A, AAT = alpha-1 antitrypsin, I.V. = intravenous, S.C. = subcutaneous, GalNAc = N-acetylgalactosamine

Upon further inspection of the RNAi drug candidates in early clinical or preclinical development (**Figure 2**), it is evident that the majority of the current applications remains restricted to easily accessible tissues (*e.g.* eye, skin) *via* local application or the liver following systemic administration^{2,38}. Indeed, in case of local delivery, the liver can be circumvented, which lowers the risk of adverse effects, while increasing the availability of the siRNA drug at the target site⁷. The eye is one of the most targeted tissues, which can be explained by its low nuclease activity and the fact that the eye is an immunologically privileged site^{38–40}. Quark Pharmaceuticals has two intravitreally injected naked siRNAs in late clinical trials (QPI-1007 and PF-655), while Sylentis, S.A. uses topical application (*i.e.* eye drops) for their naked siRNA drug candidates Tivanisiran (SYL1001) and Bamosiran (SYL040012)². Next to ocular delivery, also the skin is an interesting target, given its large surface area and the ease of administration³⁸. Both topically applied and intradermally injected formulations are currently being tested in clinical trials². Finally, other notable examples of locally delivered RNAi-based drugs are siG12D-LODER™ of Silenseed and CEQ508 of Marina Biotech. The former is an anti-KRAS siRNA, encapsulated in a PLGA polymer matrix, that is surgically implanted in pancreatic ductal adenocarcinoma tumors

and which has shown promising anti-cancer effects in combination with chemotherapy in a small phase I/II clinical trial⁴¹. The latter is an orally administered live-attenuated *Escherichia coli* that is genetically modified to produce and deliver anti- β -catenin shRNAs to the mucosal lining of the intestines⁴². Despite their promising results in early clinical stages, it will be interesting to see how such approaches will perform in phase III trials.

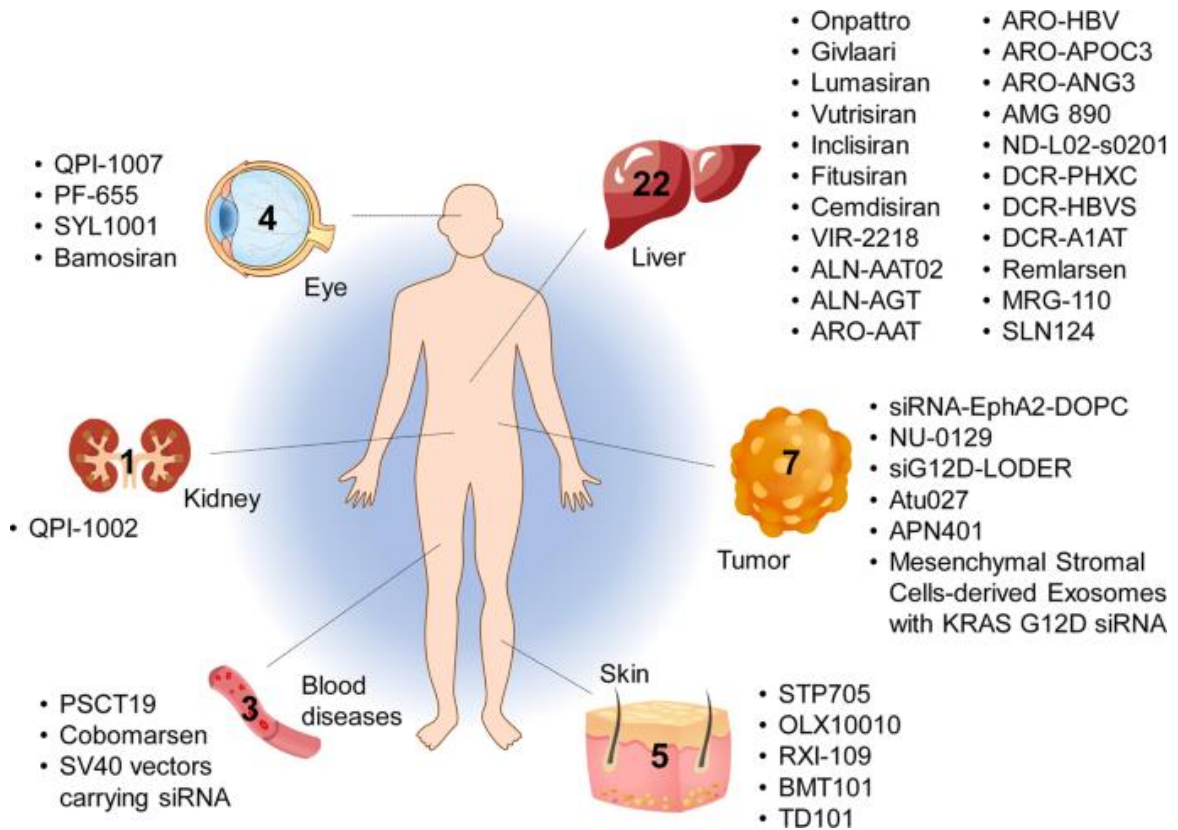


Figure 2. Target organs/tissues of siRNA and miRNA therapeutics currently being tested at different clinical stages. The therapeutic names of each of the RNAi candidates are shown next to the tissues of interest. Adapted from Hu *et al.*³⁸.

In this dissertation, we predominantly used a non-small cell lung cancer (NSCLC) cell type and a dextran nanogel siRNA delivery system in an *in vitro* setting⁴³. Notably, our group previously provided proof-of-concept that such siRNA-loaded nanogels can significantly produce siRNA knockdown *in vivo* upon local pulmonary delivery, at least if these NPs were coated with a proteolipid shell of either clinical pulmonary surfactant (PSurf)⁴⁴ or a PSurf-inspired mimic⁴⁵. As several CADs are available as dry powder inhalators or pressurized metered-dose inhalers⁴⁶, an *in vivo* inhalation strategy with the proposed adjuvant approach

could be envisioned⁴⁷. Indeed, the lung is an attractive target tissue, given that several lung(-related) diseases (*e.g.* asthma, chronic obstructive pulmonary disease, pulmonary fibrosis, lung cancer, *etc.*) originate from or are characterized by an elevated transcription of certain genes^{48–50}. In addition, an inhalation therapy would be much more convenient than systemic administration^{48,51}. However, to date, there is only one RNAi drug (ARO-ENaC, Arrowhead) in clinical development for local lung delivery and early clinical trials from Alnylam with a siRNA candidate against RSV (ALN-RSV01) were discontinued before phase III². Nevertheless, this could change rapidly as ALN-COV, the inhaled COVID-19 siRNA therapeutic candidate of Vir Biotechnology and Alnylam Pharmaceuticals, has shown to be effective in preclinical studies (by targeting a sequence in the SARS-CoV-2 genome)⁵¹.

2.2. Addressing the ongoing challenges

Despite the clear successes with the current generation of siRNA drugs for liver-related diseases, it is also evident that RNAi therapeutics could have a greatly extended impact if extrahepatic delivery becomes a clinical reality for systemically administrated formulations⁷. Hence, advanced delivery methods that lead to a higher efficacy in difficult to reach organs/tissues are still highly sought after. To enhance the potency and the safety of the next generation of RNAi formulations (or other NA drugs such as mRNA), current research especially focuses on techniques for improved systemic circulation^{52,53} and targeted delivery⁷. However, in contrast to the GalNAc-conjugates which benefited from the extremely high hepatic expression of the target receptor, other ligand-targeting approaches only had a limited success⁵⁴. Interestingly, a growing number of literature reports provided evidence that non-liver delivery is feasible in both mice and non-human primates with NPs that do not contain an active targeting ligand, but rather have differing physicochemical properties (*e.g.* different shape, size, zeta-potential, *etc.*)^{55–59}. We anticipate that specific delivery of NA molecules to non-liver tissues such as lung, muscle, brain, heart, *etc.* will continue to emerge, as the tools to identify NPs or conjugates with a tropism to new cells/tissues are now available (*e.g.* high-throughput *in vivo* assays⁶⁰, see **Chapter 1**).

In addition, as discussed throughout this thesis, endosomal escape remains a major barrier for NA therapeutics, certainly in those tissues and cell types where only a limited amount of drug accumulates^{7,61}. Boosting the intracellular delivery of the NA molecules (**Chapter 1**) might overall enhance the efficacy of the next-generation NA drugs (for both local and systemic administration)⁷. In this context, the use of small molecular adjuvants

that alleviate specific barriers within the NA delivery process, might pose an exciting alternative to the conventional NA delivery solutions⁶². Most importantly, if such adjuvants are existing drugs, a faster clinical translation could potentially be obtained⁶².

3. DRUG REPURPOSING: OLD DRUGS, NEW TRICKS

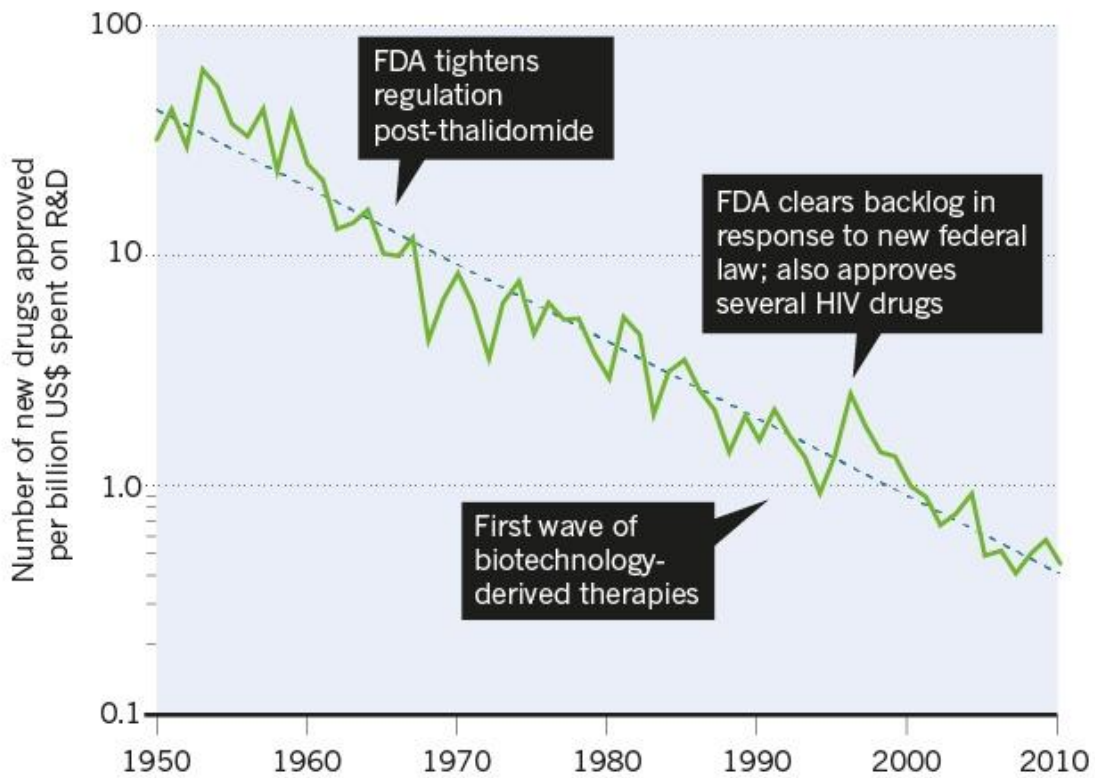
The strategy of identifying new uses for previously approved, withdrawn or abandoned drugs, or even initially failed investigational drugs, beyond their original therapeutic indication is known as drug repositioning (also called drug repurposing, reprofiling, re-tasking or rescue), a term first introduced by Ashburn and Thor in 2004⁶³. However, as discussed below, the concept was not new at the time, given the various examples of earlier repurposed drugs⁶⁴. Importantly, the repurposing approach offers several advantages over *de novo* drug discovery^{63,64}. First, as old drug(s) (candidates) previously underwent preclinical animal and sometimes early-stage human clinical trials, data regarding the pharmacokinetics, drug toxicity, potential interactions is already available, which consequently lowers, from a safety point of view, the risk of failure in new trials. Secondly, the drug development time can be lowered, as much of the preclinical testing and sometimes formulation development has already been addressed. Thirdly, despite that additional efficacy (phase III) trials and regulatory steps should be performed for a new indication, less investments could be needed in preclinical and phase I and II testing, at least if the used drug concentrations fall within the previously approved therapeutic window. Taken together, drug repurposing is generally considered to be less risky, while having a more rapid and higher return on investment than the development of totally new drug entities⁶³⁻⁶⁵. While drug repurposing requires 3-12 years and approximately US\$300 million, the *de novo* drug discovery and development process takes around 10-17 years with an estimated cost of ~ US\$2-3 billion^{63,64}. Indeed, despite the ever increasing investment in pharmaceutical research and development (R&D) in recent decades, the amount of new FDA-approved drugs per billion US dollars of R&D spending has halved approximately every 9 years since 1950 (a trend called the 'Eroom's law', **Figure 3**), indicating a decline in productivity of the pharmaceutical R&D⁶⁵⁻⁶⁷. This can, in part, be attributed to the changing regulatory requirements, high attrition rates⁶⁸ and longer development times that result in escalating costs, with estimates indicating that for every dollar spent on R&D, less than a dollar of value is returned on average^{64,69}.

The most fruitful basis for the discovery of a new drug is to start with an old drug.

Sir James Black, pharmacologist and Nobel laureate⁷⁰

EROOM'S LAW

The efficiency of research and development of new drugs in the United States halves every nine years or so. Drug developers sometimes call this Eroom's law — Moore's law for microprocessors in reverse. Repositioning drugs could help to counter this decline.



A SHORTER TIMESCALE

Because most repositioned drugs have already passed the early phases of development and clinical testing, they can potentially win approval in less than half the time and at one-quarter of the cost.



©nature

Figure 3. Pharmaceutical R&D has a productivity crisis. Can drug repurposing turn the tide? (upper part) Eroom's law: the number of new FDA-approved drugs per billion US dollars (inflation-adjusted) spent on research and development (R&D) halves roughly every 9 years⁶⁷. Drug repurposing could be an interesting strategy to counteract this decline. (lower part) Bringing a repurposed drug to the market generally requires less development time, while being associated with a lower overall cost, even after accounting for failures. Adapted from⁶⁵. (FDA = US Food and Drug Administration, R&D = research and development).

Traditionally, drug repurposing did not involve a systematic approach⁶⁴. Indeed, the most successful and best known examples of repurposed drugs were mainly based upon serendipitous clinical observations^{63,64}. For example, during the development of sildenafil as a treatment for angina pectoris, retrospective clinical experience indicated that the drug could be used for erectile dysfunctions, which eventually became the therapeutic indication for the marketed drug (Viagra®)⁶⁴. Sparked by such successes, both academia and (big) pharmaceutical companies embraced drug repurposing as a standalone drug development approach in the last decade^{64,65}. Consequently, efforts were made to rationalize the first (and very important) step of the process: selecting drug candidates for further repurposing. This step can be generally subdivided in experimental (*e.g.* **Chapter 2**) and computational strategies (*e.g.* analysis of different types of big data to generate novel hypotheses)⁶⁴. Driven by these modern drug repurposing initiatives, the field has increased tremendously, as evident from the vast increase of publications on the subject (> 1500 in 2020)⁷¹. However, the concept is probably best known by the wide audience for its use in finding medication that can join the fight against the COVID-19 pandemic⁷²⁻⁷⁷. Several existing drug(s) candidates were (and are still being) evaluated in (pre-)clinical trials to probe their anti-viral effects against SARS-CoV-2 (*e.g.* remdesivir, (hydroxy)chloroquine) or to lower the immune system's overreaction to the virus (*e.g.* dexamethasone)^{72,78-81}.

Notably, the boost in drug repurposing activity during the COVID-19 pandemic also led to the hyped '(hydroxy)chloroquine saga'⁸². Initial *in vitro* data suggested the potential efficacy of chloroquine in February 2020⁸³. This publication was followed by several other (questionable) studies investigating the effects of (hydroxy)chloroquine⁸⁴, including one infamous article from a medical group in Marseille in early March 2020⁸⁵. The authors recommended the use of a combination of hydroxychloroquine and azithromycin as a curative and preventative therapy for COVID-19, albeit their non-randomized clinical trial did only include 26 patients. Despite the limited evidence, this study led to an enormous focus

on (hydroxy)chloroquine by academia, companies and the lay press, which had serious consequences across the industrial, medical, political and societal landscape^{82,86,87}. Regulatory authorities rushed through emergency approvals without data on the drug's efficacy, pharmaceutical companies ramped up manufacturing of (hydroxy)chloroquine, while countries also started to hoard the products, altogether affecting patients that legitimately receive the drugs for autoimmune diseases such as systemic lupus erythematosus⁸². Albeit growing evidence showed a lack of efficacy for both chloroquine and hydroxychloroquine in COVID-19 treatment⁸⁸⁻⁹⁰ and while the FDA retracted the temporary approval in less than three months, several supporters keep on advocating prophylactic self-medication in combination with other supplements such as zinc salts⁸². Nevertheless, next to sildenafil (and in contrary to (hydroxy)chloroquine), there are also other successful examples of repurposed drugs, of which thalidomide (original indication 'morning sickness', now 'erythema nodosum leprosum and multiple myeloma'), zidovudine (original indication 'cancer', now 'HIV/AIDS') and minoxidil (original indication 'hypertension', now 'hair loss') are good examples⁶⁴.

“HYDROXYCHLOROQUINE & AZITHROMYCIN, taken together, have a real chance to be one of the biggest game changers in the history of medicine. The FDA has moved mountains - Thank You! Hopefully they will BOTH (H works better with A, International Journal of Antimicrobial Agents) be put in use IMMEDIATELY. PEOPLE ARE DYING, MOVE FAST, and GOD BLESS EVERYONE! @US_FDA @SteveFDA @CDCgov @DHSgov”

Donald J. Trump, 45th President of the United States of America

Finally, there are also important repurposing-specific technical, regulatory and organizational barriers that hamper progress in the repurposing field⁶⁴. For instance, obtaining commercial protection for the repurposed product might be difficult given that off-label use of generic drugs, with the same formulation and dosage form, may circumvent an obtained new method-of-use patent, consequently impacting possible profitability of the repurposed drug⁶⁴. Hence, drug repurposing will most likely continue to complement *de novo* drug discovery, rather than replacing the latter⁶⁵. Nonetheless, the former may be an especially appealing strategy in emergency situations (*e.g.* COVID-19 pandemic), where development of new molecules is almost unfeasible⁷², and for the discovery of rare disease treatments⁶⁴, where a lack of understanding of the underlying pathophysiology typically impedes rational drug development.

4. HOW TO PROCEED WITH (CAD) ADJUVANT EFFECT?

Three years ago, Joris *et al.* reported for the first time that a selection of CADs could significantly boost functional siRNA delivery from the endolysosomal compartment, which was corroborated in **Chapter 2** with our small compound screen. Most importantly, these data showed that plenty more physicochemical related compounds phenocopied these delivery effects. However, multiple questions remained on how broadly applicable the CAD adjuvant strategy could be, which was partially addressed in **Chapter 3**. Furthermore, our preliminary data in **Chapter 4**, indicated that the ‘non-CAD hit’ prazosin (PRA) could potentially be used as both a siRNA delivery enhancer and cell death inducer. In this paragraph, we will critically review our work and discuss the shortcomings of the presented adjuvant approach, while we highlight how the data obtained in this dissertation could guide future research and eventual the development of advanced delivery systems.

4.1. Recommendations for future (repurposing library) screenings

In **Chapter 2**, we screened the small drug repurposing library called “National Institutes of Health Clinical Collection” (NIHCC) for compounds that could boost the gene-silencing potential of siRNA-loaded dextran nanogels (siNGs). However, this library only contained 700 compounds and as several drug libraries with larger amounts of both approved and investigational compounds are (commercially) available⁹¹, it would be interesting to perform additional compound screens with differing chemical libraries. In addition to using different compound libraries, it might as well be useful to vary several other experimental parameters of the primary screen protocol. For instance, given the instability and reduced transfection efficiency of the used siNGs in serum-rich conditions⁹², transfection occurred in serum-free medium (Opti-MEM®). However, *in vivo*, ‘protein-rich’ biological fluids (*e.g.* blood, ascites fluids, *etc.*) affect the transfection potential of NPs *via* the formation of a protein corona⁹³. Hence, testing a (state-of-the-art) NP that has previously shown *in vivo* activity and the use of serum-containing transfection medium might more closely resemble the *in vivo* situation. In addition, as *in vitro* NP transfection data is generally a poor predictor of *in vivo* activity^{94,95}, it might be extremely interesting to perform future screenings directly in a more advanced *in vitro* cell model (*e.g.* 3D spheroids, see **Chapter 1**). Albeit such models might be more costly and less compatible with a high-throughput screening (HTS) approach, significant advances have been made to increase its feasibility⁹⁶. For example, Cutrona *et al.*

recently reported on an automated high-resolution confocal microscopy platform that can quantify NP-uptake and trafficking within spheroids in a high-throughput fashion, while simultaneously allowing the application of (non-)genetic screens⁹⁷.

4.2. Exact mechanism and general effects on cells

Half of the CADs (~56%) present in the NIHCC library were not identified as hits at 20 μ M, albeit an adjuvant effect cannot be excluded at higher concentrations. Indeed, not all CADs are effective in the same dose range^{98–100}. Nevertheless, our secondary validation data with the CADs loperamide and ketotifen revealed a clear correlation between the CAD-induced cytosolic siRNA delivery and the degree of lysosomal swelling, phospholipidosis (PLD) induction and functional inhibitor of acid sphingomyelinase (ASM) (FIASMA) activity, although we did not directly measure this enzyme activity. These diverging activities might potentially be related to differences in structure and physicochemical properties of the tested CADs, which could alter the final endolysosomal concentration^{101–108} or the efficiency with which CADs insert in lysosomal membranes (*e.g.* bulkiness of the aliphatic part of the molecule) and/or displace the ASM enzyme from the lysosomal membrane (*e.g.* steric hindrance of the basic nitrogen atom)^{109,110}. We believe that a comparison of additional CAD compounds with varying logP/pKa values and structures could offer interesting insights on the structural determinants of lysosomal accumulation, membrane insertion and the subsequent induction of the phenotypical cellular effects.

Based upon our earlier results¹⁰⁰ and the data presented in **Chapter 2-3**⁴³, we theorised that the CADs enhanced the cytosolic delivery of small nucleic acids *via* an increased permeability of the lysosomal compartment (*i.e.* lysosomal membrane permeabilization (LMP)). However, despite clearly demonstrating improved endolysosomal escape of fluorescently labeled oligonucleotides and siRNAs *via* confocal microscopy, we did not directly verify CAD-induced membrane damage of lysosomes. Interestingly, by using a galectin puncta assay, Du Rietz *et al.* recently showed that two CADs (siramesine and chloroquine) damaged differing subsets of endolysosomes, with chloroquine disrupting chol-siRNA-containing vesicles to a significantly larger extent, leading to a difference in knockdown enhancement¹¹¹. However, only a small set of CADs was investigated, hence comparing several of our identified CAD adjuvants with a similar galectin puncta assay could shed light on the underlying causes of differing activity between certain CAD adjuvants.

Our results clearly suggest that some CADs only trigger minor and transient LMP, sufficient to allow improved siRNA release in the cytosol while avoiding extensive lysosomal cell death. However, given that the combination of a CAD-responsive NP and 40 μ M desloratadine could apparently release FITC-dextran up to 150 kDa into the cytosol (**Chapter 3**), while most cell death evoking cathepsins are ~20-30 kDa, a detailed exploration of the related lysosomal repair mechanisms (*e.g.* involvement of cytosolic hydrolase inhibitors or lysophagy) could be of interest.

Next to the CADs, further research should be done on the prazosin adjuvant (**Chapter 4**). As this compound induced a distinct cellular phenotype (*e.g.* extensive vacuolization, no PLD induction) compared to typical CAD adjuvants, we hypothesized that unidentified cellular processes might contribute to the prazosin-induced boost in cytosolic siRNA delivery. For example, live-cell imaging could determine if endo(lyso)somal release mainly occurs from the formed vacuoles or from smaller endomembrane compartments. It would be equally interesting to (a) probe the size of the prazosin-induced pores in the limiting lysosomal membrane and (b) evaluate if an optimized exposure time of prazosin might lower the toxicity while maintaining the delivery effect (as previously shown for 2 h desloratadine compared to 20 h desloratadine¹⁰⁰). Furthermore, our preliminary data showed, in line with literature reports, that prazosin is an apoptotic cell death inducer. Given that the type of cancer cell death determines if an anti-tumor immune response is evoked¹¹², it would be interesting to evaluate if the prazosin-treated cancer cells are also immunogenic.

Finally, although the cell viability after CAD and prazosin exposure was probed with an ATP-based viability assay, such metabolic assays do not allow to reveal subtle changes in cell homeostasis¹¹³. Hence, it would be of utmost interest¹¹³ to perform a whole transcriptome analysis of CAD- and/or prazosin-treated cells at different time points to (a) identify the biological processes that are responsible for adjuvant activity and/or cell toxicity and (b) investigate the potential short and long(er) term effects on cell homeostasis^{113,114}.

4.3. Broader applicability

4.3.1. Cell types

We focused in **Chapter 3** on the broader applicability of the CAD adjuvant effect in different cancer cell lines. Our focus can be explained by the fact that cancer cells are interesting target cells for the CAD adjuvant treatment. First, as CADs are weak bases, they will likely

accumulate more efficiently in acidic tumors than in healthy tissues with a neutral pH^{99,115}. Secondly, lysosomes of transformed/cancer cells are usually less stable, have a lower ASM activity and show an altered membrane composition than their non-transformed counterparts, which sensitizes cancer cells to the CAD-induced LMP^{98,116,117}. Finally, several CADs have been proposed in the literature as repositioned anti-cancer drugs (*via* lysosomal cell death induction)^{98,99,116,118–120}. Hence, as discussed in detail for prazosin in **Chapter 4**, the combination of a CAD adjuvant and a therapeutic siRNA (*e.g.* targeting specific oncogenes) could potentially be used as an anti-cancer therapy, where both components complement the tumor killing effect of each other. If synergistic effects could be obtained, lower doses of each component would be required, thereby lowering the risk of adverse effects. Notably, in **Chapter 4**, we solely applied prazosin to a single cancer cell line (H1299), thus additional cancer cell types should be tested to verify that this compound can be more generally used as a cell death inducer and endolysosomal siRNA escape enhancer.

However, in case of systemic administration, endothelial cells and macrophages are the first cells encountered by nanocarriers^{54,121,122}. Our lab recently obtained data on the CAD adjuvant effect on siRNA delivery in the murine RAW 264.7 macrophage cell line, using siCD45-loaded dex-HEMA NGs (data not shown), which at least demonstrates that the approach is also effective in immune-related cell types. In addition, CAD exposure to primary epithelial cell types also induced the typical lysosomal phenotype (data not shown). Nevertheless, it would be highly interesting to further perform a detailed comparison for several CAD adjuvants in different primary and transformed cell types, thereby identifying feasible target cells and/or therapeutic indications.

4.3.2. Compatible nanocarriers and drug payloads?

Our previous work showed that the CAD adjuvant approach can boost the gene silencing potential of biodegradable dex-HEMA siNGs. In **Chapter 3** of this thesis, we further evaluated if other siRNA-loaded NPs (siNPs) can similarly benefit from the CAD adjuvant effect. Our data indicated that only NPs that resulted in a sufficient (lysosomal) amount of decomplexed siRNAs were responsive to desloratadine adjuvant treatment. Such a free fraction could be obtained with NPs that show sufficient siRNA decomplexation and/or a high extent of NP endocytosis. Hence, it would be interesting to further combine the CAD adjuvants with other NPs that meet these requirements. Albeit this requires experimental validation, we envision that siRNA formulations containing acid-cleavable bonds could

disassemble in the lysosomal compartment¹²³, potentially contributing to the lysosomal pool of free siRNAs. Other biostimuli-responsive materials^{124,125}, such as bonds sensitive to enzymatic digestion by lysosomal proteases/lipases, could likewise be evaluated. For one, phospholipase A2-sensitive liposomes have been described for intracellular delivery of NAs^{126–128}.

In addition, it would be of utmost interest to further compare the CAD adjuvant effect on several polymeric transfection reagents such as those known to induce a proton sponge effect (*e.g.* jetPEI®). Our preliminary data in **Chapter 4** suggested that CAD treatment might be less compatible with such carriers, possibly because the buffering polymers could counteract the pH-dependent lysosomal accumulation of CADs. An alternative explanation might be that the CAD-induced endo(lyso)somal leakiness prevents the buildup of osmotic pressure, thus impeding jetPEI®'s endosomal escape mechanism. Indeed, recent research from our group showed that endosomal escape efficiency by the proton-sponge mechanism is in part dependent on the degree of endosomal leakiness, which is a cell-type dependent parameter¹²⁹. Consequently, further studies should be conducted to truly establish if CAD adjuvants are (in)compatible with proton-sponge-based delivery systems. Next, in contrast to a recent study¹¹¹, we could not boost the endolysosomal escape of chol-siRNAs in our cell model and by using the CAD adjuvant desloratadine (**Chapter 4**). Evaluation of other conjugates (*e.g.* GalNAc- or dynamic poly-conjugates) and other CAD adjuvants might provide some clarification on this point.

Our data show that the CAD-induced pores only allow passage of small NAs, but not substantially larger NA therapeutics such as mRNA. However, the CAD adjuvant strategy could also be evaluated for delivery of other (small) membrane-impermeable macromolecules such as peptides and proteins (*e.g.* ~15 kDa large nanobodies¹³⁰ or ~38 kDa Cre recombinase¹³¹) in future studies. Indeed, the use of protein-based therapeutics is to date generally limited to extracellular targets and increasing the access of these biologics to intracellular targets could greatly expand their potential biomedical applications¹³².

4.4. Bridging *in vitro-in vivo* gap

A clear limitation of the presented work may be the absence of a proof-of-concept *in vivo* experiment. It should however be noted that directly translating our findings to an *in vivo* setting is not straightforward. For example, the applied siRNA-loaded NGs or PEGylated

DOTAP-DOPE liposomes, two CAD adjuvant-compatible NPs (**Chapter 3**), aggregate or disassemble in human blood^{92,133}, thus hindering systemic administration. Notwithstanding, our data in **Chapter 3** strongly contribute to our knowledge about the prerequisites a therapeutic siRNA-loaded nanoparticle (siNP) should have to be compatible with the CAD adjuvant strategy. More specifically, the nanocarrier should remain stable in extracellular media (*e.g.* bloodstream), while releasing its encapsulated siRNA following internalization. Hence, *in vivo* evaluation of CAD-promoted siRNA delivery would require dedicated NP design (as described above), which should be the next step in this line of research.

Next to the selection of an appropriate NP, another key point to consider for clinical translation is whether we can obtain the required tissue/cellular concentration of the CAD adjuvants without inducing off-target toxicity. Indeed, despite the advantageous physicochemical properties of the CADs (*e.g.* ion-trapping leads to high tissue concentration, see **Chapter 2** and above), the *in vitro* applied concentrations are relatively high and it might not be possible obtain these concentrations *in vivo* with therapeutic CAD doses. Detailed insights in the pharmacokinetics (*e.g.* time-dependent accumulation and metabolization) and pharmacodynamics (*e.g.* dose-limiting toxicity), both for CADs and the used NPs, will be required to address this question. Nevertheless, it has been observed in the literature that CADs can block ASM activity and induce lysosomal cell death in tumor models upon *in vivo* administration^{98,99,116,118}. As we show that non-lethal LMP is sufficient to considerably promote small NA delivery *in vitro*, the latter observation strongly suggests that CADs are able to reach the lysosomal compartment of target cancer cells in appropriate concentrations to allow their use as delivery-enhancing compounds. Moreover, multiple CADs have shown PLD induction *in vivo* in non-cancerous tissues¹³⁴, while antidepressant CADs (*e.g.* amitriptyline, fluoxetine) were also shown to decrease ASM activity *in vivo*, such as in the hippocampus (oral administration, mice), lungs (inhalation or intraperitoneal injection, mice) or nasal epithelial cells (oral administration, human)^{135–139}. Interestingly, it was shown that the CAD-mediated reduction of ceramide levels in the hippocampus of stressed mice played a role in the *in vivo* anti-depressive effects of these compounds^{135,140}.

In addition, given that CADs and NPs need to accumulate into the same cells to enable the adjuvant effect, incorporation of the CAD within the delivery system and/or local application might boost successful *in vivo* translation^{62,141}. Indeed, for local delivery in the eye/lung, CADs that are already used/approved for these local delivery routes (*e.g.* eye drops and

inhalators) might be used at concentrations that would not be achieved by systemic administration. Note that the majority of the above-mentioned action points do also apply to the prazosin adjuvant, albeit the latter is most probably only useful in anti-cancer applications.

Finally, in this thesis, we have evaluated the adjuvant effects in ‘simple’ 2D *in vitro* model systems (*i.e.* *in vitro* 2D cell monolayer, cancer cell lines). However, these artificial systems often fail to mimic the complex biological situation that NA therapeutics encounter upon *in vivo* administration¹⁴². Hence, several more complex *in vitro* (*e.g.* spheroids¹⁴³) and *in vivo* (*e.g.* zebrafish¹⁴²) models have been proposed to overcome this *in vitro-in vivo* gap. A brief discussion on these emerging models is provided in **Chapter 1** and, in theory, such models could also aid our adjuvant research. Nevertheless, uncertainty remains around the predictive value of each of these models. As the methodology for high-throughput *in vivo* studies (*e.g.* barcoding, see **Chapter 1**) is now available, side-by-side comparisons could establish which (characteristics of) model systems are predictive of *in vivo* delivery. Furthermore, positive data in mice models does not necessarily result in successful delivery in humans. By comparing the delivery of thousands of NPs in multiple small animal models and understanding how strain- and species-dependent characteristics affect delivery, “gold standard” animal models could potentially be identified for different diseases/target tissues¹¹⁴.

5. CONCLUSION

The widespread use of RNA therapeutics, such as siRNA drugs, is still hampered by a plethora of extra- and intracellular barriers. While state-of-the-art nanoparticle (NP)- and conjugate-based delivery systems predominantly show hepatic accumulation, endosomal entrapment of the NAs in the (target) cells remains one of the major bottlenecks. Hence, novel delivery strategies that can increase the biodistribution and/or the intracellular delivery are highly sought after. Interestingly, distinct classes of small molecules have shown potential to partially overcome these major delivery hurdles. As the repurposing of approved or abandoned drug (candidates) has several advantages over the use of entirely new chemical entities, the application of repurposed drugs as nucleic acid (NA) delivery enhancers might be a particularly appealing strategy. In this thesis, we described the screening of a repurposing library that, in line with previous findings, identified multiple cationic amphiphilic drug (CAD) adjuvants that boost intracellular siRNA delivery. We furthermore investigated the broader applicability of the CAD adjuvant approach and we demonstrated that prazosin, a hit compound that showed a differing cellular phenotype compared to our typically applied CADs, could also increase endo(lyso)somal escape. However, further research is required to better understand which NAs/NPs and target tissues/diseases could benefit from our adjuvant approach in an *in vivo*(-like) situation. In addition, the whole delivery field could benefit from correlative *in vitro-in vivo* studies to assess the predictive value of several well-established *in vitro/in vivo* model systems. Although a long road still lies ahead, we strongly believe that investigating small molecules for their delivery-enhancing effects is a valuable concept. The gained knowledge can be exploited to develop new or make existing delivery systems more efficient, altogether boosting the clinical translation of NA therapeutics.

REFERENCES

1. Eisenstein, M. Pharma's Roller-Coaster Relationship with RNA Therapies. *Nature* **2019**, *574*, S4–S6.
2. Weng, Y.; Xiao, H.; Zhang, J.; Liang, X. J.; Huang, Y. RNAi Therapeutic and Its Innovative Biotechnological Evolution. *Biotechnol. Adv.* **2019**, *37*, 801–825.
3. Khvorova, A.; Watts, J. K. The Chemical Evolution of Oligonucleotide Therapies of Clinical Utility. *Nat. Biotechnol.* **2017**, *35*, 238–248.
4. Fire, A. *et al.* Potent and Specific Genetic Interference by Double-Stranded RNA in *Caenorhabditis Elegans*. *Nature* **1998**, *391*, 806–811.
5. Elbashir, S. M. *et al.* Duplexes of 21-Nucleotide RNAs Mediate RNA Interference in Cultured Mammalian Cells. *Nature* **2001**, *411*, 494–498.
6. Caplen, N. J.; Parrish, S.; Imani, F.; Fire, A.; Morgan, R. A. Specific Inhibition of Gene Expression by Small Double-Stranded RNAs in Invertebrate and Vertebrate Systems. *Proc. Natl. Acad. Sci. U. S. A.* **2001**, *98*, 9742–9747.
7. Setten, R. L.; Rossi, J. J.; Han, S. ping. The Current State and Future Directions of RNAi-Based Therapeutics. *Nat. Rev. Drug Discov.* **2019**, *18*, 421–446.
8. Song, E. *et al.* RNA Interference Targeting Fas Protects Mice from Fulminant Hepatitis. *Nat. Med.* **2003**, *9*, 347–351.
9. Zimmermann, T. S. *et al.* RNAi-Mediated Gene Silencing in Non-Human Primates. *Nature* **2006**, *441*, 111–114.
10. Hopkin, M. RNAi Scoops Medical Nobel. *Nature* **2006**.
11. Rgen Soutschek, J. *et al.* Therapeutic Silencing of an Endogenous Gene by Systemic Administration of Modified siRNAs. **2004**, *432*, 173–178.
12. Mccaffrey, A. P. *et al.* Inhibition of Hepatitis B Virus in Mice by RNA Interference. *Nat. Biotechnol.* **2003**, *21*, 639–644.
13. Krieg, A. M. Is RNAi Dead? *Mol. Ther.* **2011**, *19*, 1001–1002.
14. Kleinman, M. E. *et al.* Sequence- and Target-Independent Angiogenesis Suppression by siRNA via TLR3. *Nature* **2008**, *452*, 591–597.
15. Pilcher, H. R. RNA Hopes Hyped? *Nature* **2003**.
16. Ledford, H. Investors Flee as Firm Scraps RNA-Interference Drug Candidate. *Nature* **2016**.
17. Ledford, H. Drug Giants Turn Their Backs on RNA Interference. *Nature* **2010**, *468*, 487.
18. Hayden, E. C. RNA Interference Rebooted. *Nature* **2014**, *508*, 443.
19. DeVincenzo, J. *et al.* A Randomized, Double-Blind, Placebo-Controlled Study of an RNAi-Based Therapy Directed against Respiratory Syncytial Virus. *Proc. Natl. Acad. Sci. U. S. A.* **2010**, *107*, 8800–8805.
20. Davis, M. E. *et al.* Evidence of RNAi in Humans from Systemically Administered siRNA via Targeted Nanoparticles. *Nature* **2010**, *464*, 1067–1070.
21. Barros, S. A.; Gollob, J. A. Safety Profile of RNAi Nanomedicines. *Adv. Drug Deliv. Rev.* **2012**, *64*, 1730–1737.
22. A Triumph of Perseverance over Interference. *Nat. Biotechnol.* **2018**, *36*, 775.
23. Coelho, T. *et al.* Safety and Efficacy of RNAi Therapy for Transthyretin Amyloidosis. *N. Engl. J. Med.* **2013**, *369*, 819–829.
24. Adams, D. *et al.* Patisiran, an RNAi Therapeutic, for Hereditary Transthyretin Amyloidosis. *N. Engl. J. Med.* **2018**, *379*, 11–21.
25. Akinc, A. *et al.* The Onpattro Story and the Clinical Translation of Nanomedicines Containing Nucleic Acid-Based Drugs. *Nat. Nanotechnol.* **2019**, *14*, 1084–1087.
26. Ledford, H. Gene-Silencing Technology Gets First Drug Approval after 20-Year Wait. *Nature* **2018**, *560*, 291–292.
27. Garber, K. Alnylam Launches Era of RNAi Drugs. *Nat. Biotechnol.* **2018**, *36*, 777–778.
28. Nikam, R. R.; Gore, K. R. Journey of siRNA: Clinical Developments and Targeted Delivery.

- Nucleic Acid Ther.* **2018**, *28*, 209–224.
29. Springer, A. D.; Dowdy, S. F. GalNAc-SiRNA Conjugates: Leading the Way for Delivery of RNAi Therapeutics. *Nucleic Acid Ther.* **2018**, *28*, 109–118.
 30. Shen, X.; Corey, D. R. Chemistry, Mechanism and Clinical Status of Antisense Oligonucleotides and Duplex RNAs. *Nucleic Acids Res.* **2018**, *46*, 1584–1600.
 31. Scott, L. J. Givosiran: First Approval. *Drugs* **2020**, *80*, 335–339.
 32. Garrelfs, S. *et al.* LB002ILLUMINATE-A, A PHASE 3 STUDY OF LUMASIRAN, AN INVESTIGATIONAL RNAI THERAPEUTIC, IN CHILDREN AND ADULTS WITH PRIMARY HYPEROXALURIA TYPE 1 (PH1). *Nephrol. Dial. Transplant.* **2020**, *35*, gfaa146.LB002.
 33. Huggett, B.; Paisner, K. The Commercial Tipping Point. *Nat. Biotechnol.* **2017**, *35*, 708–709.
 34. Ray, K. K. *et al.* Two Phase 3 Trials of Inclisiran in Patients with Elevated LDL Cholesterol. *N. Engl. J. Med.* **2020**, *382*, 1507–1519.
 35. Kosmas, C. *et al.* Inclisiran: A New Promising Agent in the Management of Hypercholesterolemia. *Diseases* **2018**, *6*, 63.
 36. Drew, L. Why Rare Genetic Diseases Are a Logical Focus for RNA Therapies. *Nature* **2019**, *574*, S16–S18.
 37. Martin, C.; Lowery, D. mRNA Vaccines: Intellectual Property Landscape. *Nat. Rev. Drug Discov.* **2020**, *19*, 578.
 38. Hu, B. *et al.* Therapeutic siRNA: State of the Art. *Signal Transduct. Target. Ther.* **2020**, *5*, 101.
 39. Bobbin, M. L.; Rossi, J. J. RNA Interference (RNAi)-Based Therapeutics: Delivering on the Promise? *Annu. Rev. Pharmacol. Toxicol.* **2016**, *56*, 103–122.
 40. Guzman-Arangué, A.; Loma, P.; Pintor, J. Small-Interfering RNAs (siRNAs) as a Promising Tool for Ocular Therapy. *Br. J. Pharmacol.* **2013**, *170*, 730–747.
 41. Golan, T. *et al.* RNAi Therapy Targeting KRAS in Combination with Chemotherapy for Locally Advanced Pancreatic Cancer Patients. *Oncotarget* **2015**, *6*, 24560–24570.
 42. Trieu, V. *et al.* First-in-Human Phase I Study of Bacterial RNA Interference Therapeutic CEQ508 in Patients with Familial Adenomatous Polyposis (FAP). *Ann. Oncol.* **2017**, *28*, v174.
 43. Van de Vyver, T. *et al.* Cationic Amphiphilic Drugs Boost the Lysosomal Escape of Small Nucleic Acid Therapeutics in a Nanocarrier-Dependent Manner. *ACS Nano* **2020**, *14*, 4774–4791.
 44. De Backer, L. *et al.* Hybrid Pulmonary Surfactant-Coated Nanogels Mediate Efficient *In Vivo* Delivery of siRNA to Murine Alveolar Macrophages. *J. Control. Release* **2015**, *217*, 53–63.
 45. Merckx, P. *et al.* Surfactant Protein B (SP-B) Enhances the Cellular siRNA Delivery of Proteolipid Coated Nanogels for Inhalation Therapy. *Acta Biomater.* **2018**, *78*, 236–246.
 46. Berlinski, A. 2019 Year in Review: Aerosol Therapy. *Respir. Care* **2020**, *65*, 705–712.
 47. Merckx, P. *et al.* Lyophilization and Nebulization of Pulmonary Surfactant-Coated Nanogels for siRNA Inhalation Therapy. *Eur. J. Pharm. Biopharm.* **2020**, *157*, 191–199.
 48. Kandil, R.; Merkel, O. M. Pulmonary Delivery of siRNA as a Novel Treatment for Lung Diseases. *Ther. Deliv.* **2019**, *10*, 203–206.
 49. Ruigrok, M. J. R.; Frijlink, H. W.; Hinrichs, W. L. J. Pulmonary Administration of Small Interfering RNA: The Route to Go? *Journal of Controlled Release*. Elsevier B.V. August 10, 2016, pp 14–23.
 50. Siegel, R. L.; Miller, K. D.; Jemal, A. Cancer Statistics, 2020. *CA. Cancer J. Clin.* **2020**, *70*, 7–30.
 51. Shaffer, C. Mist Begins to Clear for Lung Delivery of RNA. *Nat. Biotechnol.* **2020**, *38*, 1110–1112.
 52. Ouyang, B. *et al.* The Dose Threshold for Nanoparticle Tumour Delivery. *Nat. Mater.*

- 2020**, 1–10.
53. Lammers, T. Just Dose It. *Nat. Mater.* **2020**, *19*, 1257–1258.
 54. Wilhelm, S. *et al.* Analysis of Nanoparticle Delivery to Tumours. *Nat. Rev. Mater.* **2016**, *1*, 1–12.
 55. Dahlman, J. E. *et al.* *In Vivo* Endothelial siRNA Delivery Using Polymeric Nanoparticles with Low Molecular Weight. *Nat. Nanotechnol.* **2014**, *9*, 648–655.
 56. Khan, O. F. *et al.* Endothelial siRNA Delivery in Nonhuman Primates Using Ionizable Low-Molecular Weight Polymeric Nanoparticles. *Sci. Adv.* **2018**, *4*, 8409.
 57. Kauffman, K. J. *et al.* Rapid, Single-Cell Analysis and Discovery of Vectored mRNA Transfection *In Vivo* with a LoxP-Flanked TdTomato Reporter Mouse. *Mol. Ther. - Nucleic Acids* **2018**, *10*, 55–63.
 58. Cheng, Q. *et al.* Selective Organ Targeting (SORT) Nanoparticles for Tissue-Specific mRNA Delivery and CRISPR–Cas Gene Editing. *Nat. Nanotechnol.* **2020**, 1–8.
 59. Kranz, L. M. *et al.* Systemic RNA Delivery to Dendritic Cells Exploits Antiviral Defence for Cancer Immunotherapy. *Nature* **2016**, *534*, 396–401.
 60. Lokugamage, M. P.; Sago, C. D.; Dahlman, J. E. Testing Thousands of Nanoparticles *in Vivo* Using DNA Barcodes. *Curr. Opin. Biomed. Eng.* **2018**, *7*, 1–8.
 61. Dowdy, S. F. Overcoming Cellular Barriers for RNA Therapeutics. *Nat. Biotechnol.* **2017**, *35*, 222–229.
 62. Joris, F.; De Smedt, S. C.; Raemdonck, K. Small Molecules Convey Big Messages: Boosting Non-Viral Nucleic Acid Delivery with Low Molecular Weight Drugs. *Nano Today* **2017**, *16*, 14–29.
 63. Ashburn, T. T.; Thor, K. B. Drug Repositioning: Identifying and Developing New Uses for Existing Drugs. *Nat. Rev. Drug Discov.* **2004**, *3*, 673–683.
 64. Pushpakom, S. *et al.* Drug Repurposing: Progress, Challenges and Recommendations. *Nat. Rev. Drug Discov.* **2018**, *18*, 41–58.
 65. Nosengo, N. Can You Teach Old Drugs New Tricks? *Nature* **2016**, *534*, 314–316.
 66. Pammolli, F.; Magazzini, L.; Riccaboni, M. The Productivity Crisis in Pharmaceutical R&D. *Nat. Rev. Drug Discov.* **2011**, *10*, 428–438.
 67. Scannell, J. W.; Blanckley, A.; Boldon, H.; Warrington, B. Diagnosing the Decline in Pharmaceutical R&D Efficiency. *Nat. Rev. Drug Discov.* **2012**, *11*, 191–200.
 68. Waring, M. J. *et al.* An Analysis of the Attrition of Drug Candidates from Four Major Pharmaceutical Companies. *Nat. Rev. Drug Discov.* **2015**, *14*, 475–486.
 69. Health, R. on T. G.-B. R. for; Policy, B. on H. S.; Medicine, I. of. Roundtable on Translating Genomic-Based Research for Health (Board on Health Sciences Policy) Institute of Medicine. In *Drug Repurposing and Repositioning: Workshop Summary*; Johnson, S. G., Beachy, S. H., Olson, S., Berger, A. C., Eds.; National Academies Press: Washington DC, **2014**.
 70. Chong, C. R.; Sullivan, D. J. New Uses for Old Drugs. *Nature* **2007**, *448*, 645–646.
 71. Sun, W.; Sanderson, P. E.; Zheng, W. Drug Combination Therapy Increases Successful Drug Repositioning. *Drug Discov. Today* **2016**, *21*, 1189–1195.
 72. Zhou, Y.; Wang, F.; Tang, J.; Nussinov, R.; Cheng, F. Artificial Intelligence in COVID-19 Drug Repurposing. *Lancet Digit. Heal.* **2020**, *2*, e667–e676.
 73. Singh, T. U. *et al.* Drug Repurposing Approach to Fight COVID-19. *Pharmacol. Reports* **2020**, *1*, 1.
 74. Wang, X.; Guan, Y. COVID-19 Drug Repurposing: A Review of Computational Screening Methods, Clinical Trials, and Protein Interaction Assays. *Med. Res. Rev.* **2020**, med.21728.
 75. Li, G.; De Clercq, E. Therapeutic Options for the 2019 Novel Coronavirus (2019-NCoV). *Nat. Rev. Drug Discov.* **2020**, *19*, 149–150.
 76. Harrison, C. Coronavirus Puts Drug Repurposing on the Fast Track. *Nat. Biotechnol.* **2020**, *38*, 379–381.

77. Kiplin Guy, R.; DiPaola, R. S.; Romanelli, F.; Dutch, R. E. Rapid Repurposing of Drugs for COVID-19. *Science (80-.)*. **2020**, *368*, 829–830.
78. McMahon, J. H.; Udy, F. R. A. C. P. A.; Anton, F. C. I. C. M.; Peleg, Y. Remdesivir for the Treatment of Covid-19 — Preliminary Report. *N. Engl. J. Med.* **2020**, *383*, 992–994.
79. Beigel, J. H. *et al.* Remdesivir for the Treatment of Covid-19 — Final Report. *N. Engl. J. Med.* **2020**, *383*, 1813–1826.
80. Dexamethasone in Hospitalized Patients with Covid-19 — Preliminary Report. *N. Engl. J. Med.* **2020**, NEJMoa2021436.
81. Hsu, J. Covid-19: What Now for Remdesivir? *BMJ* **2020**, *371*, m4457.
82. Levin, J. M. *et al.* Artificial Intelligence, Drug Repurposing and Peer Review. *Nat. Biotechnol.* **2020**, *38*, 1127–1131.
83. Wang, M. *et al.* Remdesivir and Chloroquine Effectively Inhibit the Recently Emerged Novel Coronavirus (2019-NCoV) *in Vitro*. *Cell Res.* **2020**, *30*, 269–271.
84. Gao, J.; Tian, Z.; Yang, X. Breakthrough: Chloroquine Phosphate Has Shown Apparent Efficacy in Treatment of COVID-19 Associated Pneumonia in Clinical Studies. *Biosci. Trends* **2020**, *14*, 72–73.
85. Gautret, P. *et al.* Hydroxychloroquine and Azithromycin as a Treatment of COVID-19: Results of an Open-Label Non-Randomized Clinical Trial. *Int. J. Antimicrob. Agents* **2020**, *56*, 105949.
86. Ledford, H. Chloroquine Hype Is Derailing the Search for Coronavirus Treatments. *Nature* **2020**, *580*, 573–573.
87. Vetter, P.; Kaiser, L.; Calmy, A.; Agoritsas, T.; Huttner, A. Dexamethasone and Remdesivir: Finding Method in the COVID-19 Madness. *The Lancet Microbe* **2020**, *0*.
88. Hoffmann, M. *et al.* Chloroquine Does Not Inhibit Infection of Human Lung Cells with SARS-CoV-2. *Nature* **2020**, *585*, 588–590.
89. Funnell, S. G. P. *et al.* Emerging Preclinical Evidence Does Not Support Broad Use of Hydroxychloroquine in COVID-19 Patients. *Nat. Commun.* **2020**, *11*, 4253.
90. Kaptein, S. J. F. *et al.* Favipiravir at High Doses Has Potent Antiviral Activity in SARS-CoV-2-infected Hamsters, Whereas Hydroxychloroquine Lacks Activity. *Proc. Natl. Acad. Sci. U. S. A.* **2020**, *117*, 26955–26965.
91. Janes, J. *et al.* The ReFRAME Library as a Comprehensive Drug Repurposing Library and Its Application to the Treatment of Cryptosporidiosis. *Proc. Natl. Acad. Sci. U. S. A.* **2018**, *115*, 10750–10755.
92. Naeye, B. *et al.* Hemocompatibility of SiRNA Loaded Dextran Nanogels. *Biomaterials* **2011**, *32*, 9120–9127.
93. Dakwar, G. R. *et al.* Disregarded Effect of Biological Fluids in SiRNA Delivery: Human Ascites Fluid Severely Restricts Cellular Uptake of Nanoparticles. *ACS Appl. Mater. Interfaces* **2015**, *7*, 24322–24329.
94. Paunovska, K. *et al.* A Direct Comparison of *in Vitro* and *in Vivo* Nucleic Acid Delivery Mediated by Hundreds of Nanoparticles Reveals a Weak Correlation. *Nano Lett.* **2018**, *18*, 2148–2157.
95. Whitehead, K. A. *et al.* *In Vitro* - *In Vivo* Translation of Lipid Nanoparticles for Hepatocellular SiRNA Delivery. *ACS Nano* **2012**, *6*, 6922–6929.
96. Eglén, R. M.; Randle, D. H. Drug Discovery Goes Three-Dimensional: Goodbye to Flat High-Throughput Screening? *Assay Drug Dev. Technol.* **2015**, *13*, 262–265.
97. Cutrona, M. B.; Simpson, J. C. A High-Throughput Automated Confocal Microscopy Platform for Quantitative Phenotyping of Nanoparticle Uptake and Transport in Spheroids. *Small* **2019**, *15*, 1902033.
98. Petersen, N. H. T. *et al.* Transformation-Associated Changes in Sphingolipid Metabolism Sensitize Cells to Lysosomal Cell Death Induced by Inhibitors of Acid Sphingomyelinase. *Cancer Cell* **2013**, *24*, 379–393.

99. Ellegaard, A.-M. *et al.* Repurposing Cationic Amphiphilic Antihistamines for Cancer Treatment. *EBioMedicine* **2016**, *9*, 130–139.
100. Joris, F. *et al.* Repurposing Cationic Amphiphilic Drugs as Adjuvants to Induce Lysosomal SiRNA Escape in Nanogel Transfected Cells. *J. Control. Release* **2018**, *269*, 266–276.
101. Wishart, D. S. *et al.* DrugBank: A Comprehensive Resource for *In Silico* Drug Discovery and Exploration. *Nucleic Acids Res.* **2006**, *34*, D668–72.
102. Kessel, M.; Gieseler, F.; Woodcock, B. G. Influence of Serum Protein Binding on the Uptake and Retention of Idarubicin by Sensitive and Multidrug Resistant Human Leukemic Cells. *Eur. J. Clin. Pharmacol.* **1999**, *55*, 369–373.
103. Trainor, G. L. The Importance of Plasma Protein Binding in Drug Discovery. *Expert Opin. Drug Discov.* **2007**, *2*, 51–64.
104. Schmidt, S. *et al.* Effect of Protein Binding on the Pharmacological Activity of Highly Bound Antibiotics. *Antimicrob. Agents Chemother.* **2008**, *52*, 3994–4000.
105. Kramer, N. I.; Krismartina, M.; Rico-Rico, Á.; Blaauboer, B. J.; Hermens, J. L. M. Quantifying Processes Determining the Free Concentration of Phenanthrene in Basal Cytotoxicity Assays. *Chem. Res. Toxicol.* **2012**, *25*, 436–445.
106. Ghafourian, T.; Amin, Z. QSAR Models for the Prediction of Plasma Protein Binding. *Bioimpacts* **2013**, *3*, 21–27.
107. Trapp, S.; Rosania, G. R.; Horobin, R. W.; Kornhuber, J. Quantitative Modeling of Selective Lysosomal Targeting for Drug Design. *Eur. Biophys. J.* **2008**, *37*, 1317–1328.
108. Ufuk, A.; Somers, G.; Houston, J. B.; Galetin, A. *In Vitro* Assessment of Uptake and Lysosomal Sequestration of Respiratory Drugs in Alveolar Macrophage Cell Line NR8383. *Pharm. Res.* **2015**, *32*, 3937–3951.
109. Kornhuber, J. *et al.* Identification of New Functional Inhibitors of Acid Sphingomyelinase Using a Structure-Property-Activity Relation Model. *J. Med. Chem.* **2008**, *51*, 219–237.
110. Kornhuber, J. *et al.* Identification of Novel Functional Inhibitors of Acid Sphingomyelinase. *PLoS One* **2011**, *6*, e23852.
111. Du Rietz, H.; Hedlund, H.; Wilhelmson, S.; Nordenfelt, P.; Wittrup, A. Imaging Small Molecule-Induced Endosomal Escape of SiRNA. *Nat. Commun.* **2020**, *11*, 1809.
112. Efimova, I. *et al.* Vaccination with Early Ferroptotic Cancer Cells Induces Efficient Antitumor Immunity. *J. Immunother. cancer* **2020**, *8*, 1369.
113. Fraire, J. C. *et al.* Vapor Nanobubble Is the More Reliable Photothermal Mechanism for Inducing Endosomal Escape of SiRNA without Disturbing Cell Homeostasis. *J. Control. Release* **2020**, *319*, 262–275.
114. Paunovska, K.; Loughrey, D.; Sago, C. D.; Langer, R.; Dahlman, J. E. Using Large Datasets to Understand Nanotechnology. *Adv. Mater.* **2019**, *31*, 1902798.
115. Schrezenmeier, E.; Dörner, T. Mechanisms of Action of Hydroxychloroquine and Chloroquine: Implications for Rheumatology. *Nat. Rev. Rheumatol.* **2020**, *16*, 155–166.
116. Gulbins, E.; Kolesnick, R. N. It Takes a CAD to Kill a Tumor Cell with a LMP. *Cancer Cell* **2013**, *24*, 279–281.
117. Boya, P.; Kroemer, G. Lysosomal Membrane Permeabilization in Cell Death. *Oncogene* **2008**, *27*, 6434–6451.
118. Verdoodt, F. *et al.* Antihistamines and Ovarian Cancer Survival: Nationwide Cohort Study and *In Vitro* Cell Viability Assay. *JNCI J. Natl. Cancer Inst.* **2020**, *112*, djz217.
119. Anand, A. *et al.* Cell Death Induced by Cationic Amphiphilic Drugs Depends on Lysosomal Ca²⁺ Release and Cyclic AMP. *Mol. Cancer Ther.* **2019**, molcanther.1406.2018.
120. Groth-Pedersen, L.; Ostefeld, M. S.; Høyer-Hansen, M.; Nylandsted, J.; Jäättelä, M. Vincristine Induces Dramatic Lysosomal Changes and Sensitizes Cancer Cells to Lysosome-Destabilizing Siramesine. *Cancer Res.* **2007**, *67*, 2217–2225.
121. Campbell, F. *et al.* Directing Nanoparticle Biodistribution through Evasion and Exploitation of Stab2-Dependent Nanoparticle Uptake. *ACS Nano* **2018**, *12*, 2138–2150.

122. Hayashi, Y. *et al.* Differential Nanoparticle Sequestration by Macrophages and Scavenger Endothelial Cells Visualized *In Vivo* in Real-Time and at Ultrastructural Resolution. *ACS Nano* **2020**, *14*, 1665–1681.
123. Wu, W. *et al.* Endogenous PH-Responsive Nanoparticles with Programmable Size Changes for Targeted Tumor Therapy and Imaging Applications. *Theranostics* **2018**, *8*, 3038–3058.
124. Lu, Y.; Aimetti, A. A.; Langer, R.; Gu, Z. Bioresponsive Materials. *Nat. Rev. Mater.* **2016**, *1*, 16075.
125. You, J. O.; Almeda, D.; Ye, G. J. C.; Auguste, D. T. Bioresponsive Matrices in Drug Delivery. *J. Biol. Eng.* **2010**, *4*, 15.
126. Foged, C.; Nielsen, H. M.; Frokjaer, S. Phospholipase A2 Sensitive Liposomes for Delivery of Small Interfering RNA (SiRNA). *J. Liposome Res.* **2007**, *17*, 191–196.
127. Foged, C.; Nielsen, H. M.; Frokjaer, S. Liposomes for Phospholipase A2 Triggered SiRNA Release: Preparation and *in Vitro* Test. *Int. J. Pharm.* **2007**, *331*, 160–166.
128. Shiraishi, T.; Ghavami, M.; Nielsen, P. E. *In Vitro* Cellular Delivery of Peptide Nucleic Acid (PNA); Humana, New York, NY, **2020**; pp 173–185.
129. Vermeulen, L. M. P. *et al.* Endosomal Size and Membrane Leakiness Influence Proton Sponge-Based Rupture of Endosomal Vesicles. *ACS Nano* **2018**, *12*, 2332–2345.
130. Van Audenhove, I.; Gettemans, J. Nanobodies as Versatile Tools to Understand, Diagnose, Visualize and Treat Cancer. *EBioMedicine* **2016**, *8*, 40–48.
131. Hoess, R.; Abremski, K.; Irwin, S.; Kendall, M.; Mack, A. DNA Specificity of the Cre Recombinase Resides in the 25 KDa Carboxyl Domain of the Protein. *J. Mol. Biol.* **1990**, *216*, 873–882.
132. Zuris, J. A. *et al.* Cationic Lipid-Mediated Delivery of Proteins Enables Efficient Protein-Based Genome Editing *in Vitro* and *in Vivo*. *Nat. Biotechnol.* **2015**, *33*, 73–80.
133. Buyens, K. *et al.* A Fast and Sensitive Method for Measuring the Integrity of SiRNA-Carrier Complexes in Full Human Serum. *J. Control. Release* **2008**, *126*, 67–76.
134. Goracci, L.; Ceccarelli, M.; Bonelli, D.; Cruciani, G. Modeling Phospholipidosis Induction: Reliability and Warnings. *J. Chem. Inf. Model.* **2013**, *53*, 1436–1446.
135. Gulbins, E. *et al.* Acid Sphingomyelinase-Ceramide System Mediates Effects of Antidepressant Drugs. *Nat. Med.* **2013**, *19*, 934–938.
136. Teichgräber, V. *et al.* Ceramide Accumulation Mediates Inflammation, Cell Death and Infection Susceptibility in Cystic Fibrosis. *Nat. Med.* **2008**, *14*, 382–391.
137. Becker, K. A. *et al.* Acid Sphingomyelinase Inhibitors Normalize Pulmonary Ceramide and Inflammation in Cystic Fibrosis. *Am. J. Respir. Cell Mol. Biol.* **2010**, *42*, 716–724.
138. Becker, K. A. *et al.* Sphingolipids as Targets for Inhalation Treatment of Cystic Fibrosis. *Adv. Drug Deliv. Rev.* **2018**, *133*, 66–75.
139. Carpinteiro, A. *et al.* Pharmacological Inhibition of Acid Sphingomyelinase Prevents Uptake of SARS-CoV-2 by Epithelial Cells. *Cell Reports Med.* **2020**, *1*, 100142.
140. Adams, C. *et al.* Long-Term Pulmonary Therapy of Cystic Fibrosis-Patients with Amitriptyline. *Cell. Physiol. Biochem.* **2016**, *39*, 565–572.
141. Schirotti, D. *et al.* Effective *In Vivo* Topical Delivery of SiRNA and Gene Silencing in Intact Corneal Epithelium Using a Modified Cell Penetrating Peptide. *Mol. Ther. - Nucleic Acids* **2019**, *17*, 891–906.
142. Sieber, S. *et al.* Zebrafish as a Preclinical *in Vivo* Screening Model for Nanomedicines. *Adv. Drug Deliv. Rev.* **2019**, *151–152*, 152–168.
143. Lazzari, G.; Couvreur, P.; Mura, S. Multicellular Tumor Spheroids: A Relevant 3D Model for the: *In Vitro* Preclinical Investigation of Polymer Nanomedicines. *Polym. Chem.* **2017**, *8*, 4947–4969.

SUMMARY AND CONCLUSIONS

RNA therapeutics have the capacity to revolutionize the way we treat a myriad of disorders such as viral infections, cancer and genetic diseases. For example, messenger RNA vaccines can produce antigens to boost our immune response, as recently demonstrated in the context of the COVID-19 pandemic. On the other hand, smaller nucleic acid (NA) therapeutics, such as small interfering (siRNA) or antisense oligonucleotides (ASOs), can induce sequence-specific silencing of disease-promoting genes. However, given their instability and unfavorable physicochemical properties/pharmacokinetics, these NA molecules require appropriate delivery systems to overcome the multiple extra- and intracellular barriers upon *in vivo* administration. In this regard, several non-viral delivery carriers, such as nanoparticles (NPs) or N-acetylgalactosamine (GalNAc)-siRNA conjugates, have been developed. However, despite the recent approval of the first RNA therapeutics, state-of-the-art carriers are still associated with several delivery problems. Indeed, nanoparticles and GalNAc-siRNA conjugates predominately target the liver upon systemic administration, while endosomal sequestration limits the amount of RNA drugs that reach their intracellular targets. Hence, to fully unlock the therapeutic potential of RNA therapeutics, safe and efficient delivery strategies that improve biodistribution and increase the intracellular delivery are highly sought after. While there is a growing trend within the delivery field to develop novel nanomaterials and highly sophisticated carrier designs, it has been postulated that increasing our understanding of how (current) delivery vehicles interact with the several extra- and intracellular barriers can boost the rational development of the next generation of NA carriers.

In **Chapter 1**, we provided a general introduction to the use of several RNA therapeutics and we gave an overview of the numerous extra- and intracellular barriers encountered by these therapeutic molecules upon *in vivo* administration. Furthermore, we briefly described the most relevant delivery systems (*e.g.* nanoparticles, conjugates) that were developed over the years to tackle these delivery hurdles. We highlighted how several tools can be used to investigate the interaction of NAs or nanoparticles with the plethora of intracellular barriers. Most importantly, it was shown that both non-genetic (*e.g.* small molecules) and genetic (*e.g.* RNAi or CRISPR) tools can be applied to improve intracellular delivery by modulating each of the intracellular barriers. Albeit each of these tools could generate

knowledge about the biological mechanisms that underly the intracellular delivery process, the use of small molecules as NA delivery enhancers might be an especially appealing strategy, given that several delivery-promoting compounds are also approved drugs. In this context, our group recently reported that a selection of cationic amphiphilic drugs (CADs) could be repurposed to increase the release of lysosomal sequestered siRNA into the cytosol of lung epithelial cancer cells. Due to their physicochemical properties, these drugs accumulate inside the lysosomal compartment, where they functionally inhibit the acid sphingomyelinase (ASM) enzyme. ASM inhibition leads to lysosomal swelling and a transient lysosomal membrane permeabilization, allowing the siRNA molecules to diffuse from the lysosomal lumen into the cytosol. As many CADs are widely used (*e.g.* antihistamines, antidepressants,...), their repurposing as NA delivery enhancers could foster clinical translation of NA drugs. However, multiple questions remained on the broader applicability of such an intracellular delivery strategy, which were investigated in this thesis.

In **Chapter 2**, we reported on a drug repurposing screen (National Institutes of Health Clinical Collection) that allowed identification of 56 CAD adjuvants. Although ~56% of the CADs present in the screen were not identified as adjuvants (at a concentration of 20 μ M), our data clearly correlated the improved siRNA delivery with the induction of an acquired lysosomal storage disease phenotype by CAD hits (*i.e.* CADs that were identified as siRNA delivery-promoting compounds). Most importantly, this compound screen highlighted that the observed adjuvant effect on siRNA delivery is not limited to the previously identified CAD molecules, but that many more CADs phenocopy these effects.

Given that our previous work and the compound screen only evaluated the CAD adjuvant effect in dextran nanogel-transfected lung epithelial cancer cells, we furthermore investigated in **Chapter 3** if the CAD adjuvant approach could also be extended to other nanocarrier types, other cancer cells and other types of small NAs (ASOs or Dicer-substrate siRNAs (DsiRNAs)). Our data confirmed that several CADs share the same adjuvant effect on the cytosolic delivery of both (D)siRNAs and ASOs in distinct cancer cell lines. Importantly, we showed that the CAD adjuvant effect is carrier-specific, likely providing benefit mainly for nanoparticles that entail a substantial endolysosomal pool of decomplexed NAs to diffuse through the CAD-induced pores in the limiting endolysosomal membrane. In contrast to the governing nanomedicine model, that states that lysosomes are a dead end for siRNA

nanomedicines, our data support the rational design of nanocarriers that release their NA payload in the endolysosomal lumen with the aim to maximize the CAD adjuvant effect.

Interestingly, several hits from the compound screen, described in **Chapter 2**, did not comply with the applied CAD definition. We discussed these unrelated compounds in **Chapter 4** and we further focused on the adjuvant activity of the α 1-adrenergic receptor antagonist prazosin, which was the compound with the strongest adjuvant effect in our screen. Our data revealed that prazosin, but not the structural quinazoline-analogues doxazosin or terazosin, can strongly boost endolysosomal escape of both cholesterol-conjugated and polymer-transfected siRNA in lung epithelial cancer cells. Furthermore, prazosin had more outspoken effects on lysosomal swelling and siRNA delivery than our typical CAD adjuvant desloratadine, albeit prazosin clearly affected cell viability. In addition, prazosin-treated cells were characterized by a distinct cellular phenotype compared to CADs, which included the formation of large cytoplasmic vacuoles and the absence of phospholipidosis (PLD) induction. Hence, we hypothesized that yet unidentified cellular processes might contribute to prazosin-induced cytosolic siRNA delivery. In line with previous reports, our preliminary data indicated that prazosin also induces apoptosis in our cell model. These findings, in conjunction with the recent discovery that prazosin is able to enhance cross-presentation of tumor-associated antigens, altogether offer an interesting opportunity to further investigate prazosin as a cell death inducer, siRNA delivery enhancer and cross-presentation enhancer in the context of an anti-cancer combination treatment.

Finally, in **Chapter 5** we discussed the broader international context of this work and its relevance to the field. This chapter first described the key events in the development history of RNA interference (RNAi) therapeutics, which spans from the discovery of RNAi more than two decades ago to the recent clinical approvals of the first siRNA-based drugs. Next, we highlighted that the major hurdle for the widespread application of several NA therapeutics is the inefficient extra- and intracellular delivery in tissues beyond the liver. Given that we investigated the intracellular delivery-promoting effects of several small molecular drugs in this dissertation, we discussed the concept of drug repurposing and we further critically reviewed our presented (CAD) adjuvant approach. Most importantly, given that we only presented *in vitro* data in this thesis, future research should focus on the applicability of our adjuvant approach in an *in vivo* situation. In this context, local application and incorporation of the adjuvants in the carrier should be explored. Additionally, the broader applicability of

the prazosin adjuvant in an anti-cancer combination strategy should be investigated. Overall, even if delivery-enhancing compounds may never be used to increase the therapeutic potential of NA therapeutics in the clinic, the gained knowledge could foster the development of the next generation of delivery systems.

SAMENVATTING EN CONCLUSIES

RNA-therapieën kunnen een revolutie teweegbrengen in de manier waarop we een groot aantal aandoeningen behandelen, zoals virale infecties, kanker en genetische ziekten. Ten eerste kunnen boodschapper RNA (mRNA) vaccins antigenen produceren om onze immuunrespons te versterken, zoals onlangs is aangetoond in de context van de COVID-19 pandemie. Anderzijds kunnen kleinere nucleïnezuur therapieën, zoals ‘small interfering RNA’ (siRNA) of antisense oligonucleotiden (ASOs), sequentiespecifieke uitschakeling van ziektebevorderende genen induceren. Gezien hun instabiliteit en ongunstige fysicochemische eigenschappen, hebben deze nucleïnezuur-moleculen echter geschikte toedieningssystemen nodig om de meervoudige extra- en intracellulaire barrières bij *in vivo* toediening te overwinnen. In dit opzicht zijn verschillende niet-virale afleveringsdragers ontwikkeld, zoals nanopartikels (NPs) of N-acetylgalactosamine (GalNAc)-siRNA-conjugaten. Ondanks de recente goedkeuring van de eerste RNA-therapieën, worden de verst gevorderde afleveringsdragers echter nog steeds geassocieerd met verschillende afleveringsproblemen. Inderdaad, NPs en GalNAc-siRNA-conjugaten accumuleren voornamelijk in de lever bij systemische toediening, terwijl endosomale sekwestratie de RNA-geneesmiddelen afschermt van hun intracellulaire doel in het cytosol of de nucleus. Om het therapeutische potentieel van RNA-therapieën verder te verbreden zijn (nieuwe), veilige en efficiënte toedieningsstrategieën, die de biologische distributie verbeteren en de intracellulaire afgifte verhogen, zeer gewild. Hoewel er op het gebied van NP/nucleïnezuur aflevering een groeiende trend is om nieuwe nanomaterialen en zeer geavanceerde ontwerpen voor afleveringsdragers te ontwikkelen, kan het vergroten van onze fundamentele kennis (bv. hoe interageren de (huidige) NPs met de verschillende extra- en intracellulaire barrières) de rationele ontwikkeling van de volgende generatie nucleïnezuur-dragers verbeteren.

In **Hoofdstuk 1** hebben we een algemene inleiding gegeven over het gebruik van verschillende RNA-therapieën en hebben we een overzicht gegeven van de talrijke extra- en intracellulaire barrières die deze therapeutische moleculen tegenkomen bij *in vivo* toediening. Verder hebben we kort de meest relevante toedieningssystemen beschreven (bv. NPs, conjugaten) die in de loop der jaren zijn ontwikkeld om deze afleveringshindernissen aan te pakken. Daarnaast werd benadrukt hoe verschillende

technieken kunnen worden gebruikt om de interactie van nucleïnezuren en NPs met de verschillende intracellulaire barrières te onderzoeken. Het belangrijkste is dat werd aangetoond dat zowel niet-genetische (bv. kleine chemische stoffen) als genetische (bv. RNAi of CRISPR) technieken intracellulaire barrières kunnen moduleren en op deze manier de intracellulaire afgifte verbeteren. Hoewel elk van deze technieken kennis kunnen genereren over de biologische mechanismen die ten grondslag liggen aan het intracellulaire afgifteproces, is het gebruik van kleine chemische stoffen als nucleïnezuur-afgifte versterkers (*i.e.* adjuvantia) een bijzonder aantrekkelijke strategie, aangezien verschillende adjuvantia ook goedgekeurde geneesmiddelen zijn. In deze context heeft onze onderzoeksgroep onlangs gerapporteerd dat een selectie van kationische amfifiele geneesmiddelen (CADs) zou kunnen worden hergebruikt om de afgifte van lysosomaal geaccumuleerd siRNA in het cytosol van kleincellige longkankercellen te verhogen. Vanwege hun fysicochemische eigenschappen hopen deze geneesmiddelen zich op in het lysosomale compartiment, waar ze het zure sfigomyelinase enzym (ASM) functioneel blokkeren. ASM-remming leidt tot lysosomale zwelling en een permeabilisatie van het lysosomale membraan, waardoor de siRNA-moleculen vanuit het lysosomale lumen in het cytosol kunnen diffunderen. Aangezien veel CADs op grote schaal worden gebruikt (bv. antihistaminica, antidepressiva,...), zou hun herbestemming als adjuvantia de klinische vertaling van nucleïnezuur-geneesmiddelen kunnen bevorderen. Er waren echter nog meerdere vragen over de bredere toepasbaarheid van een dergelijke strategie, die in dit proefschrift verder werden onderzocht.

In **Hoofdstuk 2** rapporteerden we over een screening van een ‘repurposing’ geneesmiddelen bibliotheek (National Institutes of Health Clinical Collection) waarmee 56 CAD-adjuvantia konden worden geïdentificeerd. Hoewel ~56% van de CADs die in de screening aanwezig waren niet geïdentificeerd werden als adjuvantia (*i.e.* ‘hits’) bij 20 μ M, toonden onze data duidelijk dat de verbeterde siRNA afgifte het gevolg was van de inductie van een lysosomaal fosfolipidose fenotype door ‘CAD-hits’. Dit hoofdstuk benadrukte voornamelijk dat het waargenomen adjuvans effect op siRNA afgifte niet beperkt is tot de eerder geïdentificeerde CAD-moleculen, maar dat veel meer CADs dezelfde effecten teweegbrengen.

Aangezien in ons eerdere werk (en in de screening in **Hoofdstuk 2**) alleen het effect van de CAD adjuvantia in dextraan nanogel-getransfecteerde kleincellige longkankercellen werd geëvalueerd, onderzochten we in **Hoofdstuk 3** of de CAD adjuvantia ook gebruikt zouden kunnen worden voor andere NPs, andere kankercellen en andere soorten kleine nucleïnezuren (bv. ASOs). Onze data bevestigden dat meerdere CADs een adjuvans effect hebben op de cytosolische afgifte van zowel siRNAs als ASOs in verschillende kankercellijnen. De CAD adjuvantia zijn echter enkel compatibel met NPs die een aanzienlijke endolysosomale pool van gedecomplexeerde siRNAs met zich meebrengen. Deze vrije siRNAs kunnen vervolgens door de CAD-geïnduceerde poriën in het endolysosomale membraan diffunderen. In tegenstelling tot de huidige consensus, dat stelt dat lysosomen een doodlopende weg zijn voor siRNA-beladen nanogeneesmiddelen, ondersteunen onze data het rationele ontwerp van NPs die hun siRNA-lading vrijgeven in het endolysosomale lumen met als doel het CAD adjuvans effect te maximaliseren.

Verschillende ‘hits’ uit de screening, beschreven in **Hoofdstuk 2**, voldeden niet aan de definitie van een CAD. We bespraken deze niet-verwante moleculen in **Hoofdstuk 4** en we concentreerden ons verder op de adjuvans activiteit van de α 1-adrenerge receptorantagonist prazosine, de molecule met het sterkste adjuvans effect in onze screening. Onze gegevens toonden aan dat prazosine, maar niet de structurele analogen doxazosine of terazosine, de endolysosomale vrijstelling van zowel cholesterol-geconjugeerd als polymeer-getransfecteerd siRNA in kleincellige longkankercellen sterk kan stimuleren. Bovendien had prazosine sterker uitgesproken effecten op lysosomale zwelling en siRNA afgifte dan ons typische CAD adjuvantia (*i.e.* desloratadine), hoewel prazosine duidelijk toxiciteit induceerde. Bovendien werden prazosine-behandelde cellen gekenmerkt door een sterk verschillend cellulair fenotype ten opzichte van CADs, waaronder de vorming van grote cytoplasmatische vacuolen en de afwezigheid van fosfolipidose. Daarom postuleerden we dat andere, nog niet-geïdentificeerde, cellulaire processen zouden kunnen bijdragen aan de door prazosine-geïnduceerde cytosolische siRNA afgifte. In lijn met eerdere studies gaven onze voorlopige data aan dat prazosine ook apoptose induceert in ons celmodel. Deze bevindingen, in combinatie met de recente ontdekking dat prazosine in staat is om kruis-presentatie van tumor-geassocieerde antigenen te verbeteren, bieden een interessante mogelijkheid om prazosine verder te onderzoeken als een celdood induceerder, siRNA afgifte versterker en kruis-presentatie versterker in de context van een combinatie kankerbehandeling.

Ten slotte hebben we in **Hoofdstuk 5** de bredere internationale context van dit werk en de relevantie ervan voor het veld besproken. Dit hoofdstuk beschreef eerst de belangrijkste gebeurtenissen in de ontwikkelingsgeschiedenis van RNA-interferentie (RNAi)-therapieën. Vervolgens hebben we benadrukt dat de belangrijkste hindernis voor de wijdverbreide toepassing van verschillende nucleïnezuur-therapieën de inefficiënte extra- en intracellulaire afgifte in weefsels buiten de lever is. Aangezien we in dit proefschrift de intracellulaire afgifte-bevorderende effecten van verschillende geneesmiddel-moleculen hebben onderzocht, hebben we het concept van herbestemming ('repurposing') van bestaande geneesmiddelen besproken. Daarnaast hebben we het gebruik van onze (CAD) adjuvantia kritisch onder de loep genomen. Aangezien we in dit proefschrift alleen *in vitro* data hebben getoond, zou toekomstig onderzoek zich moet richten op de toepasbaarheid van zo'n adjuvantia in een *in vivo* situatie. Hierbij zou bijvoorbeeld lokale toediening en de co-inclusie van de adjuvantia (en het siRNA) in het NP onderzocht kunnen worden. Bovendien moet de bredere toepasbaarheid van het prazosine adjuvans in een combinatietherapie voor kanker verder onderzocht worden. Ter conclusie, zelfs als adjuvantia nooit gebruikt worden om het therapeutische potentieel van nucleïnezuur-therapieën in de kliniek te vergroten, dan nog kan de opgedane kennis de ontwikkeling van de volgende generatie toedieningssystemen mogelijk bevorderen.

CURRICULUM VITAE

PERSONALIA

Name	Van de Vyver
First names	Thijs
Nationality	Belgian
Place of birth	Ghent, Belgium
Date of birth	31/12/1993
Private address	Lostraat 80 9000 Ghent
Telephone	+32 (0)493 70 95 07
Professional address	Laboratory for General Biochemistry and Physical Pharmacy, Faculty of Pharmaceutical Sciences, Ghent University Ottergemsesteenweg 460 9000 Ghent Belgium
Telephone	+32 (0)9 264 80 74
Email	Thijs.VandeVyver@UGent.be Thijs.VandeVyver@gmail.com
Websites	https://be.linkedin.com/in/thijs-van-de-vyver-948440b3 https://scholar.google.be/citations?user=mROuQjwAAAAJ&hl=nl https://www.ugent.be/fw/pharmaceutics/biochemphypharm/en/team/thijs.htm https://biblio.ugent.be/person/802002393714 https://www.researchgate.net/profile/Thijs_Van_De_Vyver

DEGREES

June 2016	Ghent University, Ghent, Belgium Master of Science in Drug Development Summa cum laude Master thesis: <i>“Evaluatie geglyceerde vingernagelproteïnen via ATR-FTIR-Spectroscopie: niet-invasieve merker voor diagnose & controle van diabetes”</i> under promotorship of Prof. Dr. Joris Delanghe. Department of Clinical Chemistry, Ghent University Hospital, Ghent, Belgium
December 2014	Ghent University, Ghent, Belgium Honours Programme in Life Sciences
June 2014	Ghent University, Ghent, Belgium Bachelor in Pharmaceutical Sciences Magna cum laude
June 2011	Sint-Janscollege, Ghent, Belgium High school degree (Latin and Mathematics)

LANGUAGES

Dutch:	Native language
English:	Full professional proficiency
French:	Limited working proficiency
German:	Limited working proficiency

INTERNATIONAL PEER-REVIEWED A1 PUBLICATIONS

Published

“Cationic Amphiphilic Drugs Boost the Lysosomal Escape of Small Nucleic Acid Therapeutics in a Nanocarrier-Dependent Manner.” **Thijs Van de Vyver**, Bram Bogaert, Lynn De Backer, Freya Joris, Roberta Guagliardo, Jelter Van Hoeck, Pieterjan Merckx, Serge Van Calenbergh, Srinivas Ramishetti, Dan Peer, Katrien Remaut, Stefaan C. De Smedt, and Koen Raemdonck.
ACS Nano, 2020, 14, 4774-4791. IF₂₀₁₉ = 14.588

“Repurposing Cationic Amphiphilic Drugs as Adjuvants to Induce Lysosomal siRNA Escape in Nanogel Transfected Cells.” Freya Joris, Lynn De Backer, **Thijs Van de Vyver**, Chiara Bastiancich, Stefaan C. De Smedt, and Koen Raemdonck.
Journal of Controlled Release, 2018, 269, 266-276. IF₂₀₁₉ = 7.727

“Glycation in Human Fingernail Clippings Using ATR-FTIR Spectrometry, a New Marker for the Diagnosis and Monitoring of Diabetes Mellitus.” Renaat Coopman, **Thijs Van de Vyver**, Antoine Sadiki Kishabongo, Philippe Katchunga, Elisabeth H Van Aken, Justin Cikomola, Tinne Monteyne, Marijn Speeckaert, and Joris Delanghe.
Clinical Biochemistry, 2017, 50, 62-67. IF₂₀₁₉ = 2.573

Submitted

“Surfactant Protein B Promotes Cytosolic siRNA Delivery by Adopting a Virus-like Mechanism of Action.” Roberta Guagliardo, Jelle Penders, Agata Zamborlin, Herlinde De Keersmaecker, **Thijs Van de Vyver**, Sandrine Verstraeten, Pieterjan Merckx, Marie-Paule Mingeot-Leclercq, Mercedes Echaide, Jesús Pérez-Gil, Molly M. Stevens, Stefaan C. De Smedt, and Koen Raemdonck.
Pending revisions at *ACS Nano*. IF₂₀₁₉ = 14.588

“Hydrogel-induced Cell Membrane Disruptions Enable Direct Cytosolic Delivery of Membrane-impermeable Cargo.” Jelter Van Hoeck, **Thijs Van de Vyver**, Aranit Harizaj, Glenn Goetgeluk, Pieterjan Merckx, Jing Liu, Christian Vanhove, Mike Wels, Herlinde De Keersmaecker, Bart Vandekerckhove, Kevin Braeckmans, Stefaan C. De Smedt, and Koen Raemdonck.
Submitted to *Advanced Materials*. IF₂₀₁₉ = 27.398

NATIONAL AND INTERNATIONAL CONFERENCES WITH ORAL PRESENTATION

- December 8, 2017 Biopharmacy Day/Meeting 2017, Université Catholique de Louvain, Brussels, Belgium
“Repurposing low molecular weight drugs as adjuvants to induce lysosomal siRNA escape in nanogel transfected cells”
- April 19, 2018 Research Day and Student Research Symposium, Ghent, Belgium
“Repurposing low molecular weight drugs as adjuvants to induce lysosomal siRNA escape in nanogel transfected cells”
- April 4, 2019 Research Day and Student Research Symposium, Ghent, Belgium
“Repurposing Low Molecular Weight Drugs as Adjuvants to Induce Lysosomal Small RNA Escape in Nanoparticle Transfected Cells”
- December 17, 2019 Biopharmacy Day/Meeting 2019, Ghent University, Ghent, Belgium
“Cationic amphiphilic drugs boost the lysosomal escape of small nucleic acid therapeutics in a nanocarrier-dependent manner”

(INTER)NATIONAL CONFERENCES WITH POSTER PRESENTATION

- September 19-20, 2017 f-TALES on Nanomaterials in Biomedical Sciences, Ghent, Belgium
“Repurposing small molecular drugs as adjuvants to induce lysosomal siRNA escape in nanogel transfected cells”
- April 11-13, 2018 The 15th edition of the European Symposium on Controlled Drug Delivery, Egmond-Aan-Zee, The Netherlands
“Repurposing low molecular weight drugs as adjuvants to induce lysosomal siRNA escape in nanogel transfected cells”
- July 21-24, 2019 2019 Controlled Release Society Annual Meeting & Exposition, Valencia, Spain
“Repurposing Low Molecular Weight Drugs as Adjuvants to Induce Lysosomal Small RNA Escape in Nanoparticle Transfected Cells”

NATIONAL CONFERENCES/SYMPOSIA WITHOUT PRESENTATION

- September 7, 2017 RBSM symposium on high-dimensional fluorescence-based microscopy, Antwerp, Belgium
- October 19, 2017 Official opening of c-BIOS (Expertise Centre for Bioassay Development and Screening), Ghent, Belgium
- November 29, 2018 UCL Autumn Meeting, Université Catholique de Louvain, Brussels, Belgium

INTERNATIONAL RESEARCH EXPERIENCE

- August 2014 Internship at the Biopharmacy department of the University of Utrecht (Department of Pharmaceutics, Utrecht Institute for Pharmaceutical Sciences), under the supervision of Dr. Enrico Mastrobattista, to perform research in the context of the Honours Programme in Life Sciences

SCIENTIFIC COMMUNICATION

- November 26, 2017 *"Diabetes? Knip een vingernagel! : suikerziekte opsporen"* **Thijs Van de Vyver**. Eos magazine, Jrg. 33 (2016) nr. 2, p. 82-83.

TEACHING ACTIVITIES

- 2016-2019 Teaching assistant on the subject of Physical Pharmacy ('Fysicochemie van het Geneesmiddel', practical exercises).
- 2019-2020 Focusgroup reformation practical exercises 'Fysicochemie van het Geneesmiddel' and 'Industriële Analytische Chemie' (planned for 2021-2022).
- May 9, 2019 Assistant for visit GSK Vaccines (Cervarix/Shingrix manufacturing plant) in Wavre (Belgium) with major Biologics (Master of Science in Drug Development).
- 2016-2017 Lab instructor for the Pharmaceutical Bachelor Thesis (FaBaP).
- 2019-2020 Communication tutor for the Pharmaceutical Bachelor Thesis (FaBaP).
- 2016-2020 Supervisor of students during their Master/Honours Programme thesis:
- Pieter Laleman, Master dissertation (Master of Science in Drug Development, Ghent University, Ghent, Belgium). *"De rol van het TRPML-1 kanaal in CAD-gemedieerde lysosomale vrijstelling van siRNA"* (2017)
- Alexis Moust, Master dissertation (Master of Science in Drug Development, Ghent University, Ghent, Belgium). *"Assessing the broader applicability of different small molecule adjuvants for the delivery of small nucleic acids"* (2018)
- Luisa Schretzmayer, Master dissertation (Magistra der Pharmazie, University of Vienna, Vienna, Austria) *"The repurposing of different small molecule adjuvants for the delivery of nucleic acids is both payload- and carrier-dependent"* (2019)
- Saar Doornaert, Honours Programme in Life Sciences (Ghent University, Ghent, Belgium) *"Assessing multiple small molecule adjuvants for the enhanced delivery of siRNA, formulated in different nanocarriers"* (2020)
- 2016-2020 Supervising (e.g. 'Biochemie en biofysica I/II', 'Fysicochemie van het Geneesmiddel', 'Major Biofarmaca') and conducting ('Bionanotechnology', oral) examinations.

AWARDS, SCHOLARSHIPS AND GRANTS

- December 17, 2015 **'Eos-prize 2015'** (Eos Wetenschap - de Vlaamse Scriptieprijs)
My master thesis was selected from 152 applications to win the Eos-prize 2015 for the best thesis in exact sciences (<https://www.eoswetenschap.eu/gezondheid/thijs-van-de-vyver-wint-eos-prijs-2015>).
- September 20, 2016 **'Pharmacist and Doctor Nedeljkovic Award 2016'** (Belgisch Genootschap voor Farmaceutische Wetenschappen)
Granted annually to a graduated pharmacist and medical doctor, appointed by the president of the faculty and based on study results of the whole curriculum (best global study result from both masters).
- 2016-2020 **PhD Fellowship of the Research Foundation Flanders**
(Aspirant Fond Wetenschappelijk Onderzoek (FWO) – Vlaanderen)
- 2019-2020 Facultaire Commissie voor Wetenschappelijk Onderzoek (FCWO) mobility grants

COURSES

Cluster Communication Skills

Advanced Academic English: Effective Slides (Doctoral Schools, Ghent)

Cluster Leadership and Personal Efficiency

Leadership Foundation Course (Doctoral Schools, Ghent)

Personal Effectiveness (Doctoral Schools, Ghent)

Cluster Career Management

Career day @ Janssen Pharmaceutica

12th From PhD to Job Market: From PhD to Opportunity

Scientific Specialist Courses

Nanomaterials in Biomedical Science (Consortium of Flemish Universities)

qPCR course for beginners (Doctoral Schools, Biogazelle, Ghent)

From Pictures to Numbers: Workshop on Quantitative Fluorescence Microscopy (UAntwerpen, Wilrijk)

Laboratory Animal Science I & II (Ghent University)

Granted Experiment Manager Certificate

Summer Schools

SFNano Summer school 2017 (La Grande Motte, France)